DIFFUSION AND MASS TRANSFER IN SUPERCRITICAL FLUIDS

by

PABLO G. DEBENEDETTI

Ingeniero Químico Universidad de Buenos Aires
(1978)
S.M. Massachusetts Institute of Technology
(1981)

SUBMITTED TO THE DEPARTMENT OF
CHEMICAL ENGINEERING
IN PARTIAL FULFILLMENT OF THE REQUIREMENTS
FOR THE DEGREE OF

DOCTOR OF PHILOSOPHY

at the

MASSACHUSETTS INSTITUTE OF TECHNOLOGY

December 1984

Signature of author.....
Department of Chemical Engineering
December 1984

Certified by.....
Professor Robert C. Reid
Thesis Supervisor

.....
Professor Ulrich W. Suter
Thesis Supervisor

Accepted by.....
Chairman, Departmental Committee
on Graduate Studies

DIFFUSION AND MASS TRANSFER IN SUPERCRITICAL FLUIDS

by

Pablo Gastón Debenedetti

Submitted to the Department of Chemical Engineering on December 18th, 1984 in partial fulfillment of the requirements for the degree of Doctor of Philosophy

ABSTRACT

The different pressure dependence of fluid density and viscosity in going from the dilute gas to the dense fluid state gives rise to kinematic viscosities which, in the near supercritical region ($1<P_r\leq 4$; $1<T_r\leq 1.1$) are exceptionally low. The density gradients which exist in any mass transfer situation will, in the presence of a gravitational field, cause buoyancy-driven currents which, for a given geometry and Reynolds number, are two orders of magnitude higher than in ordinary liquids (the comparison being based upon the ratio of characteristic buoyant and inertial forces).

The diffusion coefficients of benzoic acid and naphthalene in supercritical SF_6, and of benzoic acid and 2-naphthol in supercritical CO_2 were measured with a hydrodynamic technique. Analysis of the data suggests that hydrodynamic behaviour at the molecular level is approached as a high viscosity limit. When experiments were conducted in the presence of bouyant currents, significant mass transfer enhancements were observed. The solution to the problem of diffusion in a finite rectangular duct is presented in analytical and graphical form.

An analysis of diffusion in the light of irreversible thermodynamics leads to the new concept of infinite dilution fugacity coefficient, and to an accurate and simple expression for the composition dependence of the fugacity coefficient. The form and asymptotic behaviour of this expression have interesting thermodynamic implications.

The behaviour of the system CO_2-benzoic acid at solute infinite dilution was studied by molecular dynamics simulation of the motion of 107 CO_2 and 1 benzene molecules, respectively, modelled as rigid polyatomics. The different symmetry of CO_2 and benzene required the implementation of two different algorithms within the same computer program. The binary diffusion coefficient and its temperature and density dependence, as well as solvent velocity and C-C radial distribution functions were calculated. Numerical problems were encountered when electrostatic forces were superimposed upon the site-site Lennard-Jones potential due to the orientation-sensitivity of the coulombic interactions.

Thesis Supervisors : Dr. Robert C. Reid; Dr. Ulrich W. Suter

Title : Professor of Chemical Engineering; Professor of Chemical Engineering

To Silvia

To my Father and Brother

To the memory of my Mother

To my family in Rome

To Professor Reid

ACKNOWLEDGEMENTS

It is a pleasure to express my sincere thanks to the many people and organizations who helped me throughout this work. Specifically, I am indebted to:

Professor Robert Reid, who taught me the rigorous beauty of Thermodynamics, and without whose help and encouragement I would not be venturing into the academic world. My respect for him as a human being and scientist can be summed up in one word: Master, which is what he has been to me

Professor Ulrich Suter, whose enthusiasm and insight were a constant source of inspiration

Professor Howard Brenner, for many a delightful discussion on matters technical and not so technical, and for his help and advice concerning my future career

Professors John Brady, Robert Brown and William Deen, members of my Thesis Committee, for their valuable help throughout this work

Professor Jack Longwell, who suggested the experimental technique in the course of a Friday afternoon seminar

Mario Da Silva and Dick Jankins of the Chemical Engineering Machine Shop, for their patience and skill in transforming clumsy drawings into working equipment

William Schmitt, for his inexhaustible good will and spirit of collaboration

Sanat Kumar and Thanassis Panagiotopoulos, for their uncommon insight and willingness to share thoughts, ideas and speculations

Glorianne Collver-Jacobson, for her help in typing part of the thesis

The National Science Foundation and the Nestle Products Technical Assistance Co. for their financial support

Howard Bernstein, for his friendship, which I truly value

Bach and Mozart, for their musical company

My family, for their constant love, support and understanding

My Father, who taught me the meaning and importance of goals and guidelines in life

Silvia, who gave so much and asked for so little during three long years. Her love was my constant source of strength and joy.

TABLE OF CONTENTS

TABLE OF CONTENTS (continued)

TABLE OF CONTENTS (continued)

LIST OF FIGURES

LIST OF FIGURES (continued)

LIST OF FIGURES (continued)

LIST OF FIGURES (continued)

LIST OF FIGURES (continued)

LIST OF FIGURES (continued)

LIST OF TABLES

LIST OF TABLES (continued)

1: SUMMARY

The technical feasibility of a chemical process is determined by two types of constraints: thermodynamic (equilibrium) limitations and kinetic (rate) limitations.

In supercritical fluid extraction, the thermodynamic constraint defines the maximum achievable solute concentration in the supercritical fluid, for any given temperature, pressure, and condensed phase composition.

From a kinetic point of view, on the other hand, the objective is to understand and, eventually, predict, the rate at which mass is transferred from the condensed to the supercritical phase.

The present work addresses several problems related to kinetic (or rate) aspects of supercritical fluid extraction, specifically:

- the influence of physical properties and their different behaviour at slightly supercritical conditions in determining the rate and mechanism of mass transfer in supercritical fluids
- the development of a hydrodynamic technique to measure true and apparent binary diffusion coefficients in supercritical fluids, where "apparent" denotes diffusion coefficients measured in the presence of buoyant forces
- the interpretation of experimental data, and the use of hydrodynamic theory to analyze diffusion in supercritical fluids
- an analysis of diffusion in the light of non-equilibrium thermodynamics
- the use of molecular dynamics to study the equilibrium structure and binary diffusion in mixtures under supercritical conditions and infinite dilution (i.e., conditions whereby solute-solute interactions are negligible).

1.1: PHYSICAL PROPERTIES AND MASS TRANSFER MECHANISM

A supercritical fluid is rigorously defined as one whose temperature and pressure are both above their critical values. In the present context, though, we restrict our attention to the region bounded by $1<Tr<1.1$, and $1<Pr<4$ (these are, of course, approximate numbers), where the rate of change of fluid properties such as the density, specific heat at constant

pressure, viscosity, etc. with respect to temperature and pressure is high and gives rise to behaviour which is unique to this region.

The above defined supercritical region is shown schematically in Figure 1.1, in reduced-density reduced pressure coordinates. Some of its peculiarities and their relevance to mass transfer will be discussed below.

The dimensionless isothermal compressibility,

$$K'_T = \left(\frac{\partial \ln \rho}{\partial \ln P}\right)_T \qquad (1.1)$$

is defined as the relative density change per unit relative pressure change, at constant temperature. It can be calculated from an equation of state, and is shown in Figures 1.2 to 1.5 as a function of temperature and pressure, for CO_2 and SF_6, for the van der Waals (1873) and Peng-Robinson (1976) equations of state (see Appendix 1). K'_T tends to 1 at low pressure (ideal gas region), 0 at high pressure (dense fluid region), and diverges at the critical point, where matter is infinitely compressible. The fact that K'_T is finite at low pressure and infinite at the critical point gives rise to states of matter whose density is comparable to that of an ordinary liquid, and which, simultaneously, are more compressible than a dilute gas. Such properties are characteristic of the supercritical region. As an example, at 318 K and 100 bar (Tr = 1.05; Pr = 1.36), CO_2 is ~ 280 times denser but almost three times more compressible than at 318K and 1 bar.

From the point of view of mass transfer, it is the different rates of change of density and viscosity in going from the ideal gas to the dense fluid region that give rise to unique behaviour under supercritical conditions. Figure 1.6 shows the density, viscosity and kinematic viscosity of CO_2 (T_c = 304.2 K; Pc = 73.8 bar) at 310 K (Tr = 1.02) as a function of pressure. Although the density of supercritical CO_2 is liquid-like, its viscosity, being virtually pressure independent at low pressures, is less than an order of magnitude higher than the corresponding dilute gas value. This is due to the fact that, although both quantities increase by roughly an order of magnitude near Pc, the finite compressibility of the dilute gas gives rise to an increase of approximately two orders

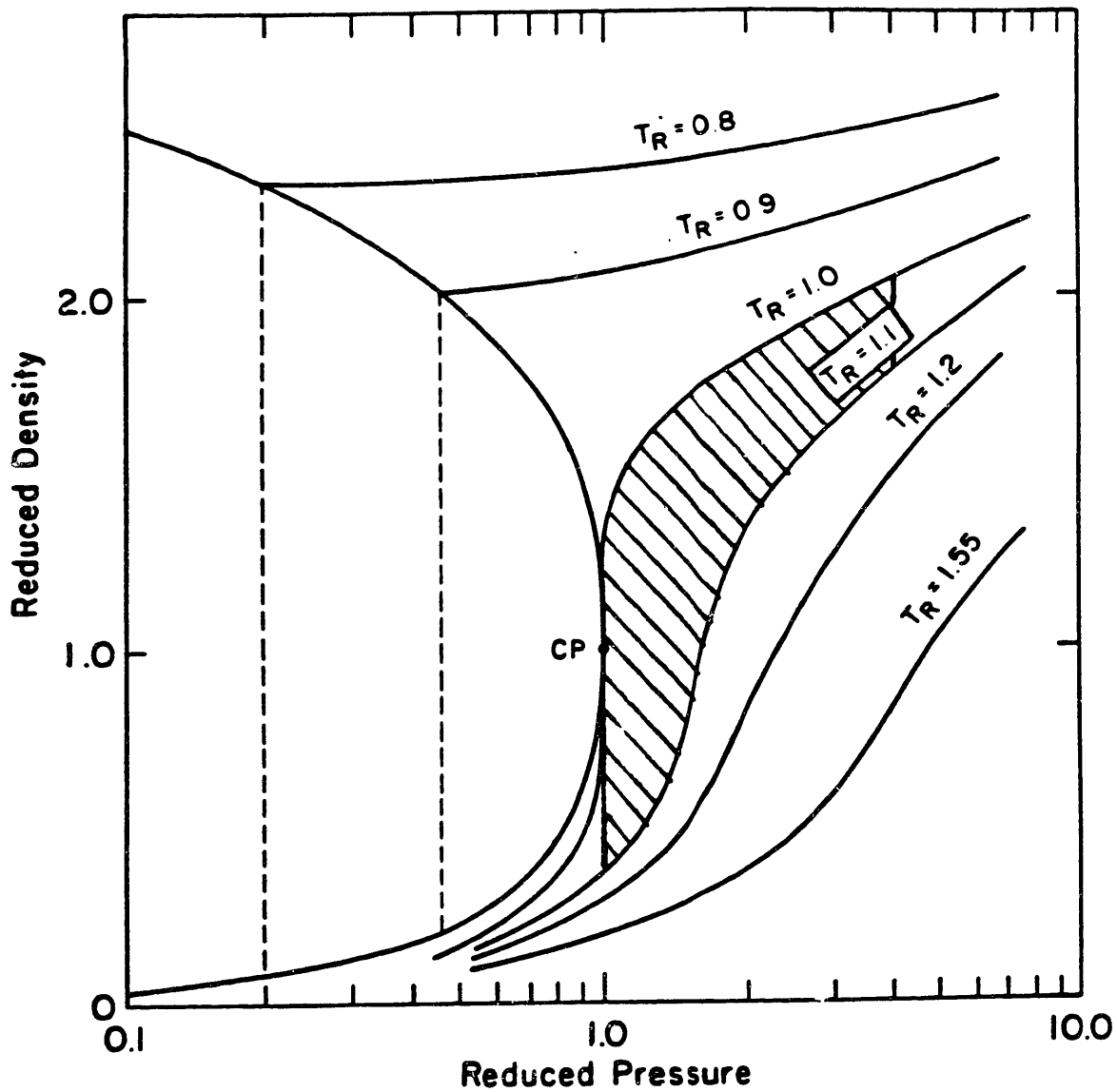

FIGURE 1.1: Schematic pressure-density diagram for a pure substance showing the region of interest in supercritical extraction.

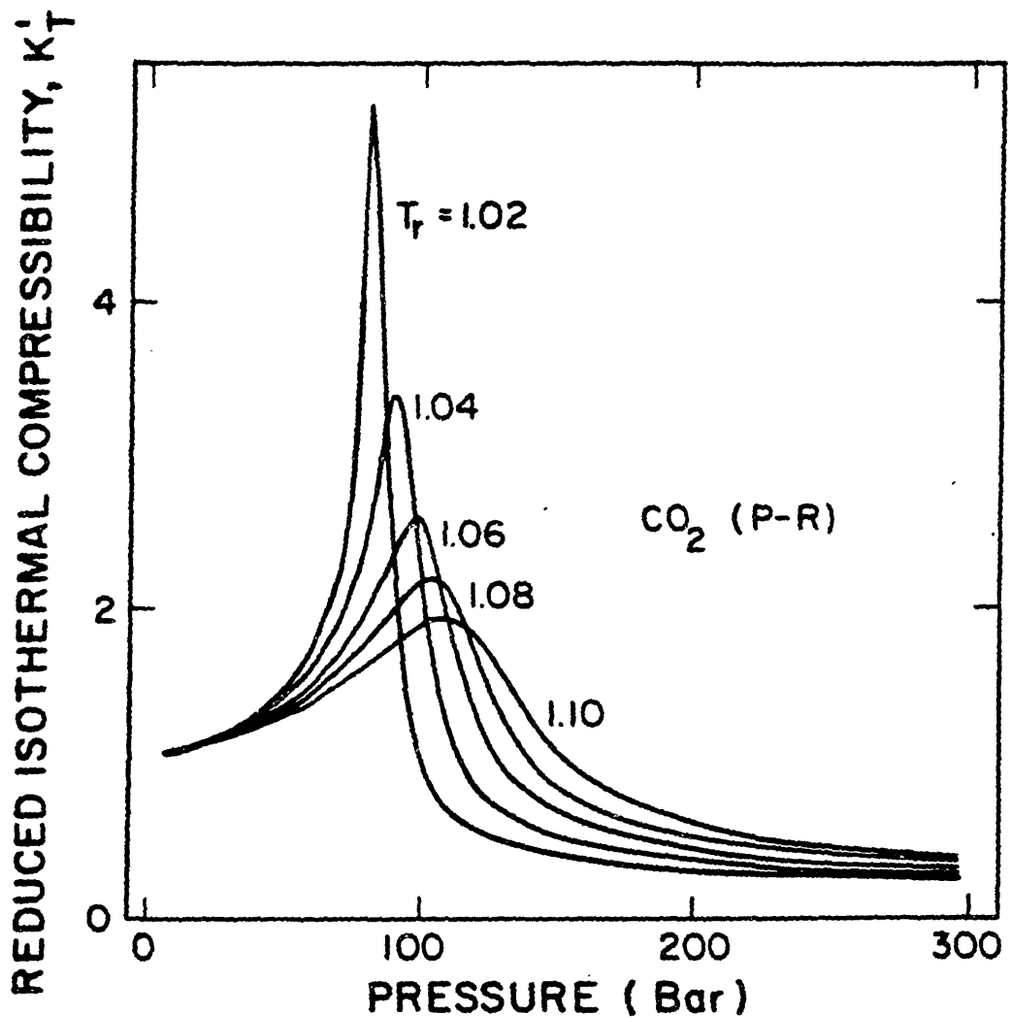

FIGURE 1.2: Dimensionless isothermal compressibility of CO_2, as modelled by the Peng-Robinson equation of state.

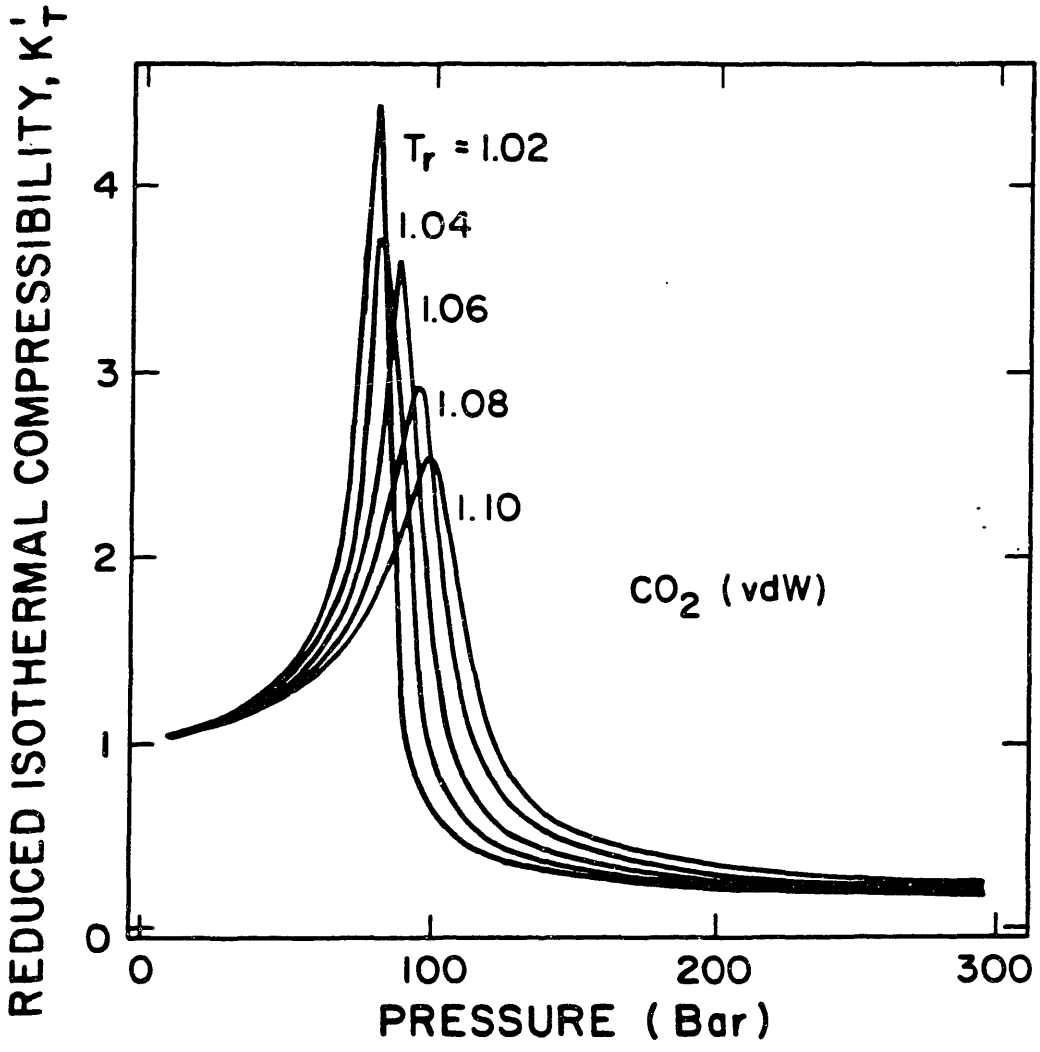

FIGURE 1.3: Dimensionless isothermal compressibility of CO_2, as modelled by the van der Waals equation of state.

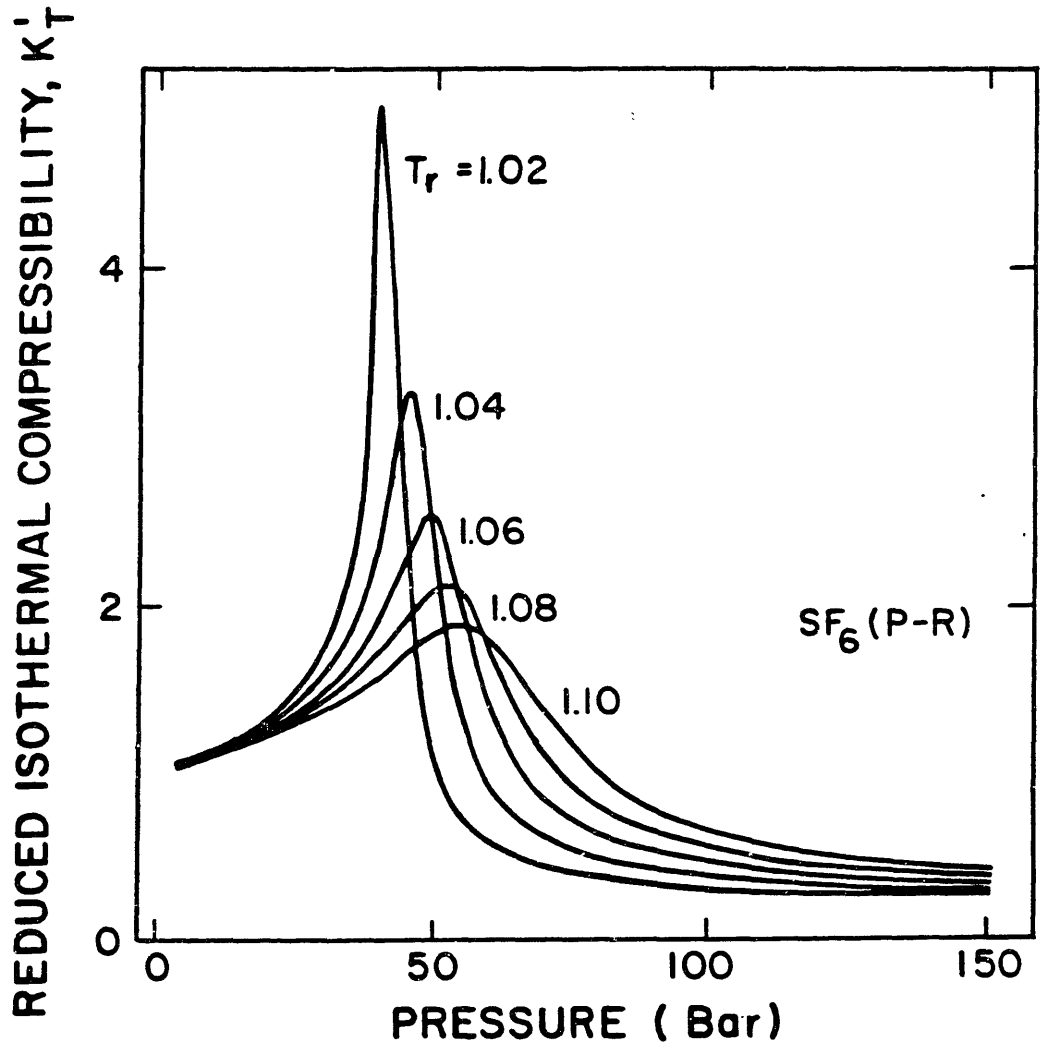

FIGURE 1.4: Dimensionless isothermal compressibility of SF_6, as modelled by the Peng-Robinson equation of state.

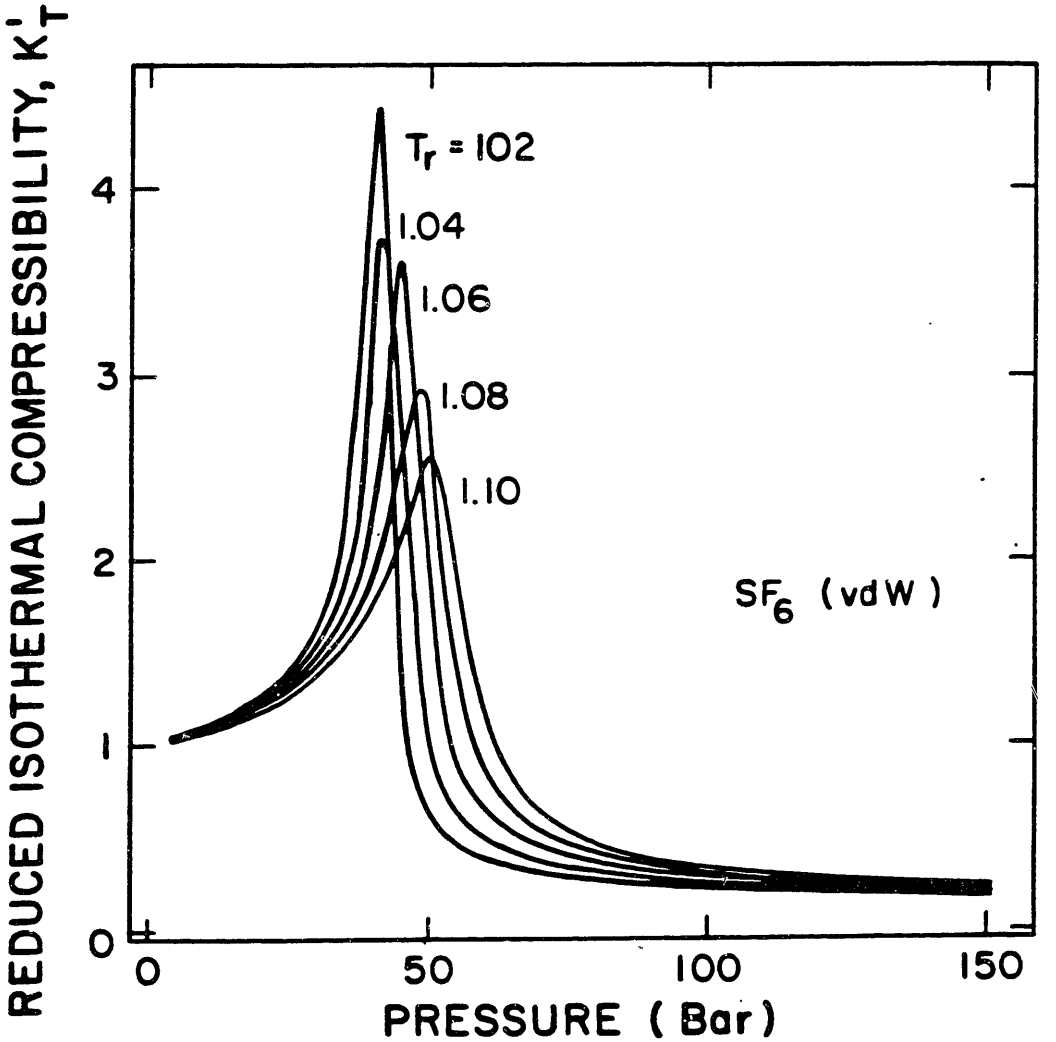

FIGURE 1.5: Dimensionless isothermal compressibility of SF_6, as modelled by the van der Waals equation of state.

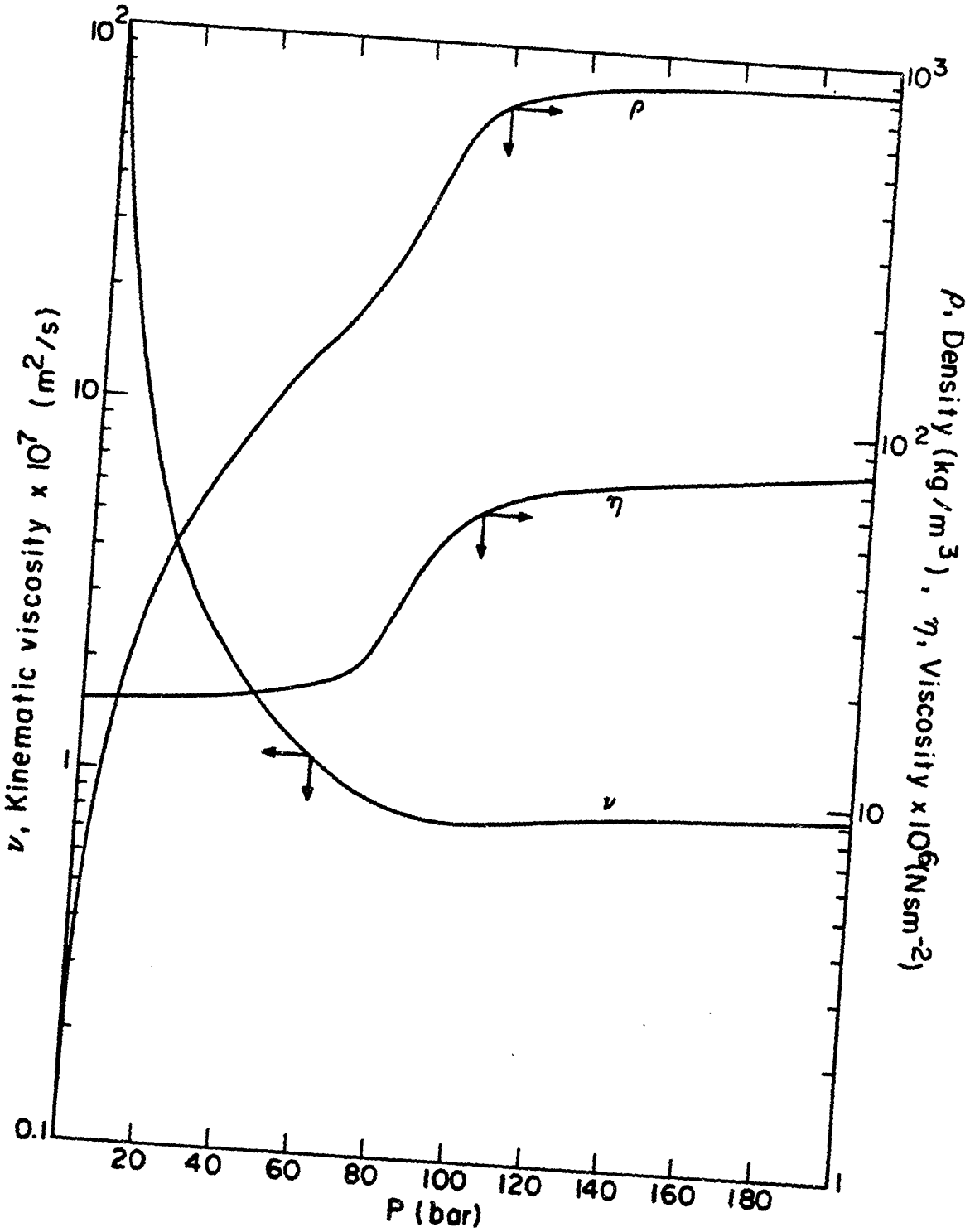

FIGURE 1.6: Density, viscosity and kinematic viscosity of CO_2 at 310K, as a function of pressure.

of magnitude in density when the pressure is raised up to values slightly lower than Pc. No such behaviour is displayed by the viscosity.

Consequently, the kinematic viscosity under supercritical conditions is very low. This is clearly shown in Figure 1.6. Liquid metals, which combine moderate viscosities with high densities, are normally associated with extremely low kinematic viscosities. This property, as will be shown below, attains even lower values in the case of supercritical fluids.

The relevance of these facts to mass transfer is best illustrated in the case of duct flow under the combined influence of a pressure gradient and gravity. We consider the situation whereby an incompressible, Newtonian fluid, under fully developed laminar flow conditions, flows inside a duct whose walls are coated with a solute that dissolves into the fluid, under the action of a concentration gradient (thermodynamic phase equilibrium exists at the interface). The aforementioned concentration gradient will give rise to a density gradient which will, in turn, alter the velocity profile. When the concentration (and density) changes are small, it is an admissible approximation to expand the density about the pure fluid value in terms of solute concentration, consider linear terms exclusively, and neglect the composition dependence of other properties (i.e., viscosity). This simplification (Boussinesq's approximation) gives rise to the following dimensionless momentum balance, (see Section 3.1).

$$\frac{2}{Re}(\nabla^+)^2 v^+ - \underline{\nabla}^+ \Pi^+ - \underline{g}' \frac{Gr}{Re^2}\frac{r}{2} = 0 \qquad (1.2)$$

where Gr ($= [(2R)^3 g\, \Delta\rho/\rho]/\nu^2$) is the Grashof number for mass transfer, and Re ($= 2R\, \langle v\rangle/\nu$), the Reynolds number.

If we now introduce the natural scales for viscous, inertial and buoyant forces,

Viscous forces ~ $\eta\, \langle v\rangle/2R$ (1.3)

Buoyant forces ~ $2R\, g\, \Delta\rho$ (1.4)

Inertial forces ~ $\langle v\rangle^2\, \rho_o$ (1.5)

the physical significance of the parameter $GrRe^{-2}$ follows immediately,

$$\frac{Gr}{Re^2} = \frac{(2R\, g\, \Delta\rho)\,(\langle v\rangle^2\, \rho_o)}{(\eta\langle v\rangle/2R)^2} \cdot \frac{(\eta\langle v\rangle/2R)^2}{(\langle v\rangle^2\, \rho_o)^2} = \frac{\text{Buoyant forces}}{\text{Inertial forces}} \qquad (1.6)$$

Consequently, if different fluids flow inside identical ducts under diffusive mass transfer conditions at any given Reynolds number, and assuming comparable density changes ($\Delta\rho/\rho$), the relative importance of natural convection (buoyant forces) scales inversely as the square of the kinematic viscosity of the fluid in question. Thus, fluids with low kinematic viscosities (i.e., supercritical fluids) can develop appreciable buoyancy driven flows even with small density gradients.

If we now compare (Figure 1.7) the properties of air, water, and mercury at ambient conditions (298K, 1 bar) with those of supercritical CO_2 at 310K and 150 bar (Tr = 1.02; Pr = 2.03) in the light of the previous discussion, some important consequences arise. We note the fact that, for ν, CO_2 has the lowest value. The fourth column is the ratio of buoyant to inertial forces at constant Reynolds number and duct geometry, scaled with the corresponding value for water. The relative importance of natural convection, therefore, is more than two orders of magnitude higher in a supercritical fluid than in ordinary liquids.

When mass transfer in the fluid phase is the controlling step, therefore, the usual design relationships for mass transfer in packed beds (Gupta and Thodos, 1962; Wilson and Geankoplis, 1966; Williamson et al., 1963) are either unsuitable on account of the absence of a Grashof number, or do not cover (Karabelas et al., 1971) the low Schmidt numbers (~ 10) which characterize diffusion of light organic solutes in supercritical fluids.

Figure 1.8 shows the importance of natural convection in vertical laminar duct flow under supercritical conditions. Although the figure itself is not limited to supercritical conditions, the values of the physical properties used to construct the actual curves are typical of supercritical fluids (ν) and of diffusion of small organic molecules (molecular weight ~ 100) in supercritical fluids (Sc = ν/). In Figure 1.8, D is the duct diameter, and L, the coated length along which diffusion takes place.

For any value of $\Delta\rho/\rho$ (interface-bulk density difference divided by mean density), the region lying above and to the right of the given curve represents tube geometries for which vertical forced laminar flow is impossible due to the presence of natural convection. For example,

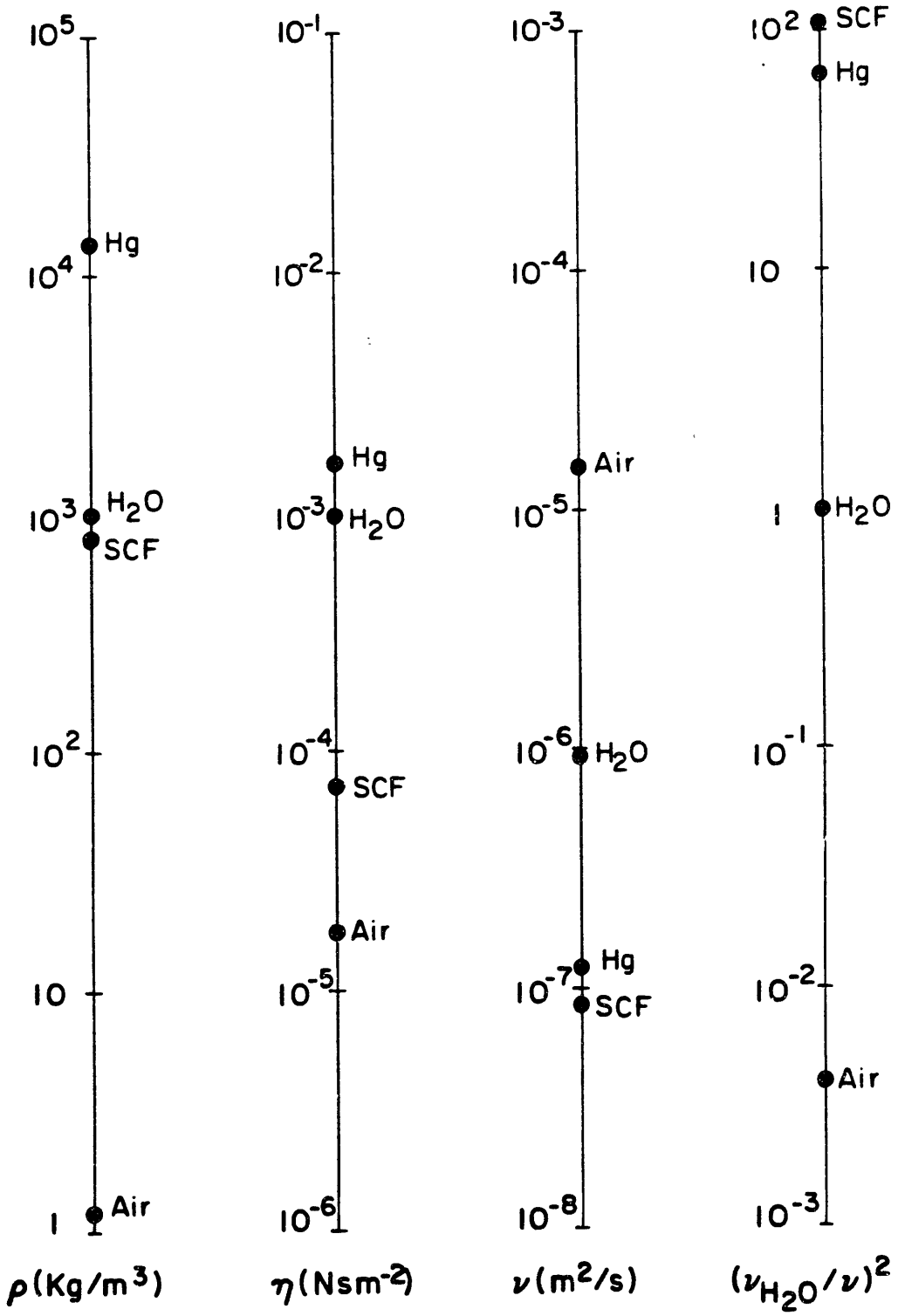

FIGURE 1.7: Comparison of physical properties of air, water, mercury (at 298K and 1 bar), and CO_2 (at 150 bar and 310 K). Relative importance of natural convection at constant Reynolds numbers.

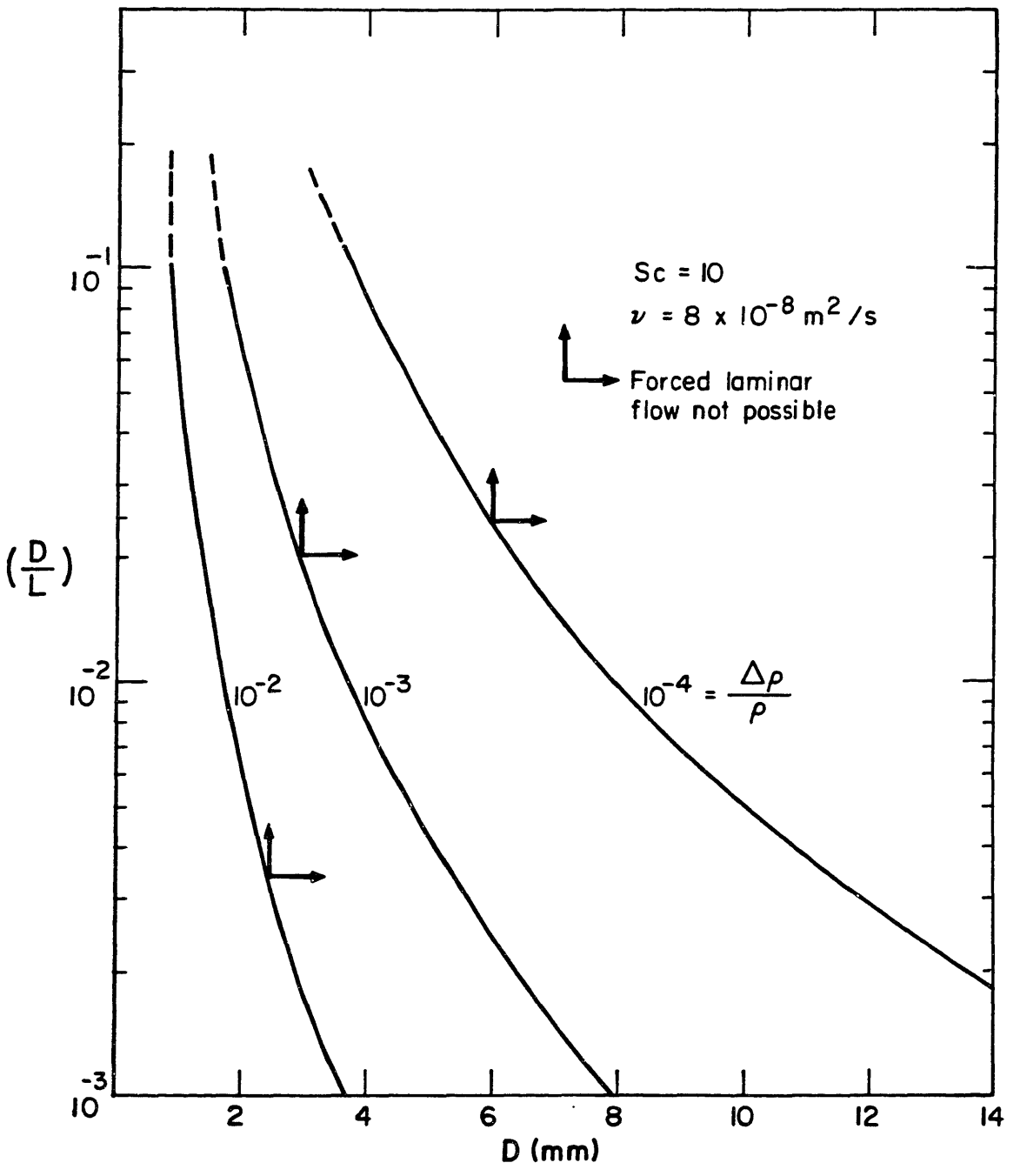

FIGURE 1.8: Cylindrical duct geometries for which forced vertical laminar flow is impossible under supercritical conditions due to natural convection.

given a relative density change as small as 10^{-3}, any aspect ratio greater than 10^{-3} makes it impossible to attain forced laminar flow in an 8mm vertical duct.

Figure 1.8 is valid for $10^{-2} < Sc\ (2R/L) < 1$ and vertical flow. If the parameter $Gr \cdot Sc(2R/L)$ (a scaled mass transfer Rayleigh number) exceeds 10^4, forced laminar flow is impossible (Metais and Eckert, 1964); this criterion has been used to obtain Figure 1.8. The condition $Gr \cdot Sc \cdot 2R/L < 10^4$ is a necessary but not sufficient criterion for forced laminar flow, so that the region lying below and to the left of each curve does not, by itself, guarantee laminar flow.

1.2: HYDRODYNAMIC EXPERIMENTS

The experimental technique involved fully developed laminar flow of a supercritical fluid in a horizontal rectangular duct (Figure 1.9), the bottom surface of which was coated with the solute of interest.

The amount of solute that, at steady state, precipitates, upon decompression, from a measured amount of solvent during the course of a carefully timed experiment is, for a given temperature, pressure (and hence equilibrium solubility of the solute in the supercritical solvent), flow rate, and duct geometry, a function of the binary diffusion coefficient.

The determination of a diffusion coefficient thus involves (at least) one equilibrium experiment, where the solubility of the solute in the supercritical fluid is measured, and a diffusion experiment.

In a diffusion experiment (Figure 1.9) a brass plate (4) is tightly fitted into an enclosure made up of two aluminium hemi-cylinders (1,2); fluid flows inside the resulting channel (3).

The test section (6) is made by casting molten solute and carefully machining and polishing after solidification. The plate also contains a section (5) where laminar flow is allowed to develop, and an outlet section (7).

Fluid by-pass of the test section is prevented by a Viton gasket (8) which forces the plate against the upper surface (9'), and by the labyrinth seal (9) which results when the hemi-cylinders are forced together (10,11) and Teflon tape is placed between the upper and lower mating

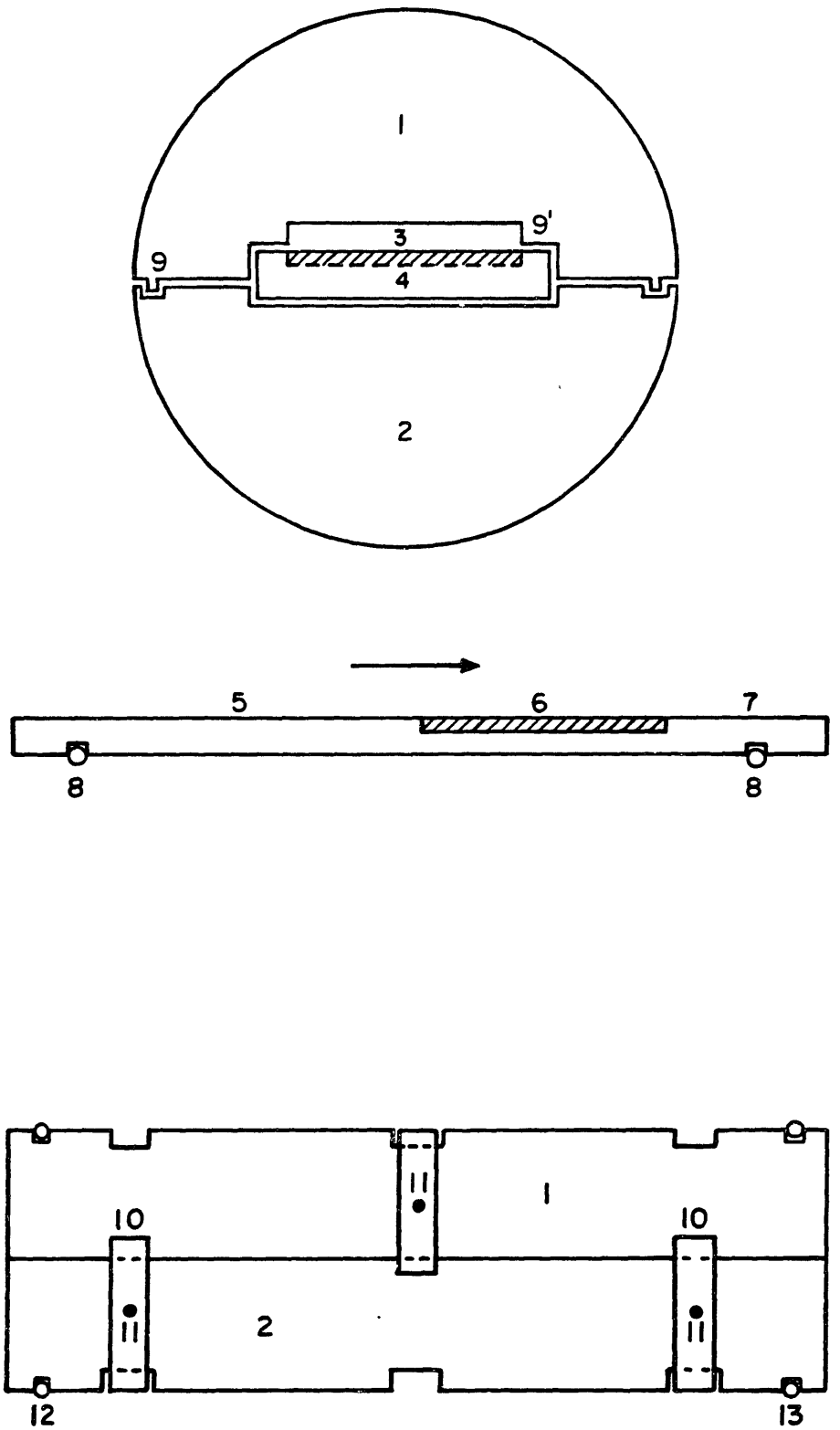

FIGURE 1.9: Schemactic diagram of flat plate for hydrodynamic experiments.

surfaces (9). The whole assembly is tightly fitted inside a 5 cm (2 inches) stainless steel pipe. O-ring 13 provides sealing, while O-ring 12 is notched: the pressure in 3 is thus equal to the pressure outside 1 and 2.

For dilute solutions, the density decreases monotonically away from the surface if

$$M_1/M_2 > \bar{V}_1/V_2 \qquad (1.7)$$

and viceversa. In Equation (1.7), M_1 and M_2 are the solute and solvent molecular weights, $\bar{V}_1$ is the solute partial molar volume, and V_2 the solvent molar volume.

The above inequality (see Section 6.3 for derivation) was satisfied under all of the experimental conditions tested (see Appendix 2). In addition, the equilibrium solubility increased with temperature for all of the systems investigated at every value of the pressure for which experiments were conducted. This implies that the solubilization was endothermic under all experimental conditions.

Consequently, when channel 3 was horizontal and constituted the duct's bottom surface, the flow was unaffected by gravity, and true binary diffusion coefficients were measured, as explained above, by weighing the amount of solute that precipitates, upon decompression, from a measured quantity of solvent, at steady state. Buoyant effects were introduced by rotating 1 and 2 (Figure 1.9) inside the steel pipe. The same experiment then gave rise to different results, which provided qualitative information on the importance of natural convection in mass transfer with supercritical fluids.

The results of such an experiment, for benzoic acid diffusing in CO_2 at 160 bar and 318K, are shown in Figure 1.10 (see also Table 6.20). The dotted line (mass transfer rate) in Figure 1.10 does not extend to 0° since the diffusion (0°) experiment was done at a different flow rate, and mass transfer rates are a function of fluid velocity. The importance of natural convection, as well as the potential for experimental error when using hydrodynamic techniques, can be seen from the fact that a 650% increase in the apparent diffusion coefficient results from a 90° rotation of the flat plate.

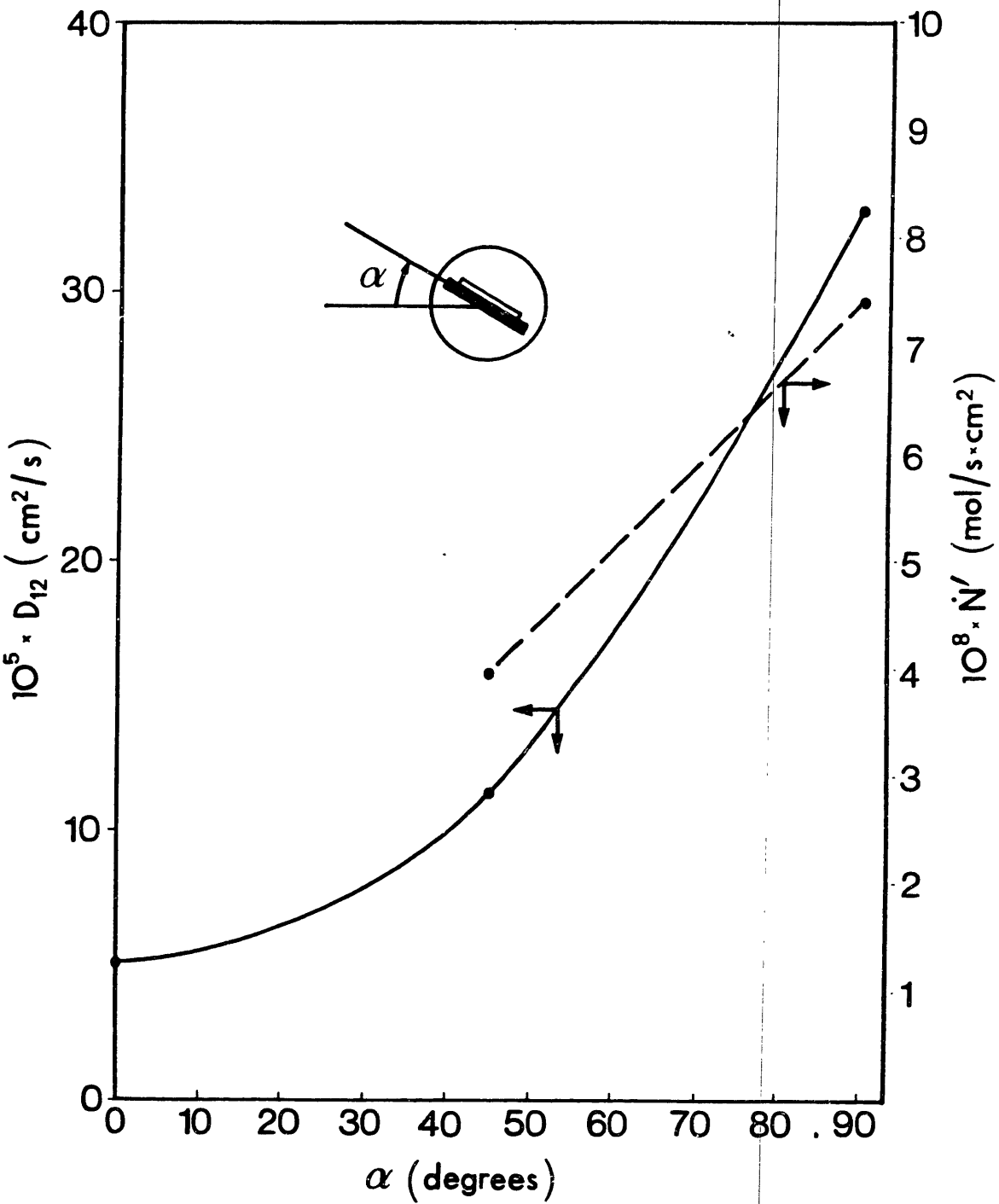

FIGURE 1.10: Effect of natural convection on the apparent diffusion coefficient and mass transfer rate; CO_2-benzoic acid; 318 K, 160 bar.

The actual calculation of a diffusion coefficient from experimental measurements implies knowledge of the solution to the problem of diffusion from a constant composition source plane into a rectangular duct where axial fully developed laminar flow of an incompressible fluid takes place.

For the geometry shown in Figure 1.11, the problem to be solved can be written in dimensionless form,

$$v^+ \frac{\partial c^+}{\partial x^+} = \left(\frac{2\beta}{\alpha}\right) Pe \left[\frac{\partial^2 c^+}{\partial x^{+2}} + \frac{\partial^2 c^+}{\partial y^{+2}} + \frac{\partial^2 c^+}{\partial z^{+2}}\right] \tag{1.8}$$

where

$$\alpha = b/a$$

$$\beta = L/2a$$

$$x^+ = x/b$$

$$y^+ = y/b \tag{1.9}$$

$$z^+ = z/b$$

$$c^+ = 1 - c/ci$$

$$v^+ = v/\langle v \rangle$$

$$Pe = \langle v \rangle L/\mathcal{D}$$

with ci, the interface solute concentration, L, the coated length, and $\langle v \rangle$, the cross section average velocity. Equation (1.8) can be simplified by performing an order of magnitude analysis, defining

$$\xi \equiv b - y \tag{1.10}$$

and using the following empirical expression for the velocity profile (Shah and London, 1978)

$$\frac{v}{v_{max}} = \left[1 - \left(\frac{|y|}{b}\right)^n\right]\left[1 - \left(\frac{|z|}{a}\right)^m\right] \tag{1.11}$$

$$m = 1.7 + 0.5\,\alpha^{-1.4}$$

$$n = 2 \qquad \alpha \leq 1/3 \tag{1.12}$$

$$n = 2 + 0.3\,(\alpha - 1/3) \qquad \alpha \geq 1/3$$

where Equations (1.12) were obtained by fitting Equation (1.11) to the finite difference solution of the momentum balance equation.

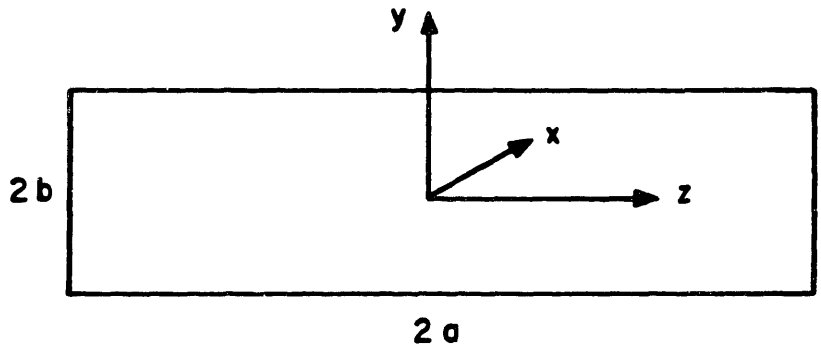

FIGURE 1.11: Geometry for the rectangular duct problem.

From order of magnitude considerations, diffusion in the axial (x) and transverse (z) directions can be considered negligible with respect to axial convection and diffusion away from the source plane (i.e., in the y direction), once the actual values of the shape factors and physical properties are taking into account (α, β, Pe; see Chapter 5).

The problem then becomes, for $\alpha < 1/3$,

$$(2\xi^{+} - \xi^{+2}) \frac{\partial c^{+}}{\partial x^{+}} = \frac{m}{m+1} \cdot \frac{4\beta}{3\alpha\ Pe} \cdot \frac{1}{[1 - (\alpha|z^{+}|)^{m}]} \frac{\partial^2 c^{+}}{\partial \xi^{+2}} \qquad (1.13)$$

Equation (1.13) can be solved by variable separation, series expansion, and integration of the resulting two dimensional solution across the transverse (z^{+}) direction. The solutions are shown graphically in Figures 1.12 and 1.13. The full expressions are given in Chapter 5. The quantities plotted in these figures are defined as

$$\langle r \rangle = \langle c \rangle / ci \qquad (1.14)$$

$$Sh = \frac{4b}{(1+\alpha)} \cdot \frac{1}{\mathfrak{D}} \cdot \int_0^1 k\, d(z/a) \qquad (1.15)$$

$$X_0 = x\mathfrak{D} / \langle v \rangle\ b^2 \qquad (1.16)$$

i.e., the relative saturation, the z-averaged local Sherwood number based on the hydraulic diameter and a modified inverse Graetz number.

The important point is that $\langle r \rangle$, the experimentally measured quantity, is a function of α(= b/a) and X_0. Thus, for a given aspect ratio, flow rate, coated length and channel height, $\langle r \rangle$ is a function of the diffusion coefficient. In an experiment, then, the ratio $\langle r \rangle$ is determined by measuring c and ci in a diffusion and an equilibrium experiment, respectively, and calculating X_0 from the mathematical expression plotted in Figure 1.12, to obtain finally, $\mathfrak{D}$, from X_0, x (= L), $\langle v \rangle$ and b^2.

1.3: EXPERIMENTAL RESULTS AND DATA ANALYSIS

The experimentally measured diffusion coefficients are shown in Figure 1.14 as a function of solvent molar density; the same data are plotted

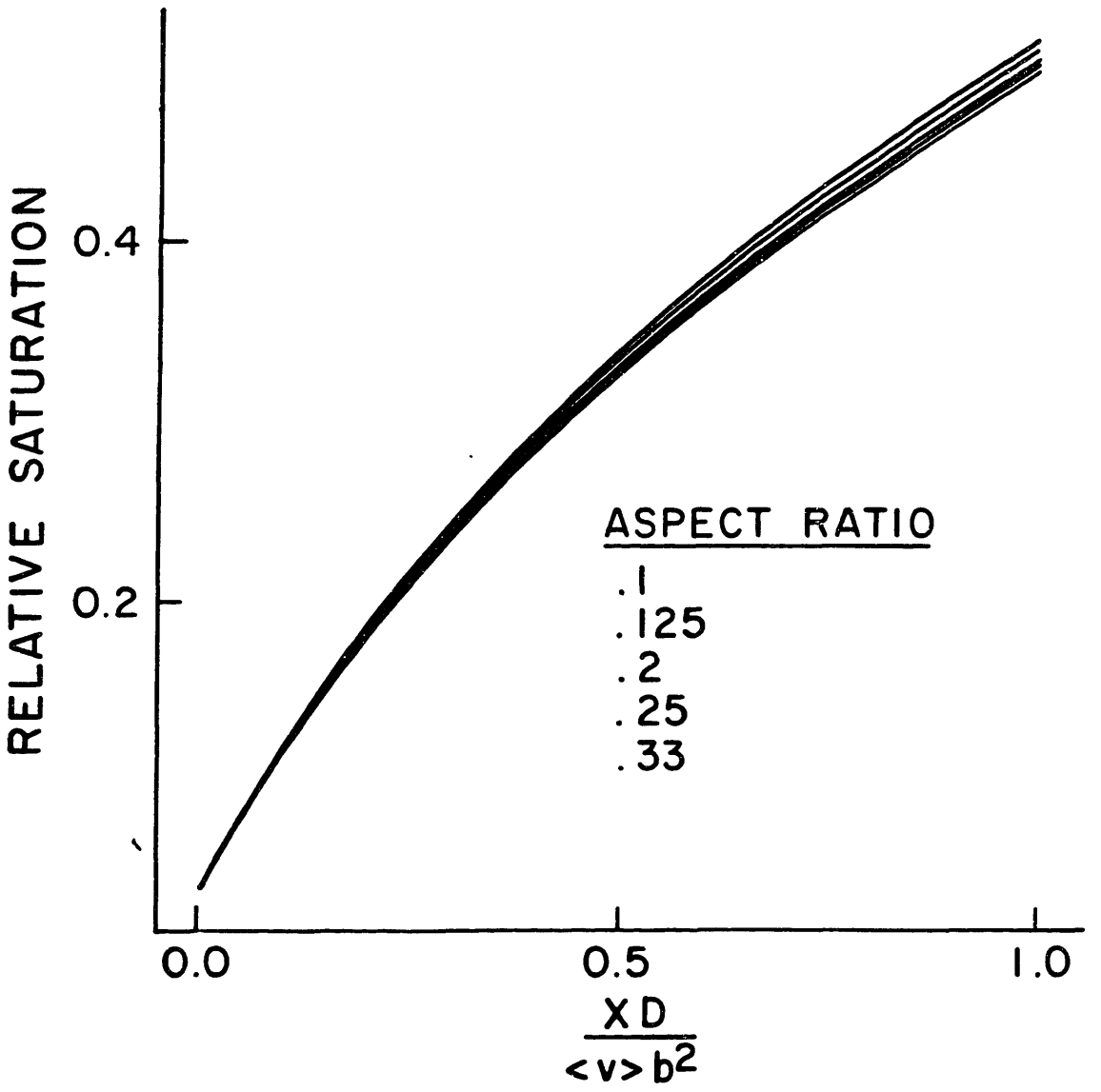

FIGURE 1.12: Relative saturation versus inverse Graetz number; solution valid for $\alpha \leq 1/3$ and high axial Peclet numbers.

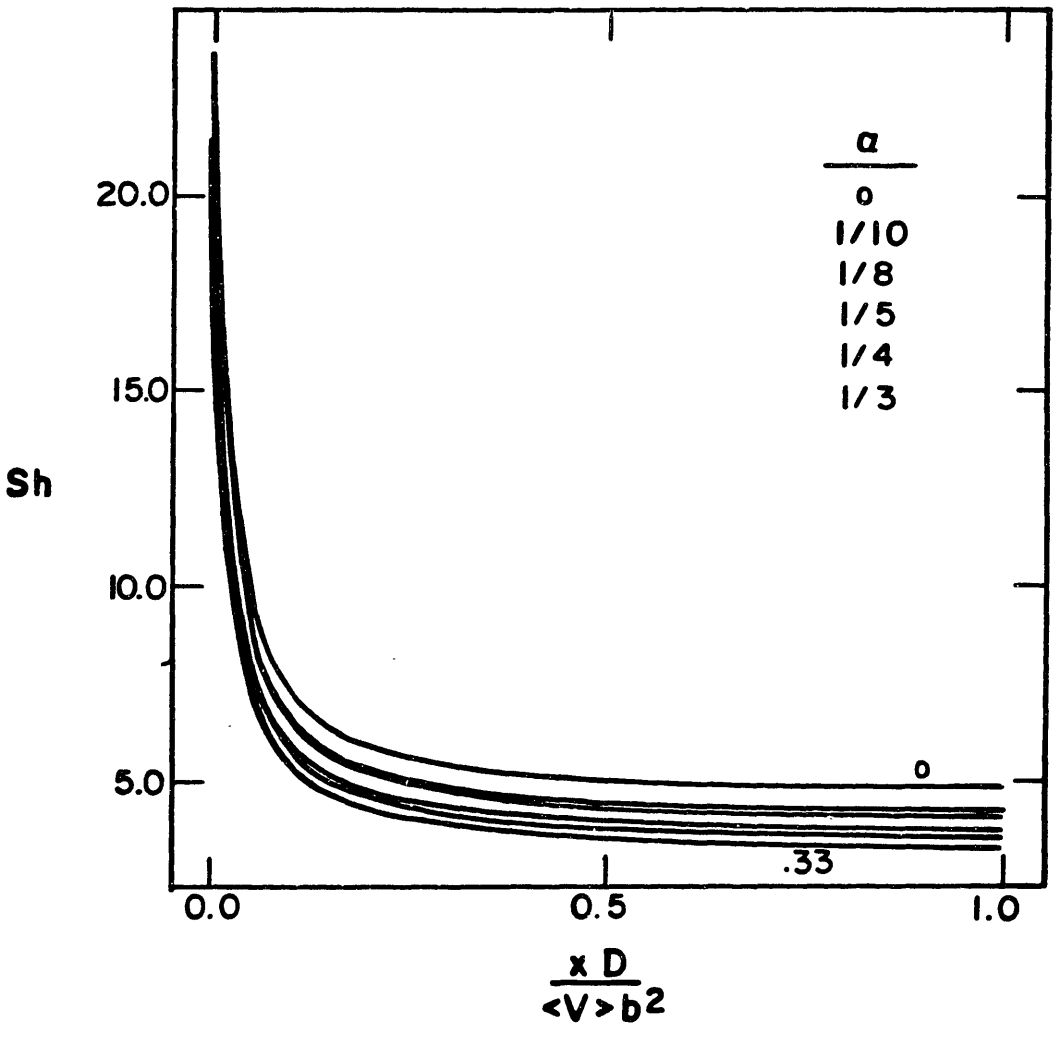

FIGURE 1.13: z-averaged local Sherwood number versus inverse Graetz number; solution valid for $\alpha \leq 1/3$ and high axial Peclet numbers.

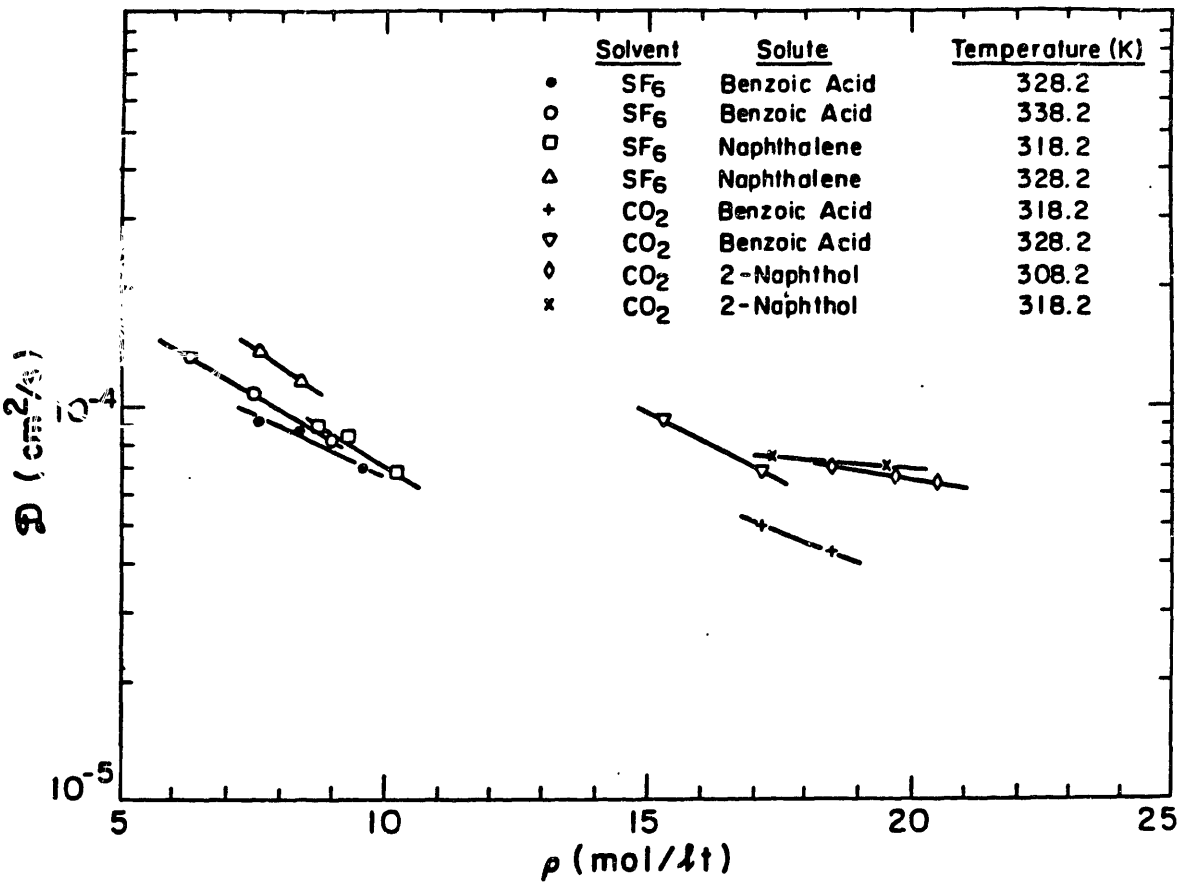

FIGURE 1.14: Experimental binary diffusion coefficients as a function of solvent molar density.

separately for each system in Figures 1.15 - 1.18. The use of density instead of pressure as an independent variable is a consequence of the molecular approach to diffusion, whereby this phenomenon is seen as the macroscopic consequence of collisions (interactions), whose frequency (for a given binary system) is a function of the molecules' average velocity (temperature) and number density (i.e., number of molecules per unit volume).

The density range over which experiments were made for any given system was too small to allow generalizations as to the observed linearity of the data when plotted in log D vs. ρ fashion.

The measured diffusion coefficients of benzoic acid were always lower, at any given density, than the corresponding values for naphthalene (in SF_6) and 2-naphthol (in CO_2), both of which are larger molecules than benzoic acid. This suggests a possible dimerization of benzoic acid in the fluid phase, a behaviour experimentally observed in CCl_4 and CCl_3H (I'Haya and Shibuya, 1965), and in its vapour, C_6H_{12}, CCl_4 and C_6H_6 (Allen et al., 1966). This hypothesis is also consistent with the exceptionally high temperature dependence of the diffusion coefficient of benzoic acid at constant density (see Figure 1.18), which shows an activation energy (6.9 Kcal/mol) in good agreement with the experimentally measured values for the dimerization of benzoic acid in cyclohexane (6.4 Kcal/mol), CCl_4 (5.5 Kcal/mol), and its own vapour phase (8.1 Kcal/mol) (Allen et al., 1966). These considerations can only be taken qualitatively, since the overall diffusion coefficient is related in a non-linear way to the dimerization constant.

Although benzoic acid association in the fluid phase has not been measured in either SF_6 or CO_2, the published equilibrium constants (Allen et al.) give rise to high associated fractions (69% at 303K in CCl_4, for example; see Chapter 6 for detailed calculations), making the dimerization hypothesis at least plausible.

At any given density, the temperature dependence of the observed diffusion coefficients is higher than the $T^{1/2}$ hard sphere prediction. However, for three of the four systems investigated, the quantity ηDT^{-1} was found to be fairly constant over the range of conditions tested, suggesting a hydrodynamic (Stokes-Einstein) description. The benzoic acid-CO_2 data, on the other hand, exhibit peculiarities which seem to

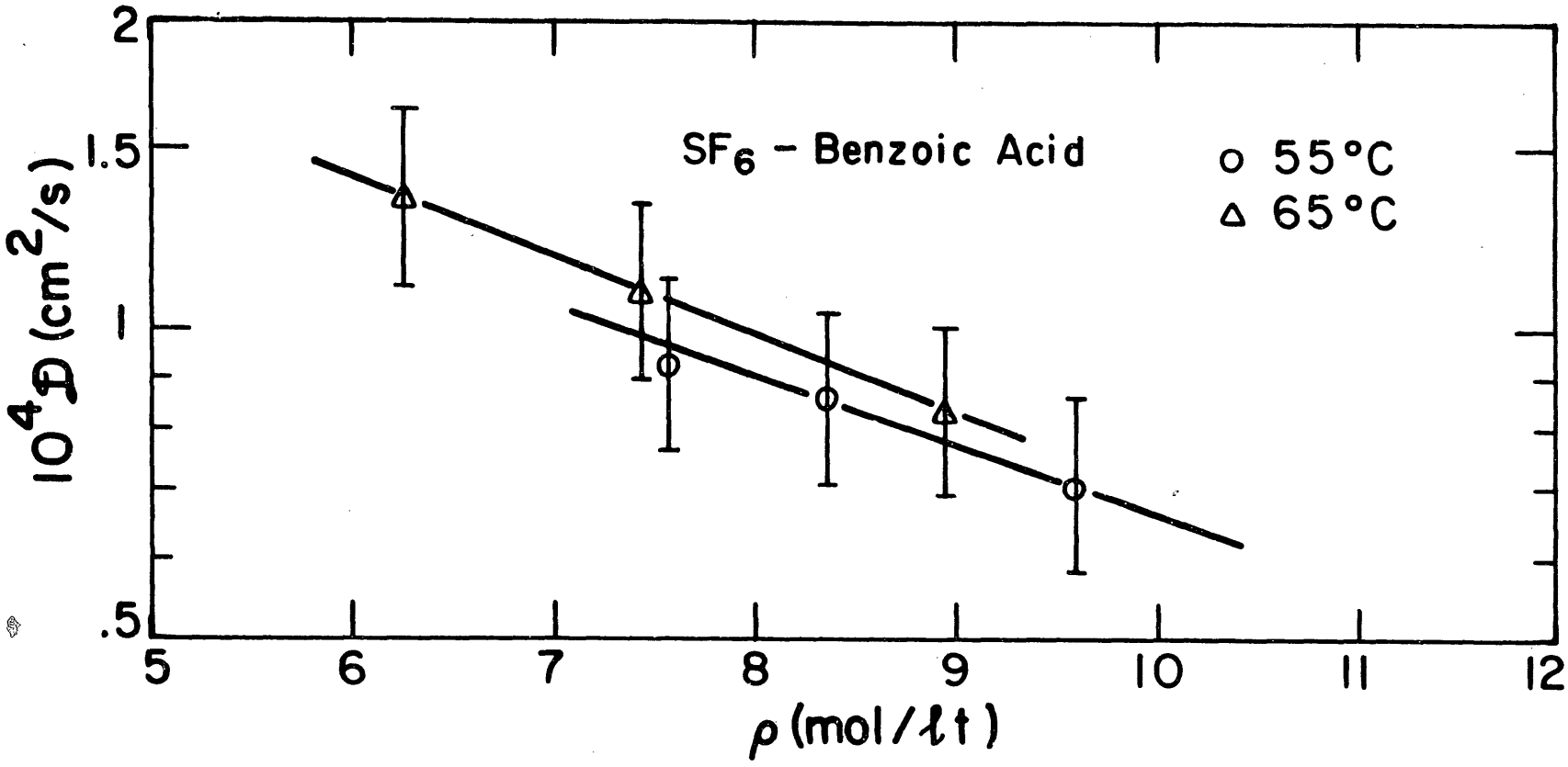

FIGURE 1.15 : Diffusion coefficients for the benzoic acid-SF_6 system.

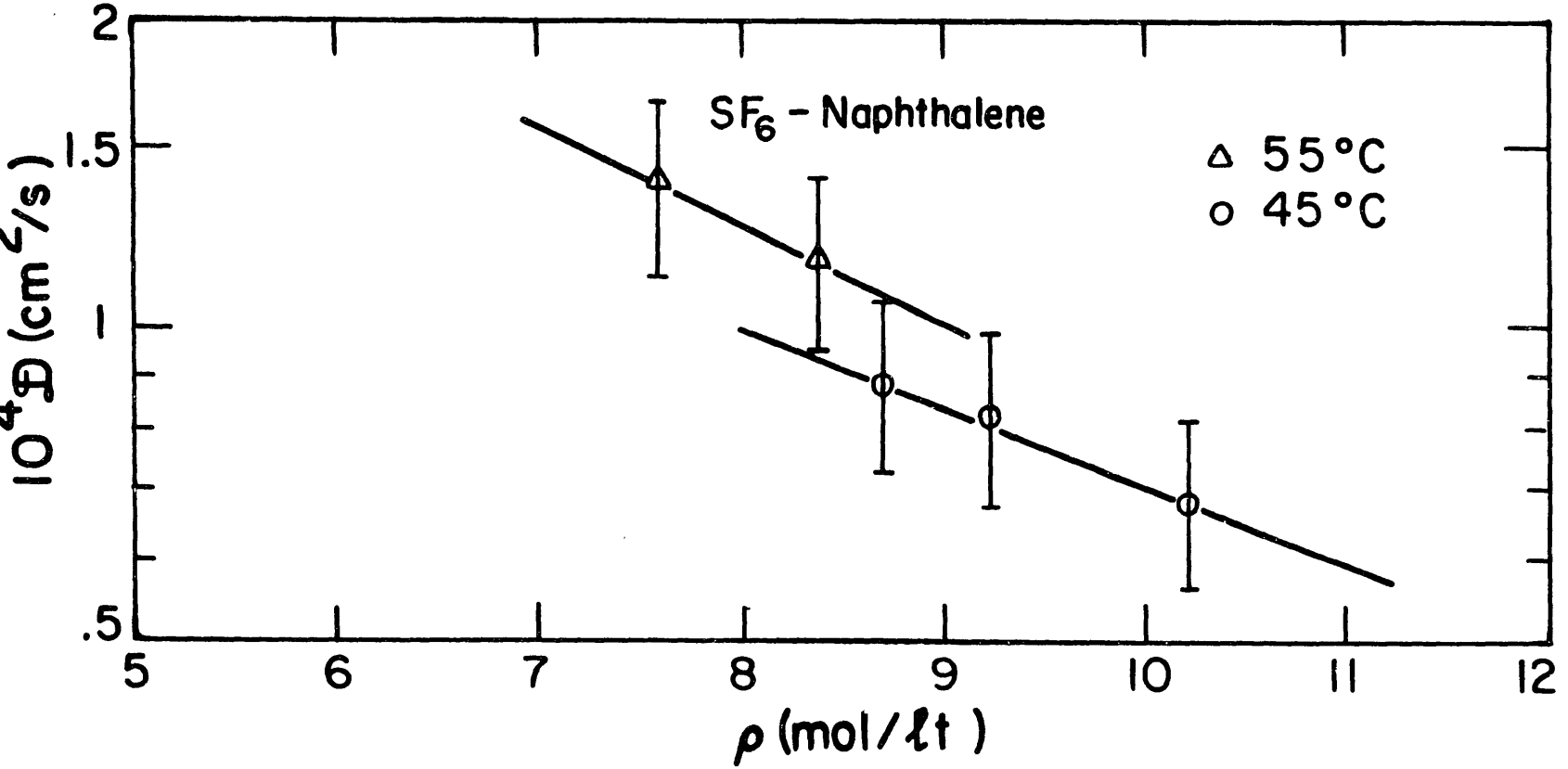

FIGURE 1.16 : Diffusion coefficients for the naphthalene-SF_6 system.

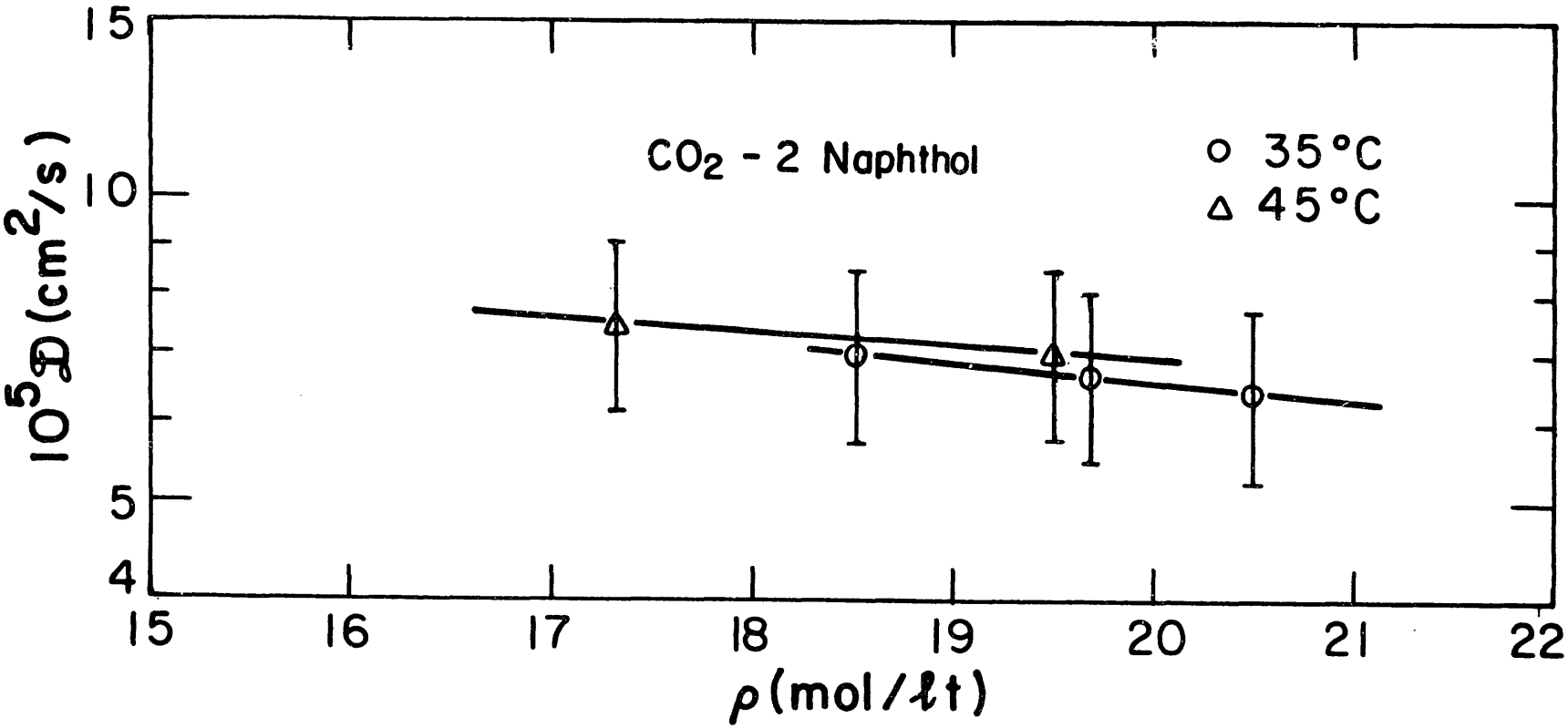

FIGURE 1.17 : Diffusion coefficients for the 2-napthol-CO_2 system.

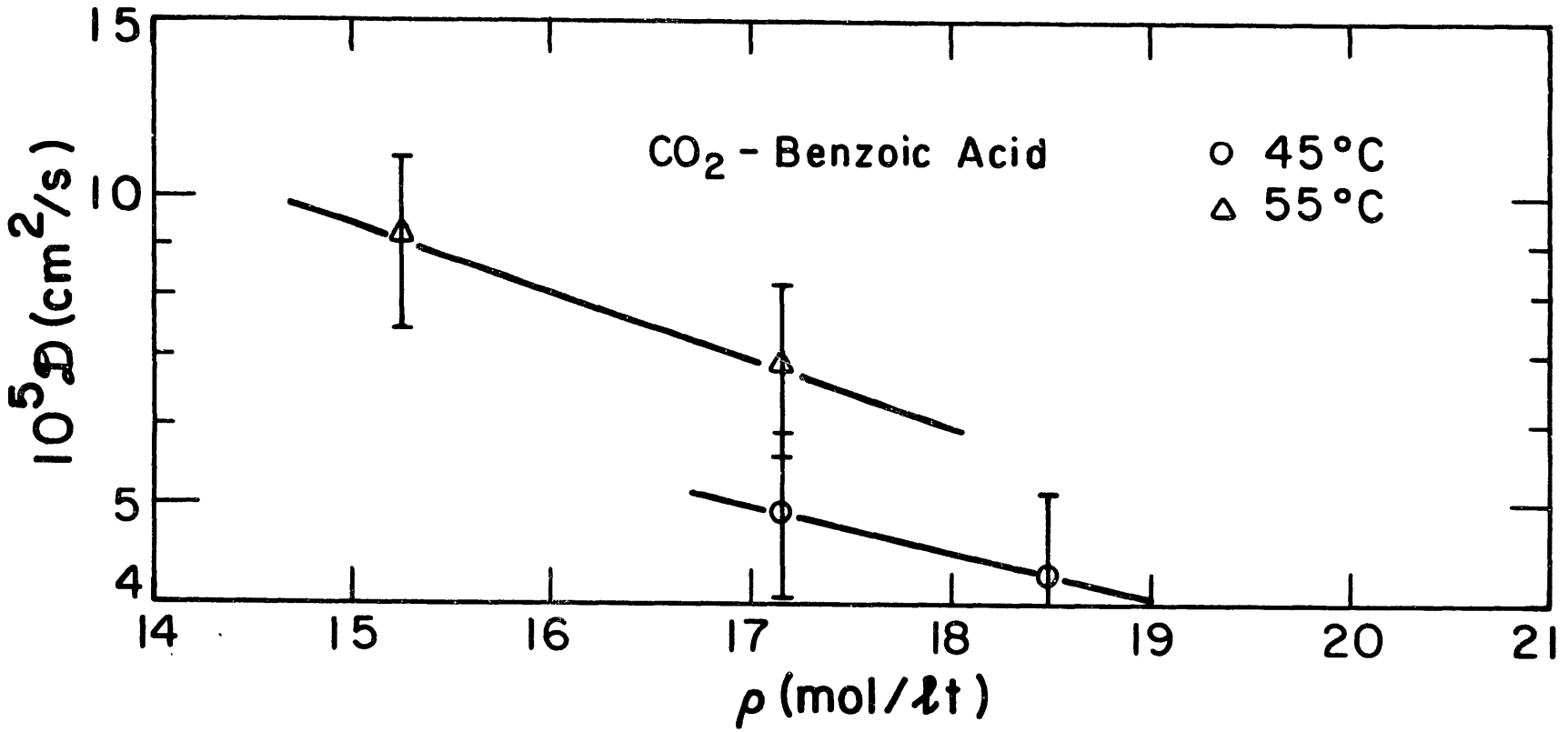

FIGURE 1.18 : Diffusion coefficients for the benzoic acid-CO_2 system.

arise from a highly temperature-sensitive effective molecular size, and cannot, therefore, be expected to show constant ηDT^{-1} values, as will be explained below.

From Tables 6.14, 6.15 and 6.16, it can be seen that ηDT^{-1} is constant to within standard deviations (expressed as percent of the mean), of 4.2% (benzoic acid - SF_6), 9.2% (naphthalene - SF_6), and 6.5% (2-Naphthol-CO_2), respectively.

The Stokes-Einstein equation (Einstein, 1905)

$$D = \frac{kT}{6\pi a\eta} \tag{1.17}$$

relates the diffusion coefficient of a spherical Brownian particle of radius a to the temperature and viscosity of the surrounding fluid, when no slip exists at the interface. Equation (1.17) implies the basic concept

$$\eta DT^{-1} = f\,[\text{size}] \tag{1.18}$$

or, in other words, for hydrodynamic behaviour, a plot of D vs. η^{-1} should yield a straight line through the origin with a slope proportional to T. Figure 1.19 shows the benzoic acid - SF_6 results plotted in this manner. As can be seen, the lines have small but finite intercepts, indicating deviation from strictly hydrodynamic behaviour, a fact already noted by Feist and Schneider (1982) in connection with their studies of diffusion in supercritical CO_2.

The general picture that emerges is sketched in Figure 1.20. Hydrodynamic behaviour is approached at high viscosities; deviations from this limiting behaviour can be correlated (but not understood) by means of empirical power law relationships of the type $D \alpha \eta^{-a}$ ($a < 1$) (Hayduck and Cheng, 1971). Supercritical viscosities fall roughly in the range $0.04 \leq \eta \leq 0.1$ cp for $1.1 \leq Pr \leq 4$ and $1 \leq Tr \leq 1.06$, which corresponds to $1 \leq 10^{-3}\ \eta^{-1} \leq 2.5$ in the units of Figure 1.20 (a typical liquid viscosity is also shown for comparison).

The exact point at which hydrodynamic behaviour breaks down (point c) cannot, at present, be predicted from first principles for any given system. However, from Figure 1.20 it can be concluded that predictive correlations based on the Stokes-Einstein equation (Wilke and Chang, 1955; Scheibel, 1954; Reddy-Doraiswamy, 1967; Lusis-Ratcliff, 1968) will

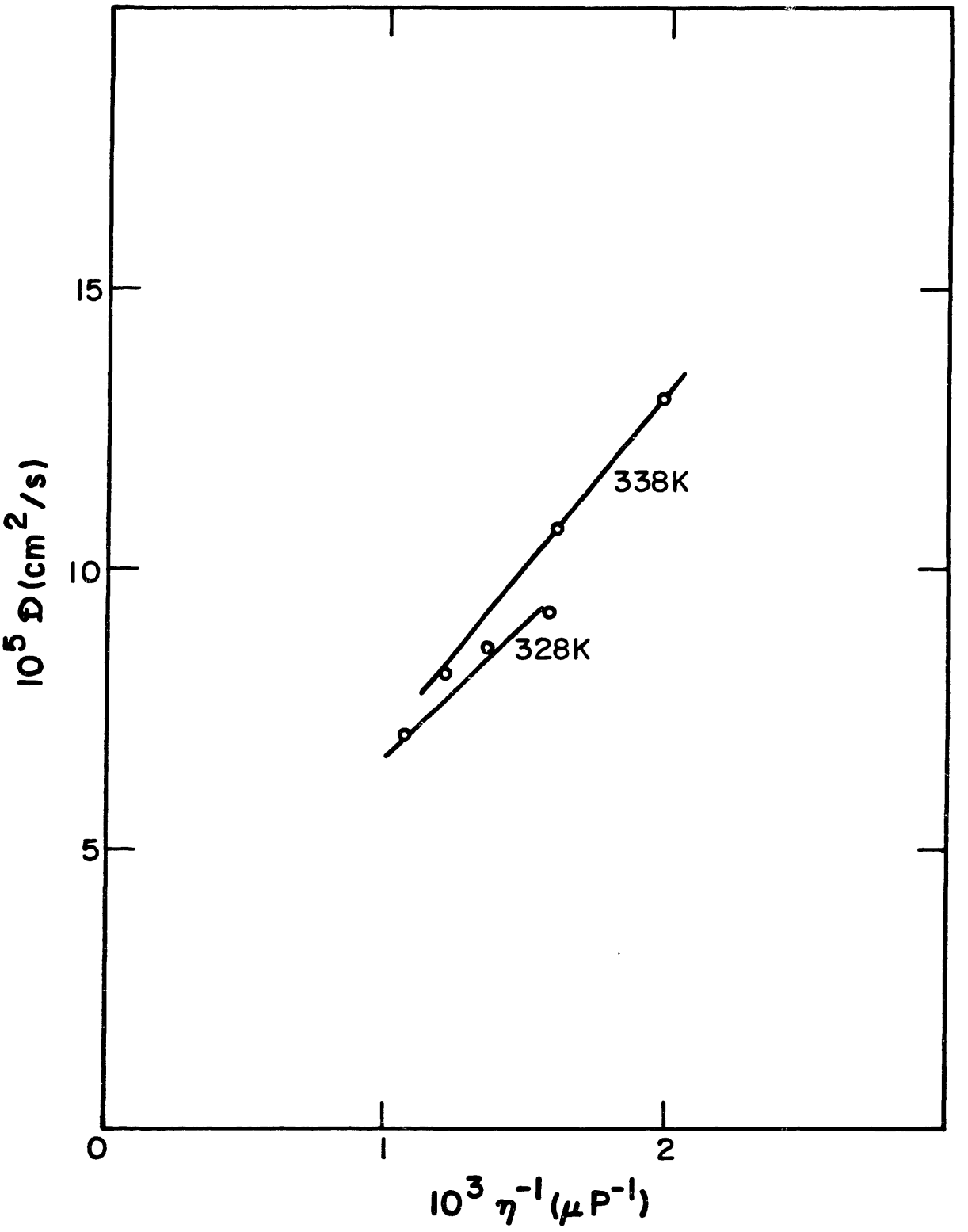

FIGURE 1.19: Diffusion coefficients of benzoic acid versus SF_6 fluidity.

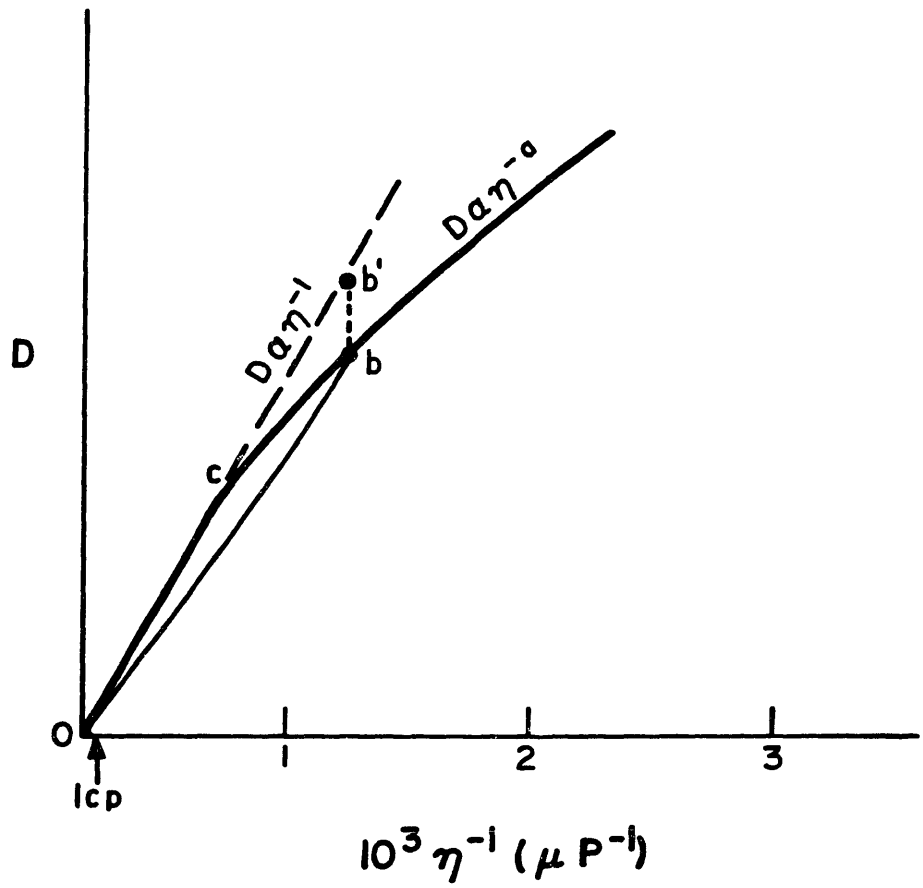

FIGURE 1.20: Hydrodynamic and power law isothermal behaviour of the diffusion coefficient as a function of fluidity.

overestimate diffusion coefficients in supercritical fluids. This was indeed found to be the case (see Chapter 6) when each of the above correlations was applied to diffusion of naphthalene in supercritical CO_2 and ethylene (Iomtev and Tsekhanskaya, 1964), benzene in supercritical CO_2 (Swaid and Schneider, 1979), as well as 2-naphthol in supercritical CO_2, and naphthalene and benzoic acid in supercritical SF_6 (this work), with the single exception of the Wilke-Chang expression for the naphthalene-ethylene system.

In addition, at high enough viscosities (or, equivalently, at high enough pressures for any given temperature), the quantity ηDT^{-1} approaches a constant value; geometrically, this is equivalent to saying that, at small η^{-1} values, the curve Ocb is well approximated by the line Ob. As an example, the measured diffusion coefficients of benzene in supercritical CO_2 (Swaid and Schneider, 1979) give rise to an ηDT^{-1} value that is constant to within a 4.6% standard deviation (expressed in percentage of the mean) when $\eta \geq 0.04$ cp, irrespective of the temperature and pressure.

Thus, at high enough viscosities, hydrodynamic behaviour is approached, and this fact can be used to extrapolate experimental data by assuming constancy of ηDT^{-1}.

1.4: DIFFUSION AND IRREVERSIBLE THERMODYNAMICS

Kinetic approaches view diffusion as a phenomenon resulting from gradients in concentration. From the point of view of irreversible thermodynamics, on the other hand, chemical potential gradients, and not concentration gradients, constitute the appropriate driving force for diffusion. The rationale behind this approach is that the uniformity of chemical potential (for any given species) throughout a system in which no impermeable boundaries exist is a condition for thermodynamic equilibrium. Consequently, if the deviations from this condition are small enough to justify the assumption of local equilibrium, it is plausible to assume a restoring (driving) force proportional to chemical potential gradients. This relationship between fluxes and thermodynamic driving forces can indeed be proved (see Appendix 5) without any additional assumption other than the local validity of thermodynamics within an overall non-equilibrium situation.

From the standpoint of irreversible thermodynamics, then, we can write, for isothermal binary diffusion with no viscous dissipation (see Chapter 7),

$$\underline{j}_1 = - \alpha \underline{\nabla} \mu \tag{1.19}$$

where $\underline{j}_1$ is a solute mass flux, μ a mixture chemical potential per unit mass,

$$\mu = \frac{\mu_1}{M_1} - \frac{\mu_2}{M_2} \tag{1.20}$$

and α, the corresponding transport coefficient. Equation (1.19) can be rewritten using the definition of μ, the Gibbs-Dubem equation, and the definition of $\hat{\phi}_1$, the fugacity coefficient,

$$\nabla \mu = \frac{1}{M_1} \nabla \mu_1 - \frac{1}{M_2} \nabla \mu_2 \tag{1.21}$$

$$0 = x_1 \nabla \mu_1 + (1 - x_1) \nabla \mu_2 \tag{1.22}$$

$$\hat{f}_1 = x_1 P \hat{\phi}_1 \tag{1.23}$$

to obtain a mathematical relationship between solute flux and solute mole fraction,

$$\underline{j}_1 = \frac{-\alpha RT}{M_1} \left[1 + \left(\frac{\partial \ln \hat{\phi}_1}{\partial \ln x_1}\right)_{T,P} \right] \left[\frac{1}{x_1} + \frac{M_1}{M_2} \frac{1}{(1 - x_1)} \right] \underline{\nabla} x_1 \tag{1.24}$$

In this thermodynamic approach, however, the transformation of Equation (1.19) into Equation (1.24) has resulted in the introduction of a term, $\left[1 + (\partial \ln \hat{\phi}_1 / \partial \ln x_1)_{T,P} \right]$, which is absent in the usual phenomenological descriptions of diffusion. Of the many equivalent phenomenological expressions, we choose (Bird et al., 1960)

$$\underline{j}_1 = - \frac{c^2 M_1 M_2}{\rho} \mathfrak{D}_{12} \underline{\nabla} x_1 \tag{1.25}$$

where c is the total molar concentration. The relationship between α and $\mathfrak{D}_{12}$, therefore, reads,

$$\mathfrak{D}_{12} = \frac{\alpha RT}{M_1^2 c} \left[\left(\frac{1 - x_1}{x_1}\right)^{1/2} + \frac{M_1}{M_2} \left(\frac{x_1}{1 - x_1}\right)^{1/2} \right]^2 \left[1 + \left(\frac{\partial \ln \hat{\phi}_1}{\partial \ln x_1}\right)_{T,P} \right] \tag{1.26}$$

It is customary to define a "thermodynamic" diffusion coefficient (D_{12}) with the same units of $\mathfrak{D}_{12}$, and such that it will equal $\mathfrak{D}_{12}$ in ideal mixtures, in which case

$$\left[1 + \left(\frac{\partial \ln \hat{\phi}_1}{\partial \ln x_1}\right)_{T,P} \right] = 1 \tag{1.27}$$

or, in other words, when $\hat{\phi}$ is composition-independent. Consequently,

$$\mathfrak{D}_{12} = D_{12} \left[1 + \left(\frac{\partial \ln \hat{\phi}_1}{\partial \ln x_1}\right)_{T,P} \right] \tag{1.28}$$

or

$$D_{12} = \frac{\alpha RT}{M_1^2 c} \left[\left(\frac{1 - x_1}{x_1}\right)^{1/2} + \frac{M_1}{M_2} \left(\frac{x_1}{1 - x_1}\right)^{1/2} \right]^2 \tag{1.29}$$

D_{12} is normally assumed (Reid et al., 1977) to be less composition-dependent than $\mathfrak{D}_{12}$. Thus, at any given temperature and pressure, a composition-independent D_{12} imposes upon α the requirement that it depend on x_1 as the dimensionless function

$$\psi(x_1) = \frac{1 + \frac{1}{c(o)} \int_0^{x_1} \left(\frac{\bar{V}_2 - \bar{V}_1}{V^2}\right) dx}{\left[\left(\frac{1 - x_1}{x_1}\right)^{1/2} + \frac{M_1}{M_2} \left(\frac{x_1}{1 - x_1}\right)^{1/2} \right]^2} \tag{1.30}$$

where V is a molar volume, and $\bar{V}_i$, a partial molar volume.

Whereas the numerator is very specifically dependent upon the binary system under consideration, the denominator is a universal function of solute mole fraction and solute/solvent weight ratio. The numerator being a finite number, we notice that $\psi(x_1)$ (and hence α) vanishes at $x_1 \to 0$ and $x_1 \to 1$, in agreement with the fact that μ (and hence $\nabla\mu$) is an undefined quantity at $x_1 \to 0$ and $x_1 \to 1$.

Figure 1.21 is a plot of the reciprocal of the denominator of Equation (1.30) (i.e., the universal part of the composition-dependence of α such that D_{12} is composition-independent). At a mole fraction of $M_1/(M_1 + M_2)$, ψ exhibits a maximum value $M_2/4\ M_1$.

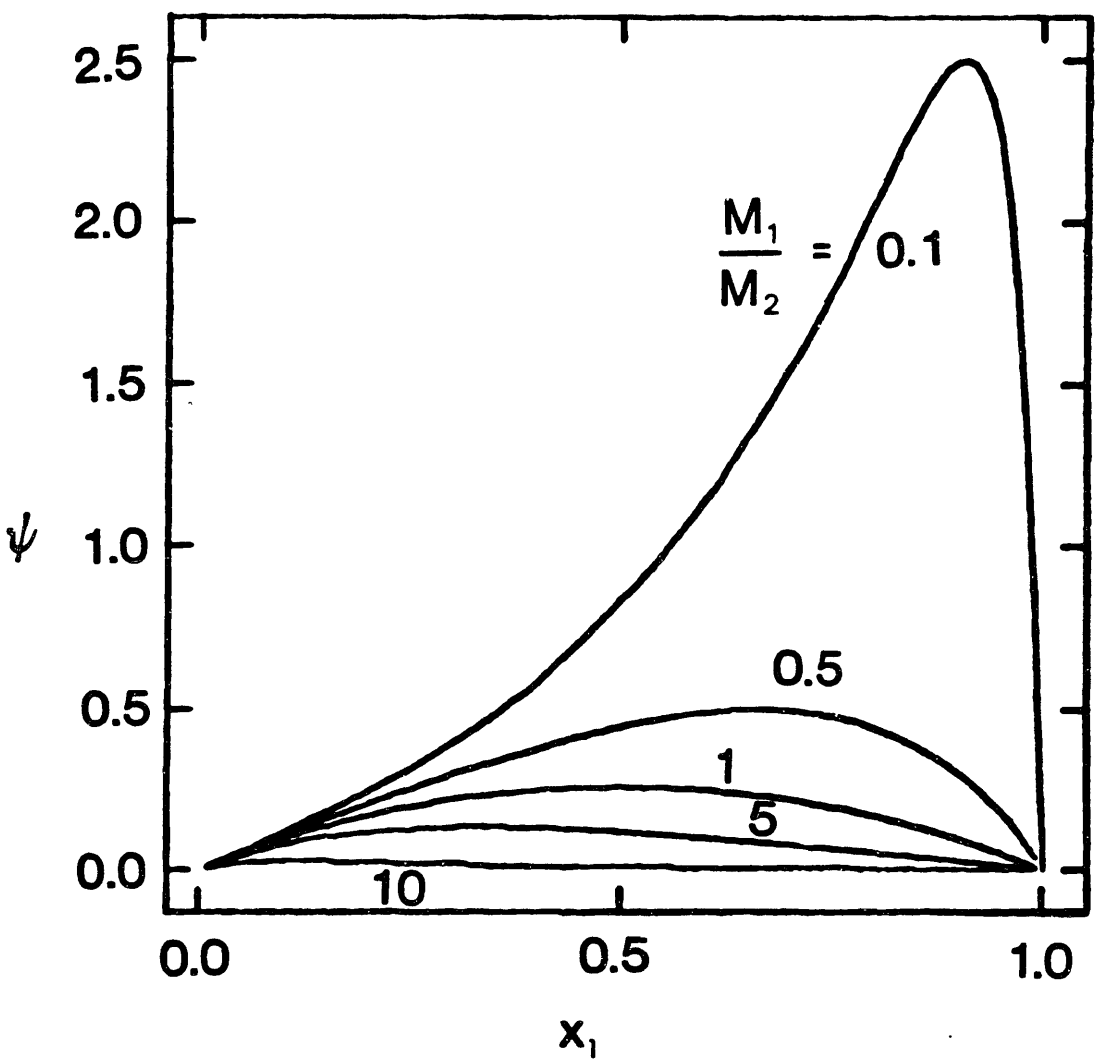

FIGURE 1.21: Universal part of composition dependence of the thermodynamic transport coefficient (α) that will give rise to a composition-independent D_{12}.

The left hand side of Equation (1.27) represents a conversion factor between "kinetic" and "thermodynamic" diffusion coefficients, whose theoretical implications are discussed in Chapter 7. Here, some of the interesting consequences of the calculated composition dependence of this function will be outlined.

The explicit form of $[1 + (\partial \ln \hat{\phi}_1 / \partial \ln x_1)_{T,P}]$ can be obtained from any given equation of state. For two-parameter cubic equations of state with composition-independent combining rules (see Chapter 7 and Appendix 1), a highly non-linear and complicated expression results (see Equation (7.27)). However, when plotted as a function x_1 (from infinite dilution to saturation) Equation (7.27) is a straight line of negative slope and unit y - intercept,

$$1 + \left(\frac{\partial \ln \hat{\phi}_1}{\partial \ln x_1}\right)_{T,P} = 1 - K x_1 \qquad (1.31)$$

or, in other words,

$$\hat{\phi}_1(x_1,T,P) = \hat{\phi}_1^{\infty}(0,T,P) \exp\left[-K(T,P)x_1\right] \qquad (1.32)$$

where

$$\hat{\phi}_1^{\infty} = \lim_{x_1 \to 0} \hat{\phi}_1(x) \qquad (1.33)$$

This functionality is shown graphically in Figure 1.22 for the benzoic acid-CO_2 system at 280 bar and 308 K between infinite dilution and saturation, and is representative of what appears to be a general feature of the thermodynamic behaviour of binary systems consisting of a non-volatile solute and a supercritical fluid (see Chapter 7).

Quite apart from the simplicity of Equation (1.31) relative to Equation (7.27), the parameter K has a physical meaning and an apparent asymptotic behaviour that could have interesting thermodynamic implications. If the linearity implied by equation (1.31) is extrapolated to the point where the factor $[1 + (\partial \ln \hat{\phi}_1 / \partial \ln x_1)_{T,P}]$ equals zero, we obtain

$$K = 1/x_1(\text{l.s.}) \qquad (1.34)$$

$$\hat{\phi}_1 = \hat{\phi}_1^{\infty} \exp[-x_1/x_1(\text{l.s.})] \qquad (1.35)$$

where x_1 (l.s.) is the composition (mole fraction) of the mixture when

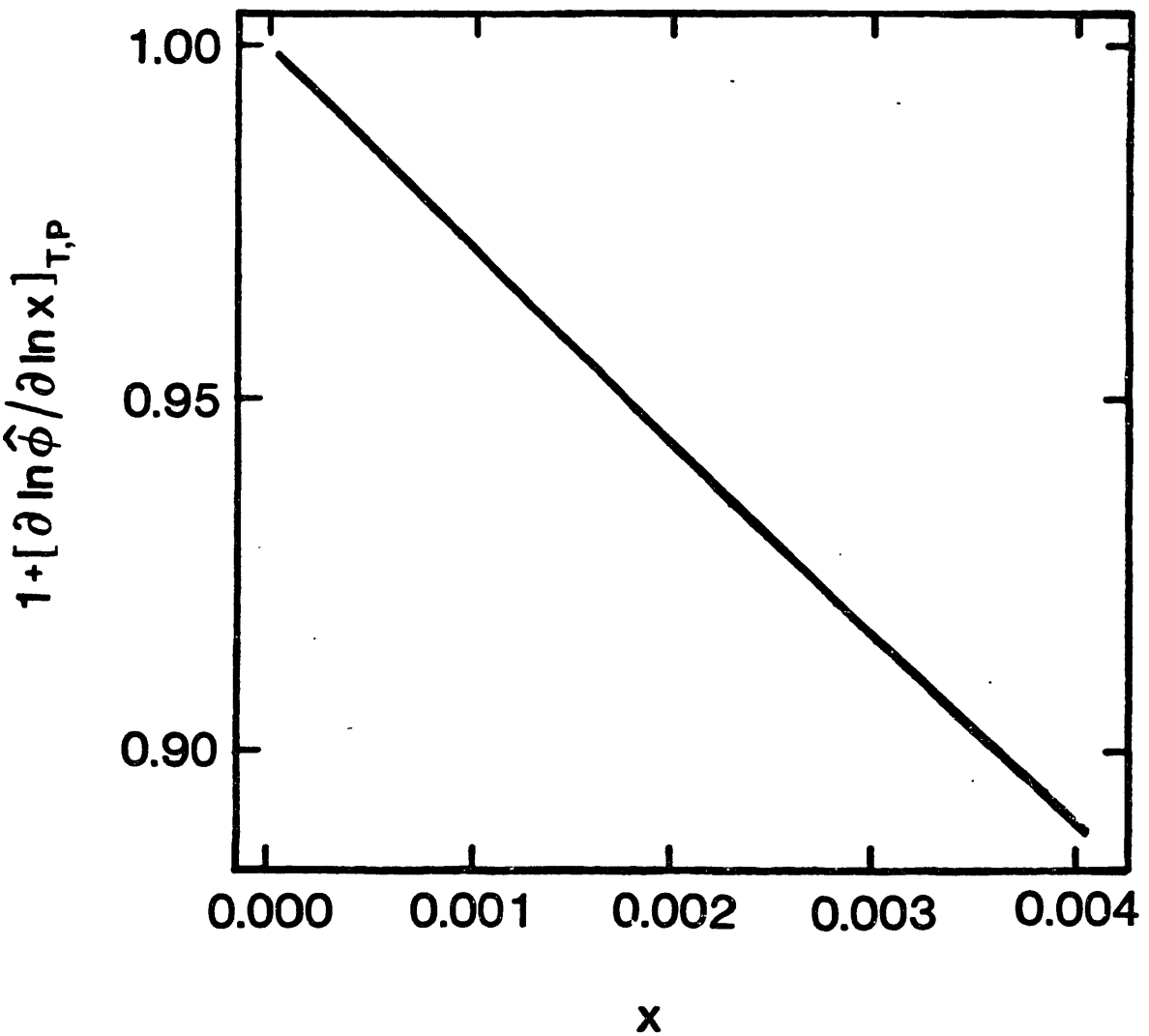

FIGURE 1.22: Linearity of the kinetic conversion factor versus solute mole fraction relationship. Benzoic acid-CO_2, 280 bar, 308 K. Peng-Robinson equation of state.

it reaches its limit of stability at the given T and P (Modell and Reid, 1983). Equation (1.35), although obtained from a linear extrapolation that may not be valid up to the limit of stability, suggests a "natural" scaling for the concentration, in analogy with the idea of corresponding states.

Furthermore, when the K values for a given system are plotted as a function of temperature and pressure (Figure 1.23), it appears that K approaches a high pressure limit which is independent of temperature (at 280 bar, the K-values in Figure 1.23 are within 6.5% of the mean).

We may summarize by saying that, according to Equation (1.32), the fugacity coefficient is the product of a composition-independent term ($\hat{\phi}_i^{\infty}$, the infinite dilution fugacity coefficient), and an exponential and explicit composition correction which is not only small, due to the small values of x_i , but appears to approach a high pressure limit which is independent of temperature.

1.5: MOLECULAR DYNAMICS SIMULATIONS

Molecular dynamics is the numerical solution of the many body problem and the use of statistical mechanics to interpret the results (i.e., evolution in time of the velocities and coordinates of the bodies (molecules) whose motion is being studied).

In this work, 107 CO_2 and 1 benzene molecules were considered (Figure 1.24) and treated as rigid polyatomics (i.e. point centers of force with no internal degrees of freedom), with pairwise additive atom-atom interactions:

$$U_{IJ} = \sum_{i \epsilon I} \sum_{j \epsilon J} U_{ij} \qquad (1.36)$$

where i and j denote sites (atoms) belonging to bodies (molecules) I and J, respectively.

The dynamic simulation of this system of interacting molecules required the solution of equations for the translational and rotational degrees of freedom. For the former, Newton's second law of motion was written

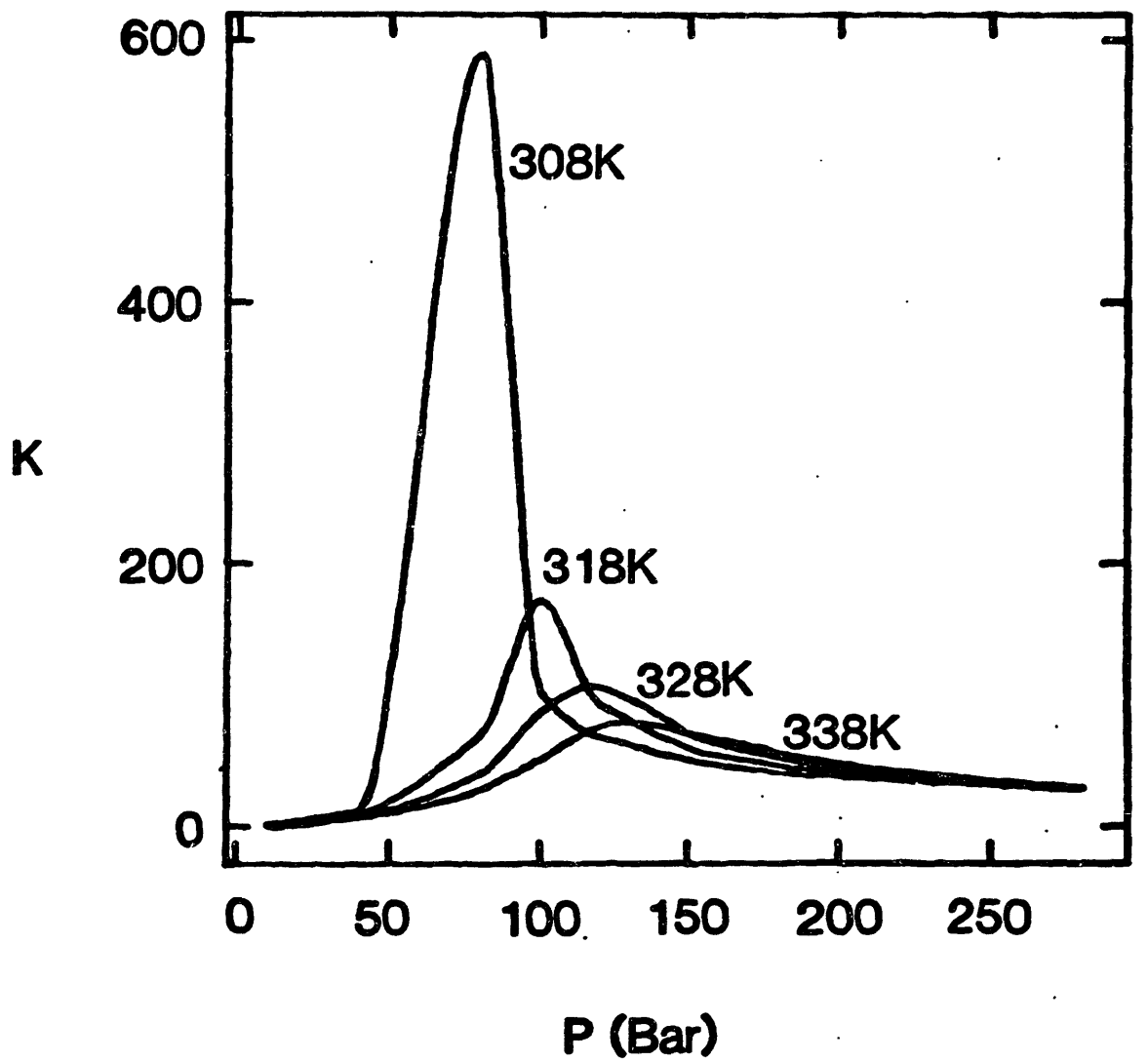

FIGURE 1.23: Pressure and temperature dependence of the exponential correction factor for the fugacity coefficient of a solute in a supercritical fluid (benzoic acid-CO_2).

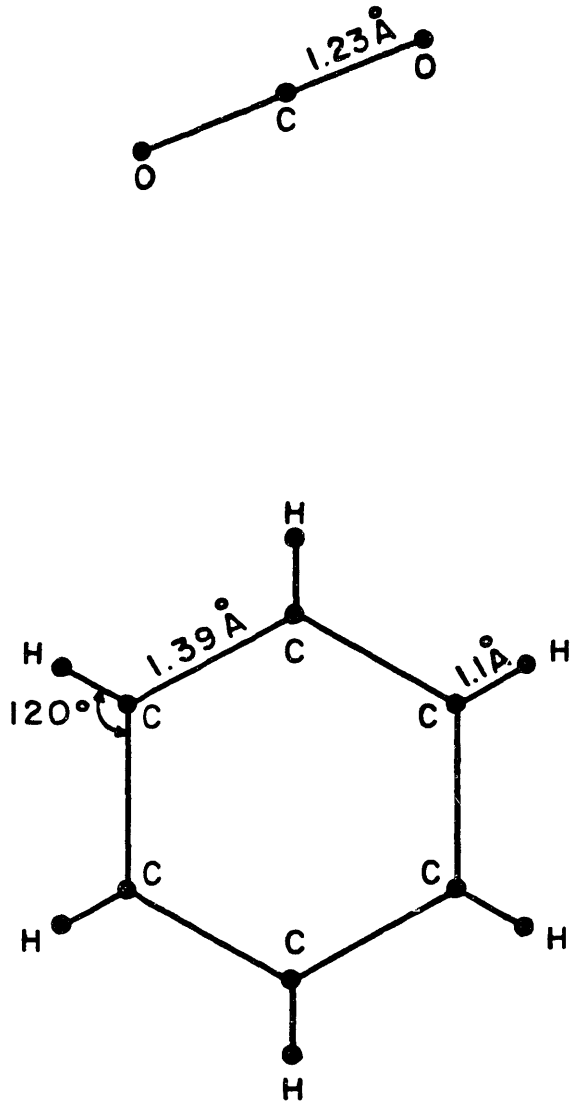

FIGURE 1.24: Geometry of the benzene and CO_2 molecules used in molecular dynamics simulations.

as two coupled first order equations,

$$\dot{\underline{v}} = m^{-1}\ \underline{f}\ (\{\underline{x}\},\ \{\underline{e}\}) \tag{1.37}$$

$$\dot{\underline{x}} = \underline{v} \tag{1.38}$$

where m, $\underline{x}$ and $\underline{v}$ denote the molecule's mass, center of mass coordinates and velocity, respectively, and the force, $\underline{f}$, is the sum of forces on the molecules' sites, and is a function of the translational $\{\underline{x}\}$ and rotational $\{\underline{e}\}$ instantaneous configuration of the system. The rotational equations for the solute, a non-linear molecule, are

$$\dot{w}_i = I_i^{-1}\ K_i\ (\{\underline{x}\},\ \{\underline{e}\}) \quad (i = 1,2,3) \tag{1.39}$$

$$\dot{\underline{\underline{e}}} = \frac{1}{2}\ \underline{\underline{e}}\ \underline{w} \tag{1.40}$$

where i denotes one of the body's principal directions, and I_i and K_i are therefore the $i^{\underline{th}}$ principal moments of inertia and the torque component along the $i^{\underline{th}}$ principal direction (which, as was the case with $\underline{f}$, is a function of the system's instantaneous configuration). In Equation (1.40), $\dot{\underline{e}}$ and $\underline{\underline{e}}$ denote, respectively a vector and a matrix whose elements are the time derivative and the instantaneous value of the four Cayley-Klein parameters (Goldstein, 1981) (with appropriate signs and ordering in the latter case), and $\underline{w}$ contains the principal angular velocity components. The Cayley-Klein parameters represent a non-singular kinematic description of the rotational degrees of freedom of the rigid body, and replace the Euler angles (Figure 1.25), which give rise to singular equations (Murad and Gubbins, 1978), unsuitable for numerical applications.

For the linear solvent, on the other hand,

$$\dot{\underline{w}} = I^{-1}\ \underline{K}\ (\{\underline{x}\},\ \{\underline{e}\}) \tag{1.41}$$

$$\dot{\underline{l}} = \underline{w} \times \underline{l} \tag{1.42}$$

where I is the line's moment of inertia, $\underline{K}$ is the torque, and $\underline{l}$ is a unit vector parallel to the line.

Equations (1.37), (1.38), (1.41) and (1.42) are frame-invariant, whereas Equations (1.39) and (1.40) refer to the body's principal axes of inertia, and imply a linear coordinate transformation at each integration

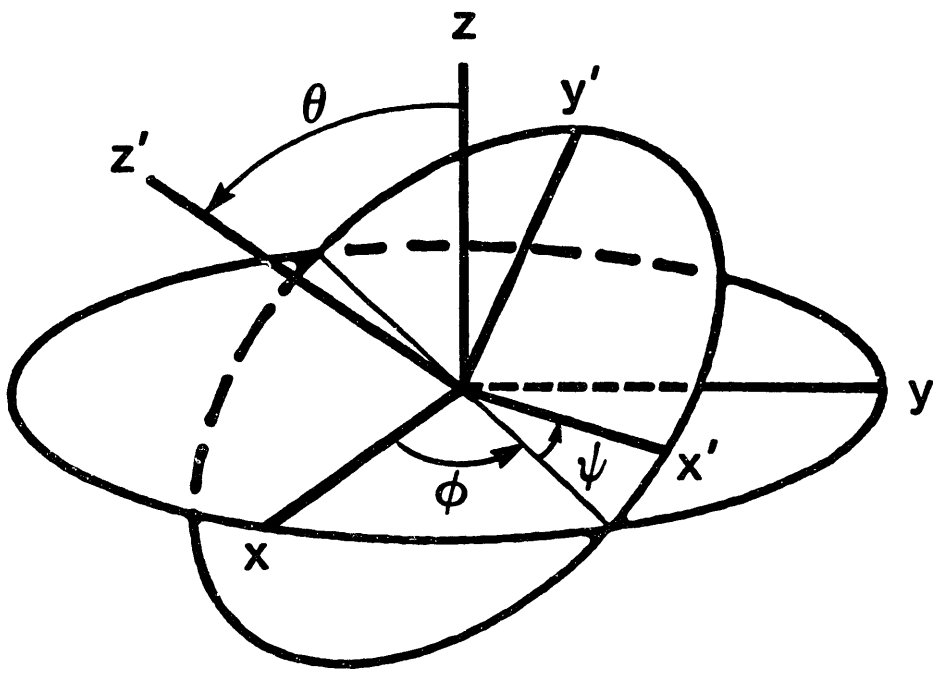

FIGURE 1.25: Euler angles.

step. The resulting system of 1297 of equations is highly coupled due to the configuration dependence of forces and torques, and was solved numerically via an Euler predictor, trapezoid corrector algorithm.

The 108 molecules were placed in a unit cell of space-filling geometry and cubic shape, and periodic boundary conditions were used throughout (Figure 1.26).

Although CO_2 has an appreciable quadrupole moment, the introduction of electrostatic forces into the model was abandoned after simulations with van der Waals forces and point monopoles exhibited large temperature and pressure fluctuations. This behaviour was ascribed to the stiffness caused by the highly orientation-dependent effective electrostatic interactions, and is illustrated in Figures 1.27 and 1.28 where the relative orientation of two CO_2 molecules is defined and the effective dimensionless (i.e., U/kT, T = 300 K) intermolecular Lennard-Jones, electrostatic and total energies (which result from the corresponding interatomic pairwise additive energies), are plotted against carbon-carbon separation. The salient features of Figure 1.28 are the orientation-sensitivity of the electrostatic potential, and the effective short range electrostatic interaction arising from elementary long-ranged Coulombic interactions.

Velocity distributions for the solvent molecules corresponding to four different run average translational temperatures,

$$\langle T(tr)\rangle = \frac{2\langle KE(tr)\rangle}{3Nk} \tag{1.43}$$

with tr denoting translation, KE, kinetic energy, and N = 107, are shown in Figures 1.29-1.32. The continuous line is the theoretical (i.e., Maxwell-Boltzmann) prediction, and the points correspond to $\langle \Delta N(\bar{v})\rangle/\Delta v$, where $\langle \Delta N\rangle$ is the average number of molecules having velocities within $\pm \Delta v/2$ of $\bar{v}$, with Δv equal to 5% of the total velocity range considered, namely, $0 < v^* < 3$, with

$$v^* = \frac{v}{\left(\frac{3k\langle T\rangle}{m}\right)^{1/2}} = \frac{v}{v_{rms}} \tag{1.44}$$

i.e., three times the root mean square velocity. The number of times the ensemble's velocities were analyzed to arrive at $\langle \Delta N\rangle$ is indicated

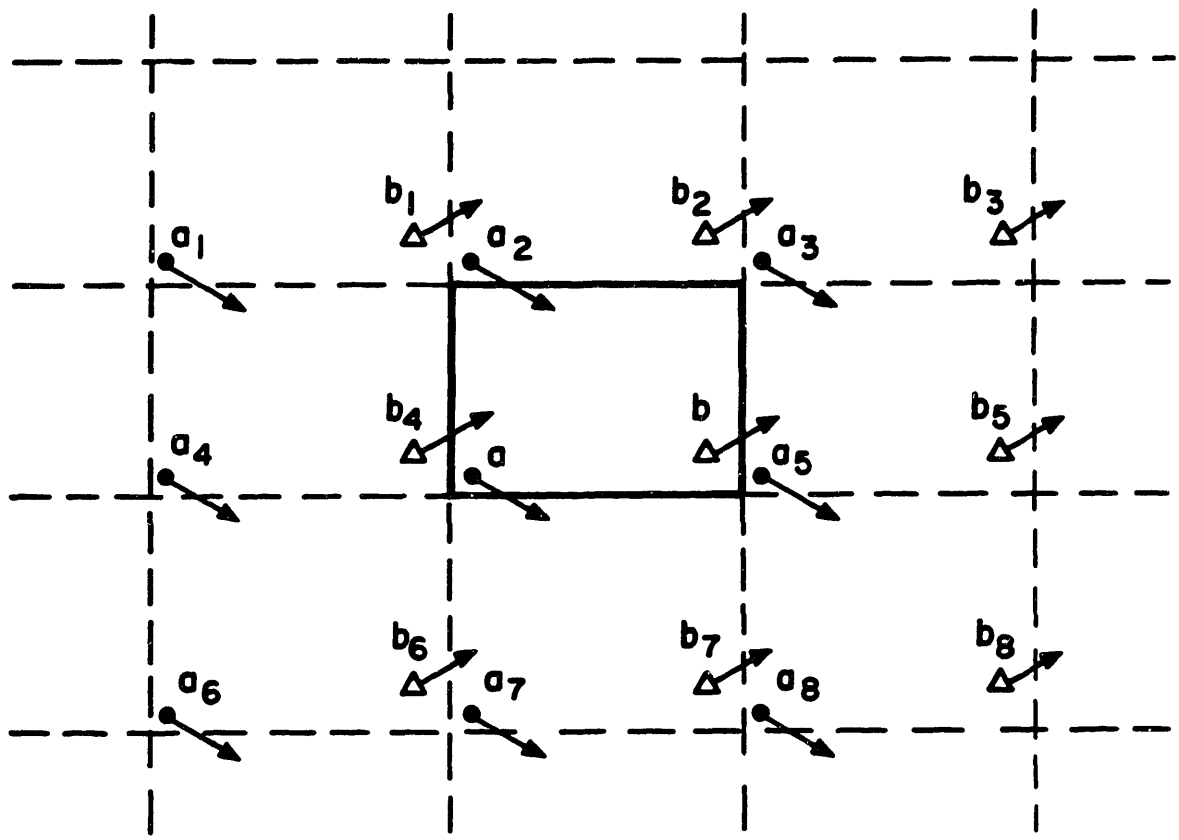

FIGURE 1.26: Two-dimensional periodic boundary conditions.

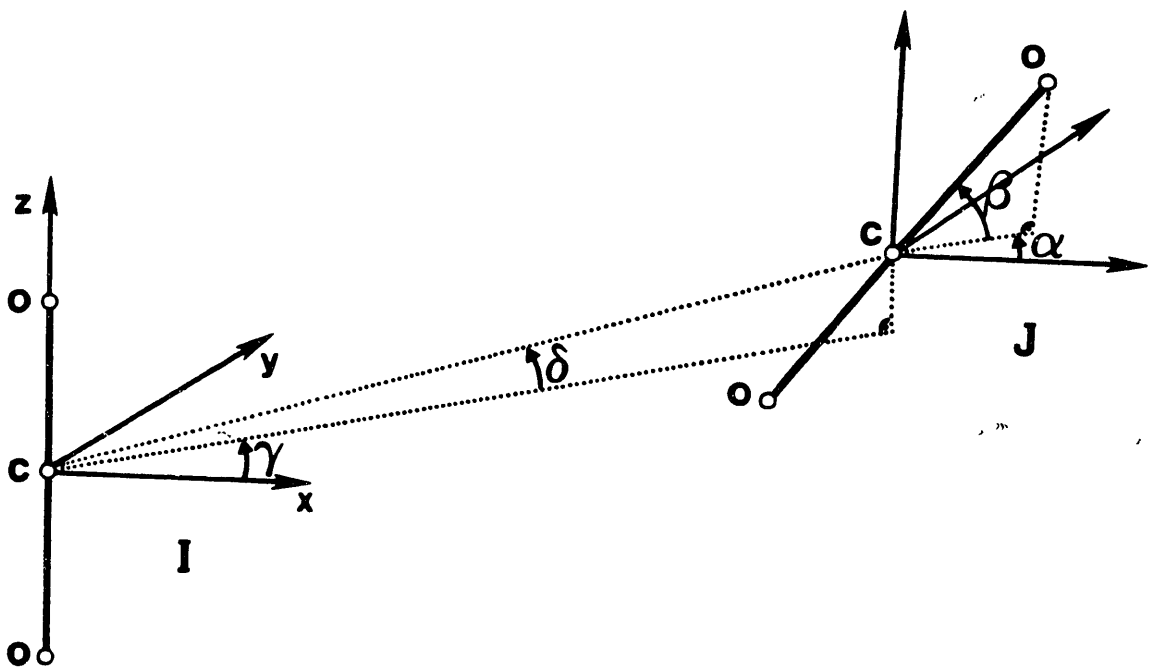

FIGURE 1.27: Kinematic description of two linear molecules.

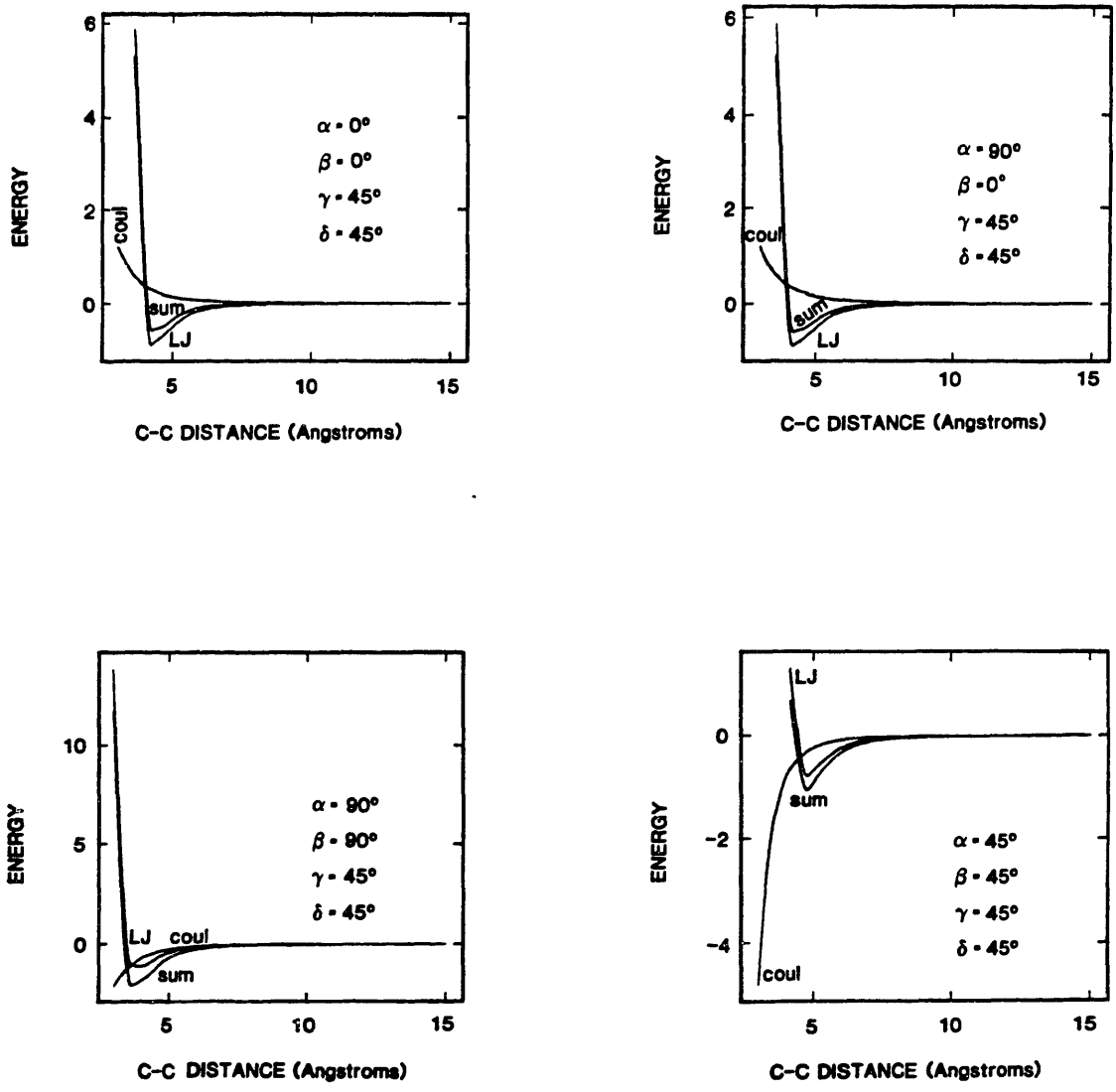

FIGURE 1.28: van der Waals, coulombic and total intermolecular interaction energy for two CO_2 molecules resulting from the sum of nine elementary atomic interactions.

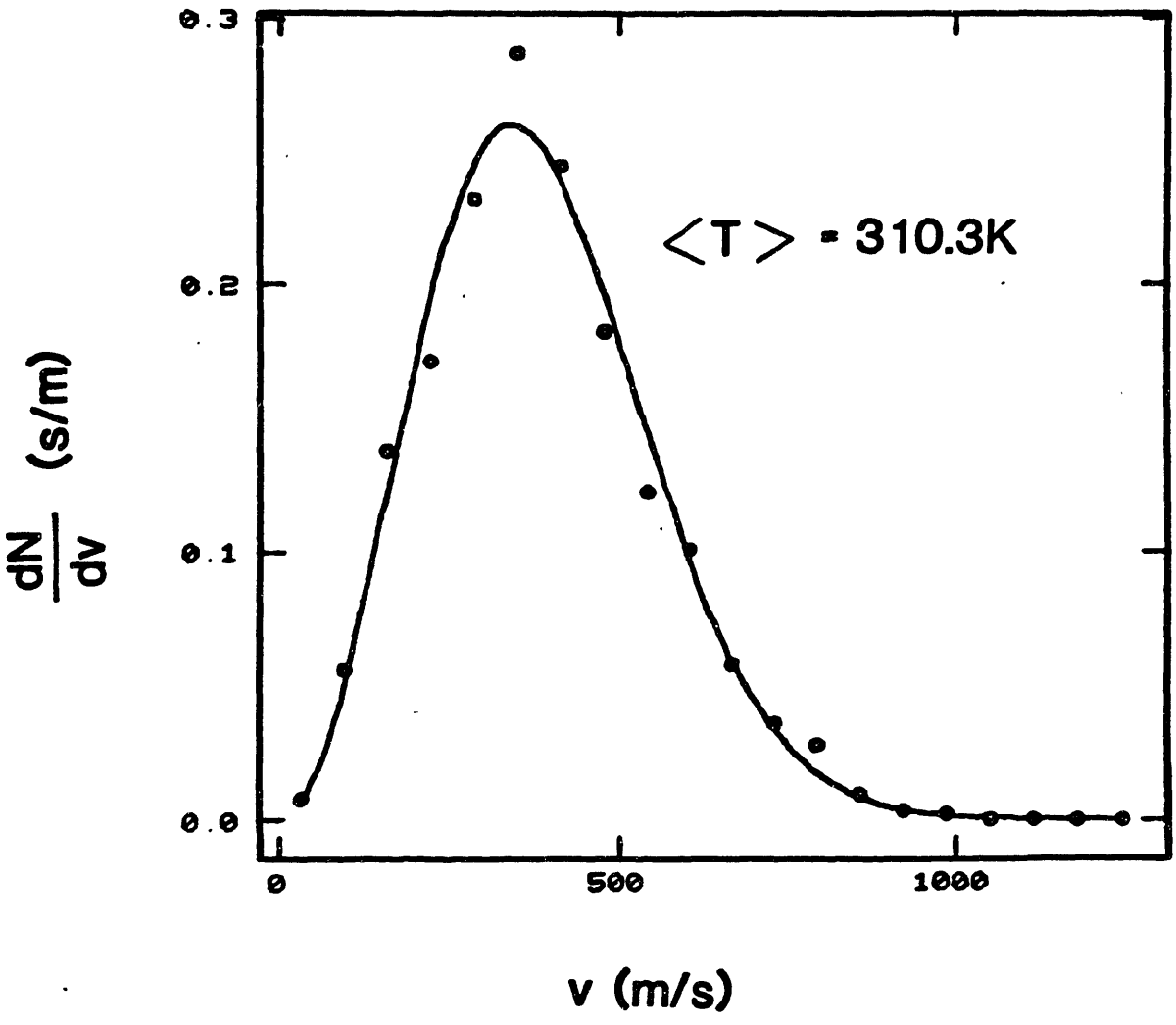

FIGURE 1.29: Maxwell-Boltzmann and computed velocity distribution; # of samplings = 64; <T> = 310.3 K.

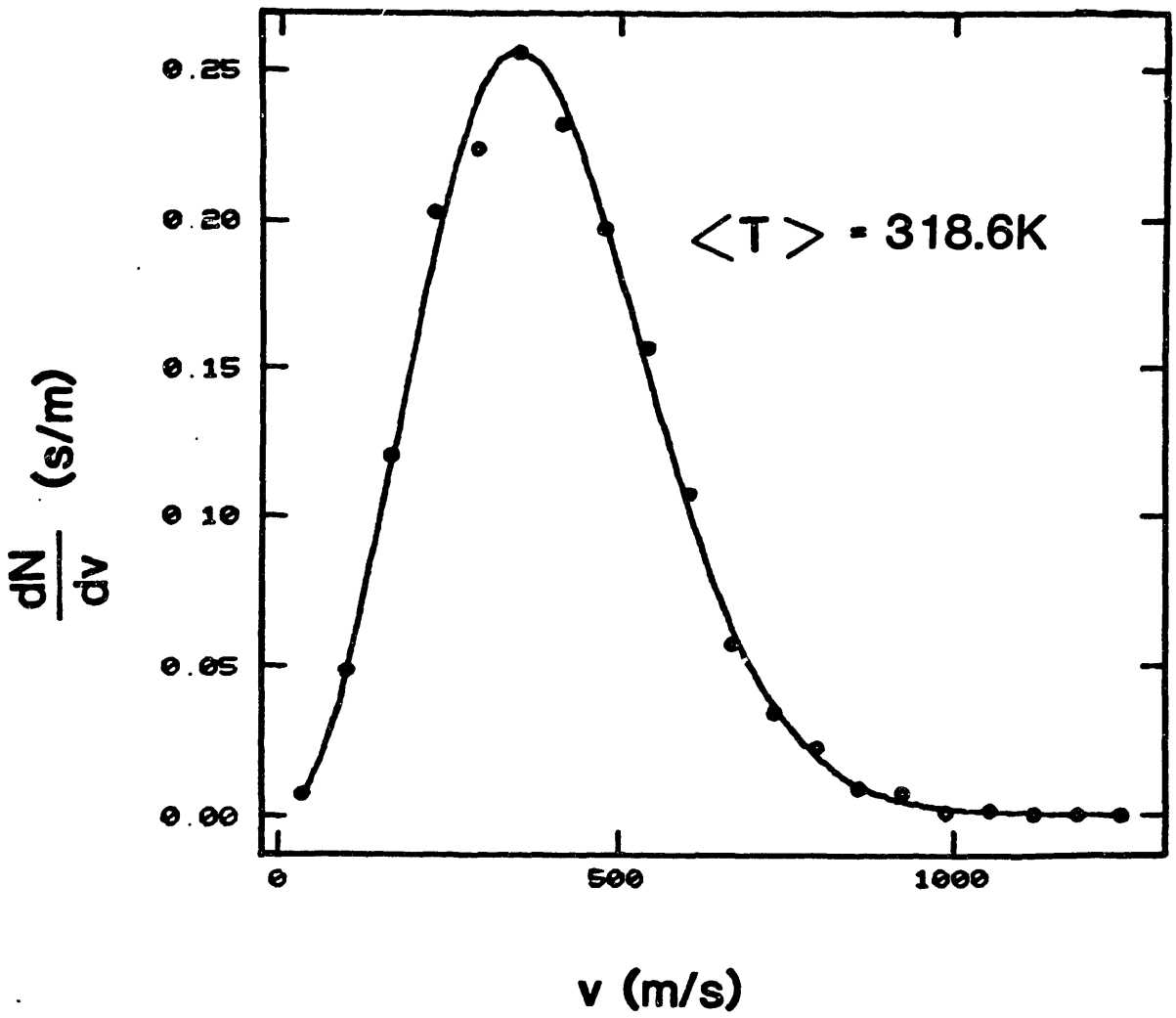

FIGURE 1.30: Maxwell-Boltzmann and computed velocity distribution; # of samplings = 67; <T> = 318.6 K.

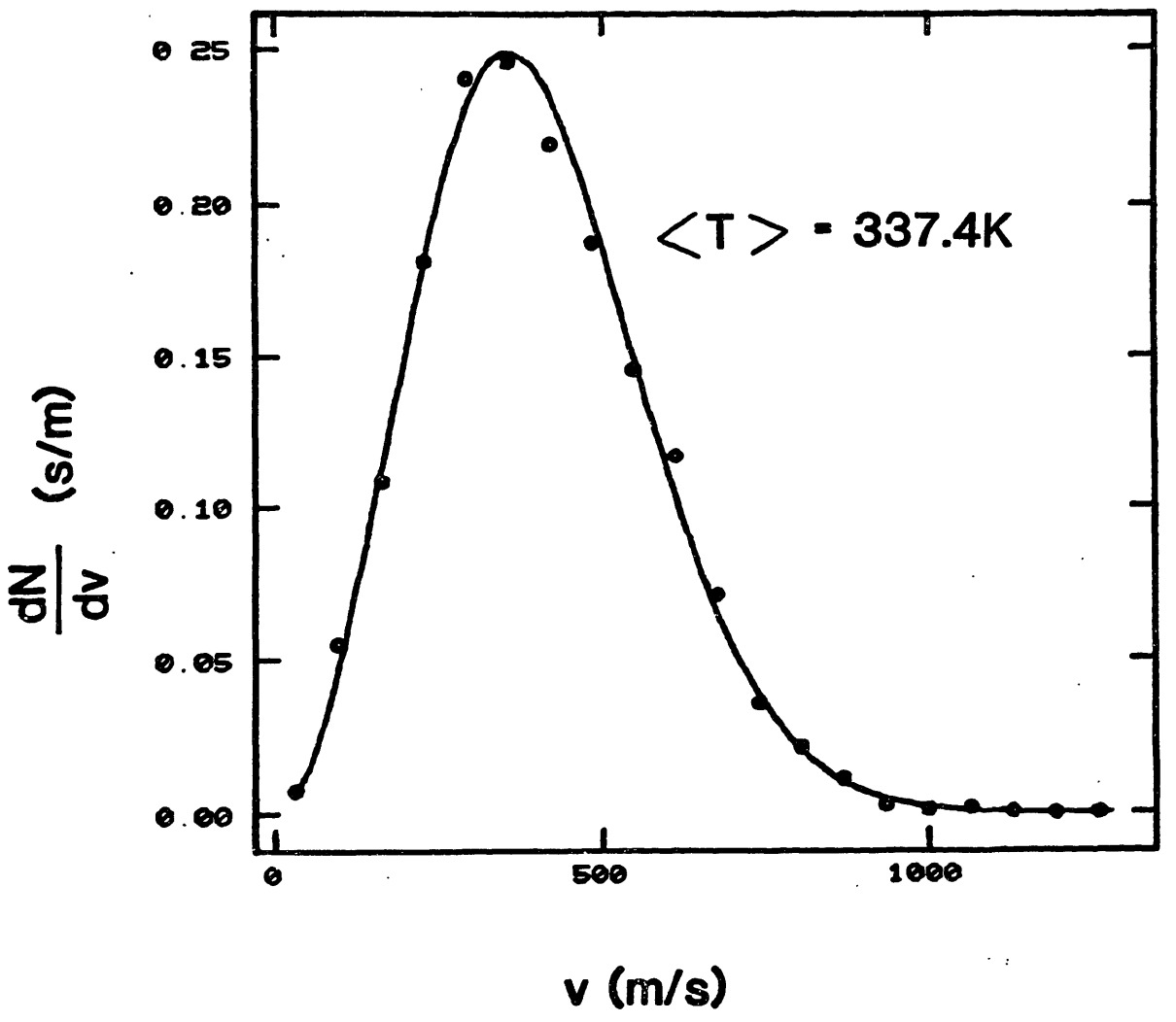

FIGURE 1.31: Maxwell-Boltzmann and computed velocity distribution; # of samplings = 67; <T> = 337.4 K.

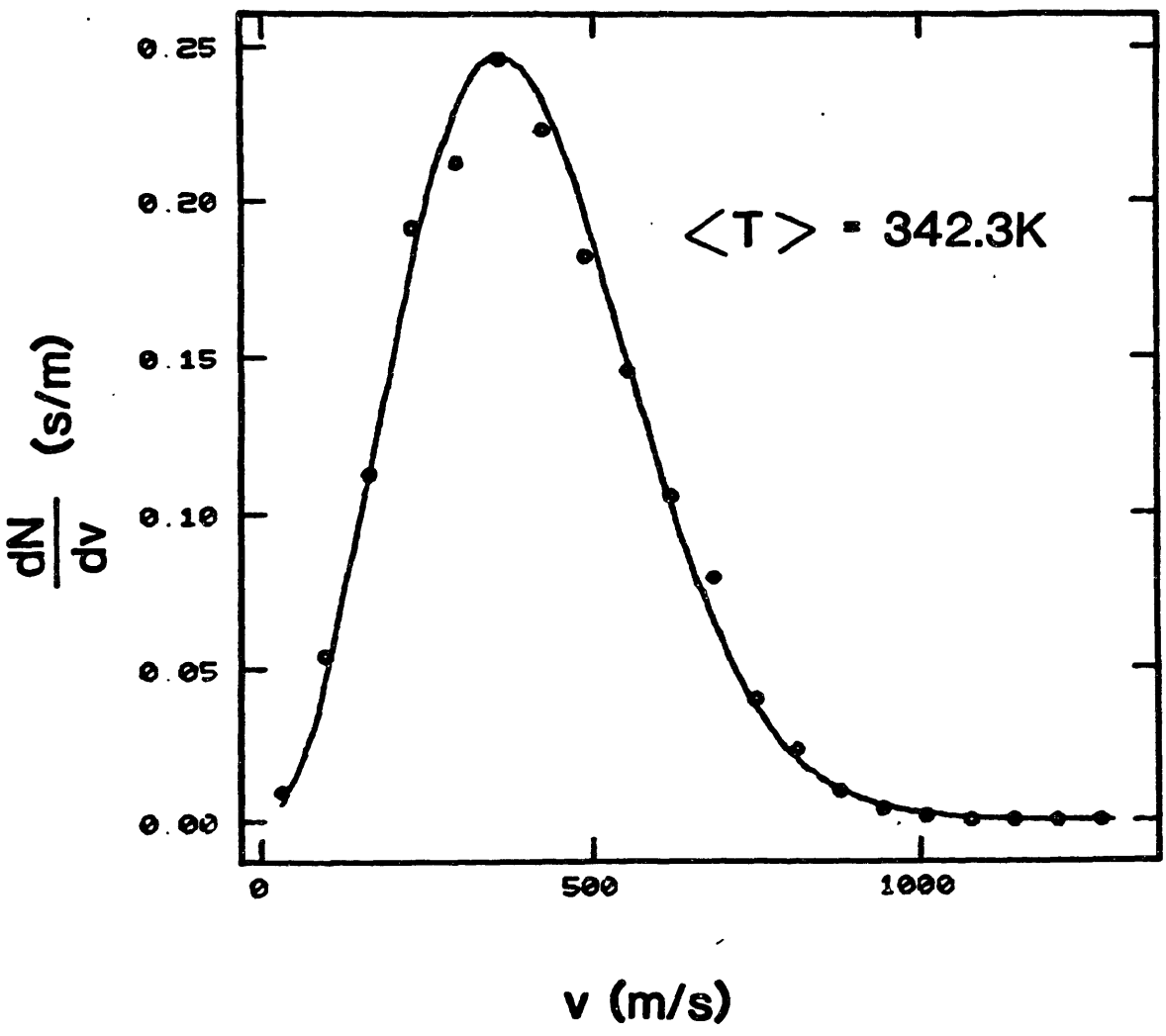

FIGURE 1.32: Maxwell-Boltzmann and computed velocity distribution; # of samplings = 64; <T> = 342.3 K.

in each case. Simulations were either started from a unimodal velocity distribution (i.e., all molecules assigned their equipartition velocities with random orientations), or from the end of a previous simulation.

The radial distribution function for the central carbon atom of the CO_2 molecule is shown in Figures 1.33 and 1.34 as a function of density and temperature. At the moderate densities considered, fluid structure is almost exclusively limited to a nearest neighbour shell whose radius is approximately 4Å. The mild secondary peak disappears at higher temperatures and lower densities.

Diffusion coefficients were calculated by creating an ensemble of solute "experiments" shifted in time and computing squared displacements at corresponding instants with respect to the respective origins (Figure 1.35). This test-particle approach (Alder et. al., 1974) allows the computation of ensemble averages from the simulation of the motion of a single solute molecule. The long time behaviour of the mean squared displacement versus time relationship yields the diffusion coefficient which is simply 1/6 of the slope of the resulting straight line (Einstein, 1905) (or, more precisely, the slope is 2dD, where d is the dimensionality of the displacements).

The temperature dependence of the squared displacement history is shown in Figure 1.36, and the results of four different simulations are plotted in Figure 1.37 in Arrhenius fashion. The regressed activation energy should be compared to the 10.9 KJ $mole^{-1}$ obtained from Swaid and Schneider's data (1979) for diffusion of benzene in supercritical CO_2 at two different temperatures. There being only one solute molecule, the temperature dependence of properties can, at best, yield semiquantitative numbers since the very concept of temperature implies a statistical distribution of velocities.

The isothermal density dependence of the squared displacement vs. time relationship, shown in Figure 1.38, displays interesting trends. The zero-displacement limit of the linear relationship defines a relaxation time, which, for a Brownian sphere, is given by (Chandrasekhar, 1943)

$$\tau = \frac{m}{6\pi\eta a} \qquad (1.45)$$

where η and a are the viscosity of the medium and the radius of the sphere,

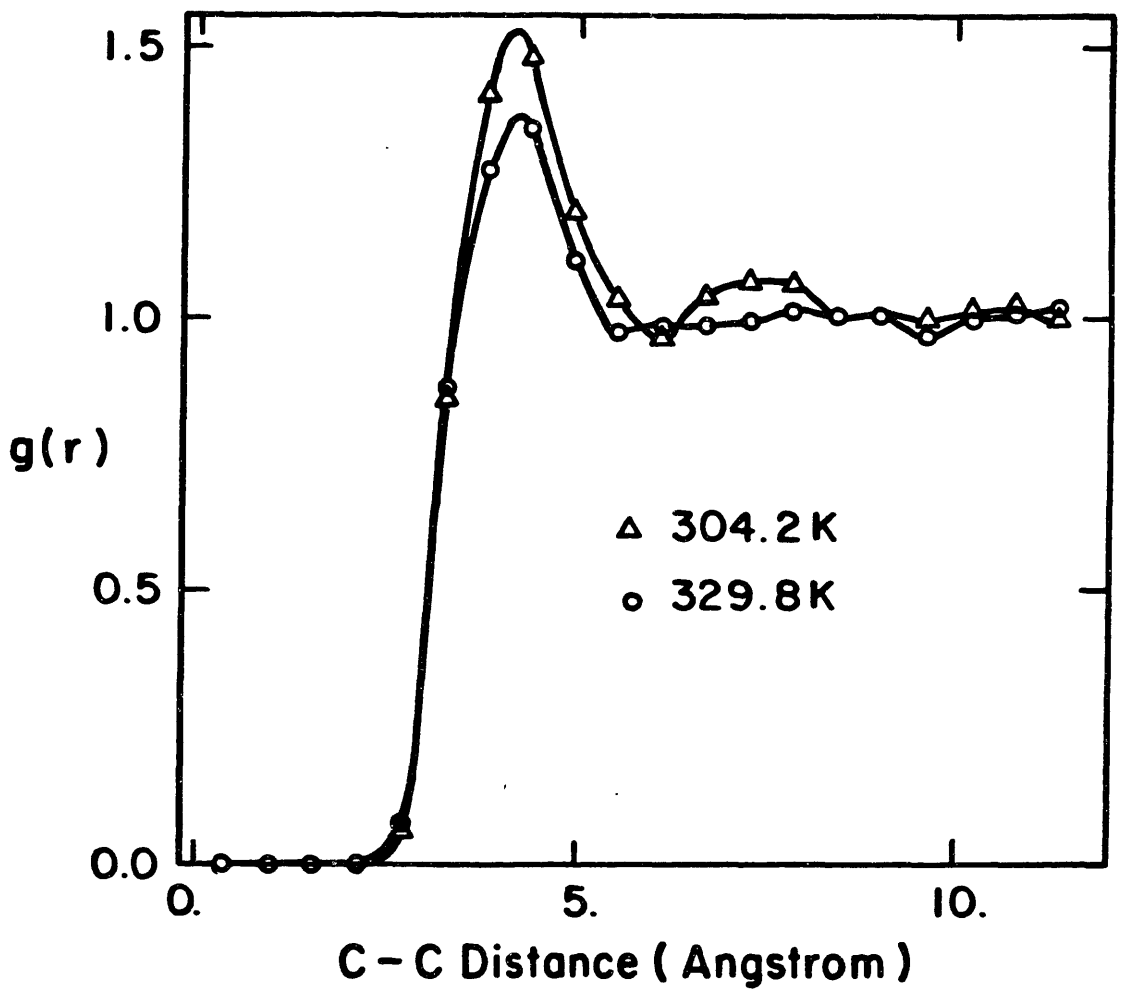

FIGURE 1.33: Effect of temperature upon the carbon-carbon radial distribution function; ρ = 13.87 mol/lt.

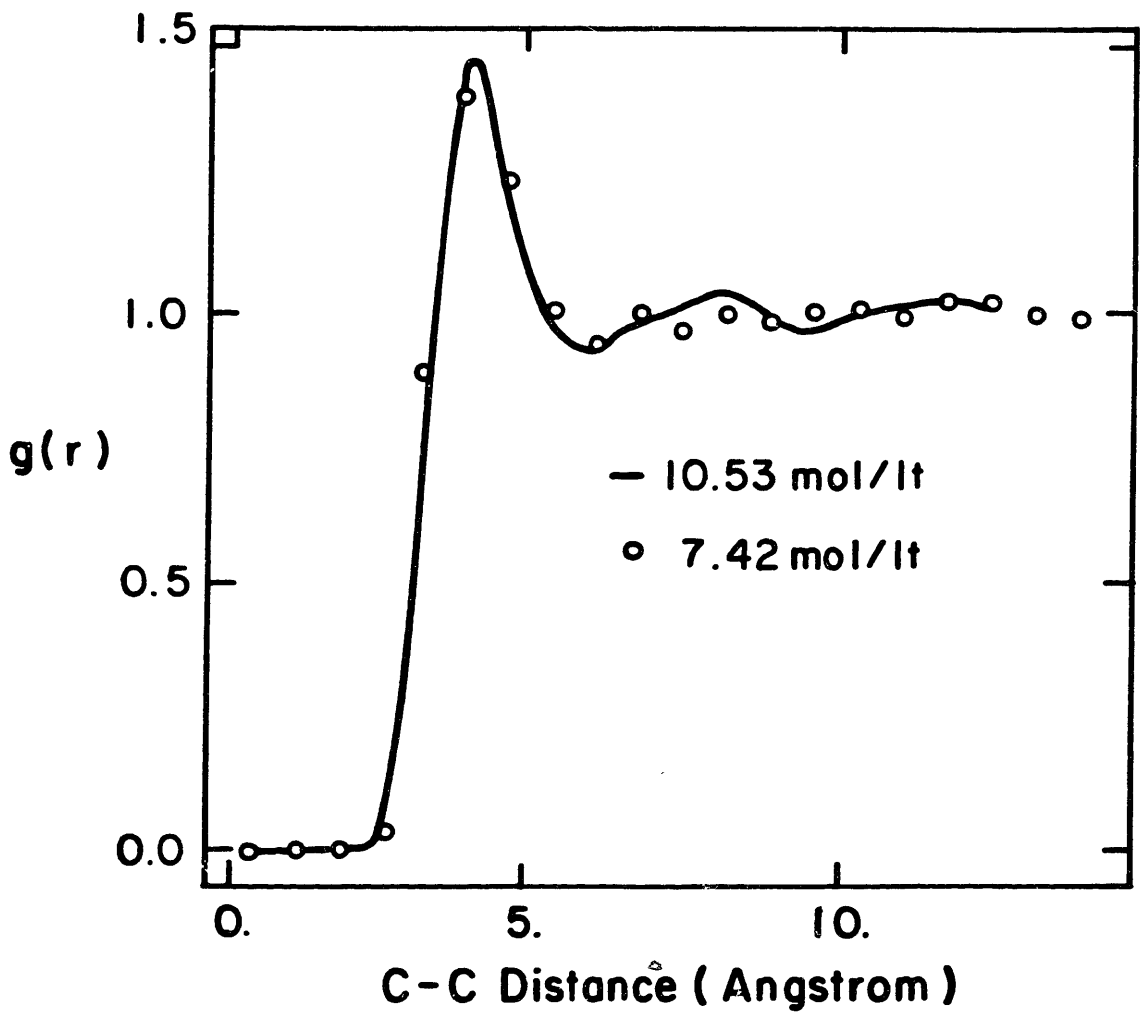

FIGURE 1.34: Effect of density upon the carbon-carbon radial distribution function; <T> ≈ 315 K.

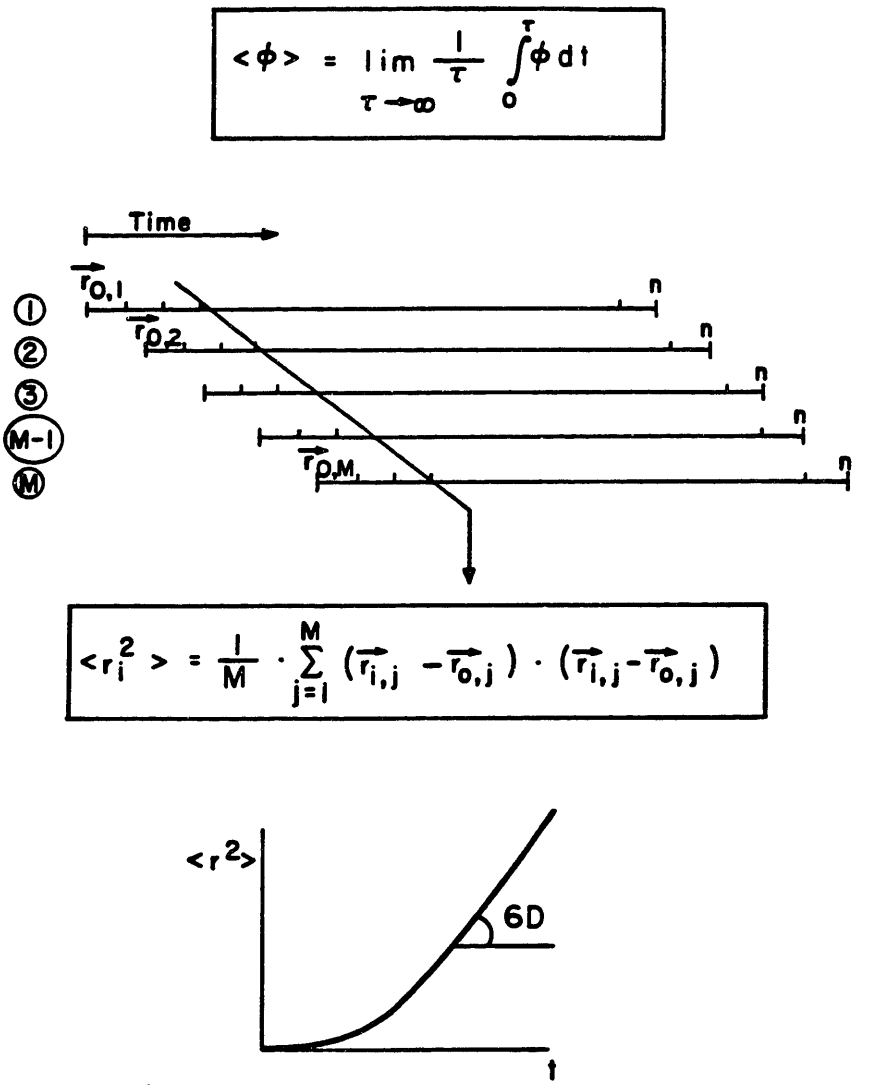

FIGURE 1.35: Ensemble generating technique.

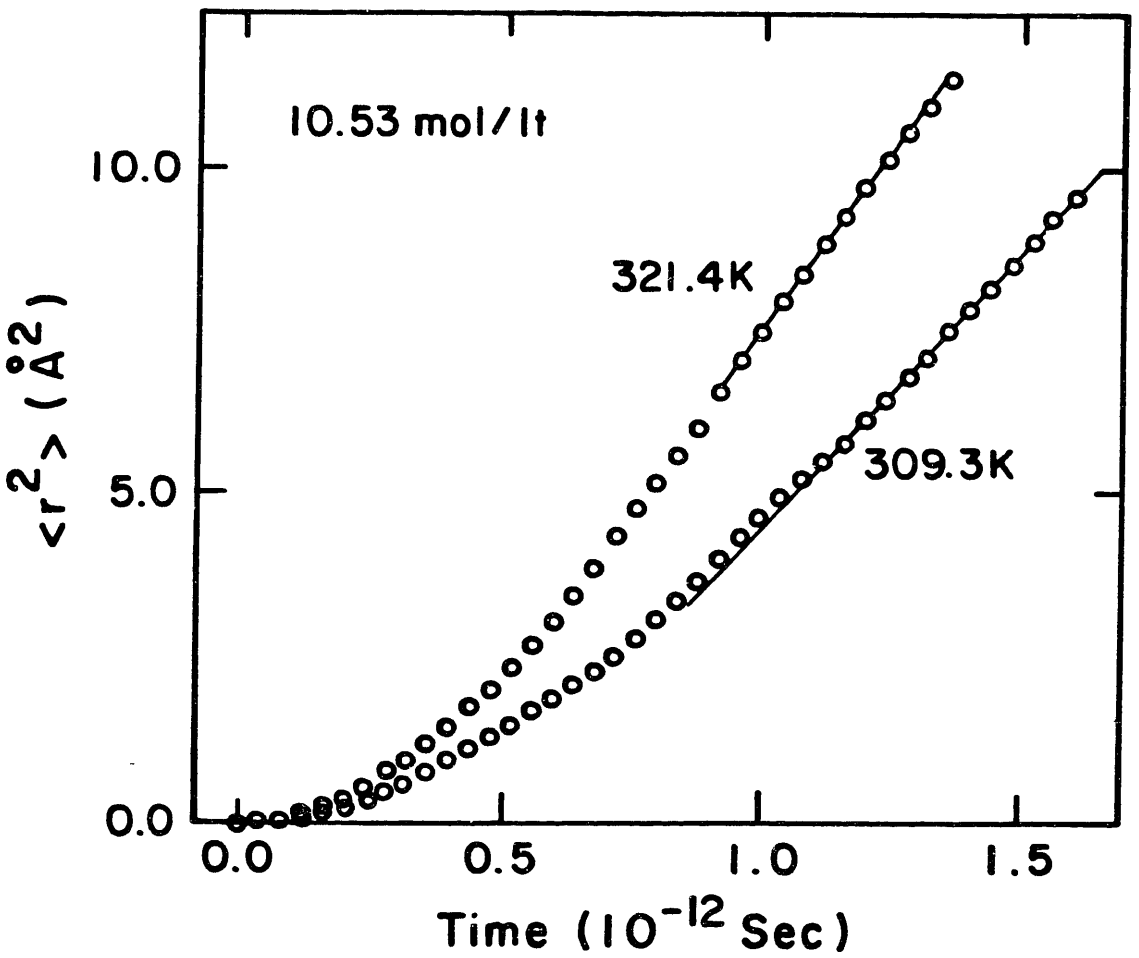

FIGURE 1.36: Effect of temperature upon the mean squared displacement versus time relationship.

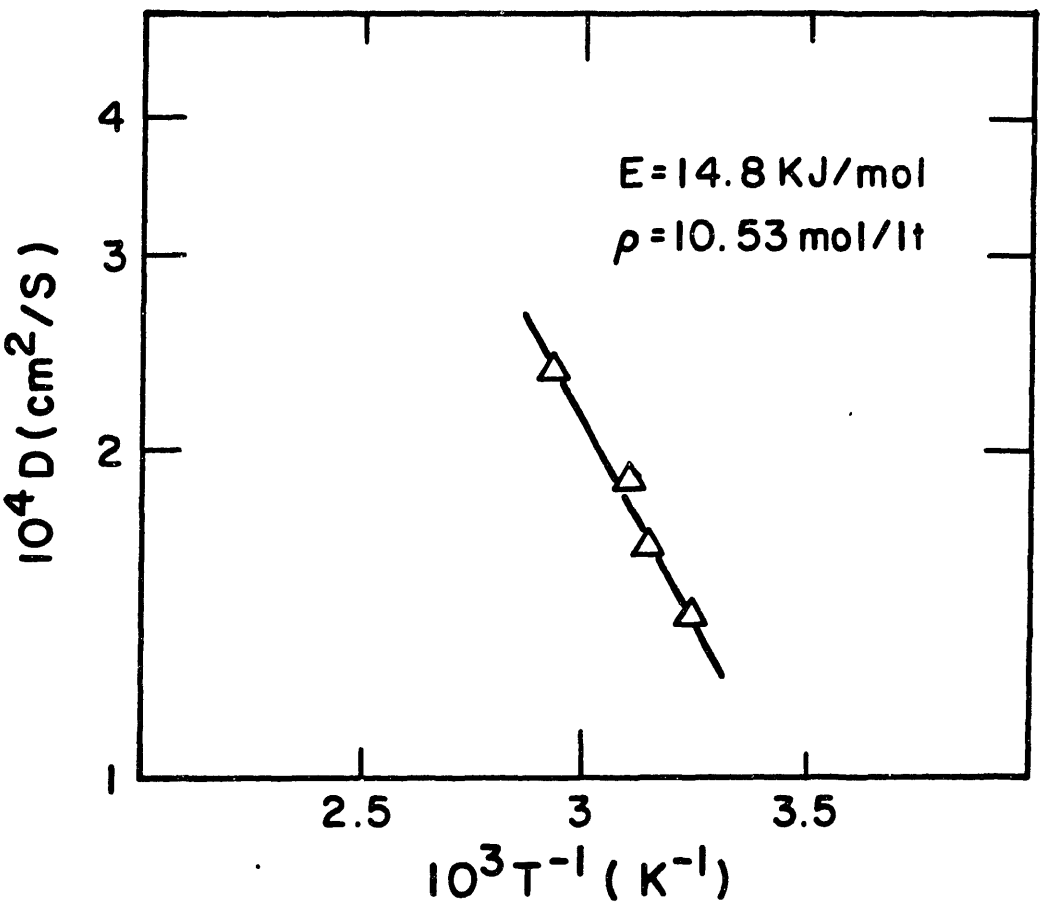

FIGURE 1.37: Arrhenius plot for the computed diffusion coefficients of benzene in CO_2.

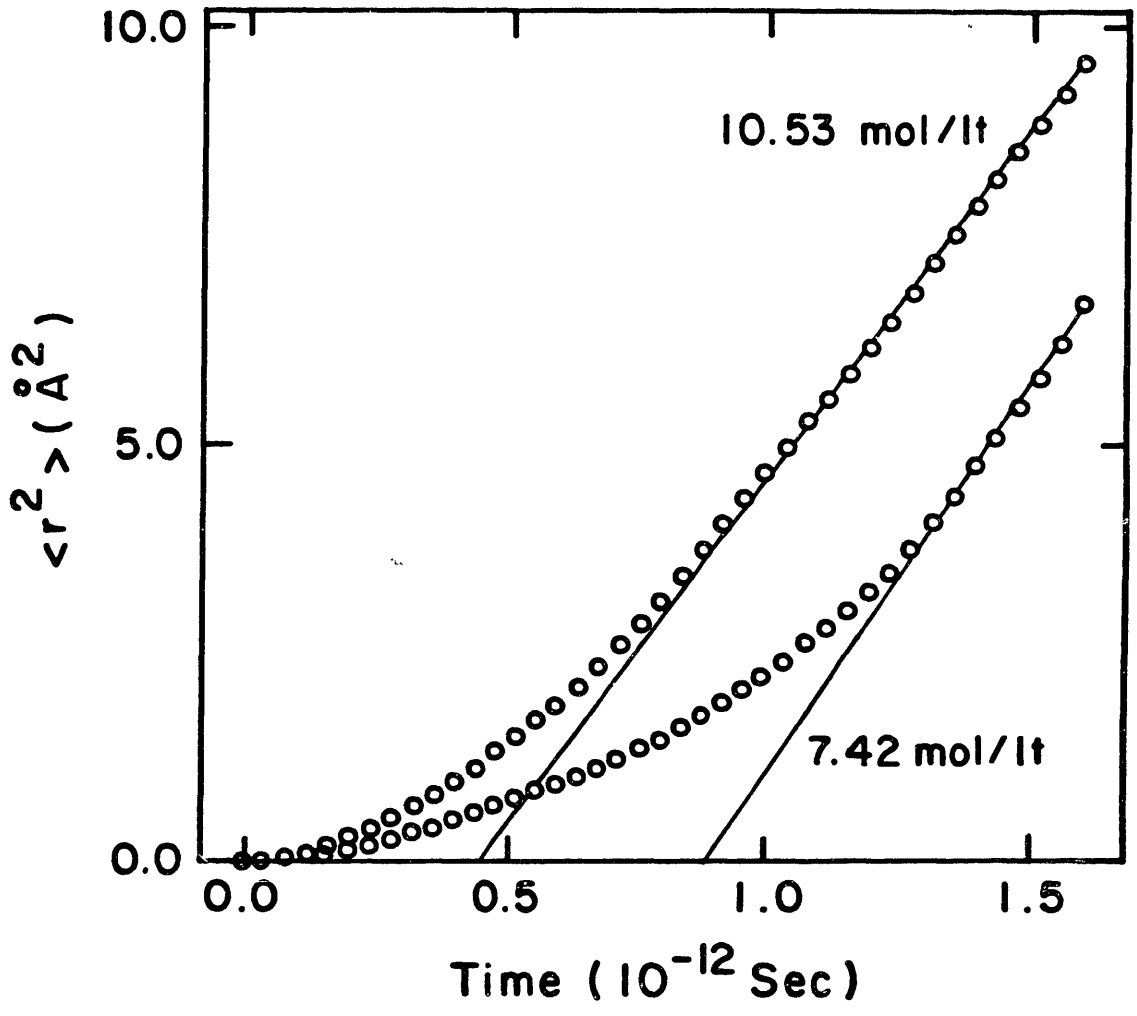

FIGURE 1.38: Effect of density upon relaxation (short time) and diffusive (long time) behaviour; benzene-CO_2; <T> - 310 K.

respectively. Furthermore, the short-time (i.e., $t \ll \tau$) behaviour of $\langle r^2 \rangle$ can be obtained from a truncated time expansion which, when squared and ensemble-averaged, yields

$$\langle r^2 \rangle = \left(\frac{3kT}{m}\right) t^2 \qquad (1.46)$$

At a given temperature, (i.e. same initial slope), then, decreasing the density (i.e., the viscosity) causes an increase in τ, which dominates the short-time behaviour, only to give rise to a higher diffusion coefficient, as expected, for $t > \tau$ (the computed diffusion coefficients are 1.396×10^{-4} cm^2/s at 10.53 mol/lt and $1.649 \times 10^{-4} cm^2/s$ at 7.42 mol/lt). Relaxation times calculated from Equation (1.45) with experimental CO_2 viscosities (.05cp at 310 K, 90 bar, 12.2 mol/lt) and 2.49 Å (i.e., center of mass to H atom distance) for a, yield values (5.5×10^{-13} sec) in excellent qualitative agreement with τ values obtained from the simulations.

A very interesting theoretical question is raised by the fact that, although in the simulations the mean squared displacement exhibits a linear behaviour at long times, the relationship $\eta D T^{-1} = f$ [size] is only an asymptotic law approached at high viscosities. This apparent paradox can be explained by noting that the long time relationship between $\langle r^2 \rangle$ and time can be derived without postulating any explicit form for the hydrodynamic drag. Alternatively (Chandrasekhar, 1943), starting from the Langevin equation, the limits $\langle r^2 \rangle \sim t^2$ ($t \to 0$) and $\langle r^2 \rangle \sim t$ ($t \to \infty$) can again be obtained without postulating any form for the drag coefficient, β, although the drag term itself is, in this approach, proportional to the particle's velocity (with an as yet undefined proportionality constant, β).

We conclude, therefore, that, if β is non-linear in η (i.e., $\beta \sim \eta^{\delta}$, for example), the Stokes-Einstein equation (or, more precisely, its form, i.e., $\eta D T^{-1} = f$ [size]) would not describe physical reality; in spite of this, though, the short and long time limits of $\langle r^2 \rangle$ would, of course, still be parabolic and linear, respectively, and the fundamental relationship between $\langle r^2 \rangle$ and D at long times would still be valid.

The breakdown of hydrodynamic behaviour in supercritical fluids, then, is associated with a "hydrodynamic" drag that can best be explained in terms of a power law relationship between the drag coefficient and viscosity.

Using the activation energy calculated from the log D vs. T^{-1} plot (Figure 1.37), we can estimate a diffusion coefficient at 313.2 K and 10.53 mol/lt from the value obtained at 309.3K and the same density. This number (1.5×10^{-4} cm^2/s) is to be compared with the value obtained by graphical interpolation of Swaid and Schneider's data at the same temperature ($2.05 \times 10^{-4} cm^2/s$).

The molecular dynamics prediction is 36.7% lower than the experimental value. This is an encouraging result, given the facts that no adjustable parameters were used in this work, and that the ensemble-generating technique involved just one solute particle.

2: INTRODUCTION

2.1: PERSPECTIVE

Research in the general area of supercritical fluids has grown considerably over the past few years (Ely and Baker, 1983). The thermodynamic aspects of this technology have, by far, received much more attention than the transport aspects.

From the point of view of transport, the goal is to understand and, eventually, predict, the rates at which mass and/or heat are transferred within the dense fluid phase. This requires knowledge of the transport properties of the mixtures involved, as well as of the particular flow situation being considered.

The present work addresses several aspects of mass transfer in supercritical fluids. The first question that must be answered, therefore, is the relevance of the problem itself, i.e., why (if at all) is mass transfer in a supercritical fluid any different from, say, liquid phase mass transfer?

Part of this answer is, of course, obvious: the physical properties of supercritical mixtures are different from liquid properties (see below). This, by itself, would justify interest in the problem, at least from the point of view of property measurement, estimation and correlation.

In addition, the unique properties of fluids in the supercritical region give rise to mass transfer mechanisms which are qualitatively different from the corresponding liquid phase case. Thus, what is required in order to understand and predict mass transfer rates in supercritical fluids is a study of the physical properties and of the peculiar convective mechanisms that arise as a consequence of those physical properties. Such an analysis has been done for heat transfer (Nishikawa and Ito, 1969; Harrison and Watson, 1976; Hauptman and Malhotra, 1980; Shitsman, 1974; Nishikawa, et al., 1973; Kakarala and Thomas, 1980; Hall, 1975), but not for mass transfer.

In this work, physical property measurement and computer simulation have been done for binary diffusion of aromatic compounds in supercritical fluids. In addition, the importance of natural convection in mass transfer

with supercritical fluids has been analyzed in the light of fluid properties, and observed experimentally.

In Table 2.1, the physical properties of a supercritical fluid (CO_2 at 150 bar and 310 K) are compared with those of air and water at ambient conditions. We notice, in the first place, the very low kinematic viscosity of the supercritical fluid. As outlined in Section 1.1 and explained in Chapter 3, this is the reason why, at any given Reynolds number, natural convection plays a much more important part in the overall transport mechanism within a supercritical fluid than it does in the case of a liquid or a gas.

In the second place, the Schmidt numbers corresponding to diffusion of typical organic solutes (molecular weight ~ 10^2) are roughly two orders of magnitude lower in a supercritical fluid than in a typical liquid, whereas Prandtl numbers are comparable.

We can therefore complete the answer to the question posed at the beginning of this section by noting that a supercritical fluid is simultaneously as dense as a liquid, more compressible than a dilute gas, possesses a kinematic viscosity that can be lower than liquid metal kinematic viscosities, Prandtl numbers similar to those of liquids, and Schmidt numbers two orders of magnitude lower than the corresponding liquid values. This is certainly more than enough to justify the study of transport in supercritical fluids.

Although the properties of supercritical fluids are a consequence of the existence of the critical point, the analysis, throughout the present work, is entirely classical. Critical phenomena (Stanley, 1971) such as the divergence of the specific heat at constant pressure or the isothermal compressibility of a pure substance at its critical point, or the vanishing of diffusive fluxes at mixture critical points (Tsekhanskaya, 1968) require entirely different theoretical approaches (Pfeuty and Toulouse, 1978; Ma, 1976). Non-classical behaviour, however, whereby fluctuations of some characteristic quantity (the order parameter) grow without limit, is restricted to very narrow regions close to criticality, and these were not explored in the present work.

Table 2.1: Comparison of physical properties of air, water and supercritical CO_2

	ρ(c) (kg/m³)	η (d) (kg/ms)	ν (m²/s)	cp(e) (m²/s²K)	k(f) (Kgm/s³K)	D(g) (m²/s)	Pr (-)	Sc (-)
Air(a)	1.17	1.78×10^{-5}	1.52×10^{-5}	1.05×10^{3}	2.62×10^{-2}	8×10^{-6}	7.1×10^{-1}	1.9
Water(a)	9.97×10^{2}	9.3×10^{-4}	9.33×10^{-7}	4.19×10^{3}	6.17×10^{-1}	10^{-9}	6.32	9.33×10^{2}
SCF (b)	7.8×10^{2}	7.03×10^{-5}	9.01×10^{-8}	3.75×10^{3}	9.13×10^{-2}	8×10^{-9}	2.90	11.3

(a) 1 bar; 298 K

(b) 150 bar; 310 K

(c) Air: ideal gas equation of state; Water: Table 3-28, p. 3-75, Perry and Green, 1984

(d) Air: Fig. 3-44, p. 3-211, Perry and Chilton, 1973; Water: Fig. 3-45, p. 3-213, Perry and Chilton, 1973; CO_2: Stephan and Lucas, 1979

(e) Air: Fig. 3-12, p. 3-130, Perry and Chilton, 1973; Water: Fig. 3-11, p. 3-129, Perry and Chilton, 1973; CO_2: Fig. 3-12, p. 3-130 and Fig. 3-53, p. 3-237, Perry and Chilton, 1973

(f) Air: Table 3-285, p. 3-215, Perry and Chilton, 1973; Water: Table 3-284, p. 3-214, Perry and Chilton, 1973; CO_2: Table 3-285, p. 3-215 and Fig. 3-59, p. 3-244, Perry and Chilton, 1973

(g) Typical values for diffusion of organic solutes (MW ~ 10^2)

2.2: DIFFUSION IN DENSE FLUIDS: THEORETICAL DIFFICULTIES

Mutual and self diffusion coefficients for low pressure gaseous systems can be estimated to within ~ 7.5% accuracy (Reid et al., 1977) from purely theoretical expressions. The starting point in this case is the Boltzmann transport equation (Hirschfelder et al., 1964; Chapman and Cowling, 1970; Huang, 1963; Pauli, 1981). The latter is a non-linear integro-differential equation for the rate of change of the distribution function and was derived by Boltzmann in its original form by considering only binary interactions of point particles and introducing the molecular chaos hypothesis, whereby the position and velocity of a particle are uncorrelated.

The Boltzmann transport equation admits a stationary solution, the Maxwell-Boltzmann distribution (see Chapter 8). The Chapman-Enskog method is a successive approximation approach to the solution of the Boltzmann transport equation, and yields expressions for the transport coefficients after considerable effort. As soon as fluid density becomes such that the mean free path is comparable to molecular dimensions, higher order interactions and the finite molecular size must be taken into account. In addition, collisional transfer (i.e., the energy and momentum transfer that takes place instantaneously in a hard sphere collision) becomes a progressively important transport mechanism which is not considered in the Boltzmann equation.

As a result, there exists no accurate kinetic theory of dense fluids that will allow, as with the dilute case, an accurate prediction of the transport coefficients. Some of the theoretical and experimental approaches to the problem will be briefly reviewed.

2.3: THEORETICAL APPROACHES

Corresponding states arguments have been applied to the correlation and extrapolation of self-diffusion data. In this case, one can use dimensional analysis arguments (Hirschfelder et al., 1964) to show that the reduced self-diffusion coefficient of a spherical non-polar molecule,

$$D^+ = D\ \sigma^{-1}(m/\varepsilon)^{1/2} \tag{2.1}$$

must be a function of the reduced temperature and volume,

$$D^+ = D^+\ (v^+, T^+) \tag{2.2}$$

where

$$v^+ = v\sigma^{-3} \tag{2.3}$$

and

$$T^+ = kT/\varepsilon \tag{2.4}$$

In Equations (2.1) to (2.4), σ and ε are a characteristic length and a characteristic energy, m is the molecular mass, and v, the molecular volume (i.e., total volume divided by number of molecules).

Even though the detailed functionality implied by Equation (2.2) may not be known, this approach provides, in principle, an extremely powerful technique for data correlation and extrapolation.

Equation (2.1) can be transformed, again through dimensional arguments, by writing

$$\sigma \sim (kTc/Pc)^{1/3} \tag{2.5}$$

$$\varepsilon \sim k\ Tc \tag{2.6}$$

$$m = ML^{-1} \tag{2.7}$$

$$k = RL^{-1} \tag{2.8}$$

where L is Avogadro's number, to arrive at D^+

$$D_r^+ = D\ M^{1/2}\ P_c{}^{1/3}\ (RT_c)^{-5/6} = D_r^+\ (Tr, Pr) \tag{2.9}$$

which is the usual starting point for corresponding states approaches to diffusion.

The extension of these ideas to binary diffusion implies, at the outset, a degree of arbitrariness in the definition of mixture critical parameters. Thus, Slattery and Bird (1958), define geometric mean critical temperatures and pressures,

$$P_{C12} \equiv (P_{C1}\ P_{C2})^{1/2} \tag{2.10}$$

$$T_{C12} \equiv (T_{C1}\ T_{C2})^{1/2} \tag{2.11}$$

whereas a more common approach is to define

$$P_{C12} = \frac{T_{C12}}{[1/2\ (T_{C1}/P_{C1})^{1/3} + 1/2\ (T_{C2}/P_{C2})^{1/3}]^3} \tag{2.12}$$

with T_{C12} as per Equation (2.11). The denominator of Equation (2.12) is equivalent to a Lorentz-Berthelot mixing rule for σ,

$$\sigma_{12} = \frac{1}{2}\ (\sigma_1 + \sigma_2) \tag{2.13}$$

The mixture molecular weight is usually defined as a modified harmonic mean,

$$\frac{2}{M_{12}} \equiv \frac{1}{M_1} + \frac{1}{M_2} \tag{2.14}$$

From this short discussion, it should be apparent that, although corresponding-states ideas can be extremely useful in correlating self-diffusion data, the extension to binary diffusion can, at best, be considered as a convenient empiricism, since the definitions of mixture parameters are somewhat arbitrary. Furthermore, for highly non-spherical molecules, a two-parameter approach (σ, ε, or T_c, P_c) is not, in general, capable of describing the system's behaviour. As an example, we consider the Slattery-Bird (1958) correlation, obtained by statistical analysis of experimental data in the light of a corresponding states approach,

$$PD\xi = 3.882 \times 10^{-4}\ T_r^{1.823} \tag{2.15}$$

with

$$\xi = \frac{M^{1/2}}{T_c^{5/6}\ P_c^{2/3}} \tag{2.16}$$

and mixture parameters as per Equations (2.10), (2.11), (2.14). Equations (2.15) and (2.16) are dimensional, with the pressures in atmospheres and D in cm^2/sec. Equation (2.15) was originally derived for self-diffusion in dilute systems, and extended to dilute binary systems by the authors.

When several dense fluid data (Table 2.2) are plotted according to Equations (2.15), (2.16), (2.10), (2.11) and (2.14) (see Figure 2.1) it can be seen that deviations are not associated with high pressures

Table 2.2: References and Experimental Conditions For Figure 2.1

System	Reference	T (K)	P (bar)
H_2-N_2	Berry and Koeller (1960)	313 —> 350	69 —> 690
CH_4-C_2H_6	Berry and Koeller (1960)	313 —> 350	69 —> 690
CH_4-N_2	Berry and Koeller (1960)	313	6.9 —> 172
C_2H_6-N_2	Berry and Koeller (1960)	313	6.9 —> 172
CO_2-C_6H_6	Swaid and Schneider (1979)	308 —> 328	80 —> 160
CO_2-n propylbenz.	Swaid and Schneider (1979)	308 —> 328	80 —> 160
CO_2-1,3,5,tri-methylbenzene	Swaid and Schneider (1979)	308 —> 328	80 —> 160
C_2H_4-$C_{10}H_8$	Iomtev and Tsekhanskaya (1964)	285 —> 308	66 —> 304
N_2-$C_{10}H_8$	Morozov and Vinkler (1975)	303 —> 313	2 —> 128
CO_2-$C_{10}H_8$	Iomtev and Tsekhanskaya (1964)	308 —> 328	83 —> 304
	Tsekhanskaya (1971)	308	80 —> 83.5
	Morozov and Vinkler (1975)	293 —> 313	5.8 —> 56

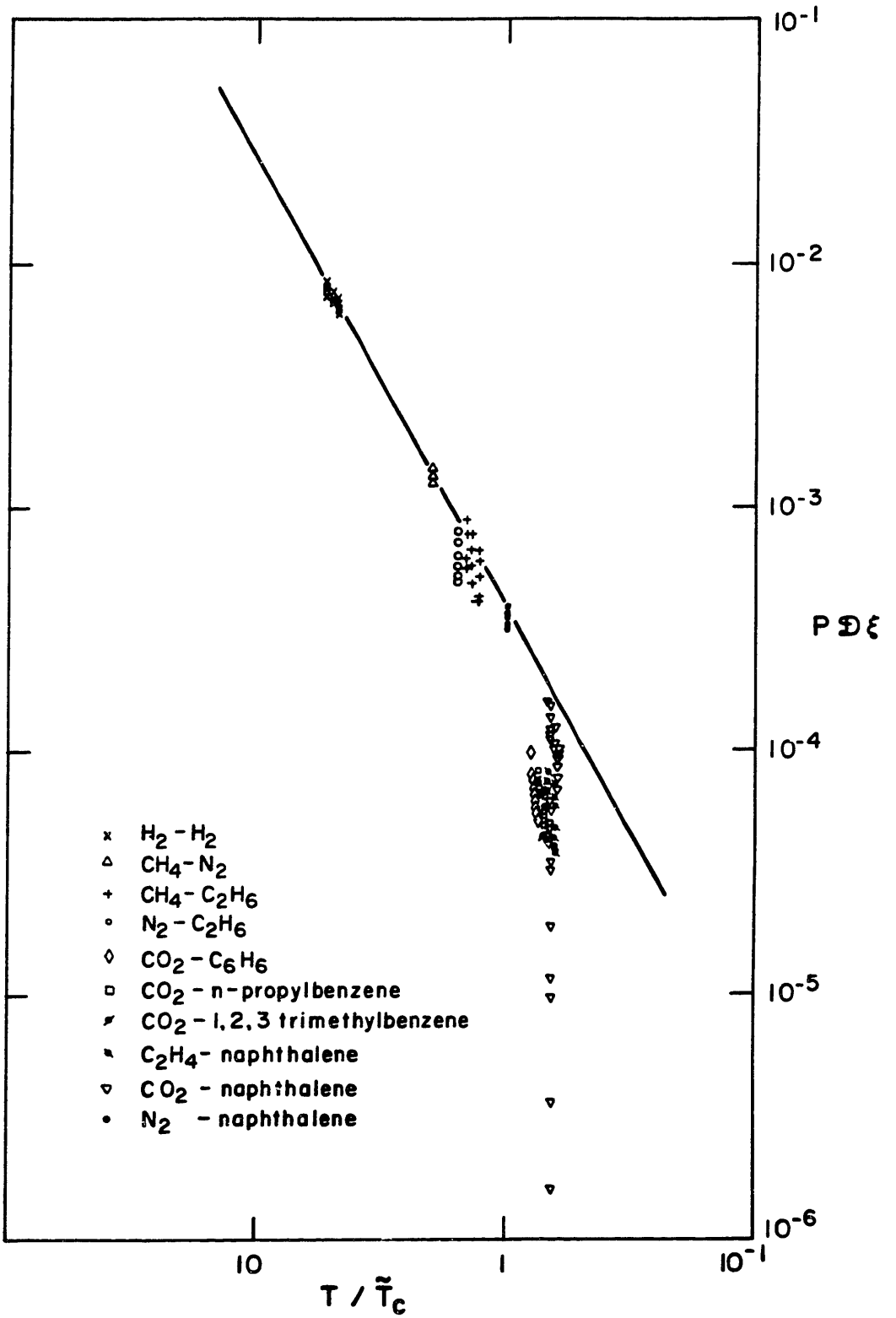

FIGURE 2.1: The Slattery-Bird correlation: a two-parameter corresponding states approach.

but with the nature of the solutes and solvents. In particular, diffusion of aromatics is poorly represented by the correlation, except for the N_2-naphthalene system. On the other hand, Berry and Koeller's (1960) data for H_2 - N_2 (69 to 690 bar), CH_4 - C_2H_6 (69 to 690 bar) and CH_4 - N_2 (7 to 172 bar) are well correlated in terms of this two parameter equation. The CO_2-naphthalene data include Tsekhanskaya's (1971) studies of the vanishing of diffusion coefficients at mixture critical points which are, a priori, beyond the scope of Equation (2.15) (see Chapter 7).

Two-parameter corresponding states arguments, therefore, should be used with extreme care in dense binary systems, and must be considered, at best, as helpful correlating guidelines. Mixture composition is not taken into account by relationships such as Equations (2.10), (2.11), (2.12) or (2.14), which can only be applied at infinite dilution.

The extension of corresponding states ideas to substances that depart from strictly conformal behaviour has received considerable attention recently. In one approach, a reference substance of well-known properties is used, and conformality with respect to the reference substance is forced through the introduction of state-dependent shape factors (Murad and Gubbins, 1977), which are either calculated iteratively or obtained from empirical fits. For mixtures, pseudo-critical properties are introduced; this leads to the appearance of cross interaction parameters, which must be regressed from experimental transport data (Murad and Gubbins, 1981). Although interesting in principle, this approach is far from standardized and requires extensive iterative calculations or empirical values for the shape factors and interaction coefficients.

Alternatively, the reduced transport coefficients (i.e., Equation (2.9) are expanded in Taylor series about a known (reference) value, using a third parameter as an expansion variable. This idea is derived from Pitzer's (1955) original work, so that the acentric factor is the most commonly used third parameter. Teja (1982) has recently proposed a modified version of this approach for binary diffusion in liquids by considering two reference fluids. Two diffusion coefficients are needed (of different solutes in a given solvent), and the resulting expression still contains an adjustable parameter.

The problem of calculating density-dependent diffusion coefficients in dense fluids is still unsolved. The Enskog (1921) theory is still widely used in spite of the fact that, in most cases, it does not predict the observed trends. In this approach, molecules are considered as hard smooth spheres, whereupon the problem again becomes tractable, since only binary collisions can exist in a hard sphere fluid. The main result of this theory, in its unmodified form, and for self-diffusion, can be written as

$$\frac{\rho D}{(\rho D)^0} = \frac{1}{\chi} \tag{2.17}$$

where superscript ^{0} indicates the dilute limit, and χ is the factor by which collision frequency in a hard sphere fluid differs from the corresponding number in a fluid composed of point particles and is given, for a hard sphere fluid, by

$$\chi = 1 + 0.625\ b_0 V^{-1} + 0.2869\ (b_0 V^{-1})^2 + 0.115\ (b_0 V^{-1})^3 + \ldots \tag{2.18}$$

where b_0 is the molar second virial coefficient,

$$b_0 = \left(\frac{2\pi\sigma^3}{3}\right)L \tag{2.19}$$

and V, the molar volume. A derivation of Equation (2.18) can be found in Chapman and Cowling (1970) and follows from geometric arguments by taking into account the increase in collision frequency due to the finite molecular size as well as the decrease in collision frequency due to the "shielding" effect that close-packed molecules exert on each other by blocking incoming molecules.

Enskog's ideas were extended to binary (1-2) diffusion by Thorne, to arrive at

$$\frac{\rho D_{12}}{(\rho D_{12})^0} = \frac{1}{\chi_{12}} \tag{2.20}$$

with

$$\chi_{12} = 1 + \frac{\pi}{12} n_1 \sigma_1^3 (8 - 3\sigma_1/\sigma_{12}) + \frac{\pi}{12} n_2\ \sigma_2^3 (8-3\ \sigma_2/\sigma_{12}) + \ldots \tag{2.21}$$

where n_1 and n_2 are number densities, and the hard sphere diameters are combined according to Equation (2.13).

As can be seen from Equation (2.18) or its binary equivalent (2.21), Enskog's theory predicts diffusivities which decrease with density more rapidly than ρ^{-1}. In addition, since χ and χ_{12} are both greater than unity, we must have, according to this theory,

$$(\rho D) < (\rho D)^{\circ} \tag{2.22}$$

always. However, experimental measurements for diffusion of aromatics in supercritical CO_2 (Swaid and Schneider, 1979), as well as aliphatic and halogenated aliphatic hydrocarbons in He (Balenovic et al., 1970) are not only consistently above the Enskog prediction, i.e.,

$$\left[\frac{\rho D}{(\rho D)^{\circ}}\right]_{exp} > \left[\frac{\rho D}{(\rho D)^{\circ}}\right]_{Enskog} \tag{2.23}$$

but, in addition, result in ratios greater than unity for several data points, a fact that cannot be explained by the Enskog theory.

The modified Enskog theory is an attempt to preserve the simplicity of the basic relationship (i.e., Equation (2.17)), while correcting for the idealizations implicit in Equation (2.18). This is done, following Enskog, by postulating that, in the hard sphere equation,

$$\chi\, b_o\, V^{-1} = z - 1 \tag{2.24}$$

where z is the compressibility factor, the pressure be replaced by the "thermal pressure", to arrive at

$$\chi\, b_o\, V^{-1} = \frac{V}{RT}\left[T\left(\frac{\partial P}{\partial T}\right)_V\right] - 1 \tag{2.25}$$

In this approach, b_o is now obtained from

$$T\left(\frac{\partial P}{\partial T}\right)_V = \frac{RT}{V}\left(1 + \chi\, b_o\, V^{-1}\right) \tag{2.26}$$

and the limit of $\chi\, b_o$ as V tends to infinity. When P-V-T data, are expressed as

$$P = \frac{RT}{V}\left[1 + \rho B(T) + \rho^2 C(T) + \ldots\right] \tag{2.27}$$

we obtain,

$$b_0 = M \left(\frac{\partial BT}{\partial T}\right)_V \tag{2.28}$$

The modified Enskog theory (Hanley et al., 1972; Hanley and Cohen, 1975) has been used successfully for simple pure dense fluids. In essence, it is an ad-hoc correction of the original theory that takes into account the actual properties of a fluid by replacing the hard sphere expression for χ (Equation (2.18)) by Equation (2.25), where χ is calculated from P-V-T data. The extension of the modified Enskog theory to binary diffusion is an interesting possibility, although, from the previous discussion, it should be evident that such an approach would constitute a semiempirical modification of an existing theory, rather than a predictive method based on first principles.

The so called van der Waals picture of transport in dense fluids (Dymond and Alder, 1966), whereby molecules are considered to interact via a spherically symmetric potential consisting of a hard core plus a long-range attractive tail, has served as a basis for a significant amount of recent work. In order to preserve this intuitive general picture, empirical correction factors have been introduced to account for non-sphericity. Thus, the idea of a rough hard sphere fluid (Chandler, 1975) "composed of spherical particles which collide impulsively, and these instantaneous collisions are capable of changing the angular momentum of a particle as well as the linear momentum" leads to a correction factor A, (the "roughness factor"), such that

$$D_{RHS} = A\, D_{SHS} \quad (A < 1) \tag{2.29}$$

where RHS and SHS denote, respectively, rough and soft hard spheres (i.e., spheres with and without rotational-translational coupling, respectively). The roughness factor is used as an adjustable parameter. From equipartition arguments it follows that A should be independent of temperature for a given system. In spite of the obvious empiricism of Equation (2.29), the rough hard sphere approach has received considerable attention (Bertucci and Flygare, 1975; De Zwaan and Jonas, 1975; Fury et al., 1979; Chen, 1983) and has been widely used for correlating purposes.

Hydrodynamic theory (Einstein, 1905) predicts, for the diffusion of a Brownian sphere of radius a in a fluid of viscosity η, at a temperature T, a diffusion coefficient given by

$$D = \frac{kT}{6\pi a\eta} \tag{2.30}$$

where the coefficient 6π corresponds to a no-slip boundary condition, and becomes 4π in the opposite case whereby the sliding friction coefficient vanishes. It has long been known that an equation of the form of (2.30), i.e.,

$$\eta D T^{-1} = f\,[\text{size}] \tag{2.31}$$

can be used to correlate and understand molecular diffusion in dense fluids. This implies the very remarkable concept of hydrodynamic behaviour at the molecular level, and is the basis of numerous empirical correlations which have been used with varied success in the study of diffusion in liquids (Wilke and Chang, 1955; Scheibel, 1954; Reddy and Doraiswamy, 1967; Lusis and Ratcliff, 1968). For non-spherical molecules of realistic shape, hydrodynamic theory cannot, in general, provide a predictive equation due to the difficulty in evaluating the drag. However, Equation (2.31) is extremely useful for correlating purposes.

The hydrodynamic limit can also be analyzed in the context of hard sphere theory (Dymond, 1974), according to which

$$D \sim T^{1/2} (V - 1.384\ V_o)\ \sigma^{-2} \tag{2.32}$$

$$\eta \sim T^{1/2} (V - 1.384\ V_o)^{-1}\ \sigma \tag{2.33}$$

where V_o is the hard sphere close-packed molar volume, and V is the molar volume. It follows that

$$D\eta\ T^{-1} \sim \sigma^{-1} \tag{2.34}$$

in agreement with hydrodynamic theory. The hard sphere fluid, then, shows hydrodynamic behaviour at the molecular level. The temperature dependence of fluid viscosity predicted by Equation (2.33), though, is obviously inconsistent with experimental evidence, whereby liquid viscosities

are strongly (i.e., activated) decreasing functions of temperature. To remedy this, temperature-dependent hard sphere diameters have been regressed from experimental data (Fury et al., 1979; Chen, 1983), but this is obviously in contradiction with the concept of a hard sphere.

From this brief survey, it can be concluded that the prediction of transport coefficients in dense fluids is, at present, an unsolved theoretical problem. Existing theories can, at best, serve as useful guidelines for data analysis and correlation.

2.4: DIFFUSION IN DENSE FLUIDS: COMPUTER SIMULATIONS

The calculation of transport coefficients via computer simulations can be done using molecular dynamics, a technique first introduced almost thirty years ago (Alder and Wainwright, 1959; Wainwright and Alder, 1958). In this approach, the dynamics of a finite number of molecules is simulated by integrating the classical equations of motion, and the resulting evolution in time of the positions (and orientations for non-spherical molecules) and velocities (including angular velocities in the case of non-spherical molecules) of the molecules is interpreted statistically.

The method, as described above, is deterministic. The dynamic aspect is necessary for the calculation of transport properties; equilibrium properties can, in addition to the dynamic approach, be obtained from statistically generated configurations from which averages can be calculated. The efficient generation of configurations with their appropriate weighing factors is accomplished by using the so-called Monte Carlo method, first introduced over thirty years ago (Metropolis et al., 1953). This represents the other important technique in the area of computer simulation of fluids, and will not be considered here since, by its very nature, it cannot be used to calculate transport properties.

Two theoretically equivalent methods can be used to compute diffusion coefficients. The Einstein expression

$$\frac{d}{dt} \langle [\underline{r}(t) - \underline{r}(0)]^2 \rangle = 2\, d\, D \qquad (2.35)$$

relates the diffusion coefficient of an ensemble of molecules to the slope of the ensemble-averaged, squared displacement versus time relationship

at long times. In Equation (2.35) (see Chapter 8 for derivation and discussion), d is the dimensionality corresponding to r, i.e., the latter can be calculated along a line, within a plane, or, as in the present work, in three dimensional space.

The calculation of a diffusion coefficient, then, involves following the motion of an ensemble of molecules during a time long enough for the ensemble-averaged squared displacement to grow linearly with time.

Alternatively, one can calculate diffusion coefficients using the time-correlation formalism (McQuarrie, 1976), whereby

$$D = \frac{1}{d} \int_0^\infty \langle \underline{v}(t) \cdot \underline{v}(0) \rangle \, dt \qquad (2.36)$$

In Equation (2.36), $\underline{v}$ is, again, a d-dimensional vector. Equation (2.36) can be derived from Equation (2.35) (McQuarrie, 1976); both methods are therefore theoretically (though not computationally) equivalent.
In this approach, then, one computes the time integral of the ensemble-averaged velocity autocorrelation, starting from a given (arbitrary) initial instant, and continuing until the autocorrelation decays to zero, whereupon the integral is invariant.

The method therefore falls into the category of computer "experiments" (Gubbins et al., 1983). This apparently contradictory classification follows from the fact that, given some initial conditions, the temporal evolution of the system is determined but cannot be known a-priori; the computer then performs the simulation (the "experiment"), whose results are finally analyzed and interpreted.

The main problems associated with the molecular dynamics approach fall into two very different categories. In the first place, for pairwise additive potentials, the duration of a simulation (given an event of fixed duration to be studied) is a quadratic function of the sample size. With current computers, tractable problems are limited to simulations representing ~ 10^{-10} seconds of real time, and sample sizes smaller than ~ 10^3 molecules (or, more generally, 10^3 sites in the case of molecular fluids). This first type of limitation is technical rather than fundamental. The relative performance of several computers for molecular dynamics applications is discussed by Ceperley (1981).

A much more fundamental limitation stems from the lack of basic knowledge in the field of intermolecular (or interatomic) potentials. Maitland et al. (1981) summarize our present state of knowledge about potential functions by considering four categories. Class I includes "functions which are considered quantitatively accurate". Ar-Ar, Kr-Kr, Ne-Ne, He-He and Ar-Kr are the only members of this group, with He-Ar, He-Kr and He-Xe described as "probably of this quality". Class II includes potential functions obtained by means of reliable methods; in this category, however, the potentials "have not been extensively tested on a wide range of properties". Members of this group include Hg-alkali metal, inert gas-alkali metal and some inert gas-inert gas (He-Ar, He-Ne, for example) potentials. Class III includes potentials ..." which result from serious attempts to describe the interactions of non-spherical polyatomic molecules". The authors recommend procedures to tackle the problem (inclusion of point monopoles, for example) but conclude that "... the most convenient representation of this anisotropy has not yet been established". Finally, in Class IV, the authors include "... the determinations not of full potential energy functions but merely the parameters that enable a model potential function to best fit selected data", and conclude that, at best "... this procedure offers a way of smoothing or of modestly extrapolating the data at hand. To invest such potentials with more value than this can lead to confusion".

The fact that the technique (i.e., molecular dynamics) is well developed, whereas the fundamental input to the simulation (i.e., the potential functions) cannot, at present, be determined with anything even approaching the same degree of confidence, makes the predictive use of the method limited at best. In the present context, the word predictive should be considered incompatible with the very concept of an adjustable parameter.

It is not surprising, therefore, that by far the most significant contribution of molecular dynamics to date has been the study of model fluids rather than the predictive calculation of properties for specific substances. Thus, important phenomena such as the long-time tails in the velocity autocorrelation function (Alder and Wainwright, 1967; Alder and Wainwright, 1970) the existence of a phase transition in a hard sphere system (Alder and Wainwright, 1962), or the equation of state for a hard

sphere or hard disk solid (Alder et al., 1968) have been successfully studied with this technique. In fact, in some cases (long-time tails), the simulated behaviour displayed hitherto unknown features which were thus first "observed" in a computer simulation and only later predicted as a general feature of dense fluid behaviour.

The generality and usefulness of such model fluid simulations are in sharp contrast with the necessarily empirical and restricted information gathered from specific fluid simulations with ad-hoc potential parameters (Stillinger and Rahman, 1974). Progress in the fundamental knowledge of interatomic and intermolecular forces should lead, eventually, to a completely predictive approach.

2.5: DIFFUSION COEFFICIENTS; EXPERIMENTAL APPROACHES

In the light of the previous discussion, it follows that experiments must necessarily play a fundamental role in the study of diffusion in dense fluids. In the particular case of supercritical fluids, the critical pressures of the solvents of interest (73.8 bar for CO_2; 50.2 bar for C_2H_4; 37.5 bar for SF_6, for example) result in high pressure operation, which makes the study of diffusion under supercritical conditions more difficult, experimentally, than the study of diffusion in liquids.

Previous studies of diffusion in supercritical fluids are summarized in Table 2.3. The weight loss method is a static technique whereby the instantaneous mass of a suspended pellet of diffusing solute is related to the cell geometry, equilibrium solubility of the solute in the solvent, diffusion time and binary diffusion coefficient through an analytical expression resulting from the solution of the appropriate diffusion problem. In view of the importance of natural convection in supercritical fluids (see Chapter 3), the assumption of a stagnant solvent may lead to errors.

The use of supercritical chromatography to study diffusion coefficients represents an application of Taylor dispersion theory (Taylor, 1953; Taylor, 1954). The diffusion coefficient of a solute injected as a pulse in trace amounts into a capillary where a solvent circulates in laminar flow can be calculated from the solute's concentration profile at the capillary's exit. The diffusion coefficient is then a function of fluid

Table 2.3: Experimental Studies of Diffusion of Organics in Supercritical Fluids

System	T (K)	P (bar)	Method	Reference
CO_2-naphthalene	308≤T≤328	83≤P≤304	Weight loss diffusion cell	Iomtev and Tsekhanskaya (1964)
C_2H_4-naphthalene	285≤T≤308	66≤P≤304	Weight loss diffusion cell	Iomtev and Tsekhanskaya (1964)
CO_2-naphthalene	308	74≤P≤84	Weight loss diffusion cell	Tsekhanskaya (1971)
CO_2-benzene	308≤T≤328	80≤P≤160	Supercritical chromatography	Swaid and Schneider (1979)
CO_2-n-propylbenzene	308≤T≤328	80≤P≤160	Supercritical chromatography	Swaid and Schneider (1979)
CO_2-1,3,5-trimethyl-benzene	308≤T≤328	80≤P≤160	Supercritical chromatography	Swaid and Schneider (1979)
CO_2-benzene	313	80≤P≤160	Supercritical chromatography	Feist and Schneider (1982)
CO_2-phenol	313	80≤P≤160	Supercritical chromatography	Feist and Schneider (1982)
CO_2-caffeine	313	80≤P≤160	Supercritical chromatography	Feist and Schneider (1982)
CO_2-naphthalene	308≤T≤333	80≤P≤160	Supercritical chromatography	Feist and Schneider (1982)
CO_2-benzene	320≤T≤342	87≤P≤107	Quasielastic light scattering	Saad and Gulari (1984)
CO_2-heptane	310≤T≤341	78≤P≤109	Quasielastic light scattering	Saad and Gulari (1984)

velocity, duct radius, concentration profile peak width and solute retention time.

This technique can be classified as hydrodynamic, since a well characterized flow situation must exist for the theory to be applicable. The effect of density non-uniformities across the duct's cross section can always be minimized by modifying the duct's aspect ratio (i.e., increasing its length to diameter ratio), making this technique preferable to diffusion cell approaches.

The use of chromatographic techniques to study binary diffusion has been applied to gaseous (Balenovic et al., 1970) as well as liquid systems (Ouano, 1972). A comprehensive review can be found in an article by Maynard and Grushka (1975).

Hydrodynamic techniques can be broadly classified as Fickian or phenomenological. This means that diffusion coefficients are obtained from the solution of a differential equation relating diffusive and convective transport in a well-characterized flow situation. Not only is concentration considered as the driving force for diffusion (see Chapter 7), but the resulting transport coefficient is an average value, resulting from the assumption of composition-independence. Thus, hydrodynamic methods should always be used at infinite dilution. This condition can always be approached with chromatographic techniques (detector sensitivity being the limiting factor) but needs to be carefully checked when diffusion occurs from a source of given composition.

In light scattering techniques, (Burstyn and Sengers, 1982; Saad and Gulari, 1984), on the other hand, the decay rate of the autocorrelation of scattered light intensity is measured at various scattering angles by means of a suitable signal detection scheme. The scattering angle is related to the wave number of concentration fluctuations through Bragg's equation, whereupon the diffusion coefficient is obtained from the relationship.

$$\Gamma = D_{12}q^2 \tag{2.37}$$

where Γ is the autocorrelation decay rate and q, the wave number. The technique has been used to study binary diffusion in liquid mixtures

both away from (Czworniak et al., 1975) and in (Burstyn and Sengers, 1982) the critical regime.

The technique is accurate and does not give rise to the experimental problems associated with hydrodynamic methods. In particular, natural convection phenomena are entirely absent due to the time scales involved. In addition, the concentration dependence of D_{12} can be measured unambiguously by performing experiments at various different concentrations. Finally, the technique has important theoretical implications, especially in the critical region, which make its use mandatory in the study of non-classical dynamic critical phenomena (Enz, 1979).

2.6: MASS TRANSFER

Little systematic work (Brunner, 1984) has been done on mass transfer into a supercritical fluid in practical situations (packed beds, liquid columns, stirred tanks, etc.). As explained in Chapter 3, significant enhancements in mass transfer rates are to be expected whenever transport in the supercritical phase is rate-limiting. This is an important and interesting problem, and should receive increasing attention in the future.

2.7: OBJECTIVES

In the previous sections, a brief review was presented on the current status of theoretical and experimental approaches to the study of transport phenomena in dense fluids. Within this general picture, the main objectives of this work can be summarized as follows:

- to understand the role of physical properties in determining both the rate and mechanism of mass transfer in supercritical fluids
- to measure binary diffusion coefficients of different organic solutes on supercritical fluids and interpret the results
- to study binary diffusion using molecular dynamics computer simulations

The experimental technique (see Chapter 4) selected in the present work is hydrodynamic. Although both chromatographic peak broadening (also a hydrodynamic method) and light scattering yield more accurate

results, the flat plate method, by allowing for the introduction of buoyant effects, made it possible to verify experimentally some of the qualitative predictions made in Chapter 3 in connection with the analysis of physical properties and natural convection.

Although important insights were gained in this way, future studies should separate the mass transfer and property measurement aspects of the problem with carefully designed hydrodynamic techniques, and, ideally, light scattering used to study the former and latter problems, respectively.

As more data become available, the understanding of diffusion in supercritical fluids will, inevitably, benefit from a more fundamental approach. In particular, the interesting theoretical implications of hydrodynamic ideas in the supercritical regime should prove to be more fruitful than the current emphasis on rough hard sphere theory.

The prediction of transport properties through the use of computer simulations is presently limited by the lack of fundamental knowledge in the area of interatomic and intermolecular potentials. In the present work, the approach chosen was somewhat different from the usual procedure: the simulations referred to specific molecules, yet no adjustable parameters were used. The results are encouraging, though accurate prediction (with no adjustable parameters) is still more a goal than a reality in the case of molecular fluids. In addition, the study of infinite dilution binary interactions poses severe problems related to computer speed and memory (see Chapters 9 and 10); the results obtained with a test-particle approach (Alder et al., 1974), again, are encouraging, but they should be considered only as a step in the right direction, which enables the study of a difficult problem without the need for a supercomputer. This is not to say, however, that the statistical significance of the answers would not improve from either a large solute ensemble or longer simulations with completely independent "experiments" (see Chapter 10). Such calculations, however, require, far more powerful computer resources than were available for this work.

3. PHYSICAL PROPERTIES AND NATURAL CONVECTION

3.1 MASS TRANSFER AND NATURAL CONVECTION;HYDRODYNAMICS

Mass transfer in a fluid is inseparable from density non-uniformities. Under the influence of gravity , density gradients give rise to natural convection currents , the relative importance of which is determined by fluid properties.

For steady laminar flow of an incompressible Newtonian fluid under the influence of gravity and an imposed pressure gradient,

$$\eta \nabla^2 \underline{v} + \rho \underline{g} - \underline{\nabla} P = 0 \qquad (3.1)$$

A second component (solute) will diffuse into the fluid if, for example, the latter is in contact with a surface from which the solute dissolves. The resulting concentration gradient will give rise to density gradients which will, in turn, alter the velocity profile. This coupling between mass and momentum transfer can be analyzed in those cases where concentration (and density) gradients are small. Expanding the density about the pure fluid value in terms of solute concentration, and truncating after the linear term,

$$\rho = \rho_o + \left(\frac{\partial \rho}{\partial c}\right)_{T,P} (c - c_o) = \rho_o[1 - \beta_m(c - c_o)] \qquad (3.2)$$

Substituting into Equation (3.1),

$$\eta \nabla^2 \underline{v} + \underline{g}\, \rho_o [1 - \beta_m c] - \underline{\nabla} P = 0 \qquad (3.3)$$

where c_o=0 has been used. Equation (3.3) has been obtained by linearizing the density and neglecting changes in viscosity. This decoupling of the mass and momentum balance equations is known as Boussinesq's approxi-

mation and is obviously restricted to small density gradients.

To illustrate Equation (3.3), let us apply it to flow in a duct of radius R and non-dimensionalize it by defining

$$\Pi = P + \rho_o g h \tag{3.4}$$

$$\Pi^+ = \Pi/\rho_o \langle v \rangle^2 \tag{3.5}$$

$$v^+ = v/\langle v \rangle \tag{3.6}$$

$$r = c/c_i \tag{3.7}$$

where $\langle v \rangle$ is the average fluid velocity in the duct, c_i is the solute concentration at the duct boundary, where phase equilibrium is assumed, and h is the height of a plane of constant hydrostatic pressure measured along the direction of gravity ($\underline{g}'$ is a unit vector collinear with the direction of gravity)

$$\underline{\nabla} h = -\underline{g}' \tag{3.8}$$

Substituting into Equation (3.3) and non-dimensionalizing, with R as length scale,

$$\frac{2}{Re} (\nabla^+)^2 \underline{v}^+ - \underline{\nabla}^+ \Pi^+ - \underline{g}' \left(\frac{Gr}{Re^2}\right) \frac{r}{2} = 0 \tag{3.9}$$

We now define $\Delta\rho$ as the difference in fluid density at the interface and in the bulk (pure solvent), and introduce the natural scales for buoyant, viscous and inertial forces,

$$\text{Bouyant forces} \sim 2R\, g\, \Delta\rho \tag{3.10}$$

$$\text{Viscous forces} \sim \eta \langle v \rangle / 2R \tag{3.11}$$

$$\text{Inertial forces} \sim \langle v \rangle^2 \rho_o \tag{3.12}$$

The physical significance of the parameter $Gr\ Re^{-2}$ follows immediately,

$$\frac{Gr}{Re^2} = \frac{(2R\ g\ \Delta\rho)(\langle v\rangle^2\ \rho_o)}{(\eta\ \langle v\rangle/2R)^2} \cdot \frac{(\eta\ \langle v\rangle/2R)^2}{(\langle v\rangle^2\ \rho_o)^2} = \frac{\text{Buoyant forces}}{\text{Inertial forces}} \qquad (3.13)$$

This ratio, then, can be used to investigate the scaling behaviour of bouyant forces. In the present context, this means comparing the relative importance of natural convection in different fluids. It is obvious that such comparisons should be made at equal Reynolds numbers.

If different fluids flow inside identical ducts under diffusive mass transfer conditions at any given Reynolds number, and assuming comparable density changes ($\Delta\rho/\rho$), the relative importance of natural convection scales inversely as the square of the kinematic viscosity of the fluid in question. Thus, fluids with low kinematic viscosities can develop appreciable buoyancy-driven flows even with small density gradients.

3.2 PHYSICAL PROPERTIES IN THE SUPERCRITICAL REGION

The role of the kinematic viscosity in determing the relative importance of natural convection has already been shown. Supercritical fluids have exceptionally small kinematic viscosities as a consequence of the very different behaviour of density and viscosity in going from the dilute gas to the dense fluid region.

In what follows, attention will be focused on the region $1 < Tr < 1.1$ $1 < Pr < 4$, where most of the changes associated with the passage from the dilute gas to the dense state occur.

The dimensionless isothermal compressibility is the relative change in density per unit relative change in pressure, at constant temperature,

$$K'_T = \left(\frac{\partial \ln \rho}{\partial \ln P}\right)_T = -\left(\frac{\partial \ln V}{\partial \ln P}\right)_T = P\ K_T \qquad (3.14)$$

For a fluid whose volumetric properties can be adequately described by a cubic equation of state, for which the most general formulation is (Schmidt and Wenzel,1980)

$$P = \frac{RT}{V-b} - \frac{a}{V^2 + uVb + wb^2} \qquad (3.15)$$

K'_T can be written as

$$K'_T = \frac{z\,(1-\kappa)}{\frac{1}{1-\kappa} - \frac{(2+u\kappa)[1-z(1-\kappa)]}{1+u\kappa+w\kappa^2}} \qquad (3.16)$$

where u,w are numerical constants which depend on the particular equation of state being used (Appendix 1) and $\kappa = bV^{-1}$. The dimensionless isothermal compressibility is unity for an ideal gas, zero for an incompressible fluid, and infinite at the critical point.

Figures 3.1 to 3.4 show the behaviour of this quantity for CO_2 and SF_6, in the region $1.01 < Tr < 1.1$, $.1 < Pr < 4$, for two different cubic equations of state. At 318 K and 100 bar (Tr = 1.05 ; Pr = 1.36), CO_2 is ~ 280 times as dense but almost three times more compressible than at 318 K and 1 bar. This unique combination of high density and high compressibility is one of the distinguishing features of supercritical extraction (Paulaitis et al.,1983).

Of more immediate concern here is the fact that the low pressure limit of the dimensionless isothermal compressibility gives rise to roughly two of the three orders of magnitude by which the density changes in going from atmospheric to supercritical conditions. This is shown in Figure 3.5, where the density, viscosity and kinematic viscosity of CO_2 at 310K (Tr = 1.02) are plotted as a function of pressure from 1 to 200 bars.

The viscosity, on the other hand, shows a very mild pressure dependence at low density (ideal gas viscosities are pressure-independent) and increases by a factor of roughly 6 in the range $.8 < Pr < 1.6$. Thus, supercritical viscosities are less than an order of magnitude higher than ideal gas viscosities.

The combined effect of liquid-like density and moderate viscosity leads to an exceptionally low kinematic viscosity. The supercritical region, then, can be viewed as an interesting transitional domain, where some fluid properties attain unique values, not necessarily intermediate

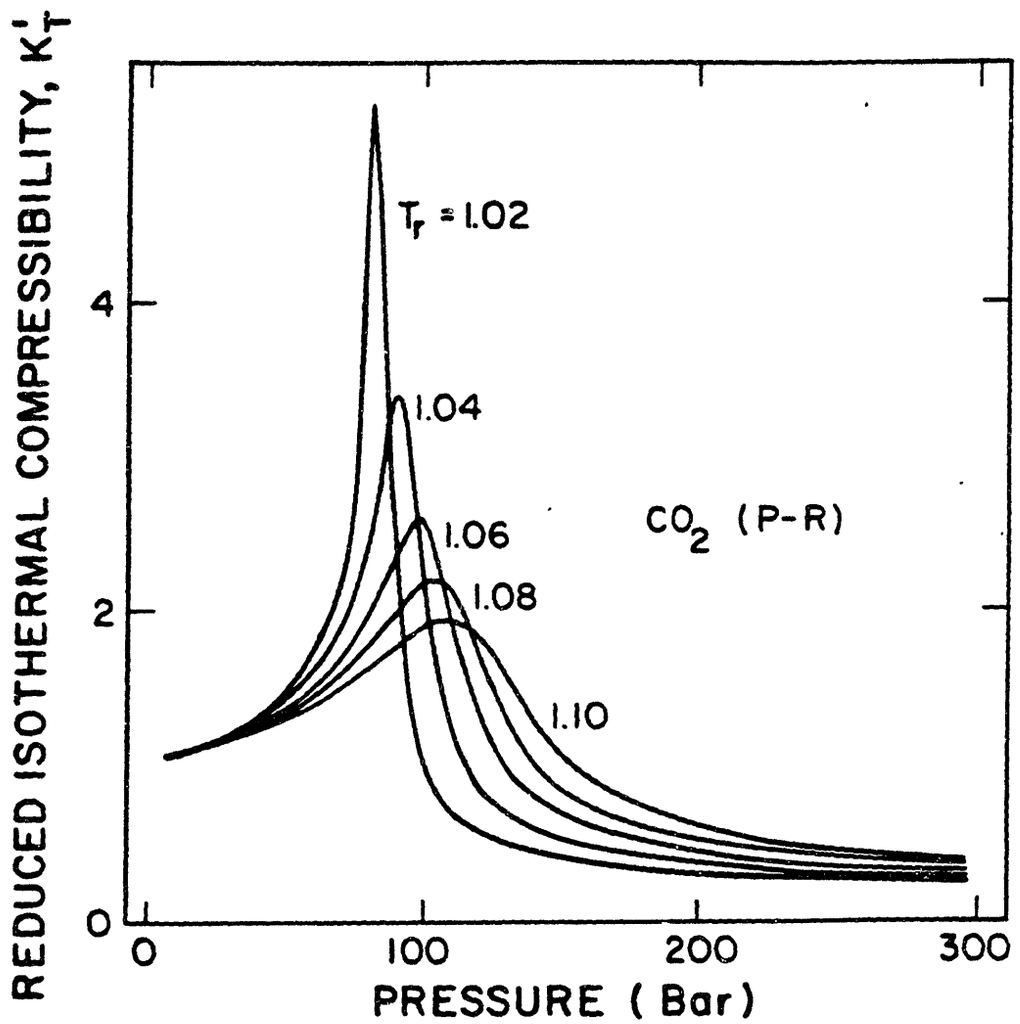

FIGURE 3.1 : Dimensionless isothermal compressibility of CO_2, as modelled by the Peng-Robinson equation of state.

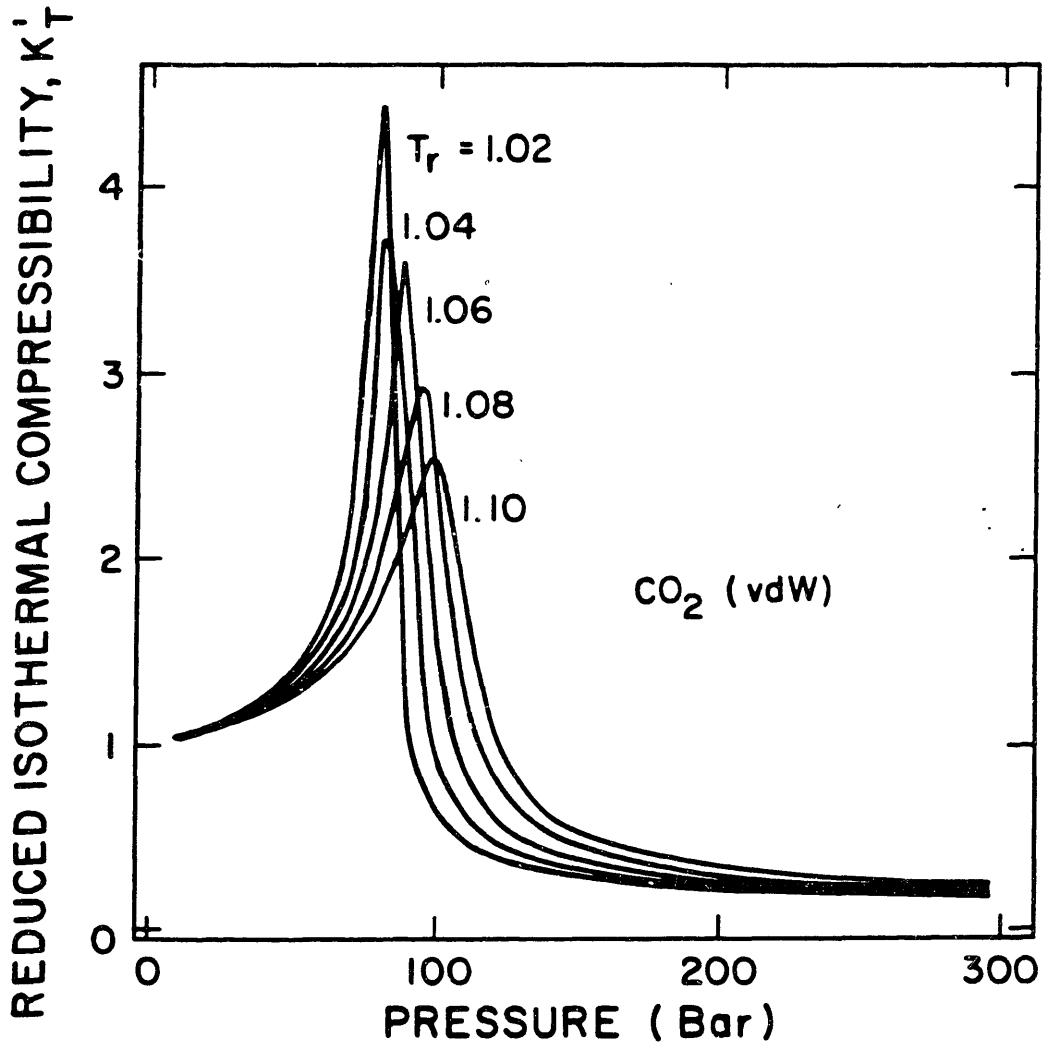

FIGURE 3.2 : Dimensionless isothermal compressibility of CO_2, as modelled by the van der Waals equation of state.

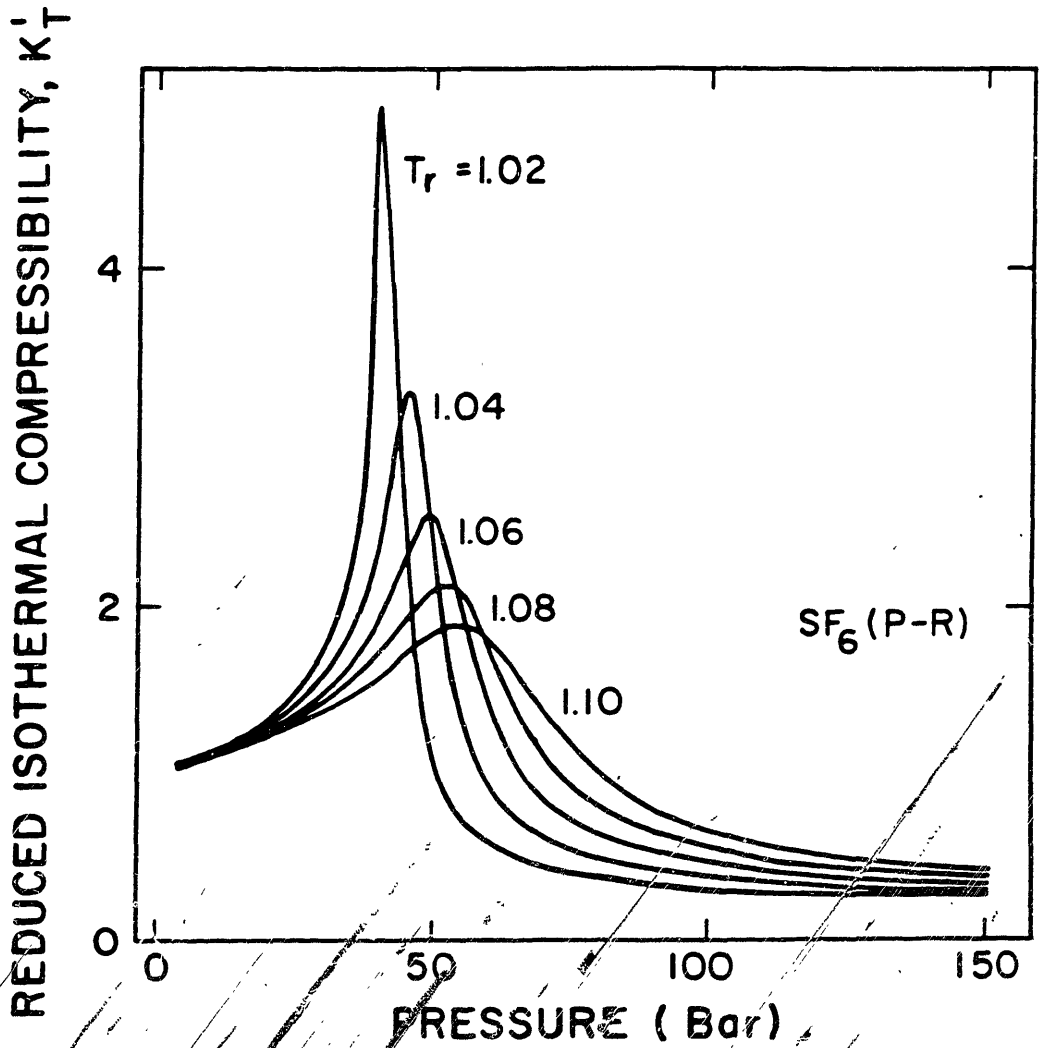

FIGURE 3.3 : Dimensionless isothermal compressibility of SF_6, as modelled by the Peng-Robinson equation of state.

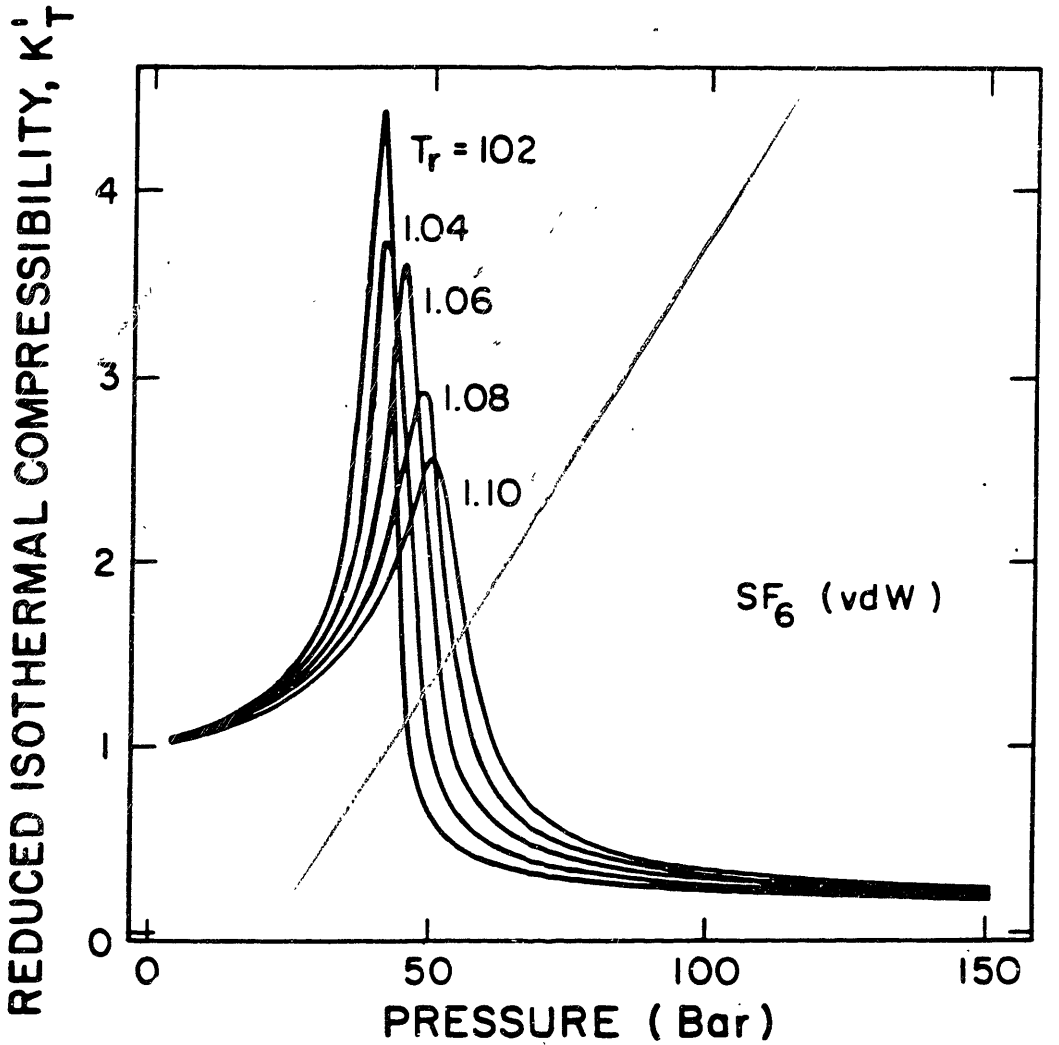

FIGURE 3.4 : Dimensionless isothermal compressibility of SF_6, as modelled by the van der Waals equation of state.

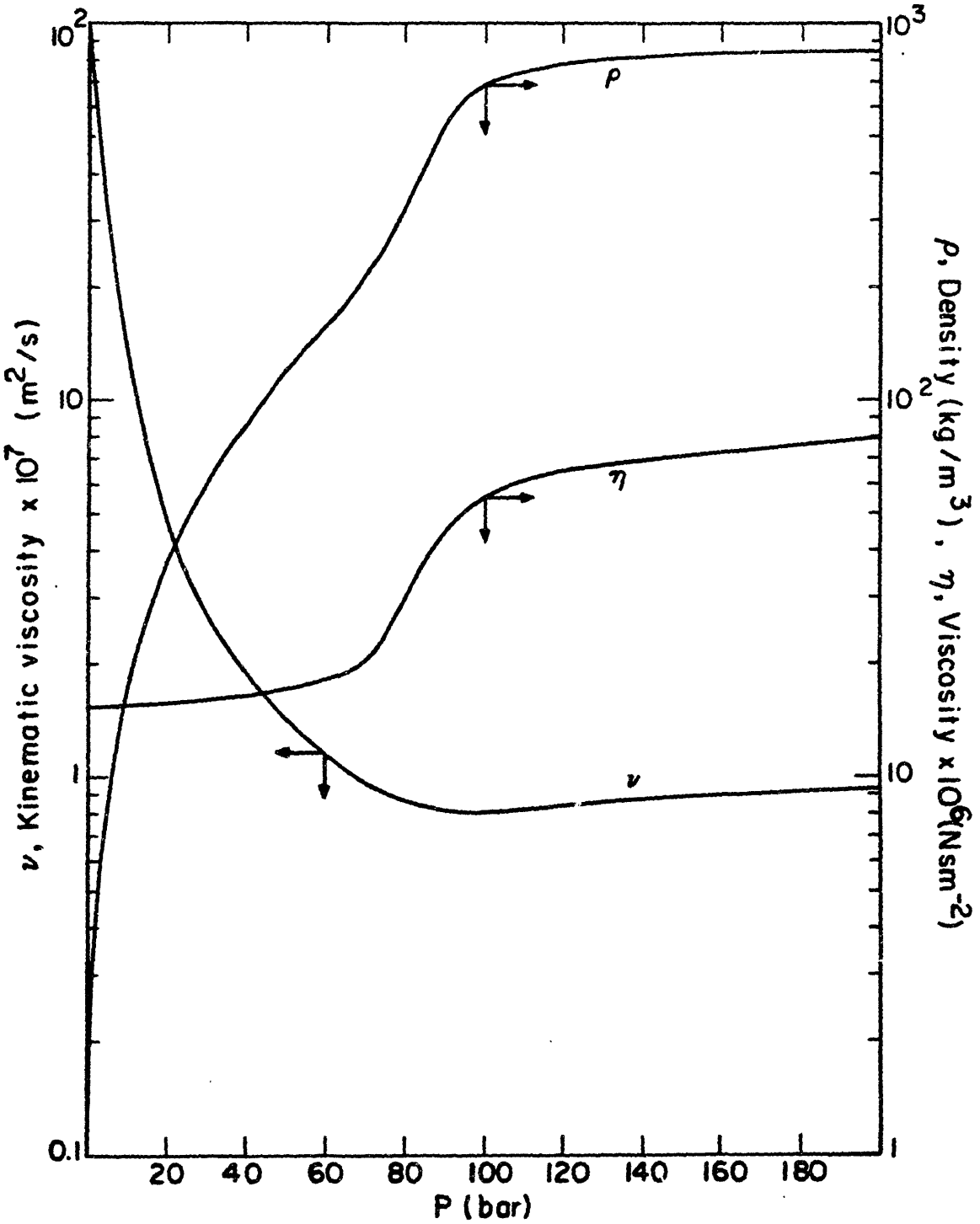

FIGURE 3.5 : Density, viscosity and kinematic viscosity of CO_2 as a function of pressure, at 310 K.

between the ideal gas and the liquid extremes.

If we now compare (Figure 3.6) the properties of air, water and mercury at 298 K and 1 bar with those of supercritical CO_2 at 310 K and 150 bar in the light of the previous discussion, some interesting consequences arise. We note the fact that, for ν, CO_2 has the lowest value (lower than for mercury, a liquid metal). The fourth column is the ratio of buoyant to inertial forces at constant Reynolds number and duct geometry, scaled with the corresponding value for water. The relative importance of natural convection, therefore, is more than two orders of magnitude higher in a supercritical fluid than in ordinary liquids.

It is important to note that this phenomenon is independent of the free convective currents that originate very close to the critical point as a consequence of the diverging fluid compressibility.

3.3 FLOW REGIMES

The extent to which natural convection controls the overall transport mechanism in a supercritical fluid is well illustrated in the case of vertical flow inside ducts.

Figure 3.7, adapted for mass transfer from heat transfer theory (Metais and Eckert,1964) shows the possible regimes that can exist for vertical flow inside a cylinder under the combined influence of buoyant forces and pressure gradients. This figure summarizes available experimental and theoretical knowledge, covers the cases of forced and free convection both aiding and opposing each other, and is valid for $10^{-2} < Sc\ D/L < 1$.

As can be seen from Figure 3.7, the hydrodynamic regime can be characterized with two parameters: the Reynolds number and the product of the aspect ratio times the Rayleigh number (which, for mass transfer, is equivalent to the product of the Schmidt and Grashof numbers). The laminar-turbulent transition in the forced and mixed regimes is shown as a dashed area of finite thickness.In the free regime, the transition occurs at an abscissa value of $\sim 10^9$.

For $Ra(2R/L) < 10^9$, then, increasing the Reynolds number (at constant abscissa value), leads to a laminar-turbulent transition. Increasing the abscissa at constant Reynolds number, on the other hand, gives rise

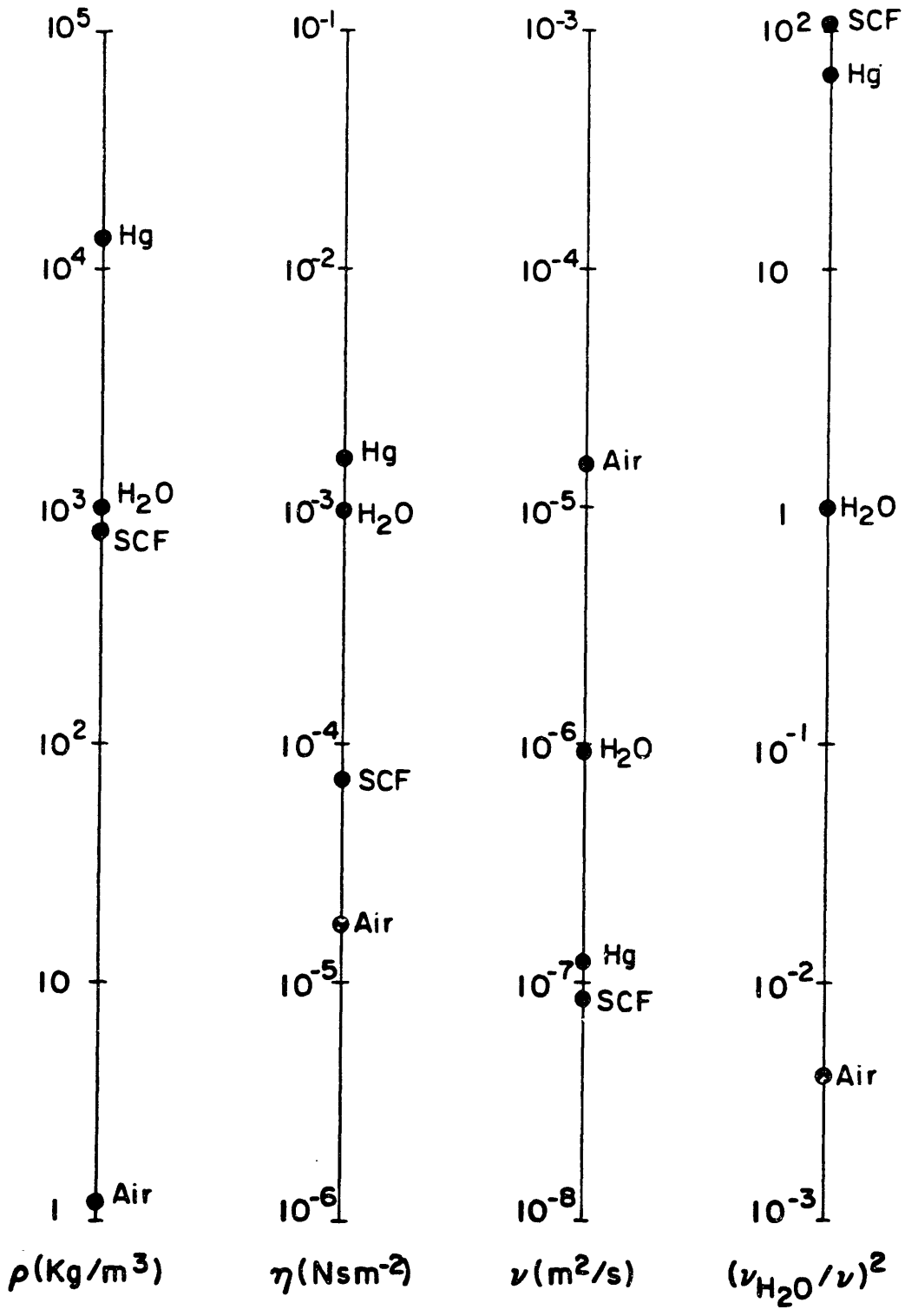

FIGURE 3.6 : Comparison of physical properties of air, water and mercury at ambient conditions with those of CO_2 at 150 bar and 310K. Relative importance of natural convection at constant Reynolds numbers.

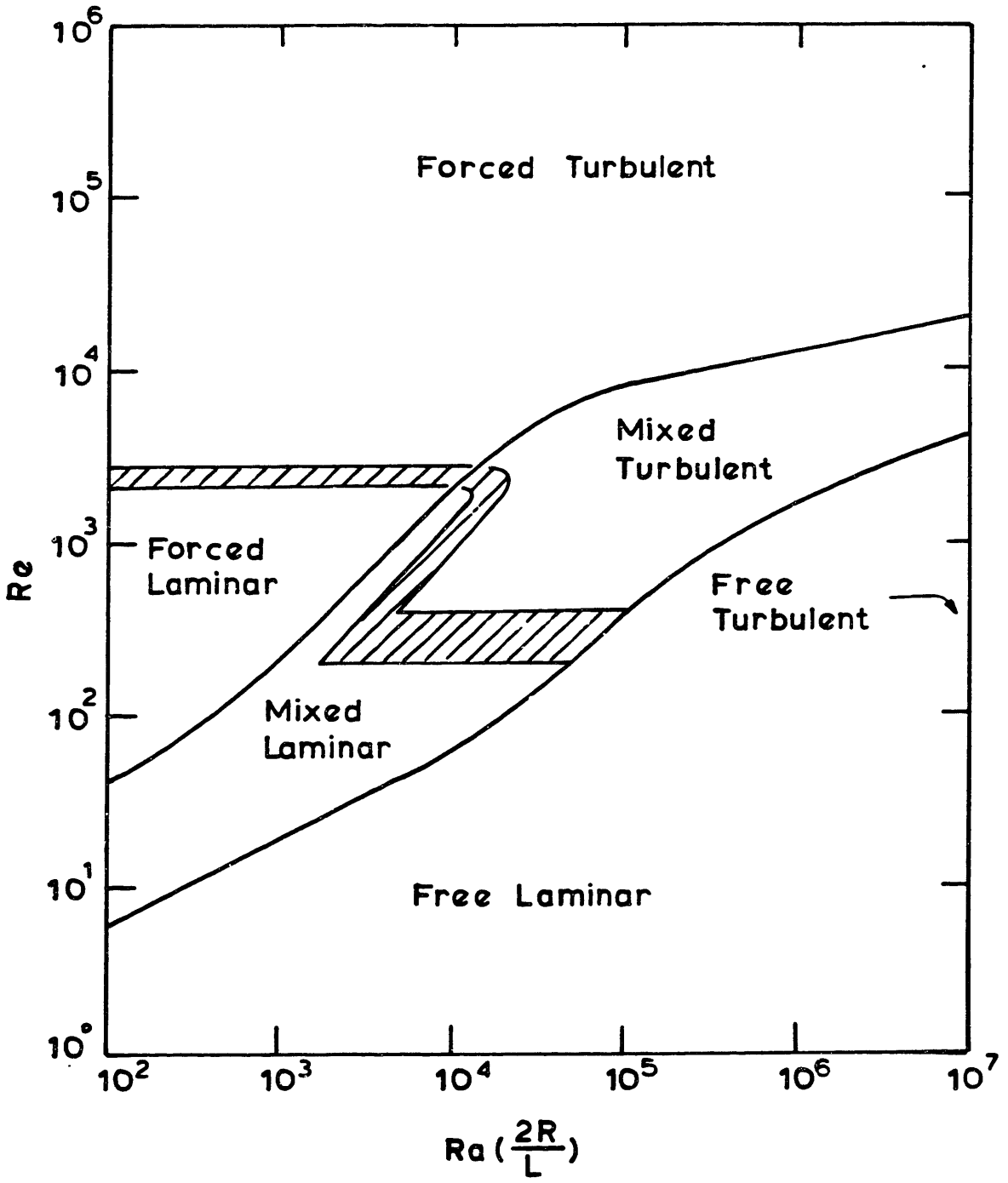

FIGURE 3.7 : Hydrodynamic regimes for vertical cylindrical duct flow.

to a forced-free transition. It is very important to notice that the forced laminar region is bounded on all sides. This means, among other things, that it is impossible to attain forced laminar flow beyond an abscissa value of ~ 10^4, no matter how low the Reynolds number is, or, in other words, that $Ra(2R/L) < 10^4$ is a necessary but not sufficient condition for forced laminar flow.

This criterion has been used in Figure 3.8, where the area lying above and to the right of each curve represents geometries for which laminar flow is impossible in supercritical operation (notice the ν and Sc values). The parameter in Figure 3.8 is the relative density change. Thus, even with negligibly small density changes (10^{-3}) and aspect ratios (10^{-3}), forced laminar flow cannot be attained for D > 8 mm. Curves are shown dotted for $D/L > 10^{-1}$ since, for Sc = 10, this is the upper limit for the validity of Figure 3.7.

For packed bed flow, the large contribution of buoyant forces suggests that the usual mass transfer correlations are unsuitable for design purposes when supercritical fluids are involved if the controlling resistance lies in the supercritical phase. Correlations which take into account buoyant forces have been published (Karabelas et al., 1971), but do not cover the low Schmidt number range characteristic of diffusion of small (MW ~ 100) organic solutes in supercritical fluids.

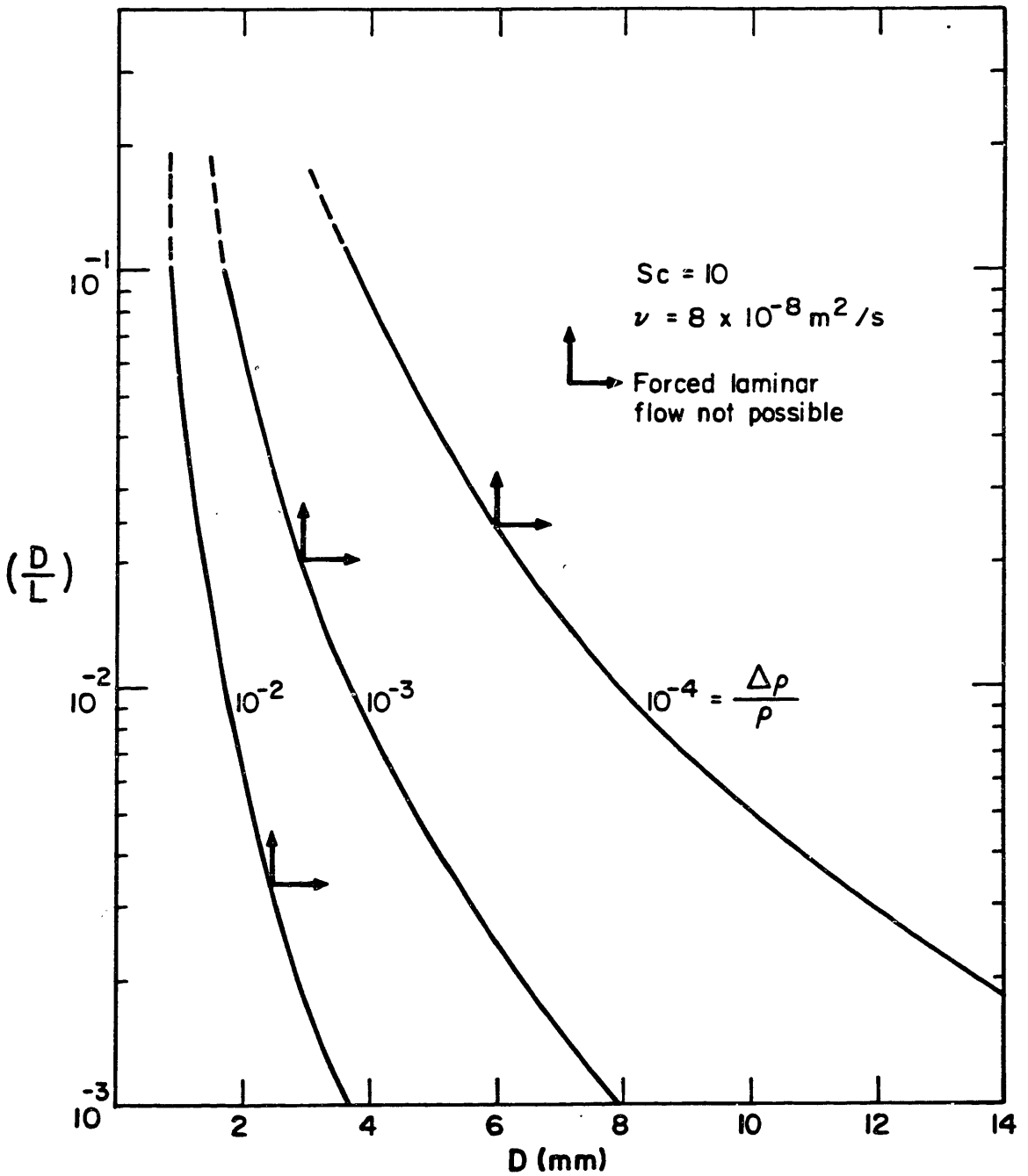

FIGURE 3.8 : Cylindrical duct geometries for which vertical forced laminar flow is impossible under supercritical conditions.

4. APPARATUS AND EXPERIMENTAL PROCEDURE

4.1 INTRODUCTION

The experimental aspects of the hydrodynamic technique used in the present work will be discussed in this Chapter. The theoretical basis will be presented in Chapter 5.

In essence, the technique involves laminar flow of a supercritical fluid within a duct of well-characterized geometry. A solid solute dissolves into the fluid from a surface at the duct boundary. Diffusion coefficients and mass transfer rates can then be calculated from a knowledge of the flow rate, duct geometry and equilibrium solubility of the solute in the supercritical fluid at the same temperature and pressure, and from the measurement of the amount of solute that, at steady state, precipitates upon decompression from a known amount of fluid.

4.2 APPARATUS

A schematic flow sheet of the experimental appartus is shown in Figure 4.1. The solvent gas is compressed by diaphragm compressor K (Aminco J46-13411) and pumped from a gas cylinder (TK2) to a 2-liter autoclave (TK1) whose pressure is maintained by an on-off controller (indicator-controller PIC) acting on the compressor's electric drive (M). A manual pressure regulator, V1 (Matheson Model 4 High Pressure Regulator or Matheson Model 3064 High Pressure Regulator) eliminates downstream pulsations. This is essential for hydrodynamic experiments.

The pressurized solvent is preheated to the desired temperature in coil CL, which is immersed in a 24 in.x 18 in.x 18 in. water bath, B1, whose temperature is maintained by heater-circulators A1 and A2 (Thermomix 1460, accurate to within 0.01°C). The pressure is displayed on a panel-mounted guage, PI (Heise guage, 0 - 400 bar, accurate to 0.5 bar). C2, the diffusion tube, is a 12 1/2 in. long 2in. Sch 160 316 stainless steel pipe with threaded ends, inside of which is located a flat plate where the diffusional process occurs. All tubing up to C2's inlet connec-

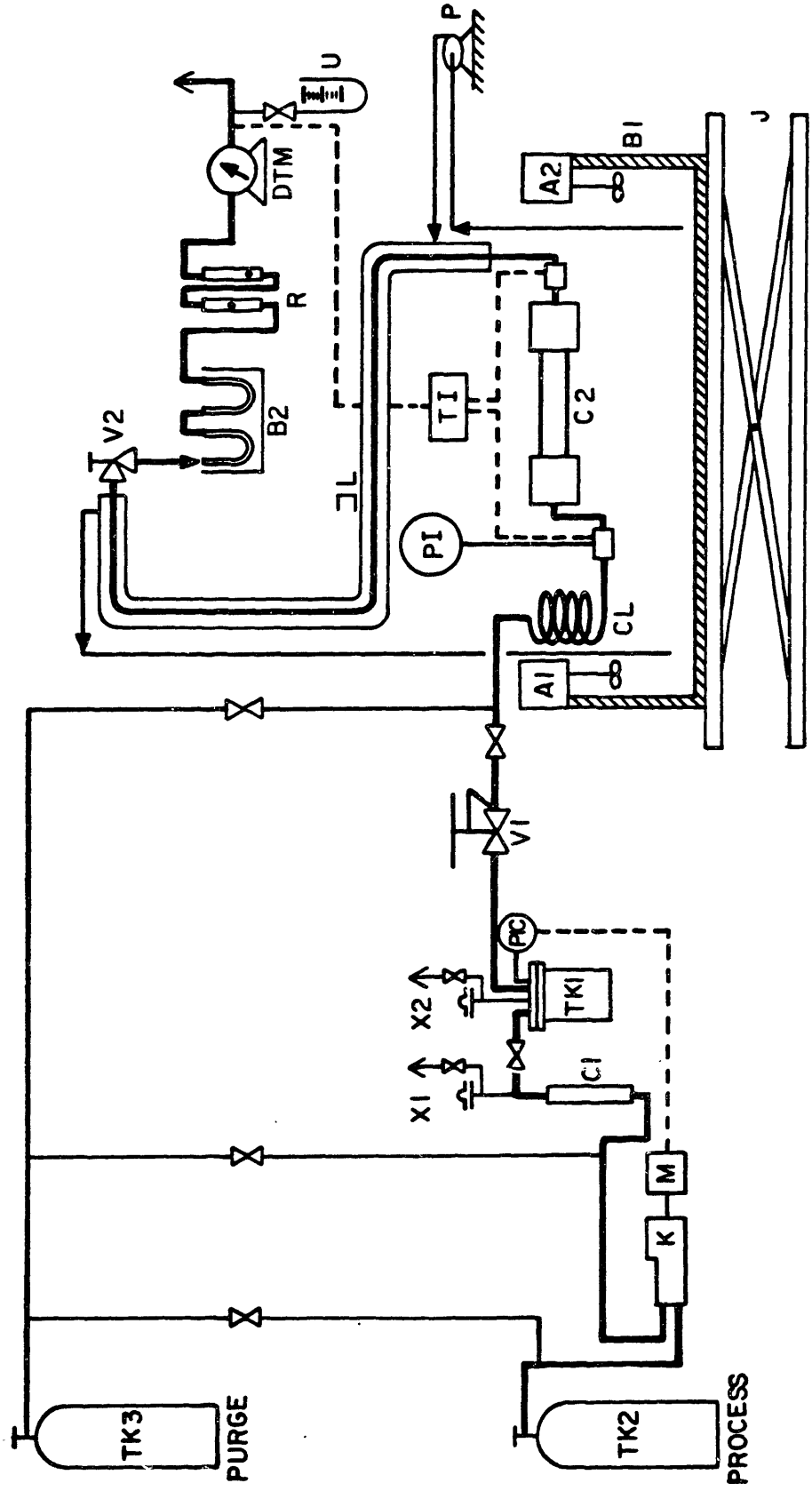

FIGURE 4.1 : Equipment flow-sheet

tion is 1/8 in. 316 stainless steel. The outlet section is 1/4 in. 316 stainless steel.

A hydraulic jack, J (American Scissor Lift), raises B1 so that, during an experiment, C2 is immersed in water; B1 is then lowered to allow easy access to C2, which must be opened between experiments to replace the flat plate.

The partially saturated fluid emerges from C2 and flows through a jacketed line (JL) up to valve V2. Bath water is circulated through the jacket by pump P to maintain the outlet line isothermal and prevent solute precipitation. V2 (30VM 4882, GA, Autoclave Engineers) is a 1/4in. manual regulating valve which controls the flow and reduces the pressure down to atmospheric. In operation, it is maintained at least 20°C above the solute's melting point in order to avoid clogging due to solid accumulation.

The precipitaed solute is collected in two glass wool packed U-tubes immersed in an ice bath (B2, a 1500ml beaker); the solvent flows through rotameters R (Matheson R 7640, Series 603 and 604), and the total amount is integrated in a dry test meter (DTM, Singer 802). The temperature at C2's inlet/outlet, and at the DTM's outlet can be read in a panel-mounted digital indicator (TI). A U-tube manometer (U) provides an accurate reading of the solvent's pressure at DTM outlet conditions.

A secondary (purge) line is also shown in Figure 4.1; its design allows separate purging of the upstream, downstream and inlet sections of the equipment. Also shown in Figure 4.1 is C1, a 1in.OD x 17in.l 316 stainless steel nipple which increases the holding capacity provided by TK1. C1 and TK1 are both protected by separate rupture discs (X1,X2).

The actual experiment involves fully developed laminar flow of a supercritical fluid inside a horizontal rectangular duct (Figure 4.2), the bottom surface of which is coated with the solute of interest. The brass plate (4) is tightly fitted into an enclosure made up of two aluminum hemi-cylinders (1,2); flow occurs inside the resulting 1in. x 1/8in. rectangular channel (3). The plate contains three sections: a section (5) where laminar flow is allowed to develop, a 1in. w x 3in. l test section (6), and an outlet section (7). The test section is made by casting the molten solute and carefully machining the surface after sol-

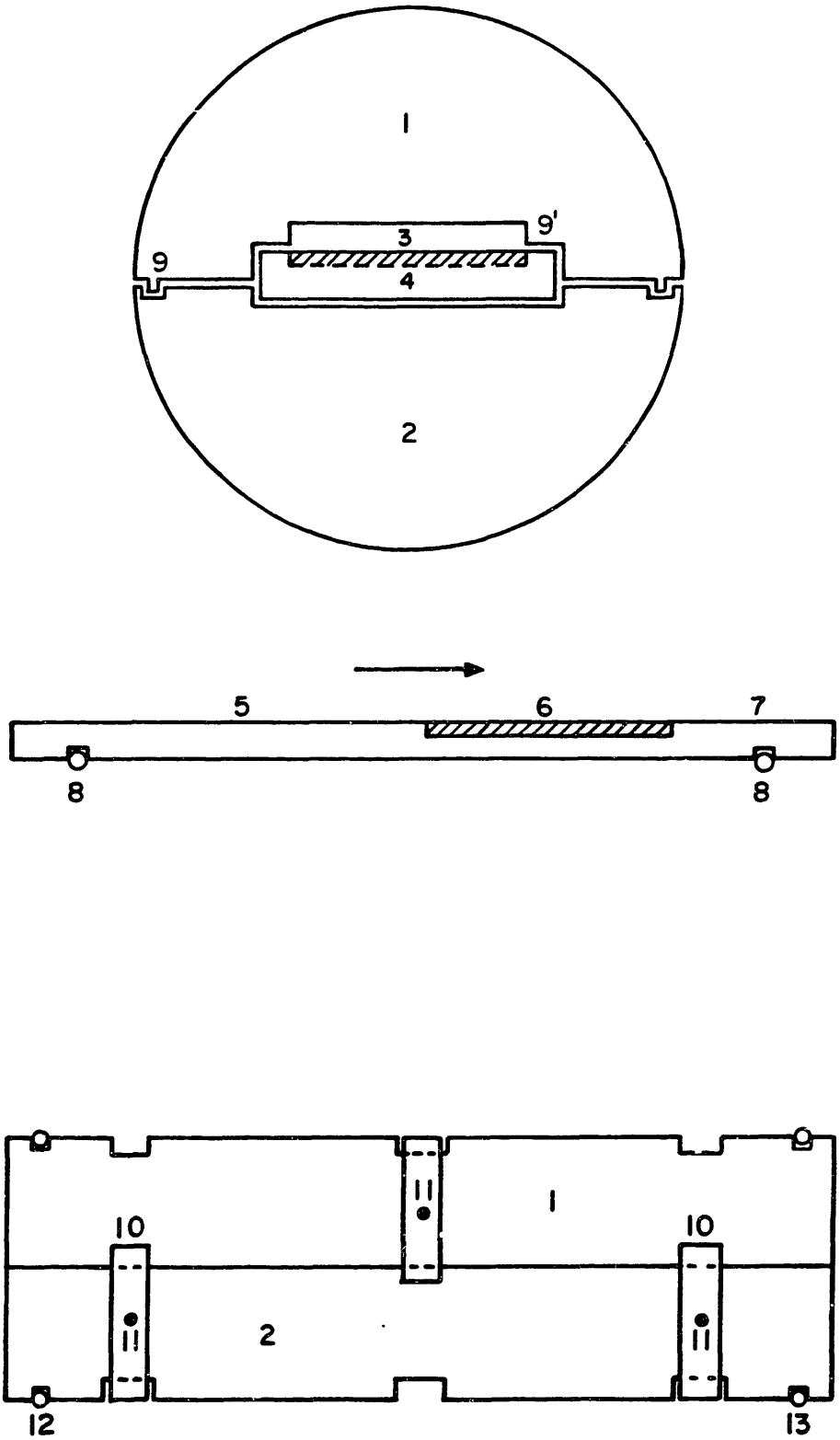

FIGURE 4.2 : Flat plate assembly for hydrodynamic experiments

idification. Fluid by-pass of the test section is prevented by a Viton gasket (8), which forces the plate against the upper surface, and by the labyrinth seal (9) which results when the hemi-cylinders are tightened (10,11) and Teflon tape is placed between the upper and lower mating surfaces (9).

The whole assembly is tightly fitted inside C2. Sealing is provided by O-ring 13, while O-ring 12 is notched: the pressure in 3 is thus equal to the pressure outside 1 and 2.

When channel 3 is horizontal, there are no buoyant effects and true binary diffusion coefficients can then be determined (this is not true in general; for the systems and experimental conditions considered in this work, however, this statement is valid in all cases; see Chapter 6 and Appendix 2 for theoretical development and proof). Arbritrarily variable buoyant forces can be introduced by rotating 1 and 2 inside C2. The same experiment should then give rise to different results, and information can be gathered on the relative importance of natural convection in supercritical fluids.

As already mentioned above, the calculation of binary diffusion coefficients requires knowledge of the equilibrium solubility of the solute in the supercritical fluid under the same conditions of temperature and pressure.

Equilbrium solubilities are measured in separate experiments. The configuration of equipment is the same as that shown in Figure 4.1, except for the fact taht C2 is replaced by a 1in. OD x 12in. l 316 stainless steel vertical column packed with the solute under investigation. B1 is also replaced by a smaller, cylindrical water bath. The supercritical fluid thus flows upward through the bed and, at low enough soovent flow rates (see below), emerges from the column saturated with the solute. The experimental procedures for equilibrium and diffusion experiments will now be discussed.

4.3 EXPERIMENTAL PROCEDURE

C2 is partially pressurized and B1 raised to its working position. Partial pressurization is attained by opening V1 (with V2 closed) and

closing the on-off valve immediately following V1 once the desired pressure has been attained. The experiment is only started after a minimum period of 2-3 hours, during which thermal uniformity inside C2 is attained. It is important to select the pressure for this thermal equilibrium period in such a way that only a negligible amount of solute is dissolved, otherwise, the test section's geometry will be altered even before the experiment begins.

TK1 is always kept at pressure at least 20 bars higher than the desired value, since V1 can only control if there is a pressure drop across its body. C2 is then pressurized, and the heated regulating valve V2 opened and manually operated to attain a constant flow rate. The precipitating solute is collected in a pair of U-tubes, the contents of which are unimportant, since at least 15 minutes are allowed for the system to attain a steady state while fluid is flowing at the desired rate, temperature and pressure. The recirculating pump is started and operates continuously throughout the duration of both this start-up stage and the actual experiment.

The back-up U-tubes are removed, and the DTM initial reading is then recorded. The actual U-tubes are the connected and an accurate timing of the experiment is started simultaneously.

It is imperative that, throughout the experiment, the flow rate be kept as constant as possible. In general, flow characteristics are good when the equilibrium solubility of the system under study is less than $\sim 10^{-4}$ mole fraction. Above this value, the flow is more uniform the lower the melting point of the solid.

Temperature and pressure readings are taken every 5 minutes. The duration of the run is determined by the need to collect at least 10mg of solute (see Appendix 2 and Chapter 6 for a more detailed discussion). Weighing is done on a Mettler H51-AR balance, accurate to 100 μg. Detailed calculations on the flat plat design, and on the duration, accuracy and limitations of the experiment are given in Appendix 2.

Equilibrium experiments are conducted in an entirely similar way, but neither accurate timing nor constancy of flow rate is important in this case. The thermal equilibrium stage is also much shorter on account of the abscence, in this case, of stagnant layers of fluid inside the

extraction column. In equilibrium experiments, on the other hand, solute precipitation inside the outlet lines is of more concern than in diffusion experiments, since the fluid is now saturated with the solute (as opposed to ~ 15-20% saturated in a typical diffusion experiment).

Flow rates for equilibrium experiments must be low to guarantee solvent saturation at the column's outlet. Typical values are 0.8 lt/min at DTM conditions (Kurnik, 1981).

5. DIFFUSION IN RECTANGULAR DUCTS

5.1 VELOCITY PROFILE; FULLY DEVELOPED FLOW

The basic geometry of the problem is shown in Figure 5.1. We consider fully developed laminar flow in the axial (x) direction inside a rectangular duct of height 2b ($-b \leq y \leq b$) and width 2a ($-a \leq z \leq a$).

The velocity profile can be expressed empirically as (Shah and London, 1978):

$$\frac{v}{v_{max}} = \left[1 - \left(\frac{|y|}{b}\right)^n\right]\left[1 - \left(\frac{|z|}{a}\right)^m\right] \tag{5.1}$$

$$m = 1.7 + 0.5\alpha^{-1.4}$$

$$n = 2 \qquad \alpha \leq 1/3 \tag{5.2}$$

$$n = 2 + .3(\alpha - 1/3) \qquad \alpha \geq 1/3$$

where

$$\alpha = b/a \tag{5.3}$$

Figure 5.2 is a plot of Equation (5.1). The expressions (5.2) were obtained by matching the finite difference solution of the momentum balance equation to the empirical form (5.1) .

From Equation (5.1) we obtain, upon integration over the duct cross section,

$$\frac{v}{\langle v \rangle} = \left(\frac{m+1}{m}\right) \cdot \left(\frac{n+1}{n}\right) \left[1 - \left(\frac{|y|}{b}\right)^n\right] \left[1 - \left(\frac{|z|}{a}\right)^m\right] \tag{5.4}$$

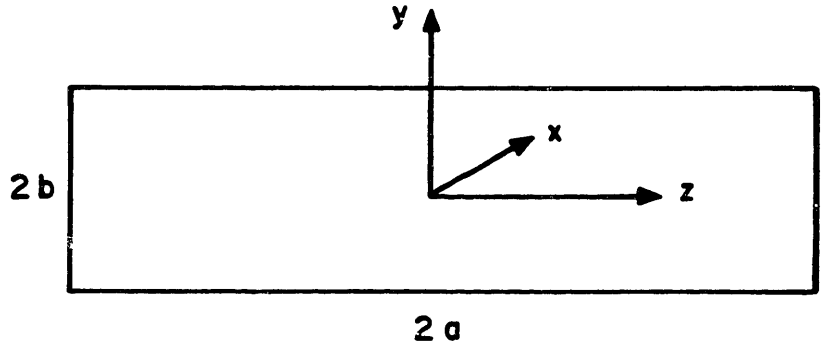

FIGURE 5.1 : Rectangular duct geometry

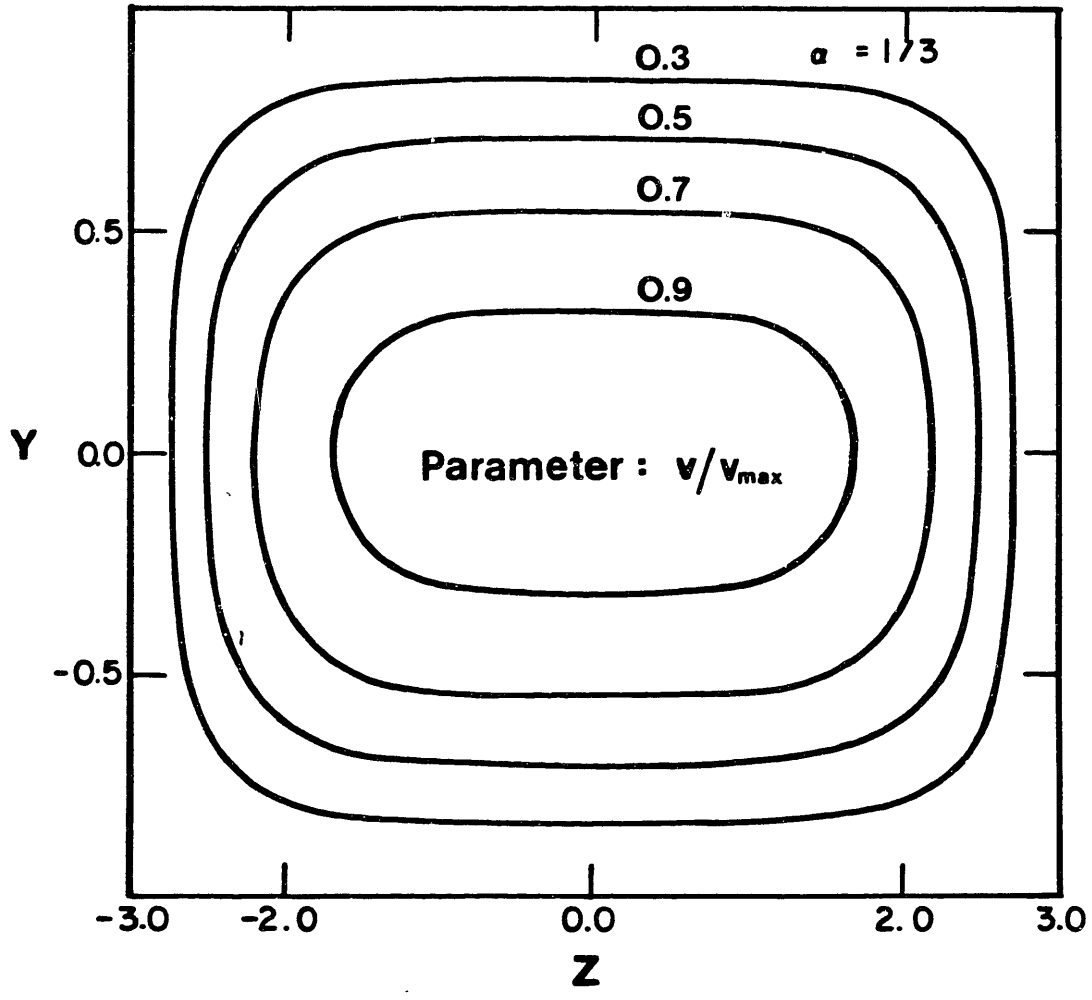

FIGURE 5.2 : Velocity profile as per Equations (5.1) and (5.2); $\alpha = 1/3$

where

$$ab\langle v\rangle = \int_0^b \int_0^a \left[1 - \left(\frac{|y|}{b}\right)^n\right]\left[1 - \left(\frac{|z|}{a}\right)^m\right] dy\, dz \tag{5.5}$$

5.2 DIFFUSION; CONSERVATION EQUATION

The steady state conservation equation for a diffusing solute is

$$v\frac{\partial c}{\partial x} = D\left(\frac{\partial^2 c}{\partial x^2} + \frac{\partial^2 c}{\partial y^2} + \frac{\partial^2 c}{\partial z^2}\right) \tag{5.6}$$

where c is the solute molar concentration and D, the binary diffusion coefficient. If we now non-dimensionalize by defining,

$$\begin{aligned} \beta &= L/2a = L\alpha/2b \\ x^+ &= x/b \\ y^+ &= y/b \\ z^+ &= z/b \\ c^+ &= (c - c_i)/(c_o - c_i) \\ v^+ &= v/\langle v\rangle \end{aligned} \tag{5.7}$$

Equation (5.6) becomes

$$Pe\left(\frac{\alpha}{2\beta}\right) v^+ \frac{\partial c^+}{\partial x^+} = \frac{\partial^2 c^+}{\partial x^{+2}} + \frac{\partial^2 c^+}{\partial y^{+2}} + \frac{\partial^2 c^+}{\partial z^{+2}} \tag{5.8}$$

$$Pe = \langle v \rangle L / D \tag{5.9}$$

In the above expressions, L is the relevant axial dimension, which will later be identified with the coated (or heated, in the equivalent heat transfer problem) length; c_i is the solute concentration at the (still undefined) solvent-solute interface, where phase equilibrium is assumed, and c_o is the solute concentration at $x = 0^-$ (which will eventually be equated to zero).

Dividing through by ($\alpha Pe/2\beta$), and taking into account that, with the definitions (5.7),

$$\begin{aligned} y^+ &\sim O(1) \\ z^+ &\sim O(\alpha^{-1}) \\ x^+ &\sim O(2\beta/\alpha) \end{aligned} \tag{5.10}$$

we have the following scales,

$$\begin{aligned} &x - \text{convection} \sim (\alpha/2\beta) \sim 2 \times 10^{-2} \\ &y - \text{diffusion} \sim (2\beta/\alpha Pe) \sim 5 \times 10^{-3} \\ &x - \text{diffusion} \sim (\alpha/2\beta Pe) \sim 2 \times 10^{-6} \\ &z - \text{diffusion} \sim (2\beta\alpha/Pe) \sim 8 \times 10^{-5} \end{aligned} \tag{5.11}$$

where $\alpha = 1/8$, $\beta = 3$, $Pe = 10^4$ have been used, corresponding to the case presently considered ($D \sim 10^{-8}$ m^2/s; $\langle v \rangle \sim 10^{-3}$ m/s; $L \sim 10^{-1}$ m; see Appendix 2). So, from order of magnitude considerations, we can neglect axial and transverse diffusion. This conclusion is by no means general. The problem now becomes, using Equation (5.4),

$$(2\xi^+ - \xi^{+2}) \frac{\partial c^+}{\partial x^+} = A(z^+) \frac{\partial^2 c^+}{\partial \xi^{+2}} \tag{5.12}$$

$$A(z^+) = \frac{4\beta}{3\alpha Pe} \cdot \left(\frac{m}{m+1} \right) \cdot \left[1 - (\alpha |z^+|) \right]^{m-1} \tag{5.13}$$

$$\xi^+ \equiv 1 - y^+$$

with boundary conditions

$$c^+(x^+,2) = 0$$

$$\left. \frac{\partial c^+}{\partial \xi^+} \right|_{(x^+,0)} = 0 \tag{5.14}$$

$$c^+(0,\xi^+) = 1$$

corresponding to a plane ($\xi = 2b$; $y = -b$) from which the solute dissolves into a Newtonian fluid moving inside the duct under steady laminar conditions. The fluid contains no solute at the entrance, and the upper plane ($\xi = 0$; $y = b$) is impermeable to mass transfer. Thermodynamic equilibrium is assumed at the source plane.

5.3 SOLUTION

Equation (5.12) can be viewed as a two- dimensional (x^+, ξ^+) problem with a coefficient, $A(z^+)$, that depends on a third dimension. Solutions to the two- dimensional problem must therefore be integrated across the third dimension's domain ($-1 < \alpha z^+ < 1$). We now separate the two- dimensional problem into an axial and a "radial" part,

$$c^+ = H(\xi^+) \cdot X(x^+) \tag{5.15}$$

and rewrite Equation (5.12)

$$\frac{1}{A(z^+)} \cdot \frac{1}{X} \cdot \frac{dX}{dx^+} = \frac{1}{H(2\xi^+ - \xi^{+2})} \cdot \frac{d^2H}{d\xi^{+2}} = -\gamma^2 \tag{5.16}$$

The full "radial" problem then becomes

$$\frac{d^2H}{d\xi^{+2}} + \gamma^2 H (2\xi^+ - \xi^{+2}) = 0 \tag{5.17}$$

$$H(2) = 0$$

$$\left(\frac{dH}{d\xi^+} \right)_0 = 0 \tag{5.18}$$

i.e., we have a homogeneous problem in ξ^+. We postulate for H a series expansion,

$$H = \sum_{i=0}^{\infty} a_i \, \xi^{+i} \tag{5.19}$$

whose coefficients a_i will obey some recurrence relationship to be found from Equation (5.17), while the first boundary condition will give rise to an eigenvalue problem. Also, from the second boundary condition, we immediately obtain, upon differentiating Equation (5.19),

$$a_1 = 0 \tag{5.20}$$

Equation (5.17), in terms of the postulated expansion, becomes

$$2a_2 + (6a_3 + 2a_0\gamma^2)\xi^+ + [12a_4 + (2a_1 - a_0)\gamma^2]\xi^{+2} +$$

$$+ [20a_5 + (2a_2 - a_1)\gamma^2]\xi^{+3} + \ldots \qquad (5.21)$$

$$+ [n(n-1)a_n + (2a_{n-3} - a_{n-4})\gamma^2]\xi^{+n-2} = 0$$

from which we obtain

$$\begin{aligned} a_2/a_0 &= 0 \\ a_3/a_0 &= -\gamma^2/3 \\ a_4/a_0 &= \gamma^2/12 \\ a_5/a_0 &= 0 \\ a_6/a_0 &= \gamma^4/45 \\ a_7/a_0 &= -\gamma^4/84 \\ a_8/a_0 &= \gamma^4/672 \\ a_9/a_0 &= -\gamma^6/1620 \\ \ldots &= \quad \ldots \end{aligned} \qquad (5.22)$$

As can be seen from the generic term in Equation (5.21), a_n/a_0 becomes a polynomial in even powers of γ for $n \geq 12$. Thus, we can write

$$\frac{a_i}{a_0} \equiv a_i' \qquad (5.23)$$

$$a_i' = \sum_{j=1}^{\infty} C_{i,j}\, \gamma^{2j} \qquad (5.24)$$

where, for example, $C_{6,2} = 1/45$; $C_{6,j} = 0$ $(j \neq 2)$. The first boundary condition in Equation (5.18) gives rise to the eigenvalue equation which,

in the light of Equation (5.24), becomes

$$1 + \sum_{i=1}^{\infty} 2^{i} \sum_{j=1}^{\infty} C_{i,j} \gamma^{2j} = 0 \qquad (5.25)$$

or, in a more convenient form,

$$1 + \sum_{j=1}^{\infty} \gamma^{2j} \sum_{i=1}^{\infty} 2^{i} C_{i,j} = 0 \qquad (5.26)$$

Eigenvalues up to 10 in magnitude require an equation of degree 40 or higher in γ. The last a'_i containing a non- vanishing $C_{i,20}$ coefficient is a'_{80} (which contains terms in γ^{40} through γ^{50}). $C_{i,j}$ values for i up to 80 and j up to 20 are shown in Appendix 3. From what has been said, we conclude that the computational equivalent of Equation (5.24), for eigenvalues ≤ 10, is

$$a'_i = \sum_{j=1}^{26} C_{i,j} \gamma^{2j} \qquad (5.27)$$

The coefficients of Equation (5.26) are listed in Table 5.1, and the first five eigenvalues, in Table 5.2. The axial problem has the formal solution,

$$X = (\text{const.}) \exp\left[-A(z^+)\, \gamma^2\, x^+\right] \qquad (5.28)$$

The two- dimensional solution, therefore, can be written, in its most general form, as

$$c^+(x^+,\xi^+) = \sum_{n=1}^{\infty} C_n \exp\left[-A(z^+)\, \gamma_n^2\, x^+\right]\left[1 + a'_{1,n} \xi^+ + a'_{2,n} \xi^{+2} + \ldots\right] \qquad (5.29)$$

Table 5.1 : Coefficients of the Eigenvalue Equation (*)

n	ζ_n
1	-1.333333333333
2	$.2793650793651$
3	$-.2319063652397 \times 10^{-1}$
4	$.1027637853035 \times 10^{-2}$
5	$-.2828429817471 \times 10^{-4}$
6	$.5302430465802 \times 10^{-6}$
7	$-.7204830258760 \times 10^{-8}$
8	$.7420607052348 \times 10^{-10}$
9	$-.5992478391541 \times 10^{-12}$
10	$.3895904572009 \times 10^{-14}$
11	$-.2082920733589 \times 10^{-16}$
12	$.9319185747388 \times 10^{-19}$
13	$-.3540455208018 \times 10^{-21}$
14	$.1156354935000 \times 10^{-23}$
15	$-.3281648836384 \times 10^{-26}$
16	$.8167183808737 \times 10^{-29}$
17	$-.1797000439336 \times 10^{-31}$
18	$.3520715535377 \times 10^{-34}$
19	$-.6181214828232 \times 10^{-37}$
20	$.9781035465679 \times 10^{-40}$

(*) $1 + \sum_{n=1}^{\infty} \gamma^{2n} \zeta_n = 0$

Table 5.2 : Eigenvalues of Equation (5.26)

.9546676

2.9743079

4.9810344

6.9845839

8.9876252

where n is an eigenvalue index, and $a'_{i,n}$ indicates the result of Equation (5.24), with $\gamma = \gamma_n$ (i.e., for the n^{th} eigenvalue). From the x^+- related boundary condition, we obtain

$$1 = \sum_{n=1}^{\infty} C_n \left[1 + a'_{1,n} \xi^+ + a'_{2,n} \xi^{+2} + \ldots \right] \equiv \sum_{n=1}^{\infty} C_n H'_n \tag{5.30}$$

Since the form of Equation (5.17) implies that the eigenfunctions, H'_n, are orthogonal with respect to the weighting function $(2\xi^+ - \xi^{+2})$, we can write (Arpaci, 1966)

$$C_n = \frac{\int_0^2 (2\xi^+ - \xi^{+2}) H'_n \, d\xi^+}{\int_0^2 (2\xi^+ - \xi^{+2}) (H'_n)^2 d\xi^+} \tag{5.31}$$

where H'_n is simply Equation (5.19) divided by a_0,

$$H'_n = 1 + a'_{1,n} \xi^+ + a'_{2,n} \xi^{+2} + \ldots \tag{5.32}$$

The numerator and denominator of Equation (5.31) will now be transformed. For the numerator, we write

$$\frac{d^2 H'_n}{d\xi^{+2}} + \gamma_n^2 H'_n (2\xi^+ - \xi^{+2}) = 0 \tag{5.33}$$

and integrate,

$$-\gamma_n^{-2} \int_0^2 \frac{d}{d\xi^+} \left(\frac{dH_n'}{d\xi^+} \right) d\xi^+ = \int_0^2 H_n' \, (2\xi^+ - \xi^{+2}) \, d\xi^+ \tag{5.34}$$

to obtain, finally,

$$-\gamma_n^{-2} \frac{dH_n}{d\xi^+} \bigg|_{\xi^+=2} = \int_0^2 H_n' \, (2\xi^+ - \xi^{+2}) \, d\xi^+ \tag{5.35}$$

where

$$\frac{dH_n'}{d\xi^+} \bigg|_0 = 0 \tag{5.36}$$

has been used. For the denominator, we multiply Equation (5.33) by $dH_n/d\gamma_n$,

$$\frac{dH_n'}{d\gamma_n} \cdot \frac{d^2 H_n'}{d\xi^{+2}} + \gamma_n^2 H_n' \frac{dH_n'}{d\gamma_n} (2\xi^+ - \xi^{+2}) = 0 \tag{5.37}$$

and integrate, to obtain

$$\frac{dH_n'}{d\gamma_n} \cdot \frac{dH_n'}{d\xi^+} \bigg|_0^2 - \int_0^2 \frac{dH_n'}{d\xi^+} \cdot \frac{d}{d\xi^+} \left(\frac{dH_n'}{d\gamma_n} \right) d\xi^+ + \tag{5.38}$$

$$+ \frac{\gamma_n^2}{2} \cdot \frac{d}{d\gamma_n} \int_0^2 (H_n')^2 \, (2\xi^+ - \xi^{+2}) \, d\xi^+ = 0$$

where use has been made of the following fact

$$\gamma_n^2 H_n' \frac{dH_n'}{d\gamma_n} = \frac{\gamma_n^2}{2} \cdot \frac{d(H_n')^2}{d\gamma_n} \tag{5.39}$$

Multiplying Equation (5.33) by H_n' and integrating,

$$H_n' \frac{dH_n'}{d\xi^+}\Big|_0^2 - \int_0^2 \left(\frac{dH_n'}{d\xi^+}\right)^2 d\xi^+ + \gamma_n^2 \int_0^2 (H_n')^2 (2\xi^+ - \xi^{+2})\, d\xi^+ = 0 \tag{5.40}$$

We now differentiate both sides of Equation (5.40) with respect to γ_n and divide by 2,

$$\frac{1}{2}\left(\frac{dH_n'}{d\gamma_n} \cdot \frac{dH_n'}{d\xi^+}\right)\Big|_0^2 + \frac{H_n'}{2} \cdot \frac{d}{d\gamma_n} \cdot \frac{dH_n'}{d\xi^+}\Big|_0^2 - \frac{1}{2}\int_0^2 \frac{d}{d\gamma_n}\left(\frac{dH_n'}{d\xi^+}\right)^2 d\xi^+ +$$

$$+ \gamma_n \int_0^2 (H_n')^2 (2\xi^+ - \xi^{+2})\, d\xi^+ + \frac{\gamma_n^2}{2} \cdot \frac{d}{d\gamma_n} \int_0^2 (H_n')^2 (2\xi^+ - \xi^{+2})\, d\xi^+ = 0 \tag{5.41}$$

Using the two "radial" boundary conditions to eliminate the second term, plus the fact that

$$\frac{d}{d\gamma_n} \cdot \left(\frac{dH_n'}{d\xi^+}\right)^2 = 2\frac{dH_n'}{d\xi^+} \cdot \frac{d}{d\gamma_n} \cdot \frac{dH_n'}{d\xi^+} = 2\frac{dH_n'}{d\xi^+} \cdot \frac{d}{d\xi^+} \cdot \frac{dH_n'}{d\gamma_n} \tag{5.42}$$

we can rewrite Equation (5.41)

$$\frac{1}{2}\cdot\frac{dH_n'}{d\gamma_n}\cdot\frac{dH_n'}{d\xi^+}\Bigg|_0^2-\int_0^2\frac{dH_n'}{d\xi^+}\cdot\frac{d}{d\xi^+}\cdot\frac{dH_n'}{d\gamma_n}\,d\xi^+ +$$

(5.43)

$$+\gamma_n\int_0^2(H_n')^2\,(2\xi^+-\xi^{+2})\,d\xi^+ +\frac{\gamma_n}{2}\cdot\frac{d}{d\gamma_n}\int_0^2(H_n')^2\,(2\xi^+-\xi^{+2})\,d\xi^+ = 0$$

Subtracting Equation (5.43) from Equation (5.38),

$$\frac{1}{2}\frac{dH_n'}{d\gamma_n}\frac{dH_n'}{d\xi^+}\Bigg|_0^2=\gamma_n\int_0^2(H_n')^2(2\xi^+-\xi^{+2})\,d\xi^+ \tag{5.44}$$

Equations (5.35) and (5.44) constitute the desired expressions, which, when substituted into Equation (5.31), yield

$$C_n=\frac{-\dfrac{1}{\gamma_n^2}\dfrac{dH_n'}{d\xi^+}\Bigg|_0^2}{\dfrac{1}{2\gamma_n}\dfrac{dH_n'}{d\gamma_n}\Bigg|_2\dfrac{dH_n'}{d\xi^+}\Bigg|_2}=\frac{-2}{\gamma_n\dfrac{dH_n'(2)}{d\gamma_n}} \tag{5.45}$$

where $(dH_n'/d\xi^+)_0 = 0$ has been used. Although the transformations are non-trivial, Equation (5.45) is much easier to use than Equation (5.31).

Substituting Equation (5.45) into Equation (5.29),

$$c^+(x^+,\xi^+,z^+) = -2\sum_{n=1}^{\infty}H_n'\left[\gamma_n\left(dH_n'/d\gamma_n\right)_2\right]^{-1}\exp\left[-A(z^+)\,\gamma_n^2\,x^+\right] \tag{5.46}$$

where $\left(dH_n'/d\gamma_n\right)_2$ means that the derivative expression should be calcula-

ted formally and evaluated at $\xi^+ = 2$.

Equation (5.46), together with the definition of H_n' (Equation (5.32)) and the numerical values of the coefficients $C_{i,j}$ (Equation (5.24), Table 5.1) and of the eigenvalues, γ_n (Table 5.2), constitute the solution to the two- dimensional (x^+, ξ^+) problem. The siplification whereby, following order of magnitude arguments, lateral diffusion was neglected, has resulted in a two-dimensional solution that must be integrated across z^+, instead of a full three-dimensional problem.

5.4 CROSS-SECTION AVERAGES

We define a cup-average concentration,

$$\langle c(x) \rangle = [\, 4ab\langle v \rangle \,]^{-1} \int_{-2b}^{2b} \int_{-2a}^{2a} c\, v\, dy\, dz \tag{5.47}$$

or, equivalently, using the definition of c^+ (Equations (5.7)),

$$\langle c^+(x^+) \rangle = [\, 4ab\langle v \rangle \,]^{-1} \int c^+\, v\, dS \tag{5.48}$$

with S denoting the duct's cross section. Using Equation (5.4) plus the fact that, for $\alpha < 1/3$, $n = 2$,

$$\langle c \rangle = \frac{m+1}{m} \cdot \frac{3}{2} \cdot \frac{1}{4ab} \cdot \alpha ab \int_{-1/\alpha}^{1/\alpha} \int_{0}^{2} [1 - (1-\xi^+)^2][1 - (\alpha|z^+|)^m]\, c\, d\xi^+\, dz^+ \tag{5.49}$$

which can be rewritten, taking into account the symmetry of the z^+ problem, as

$$\langle c \rangle = \frac{3(m+1)}{4m} \cdot \alpha \cdot \int_0^2 \int_0^{1/\alpha} [1 - (1 - \xi^+)^2][1 - (\alpha z^+)^m] \, c \, d\xi^+ \, dz^+ \qquad (5.50)$$

Using Equation (5.46), this becomes

$$\langle c^+(x^+) \rangle = \qquad (5.51)$$

$$\frac{-3\alpha(m+1)}{2m} \sum_{n=1}^{\infty} \int_0^{1/\alpha} [1 - (\alpha z^+)^m] \exp[- A(z^+) \gamma_n^2 x^+] \, dz^+ \int_0^2 \frac{[1-(1-\xi^+)^2] H_n'}{\gamma_n \left(dH_n'/d\gamma_n\right)_2} \, d\xi^+$$

The form of the z^+ integral can be made more explicit by using Equation (5.13), to obtain

$$A(z^+) \gamma_n^2 x^+ = \frac{2m\gamma_n X_o}{3(m+1)} \cdot \frac{1}{1 - (\alpha z^+)^m} \qquad (5.52)$$

where X_o is a modified inverse Graetz number,

$$X_o = \frac{x \, D}{\langle v \rangle \, b^2} \qquad (5.53)$$

and $|z^+|$ has been replaced by z^+ since integration is over positive values of the variable only.

Defining

$$X_o'(m,n) = \frac{2 \, m \, \gamma_n^2 \, X_o}{3 \, (m + 1)} \qquad (5.54)$$

the z^+ integral becomes

$$\alpha \int_0^{1/\alpha} [1 - (\alpha z^+)^m] \exp [-A(z^+) \gamma_n^2 x^+] \, dz^+ =$$

$$= \alpha \int_0^{1/\alpha} [1 - (\alpha z^+)^m] \exp \left[- \frac{X_o'(m,n)}{[1 - (\alpha z^+)^m]} \right] dz^+ = \tag{5.55}$$

$$= \int_0^1 (1 - \eta^m) \exp \left[- \frac{X_o'(m,n)}{(1 - \eta^m)} \right] d\eta \equiv \phi_n(X_o, m)$$

We now consider the ξ^+ integral in Equation (5.51),

$$\int_0^2 \frac{(2\xi^+ - \xi^{+2}) H_n'}{\gamma_n \, dH_n'/d\gamma_n \Big|_2} \, d\xi^+ = \frac{1}{\gamma_n \, dH_n'/d\gamma_n \Big|_2} \int_0^2 (2\xi^+ - \xi^{+2}) H_n' \, d\xi^+ \tag{5.56}$$

which, taking into account the definition of H_n', can be expressed, after integration, as a series

$$\frac{1}{\Gamma_n} \int_0^2 (2\xi^+ - \xi^{+2}) H_n' \, d\xi^+ = \frac{1}{\Gamma_n} \left[\frac{4}{3} + \sum_{j=4}^{\infty} (2^j/j)(2a_{j-2,n}' - a_{j-3,n}') \right] \tag{5.57}$$

where $a_{1,n}' = 0$ has been used, and Γ_n is defined below,

$$\Gamma_n \equiv \gamma_n \, dH_n'/d\gamma_n \Big|_2 \tag{5.58}$$

Taking into account the expansion, Equation (5.24),

$$\Gamma_n = \sum_{k=1}^{\infty} 2^{k+1} \sum_{j=1}^{\infty} j\, C_{k,j}\, \gamma_n^{2j} \tag{5.59}$$

$$\sum_{j=4}^{\infty} j^{-1}\, 2^j (2a'_{j-2,n} - a'_{j-3,n}) = \sum_{j=4}^{\infty} j^{-1}\, 2^j \sum_{k=1}^{\infty} (2C_{j-2,k} - C_{j-3,k})\, \gamma_n^{2k} \tag{5.60}$$

and the ξ^+ integral becomes, finally,

$$\int_0^2 \frac{(2\xi^+ - \xi^{+2})H'_n}{\Gamma_n}\, d\xi^+ = \frac{4/3 + \sum_{j=4}^{82} j^{-1}\, 2^j \sum_{k=1}^{26} (2C_{j-2,k} - C_{j-3,k})\, \gamma_n^{2k}}{\sum_{k=1}^{80} 2^{k+1} \sum_{j=1}^{26} j\, C_{k,j}\, \gamma_n^{2j}} \equiv G_n \tag{5.61}$$

where the summations contain their computational limits, as discussed in Section 5.3. Equation (5.51) now reads

$$\langle c^+(x^+) \rangle = \frac{-3(m+1)}{2m} \sum_{n=1}^{N} \phi_n(X_o, m)\, G_n \tag{5.62}$$

where N is the number of eigenvalues used. For a pure solvent at the inlet, such as we are presently considering, the cup- average relative saturation and $\langle c^+ \rangle$ are related by

$$\langle c^+ \rangle + r = 1 \tag{5.63}$$

$$r = \langle c \rangle / c_i \tag{5.64}$$

so we can write

$$r = 1 + \frac{3(m+1)}{2m} \sum_{n=1}^{N} \phi_n(X_o,m)\, G_n \tag{5.65}$$

This is the expression used to calculate binary diffusion coefficients. For a given aspect ratio (i.e., m), the relative saturation is only a function of X_o. Given <v> (solvent flow rate), x (coated length) and b (duct width), then, the measured r is only a function of D.

Finally, an expression for the local Sherwood number will be derived. We define a mass transfer coefficient, k,

$$D \left.\frac{\partial c(x,z)}{\partial \xi}\right|_{(\xi=2b)} = k\,[c_i - \langle c(x)\rangle] \tag{5.66}$$

or, after nondimensionalization and rearrangement,

$$\frac{kb}{D} = -\frac{1}{\langle c^+\rangle} \left.\frac{\partial c^+}{\partial \xi^+}\right|_{(\xi^+ = 2)} \tag{5.67}$$

The relevant length parameter is 4 times the hydraulic radius

$$4\, r_h = \frac{4(\text{Cross Section})}{\text{Wetted Perimeter}} = \frac{4(4ab)}{2(2a + 2b)} = \frac{4b}{1 + \alpha} \tag{5.68}$$

$$Sh(x^+,z^+) = -\frac{4}{1+\alpha} \cdot \frac{1}{\langle c^+\rangle} \cdot \left.\frac{\partial c^+}{\partial \xi^+}\right|_2 = \frac{4b}{1+\alpha} \cdot \frac{k}{D} \tag{5.69}$$

The z^+- averaged Sherwood number, therefore, is

$$Sh(x^+) = -\frac{4}{1+\alpha} \cdot \frac{1}{\langle c^+ \rangle} \int_0^1 \left. \frac{\partial c^+(z^+,x^+)}{\partial \xi^+} \right|_2 d(z/a) \qquad (5.70)$$

From Equation (5.46) we obtain

$$\left. \frac{\partial c^+}{\partial \xi^+} \right|_2 = -2 \sum_{n=1}^{\infty} (1 / \Gamma_n) \cdot \exp\left[-A(z^+)\, \gamma_n^2\, x^+\right] \cdot \sum_{j=1}^{\infty} j\, 2^{j-1} \sum_{k=1}^{\infty} C_{j,k}\, \gamma_n^{2k} \qquad (5.71)$$

We now define

$$A_n \equiv \frac{1}{\Gamma_n} = \frac{1}{\sum_{k=1}^{80} 2^{k+1} \sum_{j=1}^{26} j C_{k,j}\, \gamma_n^{2j}} \qquad (5.72)$$

$$B_n \equiv \sum_{k=1}^{80} k\, 2^{k-1} \sum_{j=1}^{26} C_{k,j}\, \gamma_n^{2j} \qquad (5.73)$$

where, again, the computational limits have been used in the summations. The final expression is, therefore,

$$Sh = -\frac{16m}{3(m+1)(1+\alpha)} \cdot \frac{\sum_{n=1}^{N} A_n \cdot B_n \cdot \psi_n(X_o,m)}{\sum_{n=1}^{N} G_n \cdot \phi_n(X_o,m)} \qquad (5.74)$$

with

$$\int_0^1 \exp[-A(z^+)\ \gamma_n^2\ x^+]\ d(z/a) = \int_0^1 \exp\left[-\frac{X_o'(m,n)}{(1-\eta^m)}\right] d\eta \equiv \psi_n(X_o,m) \qquad (5.75)$$

The numerical values of A_n, B_n, G_n can be found in Table 5.3. Figures 5.3 and 5.4 are plots of Equations (5.65) and (5.74), which constitute the solution to the problem of diffusion in rectangular ducts at high Peclet numbers and low aspect ratios.

ϕ_n and ψ_n, though well behaved, are non- analytic and must be evaluated numerically.

Table 5.3 : Expansion Coefficients for Cross- Section Averages

n	A	B	G
1	-.6242144449211	-.8717135423055	-.5970396020662
2	.1916121727370	1. 62136522176	$-.4033326872425\times10^{-1}$
3	-.1136094212907	-2.606320953153	$-.1209851681885\times10^{-1}$
4	$.4394766591177\times10^{-5}$	196572.6180829	$.5196364776233\times10^{-2}$
5	$.3212078027422\times10^{-10}$	26634903493.79	$.4744797120123\times10^{-2}$

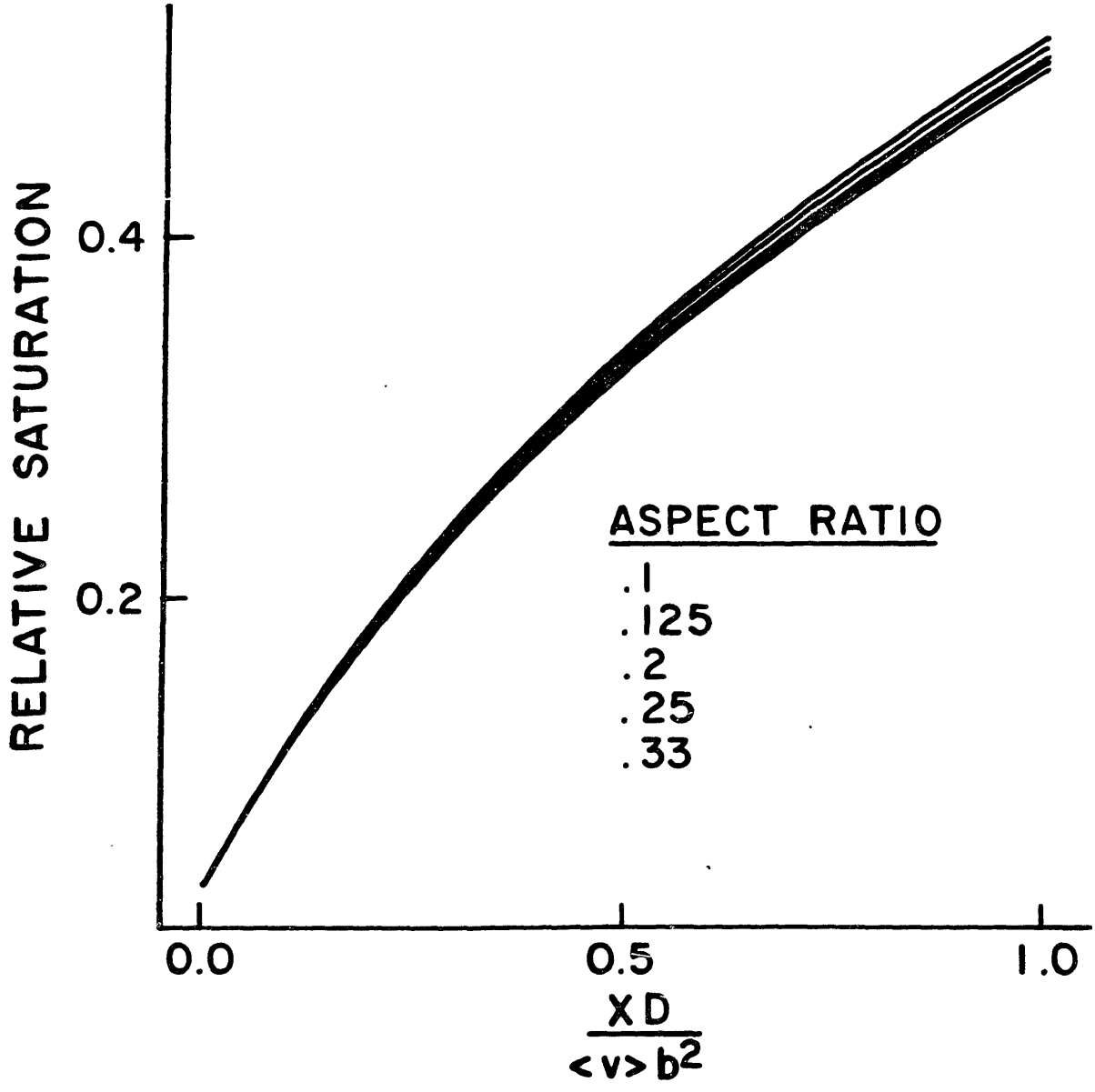

FIGURE 5.3 : Relative Saturation as a function of modified inverse Graetz number, for various aspect ratios.

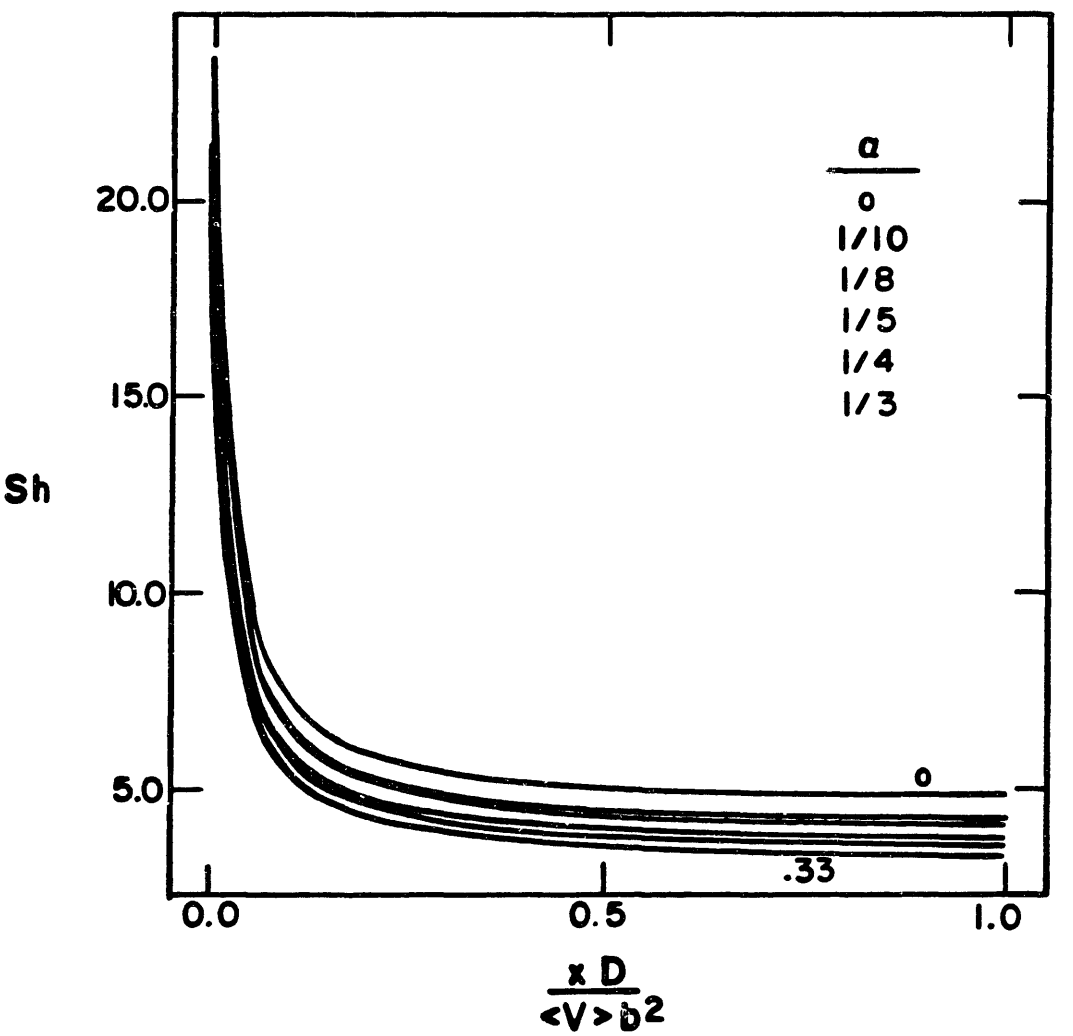

FIGURE 5.4 : Local Sherwood number (z- averaged) as a function of the modified inverse Graetz number, for various aspect ratios.

6. HYDRODYNAMIC EXPERIMENTS; RESULTS AND DISCUSSION

6.1 DIFFUSION COEFFICIENTS; RESULTS

Diffusion coefficients were measured for four different systems, using the hydrodynamic technique explained in Chapter 4. The results are summarized in Tables 6.1, 6.2, 6.3 and 6.4. The measured diffusion coefficients are shown in Figures 6.1, 6.2, 6.3, and 6.4 as a function of solvent density. The experimentally controlled variables were temperature and pressure (see Chapter 4); solvent densities were obtained via the Peng-Robinson equation of state for SF_6 (Peng and Robinson, 1976; see Appendix 1 for a discussion on cubic equations of state); CO_2 densities were obtained from the International Thermodynamic Tables of the Fluid State (Angus et al., 1976).

The approximation whereby fluid density is calculated without taking into account solute concentration is only justified for dilute systems. Equilibrium solubilities for the four systems investigated were measured with the flow technique described in detail in Chapter 4. Measured equilibrium solubilities are listed in Tables 6.5, 6.6, 6.7 and 6.8. The maximum solute weight fractions under experimental conditions (0.02 % at 338 K and 120 bar for benzoic acid in SF_6; 0.34% at 328 K and 120 bar for naphthalene in SF_6; 1.06% at 328 K and 200 bar for benzoic acid in CO_2; 0.28% at 318 K and 250 bar for 2-naphthol in CO_2) are extremely low. Under these conditions, the infinite dilution assumption introduces no analytically detectable error. Example calculations of a diffusion coefficient and an equilibrium solubility can be found in Appendix 2.

Diffusion is the macroscopic manifestation of collisions at the molecular level. The time dependence of the mean displacement of a given ensemble of particles with respect to some arbitrary initial configuration is a function of molecular velocity (temperature) and packing (density). Diffusion coefficients (see Chapter 8) can be obtained from the time evolution of the mean squared displacement of an ensemble of molecules, and should therefore be interpreted in terms of the relevant variables, i.e., temperature and density.

TABLE 6.1 DIFFUSION COEFFICIENTS OF BENZOIC ACID IN SUPERCRITICAL SULFUR HEXAFLUORIDE

T (K)	P (bar)	T_r(b) (-)	P_r(b) (-)	ρ(a) (kg/m^3)	ρ(a) (mol/lt)	ρ_r(b) (-)	10^5D (cm^2/s)	$10^5\rho$D (kg/ms)
328.2	65	1.03	1.73	1106.20	7.59	1.50	9.26	1.02
328.2	80	1.03	2.13	1222.37	8.37	1.66	8.61	1.05
328.2	120	1.03	3.19	1400.42	9.59	1.90	7.02	0.98
338.2	65	1.06	1.73	917.11	6.28	1.24	13.40	1.23
338.2	80	1.06	2.13	1083.22	7.42	1.47	10.70	1.16
338.2	120	1.06	3.19	1307.25	8.95	1.77	8.15	1.06

(a) Peng-Robinson equation of state; pure SF_6 (see Appendix 1)

(b) Critical properties from R.C.Reid, J.M.Prausnitz, T.K.Sherwood, "The Properties of Gases and Liquids", 3rd edition, 1977, Mc Graw-Hill, New York.

$T_r = T/T_c(SF_6)$

$P_r = P/P_c(SF_6)$

$\rho_r = \rho/\rho_c(SF_6)$

TABLE 6.2 DIFFUSION COEFFICIENTS OF NAPHTHALENE IN SUPERCRITICAL SULFUR HEXAFLUORIDE

T (K)	P (bar)	T_r(b) (-)	P_r(b) (-)	ρ(a) (kg/m^3)	ρ(a) (mol/lt)	ρ_r(b) (-)	10^5D (cm^2/s)	$10^5\rho$D (kg/ms)
318.2	65	1	1.73	1268.05	8.69	1.72	8.85	1.13
318.2	80	1	2.13	1349.04	9.24	1.83	8.33	1.13
318.2	120	1	3.19	1489.69	10.20	2.10	6.80	1.01
328.2	65	1.03	1.73	1106.20	7.59	1.50	13.80	1.53
328.2	80	1.03	2.13	1222.37	8.37	1.66	11.70	1.43

(a) Peng-Robinson equation of state; pure SF_6 (see Appendix 1)

(b) Critical properties from R.C.Reid, J.M.Prausnitz, T.K.Sherwood, "The Properties of Gases and Liquids", 3rd edition, 1977, Mc Graw-Hill, New York

$T_r = T/T_c(SF_6)$

$P_r = P/P_c(SF_6)$

$\rho_r = \rho/\rho_c(SF_6)$

TABLE 6.3 DIFFUSION COEFFICIENTS OF BENZOIC ACID IN SUPERCRITICAL CARBON DIOXIDE

T (K)	P (bar)	T_r(b) (-)	P_r(b) (-)	ρ(a) (kg/m3)	ρ(a) (mol/lt)	ρ_r(b) (-)	10^5D (cm^2/s)	$10^6\rho$D (kg/ms)
318.2	160	1.05	2.17	754.94	17.16	1.61	4.90	3.70
318.2	200	1.05	2.71	813.17	18.48	1.74	4.27	3.47
328.2	160	1.08	2.17	671.20	15.25	1.43	9.14	6.13
328.2	200	1.08	2.71	755.02	17.16	1.61	6.83	5.16

(a) S.Angus, B.Armstrong, K.M.de Reuck, IUPAC Commission on THermodynamics and Thermochemistry, "International Thermodynamic Tables of the Fluid State",Carbon Dioxide (Vol. 3), 1st edition, 1976, Pergamon Press, Oxford

(b) Critical Properties from R.C.Reid, J.M.Prausnitz, T.K.Sherwood, "The Properties of Gases and Liquids", 3rd edition, 1977, Mc Graw-Hill, New York

$T_r = T/T_c(CO_2)$

$P_r = P/P_c(CO_2)$

$\rho_r = \rho/\rho_c(CO_2)$

TABLE 6.4 DIFFUSION COEFFICIENTS OF 2-NAPHTHOL IN SUPERCRITICAL CARBON DIOXIDE

T (K)	P (bar)	T_r(b) (-)	P_r(b) (-)	ρ(a) (kg/m^3)	ρ(a) (mol/lt)	ρ_r(b) (-)	10^5D (cm^2/s)	10^6ρD (kg/ms)
308.2	150	1.01	2.03	815.03	18.52	1.74	7.03	5.73
308.2	200	1.01	2.71	866.21	19.69	1.85	6.63	5.74
308.2	250	1.01	3.39	901.86	20.50	1.93	6.45	5.82
318.2	165	1.05	2.24	761.76	17.31	1.63	7.43	5.66
318.2	250	1.05	3.39	857.83	19.50	1.83	7.00	6.01

(a) S.Angus, B.Armstrong, K.M.de Reuck, IUPAC Commission on Thermodynamics and Thermochemistry, "International Thermodynamic Tables of the Fluid State", Carbon Dioxide (Vol. 3), 1st edition, 1976, Pergamon Press, Oxford

(b) Critical properties from R.C.Reid, J.M.Prausnitz, T.K.Sherwood, "The Properties of Gases and Liquids", 3rd edition, 1977, Mc Graw-Hill, New York

$T_r = T/T_c(CO_2)$

$P_r = P/P_c(CO_2)$

$\rho_r = \rho/\rho_c(CO_2)$

TABLE 6.5 : EQUILIBRIUM SOLUBILITY OF BENZOIC ACID IN SF_6

T (K)	P (bar)	$10^4 x_1$ (mole fraction)
328.2	65	1.194
328.2	80	1.491
328.2	120	1.825
338.2	65	1.646
338.2	80	2.076
338.2	120	2.803

TABLE 6.6 : EQUILIBRIUM SOLUBILITY OF NAPHTHALENE IN SF_6

T (K)	P (bar)	$10^3 x_1$ (mole fraction)
318.2	65	1.978
318.2	80	2.152
318.2	120	2.445
328.2	65	3.184
328.2	80	3.513
328.2	120	3.914

TABLE 6.7 : EQUILIBRIUM SOLUBILITY OF BENZOIC ACID IN CO_2

T (K)	P (bar)	$10^3 x_1$ (mole fraction)
318.2	160	2.341
318.2	200	3.580
328.2	160	2.495
328.2	200	3.864

TABLE 6.8 : EQUILIBRIUM SOLUBILITY OF 2 NAPHTHOL IN CO_2

T (K)	P (bar)	$10^4 x_1$ (mole fraction)
308.2	150	4.460
308.2	200	5.408
308.2	250	5.910
318.2	165	5.662
318.2	250	8.655

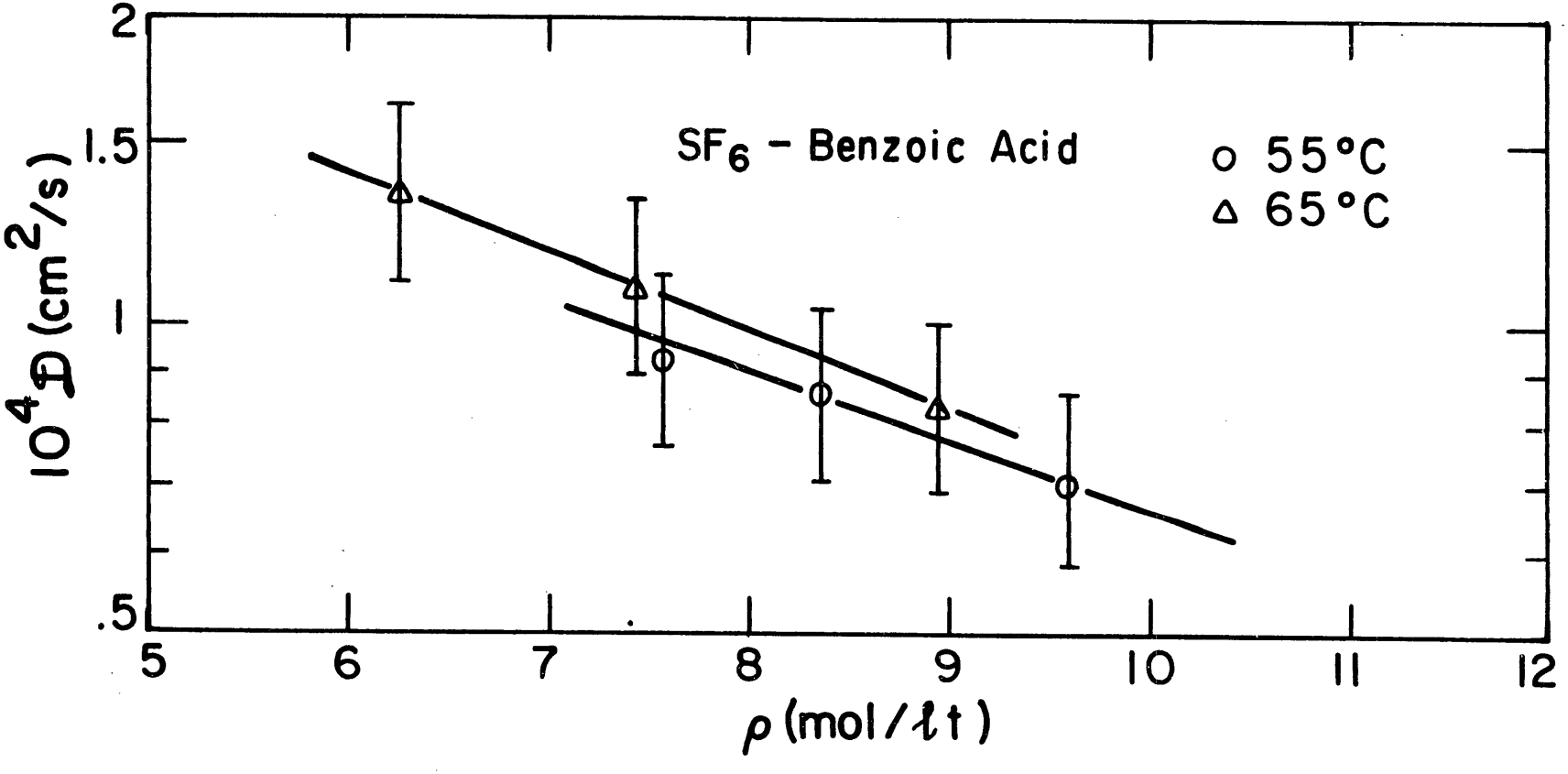

FIGURE 6.1 : Diffusion coefficients of benzoic acid in SF_6

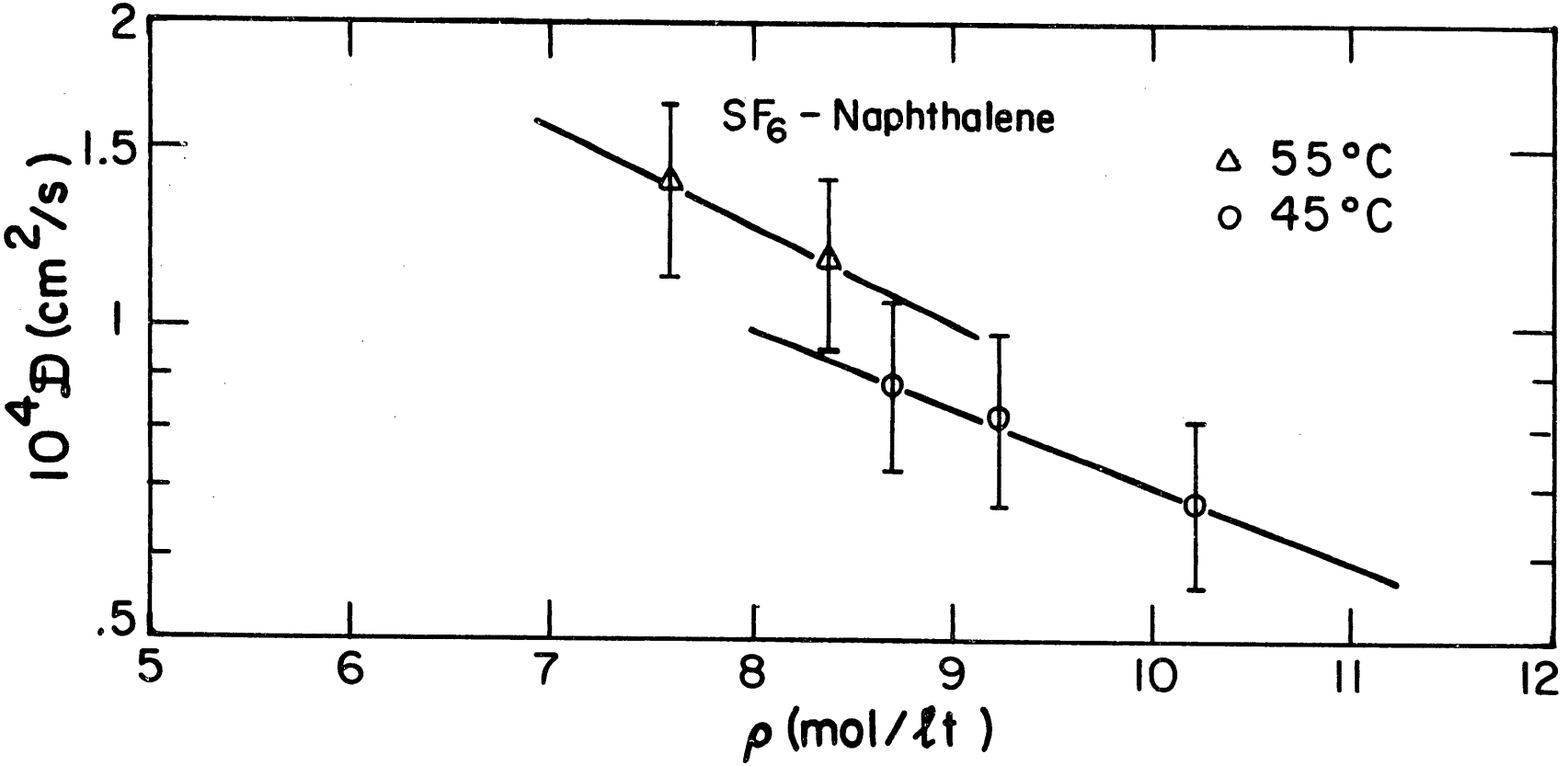

FIGURE 6.2 : Diffusion coefficients of naphthalene in SF_6

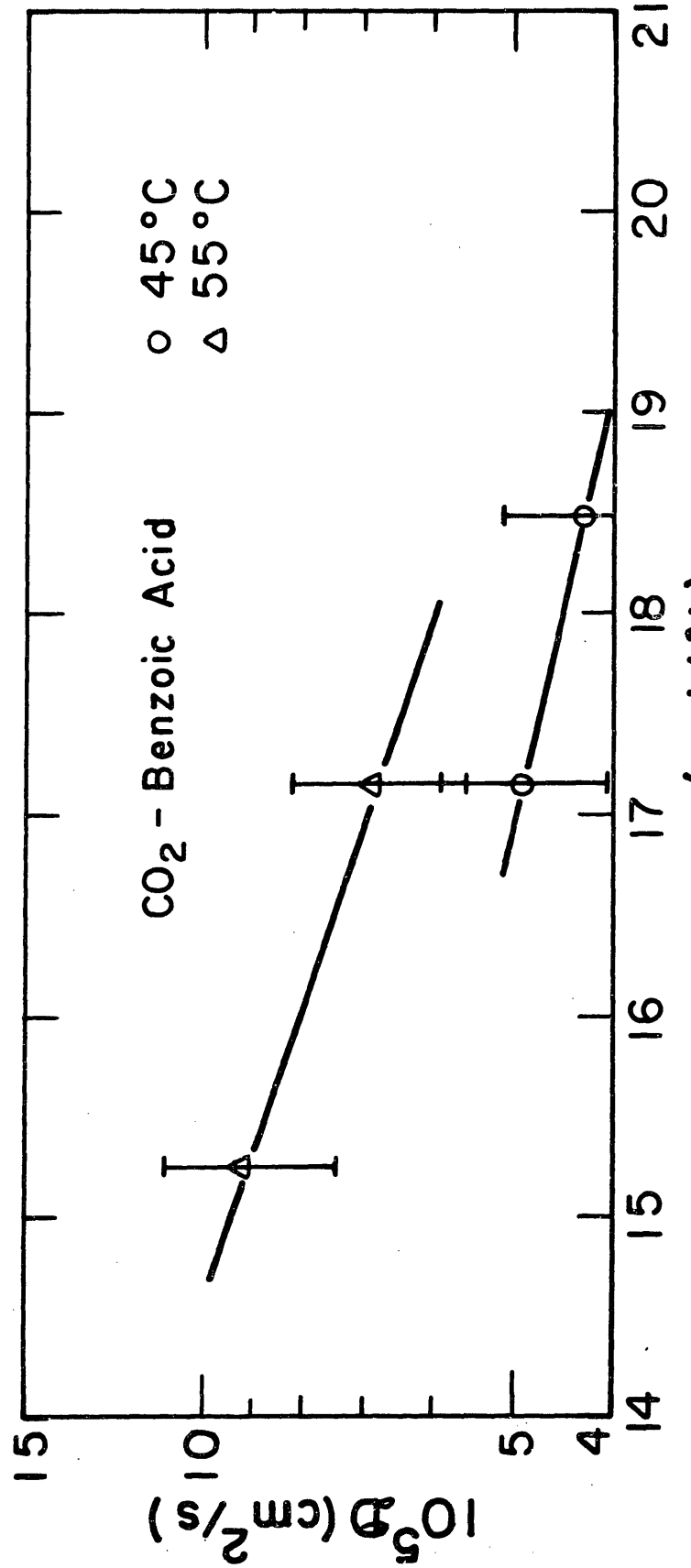

FIGURE 6.3 : Diffusion coefficients of benzoic acid in CO_2

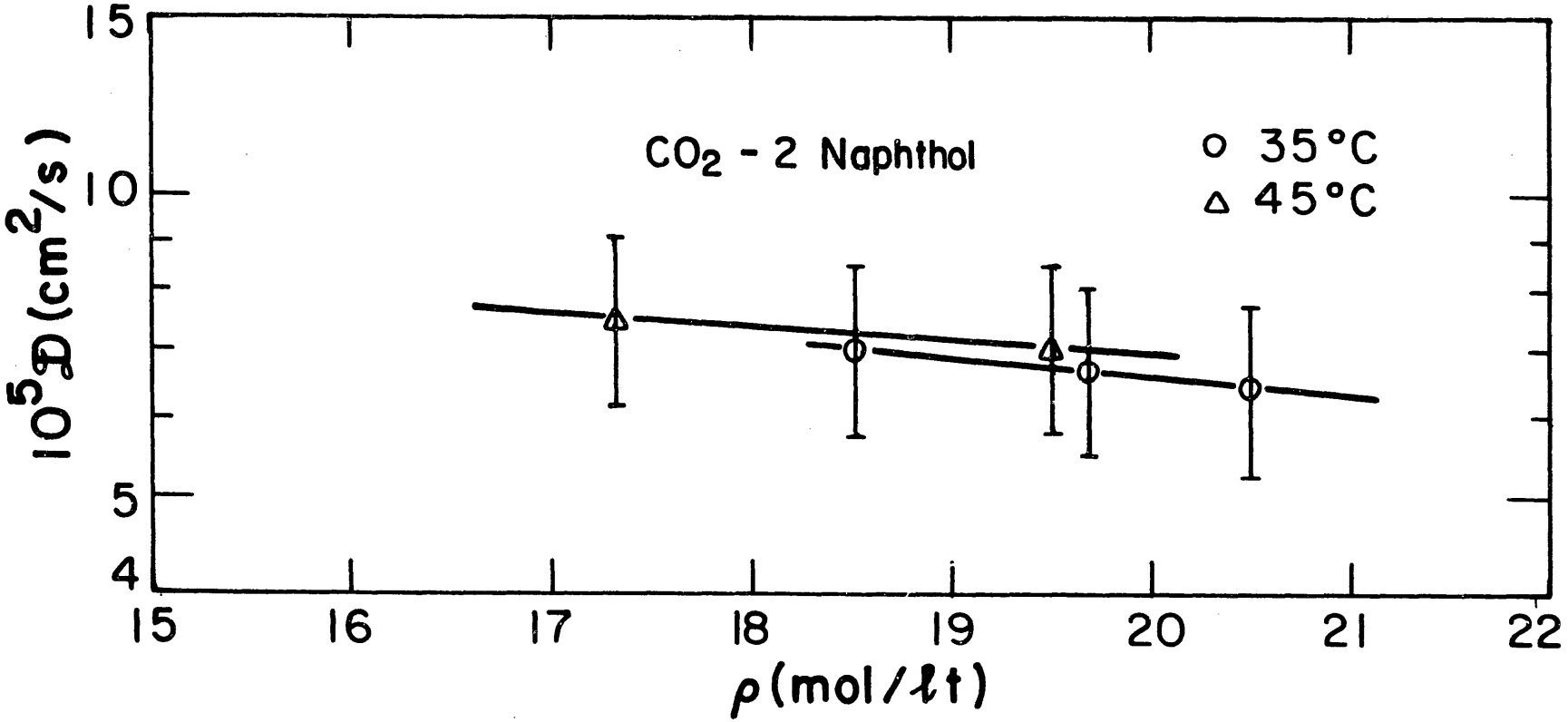

FIGURE 6.4 : Diffusion coefficients of 2-napthol in CO_2

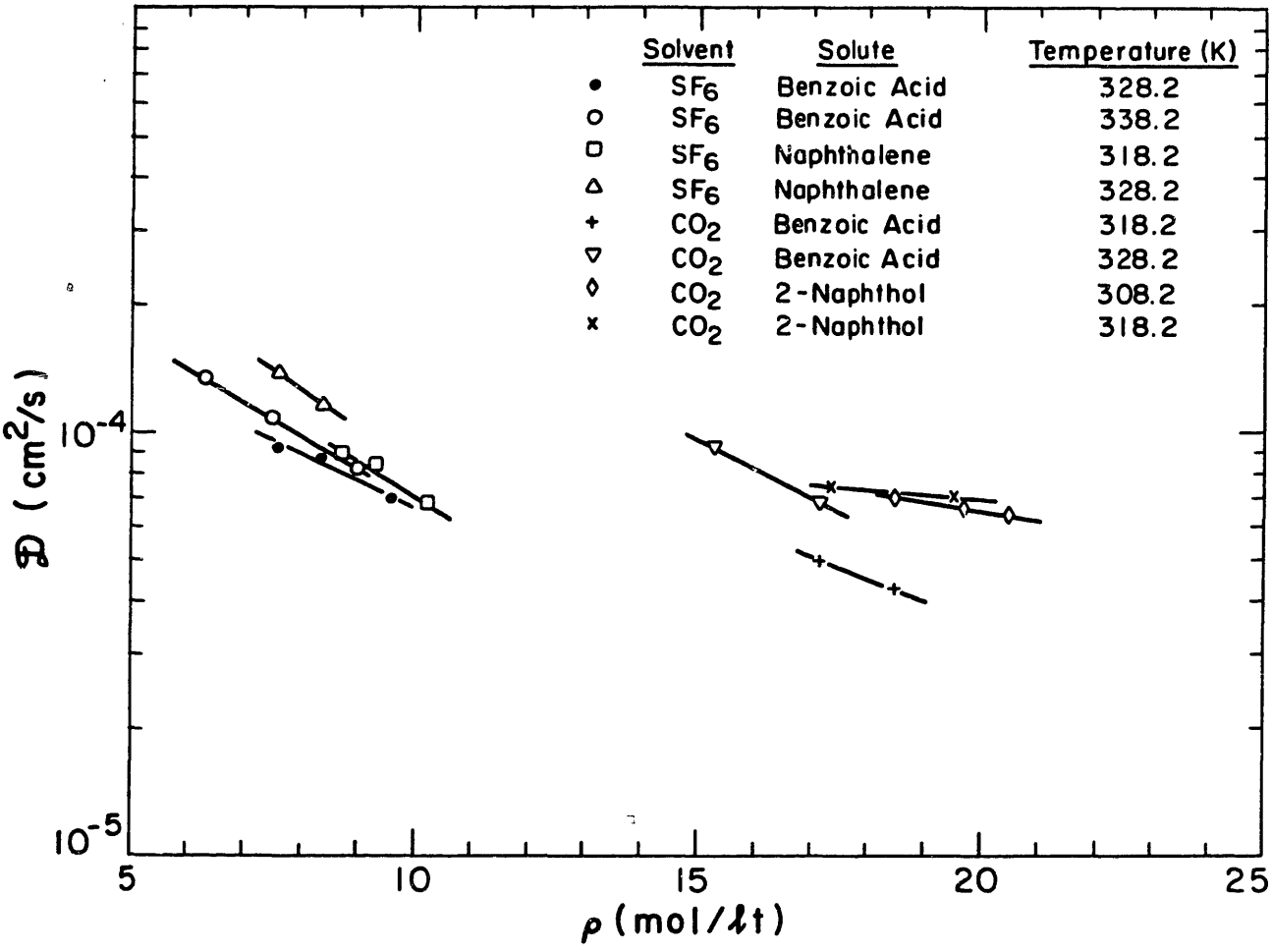

FIGURE 6.5 : Experimental diffusion coefficients as a function of solvent density

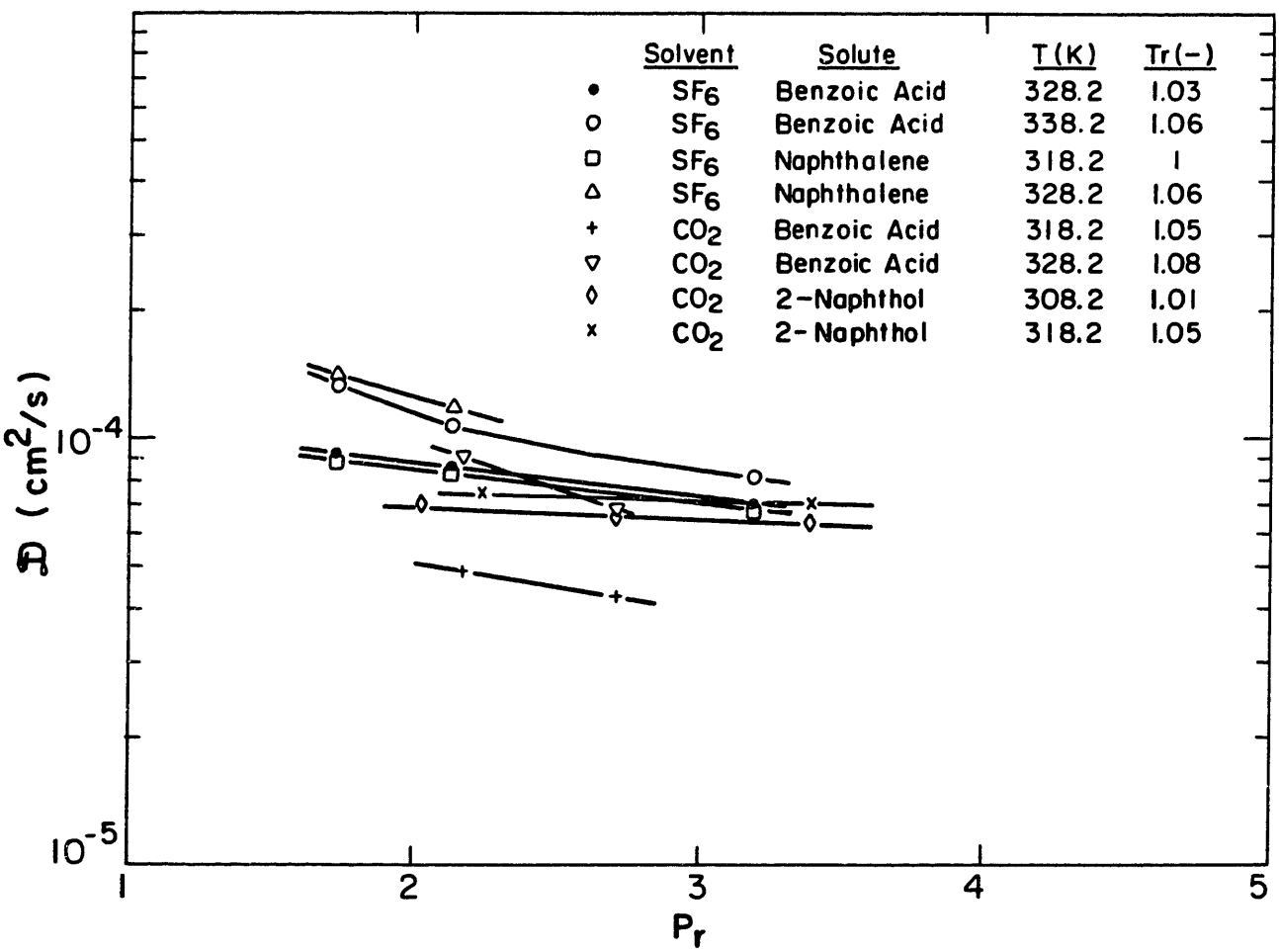

FIGURE 6.6 : Experimental diffusion coefficients as a function of solvent reduced pressure

Pressure, on the other hand, is only relevant for any particular system insofar as density is a function of pressure at any given temperature. This can be clearly seen from the fact that the measured diffusion coefficients are only slightly higher than typical binary diffusion coefficients in liquids at comparable temperatures and densities, but at ambient pressure.

For dilute systems, such as the ones presently considered, corresponding states arguments can be invoked in support of the use of solvent reduced pressure as an independent variable (Paulaitis et al., 1983). The data are therefore summarized both as a function of fluid density (Figure 6.5) and solvent reduced pressure (Figure 6.6).

At constant temperature, low density diffusion coefficients are inversely proportional to fluid density. This result can be derived theoretically (Chapman and Cowling, 1970). Furthermore, since the pressure and density of an ideal gas are directly proportional at constant temperature, a logarithmic plot of diffusion coefficients versus pressure approaches a limiting slope of -1 at low densities (Paulaitis et al., 1983). No equivalent simple relationship exists at high pressure, and the use of a semilog scale in Figure 6.6 is simply a matter of convenience. Similarly, there exists no accurate theory that will predict the isothermal density dependence of diffusion coefficients in dense fluids, as will be discussed below in connection with the Enskog theory. The linear log D vs. ρ relationship suggested by Figures 6.1, 6.2 and 6.4 (i.e., systems for which more than two points per isotherm at least at one temperature were measured) has been reported by other researchers who studied diffusion in supercritical fluids (Swaid and Schneider, 1979; Feist and Schneider, 1982). In the present case as well as in the above mentioned studies, though, the ratio of the maximum to the minimum density for any given isotherm was, at most, three; the smallness of this number suggests that the observed linearity should be interpreted with caution.

Even though benzoic acid is a smaller molecule than either naphthalene or 2-naphthol, the measured diffusion coefficients of benzoic acid in SF_6 were smaller than those of naphthalene in SF_6, and the measured diffusion coefficients of benzoic acid in CO_2 were smaller than those of 2-naphthol in CO_2, at the same density (and slightly higher temperature).

These observations suggest fluid phase association of benzoic acid, a possibility that will be discussed below in detail.

6.2 DISCUSSION

No rigorous kinetic theory for dense fluids exists that will allow an a priori calculation of transport properties. A perturbation solution of Boltzmann's transport equation constitutes the basis of the Chapman Enskog expressions for the transport coefficients in dilute fluids (Chapman and Cowling, 1970; Hirschfelder et al., 1964). Boltzmann's transport equation (Huang, 1963; Pauli, 1981) contains three fundamental assumptions:

- molecules are points and hence have only translational degrees of freedom
- the position and velocity of a molecule are uncorrelated (molecular chaos assumption)
- only binary collisions are considered

At high densities, each of these assumptions becomes progressively less plausible, and, in addition, collisional transfer (i.e., transfer occuring during an encounter) must be taken into account (Chapman and Cowling, 1970).

In spite of the fact that it cannot reproduce important experimental trends, Enskog's dense gas theory (Enskog, 1921) is widely used for correlating purposes, although never in a predictive way. It is, in fact, fairly common to report experimental data in terms of deviations from theoretical (Enskog) behaviour (Balenovic et al., 1970, for example). The simplicity and plausibility of Enskog's assumptions and of the predicted behaviour (i.e., a density correction factor whose reciprocal is linear in density) are chiefly responsible for this rather unusual situation.

In this approach, a dense atomic fluid composed of smooth hard spheres is considered. The assuption of molecular chaos is maintained, and, since hard sphere collisions are instantaneous, only binary collisions are taken into account.

As generalized by Thorne to binary diffusion, the main result of Enskog's theory for dense fluid diffusion is (Chapman and Cowling, 1970)

$$\rho D_{12} = (\rho D_{12})^{o} \chi_{12}^{-1} \tag{6.1}$$

where superscript o denotes the low density limit, and

$$\chi_{12} = 1 + \frac{n_1 \pi \sigma_1^3}{6} \left(\frac{\sigma_1 + 4\sigma_2}{\sigma_1 + \sigma_2} \right) + \frac{n_2 \pi \sigma_2^3}{6} \left(\frac{4\sigma_1 + \sigma_2}{\sigma_1 + \sigma_2} \right) + \ldots \tag{6.2}$$

with n_1, n_2, σ_1 and σ_2 denoting, respectively, solute (1) and solvent (2) number density and hard sphere diameter.

When experimental values of $(\rho D_{12})^{o}$ are not available, Equation (6.1) can still be used, with $(\rho D_{12})^{o}$ calculated from Chapman - Enskog dilute gas expressions (see below).

For infinite dilution of n_1 (solute) in n_2 (solvent), Equation (6.2) can be rewritten as

$$\chi_{12} \cong 1 + \frac{\pi n \sigma_2^3}{6} \left(\frac{4s+1}{s+1} \right) \tag{6.3}$$

$$s \equiv \sigma_1 / \sigma_2$$

where n is now the solvent number density. Equation (6.3) provides a rational basis for correlating purposes, with σ_2 as an adjustable parameter, and

$$n = \frac{L\rho}{M} \tag{6.4}$$

with L, Avogadro's number and M, solvent molecular weight. Since the

factor (4s+1)/(s+1) varies only from 1 to 4 when s varies from 0 (point solute) to ∞ (Brownian solute), σ_2 is a better choice for a regression parameter. In addition, for non-spherical solutes, s retains more physical significance than σ_2.

The low density limit of ρD was calculated from the Chapman- Enskog expression (Bird et al., 1960)

$$\frac{(\rho D_{12})^{\circ}}{M_2} = 2.2646 \times 10^{-5} \frac{\left[T\left(\frac{1}{M_1} + \frac{1}{M_2}\right)\right]^{1/2}}{\sigma_{12}^2 \, \Omega_d} \tag{6.5}$$

where D is in cm^2/s, ρ in g/cm^3, σ in Å, and T in K. An average deviation of 7.5 % was found when 114 experimental low pressure diffusion coefficients were compared with the corresponding Chapman-Enskog prediction (Reid et al., 1977). The collision integral, Ω_d, was found from Table 5-2 of Bird et al.(1960), where the 12-6 Lennard-Jones potential function has been assumed. The following combining rules were used for the intermolecular potential parameters

$$\varepsilon_{12} = (\varepsilon_1 \, \varepsilon_2)^{1/2}$$
$$\sigma_{12} = (\sigma_1 + \sigma_2)/2 \tag{6.6}$$

The ε_i and σ_i values are listed in Table 6.9 and were calculated from the following expressions (Tee et al., 1966)

$$\sigma \left(\frac{T_c}{P_c}\right)^{1/3} = 2.3551 - 0.087\omega \tag{6.7}$$

$$\frac{\varepsilon}{kT_c} = 0.7915 + 0.1693\omega \tag{6.8}$$

where P_c is in atmospheres, T_c in K, and σ in Å.

The experimental, calculated and regressed values of χ_{12} are shown

in Tables 6.10 to 6.13. The regression was done by minimizing the sum of squared deviations between χ_{12} (experimental) and Equation (6.3), with σ_2 as adjustable parameter. In the present context, experimental means observed ρD divided by theoretical (Chapman-Enskog) low pressure ρD. The s values used in the regression were calculated as the ratio of the respective $(T_c/P_c)^{1/3}$ quantities.

The experimental χ_{12} values are plotted in Figure 6.7 as a function of fluid density, and the calculated, regressed and experimental values for each system are shown in Figures 6.8, 6.9, 6.10 and 6.11.

As mentioned above, the Enskog-Thorne expression (Equation (6.3)) predicts a linear increase of χ_{12} with fluid density, which, physically, means that, at constant temperature, the diffusion coefficient decreases with density more rapidly than ρ^{-1}.

Deviations from this predicted behaviour have frequently been reported in the literature (Swaid and Schneider, 1979; Balenovic et al., 1970; O'Hern and Martin, 1955, for example) and interpreted in terms of the positive correlation of molecular velocities found by Alder and Wainwright in their molecular dynamics work (Alder and Wainwright, 1967). Although it is very qualitative in nature, the currently accepted interpretation of Alder and Wainwright's results and of observed experimental behaviour is that a large solute particle will " gather a 'cloud' of carrier molecules which move with it; since collisions by carrier molecules originate within this 'cloud', there is reduced net momentum transfer and therefore a reduced retardation of the particle..." (Balenovic et al., 1970).

This deviation from the Enskog prediction can, in some cases, lead to χ_{12} values which are less than 1 (Swaid and Schneider, 1979; Balenovic et al., 1970), a fact which cannot be predicted by Equation(6.3).

The experimental χ_{12} values shown in Figure 6.7 reveal some interesting trends. In the first place, theoretically predicted behaviour ($\chi > 1$ and increasing with ρ) is displayed by both systems where SF_6 is the solvent, whereas the CO_2-2-naphthol data do show a slightly decreasing χ vs. ρ trend. Balenovic et al.(1970) note that, whenever the same carrier gas exhibited both types of behaviour, χ decreased with ρ for large solute/solvent ratios (He - C_3H_8 ; He - C_4H_{10}) and increased with ρ for small solute/solvent size ratios (He - Ar), in qualitative

TABLE 6.9 LENNARD-JONES AND CRITICAL PARAMETERS FOR SOLUTES AND SOLVENTS

Substance (-)	T_c (K)	P_c (bar)	ω (-)	σ(a) (Å)	ε/k(b) (K)
CO_2 (c)	304.2	73.76	.225	3.762	252.36
SF_6 (c)	318.7	37.59	.286	4.752	267.68
Benzoic Acid (c)	752	45.60	.620	5.857	674.14
2-Naphthol (d)	824.8	42.90	.468	6.200	718.18
Naphthalene (d)	748.4	40.53	.302	6.155	630.62

(a) $\sigma\ (P_c/T_c)^{.33} = 2.3551 - .087\omega$ (Tee et al.,1966)

(b) $\varepsilon/kT_c = .7915 + .1693\omega$ (Tee et al.,1966)

$[\sigma]$ = Å
$[P_c]$ = atmospheres
$[T_c]$ = K
$[\varepsilon/k]$ = K
k = Boltzmann's constant
ω = acentric factor

(c) Critical constants from R.C.Reid, J.M.Prausnitz, T.K.Sherwood, "The Properties of Gases and Liquids", 3rd edition, 1977, Mc Graw-Hill, New York

(d) K.Joback, MS Thesis, Massachusetts Institute of Technology, Cambridge MA, 1984

TABLE 6.10 ENSKOG-THORNE ANALYSIS FOR THE SF_6 BENZOIC ACID SYSTEM

T (K)	P (bar)	$10^3\rho$ (mol/cm3)	$10^5 D$ (cm^2/s)	Ω (-)	$10^6(\rho D)^o$(**) (mol/cms)	χ(exp) (-)	χ(calc)(***) (-)	χ(reg)(*) (-)
328.2	65	7.577	9.26	1.642	1.093	1.558	1.681	1.472
328.2	80	8.372	8.61	1.642	1.093	1.516	1.753	1.521
328.2	120	9.592	7.02	1.642	1.093	1.623	1.862	1.597
338.2	65	6.282	13.4	1.616	1.127	1.339	1.565	1.391
338.2	80	7.419	10.7	1.616	1.127	1.420	1.667	1.462
338.2	120	8.954	8.15	1.616	1.127	1.544	1.815	1.557

(*) s = 1.248

σ_2 = 4.20 A

(**) Calculated from Equation (6.5) and Table (6.9)

(***) s = 1.233

σ_2 = 4.752 A

TABLE 6.11 ENSKOG-THORNE ANALYSIS FOR THE SF_6 NAPHTHALENE SYSTEM

T (K)	P (bar)	$10^3\rho$ (mol/cm^3)	$10^5 D$ (cm^2/s)	Ω (-)	$10^6(\rho D)^o$(**) (mol/cms)	χ(exp) (-)	χ(calc)(***) (-)	χ(reg)(*) (-)
318.2	65	8.685	8.85	1.641	1.005	1.308	1.791	1.231
318.2	80	9.240	8.33	1.641	1.005	1.306	1.842	1.245
318.2	120	10.203	6.80	1.641	1.005	1.449	1.930	1.271
328.2	65	7.577	13.80	1.613	1.039	.994	1.690	1.201
328.2	80	8.372	11.7	1.613	1.039	1.061	1.763	1.222

(*) s = 1.296

σ_2 = 3.15 A

(**) Calculated from Equation (6.5) and Table (6.9)

(***) s = 1.295

σ_2 = 4.752 A

TABLE 6.12 ENSKOG-THORNE ANALYSIS FOR THE CO_2 BENZOIC ACID SYSTEM

T (K)	P (bar)	$10^3\rho$ (mol/cm3)	10^5D (cm^2/s)	Ω (-)	$10^6(\rho D)^o$(**) (mol/cms)	χ(exp) (-)	χ(calc)(***) (-)	χ(reg)(*) (-)
318.2	160	17.158	4.90	1.643	1.869	2.223	1.814	1.947
318.2	200	18.481	4.27	1.643	1.869	2.368	1.877	2.020
328.2	160	15.255	9.14	1.616	1.930	1.384	1.724	1.842
328.2	200	17.160	6.83	1.616	1.930	1.647	1.814	1.947

(*) s = 1.587

σ_2 = 3.95 A

(**) Calculated from Equation (6.5) and Table (6.9)

(***) s = 1.557

σ_2 = 3.762 A

TABLE 6.13 ENSKOG-THORNE ANALYSIS FOR THE CO_2 2-NAPHTHOL SYSTEM

T (K)	P (bar)	$10^3\rho$ (mol/cm^3)	10^5D (cm^2/s)	Ω (-)	$10^6(\rho D)^o$(**) (mol/cms)	χ(exp) (-)	χ(calc)(***) (-)	χ(reg)(*) (-)
308.2	150	18.523	7.03	1.699	1.625	1.248	1.892	1.247
308.2	200	19.687	6.63	1.699	1.625	1.245	1.948	1.263
308.2	250	20.497	6.45	1.699	1.625	1.229	1.987	1.273
318.2	165	17.313	7.43	1.671	1.678	1.304	1.833	1.231
318.2	250	19.496	7.00	1.671	1.678	1.230	1.938	1.260

(*) s = 1.6706

σ_2 = 2.45 Å

(**) Calculated from Equation (6.5) and Table (6.9)

(***) s = 1.648

σ_2 = 3.762 Å

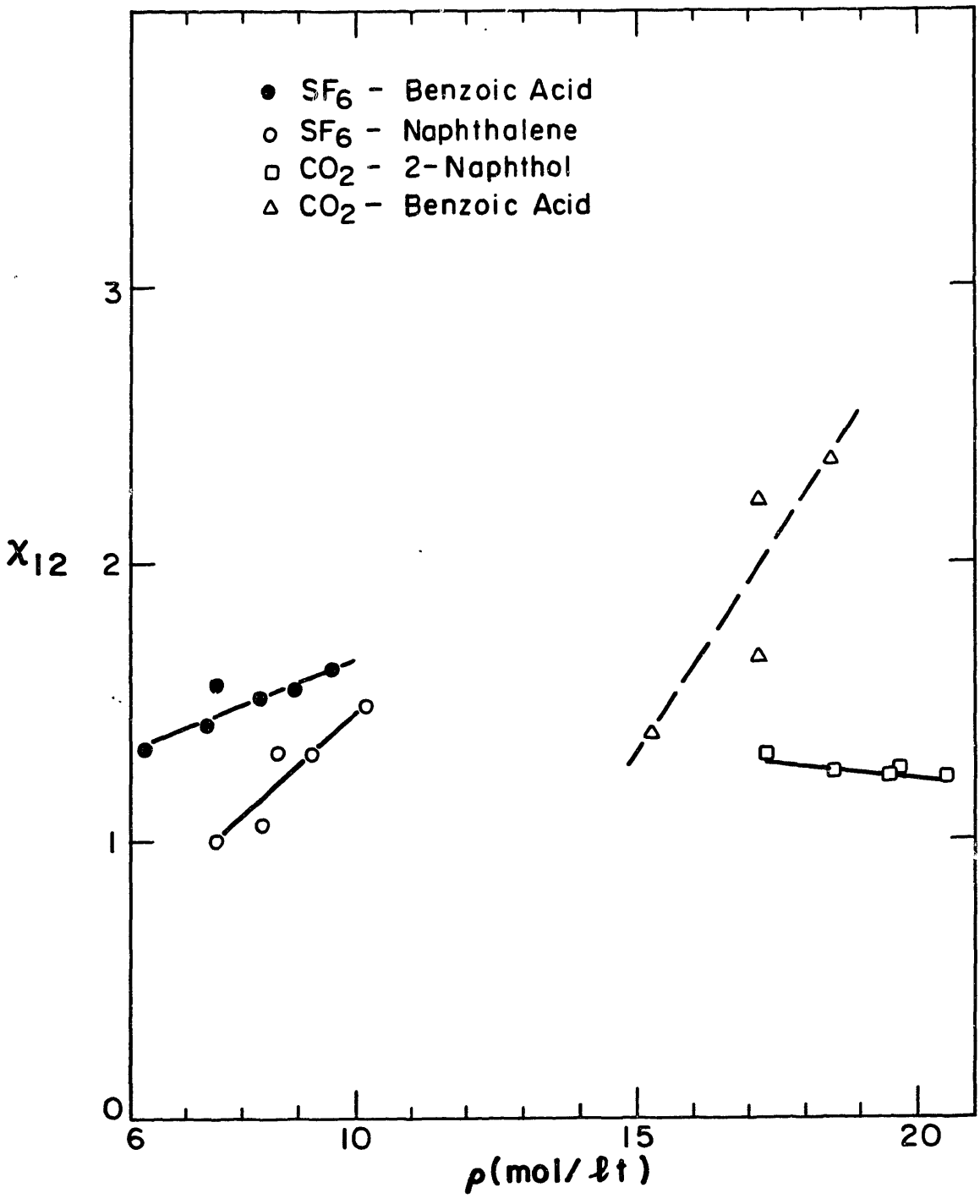

FIGURE 6.7 : Experimental Enskog-Thorne factors

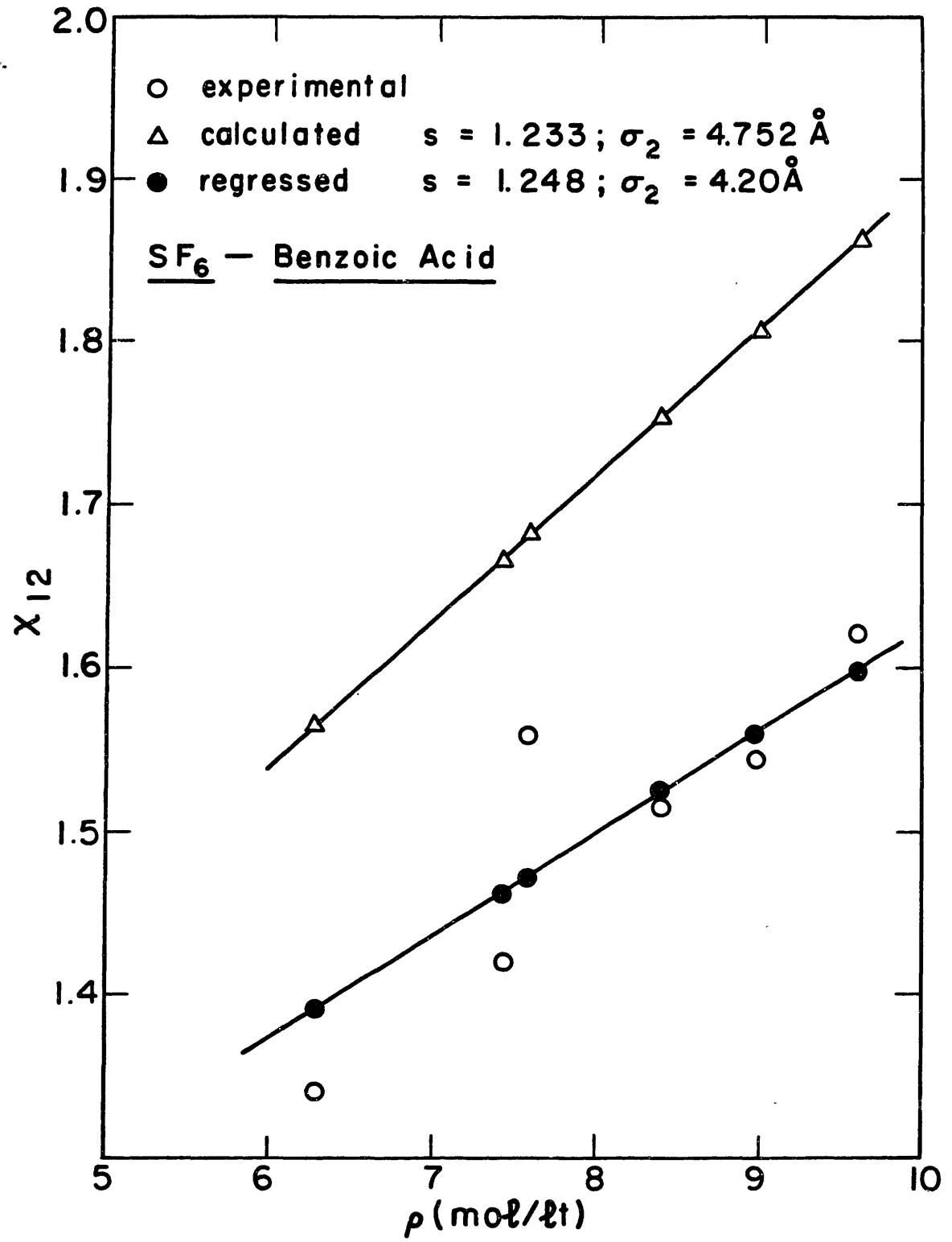

FIGURE 6.8 : Experimental, theoretical and regressed Enskog-Thorne factor for benzoic acid in SF_6

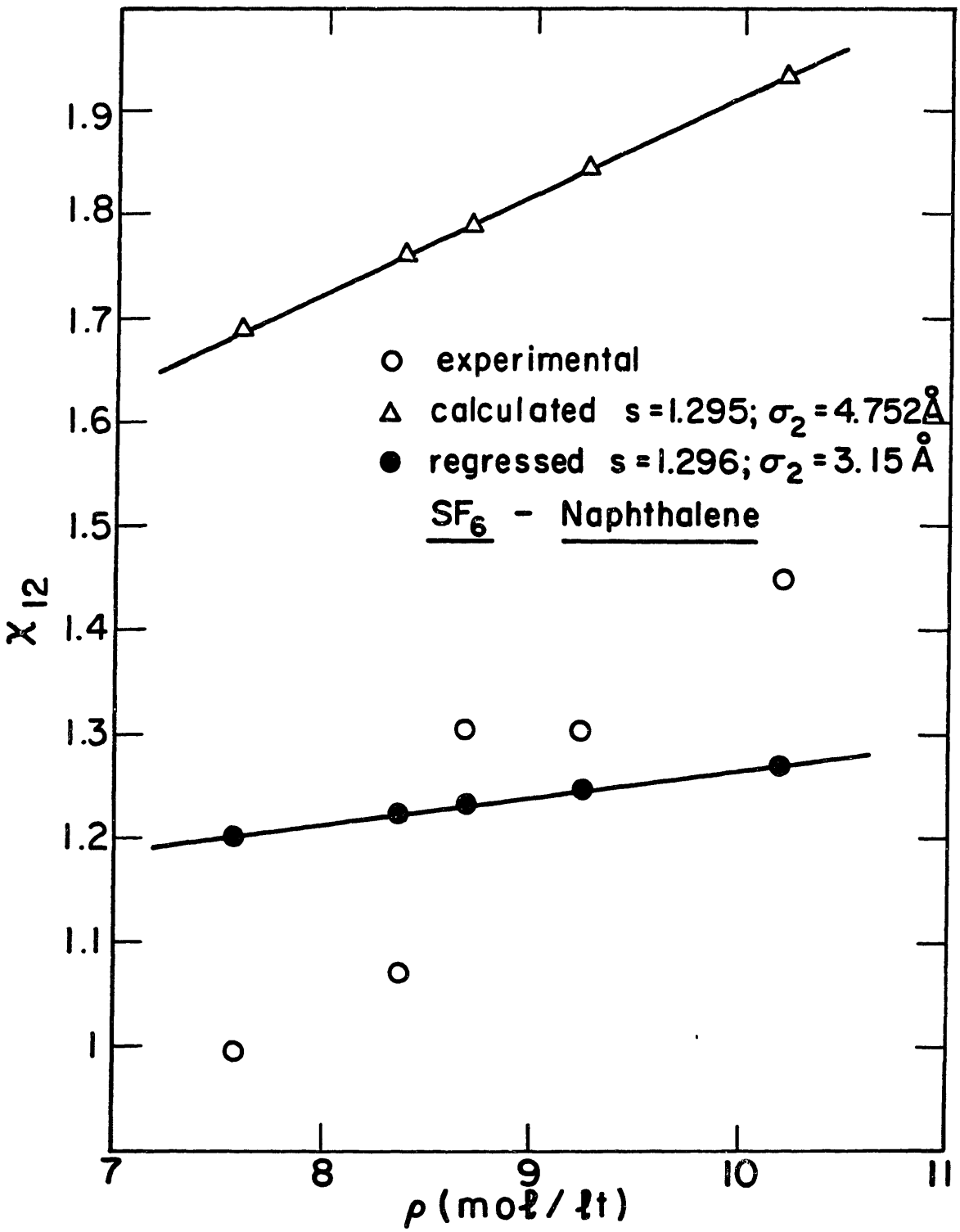

FIGURE 6.9 : Experimental, theoretical and regressed Enskog-Thorne factor for naphthalene in SF_6

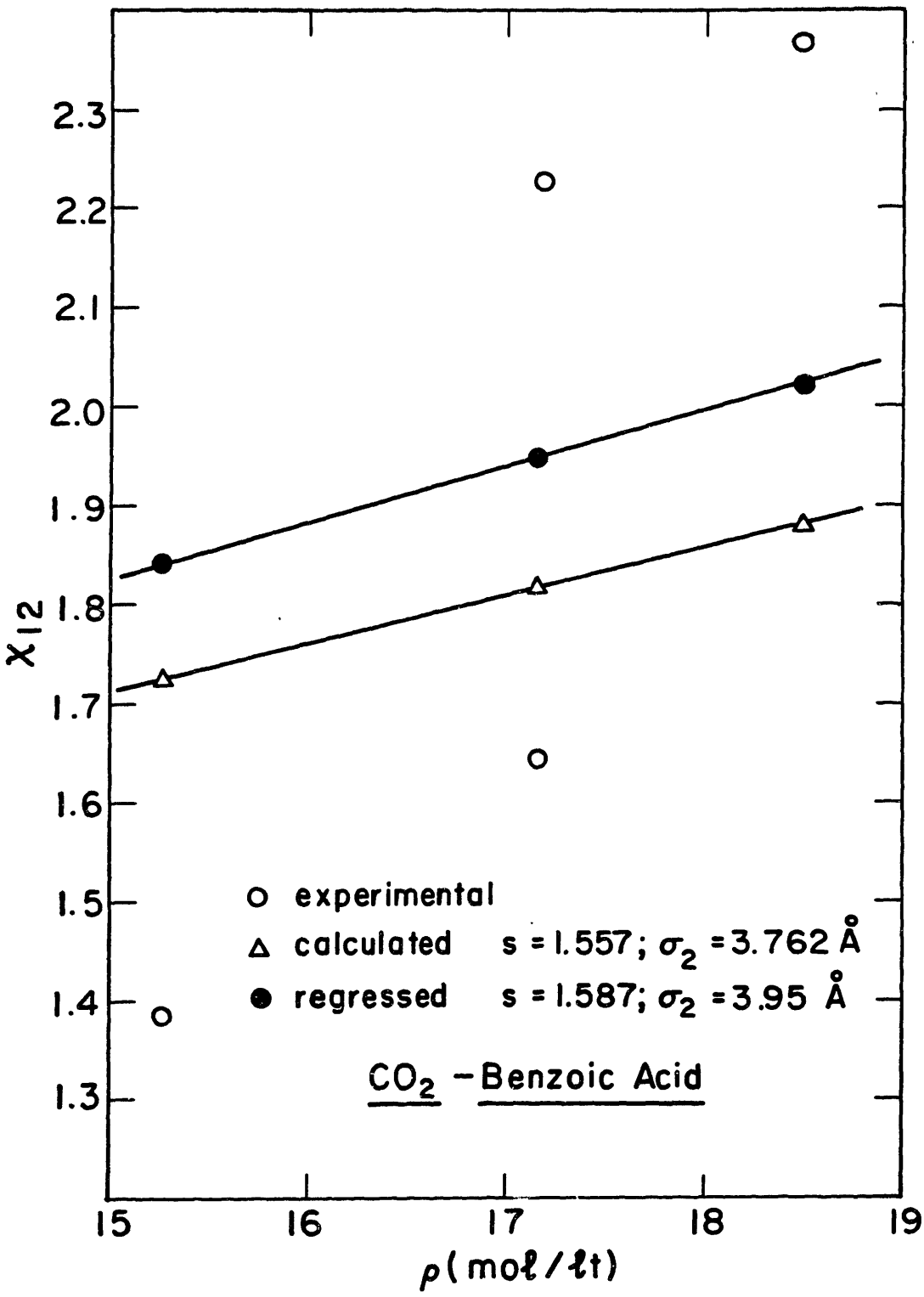

FIGURE 6.10 : Experimental, theoretical and regressed Enskog-Thorne factor for benzoic acid in CO_2

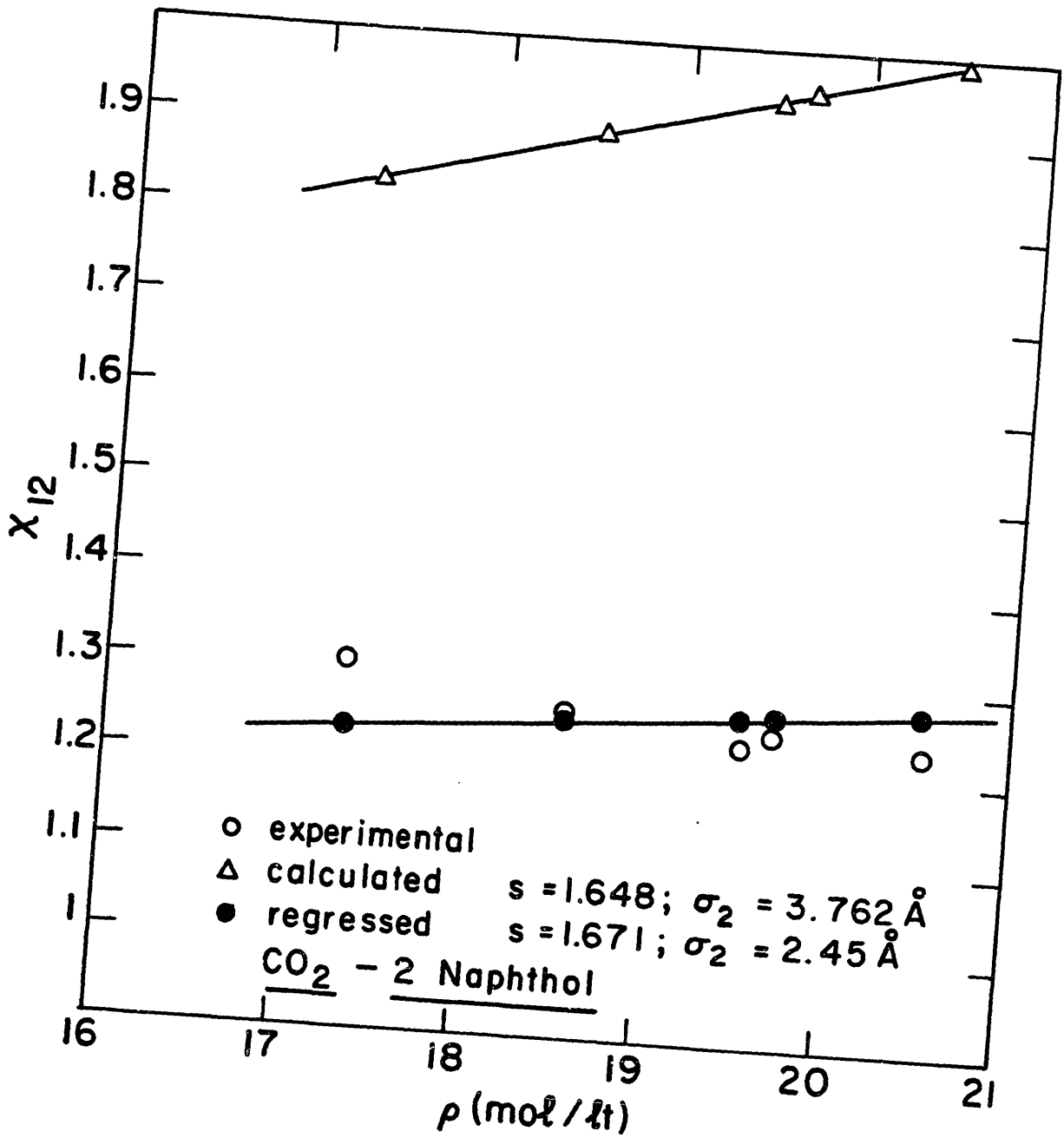

FIGURE 6.11 : Experimental, theoretical and regressed Enskog-Thorne factor for 2-naphthol in CO_2

agreement with Figure 6.7 and the interpretation of Alder and Wainwright's molecular dynamics results. The very high χ_{12} values for benzoic acid in CO_2, on the other hand, can be explained if high pressure association of benzoic acid in the fluid phase occurs, a possibility discussed below. It should also be noted that χ_{12} values for benzoic acid in SF_6 are also significantly high, again suggesting association. Furthermore, χ is an explicit function of density (and not of temperature); the fact that the intermediate density data for benzoic acid show a marked temperature dependence at constant density (see Figures 6.7 and 6.10; intermediate data points, corresponding to 318.2 K, 160 bar, and 328.2 K, 200 bar, with ρ = 17.16 mol/lt in both cases) when plotted as experimental χ vs. ρ again suggests a temperature- dependent dimerization equilibrium of benzoic acid in the fluid phase. This possibility is further substantiated below in connection with the temperature dependence of the measured diffusion coefficients.

From the previous discussion it can be concluded that the Enskog theory overpredicts the χ_{12} correction factor, a fact already observed by other researchers (Feist and Schneider, 1982; Swaid and Schneider, 1979). More significantly, though, this theory predicts a linear increase of χ with density, and χ values which are always greater than one. Correction factors which decrease with density (Figure 6.7; 2-naphthol-CO_2 system) or are less than unity (Swaid and Schneider, 1979) cannot be accounted for by the theory. This is an unfortunate situation, since the Enskog approach is the only rigorously derived predictive theory for transport in dense fluids. Modified versions of the Enskog theory, on the other hand, are really ad-hoc modifications of a hard sphere theory, and have no rigorous theoretical basis. A reliable molecular theory of transport in dense fluids is lacking, as discussed in connection with the computer simulations.

From Figure 6.5 and Tables 6.1, 6.2, 6.3 and 6.4, an interesting feature regarding the diffusion coefficients of benzoic acid in SF_6 and CO_2 arises. The measured diffusion coefficients of benzoic acid are lower, at any given density, than those of naphthalene (in SF_6) and 2-naphthol (in CO_2), both of which are larger molecules than benzoic acid. In each case, moreover, the temperature was slightly higher in the benzoic

acid experiments. This suggests association of benzoic acid in the fluid phase, a behaviour experimentally observed in CCl_4 and $CHCl_3$ (I'Haya and Shibuya, 1965) and in its own vapour, C_6H_{12}, CCl_4 and C_6H_6 (Allen et al., 1966).

The dimerization of benzoic acid can only be invoked as an explanation of observed behaviour if it is quntitatively significant. For the dimerization equilibrium, we write

$$2A = A_2 \tag{6.9}$$

or, in terms of the non-associated fraction (1-x) and the total concentration of benzoic acid, $[A^\circ]$,

$$K = \frac{(x/2)\,[A^\circ]}{\{(1-x)\,[A^\circ]\}^2} = \frac{(x/2)}{[A^\circ]\,(1-x)^2} \tag{6.10}$$

which can be rewritten as a quadratic equation

$$x^2 - x\left(2 + \frac{1}{2K\,[A^\circ]}\right) + 1 = 0 \tag{6.11}$$

Using K = 3660 l/mol (Allen et al., 1966), which corresponds to benzoic acid in CCl_4 at 303 K , and considering a total benzoic acid concentration of 7×10^{-4} mol/l as representative of the actual experimental conditions, we obtain a 31% unassociated fraction (i.e., 1-x), which increases to 61.9% at 333 K (K = 710). The dimerization constants of benzoic acid in carbon tetrachloride (Allen et al., 1966) are intermediate between the corresponding cyclohexane (5830 l/mol at 308.2 K; 1210 l/mol at 333.2 K) and benzene (462 l/mol at 303.2 K; 150 l/mol at 333.2 K) values. Even for the lowest K (i.e., in benzene, at 333.2 K), association is still significant (1-x = 0.849).

Under these circumstances, the very concept of a diffusion coefficient as a molecular property is questionable, since results simply

refer to a "molecule" that does not exist in reality and, moreover, the "effective size" of this molecule could be extremely temperature dependent.

The temperature dependence of the measured diffusion coefficients is interesting, since it provides useful insights into dense fluid behaviour, as well as a further confirmation of fluid phase association of benzoic acid. Hard sphere theory (Dymond, 1974) or its ad-hoc modification, rough hard sphere theory (Chandler, 1975) predict a $T^{1/2}$ dependence of diffusion coefficients at constant density, (slightly modified in rough hard sphere theory by allowing a mild temperature dependence of the sphere's diameter). In the hydrodynamic approach, on the other hand, the Stokes - Einstein expression is used as a starting point,

$$D = \frac{kT}{6\pi a\eta} \tag{6.12}$$

where D is the diffusion coefficient of a Brownian sphere of radius a in a continuum of viscosity η and temperature T, when no slip exists between the particle and the continuum. Since the viscosity of liquids is a very strongly decreasing function of temperature, often correlated in the Andrade form (Andrade, 1930),

$$\eta = A \exp(B/T) \tag{6.13}$$

it follows that diffusion coefficients in dense fluids should, according to this approach, exhibit a stronger tempreature dependence than predicted by hard sphere theories.

Equation (6.12) can be rewritten as

$$\frac{\eta D}{kT} = \frac{1}{6\pi a} \tag{6.14}$$

The quantities on the left hand side are all experimentally measurable. The right hand side, however, depends on the validity of the no-slip assumption and on a, which is unambiguously defined only for a truly spherical particle (molecule). Consequently, Equation (6.14) will not be used here to predict diffusion coefficients. The constancy of ηDT^{-1} for any given system, however, has important consequences that will be discussed below.

The quantity ηDT^{-1} is shown in Tables 6.14, 6.15, 6.16 and 6.17 for each of the systems investigated. For SF_6 as a solvent($1.24 < \rho_r < 2.1$), both systems exhibit fairly constant ηDT^{-1} values, suggesting that hydrodynamic arguments may be relevant. As discussed above, the ηDT^{-1} value for benzoic acid is slightly lower than for naphthalene, again suggesting association.

The CO_2 - 2-naphthol system (Table 6.16) also exhibits a fairly constant ηDT^{-1} value. The CO_2 - benzoic acid data (Table 6.17) show a pronounced temperature dependence, as can be seen from Figures 6.3 and 6.6. Although the postulated fluid phase dimerization has not been measured in CO_2, an effective activation energy for diffusion can be obtained from the two coefficients measured at the same density and two different temperatures (318K, 328K, $\rho_r = 1.61$). This value (6.9 Kcal/mol) is in good qualitative agreement with the experimental values for the dimerization of benzoic acid in cyclohexane (6.4 Kcal/mol), CCl_4 (5.5 Kcal/mol), and its own vapour phase (8.1 Kcal/mol) (Allen et al., 1966). It must be noted, however, that the overall diffusion coefficient is related in a non-linear way to the dimerization constant, so the above considerations should only be taken qualitatively.

Figure 6.12 is a plot of the measured diffusion coefficients versus reciprocal solvent viscosity. Only those isotherms for which three points were measured are included in the figure, since two points always define a line. A plot such as Figure 6.12 is a stringent test on whether diffusion in any given system can be described by an equation of the form $\eta DT^{-1} = f(\text{size})$, which implies, for any given system, a zero intercept and slopes proportional to T (for a temperature-independent molecular size).

For the benzoic acid-SF_6 system (see Table 6.14), the isotherm has

TABLE 6.14 STOKES-EINSTEIN ANALYSIS FOR THE SF_6 - BENZOIC ACID SYSTEM

T (K)	P (bar)	η^o (a) (μP)	ρ_r (-)	$10^5 D$ (cm^2/s)	Δ (b),(c) (-)	η (μP)	$10^5 D\eta T^{-1}$ (d) ($cm^2 \mu P/sK$)
328.2	65	166.91	1.50	9.26	1.787	633.65	17.88
328.2	80	166.91	1.66	8.61	1.868	737.70	19.35
328.2	120	166.91	1.90	7.02	2.001	934.63	19.99
338.2	65	171.64	1.24	13.04	1.656	504.65	19.99
338.2	80	171.64	1.47	10.7	1.772	624.12	19.75
338.2	120	171.64	1.77	8.15	1.926	823.34	19.84

(a) Low pressure viscosity from Equations (9-3.9), (9-4.3) and Appendix C; R.C.Reid, J.M.Prausnitz T.K.Sherwood, "The Properties of Gases and Liquids", 3rd edition, 1977, Mc Graw-Hill, New York

(b) $\Delta \equiv [(\eta - \eta^o)\xi + 1]^{.25}$

$\xi \equiv T_c^{1/6} / M^{1/2} P_c^{2/3}$

(c) Dense fluid viscosity from Equation (9-6.4); R.C.Reid, J.M.Prausnitz, T.K.Sherwood, "The Properties of Gases and Liquids", 3rd edition, 1977, Mc Graw-Hill, New York

(d) Mean = 19.467; Standard deviation = 0.812 (4.17 % of mean)

TABLE 6.15 STOKES-EINSTEIN ANALYSIS FOR THE SF_6 - NAPHTHALENE SYSTEM

T (K)	P (bar)	η^o (a) (μP)	ρ_r (-)	$10^5 D$ (cm^2/s)	Δ (b),(c) (-)	η (μP)	$10^5 D\eta T^{-1}$ (d) ($cm^2\mu P/sK$)
318.2	65	162.14	1.72	8.85	1.899	775.25	21.56
318.2	80	162.14	1.83	8.33	1.959	864.11	22.62
318.2	120	162.14	2.10	6.80	2.135	1172.22	25.05
328.2	65	166.91	1.50	13.80	1.787	633.65	26.64
328.2	80	166.91	1.66	11.70	1.868	737.70	26.30

(a) Low pressure viscosity from Equations (9-3.9), (9-4.3) and Appendix C; R.C.Reid, J.M.Prausnitz T.K.Sherwood, "The Properties of Gases and Liquids", 3rd edition, 1977, Mc Graw-Hill, New York

(b) $\Delta \equiv [(\eta - \eta^o)\xi + 1]^{.25}$

$\xi \equiv T_c^{1/6} / M^{1/2} P_c^{2/3}$

(c) Dense fluid viscosity from Equation (9-6.4); R.C.Reid, J.M.Prausnitz, T.K.Sherwood, "The Properties of Gases and Liquids", 3rd edition, 1977, Mc Graw-Hill, New York

(d) Mean = 24.434; Standard deviation = 2.252 (9.2 % of mean)

TABLE 6.16 STOKES-EINSTEIN ANALYSIS FOR THE CO_2 - 2-NAPHTHOL SYSTEM

T (K)	P (bar)	η^o (a) (μP)	ρ_r (-)	$10^5 D$ (cm^2/s)	Δ (b),(c) (-)	η (μP)	$10^5 D\eta T^{-1}$ (d) ($cm^2 \mu P/sK$)
308.2	150	155.61	1.74	7.03	1.910	704.61	16.07
308.2	200	155.61	1.85	6.63	1.971	784.16	16.87
308.2	250	155.61	1.93	6.45	2.019	852.16	17.83
318.2	165	160.17	1.63	7.43	1.853	641.42	14.98
318.2	250	160.17	1.83	7.00	1.959	773.22	17.01

(a) Low pressure viscosity from Equations (9-3.9), (9-4.3) and Appendix C; R.C.Reid, J.M.Prausnitz T.K.Sherwood, "The Properties of Gases and Liquids", 3rd edition, 1977, Mc Graw-Hill, New York

(b) $\Delta \equiv [(\eta - \eta^o)\xi + 1]^{.25}$

$\xi \equiv T_c^{1/6} / M^{1/2} P_c^{2/3}$

(c) Dense fluid viscosity from Equation (9-6.4); R.C.Reid, J.M.Prausnitz, T.K.Sherwood, "The Properties of Gases and Liquids", 3rd edition, 1977, Mc Graw-Hill, New York

(d) Mean = 16.552; Standard deviation = 1.078 (6.50 % of mean)

TABLE 6.17 STOKES-EINSTEIN ANALYSIS FOR THE CO_2 - BENZOIC ACID SYSTEM

T (K)	P (bar)	η^o (a) (μP)	ρ_r (-)	$10^5 D$ (cm^2/s)	Δ (b),(c) (-)	η (μP)	$10^5 D\eta T^{-1}$ (d) ($cm^2 \mu P/sK$)
318.2	160	160.17	1.61	4.90	1.842	629.05	9.69
318.2	200	160.17	1.74	4.27	1.910	709.17	9.52
328.2	160	164.68	1.43	9.14	1.752	540.32	15.05
328.2	200	164.68	1.61	6.83	1.842	633.56	13.18

(a) Low pressure viscosity from Equations (9-3.9), (9-4.3) and Appendix C; R.C.Reid, J.M.Prausnitz T.K.Sherwood, "The Properties of Gases and Liquids", 3rd edition, 1977, Mc Graw-Hill, New York

(b) $\Delta \equiv [(\eta - \eta^o)\xi + 1]^{.25}$

$\xi \equiv T_c^{1/6} / M^{1/2} P_c^{2/3}$

(c) Dense fluid viscosity from Equation (9-6.4); R.C.Reid, J.M.Prausnitz, T.K.Sherwood, "The Properties of Gases and Liquids", 3rd edition, 1977, Mc Graw-Hill, New York

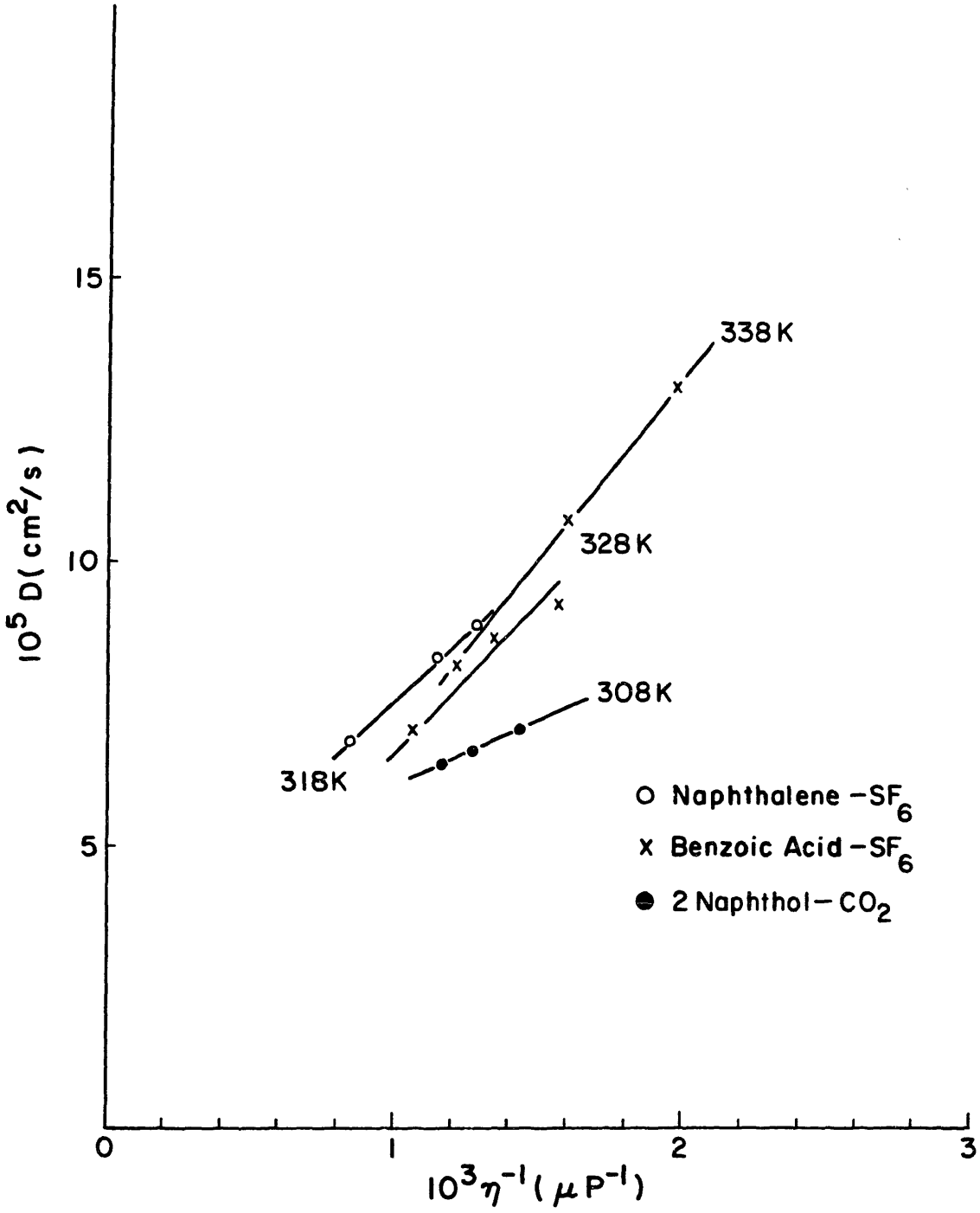

FIGURE 6.12 : Experimental diffusion coefficients as a function of reciprocal viscosity at constant temperature (hydrodynamic test)

a 1.07 intercept and a 5.57 slope (in the figure's units) when the 65 bar data point (which is two standard deviations away from the mean ηDT^{-1} value) is not considered; a 2.34 intercept and a 4.46 slope are obtained from a least squares regression including all three data points. At 338 K, the intercept is .43, and the slope, 6.38. The temperature ratio is 1.03, whereas the slope ratio is 1.145 (disregarding the 65 bar point at 328 K). The higher intercept represents less than 15% of the lowest diffusion coefficient measured for this particular system. For benzoic acid in SF_6, then, Figure 6.12 suggests that hydrodynamic behaviour is a reasonable, if not entirely accurate, description of reality. The fact that the slope ratio is higher than the temperature ratio can be explained by postulating a temperature dependent association of benzoic acid in the fluid phase. The postulated association, though, cannot be high, since the temperature dependence of the measured diffusion coefficients for this particular system is not as pronounced as in the benzoic acid-CO_2 case.

The other systems shown in Figure 6.12 exhibit a behaviour that cannot be described mathematically by a relationship of the form $\eta DT^{-1} = f(size)$, since the intercepts are clearly comparable to the actual measured diffusion coefficients.

Feist and Schneider (1982) analyzed diffusion coefficients of benzene, phenol, naphthalene and caffeine in supercritical CO_2 at 40°C and, from a D vs. η^{-1} plot concluded that the Stokes-Einstein relation did not apply, since the intercepts were non-zero. Feist and Schneider correlated their data with a power law relationship $D \sim \eta^{-a}$ ($a<1$), as proposed by Hayduck and Cheng (1971).

However, when experimental data for six binary systems consisting of an aromatic solute and a supercritical fluid were analyzed, the quantity ηDT^{-1} was found to be remarkably constant (these systems will be discussed below; the average ηDT^{-1} values and the corresponding standard deviations expressed as percentiles of the mean are shown in Table 6.19). Furthermore, Feist and Schneider's data, as read from their published plot (no tables are provided in the paper) show ηDT^{-1} values with maximum and standard deviations (in percent of the mean) of 31% and 12.4% for benzene, and 24.6% and 9.2% for naphthalene.

The above discussion and the small observed deviations in ηDT^{-1} values suggest a general picture, shown in Figure 6.13. Hydrodynamic behaviour is approached at high viscosities; deviations from this limiting behaviour can be correlated (but not understood) by means of empirical power law relationships of the type $D \alpha \eta^{-a}$ ($a < 1$) (Hayduck and Cheng,1971). Supercritical viscosities fall roughly in the range $0.04 \leq \eta \leq 0.1$ cp for $1.1 \leq P_r \leq 4$ and $1 \leq T_r \leq 1.06$, which correponds to $1 \leq 10^{-3}\ \eta^{-1} \leq 2.5$ in the fluidity units of Figure 6.13 (a typical liquid viscosity is also shown for comparison).

The exact point at which hydrodynamic behaviour breaks down (point c) cannot, at present, be predicted from first principles for any given system. However, from Figure 6.13 it can be concluded that predictive correlations based on the Stokes-Einstein equation (Wilke and Chang,1955; Scheibel,1954; Reddy-Doraiswamy,1967; Lusis-Ratcliff,1968) will overestimate diffusion coefficients in supercritical fluids.

In addition, at high enough viscosities (or, equivalently, at high enough pressures for any given temperature), the quantity ηDT_{-1} approaches a constant value; geometrically, this is equivalent to saying that, at small η^{-1} values, the curve Ocb is well approximated by the line Ob. As an example, the measured diffusion coefficients of benzene in supercritical CO_2 (Swaid and Schneider, 1979) give rise to an ηDT^{-1} value that is constant to within a 4.6% standard deviation (expressed in percentage of the mean) when $\eta \geq 0.04$ cp, irrespective of the temperature and pressure.

At high enough viscosities, hydrodynamic behaviour is approached, and this fact can be used to extrapolate experimental data by assuming constancy of ηDT^{-1}.the systems and equations tested (see detailed discussion below).

The possibility of having non-hydrodynamic behaviour and, simultaneously, a linear mean squared displacement versus time relationship is discussed in Chapters 1 and 10. In the present context, it should be pointed out that this simply means that the "drag" has a power law dependence on the viscosity.

From Figure 6.13 it can also be seen that the experimental ηDT^{-1} values should increase with viscosity at any given temperature, since tha curve Ocb lies above the straight lines corresponding to constant

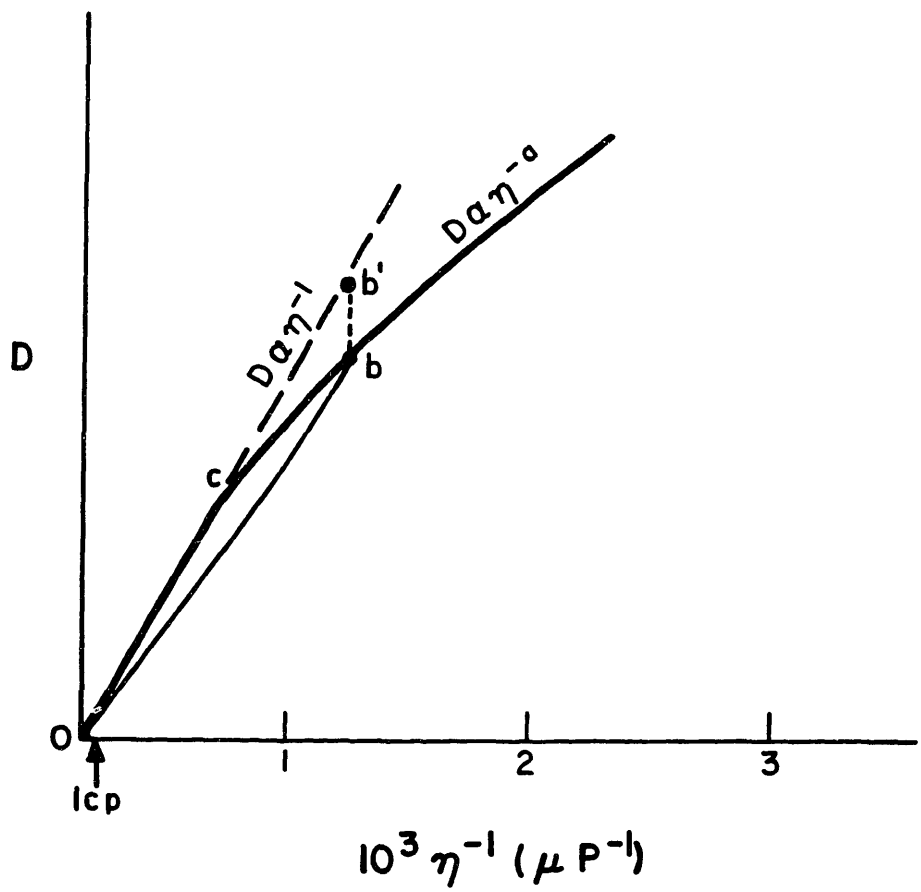

FIGURE 6.13 : Linear (hydrodynamic), power law and transition regimes for the dependence of the diffusion coefficient upon fluid viscosity at constant temperature

ηD values. This behaviour was observed in all of the systems shown in Table 6.19.

The general picture that emerges from the above discussion will now be tested by discussing the application of predictive correlations based on the Stokes-Einstein relation to the supercritical regime. Hydrodynamic expressions should, according to Figure 6.13, overestimate diffusion coefficients by some factor which is not, at present, predictable a-priori.

Several ad-hoc modifications of the Stokes-Einstein relationship have been introduced for engineering use with the purpose of extending its use to molecules of arbitrary shape, while preserving its basic form (ηDT^{-1} = f[size]).

All of these correlations have the form

$$D_{12} = K\ (T/\eta_2) \qquad (6.15)$$

where D_{12} is the infinite dilution diffusion coefficient of molecule 1 in fluid 2 (of viscosity η_2 at a temperature T). Values of K are listed in Table 6.18 for four different correlations.

The Wilke-Chang, Scheibel, Reddy-Doraiswamy and Lusis-Ratcliff correlations were tested for three of the four systems investigated (CO_2-benzoic acid was not included since this system, as explained above, cannot be studied quantitatively without knowledge of the dimerization constant), as well as for the CO_2-benzene ($308 \leq T \leq 328$ K; $80 \leq P \leq 160$ bar), (Swaid and Schneider, 1979); CO_2-naphthalene ($308 \leq T \leq 328$ K; $83 \leq P \leq 304$ bar), (Iomtev and Tsekhanskaya, 1964) and C_2H_4- naphthalene ($285 \leq T \leq 308$ K; $66 \leq P \leq 304$ bar), (Iomtev and Tsekhanskaya, 1964) systems.

The mean values of $10^5\ \eta DT^{-1}$ ($cm^2\mu P/sK$) and the corresponding standard deviations (in percentages of the mean) for the systems investigated are shown in Table 6.19. In the benzene-CO_2 experiments, chromatographic peak broadening was used, whereas weight loss within a stagnant diffusion cell of well characterized geometry was used in the naphthalene studies of Iomtev and Tsekhanskaya. The chromatographic technique is more accurate and reliable, but there is no way of introducing this into the present analysis. It must also be pointed out that, although the standard devia-

TABLE 6.18 : PROPORTIONALITY CONSTANTS FOR INFINITE DILUTION DIFFUSION COEFFICIENT CORRELATIONS (*)

	K(**)	
Wilke-Chang (1955)	$7.4 \times 10^{-8} (\phi M_B)^{1/2} V_A^{-0.6}$	
Scheibel (1954)	$8.2 \times 10^{-8}[1+(3V_B/V_A)^{2/3}]V_A^{-1/3}$	$V_A \geq 2.5V_B$
	$1.75 \times 10^{-7} V_A^{-1/3}$	$V_A < 2.5V_B$
Reddy-Doraiswamy (1967)	$10^{-7} M_B^{1/2} (V_A V_B)^{-1/3}$	$V_B \leq 1.5V_A$
	$8.5 \times 10^{-8} M_B^{1/2} (V_A V_B)^{-1/3}$	$V_B > 1.5V_A$
Lusis-Ratcliff (1968)	$8.52 \times 10^{-8}[1.4(V_B/V_A)^{1/3} + V_B/V_A] V_B^{-1/3}$	

(*) $D_{12} = K\ T/\eta_2$

D_{12} = diffusion coefficient (cm^2/s)

η_2 = viscosity (cp)

T = temperature (K)

(**) ϕ = association factor (dimensionless)

M_B = solvent molecular weight

V_A = solute molar volume at normal boiling point (cm^3/mol)

V_B = solvent molar volume at normal boiling point (cm^3/mol)

TABLE 6.19 : AVERAGE VALUES OF THE RATIOS BETWEEN PREDICTED AND EXPERIMENTAL DIFFUSION COEFFICIENTS FOR DIFFERENT HYDRODYNAMIC CORRELATIONS

	Wilke Chang	Scheibel	Reddy Doraiswamy	Lusis Ratcliff	$<10^8 \eta DT^{-1}>$ (h)	Standard Deviation (i)
SF_6-benzoic acid (a),(g)	2.50	1.79	3.01	1.80	19.47	4.17
SF_6-naphthalene (b),(g)	1.78	1.34	2.25	1.29	24.43	9.20
CO_2- 2-naphthol (c),(g)	1.44	1.60	2.33	1.68	16.55	6.50
CO_2-benzene (d),(g)	1.23	1.41	1.74	1.36	26.50	9.40
CO_2-naphthalene (e),(g)	1.33	1.48	2.15	1.55	18.16	12.90
C_2H_4-naphthalene (f),(g)	.884	1.36	1.29	1.36	21.41	6.35

(a) V_A = 128.44 cm³/mol; V_B = 69.32 cm³/mol; ϕ = 1; M_B = 146

(b) V_A = 156.01 cm³/mol; V_B = 69.32 cm³/mol; ϕ = 1; M_B = 146

(c) V_A = 155.86 cm³/mol; V_B = 32.80 cm³/mol; ϕ = 1; M_B = 44

(d) V_A = 92.87 cm³/mol; V_B = 32.80 cm³/mol; ϕ = 1; M_B = 44

(e) V_A = 156.01 cm³/mol; V_B = 32.80 cm³/mol; ϕ = 1; M_B = 44

(f) V_A = 156.01 cm³/mol; V_B = 45.35 cm³/mol; ϕ = 1; M_B = 28

(g) Molar volumes at normal boiling point calculated from the Peng-Robinson equation of state, with critical parameters from Table 6.9. Fluid viscosities calculated from Jossi et al.(1962); (see Tables (6.14-6.17)

(h) Mean of experimental values, in $cm^2 \mu P/sK$

(i) Standard deviation in percentage of the mean

tions (Table 6.19) are quite small, the constancy of ηDT^{-1} invariably improved away from the solvent's critical point (for example, at 308.2 K, deviations of up to 32% with respect to the overall mean ηDT^{-1} value occur in the CO_2-naphthalene experiments; the maximum deviatio at 328.2 K is 19%). In addition, ηDT^{-1} increased with fluid viscosity in all cases. as anticipated above.

The molar volumes at the normal boiling point can be estimated by other means than through the use of an equation of state. If the Le Bas additive volume method is used (Le Bas, 1915), the resulting K values (Table 6.18) were, in all cases, within 3% of the K values used here. The Le Bas method, though, cannot be used for SF_6 systems, since it is inaccurate for the estimation of molar volumes of simple molecules; for CO_2, the recommended value of 34 cm^3/mol was used when Le Bas-based K values were calculated (Reid et al.,1977).

Several conclusions can be drawn from Table 6.19. In the first place, all correlations overpredict observed diffusion coefficients by a considerable amount, as anticipated in connection with Figure 6.13, with the single exception of the Wilke-Chang expression for the ethylene-naphthalene case. For diffusion in CO_2, the Wilke-Chang expression is consistently less in error.

The ratio of observed to predicted diffusion coefficient cannot be excpected to remain constant over a wide range of conditions (see Figure 6.13 and the corresponding discussion). Thus, the Wilke-Chang expression with an association factor of 0.565 (obtained by averaging the three CO_2 entries in Table 6.19 under the Wilke-Chang column) gives a diffusion coefficient which is only 5.9% higher than the experimental value for benzene in CO_2 at 313 K and 80 bar (Swaid and Schneider,1979), but, at 160 bar, it overcompensates and the estimate is 14% lower than the experimental value. Once these limitations are understood, though, use of the Wilke-Chang equation with an association factor of 0.565 leads to reasonable engineering estimates of diffusion coefficients of aromatic hydrocarbons in CO_2.

For SF_6 as a solvent, both the Scheibel and Lusis-Ratcliff expressions give similar predictions, and the correction factors are smaller, under the experimental conditions, than either the Wilke-Chang or the Reddy-

Doraiswamy correction factors. Overpredictions in the benzoic acid case are exceptionally high; this is consistent with the previous discussion and the added effect of the postulated fluid phase association of benzoic acid: the effective molecular size would then be larger than indicated by the value of the size parameter used to calculate the K value in each case (Table 6.18).

The situation can be summarized by saying that, at present, no reliable predictive method exists for the calculation of diffusion coefficients in supercritical fluids. If one experimental value of D_{12} (and therefore of ηDT^{-1}) is available, it can be used to estimate diffusion coefficients in the same system under different conditions by assuming a constant ηDT^{-1} value. This extrapolation technique is not recommended for $\eta <$ 400 μP; its accuracy increases with fluid viscosity, that is to say, the experimental diffusion coefficient should be measured at the highest possible viscosity, and the constant ηDT^{-1} assumption should not be used below the recommended minimum η.

The use of predictive correlations based on the Stokes-Einstein equation is not recommended. The correction factors are always significant, and can only be generalized after analyzing large amounts of data. The emerging trends, moreover, are extremely system specific (at any rate solvent specific, since all of the solutes considered were aromatic compounds). When such data exist, useful rules can be formulated; they should never be used over a wide range of conditions, as discussed above. One such recommendation is the use of the Wilke-Chang expression with an association factor $\phi = 0.565$ for diffusion of aromatic hydrocarbons in supercritical CO_2. It is obvious, however, that the way in which this number was arrived at cannot be called predictive.

6.3 EFFECT OF NATURAL CONVECTION

The importance of natural convection in mass transfer with supercritical fluids has already been covered in Chapter 3. As discussed in Chapter 4, buoyant effects can be introduced by performing the hydrodynamic experiments with the two hemicylinders (Figure 4.2) rotated at an angle α with respect to the horizontal inside the high pressure steel enclosure.

Before analyzing the results of such experiments, the criteria for the development of stable and unstable density profiles will be analyzed. In the present context, stable signifies that density increases uniformly in the direction of gravity, and vice-versa. Thus, a stable profile will not, by itself, lead to natural convection.

We imagine a plane interface where fluid is saturated with solute, which diffuses into the bulk solvent under the influence of a concentration gradient. Let us denote the solute mole fraction by x_1, and distances from the interface, measured along a line perpendicular to the interface, by ξ. The molar volume, molecular weight and density at $\xi = 0$ are then

$$V(0) = x_1(0)\,\bar{V}_1 + [1-x_1(0)]\,\bar{V}_2 = \bar{V}_2\,[1+x_1(o)\,(\bar{V}_1/\bar{V}_2 - 1)] \tag{6.16}$$

$$M(0) = x_1(0)\,M_1 + [1-x_1(0)]\,M_2 = M_2\,[1+x_1(0)\,(M_1/M_2 - 1)] \tag{6.17}$$

$$\rho(0) = \frac{M_2\,[\,1 + x_1(0)\,(M_1/M_2 - 1)\,]}{\bar{V}_2\,[\,1 + x_1(0)\,(\bar{V}_1/\bar{V}_2 - 1)\,]} \tag{6.18}$$

Away from the interface ($\xi \to \infty$), on the other hand, we have pure solvent

$$V(\infty) = V_2 \tag{6.19}$$

$$M(\infty) = M_2 \tag{6.20}$$

$$\rho(\infty) = M_2/V_2 \tag{6.21}$$

For dilute solutions, such as we are presently considering (see Tables 6.5-6.8), we may assume

$$\bar{V}_2 \sim V_2 \neq f(x) \tag{6.22}$$

whereupon the density ratio between interface and bulk fluid becomes, simply,

$$\rho(0)/\rho(\infty) = \frac{1 + x_1(0)(M_1/M_2 - 1)}{1 + x_1(0)(\bar{V}_1/V_2 - 1)} \tag{6.23}$$

from which we conclude

$$\rho(0) > \rho(\infty) \quad <=> \quad (M_1/M_2) > \bar{V}_1/V_2 \tag{6.24}$$

Furthermore, $x_1(0)$ in Equation (6.23) is just a parameter, so that Equation (6.24) is a general criterion, i.e., whenever the solute to solvent molecular weight ratio is higher than the corresponding partial molar ratio, the local density is higher than the pure solvent density, regardless of the composition dependence of the solute partial molar volume. This criterion is valid for dilute solutions, where Equation (6.22) is an accurate description of reality.

Although Equations (6.23) and (6.24) are useful, the analysis must be pursued further to investigate the full density profile. In general, we can write

$$\frac{1}{\rho(\infty)} \cdot \frac{d\rho}{d\xi} = \left(\frac{d\rho}{dx_1} \cdot \frac{dx_1}{d\xi} \right) \cdot \frac{1}{\rho(\infty)} \tag{6.25}$$

where $(dx_1/d\xi)$ is a monotonically decreasing function of ξ at steady state. If we now define

$$A \equiv M_1/M_2 - 1 \tag{6.26}$$

$$B \equiv \bar{V}_1/V_2 - 1 \tag{6.27}$$

and neglect the composition dependence of B (which is a valid assumption for dilute solutions but, together with Equation (6.22), needs to be

modified otherwise), we obtain

$$\frac{1}{\rho(\infty)} \cdot \frac{d\rho}{dx_1} = \frac{A - B}{(1+Bx_1)^2} = \frac{M_1/M_2 - \bar{V}_1/V_2}{[\ 1 + (V_1/V_2 - 1)\ ]^2} \qquad (6.28)$$

Thus, we conclude that, for dilute solutions,

$M_1/M_2 > \bar{V}_1/V_2$ => density decreases monotonically away from the interface
$M_1/M_2 < \bar{V}_1/V_2$ => density increases monotonically away from the interface

Schematic profiles are shown in Figure 6.14. For stable profiles, then, the interface should constitute the bottom of the rectangular duct if the solute to solvent molecular weight ratio exceeds the partial molar volume ratio, and the top in the opposite case. In all of the cases presently considered, stable profiles were developed with the interface at the bottom, and, consequently, the source plane constituted the bottom of the rectangular duct; natural convection was introduced by rotating the hemicylinders away from this equilibrium configuration (see Appendix 2 for detailed calculations).

The results of such experiments are shown, for benzoic acid diffusing into CO_2 at 160 bar and 318 K, in Figure 6.15 and Table 6.20.

The dotted line in Figure 6.15 does not extend to 0^o since the diffusion experiment was done at a different flow rate. The importance of natural convection, as well as the potential for experimental error when using hydrodynamic techniques, can be seen from the fact that a 650% increase in the apparent diffusion coefficient results from a 90^o rotation of the flat plate.

6.4 SENSITIVITY ANALYSIS

Detailed examples of an equilibrium and a diffusion calculation are given in Appendix 2. The accuracy of the measured diffusion coefficients and the sensitivity to the various sources of experimental error will be discussed in this section.

A diffusion experiment involves the measurement of r, the fractional saturation at the exit of the test section (this, in turn, implies the determination, in a separate experiment, of the equilibrium solubility

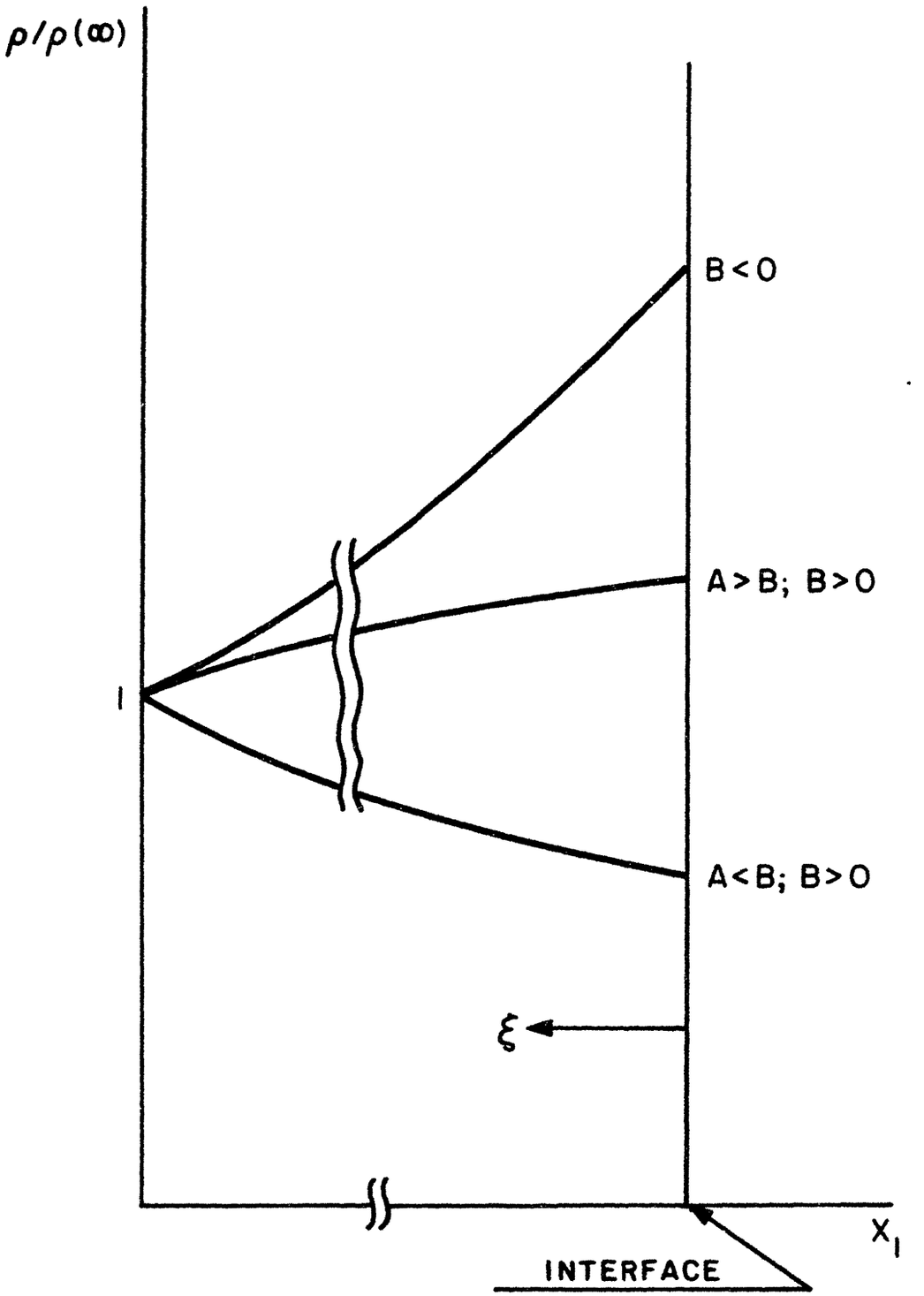

FIGURE 6.14 : Schematic density profiles for a dilute binary mixture in which a solute dissolves into the solvent from a plane ($\xi = 0$) of constant (equilibrium) composition

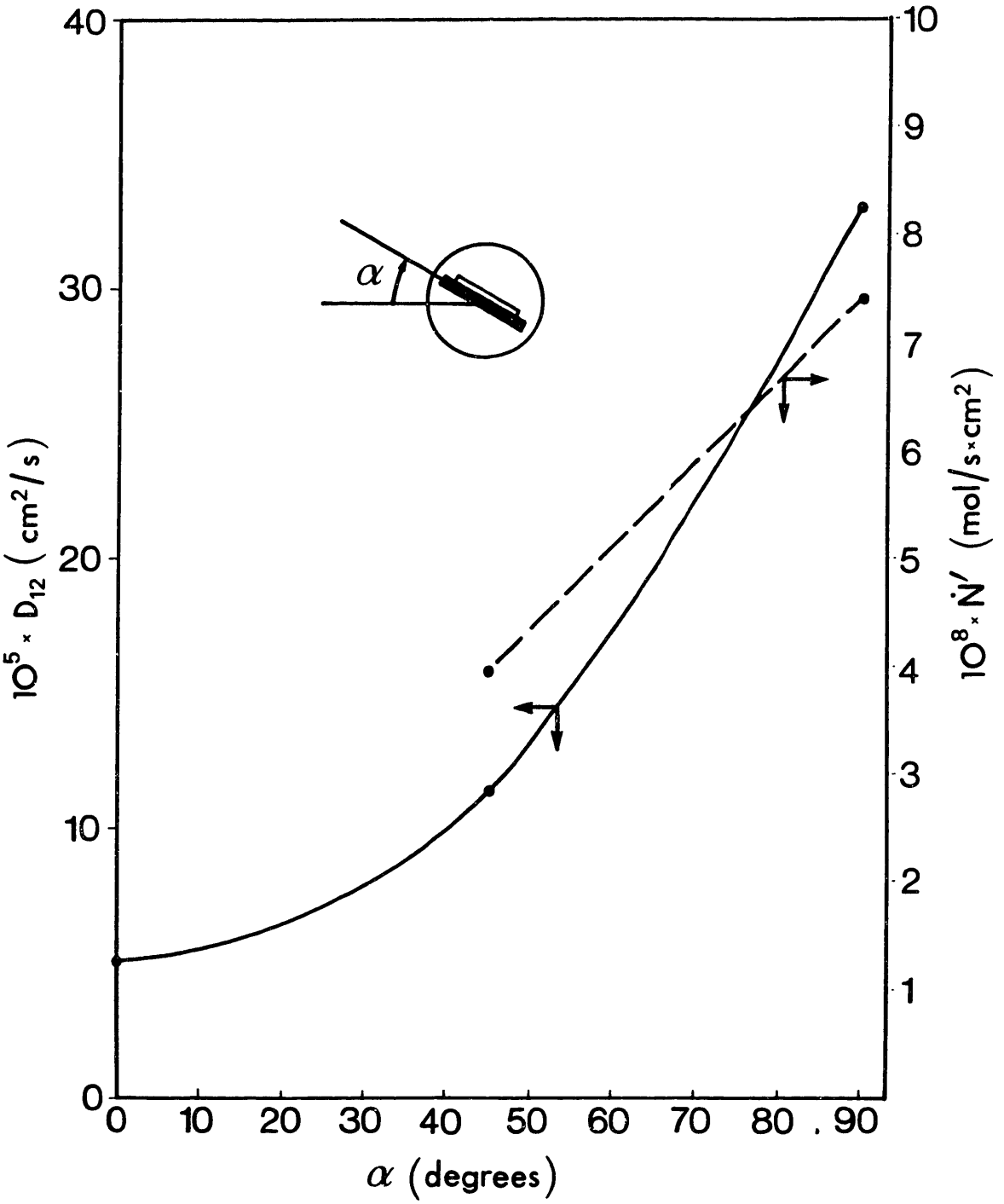

FIGURE 6.15 : Effect of natural convection on the apparent diffusion coefficient and mass transfer rate : benzoic acid-CO_2 @ 318 K and 160 bar

TABLE 6.20 EFFECT OF NATURAL CONVECTION UPON MASS TRANSFER RATE AND APPARENT DIFFUSION COEFFICIENT; CO_2 - BENZOIC ACID

160 BAR; 318K

	0°	45°	90°
$10^5 D_{12}$ (cm^2/sec)	4.9	10.9	31.8
$10^8 \dot{N}/A$ ($mol/cm^2 sec$)	2.58	3.95	7.42

of the solute in the supercritical fluid at the same temperature and pressure). For a given aspect ratio, r is a function of the parameter X_o, defined in Chapter 5 as a modified inverse Graetz number,

$$X_o = L\ D\ /\ \langle v \rangle\ b^2 \tag{6.29}$$

The relationship between r and X_o is given by Equation (4.65), and is shown graphically in Figure 4.3. In Equation (6.29), L is the coated length, $\langle v \rangle$, the mean fluid velocity, and 2b, the duct height. Since D is calculated from X_o, the sensitivity of D to errors in the determination of r is given by

$$\frac{dD}{dr} = \frac{dD}{dX_o} \cdot \frac{dX_o}{dr} = \frac{\langle v \rangle b^2}{L} \cdot \frac{dX_o}{dr} \tag{6.30}$$

from which we obtain,

$$\frac{d\ln D}{d\ln r} = \frac{d\ln X_o}{d\ln r} = \frac{1}{\dfrac{d\ln r}{d\ln X_o}} \tag{6.31}$$

The qualitative form of the dependence of r upon X_o can be deduced without recourse to algebra, once it is realized that X_o is simply a dimensionless length, so that r must grow monotonically and approach unity asymptotically as $X_o \to \infty$. The initial part of this curve is shown in Figure 5.3. The important conclusion is that the sensitivity of the measured coefficients to experimental errors in the determination of r grows without limits as r approaches unity, or, in other words, experiments should be conducted at the lowest possible value of X_o (and hence at low relative saturations).

From Equation (6.29) it can be seen that X_o can be reduced by conducting the experiments in a short duct at high fluid velocities (the duct

height is fixed by practical design considerations and will not be considered a variable). It will now be shown that there are physical constraints which dictate the optimum operating conditions.

The optimum fluid flow rate is determined by the ability of the flow regulating valve to maintain a constant flow under operating conditions, i.e., under conditions where solute deposits are melted by contact with the heated valve and pass through a tapered orfice, designed exclusively for fluid flow. In the present case, a maximum flow rate of ~ 2 liters per minute at ambient conditions could be attained with satisfactory controllability.

The coated length, on the other hand, cannot be reduced indefinitely without altering the physics of the problem, i.e., without making axial diffusion significant with respect to axial convection and vertical diffusion (this follows from the order of magnitude analysis (Section 5.3) where it was shown that axial convection scales as L^{-1}, axial diffusion as L^{-2}, and vertical diffusion as L^{0}). This, in itself, is not a physical constraint; rather, a different analytical solution would be required. However, the possibility of shortening the coated section is in fact limited by a very different constraint: the duration of a run becomes impractically long at very low values of r, given the limitation on $\langle v \rangle$.

As an example, consider an equilibrium solubility of 10^{-3} mole fraction. Then, at 15% saturation, the mole fraction at the test section's outlet is 1.5×10^{-4}, which amounts to 1.34×10^{-5} solute moles per minute for a 2 standard liters per minute solvent flow rate. For a typical solute molecular weight of 130, this means 1.74×10^{-3} g/min, or roughly half an hour to collect 0.05 g of solute, an amount of solute that would give rise to less than 2% error in weighing, (this follows from the reproducibility of the empty U-tube weighings, which was found to be approximately 0.001g). Under typical conditions, r is roughly 18%, so the potential for accuracy improvement by shortening the coated length cannot be materialized without on-line analysis (which would eliminate weighing), since weighing requires runs that soon become impractical due to their duration, when due account is taken of the absolute necessity of maintaining as constant a flow rate as possible throughout the run (it would take 1.5 hours to collect 0.05 g at 5% saturation, for example). With

the equipment described in Chapter 4, then, the minimum amount of solid that must be collected for accurate weighing, and the maximum flow rate that can be maintained with adequate controllability are the two factors which determine the accuracy of the measured diffusion coefficients.

If we now substitute typical values ($D \sim 7 \times 10^{-5}$ cm^2/sec; b = 0.15785 cm; $\langle v \rangle \sim 0.1$ cm/s; L = 7.62 cm) we obtain $X_0 = 0.21$, and r = 0.19247. Furthermore, the local slope is given by $\Delta r/\Delta X_0 \sim 0.58$, so that, finally,

$$d\ln D/d\ln r \sim (r.\Delta X_0)/(X_0.\Delta r) = 1.56 \qquad (6.32)$$

or, in other words,

$$\left|\frac{\Delta D}{D}\right| \sim 1.56 \left|\frac{\Delta r}{r}\right| \qquad (6.33)$$

In Equation (6.33), $\Delta r/r$ includes all possible sources of experimental error affecting the measured value of r, in both the equilibrium and the diffusion experiments, such as weighing errors, gas measuring errors, etc. The actual value of $|\Delta r/r|$ for a typical experiment is derived in Appendix 2. In the present context, the objectives are the derivation of Equation (6.31) and the calculation of the numerical coefficient in Equation (6.32).

From Appendix 2, therefore, we obtain 10% as a conservative estimate for $|\Delta r/r|$, which means that errors in the determination of r lead to uncertainties of $\pm$ 16% in D.

Equation (6.31) states the fact that, since D is obtained from X_0, and X_0 is linear in D, the relative errors in D caused by inaccuracies in the measurement of r are simply the relative errors in X_0 due to the same cause. The final step in the determination of D involves solving Equation (6.29) for D. The determination of $\langle v \rangle$ introduces a new source of error. The fluid velocity is obtained as follows (see Appendix 2 for an example)

$$\langle v \rangle = \frac{\text{Moles of solvent}}{\text{Run duration}} \times \frac{\text{Solvent molar volume}}{\text{Duct cross section}} \qquad (6.34)$$

In Equation (6.34), the inaccuracies in the determination of the amount of solvent gas have already been included in $\Delta r/r$, so we can write

$$\left| \frac{\Delta \langle v \rangle}{\langle v \rangle} \right| = \left| \frac{\Delta \tau}{\tau} \right| + \left| \frac{\Delta V}{V} \right| \qquad (6.35)$$

where τ is the run duration, and V, the solvent molar volume under experimental (i.e., high pressure) conditions.

A typical run lasts ~ 30 minutes; the timing has an uncertainty of ~ 15 seconds, since (see Chapter 4) a run is started after a period during which steady flow is maintained for at least 15 minutes, whereupon the actual U tubes are connected and tightened, an operation that lasts approximately 15 seconds.

The solvent molar volume was determined from the International Thermodynamic Tables of the Fluid State (Angus et al., 1976) for CO_2, and for the Peng-Robinson equation of state (Peng and Robinson, 1976) for SF_6. The error in this case is less than 5% (this figure would be much higher if runs had been done close to the critical point of the solvent; see Tables 6.1-6.4 for actual run conditions).

From the previous discussion, therefore,

$$|\Delta\langle v \rangle/\langle v \rangle| \sim 0.0083 + 0.05 = 0.0583 \sim 0.06 \qquad (6.36)$$

so that, finally,

$$\left| \frac{\Delta D}{D} \right| \sim 1.56 \times 0.1 + 0.06 = 0.216 \sim 0.22 \qquad (6.37)$$

There are, in addition to the above, two sources of error that are, however, very difficult to quantify. In the first place, erroneous num-

bers result if the angle α (Figure 6.15) is not zero. Visual inspection of the flat plate after a run was always conducted, and any diffusion runs where the solute was etched at any detectable angle were rejected. Although great care was taken to guarantee $\alpha \sim 0^{\circ}$ under operating conditions, experimental errors are inevitable and, though small, are difficult to quantify.

In the second place, experiments were conducted inside a closed tube, with no possibility for visual observation. The flow was monitored in two series rotameters (see Figure 4.1) at atmospheric pressure, but, except for the constancy of pressure and the fact that, at steady state, the flow through the rotameters reflects the molar high pressure flow, there was no way of quantifying the instantaneous constancy of fluid flow.

7. DIFFUSION AND IRREVERSIBLE THERMODYNAMICS

In the previous chapters, diffusion has been treated in a phenomenological, or kinetic, way. This characterization refers to these approaches which view diffusion as a phenomenon resulting from gradients in concentration. From the point of view of irreversible thermodynamics, however, chemical potential gradients, and not concentration gradients, constitute the appropriate driving force for diffusion. This represents an entirely different interpretation of physical reality; moreover, as will be discussed below, kinetics and thermodynamics predict opposite behaviour at mixture critical points.

The fundamentals and some of the consequences of the thermodynamic approach will be discussed in this chapter.

7.1 FORCES AND FLUXES

The integral rate of entropy creation in a closed, isolated binary system can be written as

$$\frac{d}{dt}\int \rho\, s dV = \int \frac{1}{T}\,\sigma_{ik}\,\frac{\partial v_i}{\partial x_k}\,dV - \int \left(\frac{\underline{q}-\mu\,\underline{j}_1}{T^2}\right)\cdot \underline{\nabla} T dV - \int \underline{j}_1 \cdot \frac{\underline{\nabla}\mu}{T}\,dV \qquad (7.1)$$

This relationship is derived in Appendix 5. The first integral corresponds to viscous dissipation, and σ_{ik} is therefore a stress tensor. The second integral corresponds to internal heat fluxes, with $\underline{q}$ a local heat flux vector, $\underline{j}_1$ a species 1 mass flux, and μ a mixture chemical potential per unit mixture mass,

$$\mu \equiv \frac{\mu_1}{M_1} - \frac{\mu_2}{M_2} \qquad (7.2)$$

The third integral corresponds to diffusion. Equation (7.1), then, is simply a statement of the fact that closed, isolated, macroscopic systems approach stable equilibrium through irreversible processes involving viscous dissipation, internal heat fluxes and diffusive currents.

Although viscous dissipation can be incorporated into what follows, we shall henceforth restrict our attention to the other two dissipative processes.

Equation (7.1) can be formally written as

$$\frac{d}{dt}\int \rho s dV = -\int \left[\sum_i J_i X_i\right] dV \tag{7.3}$$

where each conjugate J-X pair can be seen to represent the product of a flux (J) and a convenient driving force (X). Thus, from Equations (7.1) and (7.3), we can write

	J		X
Mass flux ($\underline{j}_1$)		$\longleftrightarrow$	$\frac{\nabla\mu}{T}$ ("force")
Energy flux ($\underline{q} - \mu\underline{j}_1$)		$\longleftrightarrow$	$\frac{\nabla T}{T^2}$ ("force")

In this context, therefore, diffusion is linked (in an as yet unspecified way) to chemical potential gradients, whereas in kinetic, mechanistic or phenomenological approaches, this thermodynamic quantity is replaced by concentration gradients.

We next address the question of the relationship between forces and fluxes. If the gradients are small enough, the problem can be treated in the linear approximation, which, in its most general form, reads

$$\underline{J} = \underline{\underline{L}}\ \underline{X} \tag{7.4}$$

i.e., each flux is a linear combination of all forces. This implies, in addition to the diagonal contributions, energy fluxes driven by chemical potential gradients, and mass fluxes driven by temperature gradients. These phenomena have been experimentally verified (Dufour and Soret effects, respectively). Onsager's reciprocity theorem (Onsager, 1931) proved the symmetry of the matrix $\underline{\underline{L}}$ (the "conductance", or transport coefficient matrix),

$$\left(\frac{\partial J_i}{\partial X_j}\right) = \left(\frac{\partial J_j}{\partial X_i}\right) \tag{7.5}$$

Considering mass and energy fluxes in the light of Equation (7.4), we write

$$\underline{j}_1 = - A' \frac{\nabla\mu}{T} - B' \frac{\nabla T}{T^2} = - \alpha \nabla\mu - \beta \nabla T \tag{7.6}$$

$$\underline{q} - \mu\underline{j}_1 = - C' \frac{\nabla\mu}{T} - D'' \frac{\nabla T}{T^2} = -\delta \nabla\mu - \gamma \nabla T \tag{7.7}$$

with

$$\delta = \beta T \tag{7.8}$$

where the last relationship follows from the symmetry of the transport coefficients.

The present analysis can carry us no further than Equations (7.6) - (7.8). As is always the case with arguments based on thermodynamics, one obtains useful relations between quantities of interest, but not actual values for the properties under study. Before turning our attention to the behaviour of the actual coefficients (α in particular), the profound significance of Equations (7.6) - (7.8) should be appreciated. We may summarize this by stating that, when viewed as a particular case of dissipative processes,

- diffusion appears to be driven by chemical potential (as opposed to concentration) gradients.
- diffusion can occur as a consequence of temperature gradients and energy fluxes as a consequence of chemical potential gradients
- the cross proportionality constants (off-diagonal terms in the conductance matrix) are equal.

7.2 RELATIONSHIP BETWEEN THERMODYNAMIC AND PHENOMENOLOGICAL APPROACHES

If we consider, for simplicity, isothermal diffusion with no viscous dissipation, we can write

$$\underline{j}_1 = -\alpha \nabla\mu \tag{7.9}$$

We next use the definition of μ, the Gibbs-Duhem equation, and the definition of fugacity coefficient,

$$\nabla\mu = \frac{1}{M_1}\nabla\mu_1 - \frac{1}{M_2}\nabla\mu_2 \tag{7.10}$$

$$0 = x_1\nabla\mu_1 + (1-x_1)\nabla\mu_2 \tag{7.11}$$

$$\hat{f}_1 = x_1 P \hat{\phi}_1 \tag{7.12}$$

to obtain

$$\underline{j}_1 = \frac{\alpha RT}{M_1}\left[1 + \left(\frac{\partial \ln\hat{\phi}_1}{\partial \ln x_1}\right)_{T,P}\right]\left[\frac{1}{x_1} + \frac{M_1}{M_2}\frac{1}{(1-x_1)}\right]\underline{\nabla}x_1 \tag{7.13}$$

On the other hand, diffusion coefficients are phenomenologically reported as proportionality constants between flux and concentration gradients. Of the many equivalent expressions, we choose (Bird et al., 1960)

$$\underline{j}_1 = -\frac{c^2 M_1 M_2}{\rho}\mathscr{D}_{12}\,\underline{\nabla}x_1 \tag{7.14}$$

Equating the last two expressions, we obtain, after some rearrangement,

$$\mathscr{D}_{12} = \frac{\alpha RT}{M_1^2 c}\left[\left(\frac{1-x_1}{x_1}\right)^{1/2} + \frac{M_1}{M_2}\left(\frac{x_1}{1-x_1}\right)^{1/2}\right]^2\left[1 + \left(\frac{\partial \ln\hat{\phi}_1}{\partial \ln x_1}\right)_{T,P}\right] \tag{7.15}$$

Since $\mathscr{D}_{12}$ has units [Length^2/time] and α, [Mass x Time/Length^3] it is customary to define a "thermodynamic" diffusion coefficient that will equal $\mathscr{D}_{12}$ in ideal mixtures, in which case (Modell and Reid, 1983)

$$\left(\frac{\partial\hat{\mu}_i}{\partial \ln x_i}\right)_{T,P} = RT \tag{7.16}$$

or, in other words, when $\hat{\phi}$ is composition-independent.
Consequently,

$$\mathscr{D}_{12} = D_{12}\left[1 + \left(\frac{\partial \ln\hat{\phi}_1}{\partial \ln x_1}\right)_{T,P}\right] = \frac{D_{12}}{RT}\left(\frac{\partial\hat{\mu}_1}{\partial \ln x_1}\right)_{T,P} \tag{7.17}$$

or

$$D_{12} = \frac{\alpha RT}{M_1^2 c}\left[\left(\frac{1-x_1}{x_1}\right)^{1/2} + \frac{M_1}{M_2}\left(\frac{x_1}{1-x_1}\right)^{1/2}\right] \tag{7.18}$$

Little can be said about the actual values of D_{12} or α. It is normally assumed that D_{12} is less composition-dependent than $\mathfrak{D}_{12}$ (Reid et al. 1977). Taking this assumption to the limit, we can now explore the composition dependence of α, that is, we force α to satisfy

$$\frac{\alpha(x_1)}{c(x_1)}\left[\left(\frac{1-x_1}{x_1}\right)^{1/2}+\frac{M_1}{M_2}\left(\frac{x_1}{1-x_1}\right)^{1/2}\right]^2 \neq f(x_1) \tag{7.19}$$

or

$$\alpha = c(x_1)\left[\left(\frac{1-x_1}{x_1}\right)^{1/2}+\frac{M_1}{M_2}\left(\frac{x_1}{1-x_1}\right)^{1/2}\right]^{-2} f(T,P,\text{ solute, solvent}) \tag{7.20}$$

In other words, a concentration-independent D_{12} imposes upon α the requirement that if depend in x_1 as the dimensionless function

$$\Psi(x_1) = \frac{1+\frac{1}{c(o)}\int_o^{x_1}\left(\frac{\bar{V}_2-\bar{V}_1}{V^2}\right)dx}{\left[\left(\frac{1-x_1}{x_1}\right)^{1/2}+\frac{M_1}{M_2}\left(\frac{x_1}{1-x_1}\right)^{1/2}\right]^2} \tag{7.21}$$

where V is now a molar volume.

Since the numerator is finite, we note that Ψ vanishes at $x_1 \to 0$ and $x_1 \to 1$, in agreement with the fact that μ (and hence $\nabla\mu$) is an undefined quantity at $x_1 \to 0$ and $x_1 \to 1$. The numerator in Equation (7.21) is very specifically dependent upon the solute and solvent under consideration. Moreover, it will yield different numerical values depending on the equation of state used in its evaluation. Since, however, the numerator is a finite number, we can focus our attention on the denominator, a universal function of the weight ratio and mixture composition. Its behaviour is shown in Figure 7.1, where the function Ψ is plotted as a function of x for various values of M_1/M_2. At a mole fraction $x_1 = M_2/(M_1 + M_2)$, Ψ has a maximum value of $M_2/4\,M_1$.

Thermodynamic and phenomenological approaches to diffusion differ in one fundamental aspect, which goes well beyond unit conversion. For

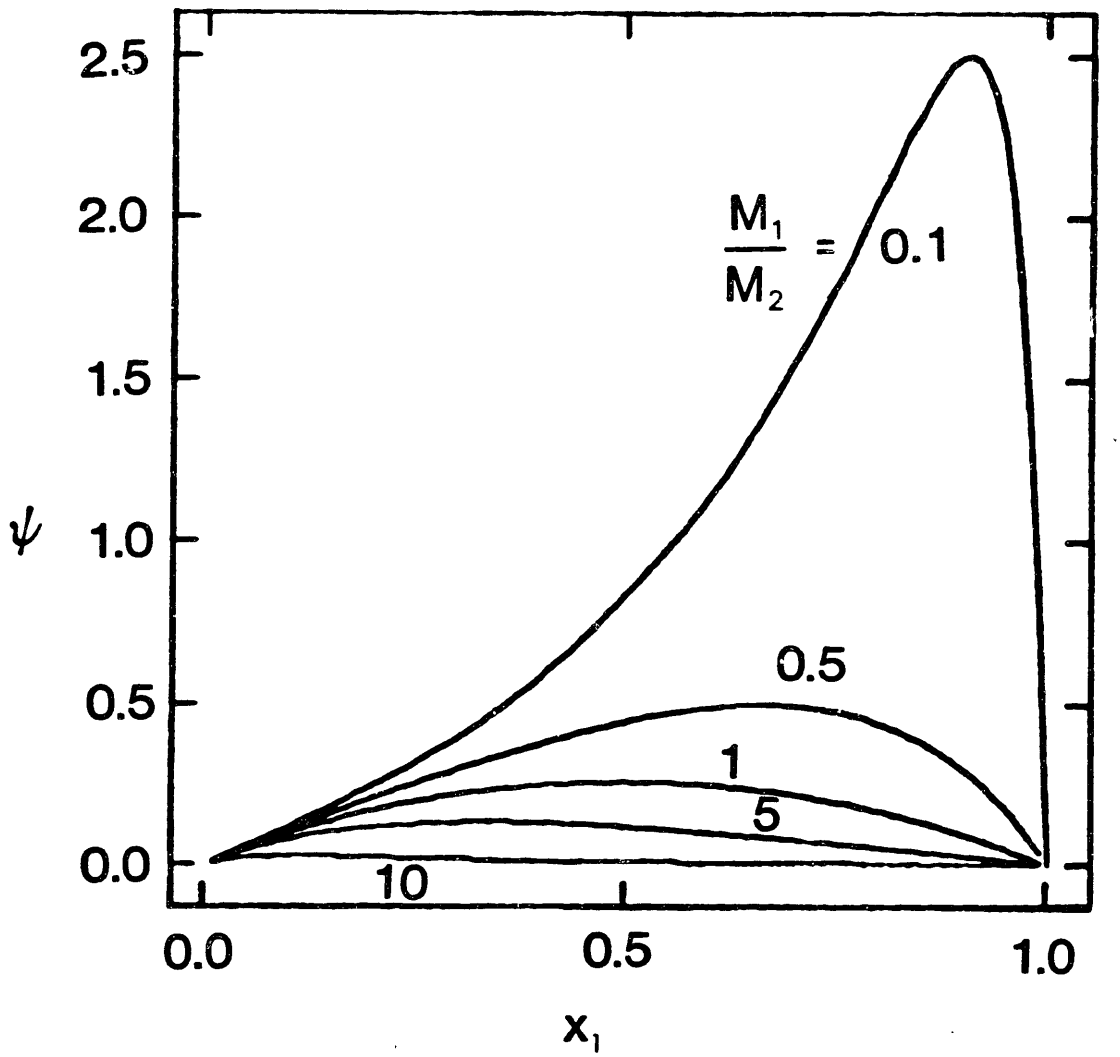

FIGURE 7.1: Universal part of the composition dependence of ψ for various weight ratios

a binary mixture, one of the many equivalent ways in which stability criteria can be expressed is (Modell and Reid, 1983)

$$\left(\frac{\partial \hat{\mu}_1}{\partial N_1}\right)_{T,P,N_2} = \frac{(N_2/N_1)RT}{N}\left[1 + \left(\frac{\partial \ln \hat{\phi}_1}{\partial \ln x_1}\right)_{T,P}\right] > 0 \qquad (7.22)$$

When the term in brackets becomes zero, the mixture reaches its limit of stability and a new phase is formed. Critical points are stable limits of stability. According to Equation (7.13), then, diffusive fluxes vanish at mixture critical points even when finite concentration gradients exist. (the same would be true for any limit of stability, but only critical points, being stable, make experimental verification simple).

The vanishing of diffusive fluxes at mixture critical points has been experimentally observed, (Tsekhanskaya (1968), Tsekhanskaya (1971)), and the results have often been reported in the light of Equation (7.14), that is, as vanishing phenomenological diffusion coefficients. From the previous discussion, it is obvious that phenomenological formulations of diffusion coefficients (i.e., Equation (7.14)) cannot account for this experimentally observed behaviour. At least in the limit where vanishing thermodynamic driving forces coexist with finite kinetic driving, forces, therefore, it appears that diffusion can be explained as an entropy generating relaxation process rather than as a kinetic phenomenon.

7.3 THE KINETIC CONVERSION FACTOR

The behaviour of the conversion factor $[1+(\partial \ln \hat{\phi}_1/\partial \ln x_1)_{TP}]$, henceforth called kinetic conversion factor, will now be analyzed. It will be assumed that the mixture under consideration can be described, in its equilibrium properties, through a cubic equation of state, for which the most general formulation is (Schmidt and Wenzel, 1980)(see Appendix 1).

$$P = \frac{RT}{V-b} - \frac{a}{V^2 + uVb + wb^2} \qquad (7.23)$$

In Equation (7.23), V is a molar quantity, u and w are numerical constants, and they vary with the particular equation of state being used. Mixture parameters a and b are obtained from pure component parameters by means of suitable mixing and combining rules, of which the most popular are (with i and j denoting i^{th} and j^{th} components, respectively,

$$a = x_i x_j a_{ij}$$

$$b = x_i b_i \tag{7.24}$$

$$a_{ij} = (a_i a_j)^{1/2} [1-k_{ij} (1-\delta_{ij})]$$

where k_{ij}, the binary interaction coefficient, is the single adjustable parameter once an equation of state is selected, and δ_{ij} is Kronecker's delta.

The methods for obtaining pure component parameters are summarized in Appendix 1, where tabulated values of v and w can also be found.

From the general thermodynamic relationship (where V is now extensive)

$$RT\ln \hat{\phi}_i = -\int_{\infty}^{V} [(\frac{\partial P}{\partial N})_{T,V,N[i]} - \frac{RT}{V}] dV - RT\ln Z \tag{7.25}$$

where N[i] means constancy of all mole numbers except for N_i, we obtain, with $A = a P/(RT)^2$; $A_{ik} = a_{ik} P/(RT)^2$; $B_i = b_i P/RT$, and $B = bP/RT$,

$$\ln \hat{\phi}_i = \frac{B_i}{B} (Z-1) - \ln (Z-B) + \frac{A}{B\sqrt{u^2-4w}} \left[\frac{2 \sum_k x_k A_{ik}}{A} - \frac{B_i}{B} \right] \ln \frac{Z + B \left(\frac{u-\sqrt{u^2-4w}}{2}\right)}{Z + B \left(\frac{u-\sqrt{u^2-4w}}{2}\right)} \tag{7.26}$$

which is valid for any cubic equation of state with mixing rules as per Equation (7.24) (provided both u and w are non-zero) and any composition and density-independent combining rule (note that A_{ik} is not defined in Equation (7.26)). From this we obtain, after considerable rearrangement

$$\left[1+\left(\frac{\partial \ln \hat{\phi}_1}{\partial \ln x_1}\right)_{T,P}\right] = 1 + x_1 \left(\frac{2\,\varepsilon}{B^4\sqrt{u^2-4w}} \ln \frac{Z + B\left(\frac{u-\sqrt{u^2-4w}}{2}\right)}{Z + B\left(\frac{u+\sqrt{u^2-4w}}{2}\right)} + \right.$$

$$\left. + (B_1-B_2)\left[\frac{B_1}{B^2}(B\eta+1-Z) - \frac{\eta-1}{Z-B} + \frac{\left(\frac{2\sum_k x_k A_{1k}}{B} - \frac{AB_1}{B^2}\right)(\eta B - Z)}{\left[Z+B\left(\frac{u-\sqrt{u^2-4w}}{2}\right)\right]\left[Z+B\left(\frac{u+\sqrt{u^2-4w}}{2}\right)\right]}\right]\right. \tag{7.27}$$

where

$$\varepsilon = (A_1-A_{12})B^3 - \{A_1x_1(2B_1-B_2) - A_2B_1(1-x_1) + A_{12}[B_1(2-3x_1) - B_2(1-x_1)]\}B^2$$
$$+ A(B_1-B_2)B_1\,B \tag{7.28}$$

$$\eta = \frac{\bar{V}_1-\bar{V}_2}{b_1-b_2} = \frac{A+(uZ+2wB)[1-(Z-B)]^2-2[1-(Z-B)]\left[\frac{x_1(A_{12}-A_1)-(1-x_1)(A_{12}-A_2)}{B_2-B_1}\right](Z-B)}{A - (2Z + uB)[1-(Z-B)]^2} \tag{7.29}$$

Equations (7.27)-(7.29) are only applicable to binary mixtures. It is hardly worth emphasizing that these expressions are, in principle, highly nonlinear in composition; in fact, x_1 appears not only in a non-trivial explicit form, but also, implicitly, through Z, A and B. However, for all of the dilute mixtures considered, the calculated kinetic conversion factor is a linear function of x_1, from infinite dilution to saturation, and for all of the equations of state tested (see below). Figure 7.2, for CO_2-Benzoic Acid at 308K and 280 bar (Peng-Robinson equation of state, k_{ij} = .0183) is typical. The significance of this observed behaviour follows at once from integration

$$1 + \left(\frac{\partial \ln \hat{\phi}_1}{\partial \ln x_1}\right)_{T,P} = 1 - K\,x_1 \tag{7.30}$$

$$\hat{\phi}_1(x_1) = \hat{\phi}_1^{\infty} \exp(-Kx_1) \tag{7.31}$$

where K is composition-independent, and

$$\hat{\phi}_1^{\infty} = \lim_{x_1 \to 0} \hat{\phi}_1(x) \tag{7.32}$$

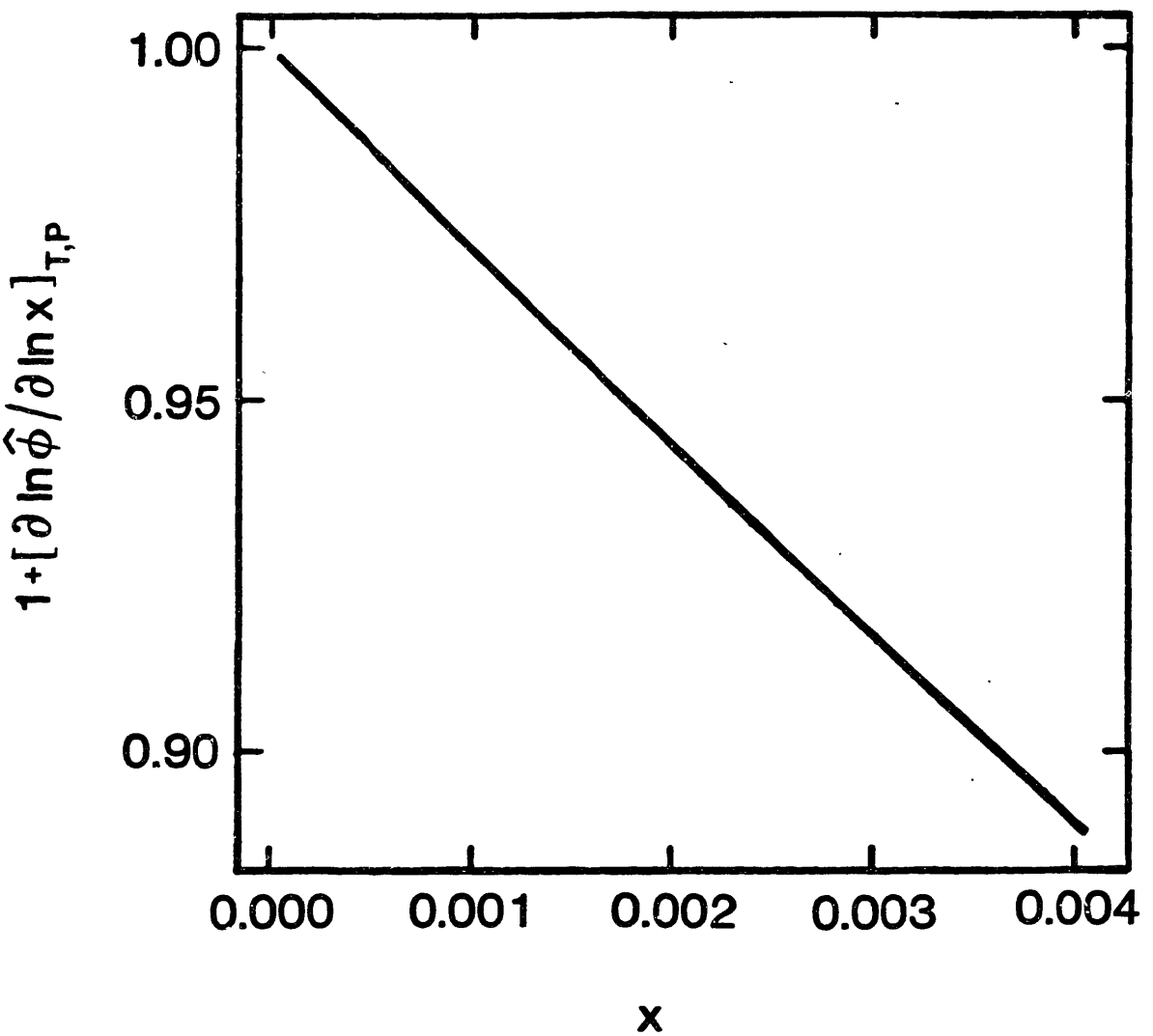

FIGURE 7.2: Composition dependence of the kinetic conversion factor from infinite dilution to saturation, as modelled by the Peng-Robinson equation of state, for CO_2-benzoic acid, at 308 K and 280 bar

In Equation (7.30), 1 has been substituted for the least-squares-regressed y-intercept, which in all cases, was greater than .999. Also, the composition-independence of $\hat{\phi}$ at low values of x has been verified in all cases. As an example, for CO_2-Benzoic Acid, the Peng-Robinson calculated $\hat{\phi}$ is 7.527×10^{-6} when $x = 10^{-10}$, and 7.525×10^{-6} when $x = 10^{-5}$, at 280 bar and 308K.

K has an interesting physical significance. Since the left hand side of Equation (7.30) vanishes at limits of stability, we write

$$1 - k\, x_1\, (\ell s.) = 0 \tag{7.33}$$

where $x_1(\ell.s.)$ is the solute mole fraction at which the mixture becomes unstable at the given T and P. In writing Equation (7.33) the assumption of a linear behaviour up to the limit of stability has been made; this is an obvious idealization, but a useful one in the present context. Equation (7.31) now becomes

$$\hat{\phi}_1\, (x_1,T,P) = \hat{\phi}_1^{\infty}\, (T,P) \exp\, [\, - x_1/x_1(\ell.s.)] \tag{7.34}$$

Within the limits of the idealization implicit in Equation (7.33), therefore, Equation (7.34) suggests a "natural" scaling of concentration, in analogy with the idea of corresponding states. Figure 7.3 is a plot of the fugacity coefficient of benzoic acid in supercritical CO_2 (308K; 280 bar; k_{ij} =.0183), from infinite dilution to saturation, calculated with Equation (7.26) and with the simplified exponential relationship (Equation (7.31)).

This remarkable agreement was observed in all of the cases tested (CO_2-benzoic acid; CO_2-2-naphthol; SF_6 - napthalene; SF_6-benzoic acid; $Pr \leq 3.4$, $1.01 \leq Tr \leq 1.1$; Peng-Robinson and Soave-Redlich Kwong equations of state).

The regressed K-values for the CO_2-Benzoic Acid system are shown in Figure 7.4 as a function of temperature and pressure. The binary interaction coefficients used in Figure 7.4 were obtained by minimizing the sum of the absolute values of $\log[x(k_{ij})] - \log[x(\text{experimental})]$ for each temperature. The experimental solubilities were taken from Kurnik (1981). The resulting values (used in Figure 7.4) are: 0.013856 (@308.2 K), 0.010308 (@318.2 K), -0.003336 (@ 328.2 K), -0.01272 (@338.2 K).

Figure 7.4 suggests that the fugacity coefficient becomes composition independent at low pressure. This is in agreement with the concept of infinite dilution fugacity coefficient, introduced above. More interestingly, though, K values approach a high pressure limit (at 280 bar, all K values are within 6.5% of the mean). If this behaviour is general, and K values can be predicted or correlated, this could simplify high pressure phase equilibrium calculations, apart from the intrinsic theoretical interest that such a trend would have.

K was found to be relatively insensitive to k_{ij} in all cases. For example, at 308 K and 120 bar, for the benzoic acid-CO_2 system, K=66.81477 for k_{ij} = .013856 (obtained by regressing experimental solubilities), and K = 68.13017 for k_{ij} = 00.

The fugacity coefficient, then, is the product of a composition-independent term ($\hat{\phi}_1^{\infty}$, the infinite dilution fugacity coefficient), and an exponential composition correction which is not only small, due to the small values of x_1, but appears to approach a high pressure limit which is independent of temperature.

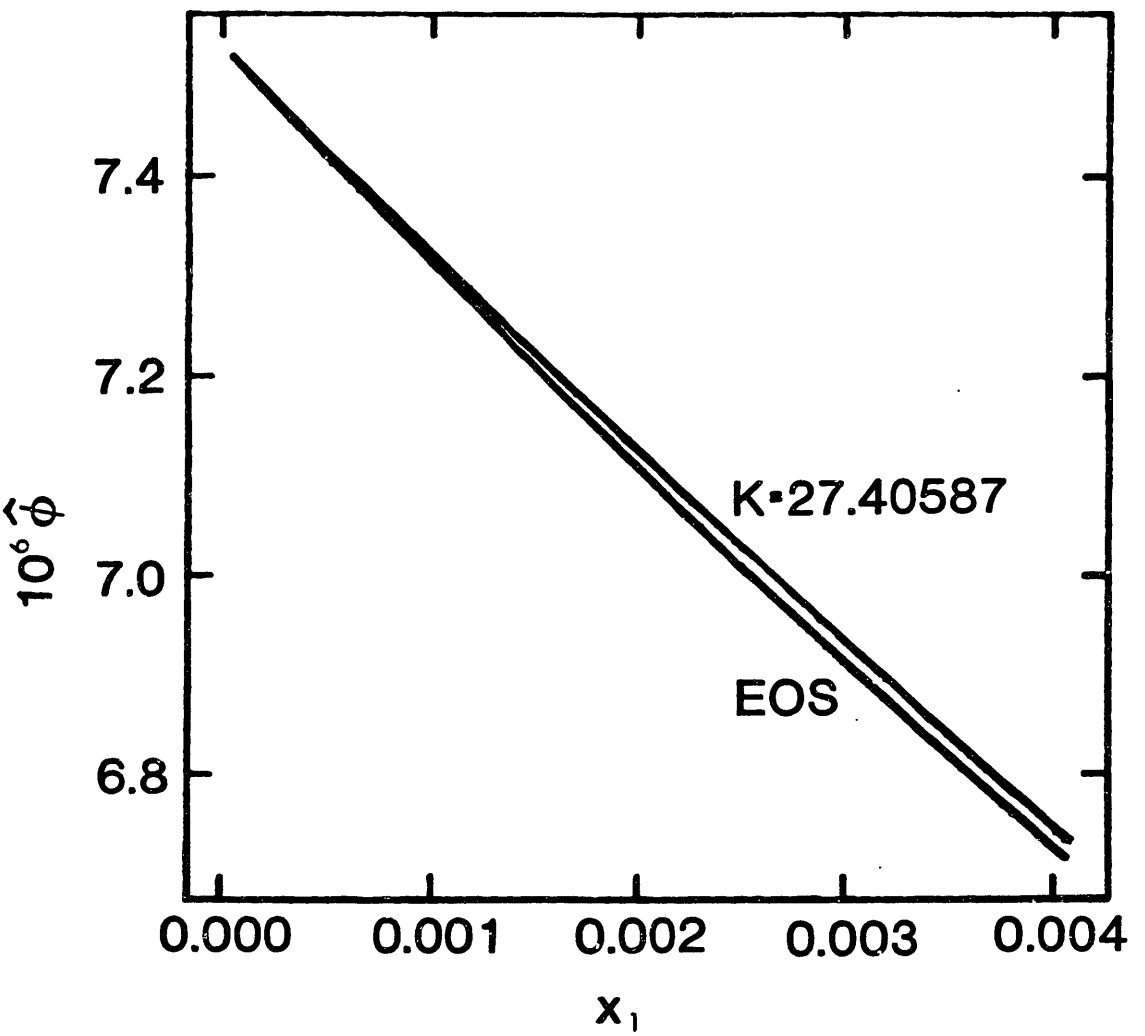

FIGURE 7.3: Fugacity coefficient of benzoic acid in CO_2, at 308 K and 280 bar, as a function of solute mole fraction, calculated with the Peng-Robinson equation of State (EOS), and with the exponential decay expression (K).

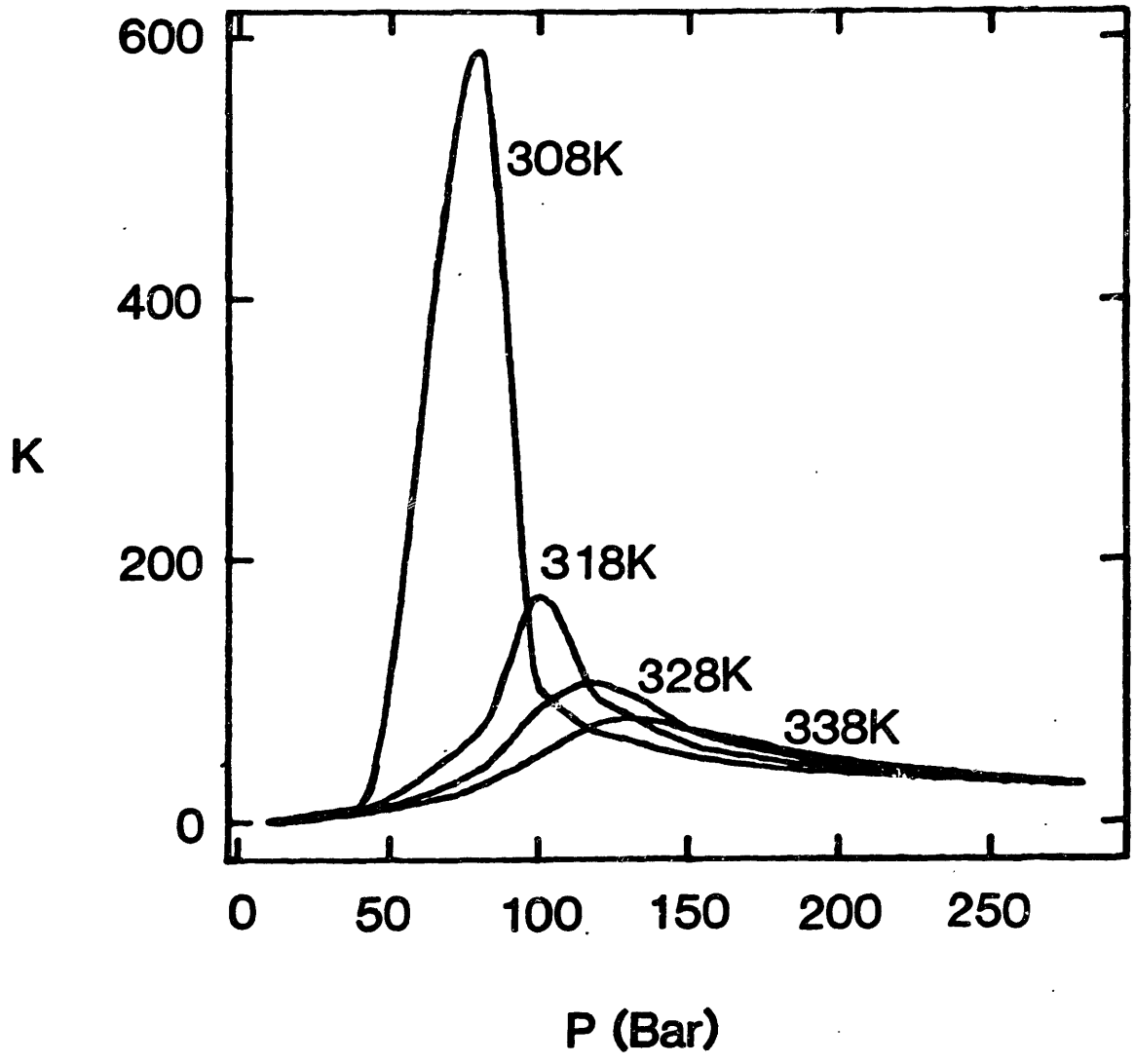

FIGURE 7.4: K values for the CO_2 benzoic acid system, as a function temperature and pressure.

DIFFUSION AND MASS TRANSFER IN SUPERCRITICAL FLUIDS

by

PABLO G. DEBENEDETTI

Ingeniero Químico Universidad de Buenos Aires
(1978)
S.M. Massachusetts Institute of Technology
(1981)

SUBMITTED TO THE DEPARTMENT OF
CHEMICAL ENGINEERING
IN PARTIAL FULFILLMENT OF THE REQUIREMENTS
FOR THE DEGREE OF

DOCTOR OF PHILOSOPHY

at the

MASSACHUSETTS INSTITUTE OF TECHNOLOGY

December 1984

Signature of author.....P. G. Debenedetti.....
Department of Chemical Engineering
December 1984

Certified by.....Robert C. Reid.....
Professor Robert C. Reid
Thesis Supervisor

.....Ulrich W. Suter.....
Professor Ulrich W. Suter
Thesis Supervisor

Accepted by.....Robert C. Reid.....
Chairman, Departmental Committee
on Graduate Studies

8 DYNAMICS OF INTERACTING BODIES : THEORETICAL FUNDAMENTALS

The dynamic simulation of a system of interacting bodies requires knowledge of the laws of classical mechanics for its implementation, and of statistical mechanics for its interpretation.

These will be discussed in this Chapter. The following sections constitute a convenient summary, where the theoretical basis of the work is presented in a concise and coherent form. It must be said at the outset, however, that the discussion, although self-contained, is by no means exhaustive, and references are given throughout to texts and articles dealing with each of the topics in detail.

8.1 KINEMATICS OF THE RIGID BODY

A rigid body is an idealization. It can be defined, when discrete, as a set of particles such that the distance between any two of them is constant. In what follows, molecules will be idealized as rigid polyatomics, that is, as point centers of force with no internal degrees of freedom.

In general, a rigid body has six degrees of freedom, this being the minimum number of independent quantities that must be specified in order to define uniquely the position of the system under investigation (Landau and Lifshitz, 1982). Three degrees of freedom pertain to the body's translational motion, and can be chosen as the coordinates of its center of mass as measured from an origin (x,y,z) fixed in space (the laboratory or inertial reference frame). The other three degrees of freedom pertain to the body's rotational motion, and describe the instantaneous angular orientation of a set of axes rigidly fixed to the body (x',y',z') with respect to the set of axes fixed in space. A possible choice of angular coordinates, known as Euler angles(θ,ψ,ϕ), is illustrated in Figure (8.1).

A vector $\underline{X}$ is transformed from the fixed to the moving frame (the latter being rigidly fixed to the body) by the linear relation

$$\underline{\underline{A}}\,\underline{X} = \underline{X}' \tag{8.1}$$

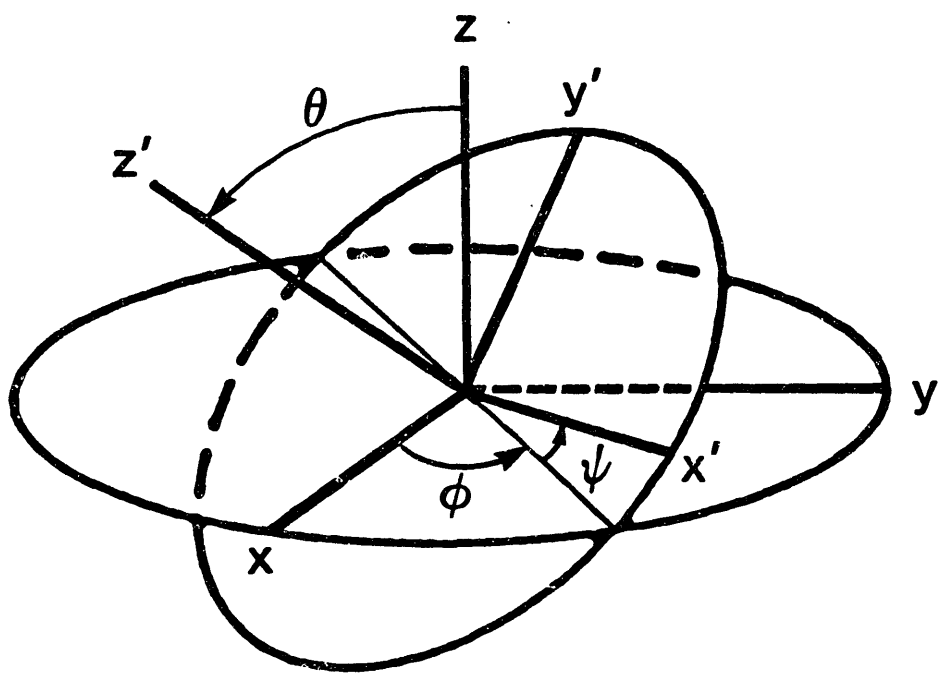

FIGURE 8.1 : Euler angles

where $\underline{\underline{A}}$ is an orthogonal transformation matrix, which , in terms of Euler angles, becomes

$$\underline{\underline{A}} = \begin{bmatrix} \cos\psi\cos\phi-\cos\theta\sin\phi\sin\psi & \cos\psi\sin\phi+\sin\psi\cos\phi\cos\theta & \sin\psi\sin\theta \\ -\sin\psi\cos\phi-\cos\psi\cos\theta\sin\phi & -\sin\psi\sin\phi+\cos\psi\cos\theta\cos\phi & \cos\psi\sin\theta \\ \sin\theta\sin\phi & -\sin\theta\cos\phi & \cos\theta \end{bmatrix} \qquad (8.2)$$

The explicit form of $\underline{\underline{A}}$ can be easily obtained as the product of the three elementary transformations defined by θ,ϕ and ψ.

The angular velocities can be expressed, in the x',y',z'system, in terms of $\dot{\phi},\dot{\psi},\dot{\theta}$, as follows (Goldstein,1981)

$$\begin{aligned} w_{x'} &= \dot{\phi}\sin\theta\sin\psi + \dot{\theta}\cos\psi \\ w_{y'} &= \dot{\phi}\sin\theta\cos\psi - \dot{\theta}\sin\psi \\ w_{z'} &= \dot{\phi}\cos\theta + \dot{\psi} \end{aligned} \qquad (8.3)$$

where,again,Equations (8.3) can be derived from elementary geometric considerations.Solving for $\dot{\phi},\dot{\theta},\dot{\psi}$, we obtain

$$\begin{aligned} \dot{\theta} &= w_{x'}\cos\psi - w_{y'}\sin\psi \\ \dot{\psi} &= w_{z'} - (1/\mathrm{tg}\theta)[w_{y'}\cos\psi + w_{x'}\sin\psi] \\ \dot{\phi} &= (1/\sin\theta)[w_{y'}\cos\psi + w_{x'}\sin\psi] \end{aligned} \qquad (8.4)$$

The expressions for the rate of change of ψ and ϕ diverge for small θ, making Euler angles unsuitable for numerical integration of the equations of motion. To overcome this problem,we introduce the so-called quaternions or Cayley-Klein parameters (Goldstein, 1981;Murad and Gubbins,1978)

$$
\begin{aligned}
e_o &= \cos\frac{\theta}{2}\cos\left[\frac{\psi+\phi}{2}\right] \\
e_1 &= \sin\frac{\theta}{2}\cos\left[\frac{\psi-\phi}{2}\right] \\
e_2 &= \sin\frac{\theta}{2}\sin\left[\frac{\phi-\psi}{2}\right] \\
e_3 &= \cos\frac{\theta}{2}\sin\left[\frac{\psi+\phi}{2}\right]
\end{aligned}
\tag{8.5}
$$

which satisfy

$$
\sum_{i=o}^{3} e_i^2 = 1 \tag{8.6}
$$

Differentiating Equations (8.5), and after considerable rearrangement, we obtain (Murad and Gubbins, 1978)

$$
\dot{\underline{e}} = \frac{1}{2}\,\underline{\underline{e}}\;\underline{w} \tag{8.7}
$$

where

$$
\dot{\underline{e}}^T = [\dot{e}_o;\dot{e}_1;-\dot{e}_2;\dot{e}_3] \tag{8.8}
$$

$$
\underline{w}^T = [w_x;w_y;w_z;\ o] \tag{8.9}
$$

$$
\underline{\underline{e}} = \begin{bmatrix} -e_1 & -e_2 & -e_3 & e_o \\ e_o & -e_3 & e_2 & e_1 \\ -e_3 & -e_o & e_1 & -e_2 \\ -e_2 & e_1 & e_o & e_3 \end{bmatrix} \tag{8.10}
$$

From the definitions (Equations (8.5)) of the Cayley-Klein parameters, we obtain

$$
\underline{\underline{A}} = \begin{bmatrix} (e_1^2+e_o^2-e_2^2-e_3^2) & 2(e_oe_3+e_1e_2) & 2(e_1e_3-e_oe_2) \\ -2(e_oe_3-e_1e_2) & (e_2^2+e_o^2-e_1^2-e_3^2) & 2(e_oe_1+e_2e_3) \\ 2(e_1e_3+e_oe_2) & -2(e_oe_1-e_2e_3) & (e_3^2+e_o^2-e_2^2-e_1^2) \end{bmatrix} \tag{8.11}
$$

Equation (8.7) is the quaternion equivalent of the Euler-based Equations (8.4), but is singularity-free, and thus provides a convenient and consistent kinematic description of the rigid body, which can be easily adapted to numerical integration of the equations of motion.

If a rigid body has a shape that justifies idealizing it as a line, the Euler angle or quaternion representation cannot be used, since a line has only two rotational degrees of freedom. The implications of this fact will be discussed below.

8.2 DYNAMICS OF THE RIGID BODY

The equations that describe the rotational motion of the rigid body assume a particularly concise form when the set of moving axes (x',y',z') coincide in direction with the body's principal axes of inertia, which will now be defined (Landau and Lifshitz, 1982).

Assuming the rigid body to be a discrete assembly of masses, the j,k^{th} component of the inertia tensor can be written as

$$I_{jk} = \Sigma m[(x_i')^2\delta_{jk} - x_j'x_k'] \tag{8.12}$$

where m denotes the generic discrete masses, the summation extending over all such masses, and x_j' is the j^{th} $(j=1,2,3)$ coordinate of the local mass with respect to a set of axes fixed to the body but otherwise undefined. The tensor defined by Equation (8.12) is symmetric and can always be diagonalized. The particular choice of (x',y',z') that diagonalizes the inertia tensor defines the principal directions; the diagonal elements are the principal moments of inertia.

The kinetic energy then becomes,

$$KE = \frac{(\Sigma m)v^2}{2} + \frac{1}{2}\left[I_1(w_1')^2 + I_2(w_2')^2 + I_3(w_3')^2 \right] \tag{8.13}$$

where v is the translational velocity of the center of mass, Σm is the total mass of the body, and 1,2,3 are the principal directions. As can be seen from Equation (8.13), the rotational contribution is now formally similar to the translational term.

The equations of motion can now be written , as follows. For translation, in the inertial reference frame,

$$\ddot{\underline{r}} = (\Sigma m)^{-1}\underline{f} \tag{8.14}$$

and for rotation, in the principal reference frame,

$$\dot{w}_i' = (I_i)^{-1}K_i' \tag{8.15}$$

where $\underline{r}$ is the position vector of the center of mass with respect to the inertial reference frame, $\underline{f}$ is the external force, i denotes the i^{th} (i=1,2,3) principal direction, and w_i', K_i' and I_i are therefore the i^{th} principal angular velocity, torque and moment of inertia, respectively.

Equations (8.14) and (8.15) are general, and are obviously independent of the kinematic description of the rigid body.

8.3 INTEGRATION OF THE EQUATIONS OF MOTION

The force $\underline{f}$ in Equation (8.14), and the principal torque component K_i' in Equation (8.15) are functions of the instantaneous position and orientation of all bodies in the system. Integration of these equations, therefore, requires expressions for the rate of change of the rotational coordinates, which will necessarily be explicit in the coordinates themselves. Thus, the expressions that will be introduced (the kinematic equations) are necessarily less general than the dynamic equations ((8.14) and (8.15)).

For a non-linear body, with quaternion kinematics, we have

$$\dot{\underline{v}} = (\Sigma m)^{-1}\ \underline{f}(\{\underline{r}\},\{e\})$$
$$\dot{\underline{x}} = \underline{v} \tag{8.16}$$

$$\dot{w}_i' = (I_i)^{-1}\ K_i'(\{\underline{r}\},\{e\}) \quad (i=1,2,3)$$
$$\dot{\underline{e}} = \frac{1}{2}\ \underline{\underline{e}}\ \underline{w}' \tag{8.17}$$

The translational equations have been written as two coupled first order equations, rather than as a single second order expression (Equation (8.14)). Also, in Equations (8.16), $\underline{f}(\{\underline{r}\},\{e\})$ denotes the dependence on all position vectors and quaternions of the force (the same is true for the torque in Equations (8.17)).

It is important to notice that Equations (8.16) are calculated in the inertial frame, whereas, in Equations (8.17), i denotes a principal direction. The torques are calculated in the inertial frame and then converted to principal torques using the quaternion-explicit form of $\underline{\underline{A}}$ (Equation (8.11))

$$\underline{K}' = \underline{\underline{A}}\ \underline{K} \tag{8.18}$$

Linear bodies have two rotational degrees of freedom; Equations (8.17) must therefore be modified. In this case, the rotational equations become

$$\dot{\underline{w}} = (I)^{-1}\ \underline{K}$$
$$\dot{\underline{l}} = \underline{w} \times \underline{l} \tag{8.19}$$

where I is now the non-vanishing principal moment of inertia and $\underline{l}$ is a unit vector, co-axial with the linear body, which specifies the instantaneous configuration of the line.

Equations (8.19) do not require a coordinate transformation, and are hence conveniently integrated in the inertial frame throughout.

The structure of the rotational Equations for a linear body follows from the fact that, for such a geometry,

$$I_1 = I_2$$

$$I_3 = 0 \qquad (8.20)$$

$$\dot{w}_3 = 0$$

i.e., two principal moments of inertia are equal and the third one vanishes; also, a line cannot rotate about its axis, and $\underline{w}$ must always lie on a plane perpendicular to the line's axis(Figure 8.2).

The actual integration of Equations (8.16) and (8.17) (or (8.19)) can be implemented in many different ways, according to the particular numerical algorithm selected.For the translational equations, a second order predictor-corrector method was chosen, with an Euler predictor and explicit trapezoid correctors,

$$\tilde{\underline{x}}^{(n+1)} = \underline{x}^{(n)} + \delta t\, \underline{v}^{(n)} \qquad (8.21)$$

$$\underline{v}^{(n+1)} = \underline{v}^{(n)} + (\Sigma m)^{-1}\, (\delta t/2)[\tilde{\underline{f}}^{(n+1)} + \underline{f}^{(n)}] \qquad (8.22)$$

$$\underline{x}^{(n+1)} = \underline{x}^{(n)} + (\delta t/2)[\underline{v}^{(n+1)} + \underline{v}^{(n)}] \qquad (8.23)$$

where $\tilde{}$ denotes predicted values, and $\tilde{\underline{f}}$ is calculated from the predicted translational and rotational coordinates. In Equations (8.21)-(8.23), the superscripts identify the integration step. For non-linear molecules,an explicit second order predictor-corrector method was also chosen,

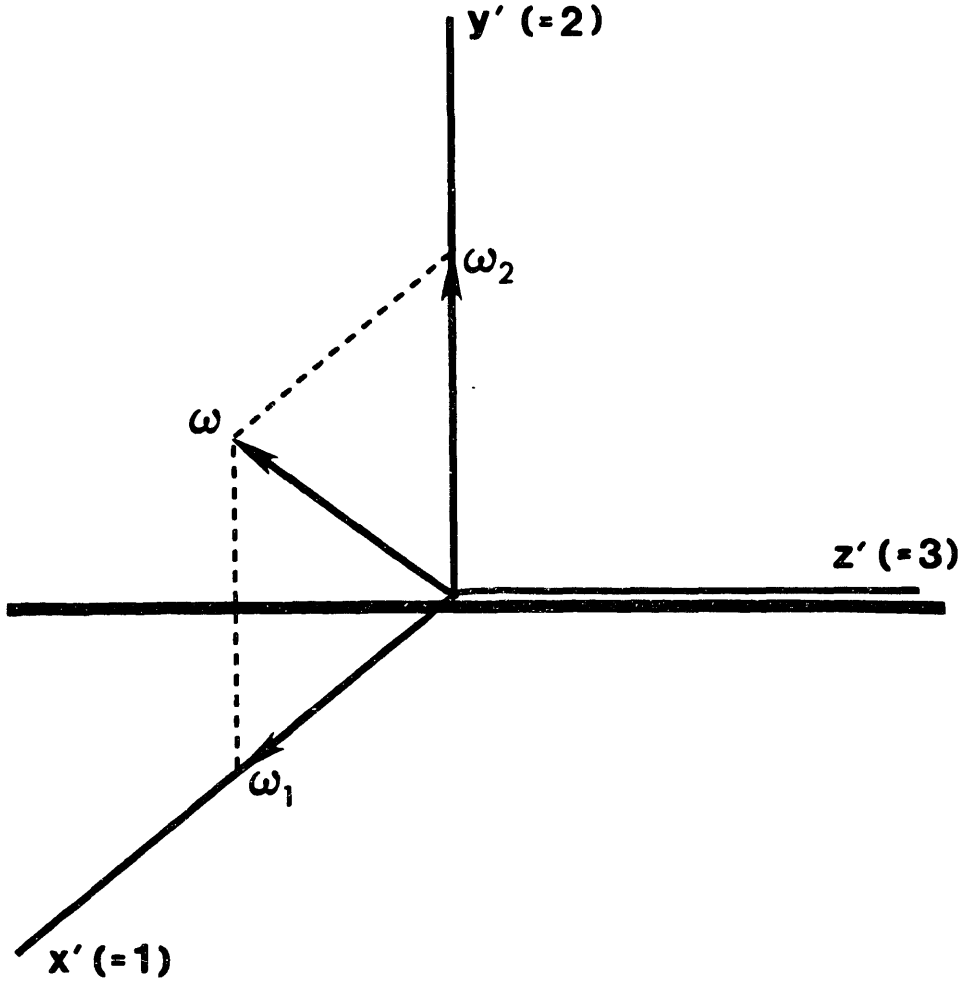

FIGURE 8.2 : Kinematic and dynamic characteristics of a linear rigid body

$$\tilde{\underline{e}}^{(n+1)} = \underline{e}^{(n)} + (\delta t/2)\, \dot{\underline{e}}^{(n)}(\underline{w}')^{(n)} \tag{8.24}$$

$$w_i'^{(n+1)} = w_i'^{(n)} + (I_i)^{-1}(\delta t/2)[(\tilde{K}_i')^{(n+1)} + (K_i')^{(n)}] \qquad (i=1,2,3) \tag{8.25}$$

$$\underline{e}^{(n+1)} = \underline{e}^{(n)} + (\delta t/4)[\tilde{\underline{e}}^{(n+1)}(\underline{w}')^{(n+1)} + \underline{e}^{(n)}(\underline{w}')^{(n)}] \tag{8.26}$$

where torques are first calculated in the inertial frame and then converted to principal torques using the quaternion-explicit form of the transformation matrix. Predicted torques are calculated from predicted coordinates and then converted from the inertial to the moving frame with the predicted transformation matrix.

For linear molecules, an implicit predictor-corrector scheme was chosen,

$$\tilde{\underline{l}}^{(n+1)} = \underline{l}^{(n)} + \delta t[\underline{w}^{(n)} \times \underline{l}^{(n)}] \tag{8.27}$$

$$\underline{w}^{(n+1)} = \underline{w}^{(n)} + (I)^{-1}(\delta t/2)[\tilde{\underline{K}}^{(n+1)} + \underline{K}^{(n)}] \tag{8.28}$$

$$\underline{l}^{(n+1)} = \underline{l}^{(n)} + (\delta t/2)[\underline{w}^{(n+1)} \times \underline{l}^{(n+1)} + \underline{w}^{(n)} \times \underline{l}^{(n)}] \tag{8.29}$$

where, as in Equation (8.25), predicted torques are calculated from predicted positions and orientations. Equation (8.29) is implicit as a consequence of the vector product in the right hand side; 3 simultaneous equations in $\underline{l}^{(n+1)}$ result.

8.4 STATISTICAL TREATMENT OF DIFFUSION

The stochastic approach to diffusion originated with Einstein's work

on the theory of Brownian motion (Einstein, 1905). Many alternative derivations of the basic relationships have since appeared, but Einstein's approach is still the simplest and most general. An illuminating and comprehensive treatment of the general area of stochastic processes can be found in Chandrasekhar's review article (Chandrasekhar, 1943).

We focus our attention on a mixture of particles of species 1 and 2, and consider the limiting case where the concentration of species 1 is so small that we can neglect 1-1 interactions. We consider a time interval, $\Delta\tau$, with the following characteristics: $\Delta\tau$ is small with respect to observed, macroscopic time, but large enough so that the velocity of any particle at a time t is independent from its velocity at a time $t-\Delta\tau$,

$$\langle \underline{v}(t+\Delta\tau).\underline{v}(t)\rangle = \langle \underline{v}(\Delta\tau).\underline{v}(0)\rangle = 0 \tag{8.30}$$

If we now identify particles with molecules, and $\Delta\tau$ with a characteristic time for a molecular interaction, then, upon observation at time intervals $\geq\Delta\tau$, the system must be described statistically rather than in a deterministic way.

At thermal equilibrium, the displacement, δ, of type 1 molecules during an interval $\Delta\tau$, projected upon any arbitrary direction, x, is subject to a probability distribution, ϕ_1, which must satisfy

$$\begin{aligned} \phi_1(\delta_x) &= \phi_1(-\delta_x) \\ \int_{-\infty}^{+\infty} \phi_1(\delta_x)\, d(\delta_x) &= 1 \end{aligned} \tag{8.31}$$

where symmetry follows from a zero net flux condition, and normalization implies that molecules must be found somewhere in space. The function ϕ_1 itself is defined in such a way that the number of molecules of species 1 that, during an interval $\Delta\tau$, experience x-displacements between δ_x and $\delta_x + d(\delta_x)$, is given by

$$dN_1(\delta_x) = N_1\, \phi_1(\delta_x)\, d(\delta_x) \tag{8.32}$$

where N_1 is the total number of type 1 molecules under consideration.

Let $f_1(x,t)$ be the z,y-averaged number of particles of species 1 per unit volume at a time t and location x. Then, we write

$$f_1(x,t+\Delta\tau) = \int_{-\infty}^{+\infty} f_1(x+\delta_x,t)\ \phi_1(\delta_x)\ d(\delta_x) \tag{8.33}$$

Equation (8.33) assumes that the kinematic description of the system at a time $t + \Delta\tau$ is independent of the system's history prior to time t. This is the single major assumption in Einstein's derivation, and, in the language of stochastic processes, is equivalent to saying that the evolution in time of $f_1(x,t)$ is a Markow chain (van Kampen, 1981).

Expanding both sides of Equation (8.33) in Taylor series,

$$f_1(x,t) + \frac{\partial f_1}{\partial t}\Delta\tau + ... =$$

$$\int_{-\infty}^{+\infty}[f_1(x,t) + \frac{\partial f_1}{\partial x}\delta_x + \frac{1}{2}\frac{\partial^2 f_1}{\partial x^2}(\delta_x)^2 + ...]\ \phi_1(\delta_x)\ d(\delta_x) \tag{8.34}$$

and taking into account that

$$\int_{-\infty}^{+\infty} f_1(x,t)\ \phi_1(\delta_x)\ d(\delta_x) = f_1(x,t)\int_{-\infty}^{+\infty}\phi_1(\delta_x)\ d(\delta_x) = f_1(x,t) \tag{8.35}$$

$$\int_{-\infty}^{+\infty}(\frac{\partial f_1}{\partial x})\ \delta_x\ \phi_1(\delta_x)\ d(\delta_x) = \frac{\partial f_1}{\partial x}\int_{-\infty}^{+\infty}\delta_x\ \phi_1(\delta_x)\ d(\delta_x) = 0 \tag{8.36}$$

we obtain

$$\frac{\partial f_1}{\partial t} = \left[\frac{1}{2\Delta\tau}\int_{-\infty}^{+\infty}(\delta_x)^2\ \phi_1(\delta_x)\ d(\delta_x)\right]\frac{\partial^2 f_1}{\partial x^2} \tag{8.37}$$

Since ϕ_1 is a probability distribution, Equation (8.37) can be rewritten as

$$\frac{\partial f_1}{\partial t} = \frac{\langle \delta_x^2 \rangle}{2\Delta\tau} \frac{\partial^2 f_1}{\partial x^2} \tag{8.38}$$

Equation (8.38), on the other hand, is a species-1 conservation equation, so we may at once write,

$$D_{12} = \frac{\langle \delta_x^2 \rangle}{2\Delta\tau} \tag{8.39}$$

or, taking into account that, since x is arbitrary and ϕ_1 symmetric,

$$\langle \delta_x^2 \rangle = \langle \delta_y^2 \rangle = \langle \delta_z^2 \rangle = \frac{\langle \delta^2 \rangle}{3} \tag{8.40}$$

$$D_{12} = \frac{\langle \delta^2 \rangle}{6\Delta\tau} \tag{8.41}$$

Equation (8.41) is the fundamental relationship to be used in the calculation of diffusion coefficients via molecular dynamics.

It is important to realize that at no point in the present derivation was the assumption of Brownian particles (i.e., particles so large that species 2 becomes a continuum relative to species 1) introduced. Although Einstein himself derived Equation (8.39) while considering Brownian motion, the major advantage of this approach is precisely the generality and plausibility of the assumptions on which it rests.

The short-time ($t < \Delta\tau$) behaviour of the system cannot be described with this treatment. An analytical equation covering the whole time range can be obtained for the special case of Brownian particles.

By splitting the force on a Brownian particle into a deterministic frictional force, proportional and opposed to the particle's velocity, and a stochastic component representative of random collisions with the

molecules that make up the continuum, (species 2) we can write a stochastic differential equation (Langevin's equation)

$$\dot{\underline{v}} = -\beta \underline{v} + \underline{A}(t) \tag{8.42}$$

from which we obtain (Chandrasekhar, 1943)

$$\langle \delta^2 \rangle \alpha [\beta t - 1 - \exp(-\beta t)] \tag{8.43}$$

For $t \to \infty$,

$$\langle \delta^2 \rangle \alpha t \tag{8.44}$$

and for $t \to 0$, expanding the exponential up to second order and simplifying,

$$\langle \delta^2 \rangle \alpha t^2 \tag{8.45}$$

It is obvious that, in writing Langevin's equation, we are introducing important restrictions which are not present in the original Einstein treatment. The long and short-time limits, however, have a fundamental significance that is independent of the assumptions built into their derivation.

For a generic particle (molecule), we write

$$\underline{\delta}(t) = \left(\frac{\partial \underline{\delta}}{\partial t}\right)_o t + \left(\frac{\partial^2 \underline{\delta}}{\partial t^2}\right)_o \frac{t^2}{2} + \ldots \tag{8.46}$$

For $t \to 0$, we can drop quadratic terms. Squaring, ensemble averaging, and using equipartition,

$$\langle \delta^2 \rangle = \frac{3kT}{m} t^2 \tag{8.47}$$

where m is the mass of the particles over which the averaging is done.

Without making any assumptions on the relative size and mass of the particles under consideration, we can say that, for times which are short with respect to the characteristic inter-particle interaction time, the dynamics is deterministic, since it can be described by Equation (8.46), and then $\langle\delta^2\rangle \alpha t^2$.

Since Equation (8.46) is time-reversal-invariant, we can call this a reversible or deterministic regime. Irreversibilities associated with molecular motion, on the other hand, are characterized by $\langle\delta^2\rangle \alpha t$, and we conclude that the onset of irreversible, stochastic behaviour, requires a finite amount of time, characteristic of interparticle interaction times. If species 2 can be regarded as a continuum, we can readily identify β^{-1} with $\Delta\tau$ (Chandrasekhar, 1943). Each degree of freedom, then, contributes to the entropy over a time greater than a characteristic relaxation time. Entropy is meaningless for $t \ll \Delta\tau$.

In Equation (8.42), and assuming the Brownian particles to be spherical, then β is given by Stokes' law,

$$\beta = \frac{6\pi\eta a}{m} \tag{8.48}$$

where η is the viscosity of the medium, a is the radius and m, the mass of the particles.

8.5 VELOCITY DISTRIBUTIONS

We define a distribution function by saying that the number of molecules of species i which, at time t, have velocities within an interval $d\underline{v}$ of $\underline{v}$ and positions within an interval $d\underline{r}$ of $\underline{r}$, is given by

$$dN_i(\underline{r},\underline{v},t) = f_i(\underline{r},\underline{v},t)\, d\underline{r}\, d\underline{v} \tag{8.49}$$

where N_i is the total number of species i molecules in the system under investigation. At equilibrium, f_i is independent of position and

time-invariant, so we write

$$n_i = \int f_i(\underline{v})\, d\underline{v} \tag{8.50}$$

where n_i is now referred to unit volume and the integral is three-dimensional and extends over all possible velocities, i.e. from $-\infty$ to $+\infty$ for each component.

The particular functional dependence that corresponds to equilibrium is the Maxwell-Boltzmann distribution,

$$f_i(\underline{v}) = n_i \left[\frac{m_i}{2\pi kT}\right]^{3/2} \exp\left[-\frac{m_i(\underline{v}.\underline{v})}{2kT}\right] \tag{8.51}$$

For a fixed volume, V, containing N_i molecules of species i, the number of molecules having velocities within a range $d\underline{v}$ of $\underline{v}$ is given by

$$dN_i = V\, f_i\, d\underline{v} = 4\pi\, V\, v^2\, f_i\, dv \tag{8.52}$$

or

$$\frac{dN_i}{dv} = 4\pi\, N_i \left[\frac{m_i}{2\pi kT}\right]^{3/2} v^2 \exp\left[-\frac{m_i v^2}{2kT}\right] \tag{8.53}$$

which is maximized for

$$v^* = \left[\frac{2kT}{m_i}\right]^{1/2} \tag{8.54}$$

The distribution f_i has a root mean square velocity,

$$v_{rms} \equiv \left[\frac{\int d^3v\, v^2\, f_i}{\int d^3v\, f_i}\right]^{1/2} = \left[\frac{3kT}{m_i}\right]^{1/2} = \langle v^2 \rangle^{1/2} \tag{8.55}$$

a mean velocity,

$$\langle v \rangle = N_i^{-1} \int_0^\infty 4\pi v^2 f_i \, dv = \left[\frac{8kT}{m_i}\right]^{1/2} \tag{8.56}$$

and a standard deviation,

$$\langle \sigma^2 \rangle^{1/2} = \left[N_i^{-1} \int_0^\infty 4\pi v^2 [v - \langle v \rangle]^2 f_i \, dv\right]^{1/2} = \left[\left(\frac{3\pi - 8}{\pi}\right) \frac{kT}{m_i}\right]^{1/2} \tag{8.57}$$

As will be explained later, setting the root mean square velocity to unity is a convenint way of defining a simulation time scale (having previously defined a simulation length scale; see Chapter 9). Then, Equation (8.53) becomes

$$\frac{dN_i}{dv} = \frac{4(3/2)^{1.5}}{\pi^{1/2}} N_i \, v^2 \exp(-1.5 \, v^2) =$$

$$= 4.146 \, N_i \, v^2 \exp(-1.5 \, v^2) \tag{8.58}$$

Equation (8.58) is plotted in Figure 8.3, with $N_i = 107$, which is the number of solvent molecules used in the simulations.

8.6 EQUIPARTITION AND VIRIAL THEOREM

For a system of N bodies with ξ degrees of freedom per body, the equipartition theorem (Huang, 1963) can be written as

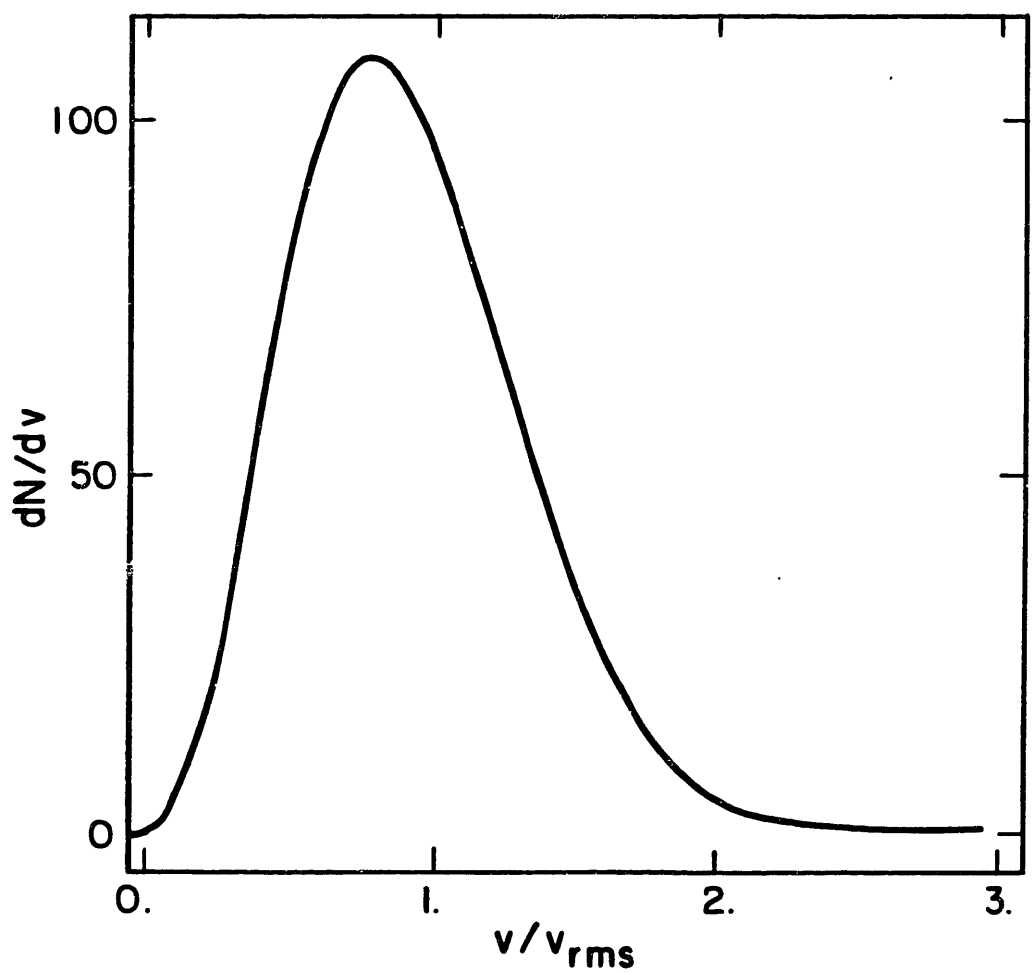

FIGURE 8.3 : Maxwell-Boltzmann velocity distribution; N=107

$$\langle p_i \frac{\partial H}{\partial p_i} \rangle = kT$$
$$\langle q_i \frac{\partial H}{\partial q_i} \rangle = kT \tag{8.59}$$

where p_i and q_i ($i = 1,\ldots,\xi N$) are generalized momenta and coordinates, and H is the system's Hamiltonian (i.e., its energy expressed as a function of coordinates and momenta). For smooth spherical or point bodies with no rotational degrees of freedom, $\xi = 3$ and $\underline{q}$ and $\underline{p}$ are simply the position and linear momentum vectors, respectively. For rigid bodies, $\xi = 6$ and $\underline{q}$ is a vector whose six components are the three cartesian coordinates of the center of mass with respect to an inertial reference frame and the three components of the rotation vector (Landau and Lifshitz, 1982) along the body's principal directions, while $\underline{p}$ is a vector whose six components are, respectively, the cartesian components of the body's linear momentum in the inertial frame, and the principal angular momentum components. Conjugate momenta and coordinates satisfy Hamilton's equations,

$$\frac{\partial H}{\partial q_i} = -\dot{p}_i \quad (i = 1,\ldots,\xi N)$$
$$\frac{\partial H}{\partial p_i} = \dot{q}_i \quad (i = 1,\ldots,\xi N) \tag{8.60}$$

Restricting our attention to the translational degrees of freedom, we consider the sum

$$\sum_{i=1}^{3N} q_i\, p_i = \Gamma \tag{8.61}$$

$$\dot{\Gamma} = \sum_{i=1}^{3N} \dot{q}_i\, p_i + \sum_{i=1}^{3N} \dot{p}_i\, q_i \tag{8.62}$$

Time-averaging,

$$\langle \dot{\Gamma} \rangle = \lim_{\tau \to \infty} \frac{1}{\tau} \int_0^{\infty} \dot{\Gamma}\, dt = \lim_{\tau \to \infty} \frac{1}{\tau} \left[\Gamma(\tau) - \Gamma(0) \right] \tag{8.63}$$

but, since Γ is not unbounded, we must have

$$\langle \dot{\Gamma} \rangle = 0 \tag{8.64}$$

which simply states the fact that the time average of a derivative of a finite quantity vanishes.

Taking into account Equations (8.64), (8.60), and (8.59),

$$\left\langle \sum_{i=1}^{3N} \dot{p}_i\, q_i \right\rangle = - \left\langle \sum_{i=1}^{3N} \dot{q}_i\, p_i \right\rangle = - \left\langle \sum_{i=1}^{3N} \frac{\partial H}{\partial p_i}\, p_i \right\rangle = -3NkT = - 2\langle KE(t) \rangle \tag{8.65}$$

where KE(t) is the translational kinetic energy. The left hand side of Equation (8.65) is the time average of the sum, over all bodies, of the scalar product of external force and position.
This can be written as the sum of two terms,

$$\left\langle \sum_{i=1}^{3N} \dot{p}_i\, q_i \right\rangle = -P \oint \underline{r}.\underline{n}'\, dF + \left\langle \sum_{i=1}^{3N} q_i\, f_i \right\rangle \tag{8.66}$$

The first term is the contribution of the collisions against the bounding surface, with $\underline{r}$ denoting not the coordinates of a molecule, but a location on the bounding surface, $\underline{n}'$ is a unit normal vector, and F denotes the bounding surface. The second summation, then, is the contribution of intermolecular forces, $\underline{f}$. We can transform the surface integral,

$$-P \oint \underline{r}.\underline{n}' \, dF = -P \int (\nabla.\underline{r}) \, dV = -3PV \tag{8.67}$$

and rewrite Equation (8.65),

$$2 \langle KE(t) \rangle + \left\langle \sum_{i=1}^{3N} q_i \, f_i \right\rangle = 3PV \tag{8.68}$$

Dividing by $2\langle KE(t)\rangle$,

$$\frac{3PV}{2\langle KE(t)\rangle} = 1 + \frac{\left\langle \sum_{i=1}^{3N} q_i \, f_i \right\rangle}{2\langle KE(t)\rangle} \tag{8.69}$$

or, equivalently,

$$Z = 1 + \frac{\left\langle \sum_{i=1}^{3N} q_i \, f_i \right\rangle}{2\langle KE(t)\rangle} = 1 + \frac{\left\langle \sum_{j=1}^{N} \underline{q}_j.\underline{f}_j \right\rangle}{2\langle KE(t)\rangle} \tag{8.70}$$

If the interparticle forces are pairwise additive, the summation can be expressed in a computationally convenient way,

$$\sum_{i=1}^{3N} q_i \, f_i = \sum_{j=1}^{N} \underline{q}_j.\underline{f}_j = \sum_{j=1}^{N} \underline{q}_j . \sum_{i \neq j} \underline{f}_{ji} = \sum_{i=1}^{N-1} \sum_{j=i+1}^{N} \underline{f}_{ij}.(\underline{q}_i - \underline{q}_j) \tag{8.71}$$

i.e., as the sum of the products of interparticle forces and interparticle separations. Equation (8.70) then becomes,

$$Z = 1 + \frac{\left\langle \sum_{i=1}^{N-1} \sum_{j=i+1}^{N} \underline{f}_{ij}.(\underline{q}_i - \underline{q}_j) \right\rangle}{2\langle KE(t)\rangle} \tag{8.72}$$

where $\underline{f}_{ij}$ is the net force on particle i exerted by particle j, and $(\underline{q}_i - \underline{q}_j)$ is a vector directed from j to i. The double sum is therefore positive when interactions are, on the average, repulsive, and negative when they are attractive.

9. COMPUTER SIMULATIONS; TECHNICAL ASPECTS

9.1 SAMPLE SIZE; BOUNDARY CONDITIONS; CUTOFF RADIUS

The goal of molecular dynamics is the study of the bulk properties of matter. This is done by following the motion of an ensemble of molecules and interpreting the "results" (i.e., the evolution in time of velocities, forces, positions, orientations and torques) statistically (see Chapters 8 and 10 for fundamentals and results, respectively).

The first question that must be addressed, therefore, is the number of molecules that will be considered in the simulation. Since we are studying bulk matter, it is obvious that this number should be as high as possible. For pairwise additive, continuously differentiable potentials, the simulation is simply a repetitive procedure whereby, at each step, every molecule "scans" all other molecules in the system, and, due to pairwise additivity,

$$\underline{F}_i = \sum_{j \neq i} \underline{f}_{ij} \tag{9.1}$$

where $\underline{F}_i$ is the net force on the ith molecule, and $\underline{f}_{ij}$ is the force exerted by the jth molecule on the ith molecule.

In the presently considered case, however, molecules are really rigidity constraints, and the forces are interatomic, so that Equation (9.1) is really computed as

$$\underline{F}_i = \sum_{j \neq i} \left[\sum_{\eta \epsilon i} \sum_{\xi \epsilon j} \underline{f}_{\eta\xi} \right] = \sum_{j \neq i} \underline{f}_{ij} \tag{9.2}$$

where η and ξ now denote atoms. Thus, for N molecules with n atoms per molecule, each integration step involves, in principle, S elementary evaluations

$$S = \frac{N(N-1)n^2}{2} \tag{9.3}$$

As will be explained below, the density of the simulated fluid has a strong influence on the average duration of a "scan", but, for the present purposes, or, at any rate, at a given density, the duration of a simulation is a quadratic function of the sample size and of molecular complexity, as measured by the number of sites per molecule.

The other factor influencing the duration of a simulation is the integration step, which is determined by numerical accuracy considerations. The run duration is only a linear function of the number of integration steps. Consequently, it is the number and complexity of the molecules that determines the size of the problem (given an event of fixed duration to be simulated).

Even with supercomputers, currently solvable problems are limited to $N \sim O(10^3)$, with n between 1 and 5, and simulations are used to study events that last $\sim 10^{-11}$ seconds, at typical liquid densities (Ceperley, 1981).

In the present case, N = 108, with one solute and 107 solvent molecules. For CO_2 as a solvent and C_6H_6 as, a solute, S = 54891 elementary evaluations per integration step, or a total of $\sim 1.7 \times 10^8$ evaluations per simulation (for a 3000 step simulation).

The choice of appropriate boundary conditions is the next important question that must be addressed. A possible choice would be to enclose the N molecules inside a perfectly reflecting rigid surface of arbitrary shape. This approach, however, suffers from a major drawback. For a spherical boundary of radius R and an effective interaction range Δr, the fraction of molecules interacting with the surface is $3\Delta r/R$. In general, the fraction of molecules that, at any given time, interact with the boundary surface is directly proportional to the product of the effective interaction range and the surface-to-volume ratio, which, in turn, is inversely proportional to some characteristic length. For a typical molecular dynamics simulation at liquid-like densities, the characteristic length can be estimated as

$$\left[\frac{1000 \text{ molecules} \times 5\times10^{-5} \text{ m}^3/\text{mol}}{6.02\times10^{23} \text{molecules/mol}}\right]^{1/3} \times 10^{10} \approx 40 \text{ Å}$$

which means that the fraction of molecules interacting with the rigid boundaries is ~ 3×10^6 times higher than in a 1 cm^3 macroscopic system, for any given effective interaction range.

This problem can be overcome by using periodic boundary conditions, which have been used in molecular dynamics since the method was originally proposed (Wainwright and Alder, 1958; Alder and Wainwright, 1959). In this approach, computations take place in a unit cell which repeats itself in space. Whenever a molecule leaves the cell, it is replaced by an "image" which enters through the opposite boundary. This is shown in Figure 9.1 for a two dimensional system with a quadrangular unit cell. Thus, periodic boundary conditions not only eliminate the artificial influence of the boundary surface, but, in effect, treat the system as infinite, although with an arbitrary periodicity assumption. In the presently considered case, the unit cell is a cube, since the problem is three-dimensional. Because of the periodicity imposed by the boundary conditions, a molecule and its images are never moved independently. Instead, in considering the interaction between any two molecules a-b (see Figure 9.1), only the closest of all possible a-b pairs must be taken into account ($a\text{-}b_4$ or $b\text{-}a_5$ in Figure 9.1; the choice between these two is arbitrary and one may conveniently assign a number to each molecule and, by convention, look at interactions between i and the possible images of j, including j itself, if $i < j$, and viceversa).

Periodicity thus introduces an important limitation: because, as explained above, a molecule and its images are not independent, the range of the intermolecular (or, in the present case, interatomic) potential cannot be infinite. This follows from simple geometric reasoning. Consider particle a (Figure 9.1) and let the cell side have unit size. Coordinates can be measured from any arbitrary origin: let us place the origin at the cell's corner nearest to a, and denote vertical coordinates by y, and horizontal coordinates by x. Then, it is obvious that, whenever

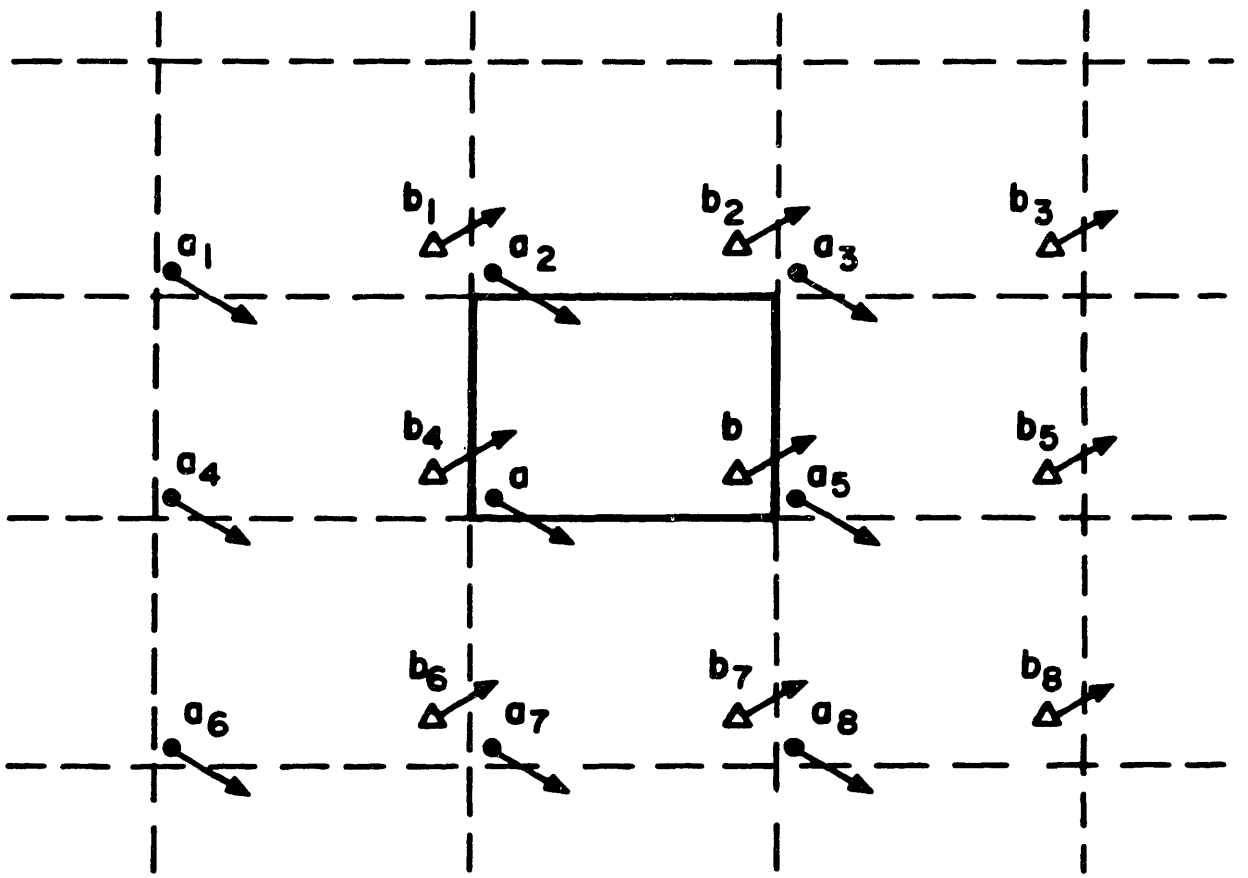

FIGURE 9.1 : Two dimensional periodic boundary conditions

$|x_b - x_a| > 1/2$, and only when this condition is met, an image b_i of b exists such that

$$|x_b - x_a| > |x_{bi} - x_a| \tag{9.4}$$

Similar considerations apply to the y (and z, in three dimensions) coordinates, so we conclude that, to avoid double counting between a molecule and its images, the range of the interparticle potential cannot exceed half the cell side's length. In the presently considered case, a and b would represent molecules, (or, more specifically, their centers of mass). Having located the closest pair, and only then, are atomic interactions taken into account. Since, for N = 108, there are 5778 pairs, and, in three dimensions, 27 possible images per pair, it follows that an efficient algorithm for locating closest pairs without actually calculating all possible distances is mandatory. Such an algorithm is shown in Figure 9.2, for a cubic cell.

The actual cutoff radius is determined more conservatively than the above considerations would suggest. When simulating the dynamics of rigid polyatomics, the cutoff distance must obey

$$r_c < \frac{1}{2} - (\sigma_a + \sigma_b) \tag{9.5}$$

where the σ's denote the maximum possible distance between a molecule's center of mass and any one of its sites. Thus, this conservative criterion guarantees that the closest possible distance between atoms of molecule a and atoms of molecule b, when b has been discarded in favor of one of its images, will never equal the cutoff radius. Since any finite cutoff distance represents a distortion of physical reality, the extreme form of Equation (9.5) may have to be relaxed whenever σ is large, at the expense of introducing slight inaccuracies in the program. In the present work, a cutoff radius of 7.4 Angstrom was used throughout (see Figure 10.1 for molecular geometry).

There is, of course, nothing fundamental about the cubic shape of the unit cell. It merely provides a simple geometric description, and

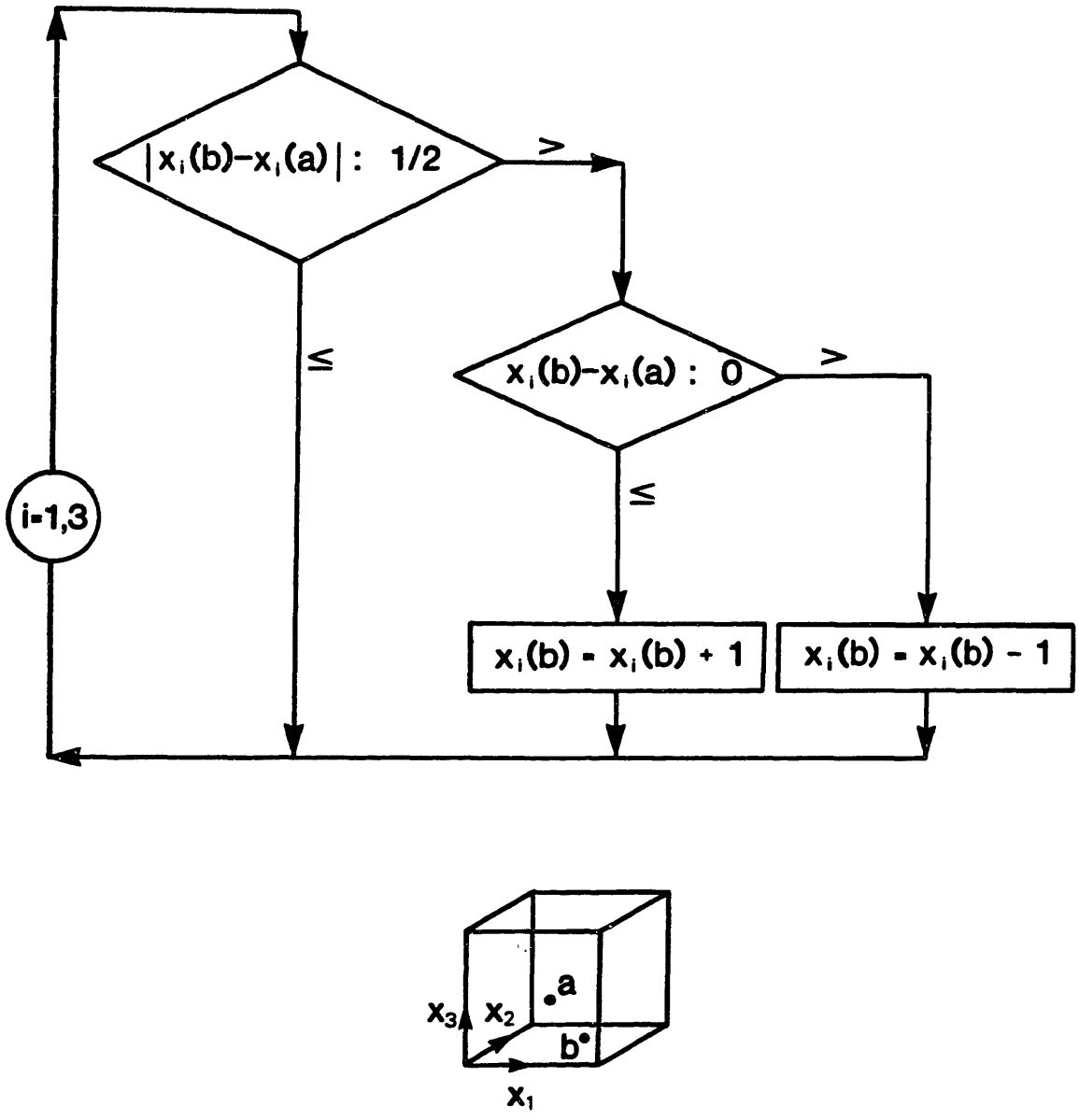

FIGURE 9.2 : Nearest image location in a three dimensional cubic cell

a convenient start-up lattice "backbone": the molecular centers of mass are arranged in a face-centered cubic lattice. This structure can be generated by spatial repetition of a unit cube containing occupied sites in four different positions (Figure 9.3). The simulation takes place in a cube of unit size which contains 1^3 elementary units such as the one depicted in Figure 9.3. Thus, molecular dynamics simulations with 32, 108, 256,..., 41^3, ... etc. molecules are common. The details of the start-up procedure are discussed in Section 9.3.

Periodic and bulk matter are obviously not equivalent concepts, although this assumption is built into the choice of periodic boundary conditions. At present, however, there is no better approach to the problem of simulating bulk matter using a small number of particles. An interesting question arises when we consider the possible influence of the unit cell's geometry upon the results. Although systematic studies have not been made, this problem should be of particular concern when molecular dynamics is used to study fluid-solid phase transitions, for example, where symmetry considerations play an important role. Thus, one can imagine simulations taking place in polyhedric space-filling unit cells, or, even more simply, in deformed cubic cells (parallelepiped cells, for example; Theodorou and Suter,1984).

In principle, one would hope the computed relaxation, transport and equilibrium properties of fluids to be independent of these considerations. This is strongly suggested by the good agreement with experiment obtained so far with molecular dynamics, unless we assume that cubic symmetry is more than an accidental choice, and disordered, isotropic matter can only be described with particular choices of symmetries, an unlikely but fascinating possibility.

9.2 TIME CONSIDERATIONS

In the area of molecular modelling of matter, computer time considerations are of fundamental importance. Without an efficient code, the simulations quickly become prohibitively expensive, and, in extreme cases, too long even in the absence of computer time cost constraints.

The core of a molecular dynamics simulation, as explained in section

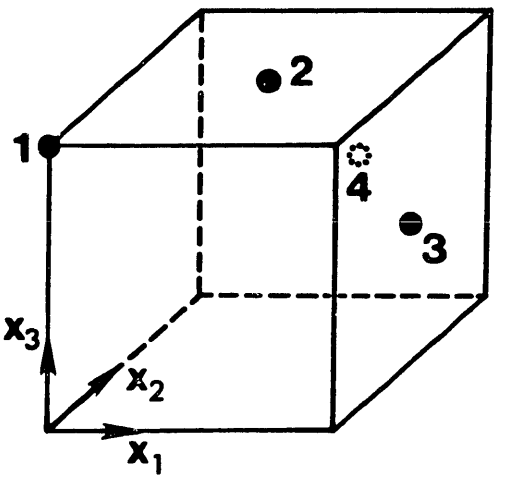

	X_1	X_2	X_3
1	0	0	1
2	1/2	1/2	1
3	1	1/2	1/2
4	1/2	1	1/2

FIGURE 9.3 : Elementary generator of face centered cubic lattice

9.1, is the "scanning" procedure, which is repeated $N(N-1)n^2/2$ times per step, or for large N, ~ $(Nn)^2/2$ times. Hence, all efforts to improve code efficiency should be focused on this part of the program.

The optimization of the N(N-1)/2 nearest image scans was already discussed and is shown in Figure 9.2. Having located the nearest image, n^2 site-site interactions must now be computed. The first step, therefore, is to check whether the particular site-site distance considered falls within the cutoff radius. Important time savings follow if the cube-sphere scan (Figure 9.4) is implemented. In this approach, the site-site distance is only calculated if each of the components of the site-site separation is less than r_c in absolute value. This is equivalent to constructing a cube of side 2 r_c whose center of symmetry coincides with one of the sites (one eighth of which is shown in Figure 9.4), such that all sites falling outside its boundaries are rejected. This cube, then, is the geometric equivalent of a necessary but not sufficient condition for a site-site separation to be $\leq r_c$. The sufficient condition, a concentric sphere of radius r_c, is then introduced, but only after having rejected all sites which do not obey the necessary condition. In addition, since a distance is the square root of the sum of three squares, the sufficiency condition is tested with respect to the square of the cutoff distance, so that a rejected site does not cause the unnecessary computation of a square root.

The last part of each elementary "scan" involves the actual calculation of a force and, if needed, an energy. Explicit calculation of the resulting expressions (see Section 9.4) would make the program prohibitively slow and inefficient. To overcome this problem, the force and potential are tabulated at the beginning of the program. There are as many tables as there are different types of site pairs (i.e., O-O, C-C, O-C for pure CO_2, simulations for example). The range $0 < r \leq r_c$ is divided into a sufficiently fine "grid" (typical simulations employ ~ 10^4 elements per table). The site separation is then assigned an integer value, I, according to

$$I = INT\ (M*R/RC) \qquad (9.6)$$

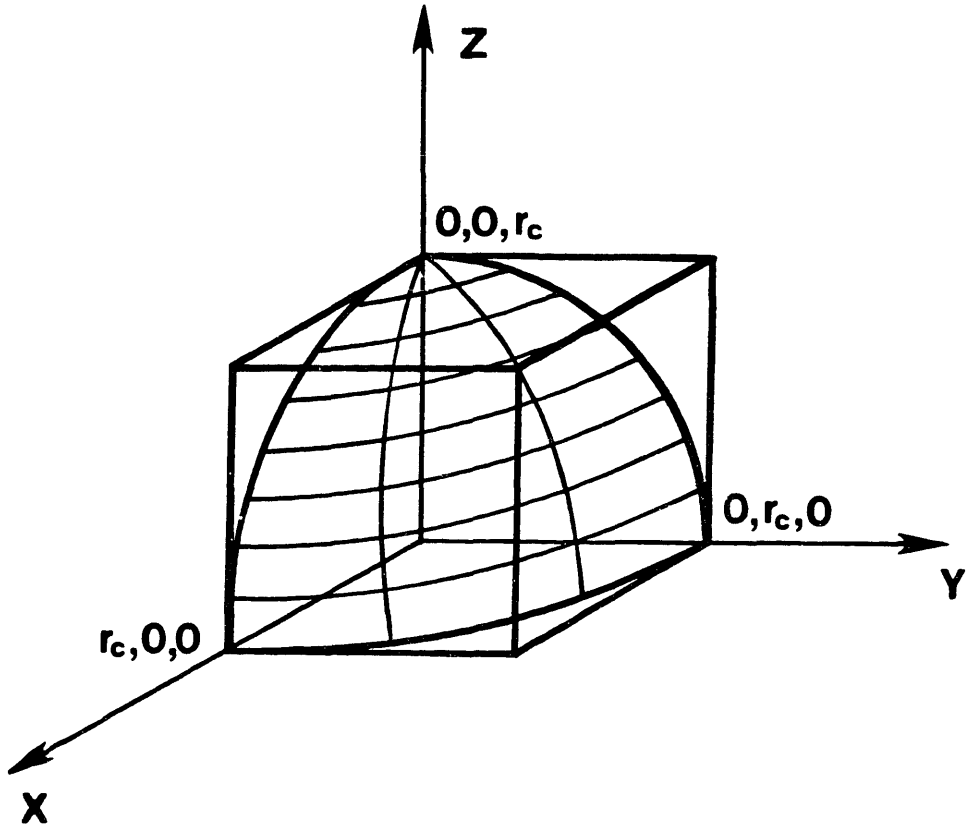

FIGURE 9.4 : Cube-sphere site-site distance test

where M is the number of elements into which the range $0 \leq r \leq r_c$ is divided, 6000 in the present work. Since M is such a high number, linear interpolation is not necessary and the force and potential calculation are therefore simply table look-ups.

To summarize, the $N(N-1)n^2/2$ "scans" per integration step constitute the rate-limiting step of the simulation, and have been optimized by

- logical nearest image search (i.e., with no algebraic operations) (Figure 9.2)
- cube-sphere site-site test (Figure 9.4)
- potential and force tabulation

The influence of density upon the duration of a run follows directly from the above considerations, once it is realized that, for a given cutoff radius, the number of sites within a sphere of radius r_c scales as the fluid density. The higher the density, then, the higher the proportion of sites for which computations have to be made, or, in other words, the lower the proportion of cube-sphere time saving rejections.

9.3 START-UP; RESCALING; RELAXATION RUNS

There are two different start-up modes: strict start-up and continuation. In strict start-up, the centers of mass of the molecules are placed in a face-centered cubic lattice, and random orientations and velocity components are assigned to them (see subroutines PUT, TURN, START, in Appendix 4). The magnitude of both angular and linear velocities are the equipartition values, i.e.,

$$v_{\text{start-up}} = (3kT/m)^{1/2} \tag{9.7}$$

$$w_{\text{start-up}} = (2kT/I)^{1/2} \tag{9.8}$$

where Equation (9.8) corresponds to the case of a linear molecule. For the general case,

$$[w_{\text{start-up}}]_i = (kT/I_i)^{1/2} \quad (i = 1,2,3) \tag{9.9}$$

where i denotes one of the principal directions. The continuation mode is used most of the time (i.e., for all of the actual simulations and most of the "relaxation" runs). Here, the initial configuration (cartesian and angular coordinates) and velocities (translational and rotational) are read from a file, generated at the end of the previous run, where this information is stored.

"Relaxation" runs are shorter (typically 500 to 800 steps) than the actual simulations. During a "relaxation" run, the system is allowed to reach an equilibrium state either from a highly ordered condition (strict start-up), or from the final state of a previous run at different conditions (continuation).

Whereas the density in any given simulation is fixed by defining a length scale (Å/simulation length units) and the number of molecules in the cube, the temperature fluctuates, since it is given by the kinetic energy

$$\langle KE(t) \rangle = \frac{3NkT}{2} \tag{9.10}$$

$$\langle KE(r) \rangle = [2(N-1) + 3] \frac{kT}{2} \tag{9.11}$$

$$\langle kT \rangle = \frac{2 \langle KE(r) + KE(t) \rangle}{(5N+1)} \tag{9.12}$$

where (N-1) linear solvent molecules and 1 non-linear solute molecule have been assumed, and KE(r) and KE(t) denote, respectively, rotational and translational kinetic energy. Since there is no reason why T will coincide with the desired value, velocities (both linear and angular) are repeatedly rescaled during a relaxation run, so as to force the system's configuration to equilibrate at the desired temperature.

The rescaling frequency is set at the beginning of the run with ten steps between rescalings a typical value. Rescaling factors are calculated as follows: let T^* be the desired temperature; then, the instantaneous total kinetic energies will, in general, be different from their equipartition

values

$$\frac{2[KE(t)]}{3NkT^*} = \alpha \neq 1 \tag{9.13}$$

$$\frac{2[KE(r)]}{3NkT^*} = \beta \neq \frac{2}{3} + \frac{1}{3N} \tag{9.14}$$

Since kinetic energies are quadratic in velocites, each linear velocity component is rescaled by a factor $\alpha^{-1/2}$, and each angular velocity component is rescaled by a factor $\beta^{-1/2}$

$$v_i(n+1) = v_i(n) \left(\frac{1}{\alpha}\right)^{1/2} \quad [i = 1, \ldots, 3N] \tag{9.15}$$

$$w_j(n+1) = w_j(n) \left(\frac{1}{\beta}\right)^{1/2} \quad j = [1, \ldots, 2(N-1) + 3] \tag{9.16}$$

9.4 INTERATOMIC POTENTIALS

The assumed form of the interatomic (or intermolecular) potential is an input to any molecular dynamics simulation.

Most of the early work involved the idealization of molecules as point centers of force interacting via pairwise additive, spherically symmetric potentials, such as the square-well (Alder and Wainwright, 1959), hard sphere (Wainwright and Alder, 1958), or Lennard-Jones (Rahman, 1964) models. Three-body interactions were first taken into account (Haile, 1978) via a triple dipole Axilrod-Teller potential.

Two different approaches regarding intermolecular potential parameters were followed in these studies. In the first approach, no attempt was made to simulate the behavior of any particular fluid; rather, the abstract Lennard-Jones or hard sphere fluids, for example, were considered as models, and their properties investigated (Verlet, 1968; Alder and Wainwright, 1962; Alder et al.,1974). These early idealizations, however, were also applied to the study of specific atomic fluids (Rahman, 1964) due to the inherent plausibility of the spherically symmetric, one-center

assumption for this particular case.

The simulation of rigid polyatomic molecules (i.e., point centers of force with no internal degrees of freedom), requires the specification of appropriate interatomic potentials. In addition, choosing the shape of the polyatomic implies abandoning the abstract approach whereby an idealized fluid (i.e., Lennard-Jones, for example), is simulated in favor of a more concrete and realistic description of a given particular fluid. What is gained in detail and predictive power is lost in generality. Although the specificity of the problem imposes severe restrictions upon the choice of interatomic potential parameters, fundamental knowledge is, in this case, even more limited than for intermolecular potential parameter estimation. Table 9.1 lists some of the approaches that have been used to select appropriate potential parameters.

We may summarize the situation by saying that molecules without significant electrostatic effects are usually modelled as multi-centered polyatomics with sites interacting via pairwise additive Lennard-Jones-type potentials; parameter selection is far from standardized, with fitting techniques still widely used. The lack of fundamental significance for the site-site parameter values is clearly shown from the fact that F-F (Singer, et al., 1977) and C-C (Murad and Gubbins, 1978) parameters had to be significantly altered (Nose and Klein, 1983) to fit the volumetric properties of CF_4.

Electrostatic effects are even more problematic. Here, the choice is between a more fundamental description involving localized point monopoles, or the use of multipole expansions. The first of these approaches (Rossky and Karplus, 1979) will be discussed below; apart from stability considerations, long-range Coulombic forces are not inherently appropriate for use with periodic boundary conditions. The use of multipoles, on the other hand (Murthy, et al., 1981) is a contradiction in terms, since it assigns certain features to the potential on an a-priori basis, the simulation of which is the very essence of the molecular dynamics approach.

In this work, site-site Lennard-Jones potentials were used, although the introduction of coulombic interactions, as will be discussed below,

TABLE 9.1: SITE-SITE POTENTIALS IN MOLECULAR DYNAMICS; PREVIOUS WORK

Van der Waals	Electrostatic	Molecule	Reference
2 site Lennard-Jones Parameters fitted to internal energy and P-V-T data		N_2	Cheung & Powles, 1975
1 site Lennard-Jones Parameters modified from previous potentials on an ad-hoc basis	4 point monopoles with modulating function	H_2O	Stillinger & Rahman, 1974
2 site Lennard-Jones Parameters modified from literature recommendations based on lattice properties		F_2, Cl_2, Br_2, CO_2	Singer et al. , 1977
5 site Lennard-Jones Parameters fitted to energy, pressure and specific heat		CH_4	Murad & Gubbins, 1978
2 site Lennard-Jones 2 site 9-6 potential 3 site Lennard-Jones Parameters fitted to lattice energy and second virial coefficient	Point quadrupole magnitude fitted to lattice energy and second virial coefficient	CO_2	Murthy et al., 1981
5 site Lennard-Jones Parameters modified from Murad & Gubbins, 1978, and Singer et al., 1977, to fit PVT data		CF_4	Nose & Klein, 1983

was also studied. Since the use of periodic boundary conditions is incompatible with infinite range potentials, truncation is necessary. In a simulation where all forces are conservative i.e., where

$$\underline{f} = - \frac{\partial U}{\partial \underline{r}} \tag{9.17}$$

with $\underline{f}$ any force and U an appropriate potential, energy is inherently conserved except for numerical inaccuracies. Therefore, truncation must always be done with this constraint in mind (unless the cutoff radius is increased to a point where this effect is negligible, with the consequent sharp increase in computation time). The shifted force potential (Street et al., 1978), shown schematically in Figure 9.5 and used in this work, is defined as follows

$$F_m = - \left[\frac{dU}{dr} + \frac{dU}{dr} \right]_{r = r_c} \qquad r \leq r_c \tag{9.18}$$

$$F_m = 0 \qquad r > r_c \tag{9.19}$$

$$U_m = - \int_{\infty}^{r} F_m(r)\, dr \tag{9.20}$$

where, for the Lennard-Jones case,

$$U = 4\varepsilon \left[\left(\frac{\sigma}{r}\right)^{12} - \left(\frac{\sigma}{r}\right)^{6} \right] \tag{9.21}$$

$$F = \frac{24\varepsilon}{\sigma} \left[2 \left(\frac{\sigma}{r}\right)^{13} - \left(\frac{\sigma}{r}\right)^{7} \right] \tag{9.22}$$

and therefore,

$$U_m = 4\varepsilon\left(\frac{\sigma}{r_c}\right)^6 \left\{ \left(\frac{\sigma}{r_c}\right)^6 \left[\left(\frac{r_c}{r}\right)^{12} - 1\right] - \left[\left(\frac{r_c}{r}\right)^6 - 1\right] + 6\left(\frac{r}{r_c} - 1\right) \left[2\left(\frac{\sigma}{r_c}\right)^6 - 1\right] \right\} \tag{9.23}$$

$$F_m = \frac{24\varepsilon}{\sigma} \left\{ 2\left(\frac{\sigma}{r}\right)^{13} \left[1 - \left(\frac{r}{r_c}\right)^{13}\right] - \left(\frac{\sigma}{r}\right)^7 \left[1 - \left(\frac{r}{r_c}\right)^7\right] \right\} \tag{9.24}$$

F_m and U_m, both through the definition (Equations (9.18) and (9.20)) and through the explicit expressions (Equations (9.22) and (9.24)) satisfy the energy conservation condition, i.e. Equation (9.17).

The Lennard-Jones force has a minimum of

$$\frac{r}{\sigma} = \left(\frac{26}{7}\right)^{1/6} = 1.244455 \tag{9.25}$$

whence

$$| F_{min} | = 2.396429\ \varepsilon/\sigma \tag{9.26}$$

so that a percent normalized force error can be defined

$$100\ \frac{|F_m - F|}{|F_{min}|} = 1001.49\ \left| \left(\frac{\sigma}{r_c}\right)^7 - 2\left(\frac{\sigma}{r_c}\right)^{13} \right| \tag{9.27}$$

Similarly, we define a percent normalized potential error,

$$100\ \frac{|U_m - U|}{\varepsilon} = 400 \left\{ \left(\frac{\sigma}{r_c}\right)^{12} - \left(\frac{\sigma}{r_c}\right)^6 + 6\left(\frac{r}{r_c} - 1\right) \left[\left(\frac{\sigma}{r_c}\right)^6 - 2\left(\frac{\sigma}{r_c}\right)^{12}\right] \right\} \tag{9.28}$$

The error in the shifted force is independent of r, in agreement with Equation (9.18), and is only a function of σ/r_c. The error in the

SHIFTED FORCE POTENTIAL (Streett et al., 1978)

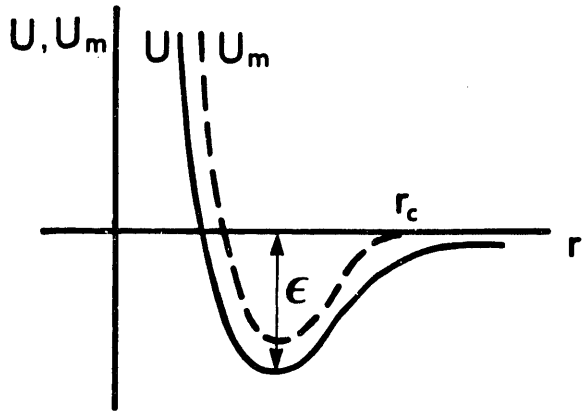

$$U_{LJ} = 4\epsilon\left[\left(\frac{\sigma}{r}\right)^{12} - \left(\frac{\sigma}{r}\right)^{6}\right]$$

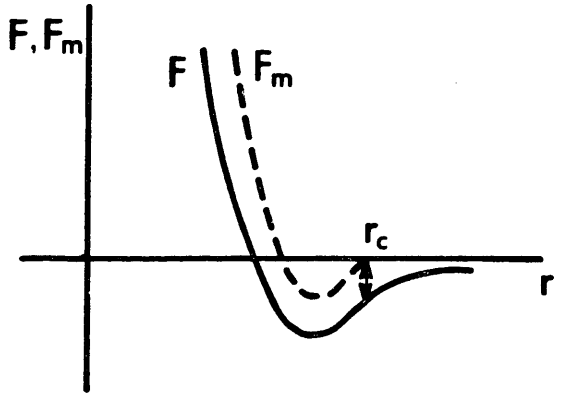

$$F_{LJ} = \frac{24\epsilon}{\sigma}\left[2\left(\frac{\sigma}{r}\right)^{13} - \left(\frac{\sigma}{r}\right)^{7}\right]$$

$$\begin{cases} F_m = -U_r' + U_r' \Big]_{r=r_c} & r \leq r_c \\ F_m = 0 & r > r_c \\ U_m = -\int_{\infty}^{r} F_m(r)\,dr \end{cases}$$

FIGURE 9.5 : The shifted force potential

potential, on the other hand, depends on r/r_c as well as on σ/r_c.

The true and shifted Lennard-Jones potentials are shown in Figure 9.6, for $r_c/\sigma = 2.4$, and Equation (9.28) is plotted in Figure 9.7 as a function of r/σ, for $2.3 < r_c/\sigma < 3.05$, covering the range used in the simulations. Equation (9.27) is shown in Figure 9.8.

As can be seen, very small errors result from using shifted potentials for $r_c/\sigma \geq 2.4$, and no discontinuities are introduced that would violate Equation (9.17). Truncation does, however, give rise to computed compressibilities which are slightly higher than would result from an infinite potential, since a weak attractive background has been artificially removed. If the radial distribution function can be taken as 1 for $r > r_c$, then, for spherical molecules, the attractive tail can be easily introduced by adding analytical correction to Equation (8.72), namely

$$\begin{array}{l}\text{long-range compressibility}\\ \text{correction for spherical}\\ \text{molecules}\end{array} = \frac{4\pi}{2[1<KE(t)>]} \cdot N \int_{r_c}^{\infty} r^3 \, n \left(- \frac{\partial U}{\partial r} \right) dr \qquad (9.29)$$

where n is a number density, and U is the intermolecular potential. An angular-average potential should be used in the above expression for non-spherical molecules.

$$<U(r)> = \frac{\int U \, e^{-U/kT} d\phi}{\int e^{-U/kT} d\phi} \qquad (9.30)$$

Given the largely empirical way in which interatomic potential parameters have been selected in the past (see Table 9.1), it was one of the objectives of the present work to use a theoretical approach rather than to fit parameters to fluid properties. The Slater-Kirkwood equation (Pitzer, 1959; Equation (9.32)) allows the calculation of site-site parameters

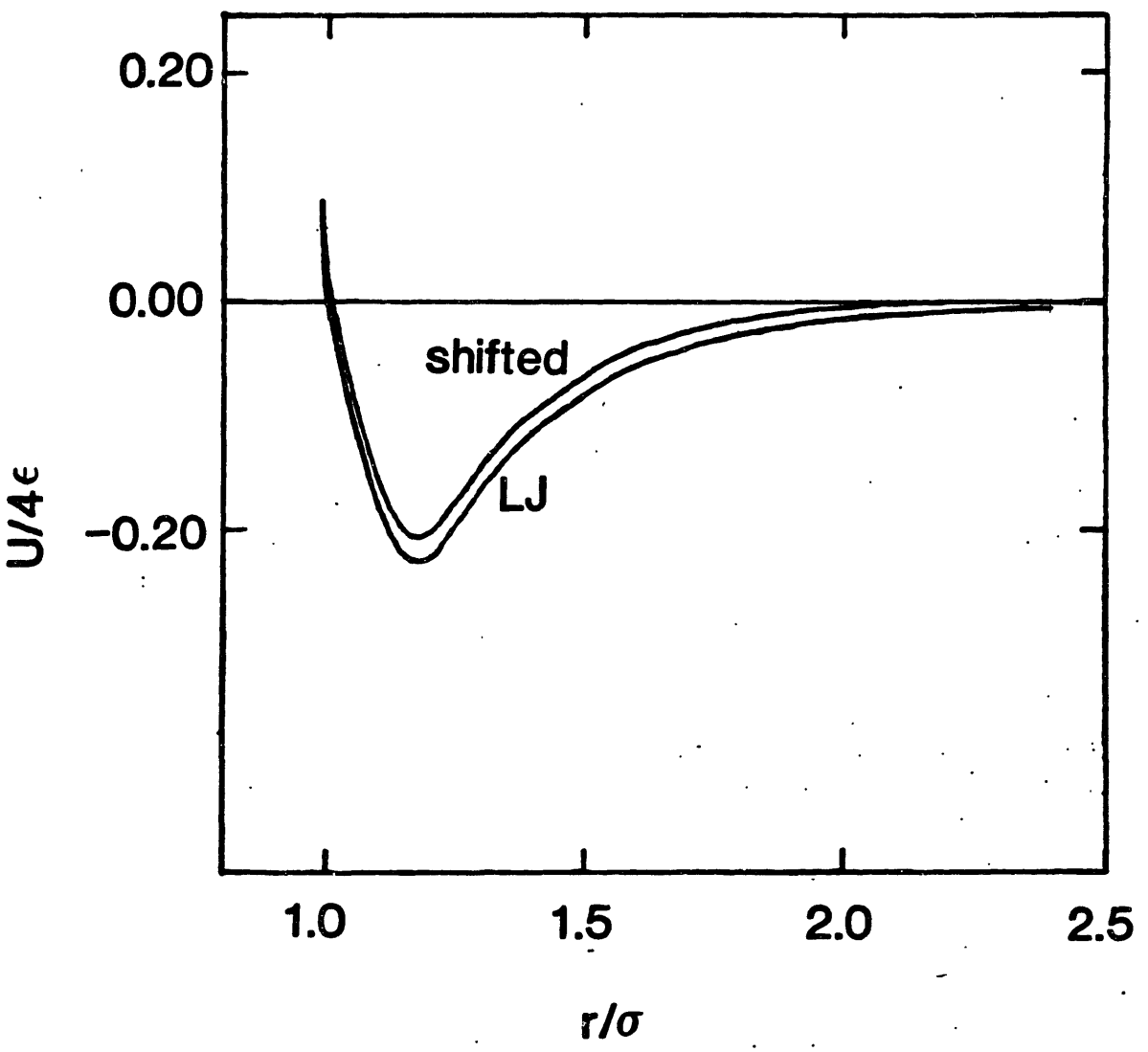

FIGURE 9.6 : True and shifted Lennard-Jones potentials; $r_c/\sigma = 2.4$

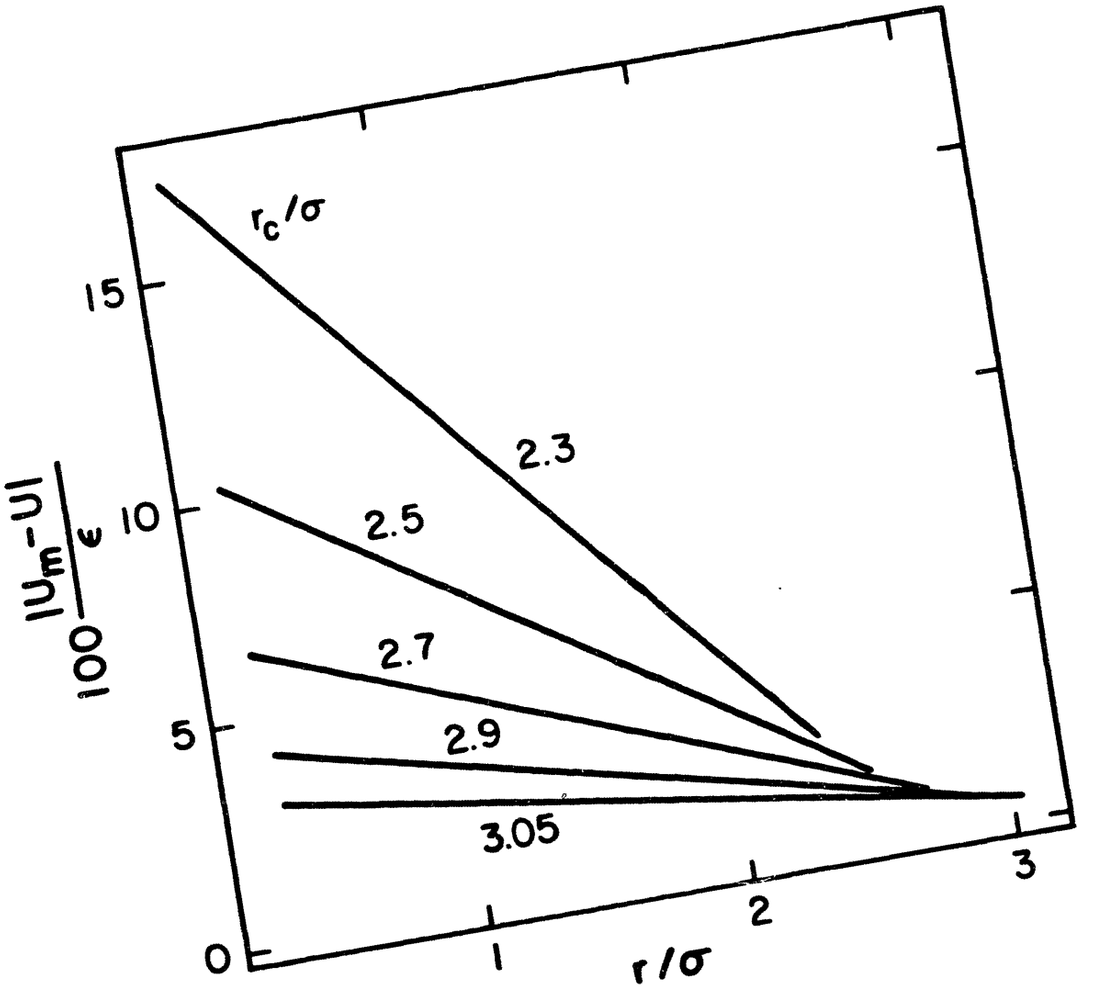

FIGURE 9.7 : Normalized error for the shifted force potential

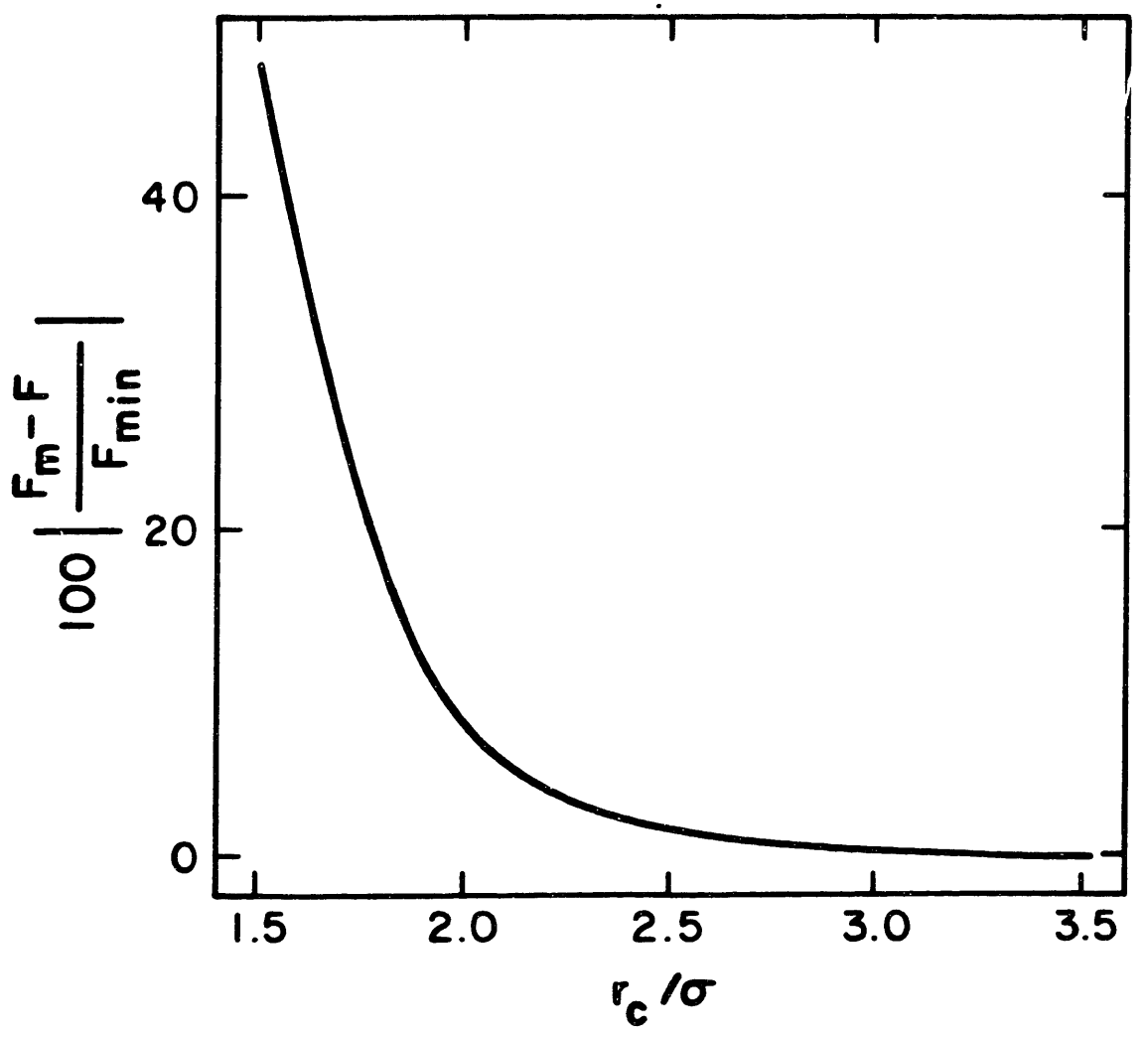

FIGURE 9.8 : Normalized force error; shifted force potential

for the general Lennard-Jones interaction between sites i and j; an additional condition (Equation (9.33)) imposes the minimization of U_{ij} at a distance equal to the sum of the van der Waals radii

$$U_{ij} = \frac{a_{ij}}{r^{12}} - \frac{C_{ij}}{r^{6}} \tag{9.31}$$

as follows,

$$C_{ij} = \frac{365 \ \alpha_i \ \alpha_j}{\left(\frac{\alpha_i}{N_i}\right)^{1/2} + \left(\frac{\alpha_j}{N_j}\right)^{1/2}} \tag{9.32}$$

$$a_{ij} = \frac{C_{ij}}{2} \left(r_{i,o} + r_{j,o}\right)^6 \tag{9.33}$$

where α is the polarizability in $Å^3$, r_0 is the van der Waals radius, in Å, and N is the outer shell effective number of electrons. From Equations (9.21) and (9.31) we obtain

$$\sigma_{ij} = \left(\frac{a_{ij}}{C_{ij}}\right)^{1/6} \tag{9.34}$$

$$\epsilon_{ij} = \frac{C^2_{ij}}{4a_{ij}} \tag{9.35}$$

The Slater-Kirkwood approach has been widely used in the molecular modeling of polymeric materials (Suter, 1979).

From Equation (9.31) it is obvious that the method assumes, at the outset, a form for U_{ij}. This represents a problem for molecules where electrostatic effects are important, since there is no theoretical way

of decoupling these effects to yield rigorous, a-priori electrostatic and van der Waals-type site-site parameters. For example, knowing the experimental quadrupole moment of CO_2 does not mean that one can model this molecule by superimposing the corresponding point monopoles to a Lennard-Jones type potential with Slater-Kirkwood parameters, since the latter already incorporate electrostatic effects through the polarizability, albeit in an oversimplified way. This, of course, means that the explicit inclusion of electrostatic forces with experimentally measured parameters cannot, at present, be done without simultaneously fitting the Lennard-Jones parameters so that the overall fluid behavior reproduces some arbitrarily selected property (generally pressure). For CO_2-benzene simulations, the site parameters for use in Equations (9.32) and (9.33) are listed in Table 9.2, and the calculated Lennard-Jones parameters are listed in Table 9.3. The length parameters σ were reduced by .15 Å in the simulations. The effects of this change are treated in Chapter 10, where the actual results are presented and discussed.

The simulation of CO_2 is not a simple problem. Apart from its linearity, which requires the implementation of a different kinematic description than for the generic rigid polyatomic, this molecule has a significant quadrupole moment (Murthy et al. 1981). In the present work, it was attempted to take this into account by introducing appropriate point monopoles, located at the Lennard-Jones sites. Severe numerical problems originated as a consequence of this, and they are discussed in Chapter 10. Here, the general aspects of long-range interactions and their molecular dynamics implementation will be treated, with CO_2 as the specific example.

The measured quadrupole movment of CO_2 (Buckingham and Disch, 1963) is -1.43448×10^{-39} Cm²; this represents a considerable electrostatic effect that should be taken into consideration (as a comparison, the corresponding value for N_2 is -4.67×10^{-40} Cm², or 307% smaller). For a C-O site separation ℓ = 1.23 Å, the quadrupole moment corresponds to partial charges (in electronic charge units)

$$Z_C = + .5912$$
$$Z_O = - .2956 \qquad (9.36)$$

TABLE 9.2: SITE PARAMETERS FOR SLATER-KIRKWOOD EQUATION

	α (Å^3)	N	r_o (Å)
C(C=O)	.97	5	1.8
O (=O)	.84	7	1.6
C (aromatic)	1.23	5	1.95
H	0.42	0.90	1.30

TABLE 9.3: CALCULATED SITE LENNARD-JONES PARAMETERS; SLATER-KIRKWOOD APPROACH

σ(Å) (*)

	C(C=O)	O (=O)	C(aromatic)	H
C(C=O)	3.207	3.029	3.341	2.762
O (=O)	3.029	2.851	3.163	2.584
C (aromatic)	3.341	3.163	——	——
H	2.762	2.584	——	——

ε/k (K)

	C(C=O)	O (=O)	C(aromatic)	H
C(C=O)	45.089	61.596	42.100	37.542
O (=O)	61.596	87.159	56.308	52.938
C (aromatic)	42.100	56.308	——	——
H	37.542	52.938	——	——

$$U = 4\varepsilon \left[\left(\frac{\sigma}{r}\right)^{12} - \left(\frac{\sigma}{r}\right)^{6} \right]$$

(*) All values were reduced by .15 Å in the simulations

It is not a-priori necessary to locate these charges exactly at the Lennard-Jones sites. However, not doing so requires the introduction of an arbitrary "switching function" (Stillinger an Rahman, 1974) that modulates the electrostatic forces in such a way that opposite charges do not collapse on each other.

The electrostatic contribution to the intermolecular potential energy for a three-site molecule such as CO_2, is given by

$$U_{coul} = \frac{e^2}{4\pi\varepsilon_0} \sum_{i=1}^{3} \sum_{j=1}^{3} \frac{Z_i Z_j}{r_{ij}} \tag{9.37}$$

where e is the electronic charge, and ε_0, the permittivity of free space.

$$e = 1.603592 \times 10^{-19} \text{ Coul} \tag{9.38}$$

$$\varepsilon_0 = 8.854 \times 10^{-12} \text{ J}^{-1} \text{ Coul}^2 \text{ m}^{-1} \tag{9.39}$$

To study the relative importance of Coulombic interactions, we concentrate on two CO_2 molecules, whose relative positions are defined in Figure 9.9.

Figures 9.10 to 9.12 show the total, Coulombic and Lennard-Jones energy, as a function of the carbon-carbon separation for different relative orientations. The energy has been normalized with kT, with T = 300 K. The absolute value of the total, Coulombic and Lennard-Jones forces are shown in figures 9.13 to 9.15, as a function of carbon-carbon separation, for the same relative orientations. Force has been normalized with kT/ℓ, with ℓ = 1.23 Å, and T = 300 K. The normalized Coulombic and Lennard-Jones components are shown in Figures 9.16 to 9.21, for the same relative orientations. The force components represent forces exerted by J on I, and are referred to the (x,y,z) coordinate set (Figure 9.9). Potential parameters used correspond to Equation (9.36) and Table 9.3.

As explained above, van der Waals and electrostatic potentials cannot be superimposed without altering the parameters; however, the conclusions that follow from Figures 9.10 to 9.21 will be used in a qualitative sense and are valid for any realistic set of parameters.

The most important conclusion to be drawn from Figures 9.10 to 9.21 is the virtual vanishing of pairwise interactions for $r > 9$ Å (this is a conservative figure; as can be seen from the Figures, interactions are very weak already at $r \sim 7.5$ Å). This fact is independent of orientation. Effective fields and forces around any given molecule would vanish even more rapidly in the presence of more than one molecule, but it is remarkable that this feature is already clearly displayed for the elementary binary interaction.

It follows immediately that, because of this cancellation, the effective electrostatic potential between two multi-site polyatomics is short-ranged and can be modelled with periodic boundary conditions. This is done by defining a shifted site-site coulombic potential,

$$\begin{aligned} U_m &= \frac{e^2 Z_i Z_j}{4\pi\varepsilon_0} \left(\frac{1}{r} - \frac{1}{r_c} \right) && r \leq r_c \\ U_m &= 0 && r \geq r_c \end{aligned} \qquad (9.40)$$

and the corresponding force,

$$\begin{aligned} F_m &= \left(\frac{e^2 Z_i Z_j}{4\pi\varepsilon_0}\right) \frac{1}{r^2} && r \leq r_c \\ F_m &= 0 && r > r_c \end{aligned} \qquad (9.41)$$

this potential gives the correct force for $r \leq r_c$, and satisfies Equation (9.17). An unshifted Coulombic potential truncated at r_c, on the other hand, gives rise to an infinite (impulsive) force which is totally unphysical and which, if overlooked, can lead to severe errors in energy conservation. A shifted force potential can also be defined; as with van der Waals

forces, such a potential would satisfy Equation (9.17) and hence energy conservation. In the present work, Equations (9.40) and (9.41) were used. The results of the inclusion of electrostatic forces are discussed in Chapter 10.

Another interesting feature that emerges from Figures 9.10 to 9.21 is the qualitatively different behavior of electrostatic and van der Waals interactions with respect to molecular orientation. For any given value of γ and δ, changes in α and/or β give rise to important changes in the electrostatic part of the interaction, whereas the van der Waals contribution is much less sensitive to orientation. This can be seen for the energy (Figures 9.10 to 9.12) and for the cartesian components of the force (Figures 9.16 to 9.18). This is a possible explanation of the difficulties encountered in simulations where coulombic forces were included.

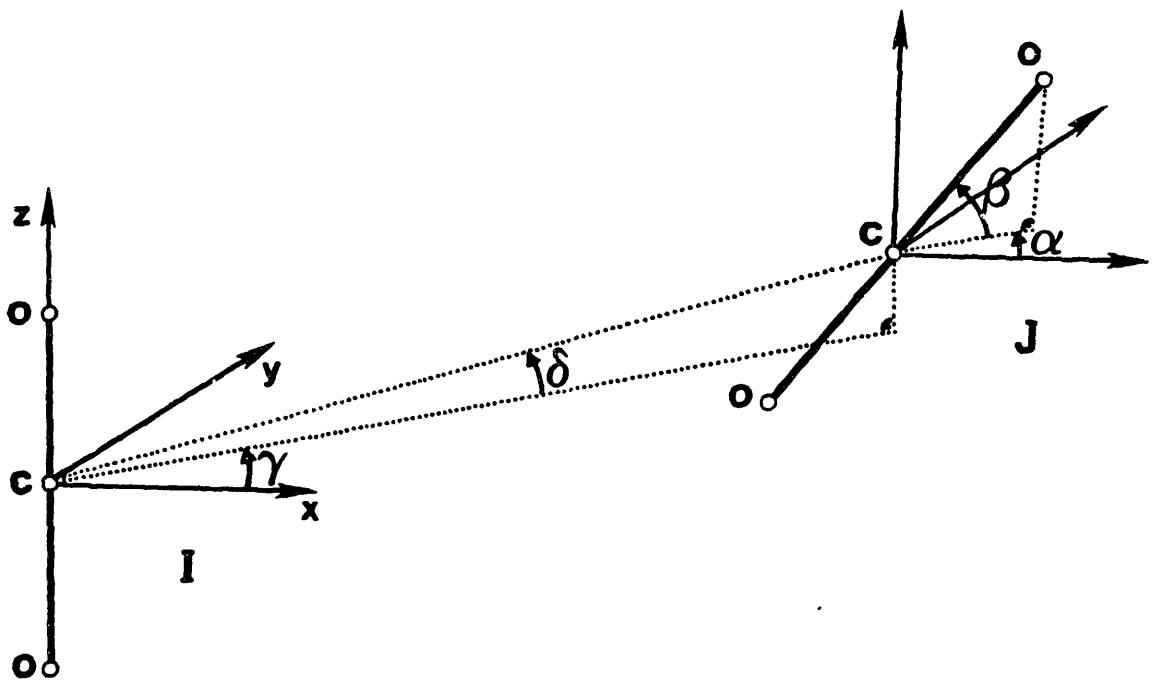

FIGURE 9.9 : Kinematic description of two linear molecules

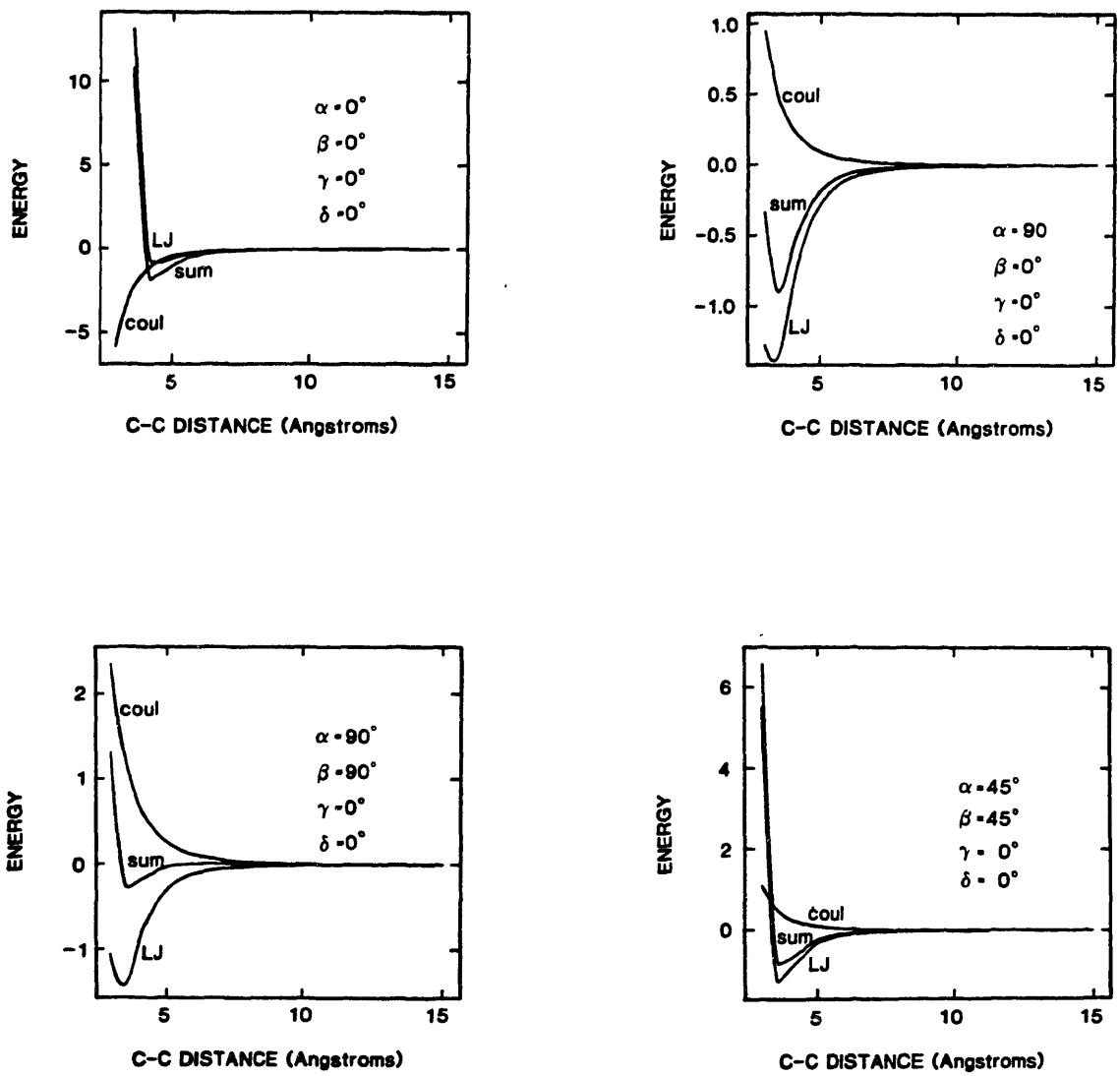

FIGURE 9.10 : van der Waals, coulombic and total energy for a binary CO_2 interaction

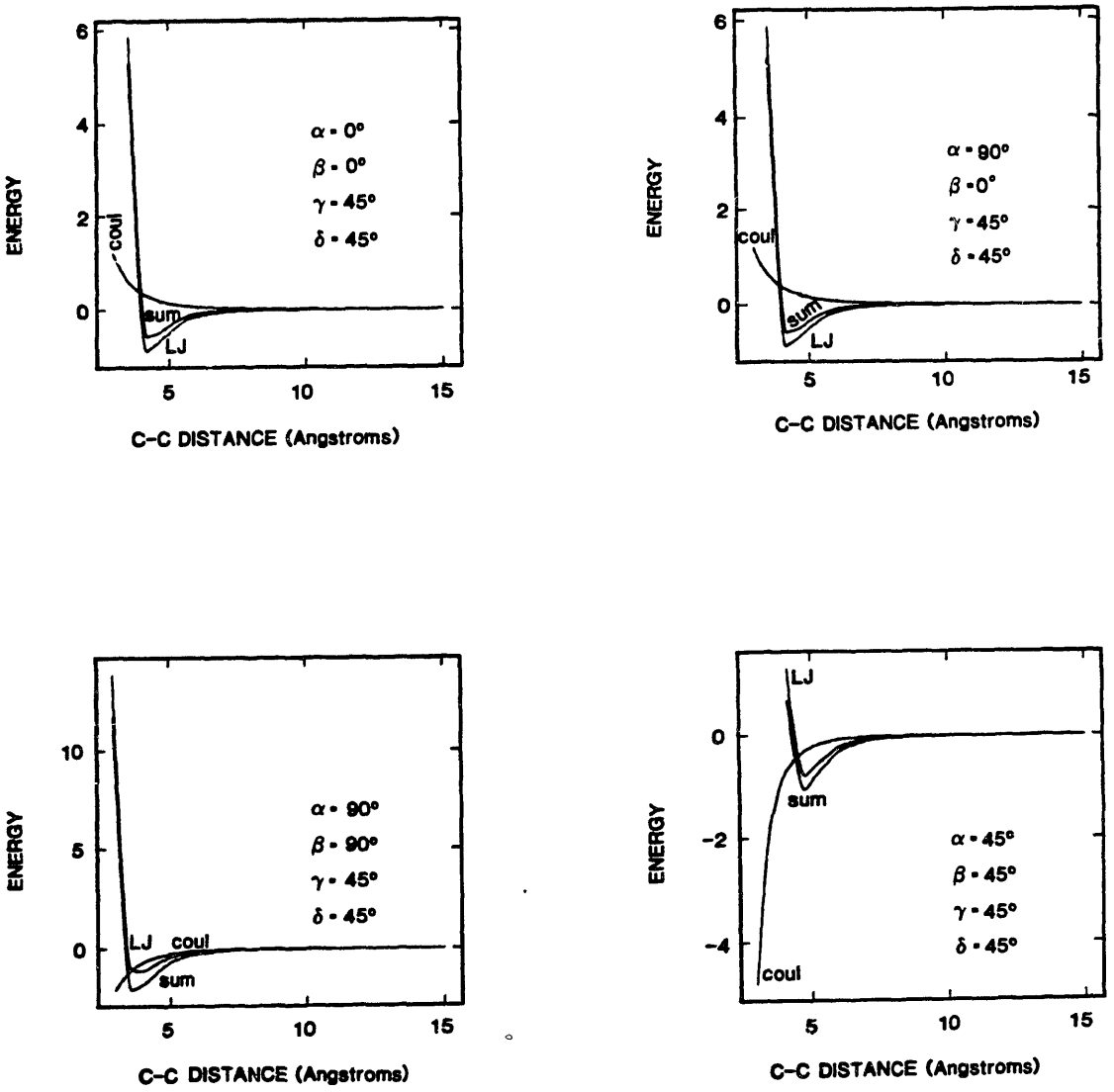

FIGURE 9.11 : van der Waals, coulombic and total energy for a binary CO_2 interaction

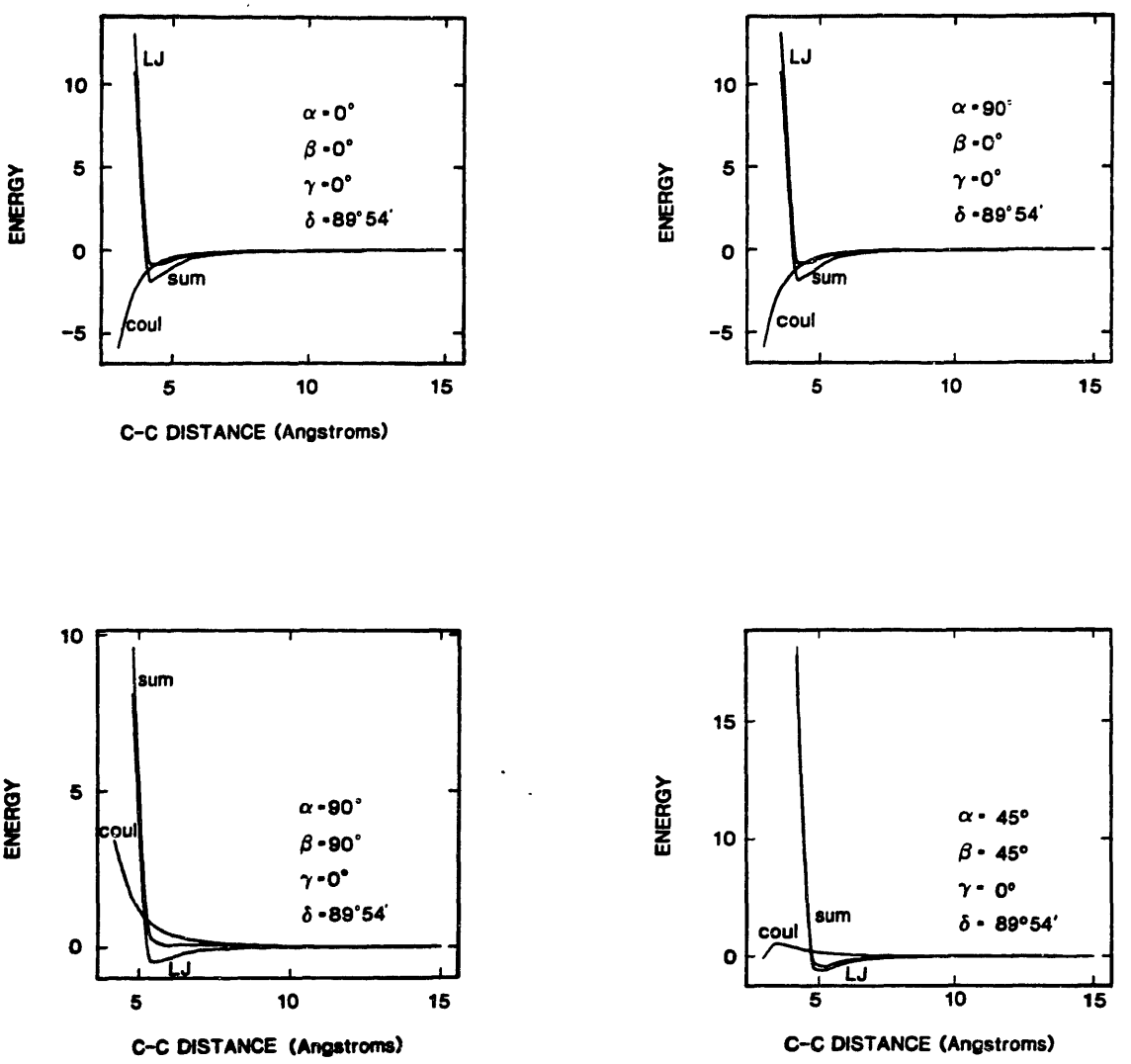

FIGURE 9.12 : van der Waals, coulombic and total energy for a binary CO_2 interaction

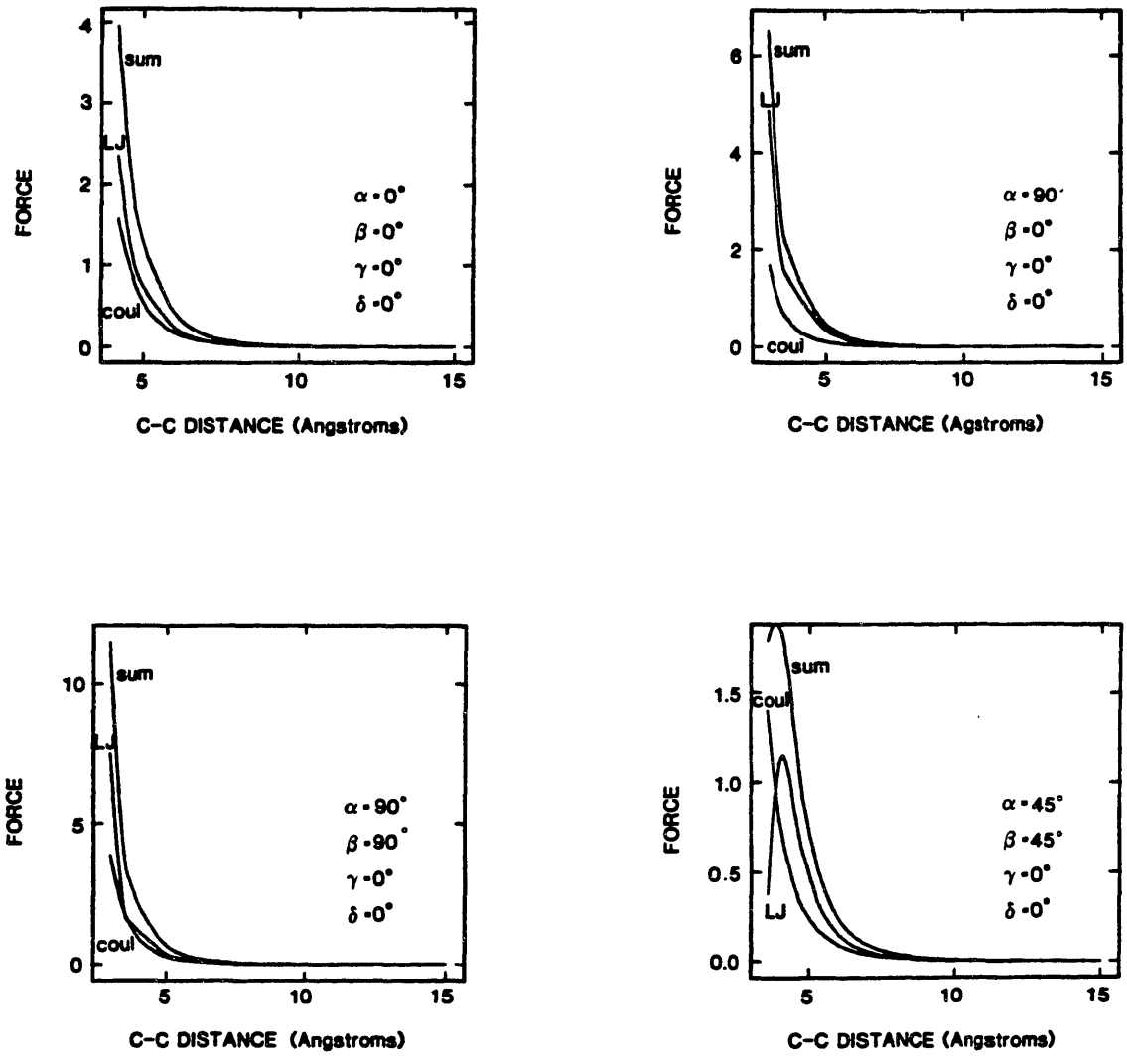

FIGURE 9.13 : Absolute value of van der Waals, coulombic and total force for a binary CO_2 interaction

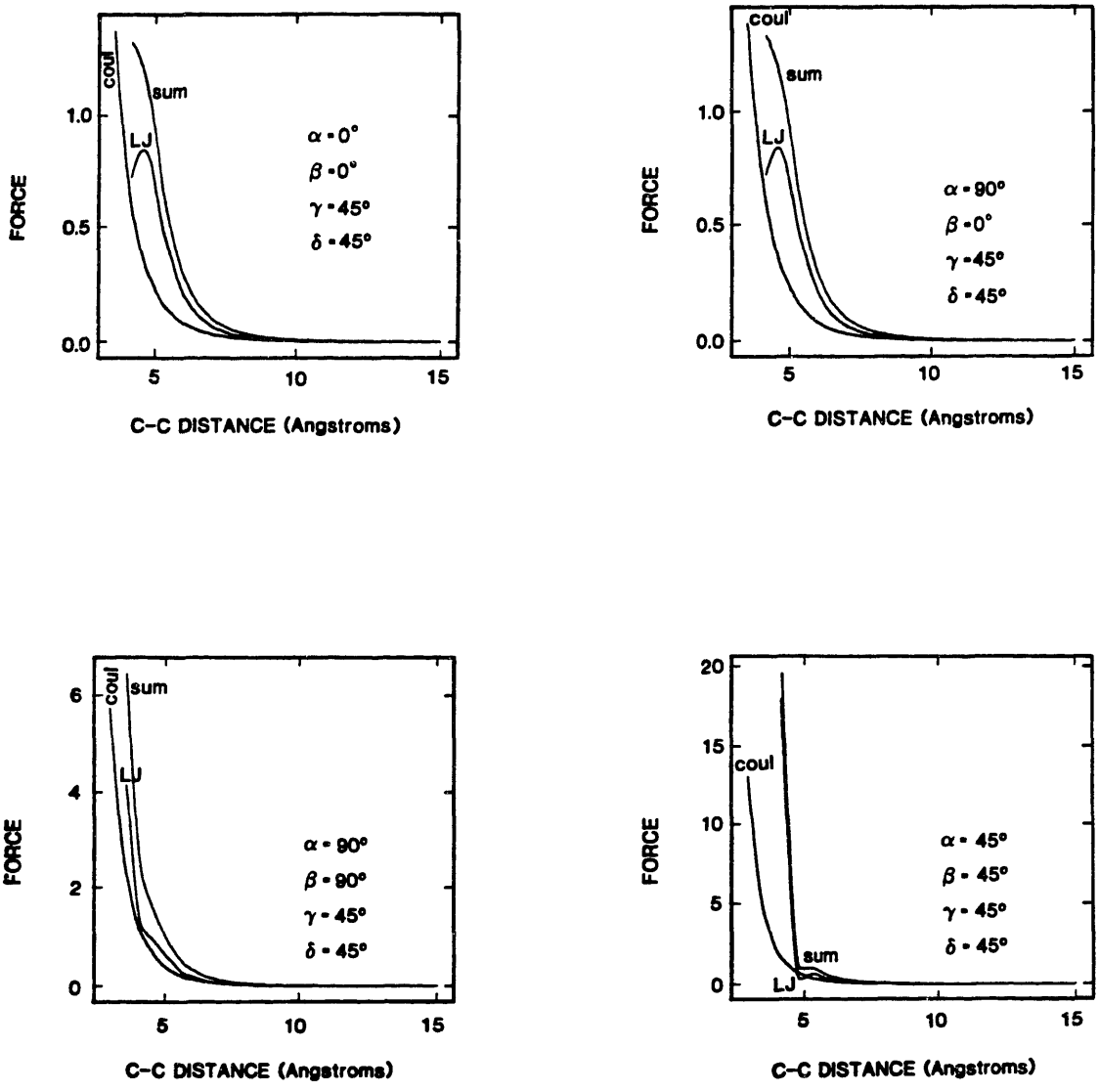

FIGURE 9.14 : Absolute value of van der Waals, coulombic and total force for a binary CO_2 interaction

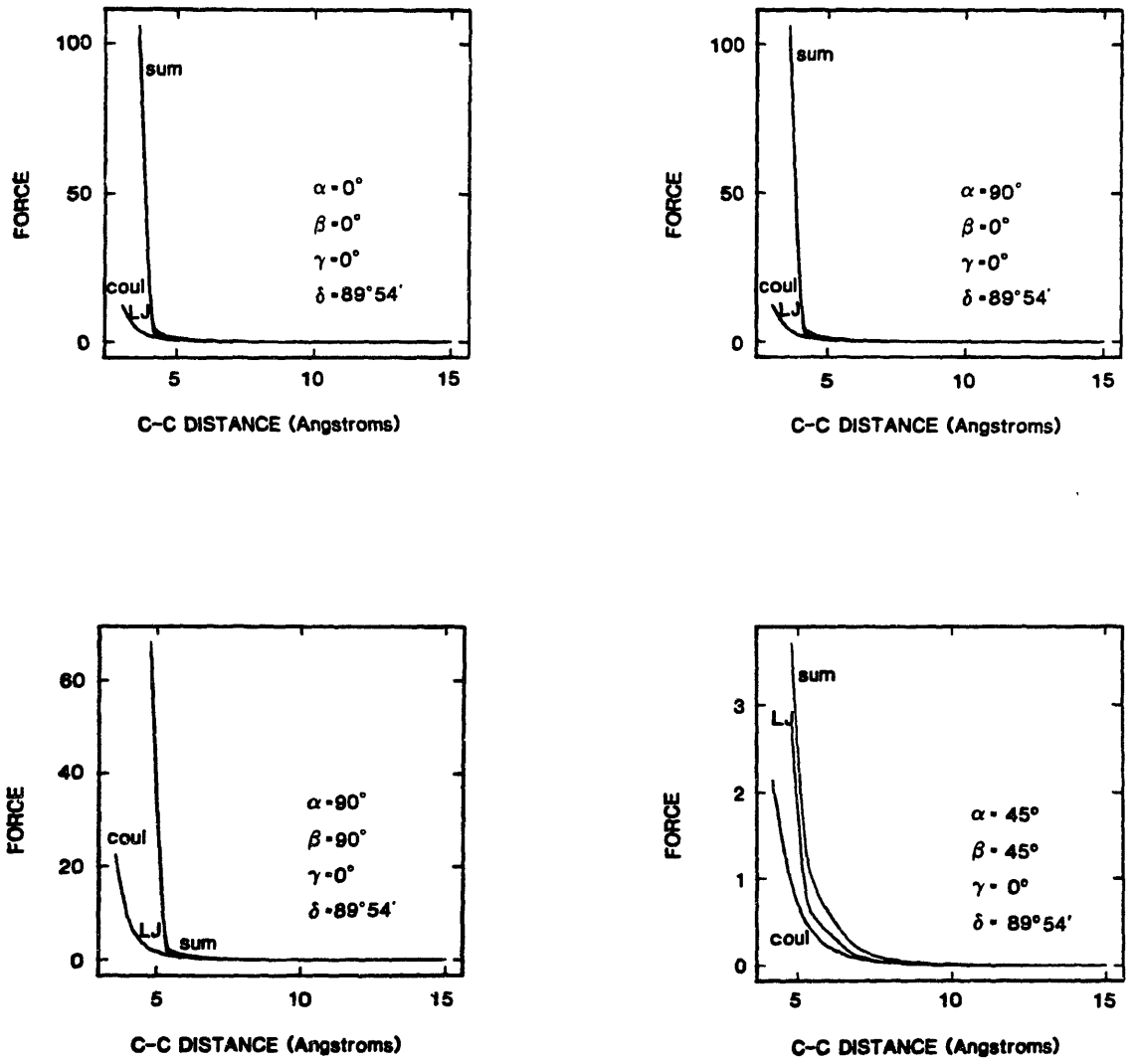

FIGURE 9.15 : Absolute value of van der Waals, coulombic and total force for a binary CO_2 interaction

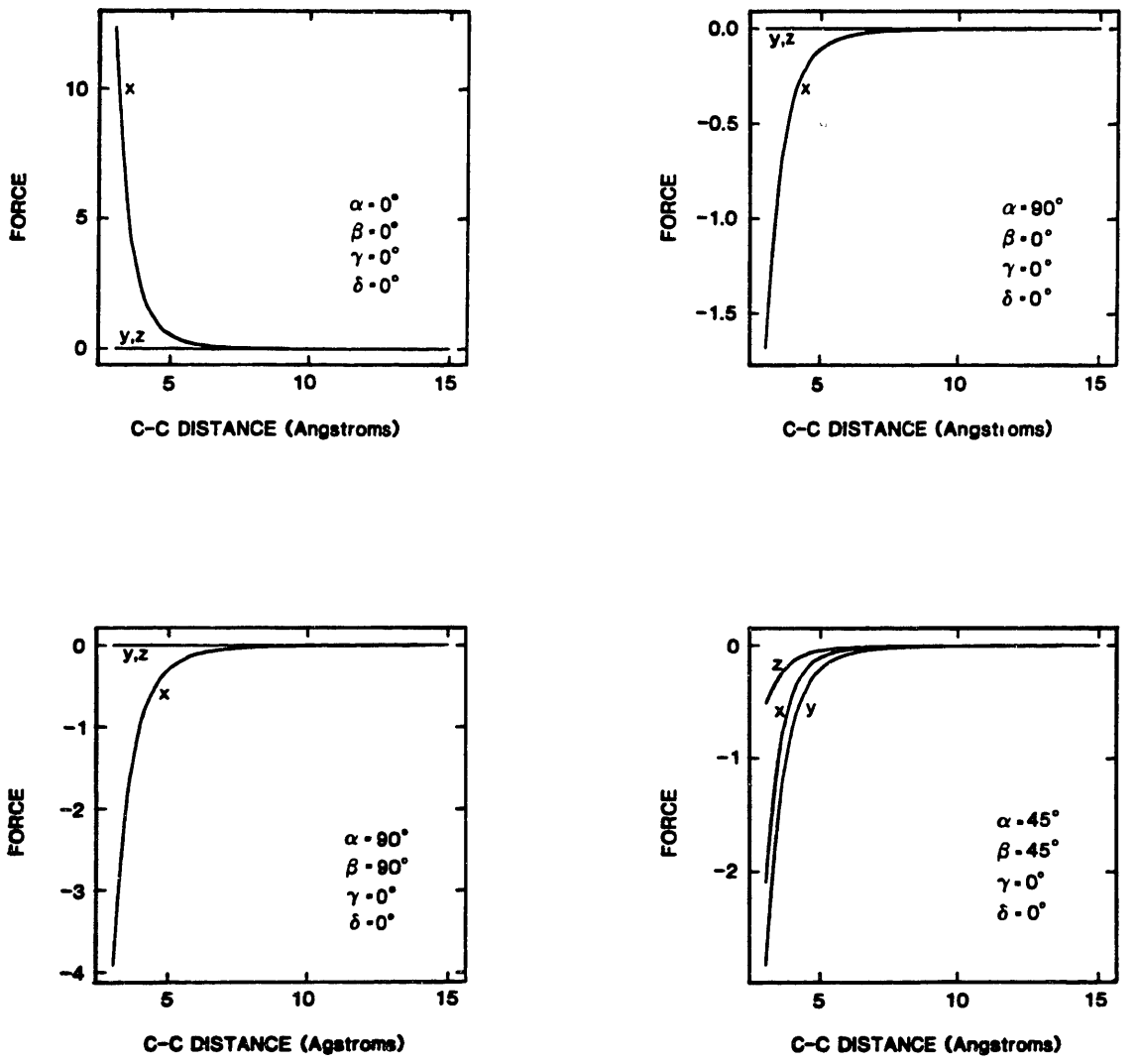

FIGURE 9.16 : Coulombic force components for a binary CO_2 interaction

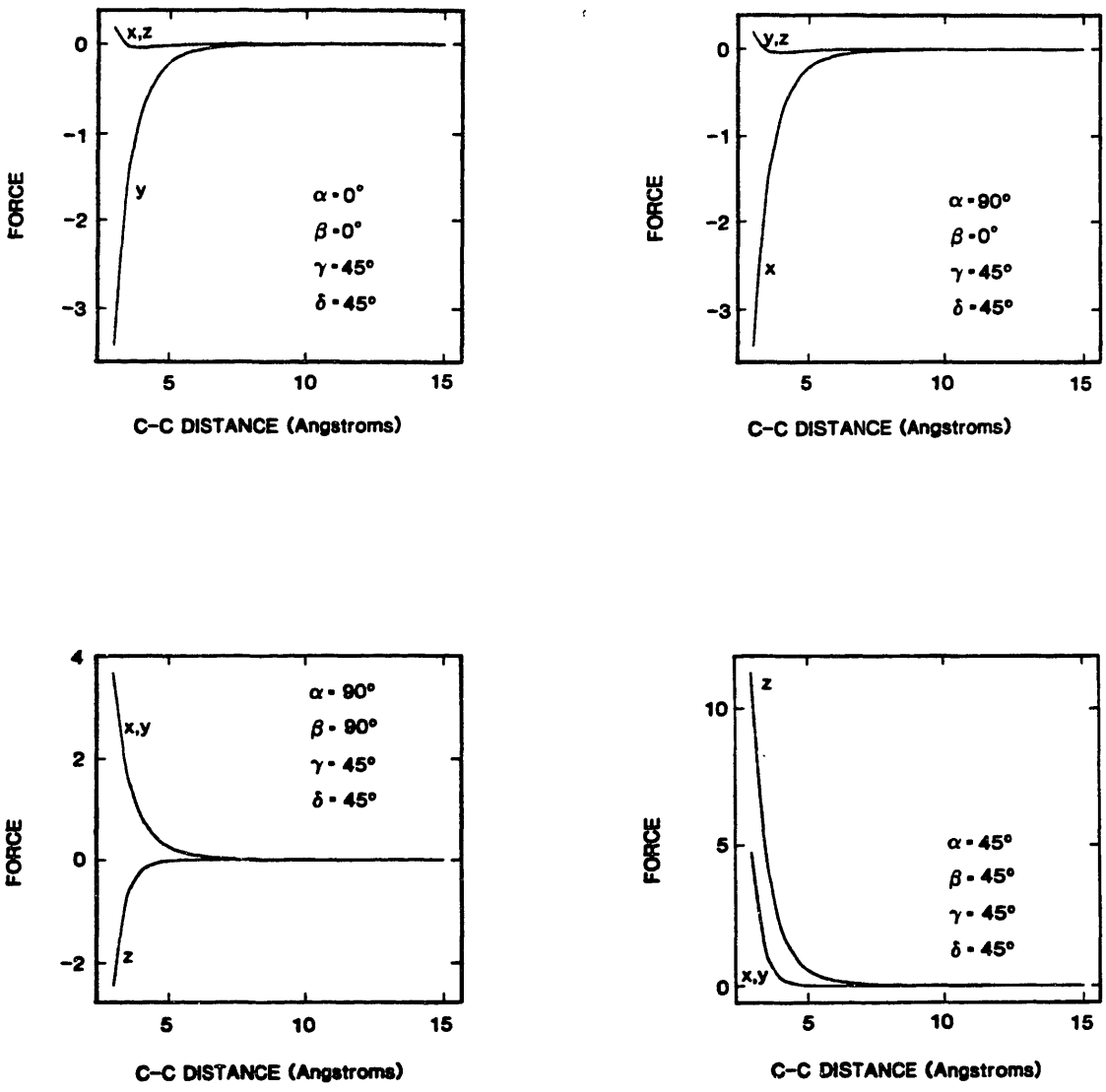

FIGURE 9.17 : Coulombic force components for a binary CO_2 interaction

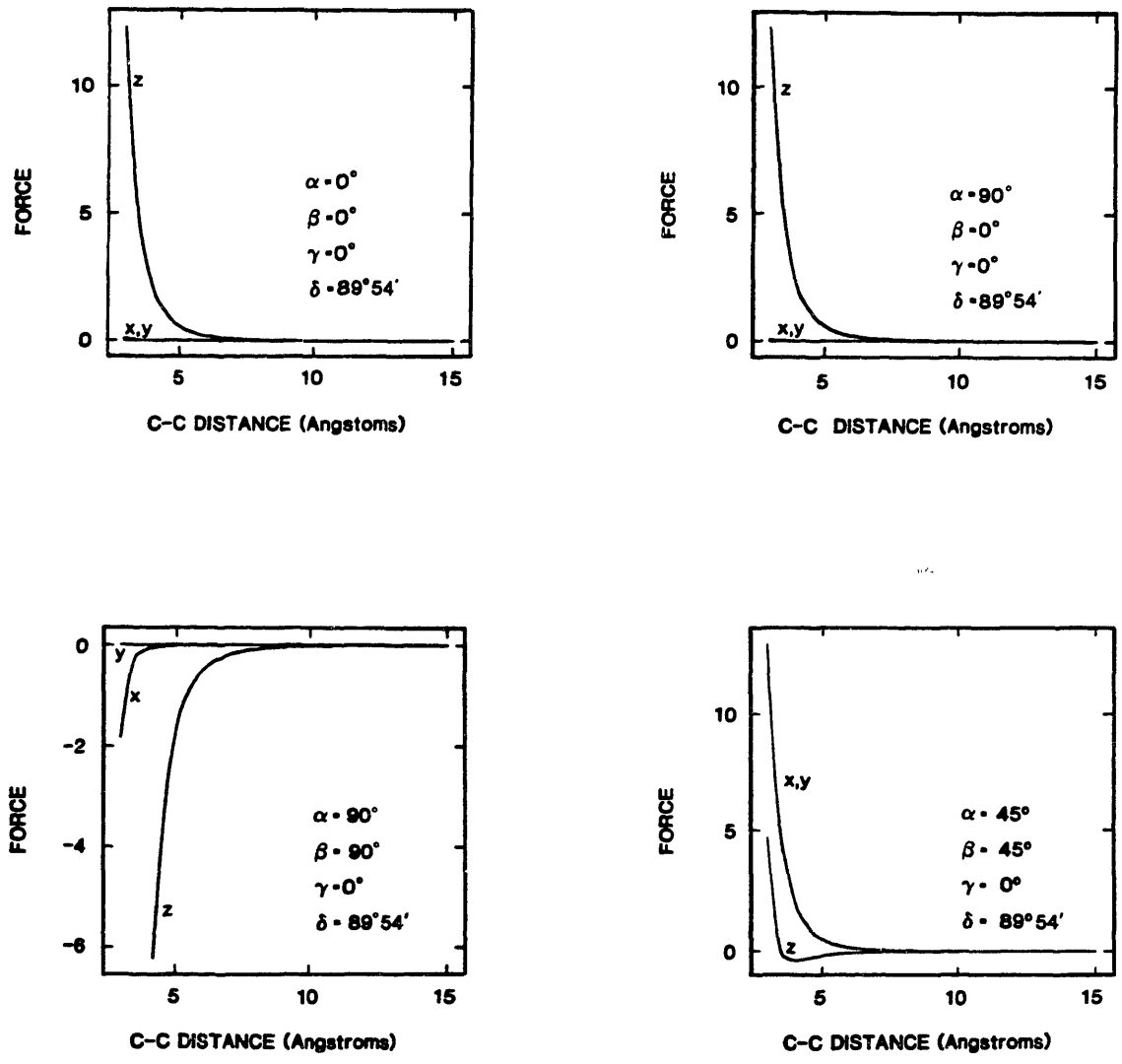

FIGURE 9.18 : Coulombic force components for a binary CO_2 interaction

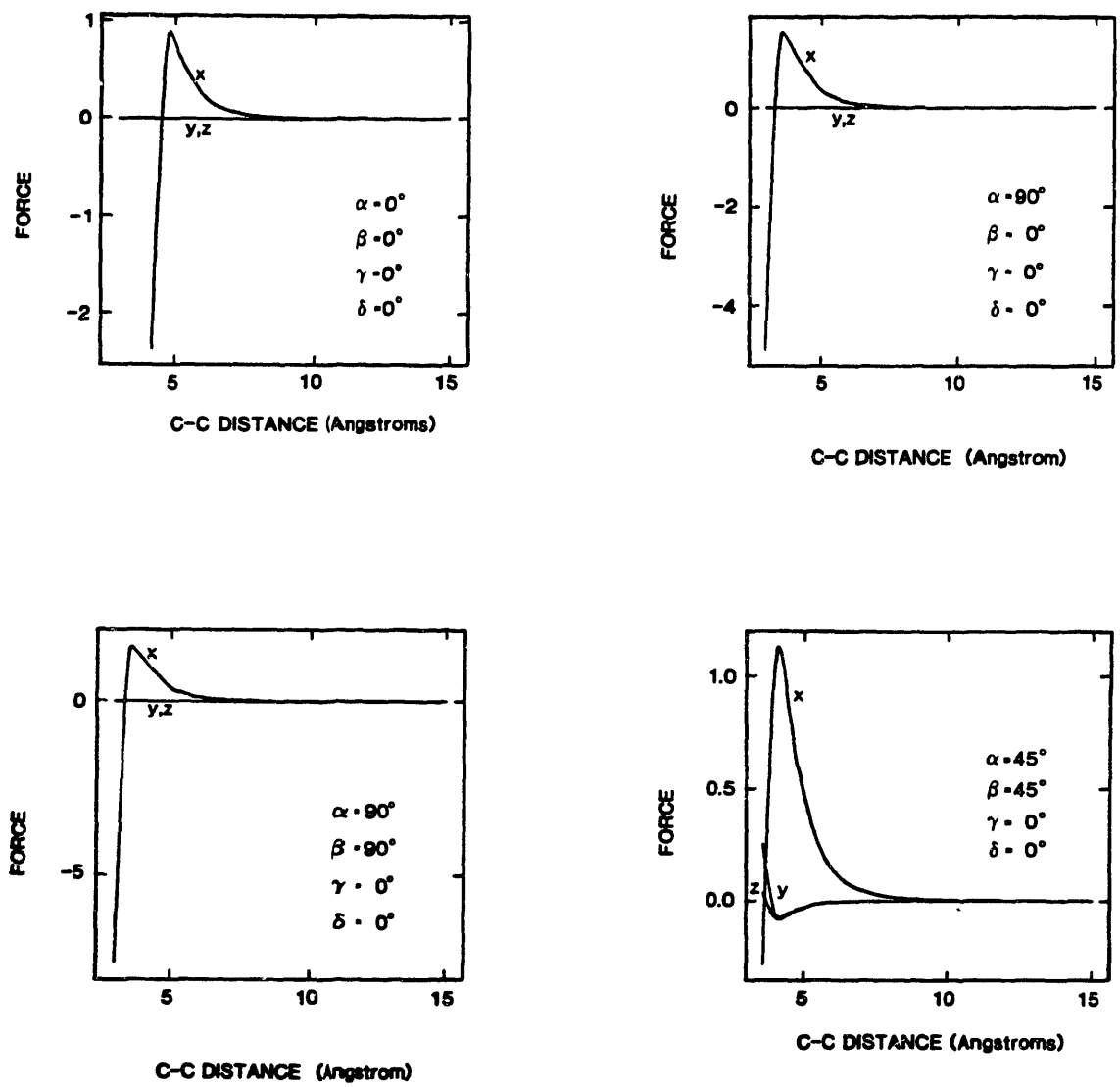

FIGURE 9.19 : Lennard-Jones force components for a binary CO_2 interaction

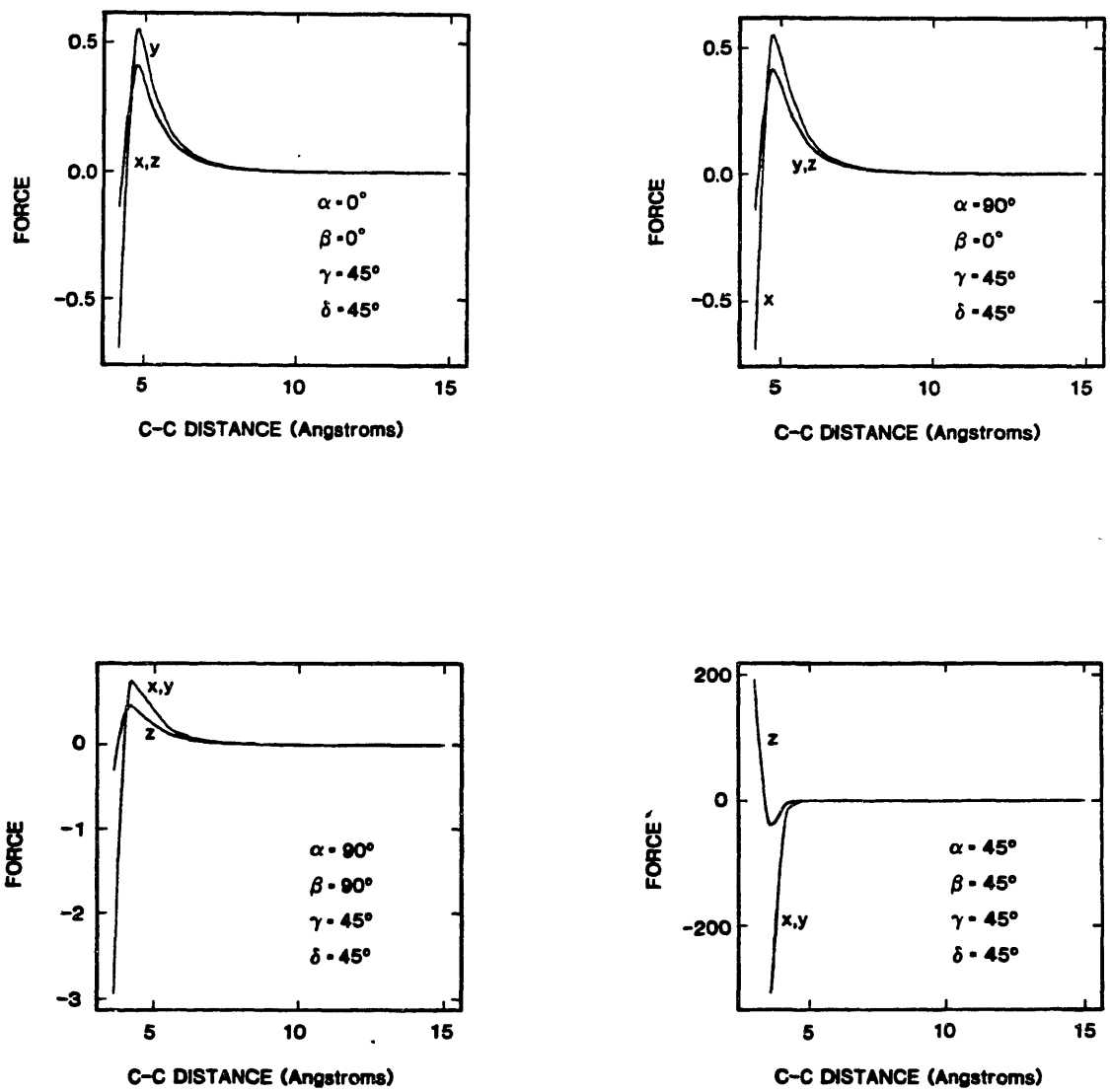

FIGURE 9.20 : Lennard-Jones force components for a binary CO_2 interaction

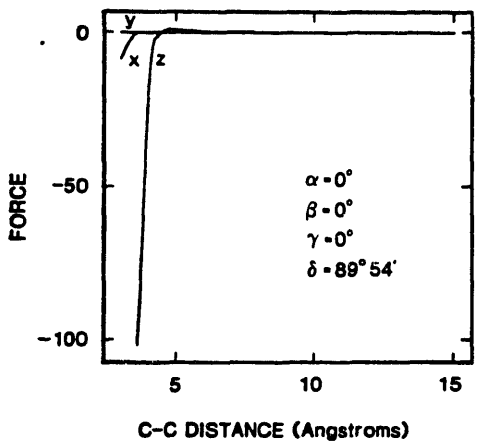

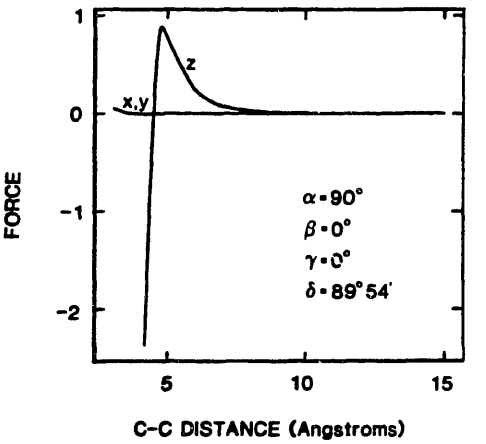

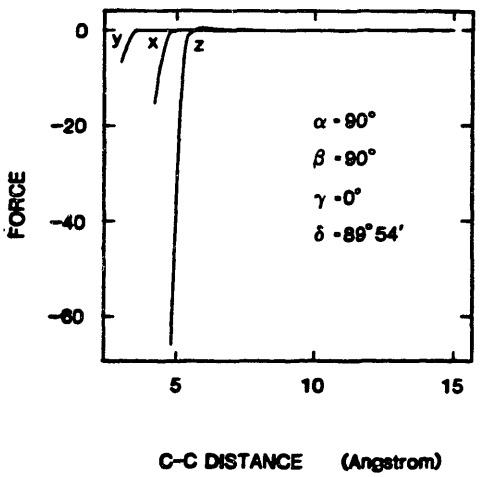

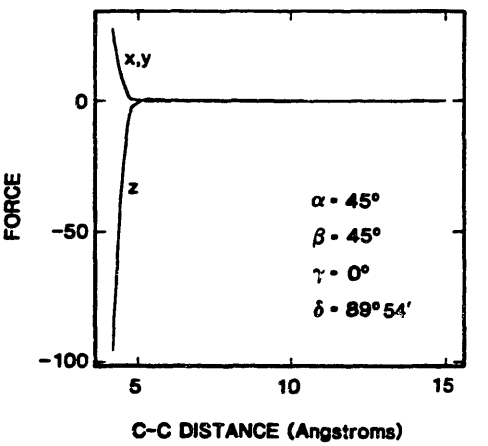

FIGURE 9.21 : Lennard-Jones force components for a binary CO_2 interaction

10: MOLECULAR DYNAMICS SIMULATIONS: RESULTS AND DISCUSSION

Unless specified otherwise, the results reported in this Chapter correspond to simulations of the motion of 108 molecules, representing 107 CO_2 and 1 benzene molecules, respectively. Interatomic potential parameters are listed in Table 9.3, and the molecular geometry is shown in Figure 10.1.

10.1: VELOCITY DISTRIBUTIONS

Velocity distributions for the 107 solvent molecules were calculated by counting the number of molecules within a certain velocity interval at different instants ("snapshots"), and averaging over the number of "snapshots". The velocity range considered was $0<v^*<3$, where v^* is expressed in units of root mean square velocity (v_{rms})

$$v^* = v \left(\frac{m}{3kT^*}\right)^{1/2} \qquad (10.1)$$

and T^* is the run's nominal temperature, i.e., that temperature towards which velocities were rescaled during the relaxation run.

The velocity range was divided into 20 intervals. Molecules with a velocity falling anywhere within a given interval were assigned a nominal velocity equal to the mid-point velocity. This implies an uncertainty of 7.5% in v_{rms} units.

In this way, the incremental number of molecules per unit velocity interval ($\Delta N/\Delta v$) can be plotted against molecular velocity, and this can be compared to the Maxwell-Boltzmann expression (Equation (8.58)).

The results are shown in Figures 10.2 to 10.7. In each case, the actual number of solvent molecules (107) was used in the Maxwell-Boltzmann expression (Equation (8.58)); this normalizes all curves in such a way that the total area equals 107. The number of "snapshots" is indicated in each case, as well as the run's average translational temperature, i.e.,

$$< T(tr) > = 2 < KE(tr) > /3Nk \qquad (10.2)$$

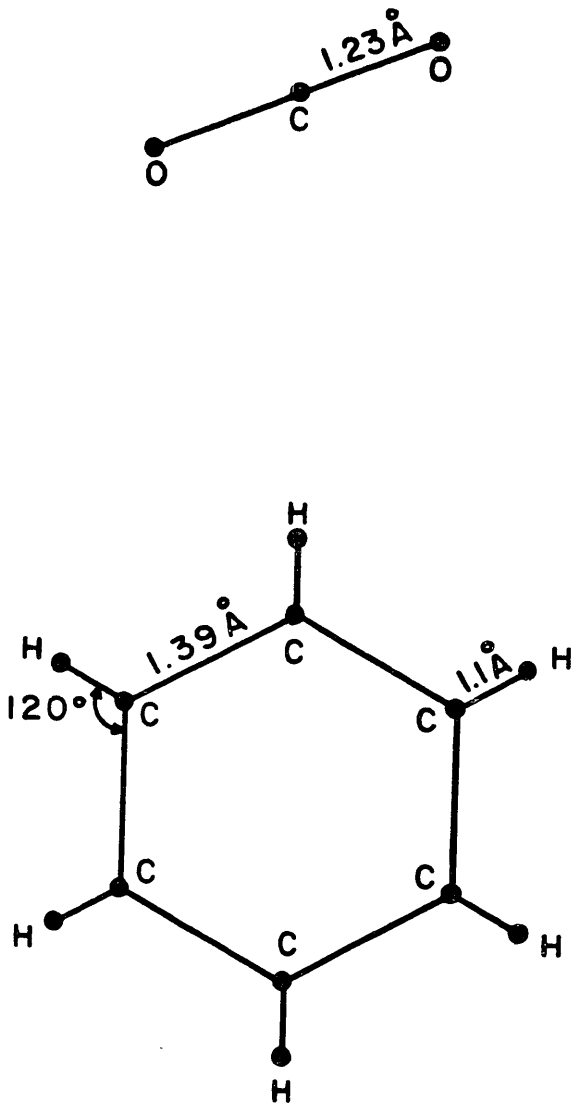

FIGURE 10.1: Geometry of benzene and CO_2 used in the simulations

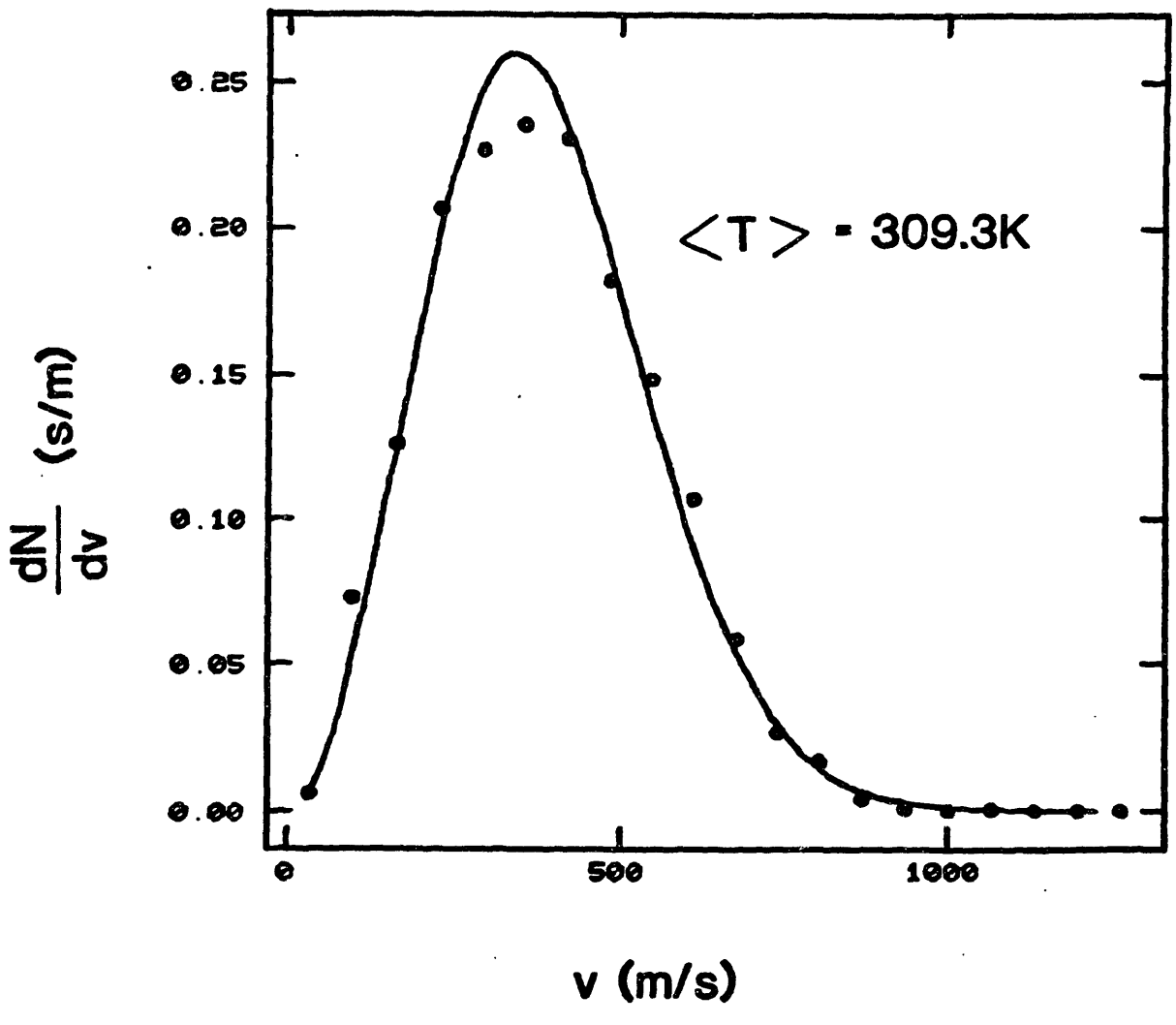

FIGURE 10.2: Theoretical and computed velocity distributions;
<T(tr)> = 309.3K; sample size = 64

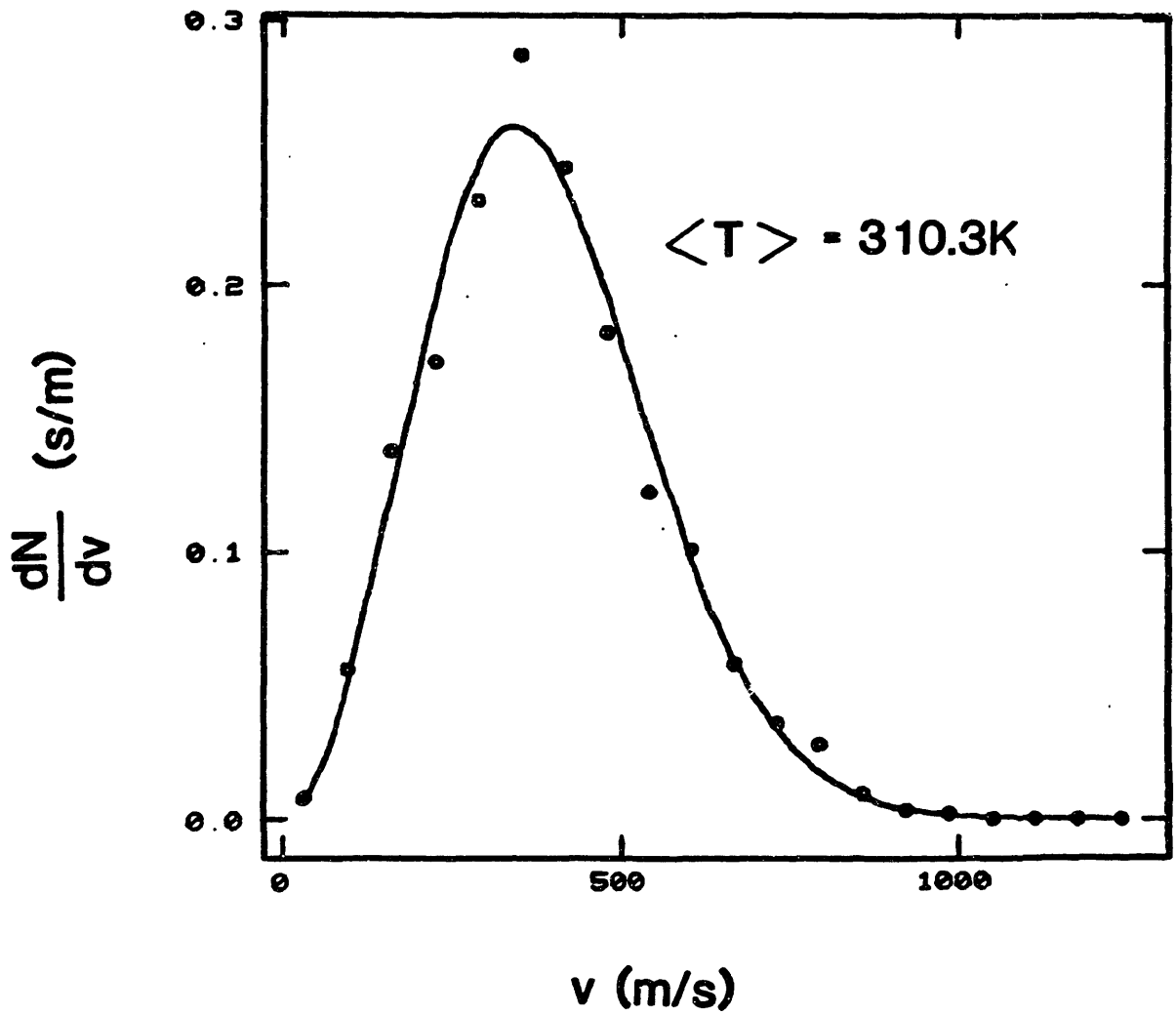

FIGURE 10.3: Theoretical and computed velocity distributions; <T(tr)> = 310.3K; sample size = 64

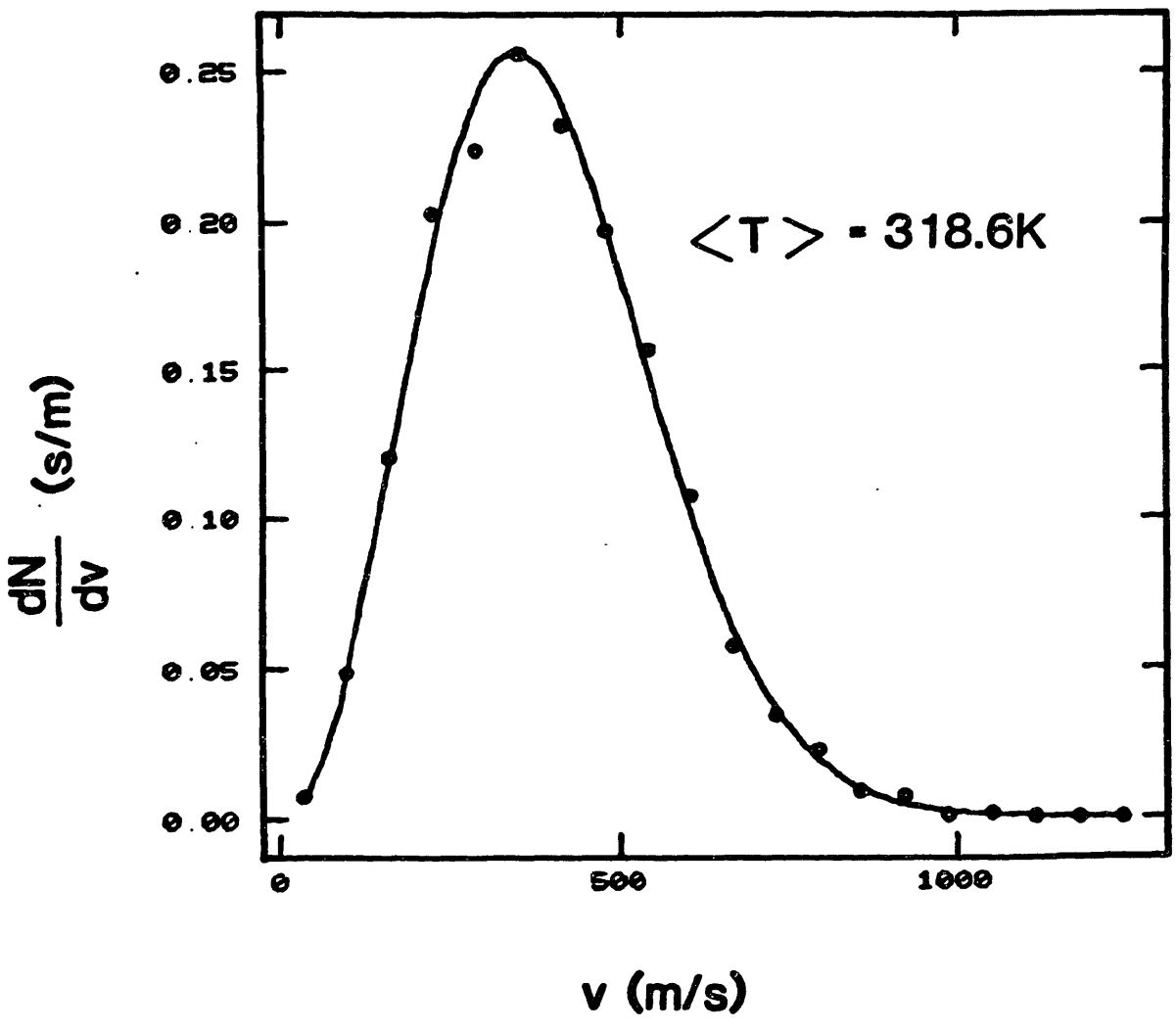

FIGURE 10.4: Theoretical and computed velocity distributions; <T(tr)> = 318.6K; sample size = 67

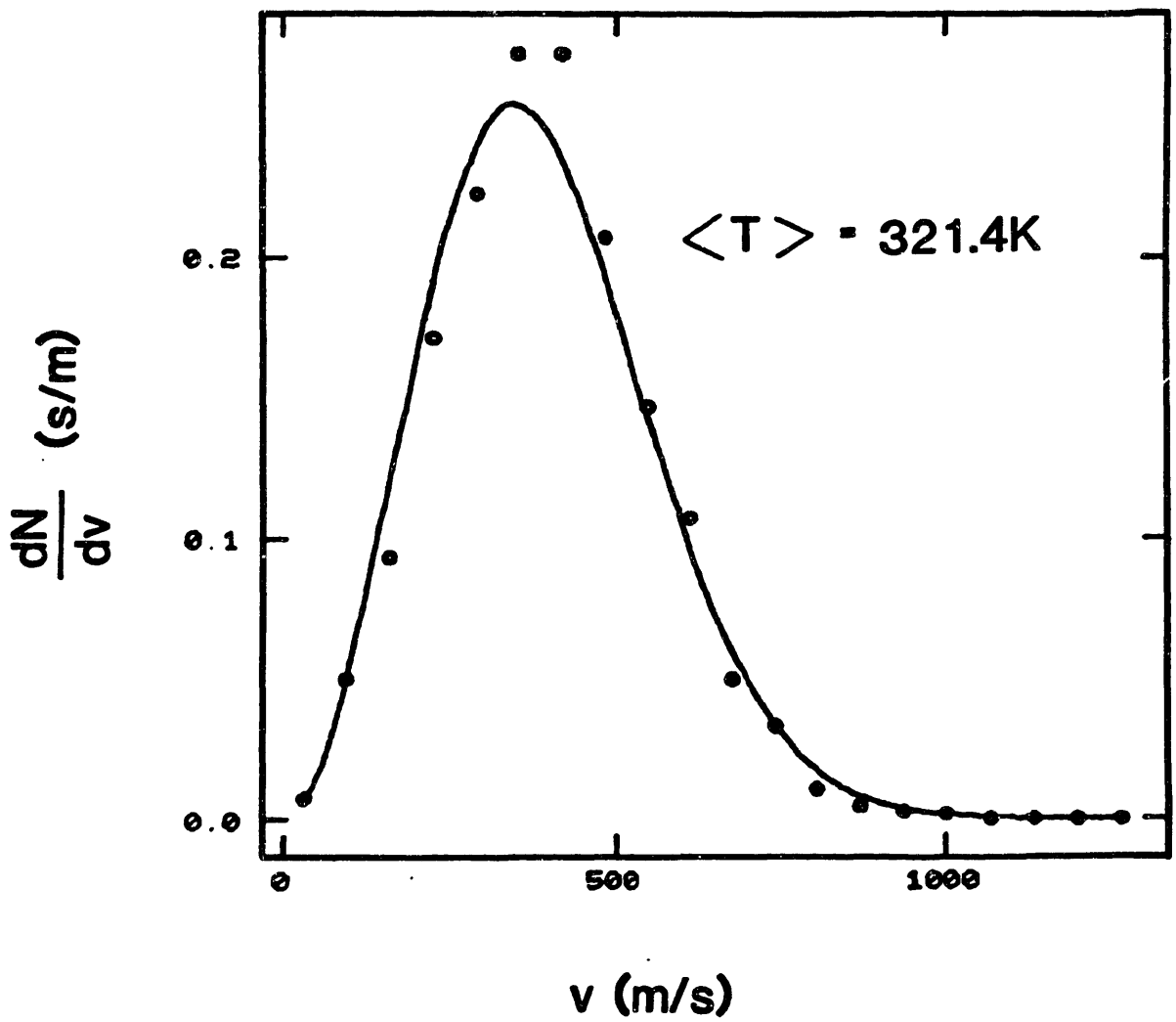

FIGURE 10.5: Theoretical and computed velocity distributions; <T(tr)> = 321.4 K; sample size = 70

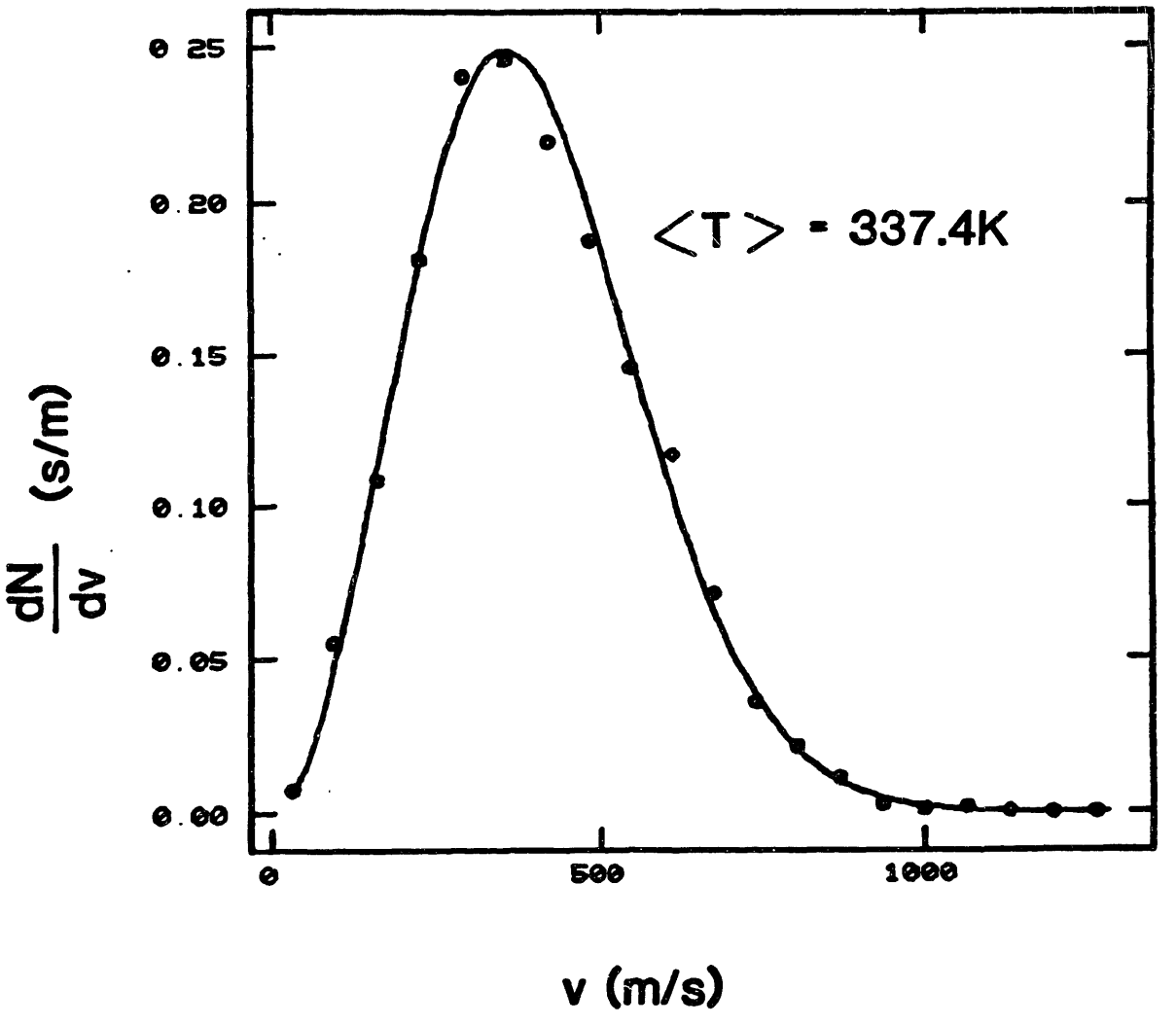

FIGURE 10.6: Theoretical and computed velocity distributions; <T(tr)> = 337.4 K; sample size = 67

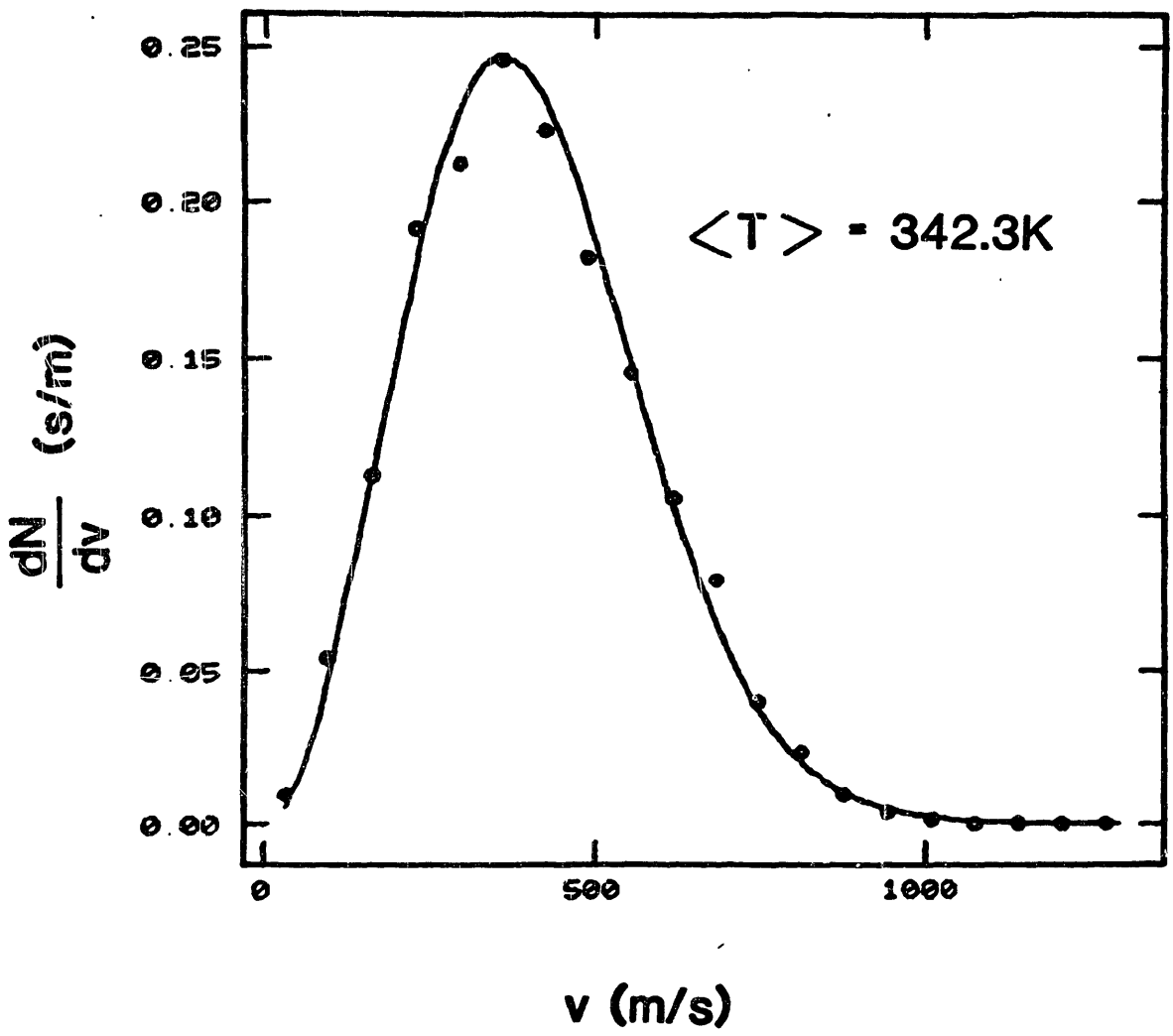

FIGURE 10.7: Theoretical and computed velocity distributions; <T(tr)> = 342.3 K; sample size = 64

where N = 107, tr denotes translation, and KE, kinetic energy. The abscissae corresponding to interval midpoints were dimensionalized with the nominal root mean square velocity (i.e., velocity corresponding to the run's nominal temperature), since this was the actual velocity scale used during the simulation. For the Maxwell-Boltzmann curve, on the other hand, the run average translational root mean square velocity was used. The curves represent, then, the theoretical and "experimental" velocity frequency distributions corresponding to a temperature <T(tr)>.

The agreement with theory is very good in all cases. As an example, in Figure 10.2, the run's nominal temperature was 328.2 K, which, for CO_2, corresponds to a root mean square velocity of 431.34 ms^{-1}; the velocity intervals for this figure, therefore, have a width of (3/20) v_{rms}, or 64.70 ms^{-1}. The maximum difference between the Maxwell-Boltzmann and the computed frequency distribution (in dN/dv units) is ~ 0.024, which corresponds to 1.5 molecules (i.e., $(\Delta N/\Delta v)\ \Delta v$), or 1.4% of the total number of molecules.

Non-zero computed dN/dv values span a velocity range which can vary from $32.5 < v < 1068$ ms^{-1} (Figure 10.2) to $32.5 < v < 1262$ ms^{-1} (Figure 10.6). In any given simulation, therefore, molecular velocities vary by factors of up to 30 or 40.

In the present case, with an integration step of 10^{-15} sec, a velocity of 32.5 ms^{-1} corresponds to 3.25×10^{-4} Å/step, which represents 4.4×10^{-5} of the cutoff radius (7.4 Å), or 26.8% of a potential tabulation length unit. For a velocity of 1262 ms^{-1}, on the other hand, the corresponding values are 1.26×10^{-2} Å/step, 1.7×10^{-3}, and 1040%, or 10.4 potential tabulation length units, repectively. Numerically, then, it can be seen that integration accuracy (i.e., energy conservation) is favoured by the statistical irrelevance of high energy molecules.

10.2: RADIAL DISTRIBUTION FUNCTIONS

Given a particle i (molecule) located at a certain point in space, the number of particles located within a spherical shell of mean radius r and width δr about i is given by

$$\frac{\delta N}{N-1} = \frac{4\pi r^2 \delta r}{V} g(r) \qquad (10.3)$$

where N is the total number of molecules in a volume V, and g(r) is the radial distribution function (McQuarrie, 1976), the most important features of which will now be summarized.

In a structureless fluid, such as an ideal gas, g(r) is unity throughout since the particles exert no influence upon each other, and hence the number of particles within any given volume about particle i is independent of i's presence, and is simply proportional to the volume considered.

Molecules interacting via van der Waals forces, on the other hand, repel each other strongly at short distances and attract each other at long distances. This leads to the establishment of local order in dense fluids (Widom, 1967; Chandler et al., 1983), whereby each molecule is, statistically speaking, surrounded by a "nearest neighbour shell" (or $g(r) > 1$, mathematically). Moreover, g(r) decays abruptly to zero as $r \to 0$ due to the steeply repulsive part of the intermolecular potential, and becomes unity at large distances, since the influence of the central molecule (i) is then negligible. Secondary peaks where g(r), though greater than 1, is smaller than at the nearest neighbour peak, arise at high densities as a consequence of close packing. These qualitative features are shown schematically in Figure 10.8. The usefulness of a function like g(r) is two fold. In the first place, for a given temperature and intermolecular potential, knowledge of g(r) implies knowledge of the compressibility (Hirschfelder et al., 1964), since this quantity, as discussed in Chapter 8 in connection with the virial theorem (Equation 8.72), is a function of the average relative positions and forces between all possible molecular pairs, and of the temperature; g(r), on the other hand, is simply the mathematical expression of the distribution of intermolecular separations. In addition to this quantitative aspect (which will not be used here) g(r) provides a very graphical description of structure and local order in the fluid.

Finally, it must be emphasized that g(r) is a statistical concept. Order in a fluid cannot be directly observed: it is always inferred by statistical arguments.

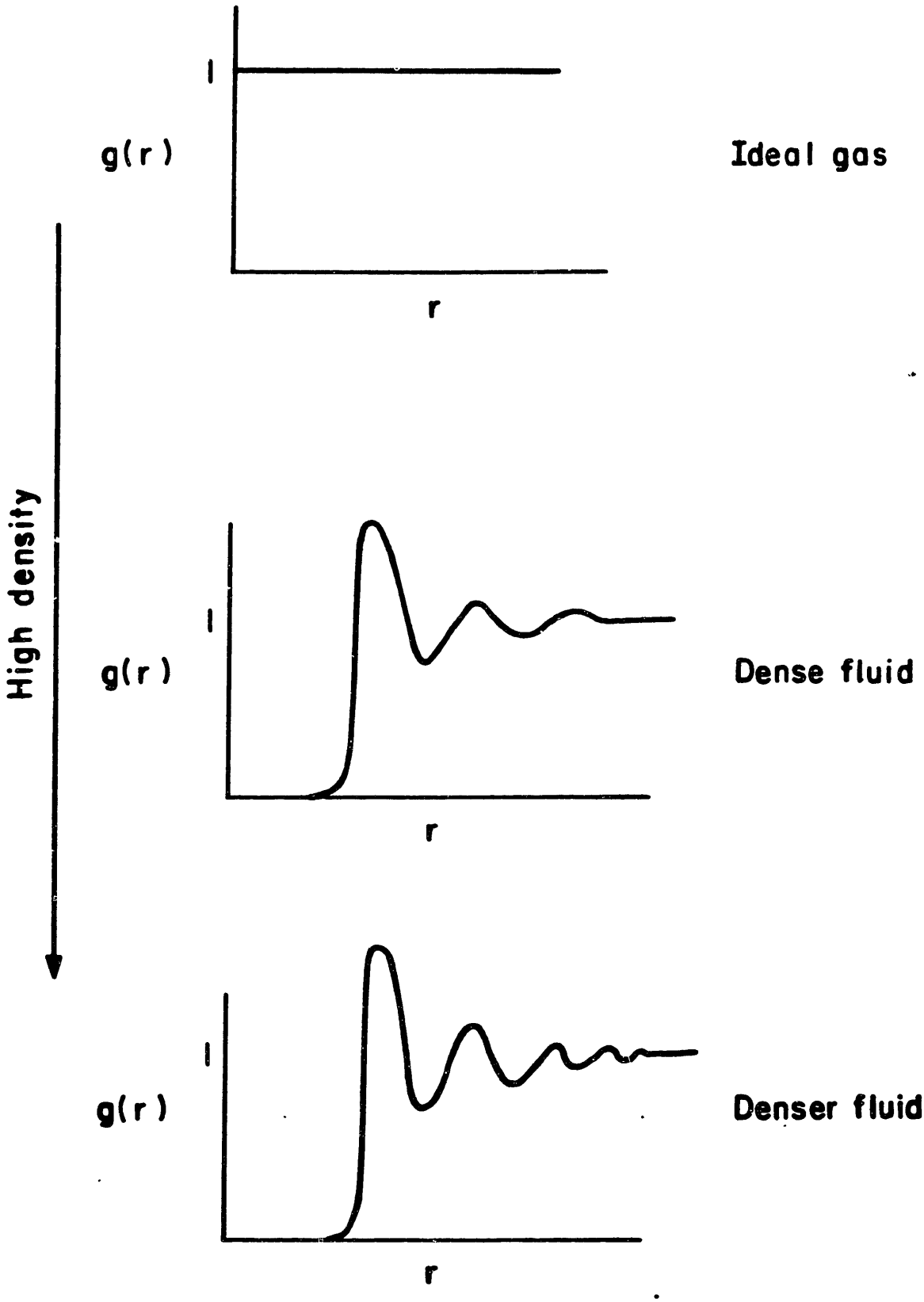

FIGURE 10.8: Qualitative features of the radial distribution function

In the simulations, the radial distribution function of the CO_2 carbon centers was computed by dividing the maximum possible intermolecular distance (i.e., half the side of the cube where the simulation takes place) into twenty equal intervals. Several "snapshots" of the system were taken, and the positions of all the CO_2 centers were recorded. For every "snapshot", all possible pairs were scanned, and the respective separations classified into one of the twenty distance intervals. Averaging over all molecules and all "snapshots", the radial distribution was obtained,

$$\langle g(\bar{r})\rangle = \frac{\langle \Delta N(\bar{r})\rangle}{4\pi \bar{r}^2 \Delta r} \cdot \frac{V}{N-1} \qquad (10.4)$$

where $\langle\ \rangle$ denotes averaging over all molecules and "snapshots", $\bar{r}$ is the mid-point of the distance interval, and Δr is (1/40)th of the cube's side.

Roughly 55 "snapshots" per simulation were taken, which, coupled with the number of solvent molecules considered (107), implies that each calculated $\langle g(\bar{r})\rangle$ curve is the average of nearly 6000 "measurements". The details of the computational procedure used to calculate radial distribution functions with periodic boundary conditions can be found in Appendix 5 (computer program NEUTRAL-2).

The nature of the solute-solvent interaction and its temperature and density dependence are ideally suited to a distribution function approach. In this case, one would compute the radial and angular distribution of CO_2 centers about the solute molecule's center. However, a smooth curve cannot be generated from a single solute particle, since the averaging can only be done over the "snapshots". These can only be increased by a limited amount (certainly not 100-fold) without making either the duration of a simulation or the computer memory requirements unacceptable. Increasing the number of solute molecules, on the other hand, is an even more impractical approach, since the number of solvent molecules must then be dramatically increased if the simulation is to be done at infinite dilution conditions.

The important conclusion, therefore, is that the study of the equilibrium aspects of solute-solvent interactions at infinite dilution requires computer speed and memory well beyond those used in the present work.

The effect of density upon the radial distribution function is shown in Figure 10.9. The higher density (10.53 mol/lt) curve was obtained from 58 "snapshots", whereas the lower (7.42 mol/lt) density curve is the average of 53 "snapshots". The run average temperatures were, respectively, 314.9 K and 316.5 K. Although the densities are moderate, and the fluid structure is limited almost exclusively to the nearest neighbour peak in both cases, it can be seen that a mild secondary peak exists at 10.53 mol/lt, whereas no structure beyond the nearest neighbour peak exists at 7.42 mol/lt.

As explained above, the interval width corresponds to (1/40)th of the cell size; since separations are assigned a nominal value equal to the interval's mid-point, this implies an uncertainty of (1/80)th of the cell size. For the densities considered in Figure 10.9, the cell size and the corresponding uncertainties are 25.73 Å and 0.32 Å (10.53 mol/lt; 6.34×10^{-3} molec/Å^3), and 28.91 Å and 0.36 Å (7.42 mol/lt; 4.4×10^{-3} molec/Å^3).

The effect of temperature at constant density is shown in Figure 10.10, corresponding to simulations at 13.87 mol/lt (8.35×10^{-3} molec/Å^3), with average run temperatures of 304.2 K and 329.8 K, respectively. The high temperature curve was obtained from 56 "snapshots"; the low temperature curve, from 53. The cell size corresponding to this density is 23.47 Å, and the length uncertainty is therefore 0.29 Å. As was the case with Figure 10.9, we see a mild secondary peak gradually disappearing, this time due to temperature.

The densities considered in these simulations are moderate. As will be explained below in connection with the calculation of diffusion coefficients, statistical problems arise at high densities, and this constitutes one of the most severe limitations of the one-molecule approach to the calculation of transport properties.

For the densities considered, therefore, we conclude that structure in the fluid phase is primarily limited to a nearest neighbour shell whose density is between 35% and 45% higher than the bulk density. The average radius of this nearest neighbour shell is roughly 4 Å . A mild outer shell (density between 3% and 7% higher than the bulk density) can be detected, under appropriate conditions; the radius of this outer shell is roughly 7.5 Å.

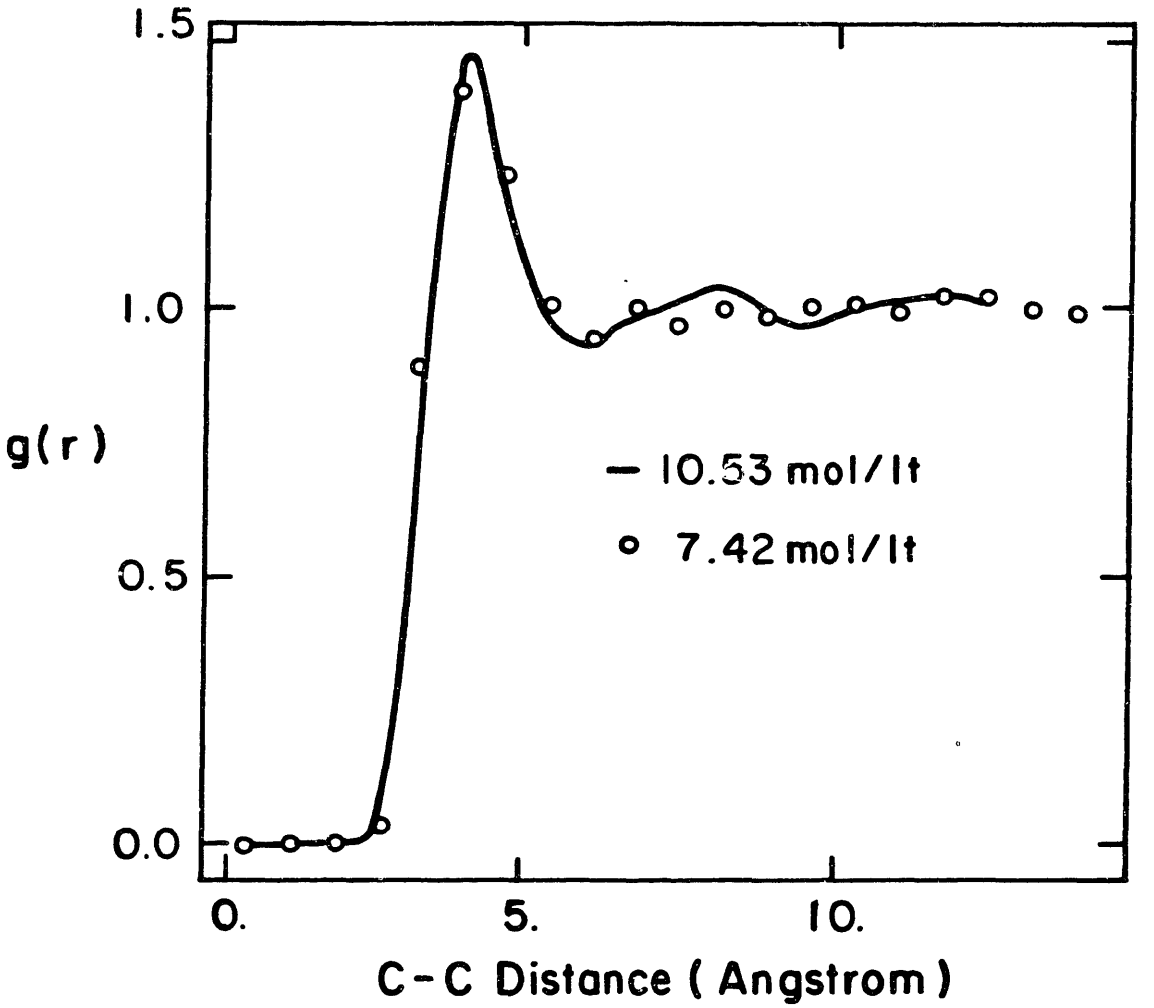

FIGURE 10.9: Effect of density upon g(r). Density = 10.53 mol/lt, <T> = 314.9 K, sample size = 58; Density = 7.42 mol/lt, <T> = 316.5 K, sample size = 53

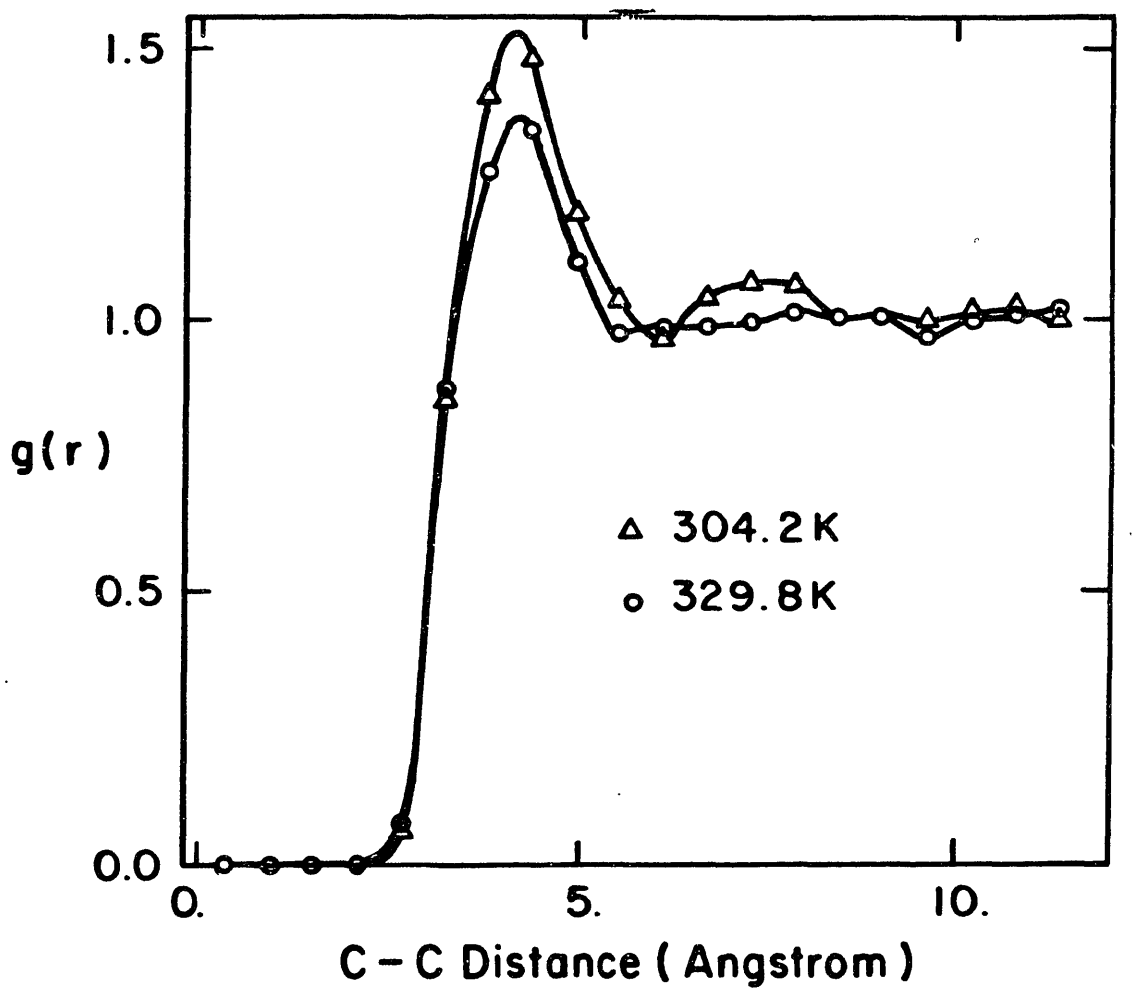

FIGURE 10.10: Effect of temperature upon g(r); Density = 13.87 mol/lt. <T> = 304.2 K, sample size = 53; <T> = 329.8 K, sample size = 56

10.3: DIFFUSION COEFFICIENTS

Diffusion coefficients were calculated by a method based on Einstein's statistical treatment of diffusion (Section 8.4). Specifically (see Equation (8.41)) the theory predicts that, for times greater than a characteristic relaxation time, the mean squared displacement of an ensemble of particles with respect to an arbitrary initial configuration increases linearly with time, the proportionality constant being 6D (or, more generally, 2dD, where d is the dimensionality of space where the diffusion under study takes place, and D is the particles' diffusion coefficient).

In the present case, with only one solute particle as the sample, the equivalence between time and ensemble averaging was invoked to generate an ensemble as explained in Figure 10.11 where ϕ is a generic property. In a simulation, M diffusion "experiments" with n time steps each were conducted. The position of the single solute particle at the beginning of each experiment was recorded, and squared displacements at corresponding time intervals were averaged over the M "experiments", to yield the generic expression for the i^{th} (i = 0, 1, ..., n) mean squared displacement, shown in Figure 10.11.

The equivalence between time and ensemble averaging is strictly applicable only if each of the M experiments is statistically independent from the rest, which, physically, requires that the experiments be non-overlapping. This was not possible in the present case since the simulations would have become too long. The reason behind this limitation lies in the duration of a single experiment, which, as will be seen from the results below, must be of the order of 1.5×10^3 integration steps (with a time step of 10^{-15}sec) in order to guarantee that the computed mean squared displacement versus time relationship covers a time span at least three times greater than the relaxation time.

Given the way in which the ensemble was generated, whenever the solute particle underwent an interaction which caused an unusual change in its configuration (position, velocity) or, in other words, a "violent collision", this event was "felt" throughout the M experiments, and deviations from linearity in the $\langle r^2 \rangle$ vs. time curve occured. This, of course, would

$$\langle \phi \rangle = \lim_{\tau \to \infty} \frac{1}{\tau} \int_0^{\tau} \phi \, dt$$

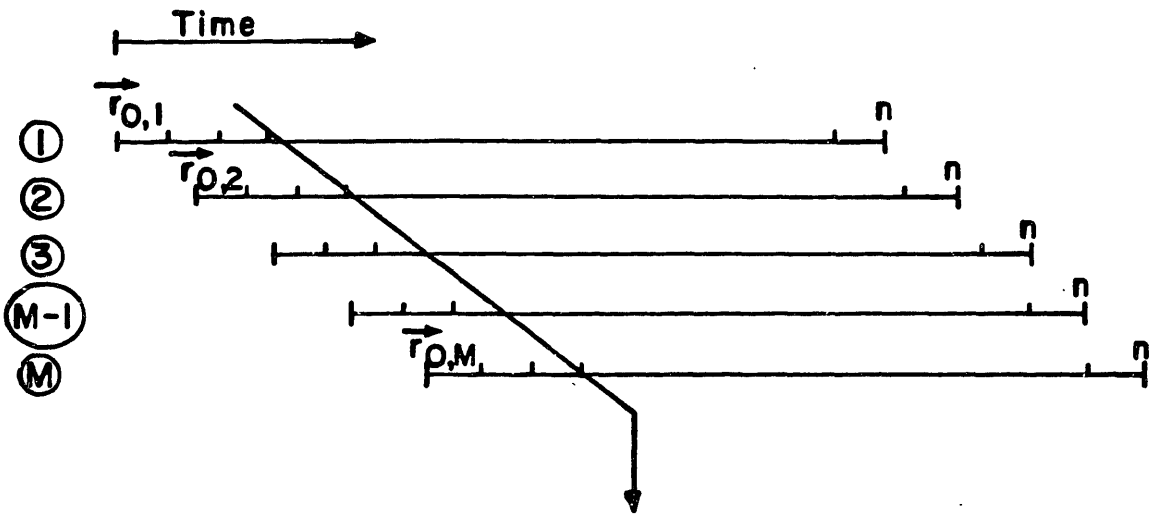

$$\langle r_i^2 \rangle = \frac{1}{M} \cdot \sum_{j=1}^{M} (\vec{r}_{i,j} - \vec{r}_{o,j}) \cdot (\vec{r}_{i,j} - \vec{r}_{o,j})$$

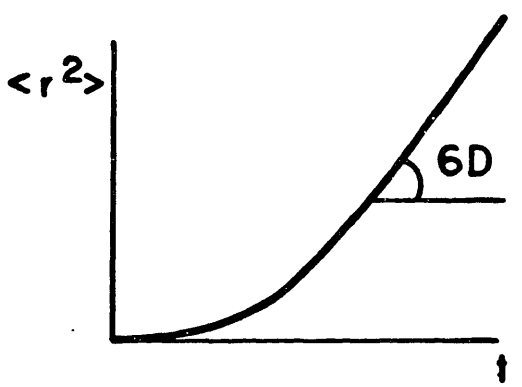

FIGURE 10.11: Ensemble generation for test-particle "experiments"

not have happened with an ensemble consisting of truly independent experiments. Since such events become more frequent the higher the density, deviations from linearity occured in a considerable proportion (~ 50%) of high density simulations. This is the reason behind the relatively moderate densities that were used in the present work.

We conclude that the generation of a time ensemble composed of strictly independent "experiments" from the dynamic simulation of the motion of one rigid polyatomic solute molecule and as few as 107 rigid polyatomic solvent molecules is already a problem which requires at least an order of magnitude increase in computer speed with respect to the machine used in the present simulations. This can be seen by comparing the length of a simulation with 21 overlapping experiments of 1600 steps each (~ 28 CPU hours for 3200 integration steps, at 31 seconds per step) with the corresponding requirements for 21 successive experiments of the same length (~ 289 CPU hours for 33600 integration steps, at the same speed). The above computer speed figure (31 seconds per step) is indicative; as explained in Chapter 9, this number is a function of the simulated density.

As discussed above in connection with the calculation of radial distribution functions, the alternative approach is to generate an ensemble by considering more than one solute molecule, with the corresponding increase in solvent molecules. Hoheisel (1983) studied binary diffusion of benzene in dense CO_2 using this approach, by considering 62 benzene and 1310 CO_2 molecules, modelled, respectively, as a one center Lennard-Jones and a one-center Lennard-Jones plus point dipole. Even with these highly simplified potentials, the simulations required the use of a Cyber 205 computer.

In the present work, 21 "experiments" were conducted in each simulation, with eighty time steps between successive "experiments", each of which lasted roughly 1600 time steps (i.e., 1.6×10^{-12} sec, with an integration step of 10^{-15} seconds). The duration of the "experiments" was varied in different simulations between a maximum of 1920 (1.92×10^{-12} sec) and a minimum of 1440 (1.44×10^{-12}sec) steps.

Squared displacements with respect to the initial positions were recorded every fourty time steps. Although the use of periodic boundary

conditions (see Chapter 9) implies a sudden shift in the coordinates of a particle whenever it leaves the cube where the simulations occurs, this was done, for the solute particle, only for force and torque calculations. For the calculation of diffusion coefficients, on the other hand, the true coordinates were recorded (i.e., the solute molecule was allowed to have coordinates greater than one and/or smaller than zero). This implies two separate book-keeping procedures for the single solute molecule (see Appendix 5, computer program LINALB).

The temperature dependence of binary diffusion coefficients in supercritical fluids, as was discussed in Chapter 6 in connection with the experimental results, cannot be described by a simple power law relationship, such as the $T^{1/2}$ dependence at constant density predicted by hard sphere theory. Diffusion coefficients exhibit an activated behaviour, which has been observed both experimentally (Feist and Schneider, 1982) and through computer simulations (Hoheisel, 1983).

Figure 10.12 is a plot of the mean squared displacement versus time for two different simulations at the same density (10.53 mol/lt, 6.34 x 10^{-3} molecules/$\mathring{A}^3$) but different temperatures. The temperatures shown in the figure are run average translational temperatures.

Four diffusion coefficients corresponding to simulations at the same density (10.53 mol/lt) are shown in Table 10.1, and are plotted in Figure 10.13 in Arrhenius fashion; the least-squares regressed activation energy is 14.8 KJ $mole^{-1}$. This number is to be compared with the 5.1 KJ $mole^{-1}$ figure obtained by Hoheisel (1983) at 13.64 mol/lt in his molecular dynamics calculations, and with the 10.9 KJ $mole^{-1}$ and 10 KJ $mole^{-1}$ (at 9.55 mol/lt and 14.45 mol/lt, respectively) calculated from the experimental measurements of Swaid and Schneider (1979), in all cases for the CO_2 - benzene system. The calculated activation energy is therefore 35.7% higher than the experimental value at a similar density.

The activation energy obtained from the Arrhenius plot should be interpreted with caution, since temperature is not a variable that can be directly controlled in a simulation. Instead, while volume and (ideally) energy are held constant, pressure and temperature fluctuate during the course of a simulation. In addition, the very concept of temperature is a statistical one, implying a distribution of velocities (see Section

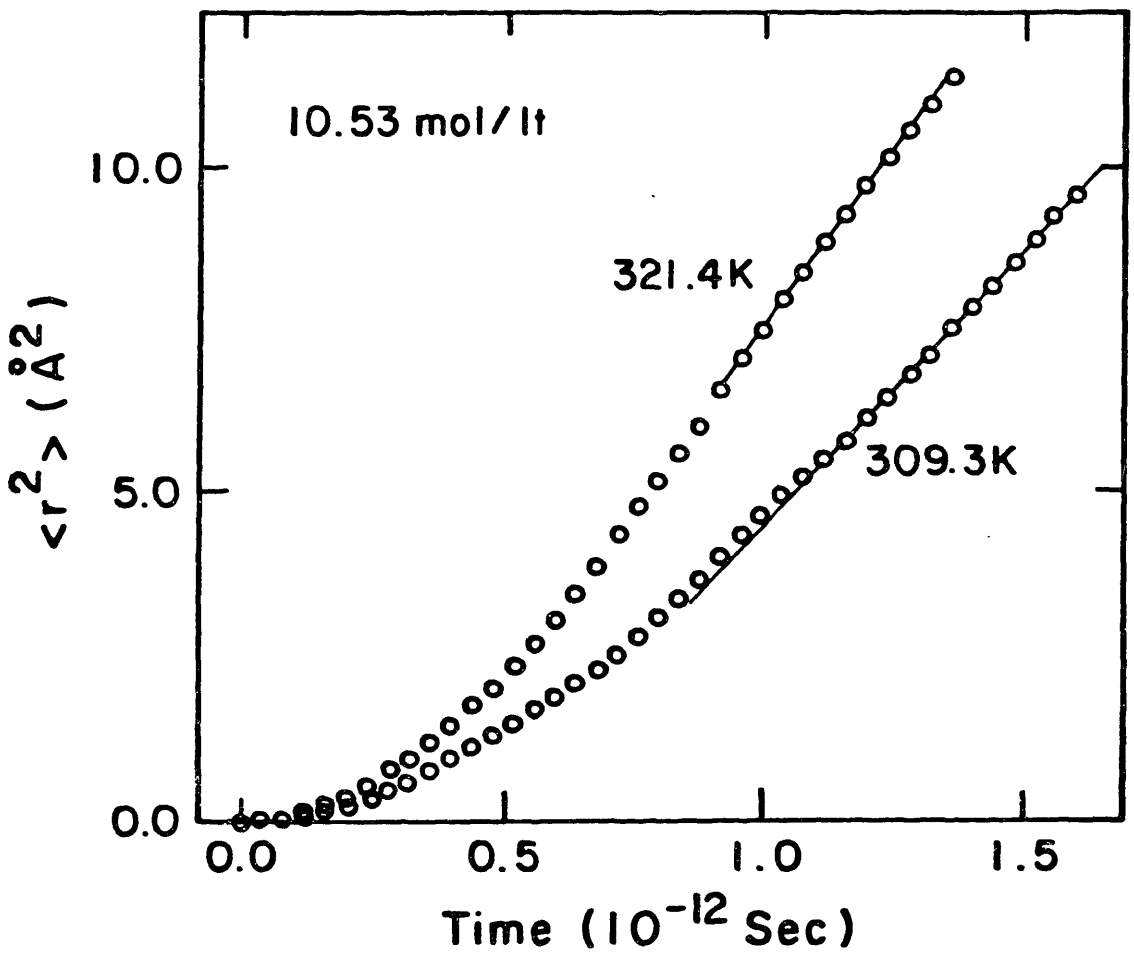

FIGURE 10.12: Temperature dependence of the mean squared displacement versus time relationship. Density = 10.53 mol/lt

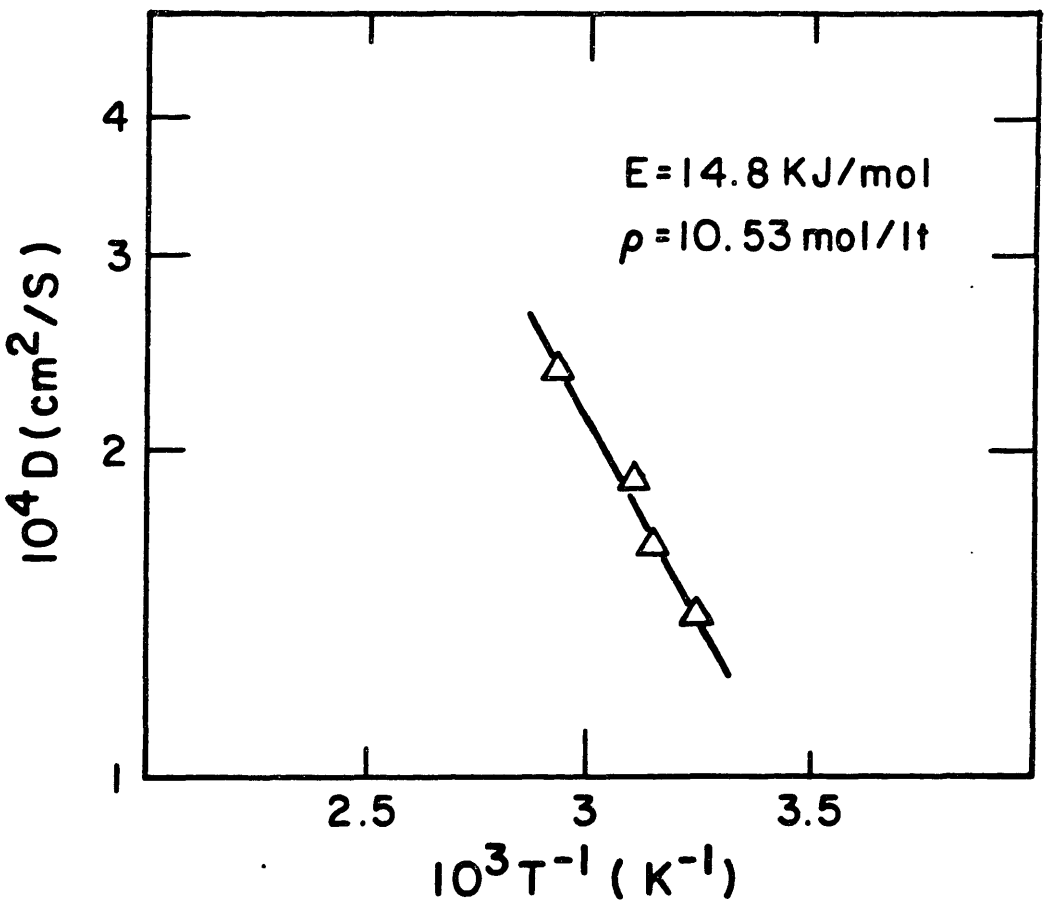

FIGURE 10.13: Arrhenius plot for four different simulations at a density of 10.53 mol/lt.

10.1), whereas there is but one solute molecule in the presently considered simulations.

If, however, we accept the activation energies calculated from Swaid and Schneider's experiments (although more than two temperatures were considered in that work, constant density data were taken at two different densities and just two temperatures in each case), we must then conclude that the presently chosen method of ensemble generation not only predicts the right trends, but also gives reasonable estimates of actual physical properties.

The calculated standard deviations in the run average translational temperature and in the run average translational (plus rotational) temperature are given in Table 10.1. These numbers were obtained from more than three hundred values, corresponding to an update of key run indicators (temperature, energy, compressibility, etc.) performed by the program every ten steps. Even though the relative standard deviations are small, they represent non-negligible numbers when converted to degrees. This aspect of the simulations is independent of energy conservation, accuracy and stability considerations, and is due to the fact that fluctuations of macroscopic properties scale inversely as the square root of the ensemble size (Landau and Lifshitz, 1980). Since the duration of a simulation is a quadratic function of sample size, we must have

$$\frac{\left[\langle\Delta\phi\rangle/\langle\phi\rangle\right]_1}{\left[\langle\Delta\phi\rangle/\langle\phi\rangle\right]_2} = \left(\frac{N_1}{N_2}\right)^{-1/2} = \left(\frac{t_1}{t_2}\right)^{-1/4} \qquad (10.5)$$

where ϕ is a generic property, N, the number of molecules in the simulation, and t, the run's duration (in CPU units). The first equality follows from statistical mechanics, the second, from pairwise additivity. From Equation (10.5) we conclude that reducing a given relative fluctuation by a factor of two requires increasing the ensemble size by a factor of four, and leads to a sixteen-fold increase in computer time (given an event of fixed duration to be simulated).

The isothermal density dependence of the measured diffusion coefficients is shown in Figure 10.14, for simulations at 310.3K, 7.42 mol/lt (4.47×10^{-3} molec/Å^3) and 309.3K, 10.53 mol/lt (6.34×10^{-3} molec/Å^3). The corresponding diffusion coefficients are shown in Table 10.2. If the

Table 10.1: DIFFUSION COEFFICIENTS CORRESPONDING TO FIGURE 10.13

$\langle T \rangle$(*) (K)	$\langle \Delta T \rangle / \langle T \rangle$(**) (-)	$\langle \Delta T \rangle / \langle T \rangle$(***) (-)	D (cm^2/s)
309.3	.0554	.0257	1.396×10^{-4}
318.6	.0368	.0171	1.608×10^{-4}
321.4	.0476	.0172	1.850×10^{-4}
342.3	.0372	.0227	2.430×10^{-4}

(*) run average translational temperature

(**) relative standard deviation (translational temperature)

(***) relative standard deviation (translational & rotational temperature)

Table 10.2: DIFFUSION COEFFICIENTS CORRESPONDING TO FIGURE 10.14

ρ (mol/lt)	D (cm^2/s)
7.42	1.649×10^{-4}
10.53	1.396×10^{-4}

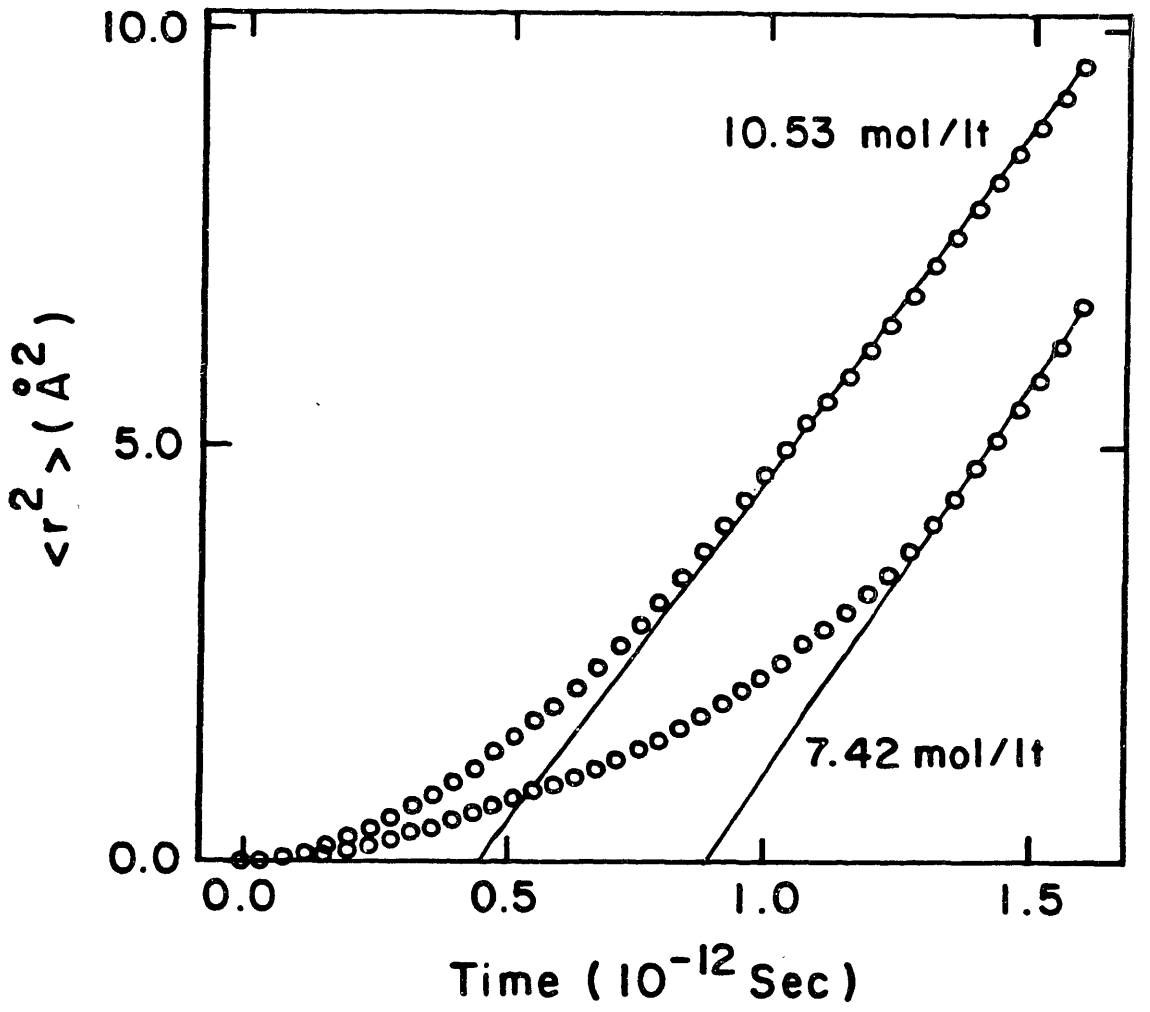

FIGURE 10.14: Density dependence of the mean squared displacement versus time relationship. $\langle T(tr) \rangle$ = 309.3 K, ρ = 10.53 mol/lt; $\langle T(tr) \rangle$ = 310.3K, ρ = 7.42 mol/lt

linear part of the mean squared displacement versus time relationship is projected to zero displacement, we obtain an abscissa intercept which can be used as an estimate of the relaxation time. Although hydrodynamic arguments (see Chapter 6) can be used only in a qualitative way, due to the moderate densities (viscosities) involved, they are extremely useful in the present context. The relaxation time for a Brownian particle (Equation (8.48)) is given by

$$\Delta\tau = \frac{m}{6\pi\eta a} \tag{10.6}$$

where m and a are, respectively, the mass and radius of the Brownian particle, and η is the viscosity of the continuum fluid.

Since the viscosity of a dense fluid increases with density at constant temperature, the trends shown in Figure 10.14 are consistent with Equation (10.6). The relaxation times are, respectively, 4.51×10^{-13} sec at 10.53 mol/lt, and 8.78×10^{-13} mol/lt at 7.42 mol/lt. At 310K, the corresponding CO_2 pressures, calculated from the Peng-Robinson equation of state, are 85.6 (10.53 mol/lt) and 80 bar (7.42 mol/lt). From Figure 3.5, it can be seen that large changes in viscosity occur precisely in this region. The detailed discussion of Chapter 6 shows that these arguments cannot be pursued further in a quantitative way, i.e., since the behaviour is not truly hydrodynamic, changes in relaxation times cannot be calculated, but only explained in terms of viscosity changes. However, as was the case with the interpretation of the experimental results, hydrodynamic arguments provide an extremely useful framework for data analysis and interpretation even when Stokes-Einstein-based expressions constitute a high viscosity limit rather than a quantitative description of molecular behaviour.

The sharp increase in relaxation times at lower densities introduces another practical limitation. As explained above, the interval between successive experiments is 8×10^{-14} sec (80 time steps), which represents ~ 18% of the relaxation time at a density of 10.53 mol/lt, and ~ 10% at the lower density. Thus, although each individual integration step is faster at low densities (see Chapter 9), the statistical independence of the individual "experiments" becomes progressively worse, and calls

for a greater inter-experiment interval, with the consequent increase in computer time for the same number of "experiments".

In addition, it can be seen from Figure 10.14 that, regardless of statistical independence considerations, the long relaxation times at low densities will give rise to results which can appear unphysical if not adequately interpreted. In fact, the very interesting behaviour illustrated in Figure 10.14 is a direct consequence of the principles discussed in Chapter 8. At short times (Equation (8.47)), the mean squared displacement is quadratic in time, and depends only on molecular mass and temperature. Thus, for a given solute and temperature, Figure 10.14 simply shows how the longer relaxation time dominates the short time behaviour of the low density experiment.

In spite of the limitations explained in detail in Chapter 6 regarding the predictive use of hydrodynamic expressions in the supercritical region, it is interesting to compare Equation (10.6) with the relaxation times obtained in the present simulations by extrapolating the linear part of the mean squared displacement versus time relationship down to zero displacement. For these purposes, we use the following property values:

$m = 1.295 \times 10^{-25}$ kg (mass of benzene molecule)

$a \sim 2.5$ Å (center of mass-to-hydrogen distance)

$\eta \sim .05$ cp (Figure 3.5, 310 K, 90 bar)

to obtain

$\Delta\tau \sim 5.5 \times 10^{-13}$ sec

in excellent qualitative agreement with the results obtained in the simulations.

A very interesting theoretical question is raised by the fact that, although in the simulations the mean squared displacement exhibits a linear behaviour at long times, the relationship $\eta D T^{-1} = f$ [size] (see Chapter 6) is only an asymptotic law approached at high viscosities. This apparent paradox can be explained by noting that the long time relationship between $\langle r^2 \rangle$ and time can be derived (see Chapter 8) without postulating any explicit form for the hydrodynamic drag. Alternatively (Chandrasekhaar, 1943, see also Chapter 8), starting from the Langevin equation, the limits $\langle r^2 \rangle \sim t^2$ $(t \to 0)$ and $\langle r^2 \rangle \sim t$ $(t \to \infty)$ can again be obtained without postulating any form for the drag coefficient, β, although the drag term

itself is, in this approach, proportional to the particle's velocity (with an as yet undefined proportionality constant, β).

We conclude, therefore, that, if β is non-linear in η (i.e., $\beta \sim \eta^{\delta}$, for example), the Stokes-Einstein equation (or, more precisely, its form, i.e., $\eta D T^{-1}$ = f [size]) would not describe physical reality; in spite of this, though, the short and long time limits of $\langle r^2 \rangle$ would, of course, still be parabolic and linear, respectively, and the fundamental relationship between $\langle r^2 \rangle$ and D at long times would still be valid.

The breakdown of hydrodynamic behaviour in supercritical fluids, then, is associated with a "hydrodynamic" drag that can best be explained in terms of a power law relationship between the drag coefficient and viscosity.

Using the activation energy calculated from the log D vs. T^{-1} plot (Figure 10.13), we can estimate a diffusion coefficient at 313.2 K and 10.53 mol/lt from the value obtained at 309.3K and the same density. This number (1.5×10^{-4} cm^2/s) is to be compared with the value obtained by graphical interpolation of Swaid and Schneider's data at the same temperature (2.05 cm^2/s).

The molecular dynamics prediction is 36.7% lower than the experimental value. This is a remarkable result, given the facts that no adjustable parameters were used in this work, and that the ensemble-generating technique involved just one solute particle.

Linearity in the mean squared displacement versus time relationship is, by itself, an indication of the correctness of the ensemble generating procedure. However, since this is, essentially, a test-particle method (Herman and Alder, 1972; Alder et al., 1974) the accuracy of the calculated diffusion coefficients should be considered semiquantitative; ensemble averaging over different runs would obviously make the predictions quantitative; this, however, contradicts the spirit of test-particle studies. Although, as shown above, the method reproduces the basic trends and even gives good estimates for the actual properties, the test-particle approach is not to be interpreted as a predictive substitute of large ensemble methods, but as a convenient way of studying the basic physical phenomena within the limits imposed by time sharing and an average mainframe computer.

10.4: SIMULATIONS WITH COULOMBIC INTERACTIONS

As mentioned in Chapter 9, the large quadrupole moment of CO_2 (-1.43×10^{-39} Cm^2) implies that electrostatic forces should be taken into account in any realistic simulation of this molecule. In this work, the approach was to superimpose localized partial charges (point monopoles) upon the van der Waals interactions, with the resulting potential centered upon the same site (i.e., the van der Waals and electrostatic sites coincide). Truncation was done as explained in Chapter 9, the plausibility of the approach being based upon the effective short range behaviour of the intermolecular interactions resulting from pairwise additive long-range interatomic interactions.

This approach introduces, at the outset, problems in the determination of site-site interaction parameters, due to the fact that the van der Walls part of the elementary binary interaction contained length and energy parameters (σ, ε) calculated from the Slater-Kirkwood formula (Suter, 1979) (Equation 9.32). This equation represents, essentially, a self-consistent method of describing site-site interactions in terms of a Lennard-Jones type potential. The fundamental fact about the Slater-Kirkwood equation, however, is that the electrostatic properties of the site are already taken into account through the polarizability and the effective number of outer shell electrons, which are used to calculate σ and ε. The redundancy of adding point monopoles is thus evident, at least in principle.

In the case of CO_2, however, the Lennard-Jones parameters calculated from the Slater-Kirkwood formula do not reproduce experimental P-V-T behaviour, at least in the supercritical region (this will be discussed below in detail). One is then forced to try to correct this apparent inability of a van der Waals potential to reproduce the thermodynamic behaviour of a substance (CO_2) for which important coulombic effects have been experimentally measured by introducing electrostatic contributions, at the expense of internal consistency.

Two characteristics of electrostatic interactions were responsible for the failure of the attempt to successfully incorporate coulombic forces into the simulations. In the first place, as was discussed at

length in Chapter 9, (see Figures 9.10 - 9.21) the effective coulombic intermolecular force and potential obtained from the elementary pairwise additive site potentials and forces are both strongly dependent upon the relative orientation of the molecules, a feature which is, generally speaking, absent in van der Waals interactions. In the second place, at distances which correspond, approximately, to the nearest neighbour peak (i.e., ~ 4 Å), although the effective van der Waals potential and force components are roughly an order of magnitude higher than the corresponding Coulombic interactions, this happens as a result of the cancellation of elementary electrostatic site-site forces and energies which are considerably greater, in absolute value, than the corresponding van der Waals elementary interactions. This is illustrated in Figure 10.15 and Table 10.3 for a specific case. Figure 10.15 shows the particular geometry, charge distribution and Lennard-Jones parameters considered; the resulting elementary energies and forces (the latter exerted on the 1-2-3 molecule along the x-y directions) are shown in Table 10.3.

We therefore, conclude that electrostatic forces introduce stiffness into the problem. Starting from the charge distribution implied by the measured quadruple moment of CO_2 $(-1.43 \times 10^{-39}$ Cm² (Murthy et al., 1981)) and the inter-site separations shown in Figure 10.1, we obtain partial charges of -0.2956 and + 0.5912 on the oxygen and carbon sites, respectively (in electronic charge units). This was originally superimposed upon the Slater-Kirkwood Lennard-Jones potential (see Table 9.3).

Although automatic rescaling during relaxation runs was not implemented until later into the project, these trial runs already showed the essential "pathology" of electrostatic simulations: large fluctuations in temperature and compressibility (the latter often preventing the attainment of a long time limit). The temperature excursions were, in general, short ranged (timewise), whereas the compressibility fluctuated over times comparable to the simulation time. After relaxation runs totalling 5000 integration steps at a density of 16.15 mol/lt, the compressibility factor, which, at the nominal temperature (310K) should have been .295, was apparently stabilized at a value of approximately 1.2 for the last 1000 steps. An extensive series of ad-hoc modifications of the van der Waals and electrostatic parameters was then tested, with the purpose of reproducing

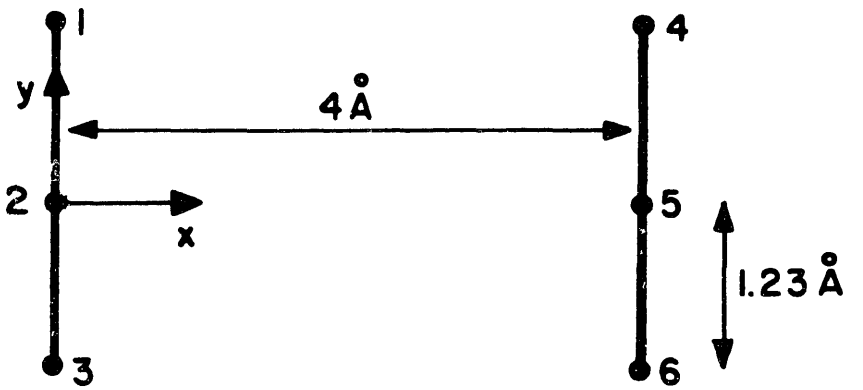

	ε/k (K)	σ (Å)
C - C	50.48	3.21
O - O	85.47	2.80
C - O	61.64	3.03

	Z (e)
C	+ 0.5912
O	- 0.2956

FIGURE 10.15: Geometry, charges and site parameters for solvent interaction case study

Table 10.3: VAN DER WAALS AND COULOMBIC INTERACTIONS FOR FIGURE 10.15

Pair	U(LJ) (10^{-20}J)	U(coul) (10^{-20}J)	fx(LJ) (10^{-12}N)	fx(coul) (10^{-12}N)	fy(LJ) (10^{-12}N)	fy(coul) (10^{-12}N)
1-4	-4.90×10^{-2}	+5.05	+6.369	-126.3	0	0
1-5	-4.38×10^{-2}	-9.735	+5.009	+226.1	-1.54	-69.53
1-6	-2.03×10^{-2}	+4.302	+2.101	-78.02	-1.292	+47.98
2-4	-4.38×10^{-2}	-9.735	+5.009	+226.1	+1.54	+69.53
2-5	-5.46×10^{-2}	+20.2	+5.203	-505.0	0	0
2-6	-4.38×10^{-2}	-9.735	+5.009	+226.1	-1.54	-69.53
3-4	-2.03×10^{-2}	+4.302	+2.101	-78.02	+1.292	-47.98
3-5	-4.38×10^{-2}	-9.735	+5.009	+226.1	+1.54	+69.53
3-6	-4.90×10^{-2}	+5.05	+6.369	-126.3	0	0
$\sum$	-3.68×10^{-1}	-3.6×10^{-2}	+42.179	-9.24	0	0

the true compressibility factor. These modifications included

- increasing the energy parameters (ε) by 20% to reduce the compressibility factor
- reducing the length parameters (σ) by - 5% to reduce the compressibility factor
- modifying the quadrupole moment by changing both the charge distribution and the site separation
- modifying all of the above parameters to reproduce the empirical three site plus point quadrupole potential parameters proposed by Murthy et al. (1981), where the point quadrupole is different from the experimental one

The essentially empirical nature of this procedure makes a detailed account of the effect of each of the above changes irrelevant for the present purposes. The essential points, however, can be summarized as follows:

- large electrostatic charges increased temperature fluctuations and gave rise to pressure fluctuations over time scales comparable to the duration of a relaxation run (~ 10^3 time steps)
- no single combination of parameters was found that could reproduce the compressibility. The best fit (and dynamic behaviour) were obtained with an ad-hoc modification of the Murthy et. al. (1981) parameters; the actual values are listed in Table 10.4. Since the compressibility factor fit (see Section 10.5), though improved with respect to the unmodified Slater-Kirkwood prediction, was still not satisfactory, this empirical approach was abandoned.

The most interesting feature of CO_2 simulations with electrostatic forces was the observation that, with the potential parameters listed in Table 10.4, temperature excursions were not coupled with poor energy conservation. In fact, the simulations which were carried out with the potential parameters as per Table 10.4 exhibited good energy conservation coupled with large temperature excursions (.928% standard deviation for

Table 10.4: EMPIRICAL SITE PARAMETERS FOR CO_2 SIMULATION

C-C	energy parameter (K)	34.8
C-C	length parameter (Å)	2.646
O-O	energy parameter (K)	99.72
O-O	length parameter (Å)	2.863
C-O	energy parameter (K)	58.92
C-O	length parameter (Å)	2.755
C-O	separation (Å)	1.16
O	charge (e)	-.214
C	charge (e)	+.428

the former, 47°C (maximum) for the latter, and, in a second run, .91% and 42°C, respectively). This seems to suggest that, although the algorithm is robust enough to handle a potential with moderate Coulombic components, the dynamics are sufficiently different as to require a much larger sample size.

The interesting and important problem of simulating the dynamics of CO_2, taking into account the significant electrostatic forces without resorting to purely empirical and time consuming fitting techniques, therefore, remains unsolved.

10.5: COMPRESSIBILITY FACTORS

Compressibility factors are calculated through the virial theorem. The expression was developed in Chapter 8 (Equation 8.72). As discussed in chapter 9, the most common approach in molecular dynamics is to obtain site or molecular parameters by fitting P-V-T behaviour. This approach was not followed here, the purpose being to perform a simulation with no adjustable parameters. This is especially justified in the case of the determination of diffusion coefficients, for which (see Chapter 6) the fundamental variables are density (and not pressure) and temperature.

Because of the significant coulombic contribution to the effective intermolecular potential of CO_2, the use of the Slater-Kirkwood parameters gives rise to compressibility factors which are considerably higher than the true values.

Table 10.5 lists results corresponding to sixteen simulations; <T> is the average translational and rotational temperature; P is the CO_2 pressure corresponding to <T> and V, as read from a P-V-T diagram derived from the International Thermodynamic Tables of the Fluid State (Angus et al., 1976) (Schmitt, private communication); Z(MD) is the compressibility factor as calculated from the simulation by averaging the instantaneous values printed every ten iterations (this value coincides, to within a fraction of one percent, with the long-time limit of the time average value calculated by the program as the simulation proceeds); P(MD) is, therefore, the pressure as calculated by the simulation; ε is the absolute value of the percent error (i.e., $\left|\frac{P_{MD}}{P} - 1\right| \times 100$). Values in parenthesis

Table 10.5: P-V-T PERFORMANCE OF SLATER-KIRKWOOD PARAMETERS

Run #	V (m^3/mol)	$\bar{T}$ (K)	P (bar)	Z(MD) (-)	P(MD) (bar)	ε (%)	ΔT_{max} (K)
1	9.4988×10^{-5}	314.9(1.71)	90	.732	201.8	124.2	29.3
2		328.9(1.72)	115	.793	228.3	98.5	25.5
3		333.7(1.45)	120	.721	210.6	75.5	22.2
4		312.2(2.57)	85	.808	220.8	159.8	36.8
5		319.9(2.50)	95	.844	236.3	148.7	38.4
7		325.7(2.41)	105	.751	214.1	103.9	34.8
8		328.2(2.27)	110	.845	242.7	120.6	32.5
9		337.1(2.27)	125	.823	242.8	94.2	33.7
10	7.21226×10^{-5}	329.8(1.84)	140	.782	297.3	112.4	28.2
11		312.9(3.04)	96	.713	257.2	167.9	44.0
12		304.2(2.29)	82	.689	241.6	194.6	40.7
13	1.3477×10^{-4}	324.8(1.86)	91	.814	163.1	79.2	33.3
14		330.8(1.72)	98	.830	169.4	72.9	32.3
15		316.46(1.30)	85	.827	161.5	90	24.1
Elec#1	6.19302×10^{-5}	340.94(3.25)	215	.680	311.3	44.8	47.2
Elec#2		322.36(2.47)	160	.597	258.4	61.5	41.4

in the temperature column indicate standard deviations expressed as percent of <T>. Elec #1 and Elec #2 denote two simulations performed with the parameters listed in Table 10.4. The last column, ΔTmax, is the maximum temperature difference that occured during the simulation.

It should be noted that the last two runs correspond to the best behaviour attained in the simulations with electrostatic charges. The average ΔTmax for non-electrostatic simulations was 32.6 K, the corresponding value for the best electrostatic simulations was 44.3 K. This confirms the previous discussion on the temperature behaviour of simulations with Coulombic forces. In addition, it must be noted that high values for non-electrostatic runs coincide with low temperature simulations (T_c=304.2K), whereas the electrostatic simulations were done at temperature levels where ΔTmax is substantially lower for the purely van der Waals simulations.

From Table 10.5 it must be concluded that the use of Slater-Kirkwood parameters is not satisfactory for the modelling of the thermodynamic properties of CO_2. The improvement obtained by introducing localized electrostatic charges indicates that potential improvement efforts should be oriented along these lines, but the problem of temperature (and pressure) fluctuations remains a significant challenge.

10.6: SUMMARY

The test particle approach predicts diffusion coefficients to within ~ 35% of experimental values, and, more importantly, reproduces the main trends, without adjustable parameters. This allows the semiquantitative study of infinite dilution diffusion processes without recourse to super-computers.

Results can be obtained, in the test particle method, within a narrow density range. At high densities, frequent deviations from linearity in the mean squared displacement versus time relationship occur, probably as a result of the insufficient statistical independence of the diffusion "experiments" in the light of the increased frequency of strong interactions. At low densities, the limitations result from the large relaxation times.

In the present work, diffusion exhibited Arrhenius behaviour; the resulting activation energy is within ~ 35% of the value calculated from

experiments at two different temperatures.

Velocity distributions are in excellent agreement with the theoretical (Maxwell-Boltzmann) prediction. Radial distribution functions have been generated for the carbon centers of the CO_2 molecules. The trends exhibited provide qualitative information on fluid structure and its density and temperature variation. Quantitative information can only be obtained from radial distributions by generating an ensemble of curves with an extremely narrow distance grid, and averaging over these histograms to eliminate the resulting noise.

The use of unmodified Slater-Kirkwood parameters is inappropriate for the modelling of P-V-T properties of CO_2; coulombic interactions must be taken into account, but this introduces stiffness which, even in cases where energy conservation is acceptable (which could only be attained by reducing the electrostatic forces), gives rise to large temperature excursions.

11 CONCLUSION

Supercritical fluids have exceptionally low kinematic viscosities. As a consequence, the inevitable density gradients which characterize mass transfer give rise, in the presence of a gravitational field, to buoyancy-driven flows which, for a given Reynolds number, are more than two orders of magnitude higher than in ordinary liquids (as measured by the ratio of characteristic buoyant to inertial forces).

Whenever the controlling resistance to mass transfer lies in the supercritical phase, significant buoyancy-driven mass transfer enhancements result. This has been verified experimentally in the present work. Future work should address this interesting aspect in a quantitative way.

Hydrodynamic behaviour at the molecular level is approached as a high viscosity (low fluidity) limit. Although constancy of ηDT^{-1} within a given system can be assumed for data extrapolation provided $\eta \geq 0.04$cp, the real need is for a fundamental theoretical understanding of the way in which the hydrodynamic limit is approached.

The concept of an infinite dilution fugacity coefficient, as well as a simple and accurate expression for the composition dependence of the solute fugacity coefficient in a binary mixture, from infinite dilution to saturation, have resulted from an analysis of diffusion in the light of irrreversible thermodynamics. These preliminary ideas merit more detailed consideration, and may have interesting thermodynamic implications.

A test-particle molecular dynamics study of binary diffusion in a rigid polyatomic ensemble with solute and solvent having different symmetry properties has been done. The results are encouraging, contain all the basic physics, and yield semiquantitative predictions for binary diffusion coefficients. The Einstein plots of mean squared displacement versus time constitute a very convenient representation of the relaxation behaviour and of the transition from a deterministic to a stochastic regime. The basic kinetic and thermodynamic characteristics of an equilibrium system (Maxwellian velocity distribution, pair distribution functions) can be obtained with as little as 108 molecules, due to the use of periodic boundary conditions.

The ensemble generating technique allows the study of infinite dilution interactions without recourse to supercomputers.

The rigorous (i.e., using a-priori site site potential parameters) dynamic simulation of CO_2, taking into account the electrostatic properties of this particular molecule represents a challenging problem. The orientation-sensitivity of the coulombic interactions make the problem stiff, and multiple time steps methods must be implemented.

APPENDIX 1 CUBIC EQUATIONS OF STATE

In the present context, an equation of state is a mathematical relationship between T,P,$\underline{V}$, and N, that is, the absolute temperature, pressure, volume and number of moles of a single phase system, which can have one or more components (throughout this Appendix, $\underline{V}$ denotes total (extensive) volume, whereas V denotes molar volume). As an example, the equation of state of an ideal gas is

$$P\underline{V} = NRT \qquad \text{(A1-1)}$$

Equation (A1-1) is an example of an analytic equation of state. Its use, however, is limited to the low pressure, high temperature region where the system behaves effectively as an ideal gas. A variety of equations of state are commonly used to describe the behaviour of real gases, dense fluids and liquids.

Cubic equations of state originate from the work of van der Waals, who proposed the equation that bears his name in his doctoral thesis (van der Waals, 1873)

$$\left(P + \frac{a}{V^2} \right).(V - b) = RT \qquad \text{(A1-2)}$$

or, in extensive form,

$$\left(P + \frac{aN^2}{\underline{V}^2} \right).(\underline{V} - Nb) = NRT \qquad \text{(A1-3)}$$

where a and b are parameters whose determination is discussed below. All existing cubic equations of state are modifications of the van der Waals equation. Their usefulness stems from the fact that a cubic polynomial in V is the simplest analytic relation that can qualitatively describe vapour-liquid equilibrium. For a single component, this means

two criticality conditions

$$\left(\frac{\partial P}{\partial V} \right)_{T=Tc} = 0 \qquad \text{(A1-4)}$$

$$\left(\frac{\partial^2 P}{\partial V^2} \right)_{T=Tc} = 0 \qquad \text{(A1-5)}$$

plus the existence of three distinct real roots in some range of temperature and pressure, bounded by an upper (critical) temperature and an upper (critical) pressure.

Although a cubic equation of state can describe qualitatively the behaviour of real gases and liquids, two important limitations should be taken into consideration. In the first place, density fluctuations become unbounded close to the critical point (Stanley, 1971), and, as a consequence, no analytic equation of state is accurate in this region, even though Equations (A1-4) and (A1-5) are still true. In the second place, an Equation such as (A1-2) cannot possibly describe phase equilibrium below the triple point of a pure substance, where the solid phase must be taken into consideration. An additional parameter and an equation of higher order in V are needed.

A cubic equation is characterized by its form and its parameters. The former can be written, in a general way (Schmidt and Wenzel, 1980)

$$P = \frac{RT}{V-b} - \frac{a}{V^2 + uVb + wb^2} \qquad \text{(A1-6)}$$

where u and w are integers. Values of u and w for several cubic equations of state are shown in Table A1-1.

Parameters a and b are determined by means of methods which, in general, are modifications of the original van der Waals approach. Applying the criticality conditions (Equations (A1-4) and (A1-5)) to Equation (A1-2), we obtain, with $T=T_c$ and $P=P_c$,

$$a = \frac{27}{64} \frac{(RT_c)^2}{P_c} \tag{A1-7}$$

$$b = \frac{RT_c}{8P_c} \tag{A1-8}$$

or, in other words, temperature-independent parameters.

Equations (A1-7) and (A1-8) can be considered particular cases of a more general type of functionality,

$$a = \alpha \, \Omega_a \frac{(RT_c)^2}{P_c} \tag{A1-9}$$

$$b = \beta \, \Omega_b \frac{RT_c}{P_c} \tag{A1-10}$$

where α, β, Ω_a and Ω_b vary according to the particular equation of state selected, and are introduced to improve agreement with experimental data. In Equations (A1-9) and (A1-10), α and β are, in general, temperature dependent whereas Ω_a and Ω_b are constants. Values of α, β, Ω_a and Ω_b are shown in Table A1-1 for several different equations of state.

Mixture parameters a and b are obtained from pure component parameters by means of suitable mixing and combining rules, of which the most commonly used are

$$\begin{aligned} a &= x_i \, x_j \, a_{ij} \\ b &= x_i \, b_i \end{aligned} \tag{A1-11}$$

$$a_{ij} = (a_i \, a_j)^{1/2} [1 - k_{ij}(1 - \delta_{ij})]$$

where k_{ij}, the binary interaction coefficient, is the single adjustable parameter once an equation of state is selected, and δ_{ij} is Kronecker's

delta.

TABLE A1-1 : PARAMETERS OF CUBIC EQUATIONS OF STATE

Equation	u	w	Ω_a	Ω_b	α	β
van der Waals (1873)	0	0	27/64	1/8	1	1
Redlich-Kwong (1949)	1	0	$[9(2^{1/3} - 1)]^{-1}$	$(2^{1/3} - 1)/3$	$T_r^{-0.5}$	1
Soave (1972)	1	0	$[9(2^{1/3} - 1)]^{-1}$	$(2^{1/3} - 1)/3$	$[1 + K_s(1 - T_r^{0.5})]^2$	1
Peng-Robinson (1976)	2	-1	.45724	.0778	$[1 + K_p(1 - T_r^{0.5})]^2$	1

$K_s = .37464 + 1.54226\ \omega - .26992\ \omega^2$

$K_p = .480 + 1.574\ \omega - .176\ \omega^2$

APPENDIX 2 EQUIPMENT DESIGN; EXPERIMENT DESIGN AND CALCULATIONS

A2.1 FLAT PLATE DESIGN

The flat plate is shown schematically in Figure 4.2. The coated section's width (2.54 cm) was determined by practical considerations: the high pressure steel tube (C2 in Figure 4.1) into which the whole assembly shown in Figure 4.2 is introduced had to be less than 5 cm (2 inches) in nominal external diameter; otherwise, the high pressure end connections would have become prohibitively expensive and much more complex than the threaded connections used in this work.

The entrance section (Figure 4.1) was designed in order to allow the development of a steady velocity profile. The hydrodynamic entrance length (Lhy) is defined (Shah and London, 1978) as "the duct length required to achieve a maximum duct section velocity of 99% of that for developed flow when the entering fluid velocity profile is uniform", and is given, in dimensionless form, by

$$L^{+}_{hy} = \frac{L_{hy}}{D_h Re} \qquad (A.2\text{-}1)$$

where D_h is the duct hydraulic diameter, and Re, the Reynolds number. In the present case, since the aluminium hemi-cylinders were shorter than the steel tube, the approximately 5 cm long empty inlet section was packed with glass wool to guarantee the flatness of the profile at the duct's entrance.

For a rectangular duct of height 2b, width 2a, and aspect ratio α = 2b/2a (see Chapter 5), the hydraulic radius is given by

$$r_h \equiv \frac{D_h}{4} = \frac{\text{Cross section}}{\text{Perimeter}} = \frac{b}{1 + \alpha} \qquad (A.2\text{-}2)$$

Furthermore, the Reynolds number can be written as

$$Re = \frac{4b}{1 + \alpha} \cdot \frac{\dot{G}}{\eta} \qquad (A.2\text{-}3)$$

where $\dot{G}$ is the mass flow rate per unit area, which, in terms of the solvent flow rate at ambient conditions becomes

$$\dot{G} = \dot{F}\ \left(\frac{lt}{min}\right) \times \frac{1}{60}\ \left(\frac{min}{sec}\right) \times \frac{1}{V_o}\ \left(\frac{mol}{lt}\right) \times M \times 10^{-3}\ \left(\frac{kg}{mol}\right) \times \frac{1}{4ab(m^2)} =$$

$$= 4.16666\ \left(\frac{\dot{F}M}{V_o\ ab}\right) \times 10^{-6} \qquad (A.2\text{-}4)$$

where V_o is the molar volume of the solvent gas at ambient conditions, which, for the present purposes, can be taken as 22.4 lt/mol, and M is the solvent's molecular weight. The hydrodynamic entry length becomes, therefore,

$$L_{hy} = L^{+}_{hy}\left(\frac{4b}{1+\alpha}\right)^2 \left(\frac{FM}{V_o\ ab}\right) \left(\frac{1}{\eta}\right) \times 4.1666 \times 10^{-6} \qquad (A.2\text{-}5)$$

Equation (A.2-5) is dimensional, and will yield L_{hy} in meters if $\dot{F}$, M, V_o, a and b have the units indicated in Equation (A.2-4), and η is expressed in kg/ms. Values of L^{+}_{hy} are tabulated in Shah and London's monograph, as a function of α; widely differing values are given, the table in question being a compilation of results from different investigators. In the present case, the most conservative (i.e., highest) value was selected,

$$L^{+}_{hy} = 0.08 \qquad (A.2\text{-}6)$$

For a typical flow rate of 2 liters per minute, $a = 1.27 \times 10^{-2}$ m, $b = 1.587 \times 10^{-3}$ m, $\alpha = 0.125$, $V_o \sim 22.4\ \frac{lt}{mol}$, $\eta \sim 5 \times 10^{-5}$ kg/ms, (a conservatively low value), L_{hy} is then given by

$$Lhy = 9.4 \times 10^{-4}\ M \quad (m) \qquad (A.2\text{-}7)$$

or, in other words, a minimum required hydrodynamic entry length of 41 mm for CO_2, and 137 mm for SF_6. Two different flat plates were used: for CO_2 experiments, the entry length was 12.70 cm, and 15.24 cm for the SF_6 experiments.

The coated length was determined by the requirement that the relative saturation at the flat plate's outlet should be neither too high (see sensitivity analysis, section 6.4) nor too low (see minimum weighing requirements in section 6.4). For an aspect ratio of 1/8, a 20% relative saturation implies $LD/\langle v\rangle\ b^2 \sim 0.2$ (see Figure 5.3). With $\langle v\rangle \sim 0.1$ cm/s, $D \sim 7 \times 10^{-5}$ cm^2/s, and b = 0.15875 cm, we obtain L = 7.2 cm. The actual value used was 7.62 cm.

Typical $\langle v\rangle$ values are obtained from the flow rate, $\dot{F}$, duct cross section, 4ab, and solvent molar density under experimental conditions. For $\dot{F} \sim 0.09$ mol/min, and 4ab = 0.80645 cm^2, and a molar density of 15 mol/lt, we obtain $\langle v\rangle$ = 0.12 cm/s, or a mean residence time of ~ 1 minute. Before every run, a period of at least 15 minutes was allowed for after opening the flow control valve, during which solvent gas was vented (see Figure 4.1) while steady conditions were gradually attained.

A2.2 SAMPLE EQUILIBRIUM AND DIFFUSION CALCULATIONS

As an example of typical equilibrium and diffusion calculations, the determination of the solubility and diffusion coefficient of benzoic acid in SF_6 at 65 bar (Pr = 1.73) and 328.2 K (Tr = 1.03) will be explained in detail.

Two equilibrium experiments were conducted simultaneously. The run duration was 40 minutes. The following numbers were obtained (values in parenthesis refer to the second experiment)

(a) Mass of benzoic acid collected (g) = .03781 (.03042)
(b) Moles of benzoic acid collected = 3.0992×10^{-4} (2.4934×10^{-4})
(c) DTM final minus initial reading (lt) = 62.703 (52.013)
(d) Atmospheric pressure (mm Hg) = 759.8
(e) Ambient temperature (°C) = 23.6
(f) Temperature-corrected ambient pressure (mm Hg) = 756.88
(value read from tables supplied by barometer manufacturer)
(g) Average temperature of DTM outlet (°C) = 24.2 (24.7)
(obtained by averaging initial and final readings)
(h) Average overpressure at DTM outlet (in) = 0.4 (0.4)

(i) Ambient pressure @ DTM outlet conditions (mm Hg) =

$$= \left[(f) + \frac{2.54 \times (h) \times 826 \times 760 \times 9.8}{101325 \times 100} \right] = 756.88 \quad (756.88)$$

(where 826 Kg/m^3 is the density of the outlet U-manometer fluid)

(j) Solvent moles through DTM =

$$= \left[\frac{(c)}{22.4179} \times \frac{273.2}{273.2 + (g)} \times \frac{(i)}{760} \right] = 2.558 \quad (2.119)$$

(where 22.4179 is the ideal gas molar volume, in moles/lt, at 1 atmosphere and 0° C)

(k) Solute mole fraction = $\left[\frac{(b)}{(b) + (j)} \right] = 1.2114 \times 10^{-4} \quad (1.1766 \times 10^{-4})$

These two results differ by 2.91%, and the average value can be taken,

(l) Average mole fraction = $\boxed{1.194 \times 10^{-4}}$

For the diffusion run, we write

(m) Mass of benzoic acid collected (g) = 0.00853

(n) DTM final minus initial reading (lt) = 77.670

(o) Atmospheric pressure (mm Hg) = 774.60

(p) Ambient temperature (°C) = 19

(q) Temperature-corrected ambient pressure (mm Hg) = 772.206

(r) Average temperature at DTM outlet (°C) = 21.6

(s) Average overpressure at DTM outlet (in) = 0.6

(t) Ambient pressure @ DTM outlet conditions (mm Hg) =

$$= \left[(q) + \frac{2.54 \times (s) \times 826 \times 760 \times 9.8}{101325 \times 100} \right] = 773.131$$

(u) Solvent moles through DTM =

$$= \left[\frac{(n)}{22.4179} \times \frac{273.2}{273.2 + (r)} \times \frac{(t)}{760} \right] = 3.26626$$

(v) Solute mole fraction = $\left[\frac{(m)/122}{(u) + (m)/122} \right] = 2.14057 \times 10^{-5}$

(w) Relative saturation = $[(v)/(\ell)] = .17928$

(x) X_0 (from mathematical solution; Chapter 5) = .188615

(y) Run duration (s) = 3600.82

(z) $$= \left[X_0 \frac{\langle v \rangle b^2}{L} \right] = \boxed{9.26 \times 10^{-5} \text{ cm}^2/\text{s}}$$

(where <v> has been calculated as follows,

$\frac{(u)}{(y)} \left(\frac{\text{mol}}{\text{s}}\right) 131.98 \frac{\text{cm}^3}{\text{mol}} \times \frac{1}{0.80645 \text{ cm}^2} = 0.1484$ cm/s; fluid density from the Peng-Robinson equation of state)

A2.3 EXPERIMENTAL ERRORS

The sensitivity of the calculated diffusion experiments with respect to experimental errors in the determination of r, the relative saturation, was analyzed in Section 6.4. In the present section, a numerical value for $|\Delta r/r|$ will be estimated.

In the first place, since r is a ratio of two mole fractions (i.e., the solute mole fraction at the exit of the test section in equilibrium and diffusion experiments), we can write, for error estimation,

$$\left|\frac{\Delta r}{r}\right| = \left|\frac{\Delta x_1}{x_1}\right|_{\text{diff}} + \left|\frac{\Delta x_1}{x_1}\right|_{\text{equil}} \qquad \text{(A2-8)}$$

where x_1 is the solute mole fraction. From Section A2.2, it follows that x_1 is determined by weighing the solid that precipitates in the

U-tubes upon decompression and measuring the corresponding amount of gas that flows through the system.

Weighings were found to be reproducible to within 0.001 g, and the amount of solute collected varied from a minimum of 0.0085 g (low pressure benzoic acid - SF_6 experiments) to values above 0.2g (high pressure benzoic acid - CO_2 experiments) for the diffusion experiments (i.e., weighing errors ranged from 0.5 to 11.8%).

Weighing errors in equilibrium experiments were always lower (for a given system, temperature and pressure) than in the corresponding diffusion experiment, since the mass of solute collected was always greater in the former case. This fact will be used below in the actual evaluation of $|\Delta r/r|$.

The determination of the amount of gas flowing through the dry test meter involved reading the instrument (accurate to ± .005 lt), and calculating the number of moles as per Section A2.2. This, in turn required reading the temperature at the test meter's outlet (thermocouple accurate to ± 0.2 °C), the pressure differential across the outlet line (U-tube manometer accurate to ± 0.1 inch), the atmospheric temperature (± 0.5 °C) and the atmospheric pressure (± 0.1 mm Hg). From Section A2.2 (item (u)), it follows that, for error analysis, we can write

$$\left|\frac{\Delta n}{n}\right| = \left|\frac{\Delta DTM}{DTM}\right| + \left|\frac{\Delta P_o}{P_o}\right| + \left|\frac{\Delta T_o}{T_o}\right| \qquad \text{(A2-9)}$$

where n is the number of solvent moles, DTM is the dry test meter reading, and P_o and T_o, the temperature and pressure at DTM outlet conditions, respectively. The ambient temperature contributed to errors in the determination of the ambient pressure since the latter was always corrected by means of a manufacturer-supplied double-entry table, the independent variables of which were temperature and pressure. Pressure errors, therefore, can be estimated as follows,

$$\left|\frac{\Delta P_o}{P_o}\right| \cong \frac{0.1\ (\text{temperature}) + 0.1\ (\text{manometer}) + 0.1\ (\text{U-tube})}{760} =$$

$$= 3.95 \times 10^{-4} \qquad \text{(A2-10)}$$

For temperature and instrument reading errors, on the other hand,

$$\left|\frac{\Delta T_o}{T_o}\right| \cong \frac{0.5}{298} = 1.678 \times 10^{-3} \qquad \text{(A2-11)}$$

$$\left|\frac{\Delta DTM}{DTM}\right| \cong \frac{0.005}{16} = 3.125 \times 10^{-4} \qquad \text{(A2-12)}$$

where a conservatively low value of solvent throughput (i.e., 16 lt) has been used (see Section A2.2 for typical values).
From Equations (A2-9) to (A2-12), we obtain, finally,

$$\left|\frac{\Delta n}{n}\right| \cong 0.0024 \qquad \text{(A2-13)}$$

The important conclusion here is that weighing errors are by far the most important in terms of their contribution to $|\Delta r/r|$, for which we can now write

$$\left|\frac{\Delta r}{r}\right| \cong 2\ [0.0024 + 0.04\ ] = 8.48 \times 10^{-2} \qquad \text{(A2-14)}$$

where a typical diffusion weighing error of 4% was used (corresponding to a collected solute amount of 0.025 g), and diffusion errors were conservatively equated to equilibrium errors.

We can therefore summarize by saying that the relative saturation can be determined to within ± 8.5%, this being a conservative estimate except for low pressure benzoic acid-SF_6 experiments, where weighing errors of up to 11% can exist in diffusion experiments due to the small amount of solute collected.

A2.4: DENSITY PROFILES

In Chapter 6, it was shown that, for dilute solutions, density decreases monotomically away from the solute-fluid interface if

$$\frac{M_1}{M_2} > \frac{\bar{V}_1}{V_2} \qquad \text{(A2-15)}$$

Where M_1 and M_2 denote solute and solvent molecular weight, respectively, while $\bar{V}_1$ and V_2 denote solute partial molar volume and solvent molar

volume, respectively. In this section, it will be shown that inequality (A2-15) was indeed satisfied for all of the conditions and systems tested, a necessary condition for the elimination of buoyant effects in the hydrodynamic experiemtns (Chapter 6).

A simple, sufficient condition will first be developed that enables to test whether (A2-15) is satisfied with minimum computations. The isothermal pressure dependence of the equilibrium solubility of solute 1 in fluid 2 is given by

$$\left(\frac{\partial \ln x_1}{\partial P}\right)_T = \left(\frac{V_1^S - \bar{V}_1}{RT}\right) \Big/ \left[1 + \left(\frac{\partial \ln \hat{\phi}_1}{\partial \ln x_1}\right)_{T,P}\right] \qquad \text{(A2-16)}$$

which simply states the fact that, if the solubility increases with pressure, the molar volume of the solid solute is larger than its partial molar volume in the fluid phase ($V_1^S > \bar{V}_1$). This provides a quick, conservative test of (A2-15) (i.e., a sufficient but not necessary condition for (A2-15) to be true),

$$\frac{M_1}{M_2} > \frac{V_1^S}{V_2} \Rightarrow \frac{M_1}{M_2} > \frac{\bar{V}_1}{V_2} \qquad \text{(A2-17)}$$

but

$$\frac{M_1}{M_2} > \frac{\bar{V}_1}{V_2} \not\Rightarrow \frac{M_1}{M_2} > \frac{V_1}{V_2} \qquad \text{(A2-18)}$$

In other words, in cases where the solubility increases with pressure, consideration of the pure solute and solvent densities provides a sufficient condition for monotomically decreasing densities away from the interface which can be easily checked.

In the general case, we write

$$V = x_1 \bar{V}_1 + (1-x_1)\bar{V}_2 \qquad \text{(A2-19)}$$

or, equivalently,

$$\frac{\bar{V}_1}{\bar{V}_2} = \frac{\frac{V}{\bar{V}_2} - (1 - x_1)}{x_1} \approx \frac{\frac{V}{V_2} - (1 - x_1)}{x_2} \qquad \text{(A2-20)}$$

where $\bar{V}_2 \approx V_2$ has been used (this is only valid in dilute solutions).

Using the Peng-Robinson equation of state (see Appendix 1) with binary interaction coefficients (k_{ij}) regressed by minimizing the sum of absolute values of log $[x_1(eq)/x_1(eos)]$, where eos denotes the equation of state prediction and $x_1(eq)$, the measured solubility, Table A2-1 was generated, with the second form of the right hand side of Equation (A2-20) used in the computations.

From Table A2-1 we conclude that inequality (A2-15) was satisfied for all of the conditions and systems tested; the flow was therefore stabilized by gravity, in all cases.

A2.5 CHEMICALS USED

The purity and suppliers of the chemicals used in this work are listed below:

Benzoic acid	Baker	99.9+ %
Naphthalene	Baker	99.9+ %
2- Naphthol	Aldrich	99%
CO_2	Matheson	99.8%
SF_6	Matheson	99.8%

TABLE A2.1: BUOYANT STABILITY CALCULATIONS

System	T (K)	P (bar)	x_1(eq)	k_{ij}	M_1/M_2	$\bar{V}_1/V_2$
SF_6-benzoic acid	328	65	1.194×10^{-4}	.128	.8356	-4.789
	328	80	1.491×10^{-4}			-2.651
	328	120	1.825×10^{-4}			-0.790
	338	65	1.646×10^{-4}	.116		-7.448
	338	80	2.076×10^{-4}			-3.901
	338	120	2.803×10^{-4}			-1.237
SF_6-naphthalene	318	65	1.978×10^{-3}	.184	.8767	-1.084
	318	80	2.152×10^{-3}			-0.325
	318	120	2.445×10^{-3}			0.515
	328	65	3.184×10^{-3}	.172		-2.663
	328	80	3.513×10^{-3}			-1.157
	328	120	3.914×10^{-3}			0.159
CO_2-benzoic acid	318	160	2.34×10^{-3}	.004	2.7727	-4.774
	318	200	3.580×10^{-3}			-2.330
	328	160	2.495×10^{-3}	-.004		-6.916
	328	200	3.864×10^{-3}			-3.472
CO_2-2 Naphthol	308	150	4.460×10^{-4}	.076	3.2727	-2.557
	308	200	5.408×10^{-4}			-0.468
	308	250	5.910×10^{-4}			0.538
	318	165	5.662×10^{-4}	.078		-3.425
	318	250	8.655×10^{-4}			-0.109

APPENDIX 3 $C_{i,j}$ COEFFICIENTS FOR EQUATION (5.27)

The following Appendix contains the $C_{i,j}$ coefficients defined in Equation (5.27), for i up to 80, and j up to 26. Coefficients corresponding to each i value are printed under the hesding "Coefficient a i ", and j should be read by lines.

!UDD!PABLO!COEFFICIENTS

COEFFICIENT a 1

.0000000000000E+00	.0000000000000E+00	.0000000000000E+00	.0000000000000E+00	.0000000000000E+00
.0000000000000E+00	.0000000000000E+00	.0000000000000E+00	.0000000000000E+00	.0000000000000E+00
.0000000000000E+00	.0000000000000E+00	.0000000000000E+00	.0000000000000E+00	.0000000000000E+00
.0000000000000E+00	.0000000000000E+00	.0000000000000E+00	.0000000000000E+00	.0000000000000E+00
.0000000000000E+00	.0000000000000E+00	.0000000000000E+00	.0000000000000E+00	.0000000000000E+00
.0000000000000E+00				

COEFFICIENT a 2

.0000000000000E+00	.0000000000000E+00	.0000000000000E+00	.0000000000000E+00	.0000000000000E+00
.0000000000000E+00	.0000000000000E+00	.0000000000000E+00	.0000000000000E+00	.0000000000000E+00
.0000000000000E+00	.0000000000000E+00	.0000000000000E+00	.0000000000000E+00	.0000000000000E+00
.0000000000000E+00	.0000000000000E+00	.0000000000000E+00	.0000000000000E+00	.0000000000000E+00
.0000000000000E+00	.0000000000000E+00	.0000000000000E+00	.0000000000000E+00	.0000000000000E+00
.0000000000000E+00				

COEFFICIENT a 3

-.3333333333333	.0000000000000E+00	.0000000000000E+00	.0000000000000E+00	.0000000000000E+00
.0000000000000E+00	.0000000000000E+00	.0000000000000E+00	.0000000000000E+00	.0000000000000E+00
.0000000000000E+00	.0000000000000E+00	.0000000000000E+00	.0000000000000E+00	.0000000000000E+00
.0000000000000E+00	.0000000000000E+00	.0000000000000E+00	.0000000000000E+00	.0000000000000E+00
.0000000000000E+00	.0000000000000E+00	.0000000000000E+00	.0000000000000E+00	.0000000000000E+00
.0000000000000E+00				

COEFFICIENT a 4

.83333333333333E-01	.0000000000000E+00	.0000000000000E+00	.0000000000000E+00	.0000000000000E+00
.0000000000000E+00	.0000000000000E+00	.0000000000000E+00	.0000000000000E+00	.0000000000000E+00
.0000000000000E+00	.0000000000000E+00	.0000000000000E+00	.0000000000000E+00	.0000000000000E+00
.0000000000000E+00	.0000000000000E+00	.0000000000000E+00	.0000000000000E+00	.0000000000000E+00
.0000000000000E+00	.0000000000000E+00	.0000000000000E+00	.0000000000000E+00	.0000000000000E+00
.0000000000000E+00				

COEFFICIENT a 5

.0000000000000E+00	.0000000000000E+00	.0000000000000E+00	.0000000000000E+00	.0000000000000E+00
.0000000000000E+00	.0000000000000E+00	.0000000000000E+00	.0000000000000E+00	.0000000000000E+00
.0000000000000E+00	.0000000000000E+00	.0000000000000E+00	.0000000000000E+00	.0000000000000E+00

!UDD!PABLO!COEFFICIENTS

.0000000000000E+00 .0000000000000E+00 .0000000000000E+00 .0000000000000E+00 .0000000000000E+00
.0000000000000E+00 .0000000000000E+00 .0000000000000E+00 .0000000000000E+00 .0000000000000E+00
.0000000000000E+00

COEFFICIENT a 6

.0000000000000E+00 .2222222222222E-01 .0000000000000E+00 .0000000000000E+00 .0000000000000E+00
.0000000000000E+00 .0000000000000E+00 .0000000000000E+00 .0000000000000E+00 .0000000000000E+00
.0000000000000E+00 .0000000000000E+00 .0000000000000E+00 .0000000000000E+00 .0000000000000E+00
.0000000000000E+00 .0000000000000E+00 .0000000000000E+00 .0000000000000E+00 .0000000000000E+00
.0000000000000E+00 .0000000000000E+00 .0000000000000E+00 .0000000000000E+00 .0000000000000E+00
.0000000000000E+00

COEFFICIENT a 7

.0000000000000E+00 -.1190476190476E-01 .0000000000000E+00 .0000000000000E+00 .0000000000000E+00
.0000000000000E+00 .0000000000000E+00 .0000000000000E+00 .0000000000000E+00 .0000000000000E+00
.0000000000000E+00 .0000000000000E+00 .0000000000000E+00 .0000000000000E+00 .0000000000000E+00
.0000000000000E+00 .0000000000000E+00 .0000000000000E+00 .0000000000000E+00 .0000000000000E+00
.0000000000000E+00 .0000000000000E+00 .0000000000000E+00 .0000000000000E+00 .0000000000000E+00
.0000000000000E+00

COEFFICIENT a 8

.0000000000000E+00 .1488095238095E-02 .0000000000000E+00 .0000000000000E+00 .0000000000000E+00
.0000000000000E+00 .0000000000000E+00 .0000000000000E+00 .0000000000000E+00 .0000000000000E+00
.0000000000000E+00 .0000000000000E+00 .0000000000000E+00 .0000000000000E+00 .0000000000000E+00
.0000000000000E+00 .0000000000000E+00 .0000000000000E+00 .0000000000000E+00 .0000000000000E+00
.0000000000000E+00 .0000000000000E+00 .0000000000000E+00 .0000000000000E+00 .0000000000000E+00
.0000000000000E+00

COEFFICIENT a 9

.0000000000000E+00 .0000000000000E+00 -.6172839506173E-03 .0000000000000E+00 .0000000000000E+00
.0000000000000E+00 .0000000000000E+00 .0000000000000E+00 .0000000000000E+00 .0000000000000E+00
.0000000000000E+00 .0000000000000E+00 .0000000000000E+00 .0000000000000E+00 .0000000000000E+00
.0000000000000E+00 .0000000000000E+00 .0000000000000E+00 .0000000000000E+00 .0000000000000E+00
.0000000000000E+00 .0000000000000E+00 .0000000000000E+00 .0000000000000E+00 .0000000000000E+00
.0000000000000E+00

!UDD!PABLO!COEFFICIENTS

COEFFICIENT a10

.0000000000000E+00	.0000000000000E+00	.5114638447972E-03	.0000000000000E+00	.0000000000000E+00
.0000000000000E+00	.0000000000000E+00	.0000000000000E+00	.0000000000000E+00	.0000000000000E+00
.0000000000000E+00	.0000000000000E+00	.0000000000000E+00	.0000000000000E+00	.0000000000000E+00
.0000000000000E+00	.0000000000000E+00	.0000000000000E+00	.0000000000000E+00	.0000000000000E+00
.0000000000000E+00	.0000000000000E+00	.0000000000000E+00	.0000000000000E+00	.0000000000000E+00
.0000000000000E+00				

COEFFICIENT a11

.0000000000000E+00	.0000000000000E+00	-.1352813852814E-03	.0000000000000E+00	.0000000000000E+00
.0000000000000E+00	.0000000000000E+00	.0000000000000E+00	.0000000000000E+00	.0000000000000E+00
.0000000000000E+00	.0000000000000E+00	.0000000000000E+00	.0000000000000E+00	.0000000000000E+00
.0000000000000E+00	.0000000000000E+00	.0000000000000E+00	.0000000000000E+00	.0000000000000E+00
.0000000000000E+00	.0000000000000E+00	.0000000000000E+00	.0000000000000E+00	.0000000000000E+00
.0000000000000E+00				

COEFFICIENT a12

.0000000000000E+00	.0000000000000E+00	.1127344877345E-04	.9352787130565E-05	.0000000000000E+00
.0000000000000E+00	.0000000000000E+00	.0000000000000E+00	.0000000000000E+00	.0000000000000E+00
.0000000000000E+00	.0000000000000E+00	.0000000000000E+00	.0000000000000E+00	.0000000000000E+00
.0000000000000E+00	.0000000000000E+00	.0000000000000E+00	.0000000000000E+00	.0000000000000E+00
.0000000000000E+00	.0000000000000E+00	.0000000000000E+00	.0000000000000E+00	.0000000000000E+00
.0000000000000E+00				

COEFFICIENT a13

.0000000000000E+00	.0000000000000E+00	.0000000000000E+00	-.1051417718084E-04	.0000000000000E+00
.0000000000000E+00	.0000000000000E+00	.0000000000000E+00	.0000000000000E+00	.0000000000000E+00
.0000000000000E+00	.0000000000000E+00	.0000000000000E+00	.0000000000000E+00	.0000000000000E+00
.0000000000000E+00	.0000000000000E+00	.0000000000000E+00	.0000000000000E+00	.0000000000000E+00
.0000000000000E+00	.0000000000000E+00	.0000000000000E+00	.0000000000000E+00	.0000000000000E+00
.0000000000000E+00				

COEFFICIENT a14

.0000000000000E+00	.0000000000000E+00	.0000000000000E+00	.4296849534945E-05	.0000000000000E+00
.0000000000000E+00	.0000000000000E+00	.0000000000000E+00	.0000000000000E+00	.0000000000000E+00
.0000000000000E+00	.0000000000000E+00	.0000000000000E+00	.0000000000000E+00	.0000000000000E+00
.0000000000000E+00	.0000000000000E+00	.0000000000000E+00	.0000000000000E+00	.0000000000000E+00

!UDD!PABLO!COEFFICIENTS

.0000000000000E+00	.0000000000000E+00	.0000000000000E+00	.0000000000000E+00	.0000000000000E+00
.0000000000000E+00				

COEFFICIENT a15

.0000000000000E+00	.0000000000000E+00	.0000000000000E+00	-.7515632515633E-06	-.8907416314824E-07
.0000000000000E+00	.0000000000000E+00	.0000000000000E+00	.0000000000000E+00	.0000000000000E+00
.0000000000000E+00	.0000000000000E+00	.0000000000000E+00	.0000000000000E+00	.0000000000000E+00
.0000000000000E+00	.0000000000000E+00	.0000000000000E+00	.0000000000000E+00	.0000000000000E+00
.0000000000000E+00	.0000000000000E+00	.0000000000000E+00	.0000000000000E+00	.0000000000000E+00
.0000000000000E+00				

COEFFICIENT a16

.0000000000000E+00	.0000000000000E+00	.0000000000000E+00	.4697270322270E-07	.1265880895511E-06
.0000000000000E+00	.0000000000000E+00	.0000000000000E+00	.0000000000000E+00	.0000000000000E+00
.0000000000000E+00	.0000000000000E+00	.0000000000000E+00	.0000000000000E+00	.0000000000000E+00
.0000000000000E+00	.0000000000000E+00	.0000000000000E+00	.0000000000000E+00	.0000000000000E+00
.0000000000000E+00	.0000000000000E+00	.0000000000000E+00	.0000000000000E+00	.0000000000000E+00
.0000000000000E+00				

COEFFICIENT a17

.0000000000000E+00	.0000000000000E+00	.0000000000000E+00	.0000000000000E+00	-.7024954503946E-07
.0000000000000E+00	.0000000000000E+00	.0000000000000E+00	.0000000000000E+00	.0000000000000E+00
.0000000000000E+00	.0000000000000E+00	.0000000000000E+00	.0000000000000E+00	.0000000000000E+00
.0000000000000E+00	.0000000000000E+00	.0000000000000E+00	.0000000000000E+00	.0000000000000E+00
.0000000000000E+00	.0000000000000E+00	.0000000000000E+00	.0000000000000E+00	.0000000000000E+00
.0000000000000E+00				

COEFFICIENT a18

.0000000000000E+00	.0000000000000E+00	.0000000000000E+00	.0000000000000E+00	.1895417005906E-07
.5821840728643E-09	.0000000000000E+00	.0000000000000E+00	.0000000000000E+00	.0000000000000E+00
.0000000000000E+00	.0000000000000E+00	.0000000000000E+00	.0000000000000E+00	.0000000000000E+00
.0000000000000E+00	.0000000000000E+00	.0000000000000E+00	.0000000000000E+00	.0000000000000E+00
.0000000000000E+00	.0000000000000E+00	.0000000000000E+00	.0000000000000E+00	.0000000000000E+00
.0000000000000E+00				

COEFFICIENT a19

!UDD!PABLO!COEFFICIENTS

.0000000000000E+00	.0000000000000E+00	.0000000000000E+00	.0000000000000E+00	-.2472247538037E-08
-.1000731994884E-08	.0000000000000E+00	.0000000000000E+00	.0000000000000E+00	.0000000000000E+00
.0000000000000E+00	.0000000000000E+00	.0000000000000E+00	.0000000000000E+00	.0000000000000E+00
.0000000000000E+00	.0000000000000E+00	.0000000000000E+00	.0000000000000E+00	.0000000000000E+00
.0000000000000E+00	.0000000000000E+00	.0000000000000E+00	.0000000000000E+00	.0000000000000E+00
.0000000000000E+00				

COEFFICIENT a20

.0000000000000E+00	.0000000000000E+00	.0000000000000E+00	.0000000000000E+00	.1236123769019E-09
.7028609990262E-09	.0000000000000E+00	.0000000000000E+00	.0000000000000E+00	.0000000000000E+00
.0000000000000E+00	.0000000000000E+00	.0000000000000E+00	.0000000000000E+00	.0000000000000E+00
.0000000000000E+00	.0000000000000E+00	.0000000000000E+00	.0000000000000E+00	.0000000000000E+00
.0000000000000E+00	.0000000000000E+00	.0000000000000E+00	.0000000000000E+00	.0000000000000E+00
.0000000000000E+00				

COEFFICIENT a21

.0000000000000E+00	.0000000000000E+00	.0000000000000E+00	.0000000000000E+00	.0000000000000E+00
-.2575187741847E-09	-.2772305108870E-11	.0000000000000E+00	.0000000000000E+00	.0000000000000E+00
.0000000000000E+00	.0000000000000E+00	.0000000000000E+00	.0000000000000E+00	.0000000000000E+00
.0000000000000E+00	.0000000000000E+00	.0000000000000E+00	.0000000000000E+00	.0000000000000E+00
.0000000000000E+00	.0000000000000E+00	.0000000000000E+00	.0000000000000E+00	.0000000000000E+00
.0000000000000E+00				

COEFFICIENT a22

.0000000000000E+00	.0000000000000E+00	.0000000000000E+00	.0000000000000E+00	.0000000000000E+00
.5172871241370E-10	.5592311823880E-11	.0000000000000E+00	.0000000000000E+00	.0000000000000E+00
.0000000000000E+00	.0000000000000E+00	.0000000000000E+00	.0000000000000E+00	.0000000000000E+00
.0000000000000E+00	.0000000000000E+00	.0000000000000E+00	.0000000000000E+00	.0000000000000E+00
.0000000000000E+00	.0000000000000E+00	.0000000000000E+00	.0000000000000E+00	.0000000000000E+00
.0000000000000E+00				

COEFFICIENT a23

.0000000000000E+00	.0000000000000E+00	.0000000000000E+00	.0000000000000E+00	.0000000000000E+00
-.5374451169646E-11	-.4755837930705E-11	.0000000000000E+00	.0000000000000E+00	.0000000000000E+00
.0000000000000E+00	.0000000000000E+00	.0000000000000E+00	.0000000000000E+00	.0000000000000E+00
.0000000000000E+00	.0000000000000E+00	.0000000000000E+00	.0000000000000E+00	.0000000000000E+00
.0000000000000E+00	.0000000000000E+00	.0000000000000E+00	.0000000000000E+00	.0000000000000E+00

!UDD!PABLO!COEFFICIENTS
.0000000000000E+00

COEFFICIENT a24

.0000000000000E+00 .0000000000000E+00 .0000000000000E+00 .0000000000000E+00 .0000000000000E+00
.2239354654019E-12 .2206337948181E-11 .1004458372782E-13 .0000000000000E+00 .0000000000000E+00
.0000000000000E+00 .0000000000000E+00 .0000000000000E+00 .0000000000000E+00 .0000000000000E+00
.0000000000000E+00 .0000000000000E+00 .0000000000000E+00 .0000000000000E+00 .0000000000000E+00
.0000000000000E+00 .0000000000000E+00 .0000000000000E+00 .0000000000000E+00 .0000000000000E+00
.0000000000000E+00

COEFFICIENT a25

.0000000000000E+00 .0000000000000E+00 .0000000000000E+00 .0000000000000E+00 .0000000000000E+00
.0000000000000E+00 -.6016269983535E-12 -.2326154792773E-13 .0000000000000E+00 .0000000000000E+00
.0000000000000E+00 .0000000000000E+00 .0000000000000E+00 .0000000000000E+00 .0000000000000E+00
.0000000000000E+00 .0000000000000E+00 .0000000000000E+00 .0000000000000E+00 .0000000000000E+00
.0000000000000E+00 .0000000000000E+00 .0000000000000E+00 .0000000000000E+00 .0000000000000E+00
.0000000000000E+00

COEFFICIENT a26

.0000000000000E+00 .0000000000000E+00 .0000000000000E+00 .0000000000000E+00 .0000000000000E+00
.0000000000000E+00 .9611940731230E-13 .2323690413121E-13 .0000000000000E+00 .0000000000000E+00
.0000000000000E+00 .0000000000000E+00 .0000000000000E+00 .0000000000000E+00 .0000000000000E+00
.0000000000000E+00 .0000000000000E+00 .0000000000000E+00 .0000000000000E+00 .0000000000000E+00
.0000000000000E+00 .0000000000000E+00 .0000000000000E+00 .0000000000000E+00 .0000000000000E+00
.0000000000000E+00

COEFFICIENT a27

.0000000000000E+00 .0000000000000E+00 .0000000000000E+00 .0000000000000E+00 .0000000000000E+00
.0000000000000E+00 -.8293906125996E-14 -.1306056100722E-13 -.2861704765760E-16 .0000000000000E+00
.0000000000000E+00 .0000000000000E+00 .0000000000000E+00 .0000000000000E+00 .0000000000000E+00
.0000000000000E+00 .0000000000000E+00 .0000000000000E+00 .0000000000000E+00 .0000000000000E+00
.0000000000000E+00 .0000000000000E+00 .0000000000000E+00 .0000000000000E+00 .0000000000000E+00
.0000000000000E+00

COEFFICIENT a28

!UDD!PABLO!COEFFICIENTS

.0000000000000E+00	.0000000000000E+00	.0000000000000E+00	.0000000000000E+00	.0000000000000E+00
.0000000000000E+00	.2962109330713E-15	.4510042255142E-14	.7482497299375E-16	.0000000000000E+00
.0000000000000E+00	.0000000000000E+00	.0000000000000E+00	.0000000000000E+00	.0000000000000E+00
.0000000000000E+00	.0000000000000E+00	.0000000000000E+00	.0000000000000E+00	.0000000000000E+00
.0000000000000E+00	.0000000000000E+00	.0000000000000E+00	.0000000000000E+00	.0000000000000E+00
.0000000000000E+00				

COEFFICIENT a29

.0000000000000E+00	.0000000000000E+00	.0000000000000E+00	.0000000000000E+00	.0000000000000E+00
.0000000000000E+00	.0000000000000E+00	-.9776672573622E-15	-.8588098052975E-16	.0000000000000E+00
.0000000000000E+00	.0000000000000E+00	.0000000000000E+00	.0000000000000E+00	.0000000000000E+00
.0000000000000E+00	.0000000000000E+00	.0000000000000E+00	.0000000000000E+00	.0000000000000E+00
.0000000000000E+00	.0000000000000E+00	.0000000000000E+00	.0000000000000E+00	.0000000000000E+00
.0000000000000E+00				

COEFFICIENT a30

.0000000000000E+00	.0000000000000E+00	.0000000000000E+00	.0000000000000E+00	.0000000000000E+00
.0000000000000E+00	.0000000000000E+00	.1295485282348E-15	.5673336338580E-16	.6578631645425E-19
.0000000000000E+00	.0000000000000E+00	.0000000000000E+00	.0000000000000E+00	.0000000000000E+00
.0000000000000E+00	.0000000000000E+00	.0000000000000E+00	.0000000000000E+00	.0000000000000E+00
.0000000000000E+00	.0000000000000E+00	.0000000000000E+00	.0000000000000E+00	.0000000000000E+00
.0000000000000E+00				

COEFFICIENT a31

.0000000000000E+00	.0000000000000E+00	.0000000000000E+00	.0000000000000E+00	.0000000000000E+00
.0000000000000E+00	.0000000000000E+00	-.9555191389397E-17	-.2374262958871E-16	-.1916849394033E-18
.0000000000000E+00	.0000000000000E+00	.0000000000000E+00	.0000000000000E+00	.0000000000000E+00
.0000000000000E+00	.0000000000000E+00	.0000000000000E+00	.0000000000000E+00	.0000000000000E+00
.0000000000000E+00	.0000000000000E+00	.0000000000000E+00	.0000000000000E+00	.0000000000000E+00
.0000000000000E+00				

COEFFICIENT a32

.0000000000000E+00	.0000000000000E+00	.0000000000000E+00	.0000000000000E+00	.0000000000000E+00
.0000000000000E+00	.0000000000000E+00	.2985997309186E-18	.6517516905107E-17	.2485755383601E-18
.0000000000000E+00	.0000000000000E+00	.0000000000000E+00	.0000000000000E+00	.0000000000000E+00
.0000000000000E+00	.0000000000000E+00	.0000000000000E+00	.0000000000000E+00	.0000000000000E+00
.0000000000000E+00	.0000000000000E+00	.0000000000000E+00	.0000000000000E+00	.0000000000000E+00
.0000000000000E+00				

!UDD!PABLO!COEFFICIENTS

COEFFICIENT a33

.0000000000000E+00	.0000000000000E+00	.0000000000000E+00	.0000000000000E+00	.0000000000000E+00
.0000000000000E+00	.0000000000000E+00	.0000000000000E+00	-.1171178327492E-17	-.1887762379748E-18
-.1245952963149E-21	.0000000000000E+00	.0000000000000E+00	.0000000000000E+00	.0000000000000E+00
.0000000000000E+00	.0000000000000E+00	.0000000000000E+00	.0000000000000E+00	.0000000000000E+00
.0000000000000E+00	.0000000000000E+00	.0000000000000E+00	.0000000000000E+00	.0000000000000E+00
.0000000000000E+00				

COEFFICIENT a34

.0000000000000E+00	.0000000000000E+00	.0000000000000E+00	.0000000000000E+00	.0000000000000E+00
.0000000000000E+00	.0000000000000E+00	.0000000000000E+00	.1324945730959E-18	.9288647287275E-19
.4003174645819E-21	.0000000000000E+00	.0000000000000E+00	.0000000000000E+00	.0000000000000E+00
.0000000000000E+00	.0000000000000E+00	.0000000000000E+00	.0000000000000E+00	.0000000000000E+00
.0000000000000E+00	.0000000000000E+00	.0000000000000E+00	.0000000000000E+00	.0000000000000E+00
.0000000000000E+00				

COEFFICIENT a35

.0000000000000E+00	.0000000000000E+00	.0000000000000E+00	.0000000000000E+00	.0000000000000E+00
.0000000000000E+00	.0000000000000E+00	.0000000000000E+00	-.8531420883390E-20	-.3090559949490E-19
-.5708537950618E-21	.0000000000000E+00	.0000000000000E+00	.0000000000000E+00	.0000000000000E+00
.0000000000000E+00	.0000000000000E+00	.0000000000000E+00	.0000000000000E+00	.0000000000000E+00
.0000000000000E+00	.0000000000000E+00	.0000000000000E+00	.0000000000000E+00	.0000000000000E+00
.0000000000000E+00				

COEFFICIENT a36

.0000000000000E+00	.0000000000000E+00	.0000000000000E+00	.0000000000000E+00	.0000000000000E+00
.0000000000000E+00	.0000000000000E+00	.0000000000000E+00	.2369839134275E-21	.7031645682613E-20
.4969269954838E-21	.1977703116109E-24	.0000000000000E+00	.0000000000000E+00	.0000000000000E+00
.0000000000000E+00	.0000000000000E+00	.0000000000000E+00	.0000000000000E+00	.0000000000000E+00
.0000000000000E+00	.0000000000000E+00	.0000000000000E+00	.0000000000000E+00	.0000000000000E+00
.0000000000000E+00				

COEFFICIENT a37

!UDD!PABLO!COEFFICIENTS

.0000000000000E+00	.0000000000000E+00	.0000000000000E+00	.0000000000000E+00	.0000000000000E+00
.0000000000000E+00	.0000000000000E+00	.0000000000000E+00	.0000000000000E+00	-.1078203809072E-20
-.2811930808711E-21	-.6946172863954E-24	.0000000000000E+00	.0000000000000E+00	.0000000000000E+00
.0000000000000E+00	.0000000000000E+00	.0000000000000E+00	.0000000000000E+00	.0000000000000E+00
.0000000000000E+00	.0000000000000E+00	.0000000000000E+00	.0000000000000E+00	.0000000000000E+00
.0000000000000E+00				

COEFFICIENT a38

.0000000000000E+00	.0000000000000E+00	.0000000000000E+00	.0000000000000E+00	.0000000000000E+00
.0000000000000E+00	.0000000000000E+00	.0000000000000E+00	.0000000000000E+00	.1063708498312E-21
.1100267936433E-21	.1108125927956E-23	.0000000000000E+00	.0000000000000E+00	.0000000000000E+00
.0000000000000E+00	.0000000000000E+00	.0000000000000E+00	.0000000000000E+00	.0000000000000E+00
.0000000000000E+00	.0000000000000E+00	.0000000000000E+00	.0000000000000E+00	.0000000000000E+00
.0000000000000E+00				

COEFFICIENT a39

.0000000000000E+00	.0000000000000E+00	.0000000000000E+00	.0000000000000E+00	.0000000000000E+00
.0000000000000E+00	.0000000000000E+00	.0000000000000E+00	.0000000000000E+00	-.6076510600705E-23
-.3034338114718E-22	-.1061206333353E-23	-.2668965068973E-27	.0000000000000E+00	.0000000000000E+00
.0000000000000E+00	.0000000000000E+00	.0000000000000E+00	.0000000000000E+00	.0000000000000E+00
.0000000000000E+00	.0000000000000E+00	.0000000000000E+00	.0000000000000E+00	.0000000000000E+00
.0000000000000E+00				

COEFFICIENT a40

.0000000000000E+00	.0000000000000E+00	.0000000000000E+00	.0000000000000E+00	.0000000000000E+00
.0000000000000E+00	.0000000000000E+00	.0000000000000E+00	.0000000000000E+00	.1519127650176E-24
.58897777756896E-23	.6790468956577E-24	.10173108233334E-26	.0000000000000E+00	.0000000000000E+00
.0000000000000E+00	.0000000000000E+00	.0000000000000E+00	.0000000000000E+00	.0000000000000E+00
.0000000000000E+00	.0000000000000E+00	.0000000000000E+00	.0000000000000E+00	.0000000000000E+00
.0000000000000E+00				

COEFFICIENT a41

.0000000000000E+00	.0000000000000E+00	.0000000000000E+00	.0000000000000E+00	.0000000000000E+00
.0000000000000E+00	.0000000000000E+00	.0000000000000E+00	.0000000000000E+00	.0000000000000E+00
-.7871618955699E-24	-.3056382122913E-24	-.1774920208724E-26	.0000000000000E+00	.0000000000000E+00
.0000000000000E+00	.0000000000000E+00	.0000000000000E+00	.0000000000000E+00	.0000000000000E+00
.0000000000000E+00	.0000000000000E+00	.0000000000000E+00	.0000000000000E+00	.0000000000000E+00
.0000000000000E+00				

!UDD!PABLO!COEFFICIENTS

COEFFICIENT a42

.0000000000000E+00	.0000000000000E+00	.0000000000000E+00	.0000000000000E+00	.0000000000000E+00
.0000000000000E+00	.0000000000000E+00	.0000000000000E+00	.0000000000000E+00	.0000000000000E+00
.6882919339874E-25	.9913679206603E-25	.187603867285BE-26	.3099843285683E-30	.0000000000000E+00
.0000000000000E+00	.0000000000000E+00	.0000000000000E+00	.0000000000000E+00	.0000000000000E+00
.0000000000000E+00	.0000000000000E+00	.0000000000000E+00	.0000000000000E+00	.0000000000000E+00
.0000000000000E+00				

COEFFICIENT a43

.0000000000000E+00	.0000000000000E+00	.0000000000000E+00	.0000000000000E+00	.0000000000000E+00
.0000000000000E+00	.0000000000000E+00	.0000000000000E+00	.0000000000000E+00	.0000000000000E+00
-.3532855000410E-26	-.2332388519434E-25	-.1339590323737E-26	-.1274373285474E-29	.0000000000000E+00
.0000000000000E+00	.0000000000000E+00	.0000000000000E+00	.0000000000000E+00	.0000000000000E+00
.0000000000000E+00	.0000000000000E+00	.0000000000000E+00	.0000000000000E+00	.0000000000000E+00
.0000000000000E+00				

COEFFICIENT a44

.0000000000000E+00	.0000000000000E+00	.0000000000000E+00	.0000000000000E+00	.0000000000000E+00
.0000000000000E+00	.0000000000000E+00	.0000000000000E+00	.0000000000000E+00	.0000000000000E+00
.8029215910023E-28	.3945085384797E-26	.6819890698944E-27	.2413927717115E-29	.0000000000000E+00
.0000000000000E+00	.0000000000000E+00	.0000000000000E+00	.0000000000000E+00	.0000000000000E+00
.0000000000000E+00	.0000000000000E+00	.0000000000000E+00	.0000000000000E+00	.0000000000000E+00
.0000000000000E+00				

COEFFICIENT a45

.0000000000000E+00	.0000000000000E+00	.0000000000000E+00	.0000000000000E+00	.0000000000000E+00
.0000000000000E+00	.0000000000000E+00	.0000000000000E+00	.0000000000000E+00	.0000000000000E+00
.0000000000000E+00	-.4670809506906E-27	-.2545009072845E-27	-.2791412906283E-29	-.3131154834023E-33
.0000000000000E+00	.0000000000000E+00	.0000000000000E+00	.0000000000000E+00	.0000000000000E+00
.0000000000000E+00	.0000000000000E+00	.0000000000000E+00	.0000000000000E+00	.0000000000000E+00
.0000000000000E+00				

COEFFICIENT a46

.0000000000000E+00	.0000000000000E+00	.0000000000000E+00	.0000000000000E+00	.0000000000000E+00

!UDD!PABLO!COEFFICIENTS

COEFFICIENT a51

.0000000000000E+00	.0000000000000E+00	.0000000000000E+00	.0000000000000E+00	.0000000000000E+00
.0000000000000E+00	.0000000000000E+00	.0000000000000E+00	.0000000000000E+00	.0000000000000E+00
.0000000000000E+00	.0000000000000E+00	-.6978528638248E-33	-.7358100995043E-32	-.9044459545593E-33
-.3886985480327E-35	-.2177134497304E-39	.0000000000000E+00	.0000000000000E+00	.0000000000000E+00
.0000000000000E+00	.0000000000000E+00	.0000000000000E+00	.0000000000000E+00	.0000000000000E+00
.0000000000000E+00				

COEFFICIENT a52

.0000000000000E+00	.0000000000000E+00	.0000000000000E+00	.0000000000000E+00	.0000000000000E+00
.0000000000000E+00	.0000000000000E+00	.0000000000000E+00	.0000000000000E+00	.0000000000000E+00
.0000000000000E+00	.0000000000000E+00	.1342024738125E-34	.9888079510354E-33	.3258326506293E-33
.3642839010771E-35	.1090697134636E-38	.0000000000000E+00	.0000000000000E+00	.0000000000000E+00
.0000000000000E+00	.0000000000000E+00	.0000000000000E+00	.0000000000000E+00	.0000000000000E+00
.0000000000000E+00				

COEFFICIENT a53

.0000000000000E+00	.0000000000000E+00	.0000000000000E+00	.0000000000000E+00	.0000000000000E+00
.0000000000000E+00	.0000000000000E+00	.0000000000000E+00	.0000000000000E+00	.0000000000000E+00
.0000000000000E+00	.0000000000000E+00	.0000000000000E+00	-.9524128443377E-34	-.9040515531687E-34
-.2502212194251E-35	-.2555513063342E-38	.0000000000000E+00	.0000000000000E+00	.0000000000000E+00
.0000000000000E+00	.0000000000000E+00	.0000000000000E+00	.0000000000000E+00	.0000000000000E+00
.0000000000000E+00				

COEFFICIENT a54

.0000000000000E+00	.0000000000000E+00	.0000000000000E+00	.0000000000000E+00	.0000000000000E+00
.0000000000000E+00	.0000000000000E+00	.0000000000000E+00	.0000000000000E+00	.0000000000000E+00
.0000000000000E+00	.0000000000000E+00	.0000000000000E+00	.6203792295223E-35	.1930392434821E-34
.1302551751147E-35	.3718285088672E-38	.1521407754930E-42	.0000000000000E+00	.0000000000000E+00
.0000000000000E+00	.0000000000000E+00	.0000000000000E+00	.0000000000000E+00	.0000000000000E+00
.0000000000000E+00				

COEFFICIENT a55

.0000000000000E+00	.0000000000000E+00	.0000000000000E+00	.0000000000000E+00	.0000000000000E+00
.0000000000000E+00	.0000000000000E+00	.0000000000000E+00	.0000000000000E+00	.0000000000000E+00

!UDD!PABLO!COEFFICIENTS

.0000000000000E+00	.0000000000000E+00	.0000000000000E+00	.0000000000000E+00	.0000000000000E+00
.0000000000000E+00	.3666420454085E-28	.7042732485734E-28	.2200589043639E-29	.1381029420056E-32
.0000000000000E+00	.0000000000000E+00	.0000000000000E+00	.0000000000000E+00	.0000000000000E+00
.0000000000000E+00	.0000000000000E+00	.0000000000000E+00	.0000000000000E+00	.0000000000000E+00
.0000000000000E+00				

COEFFICIENT a47

.0000000000000E+00	.0000000000000E+00	.0000000000000E+00	.0000000000000E+00	.0000000000000E+00
.0000000000000E+00	.0000000000000E+00	.0000000000000E+00	.0000000000000E+00	.0000000000000E+00
.0000000000000E+00	-.1708343810643E-29	-.1443758370209E-28	-.1250494201446E-29	-.2822492469798E-32
.0000000000000E+00	.0000000000000E+00	.0000000000000E+00	.0000000000000E+00	.0000000000000E+00
.0000000000000E+00	.0000000000000E+00	.0000000000000E+00	.0000000000000E+00	.0000000000000E+00
.0000000000000E+00				

COEFFICIENT a48

.0000000000000E+00	.0000000000000E+00	.0000000000000E+00	.0000000000000E+00	.0000000000000E+00
.0000000000000E+00	.0000000000000E+00	.0000000000000E+00	.0000000000000E+00	.0000000000000E+00
.0000000000000E+00	.3559049605506E-31	.2162786917632E-29	.5279214913402E-30	.3544660252518E-32
.2775846484063E-36	.0000000000000E+00	.0000000000000E+00	.0000000000000E+00	.0000000000000E+00
.0000000000000E+00	.0000000000000E+00	.0000000000000E+00	.0000000000000E+00	.0000000000000E+00
.0000000000000E+00				

COEFFICIENT a49

.0000000000000E+00	.0000000000000E+00	.0000000000000E+00	.0000000000000E+00	.0000000000000E+00
.0000000000000E+00	.0000000000000E+00	.0000000000000E+00	.0000000000000E+00	.0000000000000E+00
.0000000000000E+00	.0000000000000E+00	-.2297658842569E-30	-.1680933490643E-30	-.3058074402024E-32
-.1307472076324E-35	.0000000000000E+00	.0000000000000E+00	.0000000000000E+00	.0000000000000E+00
.0000000000000E+00	.0000000000000E+00	.0000000000000E+00	.0000000000000E+00	.0000000000000E+00
.0000000000000E+00				

COEFFICIENT a50

.0000000000000E+00	.0000000000000E+00	.0000000000000E+00	.0000000000000E+00	.0000000000000E+00
.0000000000000E+00	.0000000000000E+00	.0000000000000E+00	.0000000000000E+00	.0000000000000E+00
.0000000000000E+00	.0000000000000E+00	.1635954782128E-31	.4053162949450E-31	.1919011202665E-32
.2867760963124E-35	.0000000000000E+00	.0000000000000E+00	.0000000000000E+00	.0000000000000E+00
.0000000000000E+00	.0000000000000E+00	.0000000000000E+00	.0000000000000E+00	.0000000000000E+00
.0000000000000E+00				

```
!UDD!PABLO!COEFFICIENTS
 .0000000000000E+00   .0000000000000E+00   .0000000000000E+00   -.2440044978408E-36   -.3143339022597E-35
-.5239431837770E-36  -.3761839562919E-38  -.8077803767686E-42   .0000000000000E+00    .0000000000000E+00
 .0000000000000E+00   .0000000000000E+00   .0000000000000E+00   .0000000000000E+00    .0000000000000E+00
 .0000000000000E+00
```

COEFFICIENT a56

```
 .0000000000000E+00   .0000000000000E+00   .0000000000000E+00   .0000000000000E+00   .0000000000000E+00
 .0000000000000E+00   .0000000000000E+00   .0000000000000E+00   .0000000000000E+00   .0000000000000E+00
 .0000000000000E+00   .0000000000000E+00   .0000000000000E+00   .4357223175729E-38   .3828865324360E-36
 .1644944679425E-36   .2807553051712E-38   .2013546513416E-41   .0000000000000E+00   .0000000000000E+00
 .0000000000000E+00   .0000000000000E+00   .0000000000000E+00   .0000000000000E+00   .0000000000000E+00
 .0000000000000E+00
```

COEFFICIENT a57

```
 .0000000000000E+00   .0000000000000E+00   .0000000000000E+00   .0000000000000E+00   .0000000000000E+00
 .0000000000000E+00   .0000000000000E+00   .0000000000000E+00   .0000000000000E+00   .0000000000000E+00
 .0000000000000E+00   .0000000000000E+00   .0000000000000E+00   .0000000000000E+00  -.3372458302764E-37
-.4041760777359E-37  -.1600036245785E-38  -.3130351892445E-41  -.9532630043419E-46   .0000000000000E+00
 .0000000000000E+00   .0000000000000E+00   .0000000000000E+00   .0000000000000E+00   .0000000000000E+00
 .0000000000000E+00
```

COEFFICIENT a58

```
 .0000000000000E+00   .0000000000000E+00   .0000000000000E+00   .0000000000000E+00   .0000000000000E+00
 .0000000000000E+00   .0000000000000E+00   .0000000000000E+00   .0000000000000E+00   .0000000000000E+00
 .0000000000000E+00   .0000000000000E+00   .0000000000000E+00   .0000000000000E+00   .2024138321508E-38
 .7740654081491E-38   .7109613184215E-39   .3400473144135E-41   .5316949573594E-45   .0000000000000E+00
 .0000000000000E+00   .0000000000000E+00   .0000000000000E+00   .0000000000000E+00   .0000000000000E+00
 .0000000000000E+00
```

COEFFICIENT a59

```
 .0000000000000E+00   .0000000000000E+00   .0000000000000E+00   .0000000000000E+00   .0000000000000E+00
 .0000000000000E+00   .0000000000000E+00   .0000000000000E+00   .0000000000000E+00   .0000000000000E+00
 .0000000000000E+00   .0000000000000E+00   .0000000000000E+00   .0000000000000E+00  -.7385124026660E-40
-.1142347190961E-38  -.2492495966283E-39  -.2740194525524E-41  -.1412879428288E-44   .0000000000000E+00
 .0000000000000E+00   .0000000000000E+00   .0000000000000E+00   .0000000000000E+00   .0000000000000E+00
 .0000000000000E+00
```

!UDD!PABLO!COEFFICIENTS

COEFFICIENT a60

.0000000000000E+00	.0000000000000E+00	.0000000000000E+00	.0000000000000E+00	.0000000000000E+00
.0000000000000E+00	.0000000000000E+00	.0000000000000E+00	.0000000000000E+00	.0000000000000E+00
.0000000000000E+00	.0000000000000E+00	.0000000000000E+00	.0000000000000E+00	.1230854004443E-41
.1272134741501E-39	.6930217047732E-40	.1697069362509E-41	.2337358841330E-44	.5385666691197E-49
.0000000000000E+00	.0000000000000E+00	.0000000000000E+00	.0000000000000E+00	.0000000000000E+00
.0000000000000E+00				

COEFFICIENT a61

.0000000000000E+00	.0000000000000E+00	.0000000000000E+00	.0000000000000E+00	.0000000000000E+00
.0000000000000E+00	.0000000000000E+00	.0000000000000E+00	.0000000000000E+00	.0000000000000E+00
.0000000000000E+00	.0000000000000E+00	.0000000000000E+00	.0000000000000E+00	.0000000000000E+00
-.1032045346193E-40	-.1527292785152E-40	-.8256718258546E-42	-.2713469448283E-44	-.3182284740855E-48
.0000000000000E+00	.0000000000000E+00	.0000000000000E+00	.0000000000000E+00	.0000000000000E+00
.0000000000000E+00				

COEFFICIENT a62

.0000000000000E+00	.0000000000000E+00	.0000000000000E+00	.0000000000000E+00	.0000000000000E+00
.0000000000000E+00	.0000000000000E+00	.0000000000000E+00	.0000000000000E+00	.0000000000000E+00
.0000000000000E+00	.0000000000000E+00	.0000000000000E+00	.0000000000000E+00	.0000000000000E+00
.5742572189426E-42	.2650806045323E-41	.3197938952084E-42	.2348192013533E-44	.8885388191260E-48
.0000000000000E+00	.0000000000000E+00	.0000000000000E+00	.0000000000000E+00	.0000000000000E+00
.0000000000000E+00				

COEFFICIENT a63

.0000000000000E+00	.0000000000000E+00	.0000000000000E+00	.0000000000000E+00	.0000000000000E+00
.0000000000000E+00	.0000000000000E+00	.0000000000000E+00	.0000000000000E+00	.0000000000000E+00
.0000000000000E+00	.0000000000000E+00	.0000000000000E+00	.0000000000000E+00	.0000000000000E+00
-.1953736514989E-43	-.3575970658631E-42	-.9929696302687E-43	-.1570489823487E-44	-.1558524605977E-47
-.2757637834714E-52	.0000000000000E+00	.0000000000000E+00	.0000000000000E+00	.0000000000000E+00
.0000000000000E+00				

COEFFICIENT a64

.0000000000000E+00	.0000000000000E+00	.0000000000000E+00	.0000000000000E+00	.0000000000000E+00
.0000000000000E+00	.0000000000000E+00	.0000000000000E+00	.0000000000000E+00	.0000000000000E+00
.0000000000000E+00	.0000000000000E+00	.0000000000000E+00	.0000000000000E+00	.0000000000000E+00

```
!UDD!PABLO!COEFFICIENTS
 .30527133046 71E-45   .3667023340127E-43   .2476389538203E-43   .8304595769390E-45   .1925669081819E-47
 .1712087338996E-51    .0000000000000E+00   .0000000000000E+00   .0000000000000E+00   .0000000000000E+00
 .0000000000000E+00
```

COEFFICIENT a65

```
 .0000000000000E+00    .0000000000000E+00   .0000000000000E+00   .0000000000000E+00   .0000000000000E+00
 .0000000000000E+00    .0000000000000E+00   .0000000000000E+00   .0000000000000E+00   .0000000000000E+00
 .0000000000000E+00    .0000000000000E+00   .0000000000000E+00   .0000000000000E+00   .0000000000000E+00
 .0000000000000E+00   -.2756963437455E-44  -.4945802870714E-44  -.3522258692960E-45  -.1781214777728E-47
-.5036793539273E-51    .0000000000000E+00   .0000000000000E+00   .0000000000000E+00   .0000000000000E+00
 .0000000000000E+00
```

COEFFICIENT a66

```
 .0000000000000E+00    .0000000000000E+00   .0000000000000E+00   .0000000000000E+00   .0000000000000E+00
 .0000000000000E+00    .0000000000000E+00   .0000000000000E+00   .0000000000000E+00   .0000000000000E+00
 .0000000000000E+00    .0000000000000E+00   .0000000000000E+00   .0000000000000E+00   .0000000000000E+00
 .0000000000000E+00    .1429678203362E-45   .7846154258857E-45   .1208363219725E-45   .1279527193592E-47
 .9337035037483E-51    .1285612044156E-55   .0000000000000E+00   .0000000000000E+00   .0000000000000E+00
 .0000000000000E+00
```

COEFFICIENT a67

```
 .0000000000000E+00    .0000000000000E+00   .0000000000000E+00   .0000000000000E+00   .0000000000000E+00
 .0000000000000E+00    .0000000000000E+00   .0000000000000E+00   .0000000000000E+00   .0000000000000E+00
 .0000000000000E+00    .0000000000000E+00   .0000000000000E+00   .0000000000000E+00   .0000000000000E+00
 .0000000000000E+00   -.4556288514434E-47  -.9745308291851E-46  -.3365553002961E-46  -.7307573444969E-48
-.1223397279425E-50   -.8367115471421E-55   .0000000000000E+00   .0000000000000E+00   .0000000000000E+00
 .0000000000000E+00
```

COEFFICIENT a68

```
 .0000000000000E+00    .0000000000000E+00   .0000000000000E+00   .0000000000000E+00   .0000000000000E+00
 .0000000000000E+00    .0000000000000E+00   .0000000000000E+00   .0000000000000E+00   .0000000000000E+00
 .0000000000000E+00    .0000000000000E+00   .0000000000000E+00   .0000000000000E+00   .0000000000000E+00
 .0000000000000E+00    .6700424285933E-49   .9259034301182E-47   .7606563020953E-47   .3368988840059E-48
 .1204587058226E-50    .2586846887081E-54   .0000000000000E+00   .0000000000000E+00   .0000000000000E+00
 .0000000000000E+00
```

!UDD!PABLO!COEFFICIENTS

COEFFICIENT a69

.0000000000000E+00	.0000000000000E+00	.0000000000000E+00	.0000000000000E+00	.0000000000000E+00
.0000000000000E+00	.0000000000000E+00	.0000000000000E+00	.0000000000000E+00	.0000000000000E+00
.0000000000000E+00	.0000000000000E+00	.0000000000000E+00	.0000000000000E+00	.0000000000000E+00
.0000000000000E+00	.0000000000000E+00	-.6485292152872E-48	-.1388540861570E-47	-.1265768357291E-48
-.9250360539027E-51	-.5053466243444E-54	-.5480017238516E-59	.0000000000000E+00	.0000000000000E+00
.0000000000000E+00				

COEFFICIENT a70

.0000000000000E+00	.0000000000000E+00	.0000000000000E+00	.0000000000000E+00	.0000000000000E+00
.0000000000000E+00	.0000000000000E+00	.0000000000000E+00	.0000000000000E+00	.0000000000000E+00
.0000000000000E+00	.0000000000000E+00	.0000000000000E+00	.0000000000000E+00	.0000000000000E+00
.0000000000000E+00	.0000000000000E+00	.3148662471327E-49	.2027995013919E-48	.3895390932334E-49
.5675034953593E-51	.6998960792128E-54	.3730816353416E-58	.0000000000000E+00	.0000000000000E+00
.0000000000000E+00				

COEFFICIENT a71

.0000000000000E+00	.0000000000000E+00	.0000000000000E+00	.0000000000000E+00	.0000000000000E+00
.0000000000000E+00	.0000000000000E+00	.0000000000000E+00	.0000000000000E+00	.0000000000000E+00
.0000000000000E+00	.0000000000000E+00	.0000000000000E+00	.0000000000000E+00	.0000000000000E+00
.0000000000000E+00	.0000000000000E+00	-.9437217304130E-51	-.2333423571849E-49	-.9832727579782E-50
-.2826066624766E-51	-.7308996772386E-54	-.1209337086782E-57	.0000000000000E+00	.0000000000000E+00
.0000000000000E+00				

COEFFICIENT a72

.0000000000000E+00	.0000000000000E+00	.0000000000000E+00	.0000000000000E+00	.0000000000000E+00
.0000000000000E+00	.0000000000000E+00	.0000000000000E+00	.0000000000000E+00	.0000000000000E+00
.0000000000000E+00	.0000000000000E+00	.0000000000000E+00	.0000000000000E+00	.0000000000000E+00
.0000000000000E+00	.0000000000000E+00	.1310724625574E-52	.2064963366932E-50	.2031229410034E-50
.1154249912880E-51	.5975467852173E-54	.2483133680354E-57	.2143981705210E-62	.0000000000000E+00
.0000000000000E+00				

COEFFICIENT a73

.0000000000000E+00	.0000000000000E+00	.0000000000000E+00	.0000000000000E+00	.0000000000000E+00
.0000000000000E+00	.0000000000000E+00	.0000000000000E+00	.0000000000000E+00	.0000000000000E+00
.0000000000000E+00	.0000000000000E+00	.0000000000000E+00	.0000000000000E+00	.0000000000000E+00
.0000000000000E+00	.0000000000000E+00	.0000000000000E+00	-.1353695709120E-51	-.3413508113306E-51

!UDD!PABLO!COEFFICIENTS

-.3890499512477E-52	-.3919412185353E-54	-.3624693270110E-57	-.1523903049978E-61	.0000000000000E+00
.0000000000000E+00				

COEFFICIENT a74

.0000000000000E+00	.0000000000000E+00	.0000000000000E+00	.0000000000000E+00	.0000000000000E+00
.0000000000000E+00	.0000000000000E+00	.0000000000000E+00	.0000000000000E+00	.0000000000000E+00
.0000000000000E+00	.0000000000000E+00	.0000000000000E+00	.0000000000000E+00	.0000000000000E+00
.0000000000000E+00	.0000000000000E+00	.0000000000000E+00	.6178094811939E-53	.4618066879468E-52
.1085141882320E-52	.2096847131271E-54	.4001657596612E-57	.5168004089050E-61	.0000000000000E+00
.0000000000000E+00				

COEFFICIENT a75

.0000000000000E+00	.0000000000000E+00	.0000000000000E+00	.0000000000000E+00	.0000000000000E+00
.0000000000000E+00	.0000000000000E+00	.0000000000000E+00	.0000000000000E+00	.0000000000000E+00
.0000000000000E+00	.0000000000000E+00	.0000000000000E+00	.0000000000000E+00	.0000000000000E+00
.0000000000000E+00	.0000000000000E+00	.0000000000000E+00	-.1747632834098E-54	-.4948497739162E-53
-.2503637189162E-53	-.9251471082029E-55	-.3470258103916E-57	-.1112721522070E-60	.0000000000000E+00
.0000000000000E+00				

COEFFICIENT a76

.0000000000000E+00	.0000000000000E+00	.0000000000000E+00	.0000000000000E+00	.0000000000000E+00
.0000000000000E+00	.0000000000000E+00	.0000000000000E+00	.0000000000000E+00	.0000000000000E+00
.0000000000000E+00	.0000000000000E+00	.0000000000000E+00	.0000000000000E+00	.0000000000000E+00
.0000000000000E+00	.0000000000000E+00	.0000000000000E+00	.2299516886971E-56	.4097723699572E-54
.4761202513500E-54	.3390087395395E-55	.2423560039102E-57	.1707459687820E-60	.5723165386801E-65
.0000000000000E+00				

COEFFICIENT a77

.0000000000000E+00	.0000000000000E+00	.0000000000000E+00	.0000000000000E+00	.0000000000000E+00
.0000000000000E+00	.0000000000000E+00	.0000000000000E+00	.0000000000000E+00	.0000000000000E+00
.0000000000000E+00	.0000000000000E+00	.0000000000000E+00	.0000000000000E+00	.0000000000000E+00
.0000000000000E+00	.0000000000000E+00	.0000000000000E+00	.0000000000000E+00	-.2524363645522E-55
-.7411349092958E-55	-.1035677251729E-55	-.1386381826366E-57	-.1987014433242E-60	-.2026642383472E-64
.0000000000000E+00				

COEFFICIENT a78

!UDD!PABLO!COEFFICIENTS

```
 .0000000000000E+00    .0000000000000E+00    .0000000000000E+00    .0000000000000E+00    .0000000000000E+00
 .0000000000000E+00    .0000000000000E+00    .0000000000000E+00    .0000000000000E+00    .0000000000000E+00
 .0000000000000E+00    .0000000000000E+00    .0000000000000E+00    .0000000000000E+00    .0000000000000E+00
 .0000000000000E+00    .0000000000000E+00    .0000000000000E+00    .0000000000000E+00    .1086850041413E-56
 .9336940438395E-56    .2640475058528E-56    .6571996915879E-58    .1821873760314E-60    .4565839915160E-64
 .0000000000000E+00
```

COEFFICIENT a79

```
 .0000000000000E+00    .0000000000000E+00    .0000000000000E+00    .0000000000000E+00    .0000000000000E+00
 .0000000000000E+00    .0000000000000E+00    .0000000000000E+00    .0000000000000E+00    .0000000000000E+00
 .0000000000000E+00    .0000000000000E+00    .0000000000000E+00    .0000000000000E+00    .0000000000000E+00
 .0000000000000E+00    .0000000000000E+00    .0000000000000E+00    .0000000000000E+00   -.2910780869584E-58
-.9360666145856E-57   -.5608396124411E-57   -.2601695208182E-58   -.1349785488822E-60   -.7347680781743E-64
 .0000000000000E+00
```


COEFFICIENT a80

```
 .0000000000000E+00    .0000000000000E+00    .0000000000000E+00    .0000000000000E+00    .0000000000000E+00
 .0000000000000E+00    .0000000000000E+00    .0000000000000E+00    .0000000000000E+00    .0000000000000E+00
 .0000000000000E+00    .0000000000000E+00    .0000000000000E+00    .0000000000000E+00    .0000000000000E+00
 .0000000000000E+00    .0000000000000E+00    .0000000000000E+00    .0000000000000E+00    .3638476086980E-60
 .7282589285880E-58    .9879038500145E-58    .8641521991856E-59    .8223031157965E-61    .8989697079596E-64
 .0000000000000E+00
```

APPENDIX 4 COMPUTER PROGRAMS

A4.1 COMPUTER : TECHNICAL DETAILS

All the computer simulations were run at the Massachusetts Institute of Technology's Chemical Engineering Department Computer Facility.

The computer is a Data General "Eclipse" MV 4000 32 bit data processing system.

A4.2 COMPUTER PROGRAM EQUIL

```
!UDD!PABLO!EQUIL                                                    2-DEC-84   0:29:38  PAGE 1
      IMPLICIT REAL*8(A-H,O-Z)
      COMMON/TRAN/QM(3,3),QUAT(4)
      COMMON/VEL/VPREV(108,3)
      COMMON/COORD/XPREV(108,3)
      COMMON/DISTRI/LUDWIG(20),V(108,3),R(20),DNDV(20),VAVB,TAUSQ
      COMMON/SIT/OPREV(108,3),SLOC(350,3),ARM(4),ORPREV(108,3)
      DIMENSION II(2,2),IJ(2,2),ZIJ(4),ZINVIJ(4),ZII(3),ZINVII(3)
      DIMENSION F(6100,3),F1(6100,4),STIJ(4),STII(3)
      DIMENSION E(6100,3),E1(6100,4)
      DIMENSION NATOM(2),ISIT(2,2),ICLAS(2,12)
      DIMENSION EIJ(2,2),EII(2,2),WT(2,2),WR2(3),STSIT(12,3)
      DIMENSION SIGIJ(2,2),SIGII(2,2)
      DIMENSION XI6II(3),UII(3)
      DIMENSION KLAS1(12,3),KLAS(3,3)
      DIMENSION XI6IJ(4),UIJ(4)
      DIMENSION STEP3(2),S(3),X(108,3),ROT(4),XS(350,3)
      DIMENSION PF(350,3),XGHOST(3,3),TOTFOR(108,3),B(3)
      DIMENSION PK(108,3),PPK(3),FPREV(108,3),PPPREV(3)
      DIMENSION OME(108,3),ALFA(4,3),PKPREV(108,3),ORI(108,3),QPREV(4)
      DIMENSION RVIR(3),PFVIR(3),CHGSV(2),COULB(3),COULV(3),ABENIJ(4)
      DIMENSION ABENII(3),UCOMP(3)

      OPEN(1,FILE='MAKE')
      OPEN(20,FILE='COMMAND')
      OPEN(27,FILE='RODY')
      OPEN(86,FILE='NEWT')

C*****  INITIALIZATION & UNIT CONVERSION

C*****  THE FOLLOWING IS A LIST OF MOLECULAR PARAMETERS THAT MUST BE SPECIFIED
C*****  AS WELL AS THE CORRESPONDING UNITS IN EACH CASE

C*****  NATOM(I)  (I=1,2)  # OF DIFFERENT ATOM TYPES IN SOLUTE(1) & SOLVENT(2)
C*****  ISIT(I,J) (I=1,2;J=1,...,MAX.OF NATOM(I))  # OF SITES OF TYPE J IN
C*****            MOLECULE I.THIS MUST BE COMPLETED WITH 0'S IN INPUT FILE
C*****            IF NATOM(1) IS DIFFERENT FROM NATOM(2)
C*****  EIJ(I,J)  (I=1,...,NATOM(1);J=1,...,NATOM(2)) ENERGY PARAMETER
C*****            (IN KELVIN) FOR THE INTERACTION BETWEEN TYPE I SITE
C*****            (SOLUTE) AND TYPE J SITE IN  THE SOLVENT.THE ASSIGNMENT OF
C*****            A NUMBER TO EACH SITE TYPE IS DONE BY THE PROGRAM
C*****            BUT THE USER MUST ENTER DATA FOLLOWING A CONSISTENT ORDERING
C*****            THIS MEANS THAT ATOMIC WEIGHTS,POSITION VECTORS,SIZE AND ENER
C*****            GY PARAMETERS MUST BE CONSISTENTLY DECLARED
C*****  EII(I,J)  (I=1,...,NATOM(2);J=1,...,NATOM(2)) ENERGY PARAMETER
C*****            FOR SOLVENT SOLVENT INTERACTIONS
C*****  SIGIJ(I,J)(I=1,...,NATOM(1);J=1,...,NATOM(2))SIZE PARAMETER(A) FOR
C*****            THE INTERACTION BETWEEN SOLUTE AND SOLVENT MOLECULES
C*****  SIGII(I,J)(I=1,...,NATOM(2);J=1,...,NATOM(2))SIZE PARAMETER(A) FOR
C*****            THE INTERACTION BETWEEN SOLVENT MOLECULES
C*****  WT(I,J)   (I=1,2;J=1,...,MAX.OF NATOM(I))ATOMIC WEIGHT OF THE
C*****            Jth SITE OF THE Ith MOLECULE.THIS ARRAY MUST BE COMPLE
C*****            TED WITH 0'S IF NATOM(1) IS DIFFERENT FROM NATOM(2)
C*****  WR2(J)    (J=1,3)Jth PRINCIPAL MOMENT OF INERTIA
C*****            OF THE SOLUTE MOLECULE(IN ATOMIC WEIGHTS*Angstrom**2)
C*****  WR2SV     PRINCIPAL MOMENT OF INERTIA OF THE LINEAR SOLVENT
C*****  STSIT(I,J)(I=1,...,# OF SITES IN SOLUTE;J=1,3)Jth COMPONENT
C*****            OF THE POSITION VECTOR OF THE Ith SITE IN THE SOLUTE MOLE
C*****            CULE(A),IN A COORDINATE SYSTEM WHOSE AXES ARE THE PRINCIPAL
C*****            AXES OF INERTIA OF THE MOLECULE UNDER CONSIDERATION.THE
```

```
!UDD!PABLO!EQUIL
C*****            NUMBERING OF THE SITES MUST BE CONSISTENT WITH ALL OF THE
C*****            ABOVE ARRAYS
C*****  ARM(I)    (I=1,...,# OF SOLVENT SITES)LINEAR COORDINATE
C*****            OF THE Ith SOLVENT SITE WRT CENTER OF MASS.SITE NUMBERING
C*****            MUST BE CONSISTENT WITH ALL OF THE ABOVE ARRAYS

C*****  CHGSV(I)  (I=1,...,NATOM(2))EFFECTIVE CHARGE(IN ELECTRONS) OF
C*****            TYPE I SITE(SOLVENT)

C*****  ENTER TEMPERATURE(K),MOLAR VOLUME(M**3/MOL),TIME STEP(S) , CUTOFF
C*****  RADIUS(A), FRACTION OF SIZE PARAMETER BELOW WHICH DEFAULT
C*****  VALUES OF FORCE AND ENERGY ARE SPECIFIED AND VELOCIY SCALING FACTORS

        READ(20,FMT=*)T,VOL,TIME,RCUT,ACCU,VSCALE,ROTSCL

C*****  INITU IS THE # OF INITIALIZATION STEPS
C*****  IKODE=0 INDICATES START-UP FILE ALREADY EXISTS
C*****  IKODE=1 INDICATES INITIALIZATION MUST BE DONE
C*****  LSLAP=1 INDICATES VELOCITY RESCALING
C*****  LSLAP=0 INDICATES NO RESCALING
C*****  NSLAP=# OF STEPS BETWEEN RESCALINGS

        READ(20,FMT=*)INITU,IKODE,LSLAP,NSLAP

C*****  ENTER # OF UNIT CUBES

        READ(1,FMT=*)NCUB

C*****  CALCULATE # OF MOLECULES

        N=4*(NCUB**3)

C*****  TKT1 IS A CONVERSION FACTOR ALLOWING FOR THE SOLUTE HAVING THREE
C*****  ROTATIONAL DEGREES OF FREEDOM

        TKT=FLOAT(N)
        TKT1=1.+(2.*(TKT-1.)+3.)/(3.*TKT)

C*****  ENTER # OF DIFERENT SITE TYPES IN SOLUTE & SOLVENT MOLECULES

        READ(1,FMT=*)(NATOM(I),I=1,2)

C*****  DETERMINE MAXIMUM

        IKETZ=NATOM(2)-NATOM(1)
        IF(IKETZ.GE.0)GO TO 800
        JMAXI=NATOM(1)
        GO TO 801
 800    JMAXI=NATOM(2)
 801    CONTINUE

C*****  ENTER NUMBER OF SITES OF EACH DIFFERENT KIND,ENERGY AND SIZE PARAMETERS
C*****  AND ATOMIC WEIGHTS

        DO 802 I=1,2
        READ(1,FMT=*)(ISIT(I,J),J=1,JMAXI)
 802    CONTINUE
        DO 803 I=1,NATOM(1)
        READ(1,FMT=*)(SIGIJ(I,J),J=1,NATOM(2))
```

```
 803    CONTINUE
        DO 804 I=1,NATOM(1)
        READ(1,FMT=*)(EIJ(I,J),J=1,NATOM(2))
 804    CONTINUE
        DO 891 I=1,NATOM(2)
        READ(1,FMT=*)(SIGII(I,J),J=1,NATOM(2))
 891    CONTINUE
        DO 892 I=1,NATOM(2)
        READ(1,FMT=*)(EII(I,J),J=1,NATOM(2))
 892    CONTINUE
        DO 805 I=1,2
        READ(1,FMT=*)(WT(I,J),J=1,JMAXI)
 805    CONTINUE

C*****  CALCULATE TOTAL SITES IN SOLUTE & SOLVENT MOLECULES

        NSOLUT=0
        DO 900 I=1,NATOM(1)
        NSOLUT=NSOLUT+ISIT(1,I)
 900    CONTINUE
        NSOLVT=0
        DO 901 I=1,NATOM(2)
        NSOLVT=NSOLVT+ISIT(2,I)
 901    CONTINUE

C*****  ENTER PRINCIPAL MOMENTS OF INERTIA OF SOLUTE & SOLVENT

        READ(1,FMT=*)(WR2(J),J=1,3)
        READ(1,FMT=*)WR2SV


C*****  ENTER MOLECULAR GEOMETRY!THIS IS SPECIFIED BY MEANS OF  VECTORS
C*****  FOR THE SOLUTE,AND SCALARS FOR THE SOLVENT,GIVING SITE
C*****  COORDINATES RELATIVE TO THE CENTER OF MASS

        DO 808 I=1,NSOLUT
        READ(1,FMT=*)(STSIT(I,K),K=1,3)
 808    CONTINUE
        READ(1,FMT=*)(ARM(K),K=1,NSOLVT)

C*****  ENTER SOLVENT ATOMIC CHARGES

        READ(1,FMT=*)(CHGSV(K),K=1,NATOM(2))

C*****  CALCULATE LENGTH & TIME SCALES
C*****  SLEN IS THE LENGTH SCALE IN M/SLU

        SLEN=1.1841724E- 8*((FLOAT(N)*VOL)**.333333333)

C*****  PMOLST IS THE SOLUTE MOLECULAR WEIGHT
C*****  PMOLSV IS THE SOLVENT MOLECULAR WEIGHT

        PMOLST=0.
        PMOLSV=0.
        DO 809 K=1,JMAXI
        PMOLST=PMOLST+WT(1,K)*FLOAT(ISIT(1,K))
        PMOLSV=PMOLSV+WT(2,K)*FLOAT(ISIT(2,K))
 809    CONTINUE
        ZWTST=PMOLST/24.
```

```
      ZWTSV=PMOLSV/24.

C***** STIM IS THE TIME SCALE IN S/STU

      STIM=SLEN/(157.9341635*SQRT(T/PMOLSV))

C***** ELEC IS A COULOMBIC CONVERSION FACTOR

      ELEC=1.1572412E-2*(STIM**2)/(SLEN**3)

C***** CONVERT MOLECULAR PARAMETERS TO SIMULATION UNITS

      CONV1=PMOLSV/(36.*T)
      CONV2=1.E10*SLEN
      CONV3=12.E20*(SLEN**2)
      CONV4=PMOLSV/36.
      CONV5=24./(FLOAT(N)*PMOLSV)
      DO 810 I=1,2
      DO 811 J=1,JMAXI
      WT(I,J)=WT(I,J)/12.
  811 CONTINUE
  810 CONTINUE
      DO 816 K=1,3
      WR2(K)=WR2(K)/CONV3
  816 CONTINUE
      WR2SV=WR2SV/CONV3
      DO 812 I=1,NSOLVT
      ARM(I)=ARM(I)/CONV2
  812 CONTINUE
      DO 814 I=1,NSOLUT
      DO 815 J=1,3
      STSIT(I,J)=STSIT(I,J)/CONV2
  815 CONTINUE
  814 CONTINUE
      DO 893 I=1,NATOM(1)
      DO 894 J=1,NATOM(2)
      SIGIJ(I,J)=SIGIJ(I,J)/CONV2
      EIJ(I,J)=EIJ(I,J)*CONV1
  894 CONTINUE
  893 CONTINUE
      DO 895 I=1,NATOM(2)
      DO 896 J=1,NATOM(2)
      SIGII(I,J)=SIGII(I,J)/CONV2
      EII(I,J)=EII(I,J)*CONV1
  896 CONTINUE
  895 CONTINUE

C***** STEP IS THE TIME STEP IN STU
C***** RC IS THE CUTOFF RADIUS IN SLU

      STEP=TIME/STIM
      RC=RCUT/CONV2
      RC2=RC**2
      PELEC=ELEC/(RC**3)
      POLEC=ELEC/RC

C***** CREATE AN ARRAY THAT WILL CLASSIFY SITES ACCORDING TO TYPE

      DO 60 I=1,2
```

```
        IACCUM=0
        DO 61 J=1,NATOM(I)
        K=ISIT(I,J)
        DO 62 L=1,K
        I1=IACCUM+L
        ICLAS(I,I1)=J
 62     CONTINUE
        IACCUM=IACCUM+K
 61     CONTINUE
 60     CONTINUE

C***** CREATE AN ARRAY THAT WILL IDENTIFY SOLVENT-SOLVENT INTERACTIONS

        KJ=0
        DO 180 I=1,NATOM(2)
        ISUM=0
        DO 181 J=I,NATOM(2)
        II(I,J)=KJ+J+1-I
        IF(I.EQ.J)GO TO 182
        II(J,I)=II(I,J)
 182    CONTINUE
        ISUM=ISUM+1
 181    CONTINUE
        KJ=KJ+ISUM
 180    CONTINUE

C***** CREATE AN ARRAY THAT WILL IDENTIFY SOLVENT-SOLUTE INTERACTIONS

        DO 183 I=1,NATOM(1)
        MUSTAF=(I-1)*NATOM(2)
        DO 184 J=1,NATOM(2)
        IJ(I,J)=J+MUSTAF
 184    CONTINUE
 183    CONTINUE

C***** CREATE ARRAYS THAT WILL IDENTIFY INTERACTION TYPE GIVEN SITE TYPE

        DO 601 I=1,NSOLUT
        L=ICLAS(1,I)
        DO 602 J=1,NSOLVT
        M=ICLAS(2,J)
        KLAS1(I,J)=IJ(L,M)
 602    CONTINUE
 601    CONTINUE
        DO 603 I=1,NSOLVT
        L=ICLAS(2,I)
        DO 604 J=1,NSOLVT
        M=ICLAS(2,J)
        KLAS(I,J)=II(L,M)
 604    CONTINUE
 603    CONTINUE


C***** CALCULATE FORCE AND ENERGY CONSTANTS.THESE ARE COMBINATIONS OF SIZE
C***** AND/OR ENERGY PARAMETERS THAT APPEAR IN THE FORCE/ENERGY CALCULATION
C***** STEPS

        DO 63 I=1,NATOM(1)
        DO 64 J=1,NATOM(2)
```

```
      K=IJ(I,J)
      STIJ(K)=(SIGIJ(I,J)/RC)*ACCU
      XI6IJ(K)=(SIGIJ(I,J)/RC)**6
      AUX=(SIGIJ(I,J)/RC)**14
      ZIJ(K)=(24.*EIJ(I,J)/(SIGIJ(I,J)**2))*AUX
      UIJ(K)=4.*EIJ(I,J)*XI6IJ(K)
      ZINVIJ(K)=1./XI6IJ(K)
      WELLLJ=1./(2.*XI6IJ(K))
      UNG=WELLLJ**.1666
      DO 999 MU=1,1000
      WELL1=(UNG**13)-1.
      WELL2=(UNG**7)-1.
      WELL6=UNG**6
      WELL12=UNG**12
      SODRE=WELL1*WELL2-WELLLJ*(WELL2**2)
      SADRE=13.*WELL12*WELL2-7.*WELL6*WELL1
      UNGNEW=UNG-SODRE/SADRE
      WALL1=(UNGNEW**13)-1.
      WALL2=(UNGNEW**7)-1.
      WALL3=WALL1/WALL2-WELLLJ
      IF(ABS(WALL3).LE.1.E-8)GO TO 998
      UNG=UNGNEW
999   CONTINUE
      WRITE(86,997)
997   FORMAT(1X,'NEWTON MISBEHAVING')
      GO TO 996
998   UNG6=(UNGNEW**6)-1.
      UNG12=(UNGNEW**12)-1.
      UNGINV=(1./UNGNEW)-1.
      DEPTH=(6.*UNGINV*(2.*XI6IJ(K)-1.)+XI6IJ(K)*UNG12-UNG6)*UIJ(K)
      ABENIJ(K)=ABS(DEPTH)
64    CONTINUE
63    CONTINUE
      DO 65 I=1,NATOM(2)
      DO 66 J=I,NATOM(2)
      KIND=II(I,J)
      STII(KIND)=(SIGII(I,J)/RC)*ACCU
      XI6II(KIND)=(SIGII(I,J)/RC)**6
      UII(KIND)=4.*EII(I,J)*XI6II(KIND)
      AUX=(SIGII(I,J)/RC)**14
      ZII(KIND)=(24.*EII(I,J)/(SIGII(I,J)**2))*AUX
      ZINVII(KIND)=1./XI6II(KIND)
      WELLLJ=1./(2.*XI6II(KIND))
      UNG=WELLLJ**.166
      DO 474 MU=1,1000
      WELL1=(UNG**13)-1.
      WELL2=(UNG**7)-1.
      WELL6=UNG**6
      WELL12=UNG**12
      SODRE=WELL1*WELL2-WELLLJ*(WELL2**2)
      SADRE=13.*WELL12*WELL2-7.*WELL6*WELL1
      UNGNEW=UNG-SODRE/SADRE
      WALL1=(UNGNEW**13)-1.
      WALL2=(UNGNEW**7)-1.
      WALL3=WALL1/WALL2-WELLLJ
      IF(ABS(WALL3).LE.1.E-8)GO TO 473
      UNG=UNGNEW
474   CONTINUE
      WRITE(86,997)
```

```
      GO TO 996
 473  UNG6=(UNGNEW**6)-1.
      UNG12=(UNGNEW**12)-1.
      UNGINV=(1./UNGNEW)-1.
      DEPTH=UII(KIND)*(6.*UNGINV*(2.*XI6II(KIND)-1.)+XI6II(KIND)*UNG12-UNG6)
      ABENII(KIND)=ABS(DEPTH)
      COULB(KIND)=PELEC*CHGSV(I)*CHGSV(J)
      COULV(KIND)=POLEC*CHGSV(I)*CHGSV(J)
 66   CONTINUE
 65   CONTINUE

C***** CALCULATE FORCE TABLES FOR EACH POSSIBLE TYPE OF INTERACTION
      DO 186 I=1,NATOM(2)
      DO 187 J=I,NATOM(2)
      KIND=II(I,J)
      LOW=INT(STII(KIND)*6000.)
      UN=1./STII(KIND)
      UN14=UN**14
      UN8=UN**8
      UN6=UN**6
      UN3=UN**3
      H1=2.*XI6II(KIND)-1.
      H2=(UN6+1.)*XI6II(KIND)-1.
      IF(COULV(KIND).GT.0.)GO TO 995
      UCOMP(KIND)=ABS(COULV(KIND))*(UN-1.)
      GO TO 994
 995  UCOMP(KIND)=0.
 994  CONTINUE
      ALDO=COULV(KIND)*(UN-1.)
      POTA=UCOMP(KIND)+ABENII(KIND)
      DEFT=(6.*(1./UN-1.)*H1-UN6*(1./UN6-1.)*H2)*UII(KIND)+ALDO+POTA
      DEFLT=(2.*(UN14-UN)-(UN8-UN)*ZINVII(KIND))*ZII(KIND)+COULB(KIND)*UN3
      DO 188 MB=1,LOW
      F(MB,KIND)=DEFLT
      E(MB,KIND)=DEFT
 188  CONTINUE
      DEL=1./6000.
      BEGIN=FLOAT(LOW)/6000.
      IFALTA=5999-LOW
      DO 189 MB=1,IFALTA
      K=LOW+MB
      UN=1./(BEGIN+DEL*FLOAT(MB))
      UN14=UN**14
      UN8=UN**8
      UN6=UN**6
      UN3=UN**3
      H2=(UN6+1.)*XI6II(KIND)-1.
      F(K,KIND)=(2.*(UN14-UN)-(UN8-UN)*ZINVII(KIND))*ZII(KIND)+COULB(KIND)*UN3
      ALDA=COULV(KIND)*(UN-1.)
      E(K,KIND)=(6.*(1./UN-1.)*H1-UN6*(1./UN6-1.)*H2)*UII(KIND)+ALDA+POTA
 189  CONTINUE
      F(6000,KIND)=0.
      E(6000,KIND)=POTA
 187  CONTINUE
 186  CONTINUE
      DO 389 I=1,NATOM(1)
      DO 390 J=1,NATOM(2)
      KIND=IJ(I,J)
      LOW=INT(STIJ(KIND)*6000.)
```

```
      UN=1./STIJ(KIND)
      UN14=UN**14
      UN8=UN**8
      UN6=UN**6
      H1=2.*XI6IJ(KIND)-1.
      H2=(UN6+1.)*XI6IJ(KIND)-1.
      DEFT=(6.*(1./UN-1.)*H1-UN6*(1./UN6-1.)*H2)*UIJ(KIND)+ABENIJ(KIND)
      DEFLT=(2.*(UN14-UN)-(UN8-UN)*ZINVIJ(KIND))*ZIJ(KIND)
      DO 392 MB=1,LOW
      F1(MB,KIND)=DEFLT
      E1(MB,KIND)=DEFT
  392 CONTINUE
      DEL=1./6000.
      BEGIN=FLOAT(LOW)/6000.
      IFALTA=5999-LOW
      DO 393 MB=1,IFALTA
      K=LOW+MB
      UN=1./(BEGIN+DEL*FLOAT(MB))
      UN14=UN**14
      UN8=UN**8
      UN6=UN**6
      H2=(UN6+1.)*XI6IJ(KIND)-1.
      F1(K,KIND)=(2.*(UN14-UN)-(UN8-UN)*ZINVIJ(KIND))*ZIJ(KIND)
      E1(K,KIND)=(6.*(1./UN-1.)*H1-UN6*(1./UN6-1.)*H2)*UIJ(KIND)+ABENIJ(KIND)
  393 CONTINUE
      F1(6000,KIND)=0.
      E1(6000,KIND)=ABENIJ(KIND)
  390 CONTINUE
  389 CONTINUE
      CONST=RC/6000.

C***** CALCULATE STEP-RELATED CONSTANTS

      DO 260 I=1,2
      IF(I.EQ.1)GO TO 261
      ZWT=PMOLSV/12.
      GO TO 262
  261 ZWT=PMOLST/12.
  262 CONTINUE
      STEP3(I)=STEP/(2.*ZWT)
  260 CONTINUE
      DO 264 IAX=1,3
      S(IAX)=STEP/(2.*WR2(IAX))
  264 CONTINUE
      SSVT=STEP/(2.*WR2SV)
      STEP2=STEP/2.
      STEP4=STEP/4.
      NSITES=NSOLUT+(N-1)*NSOLVT

C***** R IS AN ARRAY CONTAINING THE VALUES OF THE VELOCITIES(IN SIM.UNITS)
C***** AT THE MID-POINT OF THE Kth INTERVAL OF THE VEL. RANGE
C***** A MAXIMUM VELOCITY OF 3 IS CONSIDERED

      DO 499 K=1,20
      VV=FLOAT(K)-1.
      R(K)=(2.*VV+1.)*.075
  499 CONTINUE
      IF(IKODE.EQ.1)GO TO 690
      DO 978 KZU=1,N
```

```
      READ(27,FMT=*)(XPREV(KZU,J),J=1,3)
      READ(27,FMT=*)(VPREV(KZU,J),J=1,3)
      READ(27,FMT=*)(OPREV(KZU,J),J=1,3)
978   CONTINUE
      DO 979 KZO=2,N
      READ(27,FMT=*)(ORPREV(KZO,J),J=1,3)
979   CONTINUE
      READ(27,FMT=*)(QPREV(L),L=1,4)
      DO 980 JK=1,4
      QUAT(JK)=QPREV(JK)
980   CONTINUE
      DO 981 JZ=2,N
      IIU=NSOLUT+(JZ-2)*NSOLVT
      DO 476 JK=1,NSOLVT
      KJ=IIU+JK
      DO 301 JL=1,3
      SLOC(KJ,JL)=ARM(JK)*ORPREV(JZ,JL)
301   CONTINUE
476   CONTINUE
981   CONTINUE
      DO 302 JZ=1,N
      DO 303 IAX=1,3
      X(JZ,IAX)=XPREV(JZ,IAX)
303   CONTINUE
302   CONTINUE
      READ(27,FMT=*)IMOVE
      READ(27,FMT=*)CLOCK
      IF(IMOVE.EQ.0)GO TO 151
      READ(27,FMT=*)ETPREV,SCPREV
      READ(27,FMT=*)DNUM,DENOM
      OPEN(30,FILE='SLSAVE')
      WRITE(30,502)
      CLOSE(30)
      ICRASH=1
      GO TO 114
151   DNUM=0.
      DENOM=0.
      OPEN(30,FILE='SLOWING')
      WRITE(30,502)
      CLOSE(30)
      ICRASH=0
      DO 306 I=1,N
      DO 307 IAX=1,3
      VPREV(I,IAX)=VSCALE*VPREV(I,IAX)
      OPREV(I,IAX)=OPREV(I,IAX)*ROTSCL
307   CONTINUE
306   CONTINUE
114   CONTINUE
      CLOSE(27)
502   FORMAT(1X,4X,'STEP',5X,'TOT.ENERG.',1X,'2KE(r)/3nkT',1X,'2KE(t)/
     K3NkT',7X,'T',10X,'Z',6X,'INST.COMPR.','QT.SQ.SUM',2X,'1stMOM.DEV.',
     K2X,'2ndMOM.DEV.',////)
      GO TO 475

C*****  INITIALIZE SOLUTE QUATERNIONS

690   DNUM=0.
      DENOM=0.
      IMOVE=0
```

```
      PQ1=SIN(1.)
      PQ2=SIN(.5)
      PQ3=SIN(.333333333)
      EULER1=3.141592654*(ABS(PQ1))
      EULER2=2.*3.141592654*(ABS(PQ2))
      EULER3=2.*3.141592654*(ABS(PQ3))
      EUL1=EULER1/2.
      EUL2=(EULER2+EULER3)/2.
      EUL3=(EULER2-EULER3)/2.
      QPREV(1)=COS(EUL1)*COS(EUL2)
      QPREV(2)=SIN(EUL1)*COS(EUL3)
      QPREV(3)=SIN(EUL1)*SIN(EUL3)
      QPREV(4)=COS(EUL1)*SIN(EUL2)
      QUAT(1)=QPREV(1)
      QUAT(2)=QPREV(2)
      QUAT(3)=QPREV(3)
      QUAT(4)=QPREV(4)

C*****  INITIALIZE SOLVENT ROTATIONAL CONFIGURATION

      CALL TURN(N,ROTSCL,CONV4,WR2SV,NSOLUT,NSOLVT)

C*****  INITIALIZE SOLUTE ANGULAR VELOCITIES TO THEIR RMS VALUES AS GIVEN
C*****  BY EQUIPARTITION

      DO 817 J=1,3
      JJ=((J+1)/2)*2
      IF(JJ.EQ.J)GO TO 616
      JNORM=-1
      GO TO 617
 616  JNORM=1
 617  CONTINUE
      QPREV(1,J)=FLOAT(JNORM)*SQRT(CONV4/WR2(J))
 817  CONTINUE

C*****  ASSIGN INITIAL POSITIONS CORRESPONDING TO A FACE-CENTERED CUBIC
C*****  LATTICE

      CALL PUT(NCUB)
      DO 836 I=1,N
      DO 837 IAX=1,3
      X(I,IAX)=XPREV(I,IAX)
 837  CONTINUE
 836  CONTINUE

C*****  INITIALIZE VELOCITIES

      CALL START(N,VSCALE)
 475  CONTINUE
      ISTART=1
      ICORR=1
      GO TO 75
 835  ISTART=0

C*****  PREDICTOR SECTION
      DO 378 IAX=1,3
      X(1,IAX)=XPREV(1,IAX)+STEP*VPREV(1,IAX)
      IF(X(1,IAX).GT.1.)GO TO 379
      IF(X(1,IAX).LT.0.)GO TO 31
```

```
      GO TO 376
379   X(1,IAX)=X(1,IAX)-1.
      GO TO 376
31    X(1,IAX)=X(1,IAX)+1.
376   CONTINUE
378   CONTINUE
      ROT(1)=QPREV(2)*OPREV(1,1)+QPREV(3)*OPREV(1,2)-QPREV(4)*OPREV(1,3)
      ROT(2)=QPREV(1)*OPREV(1,1)-QPREV(4)*OPREV(1,2)-QPREV(3)*OPREV
     K (1,3)
      ROT(3)=-QPREV(4)*OPREV(1,1)-QPREV(1)*OPREV(1,2)+QPREV(2)*OPREV(1,3)
      ROT(4)=QPREV(3)*OPREV(1,1)+QPREV(2)*OPREV(1,2)+QPREV(1)*OPREV(1,
     K 3)
      DO 618 IAX=1,4
      QUAT(IAX)=QPREV(IAX)+STEP2*ROT(IAX)
618   CONTINUE
      QTSUM=0.
      DO 436 ISUM=1,4
      QTSUM=QTSUM+QUAT(ISUM)*QUAT(ISUM)
436   CONTINUE
      ASUM=SQRT(QTSUM)
      DO 437 ISUM=1,4
      QUAT(ISUM)=QUAT(ISUM)/ASUM
437   CONTINUE
      DO 26 I=2,N
      DO 27 IAX=1,3
      X(I,IAX)=XPREV(I,IAX)+STEP*VPREV(I,IAX)
      IF(X(I,IAX).GT.1.)GO TO 28
      IF(X(I,IAX).LT.0.)GO TO 29
      GO TO 30
28    X(I,IAX)=X(I,IAX)-1.
      GO TO 30
29    X(I,IAX)=X(I,IAX)+1.
30    CONTINUE
27    CONTINUE
      ORI(I,1)=ORPREV(I,1)+STEP*(OPREV(I,2)*ORPREV(I,3)-OPREV(I,3)*
     K ORPREV(I,2))
      ORI(I,2)=ORPREV(I,2)+STEP*(OPREV(I,3)*ORPREV(I,1)-OPREV(I,1)*ORPREV
     K (I,3))
      ORI(I,3)=ORPREV(I,3)+STEP*(OPREV(I,1)*ORPREV(I,2)-OPREV(I,2)*
     K ORPREV(I,1))
      RNORM=0.
      DO 626 KU=1,3
      RNORM=RNORM+ORI(I,KU)*ORI(I,KU)
626   CONTINUE
      RNOR=1./SQRT(RNORM)
      DO 627 KU=1,3
      ORI(I,KU)=ORI(I,KU)*RNOR
627   CONTINUE
      ISTOR=NSOLVT+(I-2)*NSOLVT
      DO 819 J=1,NSOLVT
      MU=ISTOR+J
      DO 666 IAX=1,3
      SLOC(MU,IAX)=ARM(J)*ORI(I,IAX)
666   CONTINUE
819   CONTINUE
26    CONTINUE
      ICORR=0
75    CONTINUE
```

```
C*****  CALCULATE SITE POSITIONS IN INERTIAL REFERENCE FRAME

        CALL Q
        DO 90 L=1,NSOLUT
        DO 91 IAX=1,3
        Z=0.
        DO 92 LL=1,3
        Z=Z+QM(LL,IAX)*STSIT(L,LL)
 92     CONTINUE
        XS(L,IAX)=Z+X(1,IAX)
 91     CONTINUE
 90     CONTINUE
        DO 93 J=2,N
        JSTOR=NSOLUT+(J-2)*NSOLVT
        DO 10 K=1,NSOLVT
        MU=JSTOR+K
        DO 9 IAX=1,3
        XS(MU,IAX)=SLOC(MU,IAX)+X(J,IAX)
 9      CONTINUE
 10     CONTINUE
 93     CONTINUE

C*****  SET FORCES TO ZERO

        DO 80 NST=1,NSITES
        DO 81 IAX=1,3
        PF(NST,IAX)=0.
 81     CONTINUE
 80     CONTINUE

C*****  ITERATE OVER ALL POSSIBLE PAIRS OF MOLECULES

C*****  SET POTENTIAL ENERGY TO ZERO

        SCALAR=0.
        ENE=0.
        DO 401 J=2,N
        JSTOR=NSOLUT+(J-2)*NSOLVT
        DO 402 IAX=1,3
        DEL=X(J,IAX)-X(1,IAX)
        IF(ABS(DEL).LE.0.5)GO TO 406
        IF(DEL.GT.0.)GO TO 407
        RVIR(IAX)=DEL+1.
        DO 463 K=1,NSOLVT
        KIN=JSTOR+K
        XGHOST(K,IAX)=XS(KIN,IAX)+1.
 463    CONTINUE
        GO TO 408
 407    CONTINUE
        RVIR(IAX)=DEL-1.
        DO 464 K=1,NSOLVT
        KIN=JSTOR+K
        XGHOST(K,IAX)=XS(KIN,IAX)-1.
 464    CONTINUE
        GO TO 408
 406    CONTINUE
        RVIR(IAX)=DEL
        DO 494 K=1,NSOLVT
        KIN=JSTOR+K
```

```
      XGHOST(K,IAX)=XS(KIN,IAX)
 494  CONTINUE
 408  CONTINUE
      PFVIR(IAX)=0.
 402  CONTINUE
      DO 411 L=1,NSOLUT
      DO 412 K=1,NSOLVT
      KIN=JSTOR+K
      KIND=KLAS1(L,K)
      DIST=0.
      DO 413 IAX=1,3
      TROL=XS(L,IAX)-XGHOST(K,IAX)
      IF(ABS(TROL).GT.RC)GO TO 414
      DIST=DIST+TROL*TROL
 413  CONTINUE
      IF(DIST.GT.RC2)GO TO 414
      SEPN=SQRT(DIST)
      MN=INT(SEPN/CONST)
      FCE=F1(MN,KIND)
      ENE=ENE+E1(MN,KIND)
      DO 418 IAX=1,3
      ADD=FCE*(XS(L,IAX)-XGHOST(K,IAX))
      PF(L,IAX)=PF(L,IAX)+ADD
      PF(KIN,IAX)=PF(KIN,IAX)-ADD
      PFVIR(IAX)=PFVIR(IAX)-ADD
 418  CONTINUE
 414  CONTINUE
 412  CONTINUE
 411  CONTINUE
      IF(ICORR.EQ.0)GO TO 510
      DO 512 IAX=1,3
      SCALAR=SCALAR+PFVIR(IAX)*RVIR(IAX)
 512  CONTINUE
 510  CONTINUE
 401  CONTINUE
      DO 1 I=2,N-1

C*****  NUMBER OF SITES PER MOLECULE CAN BE EITHER NSOLUT OR NSOLVT

      ISTOR=NSOLUT+(I-2)*NSOLVT
      DO 4 J=I+1,N
      JSTOR=NSOLUT+(J-2)*NSOLVT

C*****  SEARCH FOR NEAREST J

      DO 5 IAX=1,3
      DEL=X(J,IAX)-X(I,IAX)
      IF(ABS(DEL).LE.0.5)GO TO 6
      IF(DEL.GT.0.)GO TO 7
      RVIR(IAX)=DEL+1.
      DO 563 K=1,NSOLVT
      KIN=JSTOR+K
      XGHOST(K,IAX)=XS(KIN,IAX)+1.
 563  CONTINUE
      GO TO 8
 7    CONTINUE
      RVIR(IAX)=DEL-1.
      DO 94 K=1,NSOLVT
      KIN=JSTOR+K
```

```
      XGHOST(K,IAX)=XS(KIN,IAX)-1.
 94   CONTINUE
      GO TO 8
 6    CONTINUE
      RVIR(IAX)=DEL
      DO 95 K=1,NSOLVT
      KIN=JSTOR+K
      XGHOST(K,IAX)=XS(KIN,IAX)
 95   CONTINUE
 8    CONTINUE
      PFVIR(IAX)=0.
 5    CONTINUE

C*****  CALCULATE DISTANCE BETWEEN ALL POSSIBLE I-J SITE PAIRS

      DO 11 L=1,NSOLVT
      LII=ISTOR+L
      DO 12 K=1,NSOLVT
      KII=JSTOR+K
      KIND=KLAS(L,K)
      DIST=0.
      DO 13 IAX=1,3
      TROL=XS(LII,IAX)-XGHOST(K,IAX)
      IF(ABS(TROL).GT.RC)GO TO 14
      DIST=DIST+TROL*TROL
 13   CONTINUE
      IF(DIST.GT.RC2)GO TO 14
      SEPN=SQRT(DIST)
      MN=INT(SEPN/CONST)
      FCE=F(MN,KIND)
      ENE=ENE+E(MN,KIND)
      DO 18 IAX=1,3
      ADD=FCE*(XS(LII,IAX)-XGHOST(K,IAX))
      PF(LII,IAX)=PF(LII,IAX)+ADD
      PF(KII,IAX)=PF(KII,IAX)-ADD
      PFVIR(IAX)=PFVIR(IAX)-ADD
 18   CONTINUE
 14   CONTINUE
 12   CONTINUE
 11   CONTINUE
      IF(ICORR.EQ.0)GO TO 511
      DO 899 IAX=1,3
      SCALAR=SCALAR+PFVIR(IAX)*RVIR(IAX)
 899  CONTINUE
 511  CONTINUE
  4   CONTINUE
  1   CONTINUE

C*****  CALCULATE TOTAL FORCE ON EACH MOLECULE

      DO 70 I=1,N
      IF(I.NE.1)GO TO 71
      ISTOR=0
      ISITI=NSOLUT
      GO TO 72
 71   ISITI=NSOLVT
      ISTOR=(I-2)*NSOLVT+NSOLUT
 72   CONTINUE
      DO 73 IAX=1,3
```

```
      TOTFOR(I,IAX)=0.
      DO 74 K=1,ISITI
      MU=ISTOR+K
      TOTFOR(I,IAX)=TOTFOR(I,IAX)+PF(MU,IAX)
 74   CONTINUE
 73   CONTINUE
 70   CONTINUE

C***** TORQUE CALCULATION IN INERTIAL COORDINATES
C***** SOLUTE
C***** SET TORQUES TO ZERO

      DO 300 IAX=1,3
      PK(1,IAX)=0.
 300  CONTINUE
      DO 22 J=1,NSOLUT
      DO 23 IAX=1,3
      B(IAX)=XS(J,IAX)-X(1,IAX)
      IF(ABS(B(IAX)).LT.1.E-15)B(IAX)=0.
 23   CONTINUE
      PK(1,1)=PK(1,1)+B(2)*PF(J,3)-B(3)*PF(J,2)
      PK(1,2)=PK(1,2)+B(3)*PF(J,1)-B(1)*PF(J,3)
      PK(1,3)=PK(1,3)+B(1)*PF(J,2)-B(2)*PF(J,1)
 22   CONTINUE

C***** CONVERT TO PRINCIPAL TORQUES

      DO 24 K=1,3
      PPK(K)=0.
      DO 25 L=1,3
      PPK(K)=PPK(K)+QM(K,L)*PK(1,L)
 25   CONTINUE
 24   CONTINUE

C***** SOLVENT TORQUE CALCULATION

      DO 19 I=2,N
      DO 20 IAX=1,3
      PK(I,IAX)=0.
 20   CONTINUE
      ISTOR=NSOLUT+(I-2)*NSOLVT
      DO 21 J=1,NSOLVT
      K=ISTOR+J
      PK(I,1)=PK(I,1)+SLOC(K,2)*PF(K,3)-SLOC(K,3)*PF(K,2)
      PK(I,2)=PK(I,2)+SLOC(K,3)*PF(K,1)-SLOC(K,1)*PF(K,3)
      PK(I,3)=PK(I,3)+SLOC(K,1)*PF(K,2)-SLOC(K,2)*PF(K,1)
 21   CONTINUE
      FORBID=PK(I,1)*ORI(I,1)+PK(I,2)*ORI(I,2)+PK(I,3)*ORI(I,3)
      PK(I,1)=PK(I,1)-FORBID*ORI(I,1)
      PK(I,2)=PK(I,2)-FORBID*ORI(I,2)
      PK(I,3)=PK(I,3)-FORBID*ORI(I,3)
 19   CONTINUE
      IF(ICORR.EQ.0)GO TO 77
      DO 79 IAX=1,3
      FPREV(1,IAX)=TOTFOR(1,IAX)
      PPPREV(IAX)=PPK(IAX)
 79   CONTINUE
      DO 78 I=2,N
      DO 778 IAX=1,3
```

```
      FPREV(I,IAX)=TOTFOR(I,IAX)
      PKPREV(I,IAX)=PK(I,IAX)
778   CONTINUE
 78   CONTINUE
      GO TO 76
77    CONTINUE

C*****  CORRECTOR SECTION

      DO 32 I=1,N
      IF(I.NE.1)GO TO 38
      IN=1
      GO TO 39
38    IN=2
39    CONTINUE
      DO 33 IAX=1,3
      V(I,IAX)=VPREV(I,IAX)+STEP3(IN)*(TOTFOR(I,IAX)+FPREV(I,IAX))
      X(I,IAX)=XPREV(I,IAX)+STEP2*(V(I,IAX)+VPREV(I,IAX))
      IF(X(I,IAX).GT.1.)GO TO 34
      IF(X(I,IAX).LT.0.)GO TO 35
      GO TO 36
34    X(I,IAX)=X(I,IAX)-1.
      GO TO 36
35    X(I,IAX)=X(I,IAX)+1.
36    CONTINUE
      VPREV(I,IAX)=V(I,IAX)
      XPREV(I,IAX)=X(I,IAX)
33    CONTINUE
32    CONTINUE
      DO 768 IAX=1,3
      OME(1,IAX)=OPREV(1,IAX)+S(IAX)*(PPK(IAX)+PPPREV(IAX))
768   CONTINUE
      DO 794 IAX=1,3
      DO 131 K=1,4
      ALFA(K,IAX)=QUAT(K)*OME(1,IAX)+QPREV(K)*OPREV(1,IAX)
131   CONTINUE
794   CONTINUE
      QUAT(1)=QPREV(1)+STEP4*(-ALFA(2,1)+ALFA(3,2)-ALFA(4,3))
      QUAT(2)=QPREV(2)+STEP4*(ALFA(1,1)-ALFA(4,2)-ALFA(3,3))
      QUAT(3)=QPREV(3)+STEP4*(-ALFA(4,1)-ALFA(1,2)+ALFA(2,3))
      QUAT(4)=QPREV(4)+STEP4*(ALFA(3,1)+ALFA(2,2)+ALFA(1,3))

C*****  RENORMALIZE QUATERNIONS

      QSUM=0.
      DO 433 ISUM=1,4
      QSUM=QSUM+QUAT(ISUM)*QUAT(ISUM)
433   CONTINUE
      ASUM=SQRT(QSUM)
      DO 434 ISUM=1,4
      QUAT(ISUM)=QUAT(ISUM)/ASUM
      QPREV(ISUM)=QUAT(ISUM)
434   CONTINUE

      DO 797 I=2,N
      ISTOR=NSOLUT+(I-2)*NSOLVT
      DO 799 IAX=1,3
      OME(I,IAX)=OPREV(I,IAX)+SSVT*(PK(I,IAX)+PKPREV(I,IAX))
799   CONTINUE
```

```
      AUX1=STEP2*OME(I,3)
      AUX2=-STEP2*OME(I,2)
      AUX4=-STEP2*OME(I,3)
      AUX5=STEP2*OME(I,1)
      AUX7=STEP2*OME(I,2)
      AUX8=-STEP2*OME(I,1)
      AUX0=(1.-AUX5*AUX8)-AUX1*(AUX4-AUX5*AUX7)+AUX2*(AUX4*AUX8-AUX7)
      AUX3=(ORPREV(I,1)+STEP2*(OPREV(I,2)*ORPREV(I,3)-OPREV(I,3)*
     K ORPREV(I,2)))
      AUX6=(ORPREV(I,2)+STEP2*(OPREV(I,3)*ORPREV(I,1)-OPREV(I,1)*ORPREV(I
     K ,3)))
      AUX9=(ORPREV(I,3)+STEP2*(OPREV(I,1)*ORPREV(I,2)-OPREV(I,2)*ORPREV
     K (I,1)))
      AUX10=AUX3*(1.-AUX5*AUX8)-AUX1*(AUX6-AUX5*AUX9)+AUX2*(AUX6*AUX8-AUX9)
      AUX11=(AUX6-AUX5*AUX9)-AUX3*(AUX4-AUX5*AUX7)+AUX2*(AUX4*AUX9-AUX6*
     K AUX7)
      AUX12=(AUX9-AUX6*AUX8)-AUX1*(AUX4*AUX9-AUX6*AUX7)+AUX3*(AUX4*AUX8-
     K AUX7)
      ORI(I,1)=AUX10/AUX0
      ORI(I,2)=AUX11/AUX0
      ORI(I,3)=AUX12/AUX0
      RNO=0.
      DO 628 KO=1,3
      RNO=RNO+ORI(I,KO)*ORI(I,KO)
 628  CONTINUE
      RNU=1./SQRT(RNO)
      DO 629 KO=1,3
      ORI(I,KO)=ORI(I,KO)*RNU
 629  CONTINUE
      DO 465 J=1,NSOLVT
      MU=ISTOR+J
      DO 549 IAX=1,3
      SLOC(MU,IAX)=ORI(I,IAX)*ARM(J)
 549  CONTINUE
 465  CONTINUE
      ORPREV(I,1)=ORI(I,1)
      ORPREV(I,2)=ORI(I,2)
      ORPREV(I,3)=ORI(I,3)
 797  CONTINUE
      DO 468 I=1,N
      DO 132 IAX=1,3
      OPREV(I,IAX)=OME(I,IAX)
 132  CONTINUE
 468  CONTINUE

C***** CALCULATE TORQUE & FORCE WITH CORRECTED COORDINATES

      ICORR=1
      GO TO 75
  76  CONTINUE
      IF(ISTART.EQ.1)GO TO 835

C***** MOLECULE MOVING SECTION ENDS

      IF(IMOVE.EQ.INITU)GO TO 500
      IMOVE=IMOVE+1
      ETRAN=0.
      VSQRE=0.
      DO 826 IAX=1,3
```

```
      VSQRE=VSQRE+V(1,IAX)*V(1,IAX)
826   CONTINUE
      ETRAN=ETRAN+VSQRE*ZWTST
      DO 827 I=2,N
      VSQRE=0.
      DO 828 IAX=1,3
      VSQRE=VSQRE+V(I,IAX)*V(I,IAX)
828   CONTINUE
      ETRAN=ETRAN+VSQRE*ZWTSV
827   CONTINUE
      IF(IMOVE.EQ.1)GO TO 529
      DENOM=DENOM+(ETPREV+ETRAN)*STEP2
      DNUM=DNUM+(SCPREV+SCALAR)*STEP2
      COMPR=1.+DNUM/(2.*DENOM)
      ZNOW=1.+SCALAR/(2.*ETRAN)
529   ETPREV=ETRAN
      SCPREV=SCALAR
      JMVA=(IMOVE/10)*10
      IF(JMVA.NE.IMOVE)GO TO 835

C*****  EROT=ROTATIONAL KINETIC ENERGY(SEU)

      EROT=0.
      DO 526 IAX=1,3
      EROT=EROT+WR2(IAX)*OME(1,IAX)*OME(1,IAX)
526   CONTINUE
      DO 527 I=2,N
      DO 528 IAX=1,3
      EROT=EROT+WR2SV*OME(I,IAX)*OME(I,IAX)
528   CONTINUE
527   CONTINUE
      EROT=EROT/2.
      ETOT=ENE+EROT+ETRAN
      TROT=CONV5*EROT
      TTRAN=CONV5*ETRAN
      EQPART=TROT/TTRAN
      THERM=((TROT+TTRAN)/TKT1)*T
      CALL BOLTZ(N)
      DELV=108.5401882*ABS(VAVG-.921317732)
      DEL2V=661.4909979*ABS(TAUSQ-.151173637)
      IF(ICRASH.EQ.1)GO TO 323
      OPEN(30,FILE='SLOWING',POSITION='END')
      GO TO 324
323   OPEN(30,FILE='SLSAVE',POSITION='END')
324   CONTINUE
      WRITE(30,501)IMOVE,ETOT,TROT,TTRAN,THERM,COMPR,ZNOW,QSUM,DELV,DEL2V
501   FORMAT(1X,3X,I5,5X,G11.4,1X,G11.4,1X,G11.4,1X,G11.4,1X,G11.4,1X,G11.4,
     K  1X,G11.4,1X,G11.4,1X,G11.4)
      CLOSE(30)
      IF(LSLAP.EQ.0)GO TO 921
      K23=(IMOVE/NSLAP)*NSLAP
      IF(K23.NE.IMOVE)GO TO 921
      Z62=.6666/TROT
      Z63=1./TTRAN
      Z64=SQRT(Z62)
      Z65=SQRT(Z63)
      DO 637 I=1,N
      DO 317 J=1,3
      VPREV(I,J)=VPREV(I,J)*Z65
```

```
      OPREV(I,J)=OPREV(I,J)*Z64
317   CONTINUE
637   CONTINUE
921   CONTINUE
      ISZAVE=(IMOVE/50)*50
      IF(ISZAVE.NE.IMOVE)GO TO 773
      CLOCK=0.
      ILUM=IMOVE
      GO TO 177
773   CONTINUE
      GO TO 835
500   CONTINUE
      ILUM=IMOVE
      CLOCK=0.
177   CONTINUE
      OPEN(27,FILE='RODY')
      DO 384 KZU=1,N
      WRITE(27,FMT=*)(X(KZU,J),J=1,3)
      WRITE(27,FMT=*)(V(KZU,J),J=1,3)
      WRITE(27,FMT=*)(OME(KZU,J),J=1,3)
384   CONTINUE
      DO 385 KZO=2,N
      WRITE(27,FMT=*)(ORI(KZO,J),J=1,3)
385   CONTINUE
      WRITE(27,FMT=*)(QUAT(L),L=1,4)
      WRITE(27,FMT=*)ILUM
      WRITE(27,FMT=*)CLOCK
      WRITE(27,FMT=*)ETPREV,SCPREV
      WRITE(27,FMT=*)DNUM,DENOM
      CLOSE(27)
      IF(IMOVE.NE.INITU)GO TO 835
996   CONTINUE
      STOP
      END
```

A4.3 SUBROUTINE Q

```
!UDD!PABLO!Q
        SUBROUTINE Q                                                    29-OCT-84  14:37:16  PAGE 1
        IMPLICIT REAL*8(A-H,O-Z)
        COMMON/TRAN/QM(3,3),QUAT(4)

C***** SUBROUTINE Q CALCULATES THE ELEMENTS OF THE 3*3 TRANSFORMATION MATRIX
C***** FOR THE SOLUTE MOLECULE.THE TRANSFORMATION MATRIX CONVERTS ANY VECTOR
C***** FROM THE INERTIAL TO THE PRINCIPAL REFERENCE FRAME.
C***** QUAT ARE THE FOUR QUATERNIONS THAT SPECIFY THE ROTATIONAL CONFIGURATION
C***** OF THE SOLUTE MOLECULE IN A REFERENCE FRAME FIXED AT ITS CENTER OF MASS


        QM(1,1)=QUAT(2)*QUAT(2)+QUAT(1)*QUAT(1)-QUAT(3)*QUAT(3)-QUAT(4)*
     K  QUAT(4)
        QM(1,2)=2.*(QUAT(4)*QUAT(1)-QUAT(3)*QUAT(2))
        QM(1,3)=2.*(QUAT(2)*QUAT(4)+QUAT(3)*QUAT(1))
        QM(2,1)=-2.*(QUAT(3)*QUAT(2)+QUAT(4)*QUAT(1))
        QM(2,2)=QUAT(3)*QUAT(3)+QUAT(1)*QUAT(1)-QUAT(2)*QUAT(2)-QUAT(4)*
     K  QUAT(4)
        QM(2,3)=2.*(QUAT(2)*QUAT(1)-QUAT(3)*QUAT(4))
        QM(3,1)=2.*(QUAT(2)*QUAT(4)-QUAT(1)*QUAT(3))
        QM(3,2)=-2.*(QUAT(3)*QUAT(4)+QUAT(2)*QUAT(1))
        QM(3,3)=QUAT(4)*QUAT(4)+QUAT(1)*QUAT(1)-QUAT(3)*QUAT(3)-QUAT(2)*
     K  QUAT(2)
        RETURN
        END
```

A4.4 SUBROUTINE PUT

```
!UDD!PABLO!PUT
        SUBROUTINE PUT(L)
        IMPLICIT REAL*8(A-H,O-Z)
        COMMON/COORD/XPREV(108,3)
        DIMENSION DUM(3)

C********SUBROUTINE PUT ASSIGNS INITIAL POSITIONS TO THE 4*(L**3) MOLECULES
C********ACCORDING TO A FACE CENTERED CUBIC ARRANGEMENT.L IS THE NUMBER OF
C********ELEMENTARY CUBIC UNITS(WITH 4 MOLECULES PER CUBE)!THERE ARE
C********L**3 UNIT CUBES.
C********THE COORDINATES ARE ASSIGNED ACCORDING TO MOLECULE 'TYPE'!IN A
C********1x1x1 CUBE,THE 'TYPES' ARE
C********TYPE1->(0,0,1)
C********TYPE2->(1/2,1/2,1)
C********TYPE3->(1,1/2,1/2)
C********TYPE4->(1/2,1,1/2)

        LAYER=(L**2)*4
        BLOCK=FLOAT(L)
        SIZE=1./(BLOCK)

C********ITERATE ALONG Z AXIS

        DO 70 K=1,L
        LYR=(K-1)*LAYER

C********ITERATE ALONG Y AXIS

        DO 71 J=1,L
        IND=(J-1)*4

C********ITERATE ALONG X AXIS

        DO 72 I=1,L
        ITYP1=(IND*L+I)+LYR
        ITYP2=ITYP1+L
        ITYP3=ITYP2+L
        ITYP4=ITYP3+L
        XPREV(ITYP1,1)=SIZE*(FLOAT(I)-1.)
        XPREV(ITYP1,2)=SIZE*(FLOAT(J)-1.)
        XPREV(ITYP1,3)=SIZE*FLOAT(K)
        XPREV(ITYP2,1)=(SIZE/2.)*(2.*FLOAT(I)-1.)
        XPREV(ITYP2,2)=(SIZE/2.)*(2.*FLOAT(J)-1.)
        XPREV(ITYP2,3)=XPREV(ITYP1,3)
        XPREV(ITYP3,1)=SIZE*FLOAT(I)
        XPREV(ITYP3,2)=XPREV(ITYP2,2)
        XPREV(ITYP3,3)=(SIZE/2.)*(2.*FLOAT(K)-1.)
        XPREV(ITYP4,1)=XPREV(ITYP2,1)
        XPREV(ITYP4,2)=SIZE*FLOAT(J)
        XPREV(ITYP4,3)=XPREV(ITYP3,3)
 72     CONTINUE
 71     CONTINUE
 70     CONTINUE

C*****  FOR 108 MOLECULES,THE SINGLE SOLUTE MOLECULE(#1) IS INTER
C*****  CHANGED WITH MOLECULE # 53,LOCATED @ THE CENTER OF THE CUBE,TO AVOID
C*****  STARTING THE SIMULATION WITH THE SOLUTE NEAR ONE OF THE BOUNDARY
C*****  SURFACES

        DO 73 IAX=1,3
```

```
!UDD!PABLO!PUT
        DUM(IAX)=XPREV(53,IAX)
        XPREV(53,IAX)=XPREV(1,IAX)
        XPREV(1,IAX)=DUM(IAX)
  73    CONTINUE

        RETURN
        END
```

A4.5 SUBROUTINE START

```
!UDR!PABLO!START
      SUBROUTINE START(L,A)
      IMPLICIT REAL*8(A-H,O-Z)
      COMMON/VEL/VPREV(108,3)
      DIMENSION BEEN(108,2)

C*****  SUBROUTINE START ASSIGNS INITIAL VELOCITIES TO ALL MOLECULES.
C*****  FOR EACH MOLECULE THE COMPONENTS ARE 'SEMI RANDOMIZED',BUT THE
C*****  MAGNITUDE OF ALL VELOCITIES CAN BE SET TO ANY ARBITRARY REAL
C*****  NUMBER,COMMON TO ALL MOLECULES
C*****  L IS THE # OF MOLECULES
C*****  A IS THE MAGNITUDE OF THE VELOCITY

      BEEN(1,1)=.425835
      BEEN(2,1)=.363355
      BEEN(3,1)=.600685
      BEEN(4,1)=.040445
      BEEN(5,1)=.296785
      BEEN(6,1)=.163425
      BEEN(7,1)=.485925
      BEEN(8,1)=.255475
      BEEN(9,1)=.631775
      BEEN(10,1)=.752255
      BEEN(11,1)=.973445
      BEEN(12,1)=.703285
      BEEN(13,1)=.581165
      BEEN(14,1)=.919645
      BEEN(15,1)=.262405
      BEEN(16,1)=.446435
      BEEN(17,1)=.832875
      BEEN(18,1)=.973915
      BEEN(19,1)=.928235
      BEEN(20,1)=.775785
      BEEN(21,1)=.660235
      BEEN(22,1)=.382775
      BEEN(23,1)=.745235
      BEEN(24,1)=.711185
      BEEN(25,1)=.848925
      BEEN(26,1)=.139565
      BEEN(27,1)=.988995
      BEEN(28,1)=.923155
      BEEN(29,1)=.657835
      BEEN(30,1)=.596405
      BEEN(31,1)=.997765
      BEEN(32,1)=.757235
      BEEN(1,2)=.388795
      BEEN(2,2)=.355445
      BEEN(3,2)=.995635
      BEEN(4,2)=.854045
      BEEN(5,2)=.049135
      BEEN(6,2)=.625475
      BEEN(7,2)=.784065
      BEEN(8,2)=.010175
      BEEN(9,2)=.861875
      BEEN(10,2)=.220725
      BEEN(11,2)=.583145
      BEEN(12,2)=.602985
      BEEN(13,2)=.723945
      BEEN(14,2)=.696685
```

```
!UDD!PABLO!START
      BEEN(15,2)=.124745
      BEEN(16,2)=.930595
      BEEN(17,2)=.020535
      BEEN(18,2)=.298075
      BEEN(19,2)=.636455
      BEEN(20,2)=.127925
      BEEN(21,2)=.835685
      BEEN(22,2)=.102275
      BEEN(23,2)=.994715
      BEEN(24,2)=.747295
      BEEN(25,2)=.220755
      BEEN(26,2)=.102335
      BEEN(27,2)=.215755
      BEEN(28,2)=.203255
      BEEN(29,2)=.213175
      BEEN(30,2)=.571245
      BEEN(31,2)=.280675
      BEEN(32,2)=.911525
      DO 20 JUT=1,5
      LMIN=33+(JUT-1)*16
      IF(JUT.EQ.5)GO TO 21
      LMAX=LMIN+15
      GO TO 22
 21   LMAX=LMIN+11
 22   CONTINUE
      LDEL=LMAX-LMIN+1
      DO 23 K=1,LDEL
      JK=K-1+LMIN
      BEEN(JK,1)=(BEEN(K,1)+BEEN(K+JUT,2))/2.
      BEEN(JK,2)=(BEEN(K,2)+BEEN(K+JUT,1))/2.
 23   CONTINUE
 20   CONTINUE
      DO 1 I=1,L
      S=(LOG(BEEN(I,1)))*(-2.)
      S2=(LOG(BEEN(I,2)))*(-2.)
      SEED2=SQRT(S2)
      SEED=SQRT(S)
      SGN1=COS(6.28318530B*BEEN(I,2))
      SGN2=SIN(6.28318530B*BEEN(I,2))
      SGN3=COS(6.28318530B*BEEN(I,1))
      VPREV(I,1)=SEED*SGN1
      VPREV(I,2)=SEED*SGN2
      P=VPREV(I,1)*VPREV(I,1)
      VPREV(I,3)=SEED2*SGN3
      Q=VPREV(I,2)*VPREV(I,2)
      W=VPREV(I,3)*VPREV(I,3)
      R=SQRT(P+Q+W)
      VPREV(I,1)=(VPREV(I,1)/R)*A
      VPREV(I,2)=(VPREV(I,2)/R)*A
      VPREV(I,3)=(VPREV(I,3)/R)*A
 1    CONTINUE
      RETURN
      END
```

A4.6 SUBROUTINE TURN

```
!UDD!PABLO!TURN                                                    2-DEC-84   0:45:54  PAGE 1
      SUBROUTINE TURN(N,ROTSCL,CONV4,WR2SV,NSOLUT,NSOLVT)
      IMPLICIT REAL*8(A-H,O-Z)
      COMMON/SIT/OPREV(108,3),SLOC(350,3),ARM(4),ORPREV(108,3)

C*****  SUBROUTINE TURN GENERATES TWO UNITARY PERPENDICULAR VECTORS
C*****  PER LINEAR SOLVENT MOLECULE;THESE SPECIFY THE DIRECTION OF THE
C*****  MOLECULAR AXIS AND THE DIRECTION OF THE ANGULAR VELOCITY,RESPECTIVELY.
C*****  THE MAGNITUDE OF THE ANGULAR VELOCITY VECTOR IS THE EQUIPARTITION
C*****  VALUE TIMES A CONSTANT SPECIFIED BY THE USER.

      S=1.414213562*ROTSCL*SQRT(CONV4/WR2SV)
      DO 1 I=2,N
      R=FLOAT(I)
      A=COS(R)
      B=SIN(R)
      C=COS(2.*R)
      D=SIN(2.*R)
      E=COS(.5*R)
      X=COS(6.28318530*B)
      Y=SIN(6.28318530*A)
      Z=SIN(6.28318530*C)
      W1=COS(6.28318530*D)
      W2=SIN(6.28318530*E)
      W3=-(X*W1+Y*W2)/Z
      BIGR=X*X+Y*Y+Z*Z
      BIGW=W1*W1+W2*W2+W3*W3
      BIX=SQRT(BIGR)
      BIW=SQRT(BIGW)
      ORPREV(I,1)=X/BIX
      ORPREV(I,2)=Y/BIX
      ORPREV(I,3)=Z/BIX
      OPREV(I,1)=(W1/BIW)*S
      OPREV(I,2)=(W2/BIW)*S
      OPREV(I,3)=(W3/BIW)*S
      J=NSOLUT+(I-2)*NSOLVT
      DO 2 K=1,NSOLVT
      KJ=J+K
      SLOC(KJ,1)=ARM(K)*ORPREV(I,1)
      SLOC(KJ,2)=ARM(K)*ORPREV(I,2)
      SLOC(KJ,3)=ARM(K)*ORPREV(I,3)
2     CONTINUE
1     CONTINUE
      RETURN
      END
```

A4.7 SUBROUTINE BOLTZ

```
      SUBROUTINE BOLTZ(N)
      IMPLICIT REAL*8(A-H,O-Z)
      COMMON/DISTRI/LUDWIG(20),V(108,3),R(20),DNDV(20),VAVG,TAUSQ
      DIMENSION VEL(108)

C*****  SUBROUTINE BOLTZ CALCULATES THE VELOCITY DISTRIBUTION,ITS MEAN
C*****  & ITS SECOND MOMENT,FOR THE SOLVENT MOLECULES
C*****  VELOCITIES BETWEEN 0 AND 3 (SIMULATION UNITS) ARE
C*****  CONSIDERED;THE INTERVAL IS BROKEN INTO 20 VELOCITY INCREMENTS

      S=FLOAT(N-1)
      DO 1 K=1,20
      LUDWIG(K)=0
 1    CONTINUE
      DO 3 I=2,N
      SUM=0.
      DO 2 J=1,3
      SUM=SUM+V(I,J)*V(I,J)
 2    CONTINUE
      VEL(I)=SQRT(SUM)
      KLASIF=INT(6.666666666*VEL(I))+1
      LUDWIG(KLASIF)=LUDWIG(KLASIF)+1
 3    CONTINUE
      ZUM=0.
      DO 4 K=1,20
      ZUM=ZUM+R(K)*(FLOAT(LUDWIG(K)))
 4    CONTINUE
      VAVG=ZUM/S
      WUM=0.
      DO 5 K=1,20
      VSQ=(R(K)-VAVG)*(R(K)-VAVG)
      WUM=WUM+VSQ*(FLOAT(LUDWIG(K)))
 5    CONTINUE
      DO 6 K=1,20
      DNDV(K)=6.666666666*FLOAT(LUDWIG(K))
 6    CONTINUE
      TAUSQ=WUM/S
      RETURN
      END
```

A4.8 COMPUTER PROGRAM LINALB

```
!UDD!PABLO!LINALB
      IMPLICIT REAL*8(A-H,O-Z)
      COMMON/TRAN/QM(3,3),QUAT(4)
      COMMON/DISTRI/LUDWIG(20),V(108,3),R(20),DNDV(20),VAVG,TAUSQ
      DIMENSION II(2,2),IJ(2,2),ZIJ(4),ZINVIJ(4),ZII(3),ZINVII(3)
      DIMENSION F(6100,3),F1(6100,4),STIJ(4),STII(3)
      DIMENSION E(6100,3),E1(6100,4)
      DIMENSION NATOM(2),ISIT(2,2),ICLAS(2,12)
      DIMENSION EIJ(2,2),EII(2,2),WT(2,2),WR2(3),STSIT(12,3)
      DIMENSION SIGIJ(2,2),SIGII(2,2)
      DIMENSION XI6II(3),UII(3)
      DIMENSION KLAS1(12,3),KLAS(3,3)
      DIMENSION XI6IJ(4),UIJ(4)
      DIMENSION STEP3(2),S(3),X(108,3),XREAL(3),XPREAL(3),ROT(4),XS(350,3)
      DIMENSION PF(350,3),XGHOST(3,3),TOTFOR(108,3),B(3)
      DIMENSION PK(108,3),PPK(3),FPREV(108,3),PPPREV(3)
      DIMENSION OME(108,3),ALFA(4,3),PKPREV(108,3),ORI(108,3)
      DIMENSION BROWN(25,90),XO(25,3)
      DIMENSION BRAV(90),DNDMAX(20)
      DIMENSION OPREV(108,3),SLOC(350,3),ARM(4),ORPREV(108,3)
      DIMENSION OPREV(4),VPREV(108,3),XPREV(108,3)
      DIMENSION RVIR(3),PFVIR(3),CHGSV(2),COULB(3),COULV(3)
      DIMENSION ABENIJ(4),ABENII(3),UCOMP(4)

      OPEN(1,FILE='BUILD')
      OPEN(20,FILE='CONTROL')
      OPEN(25,FILE='ALBMEAN')
      OPEN(86,FILE='NEWT')


C*****  INITIALIZATION & UNIT CONVERSION

C*****  THE FOLLOWING IS A LIST OF MOLECULAR PARAMETERS THAT MUST BE SPECIFIED
C*****  AS WELL AS THE CORRESPONDING UNITS IN EACH CASE

C*****  NATOM(I)  (I=1,2)  # OF DIFFERENT ATOM TYPES IN SOLUTE(1) & SOLVENT(2)
C*****  ISIT(I,J) (I=1,2;J=1,...MAX.OF NATOM(I))  # OF SITES OF TYPE J IN
C*****            MOLECULE I.THIS MUST BE COMPLETED WITH 0'S IN INPUT FILE
C*****            IF NATOM(1) IS DIFFERENT FROM NATOM(2)
C*****  EIJ(I,J)  (I=1,...,NATOM(1);J=1,...,NATOM(2)) ENERGY PARAMETER
C*****            (IN KELVIN) FOR THE INTERACTION BETWEEN TYPE I SITE
C*****            (SOLUTE) AND TYPE J SITE IN  THE SOLVENT.THE ASSIGNMENT OF
C*****            A NUMBER TO EACH SITE TYPE IS DONE BY THE PROGRAM
C*****            BUT THE USER MUST ENTER DATA FOLLOWING A CONSISTENT ORDERING
C*****            THIS MEANS THAT ATOMIC WEIGHTS,POSITION VECTORS,SIZE AND ENER
C*****            GY PARAMETERS MUST BE CONSISTENTLY DECLARED
C*****  EII(I,J)  (I=1,...,NATOM(2);J=1,...,NATOM(2)) ENERGY PARAMETER
C*****            FOR SOLVENT SOLVENT INTERACTIONS
C*****  SIGIJ(I,J)(I=1,...,NATOM(1);J=1,...,NATOM(2))SIZE PARAMETER(A) FOR
C*****            THE INTERACTION BETWEEN SOLUTE AND SOLVENT MOLECULES
C*****  SIGII(I,J)(I=1,...,NATOM(2);J=1,...,NATOM(2))SIZE PARAMETER(A) FOR
C*****            THE INTERACTION BETWEEN SOLVENT MOLECULES
C*****  WT(I,J)   (I=1,2;J=1,...,MAX.OF NATOM(I))ATOMIC WEIGHT OF THE
C*****            Jth SITE OF THE Ith MOLECULE.THIS ARRAY MUST BE COMPLE
C*****            TED WITH 0'S IF NATOM(1) IS DIFFERENT FROM NATOM(2)
C*****  WR2(J)    (J=1,3)Jth PRINCIPAL MOMENT OF INERTIA
C*****            OF THE SOLUTE MOLECULE(IN ATOMIC WEIGHTS*Angstrom**2)
C*****  WR2SV     PRINCIPAL MOMENT OF INERTIA OF THE LINEAR SOLVENT
C*****  STSIT(I,J)(I=1,...,# OF SITES IN SOLUTE;J=1,3)Jth COMPONENT
C*****            OF THE POSITION VECTOR OF THE Ith SITE IN THE SOLUTE MOLE
```

```
C*****            CULE(A),IN A COORDINATE SYSTEM WHOSE AXES ARE THE PRINCIPAL
C*****            AXES OF INERTIA OF THE MOLECULE UNDER CONSIDERATION.THE
C*****            NUMBERING OF THE SITES MUST BE CONSISTENT WITH ALL OF THE
C*****            ABOVE ARRAYS
C*****  ARM(I)    (I=1,...,# OF SOLVENT SITES)LINEAR COORDINATE
C*****            OF THE Ith SOLVENT SITE WRT CENTER OF MASS.SITE NUMBERING
C*****            MUST BE CONSISTENT WITH ALL OF THE ABOVE ARRAYS
C*****  CHGSV(I)  (I=1,...,NATOM(2))CHARGE(IN EFFECTIVE ELECTRONS)
C*****            IN SITE TYPE I(SOLVENT)

C*****  ENTER TEMPERATURE(K),MOLAR VOLUME(M**3/MOL),TIME STEP(S) , CUTOFF
C*****  RADIUS(A), FRACTION OF SIZE PARAMETER BELOW WHICH DEFAULT
C*****  VALUES OF FORCE AND ENERGY ARE SPECIFIED AND VELOCITY SCALING FACTOR

        READ(20,FMT=*)T,VOL,TIME,RCUT,ACCU,VSCALE,ROTSCL

C*****  NGIBBS=#OF DIFFUSION EXPERIMENTS
C*****  IDELTA=#OF STEPS BETWEEN EXPERIMENTS
C*****  INUM=#OF GROUPS OF IDELTAS PER EXPERIMENT
C*****  IBOLTZ=VELOCITY DISTRIBUTION WILL BE CALCULATED EVERY IBOLTZ STEPS
C*****  IBROWN=# OF EINSTEIN POINTS PER EXPERIMENT(EVERY 40
C*****  STEPS
C*****  IDELTA*INUM MUST BE A MULTIPLE OF 40
C*****  POSITIONS OF ALL MOLECULES ARE RECORDED EVERY ISPACE STEPS
C*****  IW IS AN EXPERIMENT COUNTER
C*****  IDEMAS=1 IMPLIES NEUTRAL MOLECULES;ONLY CENTER OF MASS
C*****  COORDINATES ARE TO BE RECORDED FOR RADIAL DISTRIBUTION CALCULATION
C*****  IDEMAS=0 IMPLIES CHARGED MOLECULE;CENTER OF MASS AND ORIENTA-
C*****  TION TO BE STORED

        READ(20,FMT=*)NGIBBS,IDELTA,INUM,IBOLTZ,ISPACE,IDEMAS
        IJOSIA=(NGIBBS+INUM-2)*IDELTA+1
        GIBBS=FLOAT(IDELTA)
        IDEL1=IDELTA+1
        IDEL2=INUM*IDELTA+1
        INUM2=2-INUM
        YALE=FLOAT(NGIBBS)
        IFIN=(NGIBBS+INUM-1)*IDELTA
        IBROWN=(IDELTA*INUM)/40+1
        IW=0

C*****  ENTER # OF UNIT CUBES

        READ(1,FMT=*)NCUB

C*****  CALCULATE # OF MOLECULES

        N=4*(NCUB**3)


C*****  TKT1 IS A CONVERSION FACTOR THAT ALLOWS FOR THE SOLUTE HAVING 3
C*****  ROTATIONAL DEGREES OF FREEDOM

        TKT=FLOAT(N)
        TKT1=1.+(2.*(TKT-1.)+3.)/(3.*TKT)


C*****  ENTER # OF DIFERENT SITE TYPES IN SOLUTE & SOLVENT MOLECULES
```

```
      READ(1,FMT=*)(NATOM(I),I=1,2)

C*****  DETERMINE MAXIMUM

      IKETZ=NATOM(2)-NATOM(1)
      IF(IKETZ.GE.0)GO TO 800
      JMAXI=NATOM(1)
      GO TO 801
 800  JMAXI=NATOM(2)
 801  CONTINUE

C*****  ENTER NUMBER OF SITES OF EACH DIFFERENT KIND,ENERGY AND SIZE PARAMETERS
C*****  AND ATOMIC WEIGHTS

      DO 802 I=1,2
      READ(1,FMT=*)(ISIT(I,J),J=1,JMAXI)
 802  CONTINUE
      DO 803 I=1,NATOM(1)
      READ(1,FMT=*)(SIGIJ(I,J),J=1,NATOM(2))
 803  CONTINUE
      DO 804 I=1,NATOM(1)
      READ(1,FMT=*)(EIJ(I,J),J=1,NATOM(2))
 804  CONTINUE
      DO 891 I=1,NATOM(2)
      READ(1,FMT=*)(SIGII(I,J),J=1,NATOM(2))
 891  CONTINUE
      DO 892 I=1,NATOM(2)
      READ(1,FMT=*)(EII(I,J),J=1,NATOM(2))
 892  CONTINUE
      DO 805 I=1,2
      READ(1,FMT=*)(WT(I,J),J=1,JMAXI)
 805  CONTINUE

C*****  CALCULATE TOTAL SITES IN SOLUTE & SOLVENT MOLECULES

      NSOLUT=0
      DO 900 I=1,NATOM(1)
      NSOLUT=NSOLUT+ISIT(1,I)
 900  CONTINUE
      NSOLVT=0
      DO 901 I=1,NATOM(2)
      NSOLVT=NSOLVT+ISIT(2,I)
 901  CONTINUE

C*****  ENTER PRINCIPAL MOMENTS OF INERTIA OF SOLUTE & SOLVENT

      READ(1,FMT=*)(WR2(J),J=1,3)
      READ(1,FMT=*)WR2SV


C*****  ENTER MOLECULAR GEOMETRY;THIS IS SPECIFIED BY MEANS OF  VECTORS
C*****  FOR THE SOLUTE,AND SCALARS FOR THE SOLVENT,GIVING SITE
C*****  COORDINATES RELATIVE TO THE CENTER OF MASS

      DO 808 I=1,NSOLUT
      READ(1,FMT=*)(STSIT(I,K),K=1,3)
 808  CONTINUE
      READ(1,FMT=*)(ARM(K),K=1,NSOLVT)
      READ(1,FMT=*)(CHGSV(K),K=1,NATOM(2))
```

```
C*****  CALCULATE LENGTH & TIME SCALES
C*****  SLEN IS THE LENGTH SCALE IN M/SLU

        SLEN=1.1841724E- 8*((FLOAT(N)*VOL)**.333333333)

C*****  PMOLST IS THE SOLUTE MOLECULAR WEIGHT
C*****  PMOLSV IS THE SOLVENT MOLECULAR WEIGHT

        PMOLST=0.
        PMOLSV=0.
        DO 809 K=1,JMAXI
        PMOLST=PMOLST+WT(1,K)*FLOAT(ISIT(1,K))
        PMOLSV=PMOLSV+WT(2,K)*FLOAT(ISIT(2,K))
 809    CONTINUE
        ZWTST=PMOLST/24.
        ZWTSV=PMOLSV/24.

C*****  STIM IS THE TIME SCALE IN S/STU

        STIM=SLEN/(157.9341635*SQRT(T/PMOLSV))

C*****  ELEC IS A COULOMBIC CONVERSION FACTOR

        ELEC=(1.1572412E-2)*(STIM**2)/(SLEN**3)

C*****  CONVERT MOLECULAR PARAMETERS TO SIMULATION UNITS

        CONV1=PMOLSV/(36.*T)
        CONV2=1.E10*SLEN
        CONV3=12.E20*(SLEN**2)
        CONV4=PMOLSV/36.
        CONV5=24./(FLOAT(N)*PMOLSV)
        DO 810 I=1,2
        DO 811 J=1,JMAXI
        WT(I,J)=WT(I,J)/12.
 811    CONTINUE
 810    CONTINUE
        DO 816 K=1,3
        WR2(K)=WR2(K)/CONV3
 816    CONTINUE
        WR2SV=WR2SV/CONV3
        DO 812 I=1,NSOLVT
        ARM(I)=ARM(I)/CONV2
 812    CONTINUE
        DO 814 I=1,NSOLUT
        DO 815 J=1,3
        STSIT(I,J)=STSIT(I,J)/CONV2
 815    CONTINUE
 814    CONTINUE
        DO 893 I=1,NATOM(1)
        DO 894 J=1,NATOM(2)
        SIGIJ(I,J)=SIGIJ(I,J)/CONV2
        EIJ(I,J)=EIJ(I,J)*CONV1
 894    CONTINUE
 893    CONTINUE
        DO 895 J=1,NATOM(2)
        DO 896 J=1,NATOM(2)
        SIGII(I,J)=SIGII(I,J)/CONV2
```

```
      EII(I,J)=EII(I,J)*CONV1
 896  CONTINUE
 895  CONTINUE

C***** STEP IS THE TIME STEP IN STU
C***** CLOCK=ACCUMULATED TIME (SIMULATION UNITS)

      STEP=TIME/STIM
      CLOCK=0.

C***** RC IS THE CUTOFF RADIUS IN SLU

      RC=RCUT/CONV2
      RC2=RC**2
      PELEC=ELEC/(RC**3)
      POLEC=ELEC/RC

C***** CREATE AN ARRAY THAT WILL CLASSIFY SITES ACCORDING TO TYPE

      DO 60 I=1,2
      IACCUM=0
      DO 61 J=1,NATOM(I)
      K=ISIT(I,J)
      DO 62 L=1,K
      I1=IACCUM+L
      ICLAS(I,I1)=J
 62   CONTINUE
      IACCUM=IACCUM+K
 61   CONTINUE
 60   CONTINUE

C***** CREATE AN ARRAY THAT WILL IDENTIFY SOLVENT-SOLVENT INTERACTIONS

      KJ=0
      DO 180 I=1,NATOM(2)
      ISUM=0
      DO 181 J=I,NATOM(2)
      II(I,J)=KJ+J+1-I
      IF(I.EQ.J)GO TO 182
      II(J,I)=II(I,J)
 182  CONTINUE
      ISUM=ISUM+1
 181  CONTINUE
      KJ=KJ+ISUM
 180  CONTINUE

C***** CREATE AN ARRAY THAT WILL IDENTIFY SOLVENT-SOLUTE INTERACTIONS

      DO 183 I=1,NATOM(1)
      MUSTAF=(I-1)*NATOM(2)
      DO 184 J=1,NATOM(2)
      IJ(I,J)=J+MUSTAF
 184  CONTINUE
 183  CONTINUE

C***** CREATE ARRAYS THAT WILL IDENTIFY INTERACTION TYPE GIVEN SITE TYPE

      DO 601 I=1,NSOLUT
      L=ICLAS(1,I)
```

```
      DO 602 J=1,NSOLVT
      M=ICLAS(2,J)
      KLAS1(I,J)=IJ(L,M)
602   CONTINUE
601   CONTINUE
      DO 603 I=1,NSOLVT
      L=ICLAS(2,I)
      DO 604 J=1,NSOLVT
      M=ICLAS(2,J)
      KLAS(I,J)=II(L,M)
604   CONTINUE
603   CONTINUE


C*****  CALCULATE FORCE AND ENERGY CONSTANTS.THESE ARE COMBINATIONS OF SIZE
C*****  AND/OR ENERGY PARAMETERS THAT APPEAR IN THE FORCE/ENERGY CALCULATION
C*****  STEPS

      DO 63 I=1,NATOM(1)
      DO 64 J=1,NATOM(2)
      K=IJ(I,J)
      STIJ(K)=(SIGIJ(I,J)/RC)*ACCU
      XI6IJ(K)=(SIGIJ(I,J)/RC)**6
      AUX=(SIGIJ(I,J)/RC)**14
      ZIJ(K)=(24.*EIJ(I,J)/(SIGIJ(I,J)**2))*AUX
      UIJ(K)=4.*EIJ(I,J)*XI6IJ(K)
      ZINVIJ(K)=1./XI6IJ(K)
      WELLLJ=1./(2.*XI6IJ(K))
      UNG=WELLLJ**.1666
      DO 999 MU=1,150
      WELL1=(UNG**13)-1.
      WELL2=(UNG**7)-1.
      WELL6=UNG**6
      WELL12=UNG**12
      SODRE=WELL1*WELL2-WELLLJ*(WELL2**2)
      SADRE=13.*WELL12*WELL2-7.*WELL6*WELL1
      UNGNEW=UNG-SODRE/SADRE
      WALL1=(UNGNEW**13)-1.
      WALL2=(UNGNEW**7)-1.
      WALL3=WALL1/WALL2-WELLLJ
      IF(ABS(WALL3).LE.1.E-8)GO TO 998
      UNG=UNGNEW
999   CONTINUE
      WRITE(86,997)
997   FORMAT(1X,'NEWTON MISBEHAVING')
      GO TO 996
998   UNG6=(UNGNEW**6)-1.
      UNG12=(UNGNEW**12)-1.
      UNGINV=(1./UNGNEW)-1.
      DEPTH=(6.*UNGINV*(2.*XI6IJ(K)-1.)+XI6IJ(K)*UNG12-UNG6)*UIJ(K)
      ABENIJ(K)=ABS(DEPTH)
64    CONTINUE
63    CONTINUE
      DO 65 I=1,NATOM(2)
      DO 66 J=I,NATOM(2)
      KIND=II(I,J)
      STII(KIND)=(SIGII(I,J)/RC)*ACCU
      XI6II(KIND)=(SIGII(I,J)/RC)**6
      UII(KIND)=4.*EII(I,J)*XI6II(KIND)
```

```
        AUX=(SIGII(I,J)/RC)**14
        ZII(KIND)=(24.*EII(I,J)/(SIGII(I,J)**2))*AUX
        ZINVII(KIND)=1./XI6II(KIND)
        WELLLJ=1./(2.*XI6II(KIND))
        UNG=WELLLJ**.166
        DO 474 MU=1,150
        WELL1=(UNG**13)-1.
        WELL2=(UNG**7)-1.
        WELL6=UNG**6
        WELL12=UNG**12
        SODRE=WELL1*WELL2-WELLLJ*(WELL2**2)
        SADRE=13.*WELL12*WELL2-7.*WELL6*WELL1
        UNGNEW=UNG-SODRE/SADRE
        WALL1=(UNGNEW**13)-1.
        WALL2=(UNGNEW**7)-1.
        WALL3=WALL1/WALL2-WELLLJ
        IF(ABS(WALL3).LE.1.E-8)GO TO 472
        UNG=UNGNEW
 474    CONTINUE
        WRITE(86,997)
        GO TO 996
 472    UNG6=(UNGNEW**6)-1.
        UNG12=(UNGNEW**12)-1.
        UNGINV=(1./UNGNEW)-1.
        DEPTH=UII(KIND)*(6.*UNGINV*(2.*XI6II(KIND)-1.)+XI6II(KIND)*UNG12-UNG6)
        ABENII(KIND)=ABS(DEPTH)
        COULB(KIND)=PELEC*CHGSV(I)*CHGSV(J)
        COULV(KIND)=POLEC*CHGSV(I)*CHGSV(J)
 66     CONTINUE
 65     CONTINUE

C*****  CALCULATE FORCE TABLES FOR EACH POSSIBLE TYPE OF INTERACTION
        DO 186 I=1,NATOM(2)
        DO 187 J=I,NATOM(2)
        KIND=II(I,J)
        LOW=INT(STII(KIND)*6000.)
        UN=1./STII(KIND)
        UN14=UN**14
        UN8=UN**8
        UN6=UN**6
        UN3=UN**3
        H1=2.*XI6II(KIND)-1.
        H2=(UN6+1.)*XI6II(KIND)-1.
        IF(COULV(KIND).GT.0.)GO TO 995
        UCOMP(KIND)=ABS(COULV(KIND))*(UN-1.)
        GO TO 994
 995    UCOMP(KIND)=0.
 994    CONTINUE
        ALDO=COULV(KIND)*(UN-1.)
        POTA=UCOMP(KIND)+ABENII(KIND)
        DEFT=(6.*(1./UN-1.)*H1-UN6*(1./UN6-1.)*H2)*UII(KIND)+ALDO+POTA
        DEFLT=(2.*(UN14-UN)-(UN8-UN)*ZINVII(KIND))*ZII(KIND)+COULB(KIND)*UN3
        DO 188 MB=1,LOW
        F(MB,KIND)=DEFLT
        E(MB,KIND)=DEFT
 188    CONTINUE
        DEL=1./6000.
        BEGIN=FLOAT(LOW)/6000.
        IFALTA=5999-LOW
```

```
      DO 189 MB=1,IFALTA
      K=LOW+MB
      UN=1./(BEGIN+DEL*FLOAT(MB))
      UN14=UN**14
      UN8=UN**8
      UN6=UN**6
      UN3=UN**3
      H2=(UN6+1.)*XI6II(KIND)-1.
      ALDA=COULV(KIND)*(UN-1.)
      F(K,KIND)=(2.*(UN14-UN)-(UN8-UN)*ZINVII(KIND))*ZII(KIND)+COULB(KIND)*UN3
      E(K,KIND)=(6.*(1./UN-1.)*H1-UN6*(1./UN6-1.)*H2)*UII(KIND)+ALDA+POTA
189   CONTINUE
      F(6000,KIND)=0.
      E(6000,KIND)=POTA
187   CONTINUE
186   CONTINUE
      DO 389 I=1,NATOM(1)
      DO 390 J=1,NATOM(2)
      KIND=IJ(I,J)
      LOW=INT(STIJ(KIND)*6000.)
      UN=1./STIJ(KIND)
      UN14=UN**14
      UN8=UN**8
      UN6=UN**6
      H1=2.*XI6IJ(KIND)-1.
      H2=(UN6+1.)*XI6IJ(KIND)-1.
      DEFT=(6.*(1./UN-1.)*H1-UN6*(1./UN6-1.)*H2)*UIJ(KIND)+ABENIJ(KIND)
      DEFLT=(2.*(UN14-UN)-(UN8-UN)*ZINVIJ(KIND))*ZIJ(KIND)
      DO 392 MB=1,LOW
      F1(MB,KIND)=DEFLT
      E1(MB,KIND)=DEFT
392   CONTINUE
      DEL=1./6000.
      BEGIN=FLOAT(LOW)/6000.
      IFALTA=5999-LOW
      DO 393 MB=1,IFALTA
      K=LOW+MB
      UN=1./(BEGIN+DEL*FLOAT(MB))
      UN14=UN**14
      UN8=UN**8
      UN6=UN**6
      H2=(UN6+1.)*XI6IJ(KIND)-1.
      F1(K,KIND)=(2.*(UN14-UN)-(UN8-UN)*ZINVIJ(KIND))*ZIJ(KIND)
      E1(K,KIND)=(6.*(1./UN-1.)*H1-UN6*(1./UN6-1.)*H2)*UIJ(KIND)+ABENIJ(KIND)
393   CONTINUE
      F1(6000,KIND)=0.
      E1(6000,KIND)=ABENIJ(KIND)
390   CONTINUE
389   CONTINUE
      CONST=RC/6000.

C*****  CALCULATE STEP-RELATED CONSTANTS

      DO 260 I=1,2
      IF(I.EQ.1)GO TO 261
      ZWT=PMOLSV/12.
      GO TO 262
261   ZWT=PMOLST/12.
262   CONTINUE
```

390

```
      STEP3(I)=STEP/(2.*ZWT)
 260  CONTINUE
      DO 264 IAX=1,3
      S(IAX)=STEP/(2.*WR2(IAX))
 264  CONTINUE
      SSVT=STEP/(2.*WR2SV)
      STEP2=STEP/2.
      STEP4=STEP/4.
      NSITES=NSOLUT+(N-1)*NSOLVT

C***** R IS AN ARRAY CONTAINING THE VALUES OF THE VELOCITIES(IN SIM.UNITS)
C***** AT THE MID-POINT OF THE Kth INTERVAL OF THE VEL. RANGE
C***** A MAXIMUM VELOCITY OF 3 IS CONSIDERED
C***** DNDMAX IS AN ARRAY WHOSE ELEMENTS GIVE THE DISCRETIZED M-B
C***** DISTRIBUTION

      DO 499 K=1,20
      VV=FLOAT(K)-1.
      R(K)=(2.*VV+1.)*.075
      AMB=R(K)**2
      DNDMAX(K)=(11.72646*AMB*FLOAT(N-1))/EXP(3.*AMB)
 499  CONTINUE

      OPEN(27,FILE='READY')
      DO 817 KZU=1,N
      READ(27,FMT=*)(XPREV(KZU,J),J=1,3)
      READ(27,FMT=*)(VPREV(KZU,J),J=1,3)
      READ(27,FMT=*)(OPREV(KZU,J),J=1,3)
 817  CONTINUE
      DO 836 KZO=2,N
      READ(27,FMT=*)(ORPREV(KZO,J),J=1,3)
 836  CONTINUE
      READ(27,FMT=*)(QPREV(L),L=1,4)
      DO 616 JK=1,4
      QUAT(JK)=QPREV(JK)
 616  CONTINUE
      DO 617 JZ=2,N
      IIU=NSOLUT+(JZ-2)*NSOLVT
      DO 837 JK=1,NSOLVT
      KJ=IIU+JK
      DO 301 JL=1,3
      SLOC(KJ,JL)=ARM(JK)*ORPREV(JZ,JL)
 301  CONTINUE
 837  CONTINUE
 617  CONTINUE
      DO 302 JZ=1,N
      DO 303 IAX=1,3
      X(JZ,IAX)=XPREV(JZ,IAX)
 303  CONTINUE
 302  CONTINUE
      READ(27,FMT=*)IMOVE
      READ(27,FMT=*)CLOCK
      IF(IMOVE.NE.0)GO TO 305
      OPEN(22,FILE='DISTRIB')
      DO 378 I=1,20
      WRITE(22,550)R(I),DNDMAX(I)
 378  CONTINUE
      CLOSE(22)
      OPEN(31,FILE='INSPACE')
```

```
      WRITE(31,879)IMOVE
      CLOSE(31)
      DO 304 IAX=1,3
      XPREAL(IAX)=XPREV(1,IAX)
304   CONTINUE
      OPEN(21,FILE='ENERGY')
      WRITE(21,502)
      CLOSE(21)
502   FORMAT(1X,4X,'TIME',5X,'TOT.ENERG.',2X,'2KE(r)/3NkT',1X,'2KE(t)/3NkT',
     K  4X,'r/t',10X,'T',11X,'Z',6X,'INST.COMPR.',1X,'1st MOM.DEV.',1X,'2nd
     k  MOM.DEV.',///)
      DO 306 I=1,N
      DO 307 IAX=1,3
      VPREV(I,IAX)=VSCALE*VPREV(I,IAX)
      OPREV(I,IAX)=ROTSCL*OPREV(I,IAX)
307   CONTINUE
306   CONTINUE
      DNUM=0.
      DENOM=0.
      CLOSE(27)
      GO TO 362
305   CONTINUE
      READ(27,FMT=*)(XPREAL(IAX),IAX=1,3)
      READ(27,FMT=*)ETPREV,SCPREV
      READ(27,FMT=*)DNUM,DENOM
      CLOSE(27)
      OPEN(21,FILE='ENERGY',POSITION='END')
      WRITE(21,879)IMOVE
      CLOSE(21)
      OPEN(28,FILE='EXPERI')
      DO 360 K=1,NGIBBS
      READ(28,356)(XO(K,IAX),IAX=1,3)
      DO 361 J=1,IBROWN
      READ(28,355)BROWN(K,J)
361   CONTINUE
360   CONTINUE
      CLOSE(28)
      OPEN(31,FILE='INSPACE',POSITION='END')
      WRITE(31,879)IMOVE
      CLOSE(31)
      OPEN(22,FILE='DISTRIB',POSITION='END')
      WRITE(22,879)IMOVE
879   FORMAT(1X,'CRASH]RESTART @ STEP #  ',I4,///)
      CLOSE(22)
362   CONTINUE

      ISTART=1
      ICORR=1
      GO TO 75
835   ISTART=0

C*****  PREDICTOR SECTION
      ROT(1)=QPREV(2)*OPREV(1,1)+QPREV(3)*OPREV(1,2)-QPREV(4)*OPREV(1,3)
      ROT(2)=QPREV(1)*OPREV(1,1)-QPREV(4)*OPREV(1,2)-QPREV(3)*OPREV
     K  (1,3)
      ROT(3)=-QPREV(4)*OPREV(1,1)-QPREV(1)*OPREV(1,2)+QPREV(2)*OPREV(1,3)
      ROT(4)=QPREV(3)*OPREV(1,1)+QPREV(2)*OPREV(1,2)+QPREV(1)*OPREV(1,
     K  3)
      DO 618 IAX=1,4
```

```
      QUAT(IAX)=QPREV(IAX)+STEP2*ROT(IAX)
 618  CONTINUE
      QTSUM=0.
      DO 436 ISUM=1,4
      QTSUM=QTSUM+QUAT(ISUM)*QUAT(ISUM)
 436  CONTINUE
      ASUM=SQRT(QTSUM)
      DO 437 ISUM=1,4
      QUAT(ISUM)=QUAT(ISUM)/ASUM
 437  CONTINUE
      DO 26 I=1,N
      DO 27 IAX=1,3
      X(I,IAX)=XPREV(I,IAX)+STEP*VPREV(I,IAX)
      IF(X(I,IAX).GT.1.)GO TO 28
      IF(X(I,IAX).LT.0.)GO TO 29
      GO TO 30
 28   X(I,IAX)=X(I,IAX)-1.
      GO TO 30
 29   X(I,IAX)=X(I,IAX)+1.
 30   CONTINUE
 27   CONTINUE
 26   CONTINUE
      DO 379 I=2,N
      ORI(I,1)=ORPREV(I,1)+STEP*(OPREV(I,2)*ORPREV(I,3)-OPREV(I,3)*
     K ORPREV(I,2))
      ORI(I,2)=ORPREV(I,2)+STEP*(OPREV(I,3)*ORPREV(I,1)-OPREV(I,1)*ORPREV
     K (I,3))
      ORI(I,3)=ORPREV(I,3)+STEP*(OPREV(I,1)*ORPREV(I,2)-OPREV(I,2)*
     K ORPREV(I,1))
      RNORM=0.
      DO 626 KU=1,3
      RNORM=RNORM+ORI(I,KU)*ORI(I,KU)
 626  CONTINUE
      RNOR=1./SQRT(RNORM)
      DO 627 KU=1,3
      ORI(I,KU)=ORI(I,KU)*RNOR
 627  CONTINUE
      ISTOR=NSOLUT+(I-2)*NSOLVT
      DO 819 J=1,NSOLVT
      MU=ISTOR+J
      DO 666 IAX=1,3
      SLOC(MU,IAX)=ARM(J)*ORI(I,IAX)
 666  CONTINUE
 819  CONTINUE
 379  CONTINUE
      ICORR=0
 75   CONTINUE

C*****  CALCULATE SITE POSITIONS IN INERTIAL REFERENCE FRAME

      CALL Q
      DO 90 L=1,NSOLUT
      DO 91 IAX=1,3
      Z=0.
      DO 92 LL=1,3
      Z=Z+QM(LL,IAX)*STSIT(L,LL)
 92   CONTINUE
      XS(L,IAX)=Z+X(1,IAX)
 91   CONTINUE
```

```
 90     CONTINUE
        DO 93 J=2,N
        JSTOR=NSOLUT+(J-2)*NSOLVT
        DO 10 K=1,NSOLVT
        MU=JSTOR+K
        DO 9 IAX=1,3
        XS(MU,IAX)=SLOC(MU,IAX)+X(J,IAX)
 9      CONTINUE
 10     CONTINUE
 93     CONTINUE

C*****  SET FORCES TO ZERO

        DO 80 NST=1,NSITES
        DO 81 IAX=1,3
        PF(NST,IAX)=0.
 81     CONTINUE
 80     CONTINUE

C*****  ITERATE OVER ALL POSSIBLE PAIRS OF MOLECULES

C*****  SET POTENTIAL ENERGY TO ZERO

        SCALAR=0.
        ENE=0.
        DO 401 J=2,N
        JSTOR=NSOLUT+(J-2)*NSOLVT
        DO 402 IAX=1,3
        DEL=X(J,IAX)-X(1,IAX)
        IF(ABS(DEL).LE.0.5)GO TO 406
        IF(DEL.GT.0.)GO TO 407
        RVIR(IAX)=DEL+1.
        DO 463 K=1,NSOLVT
        KIN=JSTOR+K
        XGHOST(K,IAX)=XS(KIN,IAX)+1.
 463    CONTINUE
        GO TO 408
 407    CONTINUE
        RVIR(IAX)=DEL-1.
        DO 464 K=1,NSOLVT
        KIN=JSTOR+K
        XGHOST(K,IAX)=XS(KIN,IAX)-1.
 464    CONTINUE
        GO TO 408
 406    CONTINUE
        RVIR(IAX)=DEL
        DO 494 K=1,NSOLVT
        KIN=JSTOR+K
        XGHOST(K,IAX)=XS(KIN,IAX)
 494    CONTINUE
 408    CONTINUE
        PFVIR(IAX)=0.
 402    CONTINUE
        DO 411 L=1,NSOLUT
        DO 412 K=1,NSOLVT
        KIN=JSTOR+K
        KIND=KLAS1(L,K)
        DIST=0.
        DO 413 IAX=1,3
```

```
      TROL=XS(L,IAX)-XGHOST(K,IAX)
      IF(ABS(TROL).GT.RC)GO TO 414
      DIST=DIST+TROL*TROL
413   CONTINUE
      IF(DIST.GT.RC2)GO TO 414
      SEPN=SQRT(DIST)
      MN=INT(SEPN/CONST)
      FCE=F1(MN,KIND)
      ENE=ENE+E1(MN,KIND)
      DO 410 IAX=1,3
      ADD=FCE*(XS(L,IAX)-XGHOST(K,IAX))
      PF(L,IAX)=PF(L,IAX)+ADD
      PF(KIN,IAX)=PF(KIN,IAX)-ADD
      PFVIR(IAX)=PFVIR(IAX)-ADD
410   CONTINUE
414   CONTINUE
412   CONTINUE
411   CONTINUE
      IF(ICORR.EQ.0)GO TO 510
      DO 512 IAX=1,3
      SCALAR=SCALAR+PFVIR(IAX)*RVIR(IAX)
512   CONTINUE
510   CONTINUE
401   CONTINUE
      DO 1 I=2,N-1

C*****  NUMBER OF SITES PER MOLECULE CAN BE EITHER NSOLUT OR NSOLVT

      ISTOR=NSOLUT+(I-2)*NSOLVT
      DO 4 J=I+1,N
      JSTOR=NSOLUT+(J-2)*NSOLVT

C*****  SEARCH FOR NEAREST J

      DO 5 IAX=1,3
      DEL=X(J,IAX)-X(I,IAX)
      IF(ABS(DEL).LE.0.5)GO TO 6
      IF(DEL.GT.0.)GO TO 7
      RVIR(IAX)=DEL+1.
      DO 773 K=1,NSOLVT
      KIN=JSTOR+K
      XGHOST(K,IAX)=XS(KIN,IAX)+1.
773   CONTINUE
      GO TO 8
7     CONTINUE
      RVIR(IAX)=DEL-1.
      DO 94 K=1,NSOLVT
      KIN=JSTOR+K
      XGHOST(K,IAX)=XS(KIN,IAX)-1.
94    CONTINUE
      GO TO 8
6     CONTINUE
      RVIR(IAX)=DEL
      DO 95 K=1,NSOLVT
      KIN=JSTOR+K
      XGHOST(K,IAX)=XS(KIN,IAX)
95    CONTINUE
8     CONTINUE
      PFVIR(IAX)=0.
```

```
 5      CONTINUE

C*****  CALCULATE DISTANCE BETWEEN ALL POSSIBLE I-J SITE PAIRS

        DO 11 L=1,NSOLVT
        LII=ISTOR+L
        DO 12 K=1,NSOLVT
        KII=JSTOR+K
        KIND=KLAS(L,K)
        DIST=0.
        DO 13 IAX=1,3
        TROL=XS(LII,IAX)-XGHOST(K,IAX)
        IF(ABS(TROL).GT.RC)GO TO 14
        DIST=DIST+TROL*TROL
 13     CONTINUE
        IF(DIST.GT.RC2)GO TO 14
        SEPN=SQRT(DIST)
        MN=INT(SEPN/CONST)
        FCE=F(MN,KIND)
        ENE=ENE+E(MN,KIND)
        DO 18 IAX=1,3
        ADD=FCE*(XS(LII,IAX)-XGHOST(K,IAX))
        PF(LII,IAX)=PF(LII,IAX)+ADD
        PF(KII,IAX)=PF(KII,IAX)-ADD
        PFVIR(IAX)=PFVIR(IAX)-ADD
 18     CONTINUE
 14     CONTINUE
 12     CONTINUE
 11     CONTINUE
        IF(ICORR.EQ.0)GO TO 511
        DO 899 IAX=1,3
        SCALAR=SCALAR+PFVIR(IAX)*RVIR(IAX)
 899    CONTINUE
 511    CONTINUE
  4     CONTINUE
  1     CONTINUE

C*****  CALCULATE TOTAL FORCE ON EACH MOLECULE

        DO 70 I=1,N
        IF(I.NE.1)GO TO 71
        ISTOR=0
        ISITI=NSOLUT
        GO TO 72
 71     ISITI=NSOLVT
        ISTOR=(I-2)*NSOLVT+NSOLUT
 72     CONTINUE
        DO 73 IAX=1,3
        TOTFOR(I,IAX)=0.
        DO 74 K=1,ISITI
        MU=ISTOR+K
        TOTFOR(I,IAX)=TOTFOR(I,IAX)+PF(MU,IAX)
 74     CONTINUE
 73     CONTINUE
 70     CONTINUE

C*****  TORQUE CALCULATION IN INERTIAL COORDINATES
C*****  SOLUTE
C*****  SET TORQUES TO ZERO
```

```
      DO 300 IAX=1,3
      PK(1,IAX)=0.
300   CONTINUE
      DO 22 J=1,NSOLUT
      DO 23 IAX=1,3
      B(IAX)=XS(J,IAX)-X(1,IAX)
      IF(ABS(B(IAX)).LT.1.E-15)B(IAX)=0.
23    CONTINUE
      PK(1,1)=PK(1,1)+B(2)*PF(J,3)-B(3)*PF(J,2)
      PK(1,2)=PK(1,2)+B(3)*PF(J,1)-B(1)*PF(J,3)
      PK(1,3)=PK(1,3)+B(1)*PF(J,2)-B(2)*PF(J,1)
22    CONTINUE

C*****  CONVERT TO PRINCIPAL TORQUES

      DO 24 K=1,3
      PPK(K)=0.
      DO 25 L=1,3
      PPK(K)=PPK(K)+QM(K,L)*PK(1,L)
25    CONTINUE
24    CONTINUE

C*****  SOLVENT TORQUE CALCULATION

      DO 19 I=2,N
      DO 20 IAX=1,3
      PK(I,IAX)=0.
20    CONTINUE
      ISTOR=NSOLUT+(I-2)*NSOLVT
      DO 21 J=1,NSOLVT
      K=ISTOR+J
      PK(I,1)=PK(I,1)+SLOC(K,2)*PF(K,3)-SLOC(K,3)*PF(K,2)
      PK(I,2)=PK(I,2)+SLOC(K,3)*PF(K,1)-SLOC(K,1)*PF(K,3)
      PK(I,3)=PK(I,3)+SLOC(K,1)*PF(K,2)-SLOC(K,2)*PF(K,1)
21    CONTINUE
      FORBID=PK(I,1)*ORI(I,1)+PK(I,2)*ORI(I,2)+PK(I,3)*ORI(I,3)
      PK(I,1)=PK(I,1)-FORBID*ORI(I,1)
      PK(I,2)=PK(I,2)-FORBID*ORI(I,2)
      PK(I,3)=PK(I,3)-FORBID*ORI(I,3)
19    CONTINUE
      IF(ICORR.EQ.0)GO TO 77
      DO 79 IAX=1,3
      FPREV(1,IAX)=TOTFOR(1,IAX)
      PPPREV(IAX)=PPK(IAX)
79    CONTINUE
      DO 78 I=2,N
      DO 778 IAX=1,3
      FPREV(I,IAX)=TOTFOR(I,IAX)
      PKPREV(I,IAX)=PK(I,IAX)
778   CONTINUE
 78   CONTINUE
      GO TO 76
77    CONTINUE

C*****  CORRECTOR SECTION

      DO 340 IAX=1,3
      V(1,IAX)=VPREV(1,IAX)+STEP3(1)*(TOTFOR(1,IAX)+FPREV(1,IAX))
```

```
      X(1,IAX)=XPREV(1,IAX)+STEP2*(V(1,IAX)+VPREV(1,IAX))
      XREAL(IAX)=XPREAL(IAX)+STEP2*(V(1,IAX)+VPREV(1,IAX))
      IF(X(1,IAX).GT.1.)GO TO 344
      IF(X(1,IAX).LT.0.)GO TO 345
      GO TO 346
344   X(1,IAX)=X(1,IAX)-1.
      GO TO 346
345   X(1,IAX)=X(1,IAX)+1.
346   CONTINUE
      VPREV(1,IAX)=V(1,IAX)
      XPREV(1,IAX)=X(1,IAX)
      XPREAL(IAX)=XREAL(IAX)
340   CONTINUE
      DO 32 I=2,N
      DO 33 IAX=1,3
      V(I,IAX)=VPREV(I,IAX)+STEP3(2)*(TOTFOR(I,IAX)+FPREV(I,IAX))
      X(I,IAX)=XPREV(I,IAX)+STEP2*(V(I,IAX)+VPREV(I,IAX))
      IF(X(I,IAX).GT.1.)GO TO 34
      IF(X(I,IAX).LT.0.)GO TO 35
      GO TO 36
34    X(I,IAX)=X(I,IAX)-1.
      GO TO 36
35    X(I,IAX)=X(I,IAX)+1.
36    CONTINUE
      VPREV(I,IAX)=V(I,IAX)
      XPREV(I,IAX)=X(I,IAX)
33    CONTINUE
32    CONTINUE
      DO 768 IAX=1,3
      OME(1,IAX)=OPREV(1,IAX)+S(IAX)*(PPK(IAX)+PPPREV(IAX))
768   CONTINUE
      DO 794 IAX=1,3
      DO 131 K=1,4
      ALFA(K,IAX)=QUAT(K)*OME(1,IAX)+QPREV(K)*OPREV(1,IAX)
131   CONTINUE
794   CONTINUE
      QUAT(1)=QPREV(1)+STEP4*(-ALFA(2,1)+ALFA(3,2)-ALFA(4,3))
      QUAT(2)=QPREV(2)+STEP4*(ALFA(1,1)-ALFA(4,2)-ALFA(3,3))
      QUAT(3)=QPREV(3)+STEP4*(-ALFA(4,1)-ALFA(1,2)+ALFA(2,3))
      QUAT(4)=QPREV(4)+STEP4*(ALFA(3,1)+ALFA(2,2)+ALFA(1,3))

C*****  RENORMALIZE QUATERNIONS

      QSUM=0.
      DO 433 ISUM=1,4
      QSUM=QSUM+QUAT(ISUM)*QUAT(ISUM)
433   CONTINUE
      ASUM=SQRT(QSUM)
      DO 434 ISUM=1,4
      QUAT(ISUM)=QUAT(ISUM)/ASUM
      QPREV(ISUM)=QUAT(ISUM)
434   CONTINUE

      DO 797 I=2,N
      ISTOR=NSOLUT+(I-2)*NSOLVT
      DO 799 IAX=1,3
      OME(I,IAX)=OPREV(I,IAX)+SSVT*(PK(I,IAX)+PKPREV(I,IAX))
799   CONTINUE
      AUX1=STEP2*OME(I,3)
```

```
      AUX2=-STEP2*OME(I,2)
      AUX4=-STEP2*OME(I,3)
      AUX5=STEP2*OME(I,1)
      AUX7=STEP2*OME(I,2)
      AUX8=-STEP2*OME(I,1)
      AUX0=(1.-AUX5*AUX8)-AUX1*(AUX4-AUX5*AUX7)+AUX2*(AUX4*AUX8-AUX7)
      AUX3=(ORPREV(I,1)+STEP2*(OPREV(I,2)*ORPREV(I,3)-OPREV(I,3)*
     K ORPREV(I,2)))
      AUX6=(ORPREV(I,2)+STEP2*(OPREV(I,3)*ORPREV(I,1)-OPREV(I,1)*ORPREV(I
     K ,3)))
      AUX9=(ORPREV(I,3)+STEP2*(OPREV(I,1)*ORPREV(I,2)-OPREV(I,2)*ORPREV
     K (I,1)))
      AUX10=AUX3*(1.-AUX5*AUX8)-AUX1*(AUX6-AUX5*AUX9)+AUX2*(AUX6*AUX8-AUX9)
      AUX11=(AUX6-AUX5*AUX9)-AUX3*(AUX4-AUX5*AUX7)+AUX2*(AUX4*AUX9-AUX6*
     K AUX7)
      AUX12=(AUX9-AUX6*AUX8)-AUX1*(AUX4*AUX9-AUX6*AUX7)+AUX3*(AUX4*AUX8-
     K AUX7)
      ORI(I,1)=AUX10/AUX0
      ORI(I,2)=AUX11/AUX0
      ORI(I,3)=AUX12/AUX0
      RNO=0.
      DO 628 KO=1,3
      RNO=RNO+ORI(I,KO)*ORI(I,KO)
 628  CONTINUE
      RNU=1./SQRT(RNO)
      DO 629 KO=1,3
      ORI(I,KO)=ORI(I,KO)*RNU
 629  CONTINUE
      DO 465 J=1,NSOLVT
      MU=ISTOR+J
      DO 549 IAX=1,3
      SLOC(MU,IAX)=ORI(I,IAX)*ARM(J)
 549  CONTINUE
 465  CONTINUE
      ORPREV(I,1)=ORI(I,1)
      ORPREV(I,2)=ORI(I,2)
      ORPREV(I,3)=ORI(I,3)
 797  CONTINUE
      DO 468 I=1,N
      DO 132 IAX=1,3
      OPREV(I,IAX)=OME(I,IAX)
 132  CONTINUE
 468  CONTINUE

C***** CALCULATE TORQUE & FORCE WITH CORRECTED COORDINATES

      ICORR=1
      GO TO 75
  76  CONTINUE
      IF(ISTART.EQ.1)GO TO 835

C***** MOLECULE MOVING SECTION ENDS

      CLOCK=CLOCK+STEP
      IMOVE=IMOVE+1
      IENERG=(IMOVE/10)*10
      IVELOC=(IMOVE/IBOLTZ)*IBOLTZ
      KSPACE=(IMOVE/ISPACE)*ISPACE
      ETRAN=0.
```

```
      VSQRE=0.
      DO 826 IAX=1,3
      VSQRE=VSQRE+V(1,IAX)*V(1,IAX)
826   CONTINUE
      ETRAN=ETRAN+VSQRE*ZWTST
      DO 827 I=2,N
      VSQRE=0.
      DO 828 IAX=1,3
      VSQRE=VSQRE+V(I,IAX)*V(I,IAX)
828   CONTINUE
      ETRAN=ETRAN+VSQRE*ZWTSV
827   CONTINUE
      IF(IMOVE.EQ.1)GO TO 529
      DENOM=DENOM+(ETPREV+ETRAN)*STEP2
      DNUM=DNUM+(SCPREV+SCALAR)*STEP2
      ZNOW=1.+SCALAR/(2.*ETRAN)
      COMPR=1.+DNUM/(2.*DENOM)
529   ETPREV=ETRAN
      SCPREV=SCALAR
      IF(IENERG.NE.IMOVE)GO TO 500

C*****  EROT=ROTATIONAL KINETIC ENERGY(SEU)

      EROT=0.
      DO 526 IAX=1,3
      EROT=EROT+WR2(IAX)*OME(1,IAX)*OME(1,IAX)
526   CONTINUE
      DO 527 I=2,N
      DO 528 IAX=1,3
      EROT=EROT+WR2SV*OME(I,IAX)*OME(I,IAX)
528   CONTINUE
527   CONTINUE
      EROT=EROT/2.
      ETOT=ENE+EROT+ETRAN
      TROT=CONV5*EROT
      TTRAN=CONV5*ETRAN
      EQPART=TROT/TTRAN
      THERM=((TROT+TTRAN)/TKT1)*T
      CALL BOLTZ(N)
      DELV=108.5401882*ABS(VAVG-.921317732)
      DEL2V=661.4909979*ABS(TAUSQ-.151173637)
      OPEN(21,FILE='ENERGY',POSITION='END')
      WRITE(21,501)CLOCK,ETOT,TROT,TTRAN,EQPART,THERM,COMPR,ZNOW,DELV,DEL2V
      CLOSE(21)
501   FORMAT(1X,1X,G11.4,1X,G11.4,1X,G11.4,1X,G11.4,1X,G11.4,1X,G11.4,1X,G11
     K  .4,1X,G11.4,1X,G11.4,1X,G11.4)
500   IX=IMOVE-1
      YX=FLOAT(IX)
      IY=IX/IDELTA
      IZ=IY*IDELTA
      IP=(IX/40)*40
      IF(IW.EQ.NOIBBS) GO TO 690
      IF(IZ.NE.IX)GO TO 670
      J2=-1
      IW=IY+1
      BROWN(IW,1)=0.
      DO 671 I=1,3
      XO(IW,I)=XREAL(I)
671   CONTINUE
```

400

```
      GO TO 676
690   IF(IZ.NE.IX)GO TO 670
      J2=-1
      GO TO 676
670   IF(IP.NE.IX)GO TO 350
      J2=0
676   CONTINUE
      IF(IMOVE.GE.IDEL1)GO TO 672
      JMIN=1
      JMAX=1
      GO TO 673
672   IF(IMOVE.GT.IDEL2)GO TO 675
      JMIN=1
      JMAX=INT(YX/GIBBS)+1
      GO TO 673
675   IF(IMOVE.LE.IJOSIA)GO TO 677
      JMIN=NGIBBS
      JMAX=NGIBBS
      GO TO 673
677   JMIN=INT(YX/GIBBS)+INUM2+J2
      JMAX=NGIBBS
673   CONTINUE
      DO 351 JEXP=JMIN,JMAX
      IJXP=(IX-(JEXP-1)*IDELTA)/40+1
      IF(IJXP.EQ.1)GO TO 353
      SUMD=0.
      DO 352 IAX=1,3
      AQ=XREAL(IAX)-XO(JEXP,IAX)
      SUMD=SUMD+AQ*AQ
352   CONTINUE
      BROWN(JEXP,IJXP)=SUMD
353   CONTINUE
351   CONTINUE
350   CONTINUE
      IF(IMOVE.GT.IFIN)GO TO 590
      ISAVE=(IX/50)*50
      IF(ISAVE.NE.IX)GO TO 308
      OPEN(27,FILE='READY')
      DO 320 KZU=1,N
      WRITE(27,FMT=*)(X(KZU,J),J=1,3)
      WRITE(27,FMT=*)(V(KZU,J),J=1,3)
      WRITE(27,FMT=*)(OME(KZU,J),J=1,3)
320   CONTINUE
      DO 321 KZO=2,N
      WRITE(27,FMT=*)(ORI(KZO,J),J=1,3)
321   CONTINUE
      WRITE(27,FMT=*)(QUAT(L),L=1,4)
      WRITE(27,FMT=*)IMOVE
      WRITE(27,FMT=*)CLOCK
      WRITE(27,FMT=*)(XREAL(IAX),IAX=1,3)
      WRITE(27,FMT=*)ETPREV,SCPREV
      WRITE(27,FMT=*)DNUM,DENOM
      CLOSE(27)
      OPEN(28,FILE='EXPERI')
      DO 354 K=1,NGIBBS
      WRITE(28,356)(XO(K,IAX),IAX=1,3)
      DO 357 J=1,IBROWN
      WRITE(28,355)BROWN(K,J)
357   CONTINUE
```

```
$UDD:[PABLO]LINALP
 354    CONTINUE
        CLOSE(28)
 308    CONTINUE
 355    FORMAT(1X,G14.7)
 356    FORMAT(1X,G14.7,1X,G14.7,1X,G14.7)
        IF(KSPACE.NE.IMOVE)GO TO 599
        IF(IDEMAS.EQ.1)GO TO 314
        CALL Q
        OPEN(31,FILE='INSPACE',POSITION='END')
        DO 399 K=2,N
        WRITE(31,FMT=*)(X(K,L),L=1,3)
        WRITE(31,FMT=*)(ORI(K,L),L=1,3)
 399    CONTINUE
        GO TO 315
 314    CONTINUE
        OPEN(31,FILE='INSPACE',POSITION='END')
        DO 316 K=2,N
        WRITE(31,FMT=*)(X(K,L),L=1,3)
 316    CONTINUE
 315    CONTINUE
        CLOSE(31)
 599    CONTINUE
        IF(IVELOC.NE.IMOVE)GO TO 835
        CALL BOLTZ(N)
        OPEN(22,FILE='DISTRIB',POSITION='END')
        DO 31 I=1,20
        WRITE(22,550)R(I),DNDV(I)
 31     CONTINUE
        CLOSE(22)
 550    FORMAT(1X,G14.7,',',G14.7)
        GO TO 835
 590    CONTINUE
        DO 380 J=1,IBROWN
        ZAX=0.
        DO 381 I=1,NOIBBS
        ZAX=ZAX+BROWN(I,J)
 381    CONTINUE
        BRAV(J)=ZAX/YALE
 380    CONTINUE
        OPEN(28,FILE='EXPERI')
        DO 562 K=1,NOIBBS
        WRITE(28,356)(XO(K,IAX),IAX=1,3)
        DO 563 J=1,IBROWN
        WRITE(28,355)BROWN(K,J)
 563    CONTINUE
 562    CONTINUE
        DO 473 I=1,IBROWN
        J=I-1
        WRITE(25,566)J,BRAV(I)
 473    CONTINUE
 566    FORMAT(1X,I4,',',G14.7)
 996    CONTINUE
        STOP
        END
```

A4.9 COMPUTER PROGRAM NEUTRAL-2

```
!UDD!PABLO!NEUTRAL_2                                                    11-OCT-84  10:59:42  PAGE 1
      IMPLICIT INTEGER*4(I-N)
      IMPLICIT REAL*8(A-H,O-Z)
      DIMENSION XC(200,3),DEL(5),M(30)
      DIMENSION SPHORE(30),G11(30),RADIUS(30)

C*****  NEUTRAL_2 CALCULATES THE RADIAL DISTRIBUTION FUNCTION

      OPEN(1,FILE='INSPACE')
      OPEN(2,FILE='NUMBER')

      READ(2,FMT=*)SCALE
      READ(2,FMT=*)N,IN

C*****  N=# OF MOLECULES(107)
C*****  IN=# OF 'PICTURES' OVER WHICH AVERAGING IS TO BE DONE
C*****  SCALE=Angstroms/SLU

      DO 12 ILENG=1,20
      RHE=2.*FLOAT(ILENG)-1.
      RHO=.0125*RHE
      RADIUS(ILENG)=RHO*SCALE
      SPHORE(ILENG)=.314159266*(RHO**2)
      M(ILENG)=0
 12   CONTINUE
      DO 1 KOUNT=1,IN
      IF(KOUNT.GT.IN)GO TO 999
      DO 2 I=1,N
      READ(1,FMT=*)(XC(I,IAX),IAX=1,3)
 2    CONTINUE
      DO 80 I=1,N
      IF(I.GT.N)GO TO 1
      DO 20 J=1,N
      IF(J.GT.N)GO TO 80
      IF(I.EQ.J)GO TO 600
      DO 21 IAX=1,3
      DEL(IAX)=XC(J,IAX)-XC(I,IAX)
      PEL=DEL(IAX)
      IF(ABS(PEL).LE.0.5)GO TO 16
      IF(PEL.GT.0.)GO TO 17
      DEL(IAX)=DEL(IAX)+1.
      GO TO 16
 17   CONTINUE
      DEL(IAX)=DEL(IAX)-1.
 16   CONTINUE
 21   CONTINUE
      SEPN=0.
      DO 18 K=1,3
      SEPN=SEPN+DEL(K)*DEL(K).
 18   CONTINUE
      SAPN=SQRT(SEPN)
      ILUM=INT(40.*SAPN)+1
      M(ILUM)=M(ILUM)+1
 600  CONTINUE
 20   CONTINUE
 80   CONTINUE
 1    CONTINUE
 999  CONTINUE
      TAT=FLOAT(N)*FLOAT(N-1)
      TUT=FLOAT(IN)
```

```
      DO 30 KI=1,20
      G11(KI)=(FLOAT(M(KI)))/TUT
      G11(KI)=(G11(KI)/SPHORE(KI))/TAT
30    CONTINUE
      OPEN(21,FILE='RADIAL')
      DO 32 IJO=1,20
      WRITE(21,50)RADIUS(IJO),G11(IJO)
32    CONTINUE
50    FORMAT(1X,G14.7,',',G14.7)
      STOP
      END
```

APPENDIX 5: THE INTEGRAL ENTROPY BALANCE IN IRREVERSIBLE THERMODYNAMICS

The following derivations follow closely the treatment of the subject by Landau and Lifshitz (1982).

A5.1: MASS BALANCE; CONSERVATION EQUATIONS

For an arbitrary volume V, fixed in space, conservation of species 1 can be written as

$$\frac{\partial}{\partial t}\int \rho\omega_1 \, dV = -\oint (\rho\omega_1 \, \underline{v} \cdot \underline{n}) \, df - \oint \underline{j}1 \cdot \underline{n} \, df \qquad (A.5\text{-}1)$$

The first term on the right hand side is the convective transport of species 1; the second term corresponds to diffusive transport. The derivation of a differential equation for the conservation of species 1 is the first step in our analysis: we are ultimately interested in a relationship between the diffusive flux and the appropriate driving force(s).

Using Green's theorem, we rewrite Equation (A.5-1),

$$\frac{\partial}{\partial t}\int \rho\omega_1 \, dV = -\int \underline{\nabla} \cdot (\rho\omega_1 \underline{v} + \underline{j}_1) \, dV \qquad (A.5\text{-}2)$$

Therefore,

$$\int [\frac{\partial \rho\omega_1}{\partial t} + \nabla \cdot (\rho\omega_1 \, \underline{v} + \underline{j}_1)] \, dV = 0 \qquad (A.5\text{-}3)$$

But this is independent of our choice of V; we must therefore have

$$\frac{\partial \rho\omega_1}{\partial t} + \nabla \cdot (\rho\omega_1 \, \underline{v} + \underline{j}_1) = 0 \qquad (A.5\text{-}4)$$

Invoking continuity for the fluid as a whole,

$$\frac{\partial \rho}{\partial t} + \nabla \cdot \rho\underline{v} = 0 \qquad (A.5\text{-}5)$$

The required equation follows from combining the last two expressions

$$\rho \, (\frac{\partial \omega_1}{\partial t} + \underline{v} \cdot \underline{\nabla}\omega_1) + \nabla \cdot \underline{j}_1 = 0 \qquad (A.5\text{-}6)$$

or, in a more concise form,

$$\rho \frac{D\omega_1}{Dt} + \underline{\nabla} \cdot \underline{j}_1 = 0 \qquad \text{(A.5-7)}$$

where D/Dt is the material derivative operator.

A5.2: THERMODYNAMIC DEFINITIONS

When diffusion is analyzed from the perspective of irreversible thermodynamics, it is convenient to introduce a mixture chemical potential. We start from the fundamental equation for a binary system,

$$dU = TdS - PdV + \mu_1 \, dN_1 + \mu_2 \, dN_2 \qquad \text{(A.5-8)}$$

If we impose the constraint of constant mass, we have

$$dN_2 = - \left(\frac{M_1}{M_2}\right) dN_1 \qquad \text{(A.5-9)}$$

and Equation (A.5-8) referred to unit mass of fluid, now reads

$$du = Tds - Pdv + \mu d\omega_1 \qquad \text{(A.5-10)}$$

with

$$\mu \equiv \frac{\mu_1}{M_1} - \frac{\mu_2}{M_2} \qquad \text{(A.5-11)}$$

A5.3: ENERGY AND ENTROPY RELATIONSHIPS

Diffusion is one of the dissipative processes that contribute to entropy generation in a fluid. We must therefore obtain an expression for the rate of entropy generation. Starting from a differential energy balance, we will use continuity, thermodynamics and the equations of motion to obtain a differential entropy balance. The integrated form of this equation gives the rate of entropy generation as a result of dissipative processes. We first derive the differential balances.

Consider a volume element fixed in space. Energy conservation yields

$$\frac{\partial}{\partial t} \left[\rho \left(\frac{v^2}{2} + u\right)\right] = - \underline{\nabla} \cdot \left[\rho \underline{v} \left(\frac{v^2}{2} + h\right) - \underline{v} \cdot \underline{\underline{\sigma}} + \underline{q}\right] \qquad \text{(A.5-12)}$$

The right hand side is the sum of reversible convective transport, irreversible viscous dissipation, and irreversible heat transfer. We now rewrite the left hand side,

$$\frac{\partial}{\partial t}\left[\rho\left(\frac{v^2}{2}+u\right)\right]=\frac{1}{2}v^2\frac{\partial\rho}{\partial t}+\rho\,\underline{v}\cdot\frac{\partial\underline{v}}{\partial t}+\rho\frac{\partial u}{\partial t}+u\frac{\partial\rho}{\partial t} \qquad (A.5\text{-}13)$$

and use continuity to transform the 1st and 4th terms in the right hand side, thermodynamics for the 3rd term, and the equations of motion for the 2nd term. Starting with the latter,

$$\rho\underline{v}\cdot\frac{\partial\underline{v}}{\partial t}=\rho v_i\frac{\partial v_i}{\partial t}=-v_i\frac{\partial P}{\partial x_i}+v_i\frac{\partial\sigma_{ik}}{\partial x_k}-\rho v_i\left[(\underline{v}\cdot\underline{\nabla})v_i\right] \qquad (A.5\text{-}14)$$

The 1st and 4th terms in Equation (A.5-13) can be rewritten, using continuity, as follows,

$$\frac{v^2}{2}\frac{\partial\rho}{\partial t}+u\frac{\partial\rho}{\partial t}=-\left(u+\frac{1}{2}v^2\right)\underline{\nabla}\cdot\rho\underline{v} \qquad (A.5\text{-}15)$$

Because of Equation (A.5-10) we can put (3rd term of Equation (A.5-13)),

$$\rho\frac{\partial u}{\partial t}=\rho T\frac{\partial s}{\partial t}+\frac{P}{\rho}\frac{\partial\rho}{\partial t}+\rho u\frac{\partial\omega_i}{\partial t} \qquad (A.5\text{-}16)$$

and substitute Equations (A.5-14), (A.5-15) and (A.5-16), and the thermodynamic relation

$$\frac{\partial P}{\partial x_i}=\rho\left[\frac{\partial h}{\partial x_i}-T\frac{\partial s}{\partial x_i}-\mu\frac{\partial\omega_i}{\partial x_i}\right] \qquad (A.5\text{-}17)$$

into Equation (A.5-13), to obtain

$$\begin{aligned}\frac{\partial}{\partial t}\left[\rho\left(\frac{v^2}{2}+u\right)\right]=&-\left(u+\frac{v^2}{2}\right)\underline{\nabla}\cdot\rho\,\underline{v}+\rho T\frac{\partial s}{\partial t}+\frac{P}{\rho}\frac{\partial\rho}{\partial t}+\\&+\rho\mu\frac{\partial\omega_i}{\partial t}-\rho v_i\left[\frac{\partial h}{\partial x_i}-T\frac{\partial s}{\partial x_i}-\mu\frac{\partial\omega_i}{\partial x_i}\right]+\\&+v_i\frac{\partial\sigma_{ik}}{\partial x_k}-\rho v_i\left[(\underline{v}\cdot\underline{\nabla})\,v_i\right]\end{aligned} \qquad (A.5\text{-}18)$$

which can be simplified with the help of Equation (A.5-6) and the identity

$$\rho\,v_i\left[(\underline{v}\cdot\underline{\nabla})\,v_i\right]=\rho\,\underline{v}\cdot\underline{\nabla}\left(\frac{1}{2}v^2\right) \qquad (A.5\text{-}19)$$

to obtain

$$\frac{\partial}{\partial t}\rho\left(u+\frac{v^2}{2}\right) = -\underline{\nabla}\cdot\left[\rho\underline{v}\left(h+\frac{v^2}{2}\right)\right] - \mu\,\underline{\nabla}\cdot\underline{j}_1 + \rho T\left[\frac{\partial s}{\partial t}+\underline{v}\cdot\underline{\nabla}s\right] + v_i\frac{\partial\sigma_{ik}}{\partial x_k} \qquad (A.5\text{-}20)$$

Adding and subtracting $\underline{\nabla}\cdot\underline{q}$, and noting that

$$v_i\frac{\partial\sigma_{ik}}{\partial x_k} = \underline{\nabla}\cdot(\underline{v}\cdot\underline{\underline{\sigma}}) - \sigma_{ik}\frac{\partial v_i}{\partial x_k} \qquad (A.5\text{-}21)$$

we obtain the important relationship

$$\frac{\partial}{\partial t}\left[\rho\left(u+\frac{v^2}{2}\right)\right] = -\underline{\nabla}\cdot\left[\rho\underline{v}\left(h+\frac{v^2}{2}\right)\right] - \underline{v}\cdot\underline{\underline{\sigma}} + \underline{q}] + \rho T\left(\frac{\partial s}{\partial t}+\underline{v}\cdot\underline{\nabla}s\right) - \mu\,\underline{\nabla}\cdot\underline{j}_1 + \underline{\nabla}\cdot\underline{q} - \sigma_{ik}\frac{\partial v_i}{\partial x_k} \qquad (A.5\text{-}22)$$

Comparing Equations (A.5-12) and (A.5-22),

$$\rho T\frac{Ds}{Dt} = \sigma_{ik}\frac{\partial v_i}{\partial x_k} - \underline{\nabla}\cdot(\underline{q}-\mu\underline{j}_1) - \underline{j}_1\cdot\underline{\nabla}\mu \qquad (A.5\text{-}23)$$

This is the required differential entropy balance.

A5.4: THE INTEGRAL ENTROPY BLAANCE

The rate of change of entropy in a volume fixed in space is given by

$$\frac{d}{dt}\int\rho s\,dV = \int\frac{\partial}{\partial t}(\rho s)dV = \int\left(\rho\frac{\partial s}{\partial t}+s\frac{\partial\rho}{\partial t}\right)dV$$

The integrand, using Equation (A.5-23) and continuity, can be written as follows,

$$\rho\frac{\partial s}{\partial t}+s\frac{\partial\rho}{\partial t} = \frac{1}{T}\left[\sigma_{ik}\frac{\partial v_i}{\partial x_k} - \underline{\nabla}\cdot(\underline{q}-\mu\underline{j}_1) - \underline{j}_1\cdot\underline{\nabla}\mu\right] - \underline{\nabla}\cdot\rho s\underline{v} \qquad (A.5\text{-}24)$$

Therefore,

$$\frac{d}{dt}\int \rho s dV = -\int(\underline{\nabla}\cdot\rho s\underline{v})\,dV + \int \frac{1}{T}\left[\sigma_{ik}\frac{\partial v_i}{\partial x_k} - \underline{\nabla}\cdot(\underline{q}-\mu\underline{j}_1) - \underline{j}_1\cdot\underline{\nabla}\mu\right]dV \tag{A.5-25}$$

The left hand side of Equation (A.5-25) (and hence the right hand side) is positive or zero for any isolated system. Restricting our attention to this case,

$$\int\underline{\nabla}\cdot\rho s\,\underline{v}\,dV = \oint(\rho s\,\underline{v}\cdot\underline{n})df = 0 \tag{A.5-26}$$

since there can be no flow across the boundaries of an isolated system. Similarly,

$$\int\frac{1}{T}\underline{\nabla}\cdot(\underline{q}-\mu\underline{j}_1)\,dV = \int\underline{\nabla}\cdot\left(\frac{\underline{q}-\mu\underline{j}_1}{T}\right)dV + \int\left(\frac{\underline{q}-\mu\underline{j}_1}{T^2}\right)\cdot\underline{\nabla}T dV =$$

$$\oint\left[\left(\frac{\underline{q}-\mu\underline{j}_1}{T}\right)\cdot\underline{n}\right]df + \int\left(\frac{\underline{q}-\mu\underline{j}_1}{T^2}\right)\cdot\underline{\nabla}T\,dV = \int\left(\frac{\underline{q}-\mu\underline{j}_1}{T^2}\right)\cdot\underline{\nabla}T\,dV \tag{A.5-27}$$

where isolation has again been invoked to eliminate the surface integral. The integral entropy balance for an isolated binary system then becomes

$$\frac{d}{dt}\int\rho s\,dV = \int\frac{1}{T}\sigma_{ik}\frac{\partial v_i}{\partial x_k}dV - \int\left(\frac{\underline{q}-\mu\underline{j}_1}{T^2}\right)\cdot\underline{\nabla}T dV - \int\underline{j}_1\cdot\frac{\underline{\nabla}\mu}{T}\,dV \tag{A.5-28}$$

Closed, isolated, macroscopic systems approach stable equilibrium in an irreversible way, the mechanisms involved being viscous dissipation, heat flow and diffusion (first, second and third integral, respectively, in the right hand side of Equation (A.5-28)).

NOTATION

A = roughness factor (Chapter 2), dimensionless

A = z-dependent coefficient (Chapter 5), dimensionless

A = defined in Equation (6.26), dimensionless

A = reduced attractive parameter in a cubic equation of state (Chapter 7) dimensionless

A = inertial-principal transformation matrix (Chapter 8), dimensionless

A_n = expansion coefficient defined in Equation (5.72), dimensionless

a = rectangular duct half-width, L

a = radius of a Brownian sphere (Equation 1.17; Section 1.5; Chapter 2; Chapter 6; Chapter 8), L

a = attractive parameter for cubic equations of state (Chapter 3; Chapter 7; Appendix 1), ML^5/t^2mol^2

a_i = ith coefficient of series expansion (Equation (5.19)), dimensionless

a'_i = scaled ith coefficient (a_i/a_o) (Chapter 5), dimensionless

$a'_{i,n}$ = scaled ith coefficient evaluated with the nth eigenvalue (Equation (5.24)), dimensionless

a_{ij} = parameter for a 12-6 type interaction energy (Equation (9.31)), ML^{14}/t^2

B = empirical linear coefficient in a density-explicit virial expansion (Chapter 2), L^3/M

B = defined in Equation (6.27), dimensionless

B = reduced repulsive parameter in cubic equation of state (Chapter 7), dimensionless

B_n = expansion coefficient (Equation (5.73)), dimensionless

b = rectangular duct half-height, L

b = repulsive parameter for cubic equations of state (Chapter 3; Chapter 7; Appendix 1), L^3/mole

b_o = molar second virial coefficient, L^3/mole

C = empirical quadratic coefficient in a density-explicit virial expansion (Chapter 2), L^6/M^2

C_n = expansion coefficient (Equation (5.29)), dimensionless

$C_{i,j}$ = expansion coefficient (Equation (5.24)), dimensionless

C_{ij} = parameter for a 12-6 type interaction energy (Equation (9.31)), ML^8/t^2

c = solute molar concentration, moles/L^3

c = total molar concentration (Section 1.4; Chapter 7), moles/L^3

c_i = interface solute molar concentration, moles/L^3

c^+ = $1 - c/c_i$ [or $(c-c_i)/(c_o-c_i)$; but $c_o = 0$ throughout], dimensionless

c_o = inlet solute molar concentration, moles/L^3

D = duct diameter (Section 1.1; Chapter 3), L

D = diffusion coefficient, L^2/t

$\mathcal{D}$ = diffusion coefficient, L^2/t

D_h = hydraulic diameter, L

d = dimensionality of space, dimensionless

e_i = ith (i = 0,1,2,3) Cayley-Klein parameter, dimensionless

F = force (Section 9.1; Section 9.4), ML/t^2

F_m = modified force for shifted force potential (Chapter 9), ML/t^2

f = force, ML/t^2

f = fugacity (Section 1.4; Chapter 7), M/Lt^2

f = distribution function (Section 8.5), t^3/L^6

f = area element (Appendix 5), L^2

G_n = expansion coefficient, defined in Equation (5.61), dimensionless

Gr = Grashof number $[(2R)^3 g (\Delta\rho/\rho)/\nu^2]$, dimensionless

g = radial distribution function, dimensionless

g = acceleration due to gravity (Section 1.1; Chapter 3), L/t^2

$\underline{g}'$ = unit vector, parallel to gravity, dimensionless

H = "radial" part of two-dimensional solution to rectangular duct diffusion problem, dimensionless

H = Hamiltonian (Chapter 8), ML^2/t^2

H_n' = scaled "radial" expansion, defined in Equation (5.32), dimensionless

h = relative height of constant hydrostatic head plane, L

h = enthalpy per unit mass (Appendix 5), L^2/t^2

I = moment of inertia, ML^2

J = generalized flux in irreversible thermodynamics (Chapter 7), variously defined

j = mass flux, M/L^2t

K = torque, ML^2/t^2

K = proportionality constant for semi-empirical hydrodynamic expressions for the diffusion coefficient (Table 6.18), variously defined

K = exponential decay factor for solute fugacity coefficient (Section 1.4; Chapter 7), dimensionless

K_T = isothermal compressibility, Lt^2/M

K_T' = reduced isothermal compressibility, dimensionless

k = Boltzmann's constant, ML^2/t^2K

k = mass transfer coefficient (Section 1.2; Chapter 5), L/t

k = thermal conductivity (Table 2.1), ML/t^3K

k_{ij} = binary interaction coefficient, dimensionless

L = coated length in duct flow, L

L = Avogadro's number (Chapter 2; Section 6.2), $mole^{-1}$

L = generalized transport coefficient (Chapter 7), variously defined

$\underline{l}$ = unit vector, parallel to linear molecule, dimensionless

M = molecular weight, M/mole

m = mass, M

m = velocity profile exponent (Section 1.2; Chapter 5), dimensionless

N = # of molecules in a simulation

N = # of moles (Chapter 7; Appendix 1; Appendix 5)

$\dot{N}'$ = molar flux, moles/L^2t

n = velocity profile exponent, dimensionless

n = number density (Chapter 2; Chapter 6), $1/L^3$

n = unit normal vector (Appendix 5), dimensionless

P = pressure, M/Lt^2

p = linear momentum, ML/t

Pe = Peclet number ($\langle v \rangle$ L/D), dimensionless

q = heat flux, M/t^3

q = generalized coordinate (Chapter 8), L

q = wave number (Chapter 2), $1/L$

R = gas constant, ML^2/t^2 mole K

R = duct radius (Section 1.1; Section 3.1; Section 3.3), L

Re = Reynolds number ($2R \langle v \rangle/\nu$), dimensionless

Ra = Raleigh number $\left[(2R)^3 g \Delta\rho/\rho /\nu D\right]$, dimensionless

r = position, displacement, relative position (variously defined), L

r = relative saturation (c/ci) (Section 1.1; Section 1.2; Chapter 3; Chapter 5; Chapter 6; Appendix 2), dimensionless

r_c = cutoff radius, L

r_h = hydraulic radius, L

Sc = Schmidt number (ν/D), dimensionless

Sh = Sherwood number ($4\ r_h\ k/D$), dimensionless

s = entropy per unit mass, L^2/t^2K

s = hard sphere solute/solvent ratio (Chapter 6), dimensionless

T = absolute temeprature

T^+ = reduced temperature (kT/ε), dimensionless

t = time, t

U = interaction energy, ML^2/t^2

U = internal energy (Appendix 5), ML^2/t^2

u = numerical constant for cubic equation of state, dimensionless

u = internal energy per unit mass, (Appendix 5), L^2/t^2

V = molar volume, L^3/mole

V = total volume (Equation (7.1); Equation (7.25); Chapter 8; Appendix 5), L^3

V_o = close-packed molar volume for a hard-sphere fluid, L^3/mole

v = velocity, L/t

$\langle v \rangle$ = cross section-average velocity, L/t

v^+ = reduced velocity ($v/\langle v \rangle$), dimensionless

v = molecular volume (Section 2.3), L^3

v^+ = reduced molecular volume (v/σ^3) (Section 2.3), dimensionless

v = molar volume (Appendix 5), L^3/mole

w = angular velocity, 1/t

w = numerical constant for a cubic equation of state (Chapter 3; Chapter 7; Appendix 1), dimensionless

X = axial part of two-dimensional solution to rectangular duct diffusion problem, dimensionless

X = generalized force (Chapter 7), variously defined

X_o = modified inverse Graetz number ($xD/\langle v \rangle b^2$), dimensionless

x = duct axial coordinate, L

x^+ = dimensionless axial coordinate (x/b)

x_i = species i mole fraction (Chapter 6; Section 1.4, Chapter 7), dimensionless

x = inertial coordinate (Section 1.5; Chapter 8), L

x' = principal coordinate, L

y = duct "radial" coordinate, L

y^+ = dimensionless "radial" coordinate (y/b)

y = inertial coordinate (Chapter 8), L

y' = principal coordinate, L

z = duct transverse coordinate, L

z^+ = dimensionless duct transverse coordinate (z/b)

z = inertial coordinate (Chapter 8), L

z' = principal coordinate, L

z = compressibility factor (RV/RT) (Chapter 2; Chapter 3; Chapter 7; Section 8.6), dimensionless

Greek Symbols

α = aspect ratio for rectangular duct (b/a), dimensionless

α = transport coefficient, (Section 1.4; Chapter 7), Mt/L^3

α = flat plate inclination with respect to horizontal position (Figure 1.10; Figure 6.15), degrees

α_i = polarizability of site i (Equation 9.32), L^3

α = angle used in specifying the relative orientation of two linear molecules (Figures 9.9 to 9.21), degrees

α = coefficient of the attractive parameter in a cubic equation of state (Appendix 1), dimensionless

β = aspect ratio for rectangular duct (L/2a), dimensionless

β_m = mass coefficient of volume expansion (Section 3.2), L^3/mole

β = transport coefficient (Chapter 7), M/Lt K

β = frictional time constant (Chapter 8), t^{-1}

β = angle used in specifying the relative orientation of two linear molecules (Figures 9.9 to 9.21), degrees

β = coefficient of the size parameter in a cubic equation of state (Appendix 1), dimensionless

Γ = scattered light autocorrelation decay rate, t^{-1}

Γ_n = defined in Equation (8.61), ML^2/t

γ_n = nth eigenvalue (Chapter 5), dimensionless

γ = transport coefficient (Chapter 7), ML/t^3K

γ = angle used in specifying the relative orientation of two linear molecules (Figures 9.9 to 9.21), degrees

δ = transport coefficient (Chapter 7), M/Lt

δ = displacement (Chapter 8), L

δ = angle used in specifying the relative orientation of two linear molecules (Figures 9.9 to 9.21), degrees

ε = energy parameter for interaction potential, ML^2/t^2

η = viscosity, M/Lt

θ = Euler angle, dimensionless

μ = chemical potential per unit mass, L^2/t^2

μ_i = species i chemical potential, ML^2/t^2 mole

ν = kinematic viscosity, L^2/t

ξ = transformed coordinate for duct flow (b-y), L

ξ^+ = dimensionless transformed coordinate ($1-y^+$)

ξ = defined in text (Chapter 2)

ξ = distance measured away from a constant composition solute source plance (Chapter 6), L

Π = modified pressure ($P_o + \rho gh$), M/Lt^2

Π^+ = dimensionless modified pressure $[\Pi/\rho_o \langle v \rangle^2]$

ρ = density, M/L^3

$\Delta\rho$ = interface-bulk density difference, M/L^3

σ = size parameter for a binary interaction, L

σ_{ij} = ijth component of stress tensor (Chapter 7; Appendix 5), M/Lt^2

τ = relaxation time, t

ϕ = fugacity coefficient, dimensionless

ϕ_n = cross section-average integral (Equation (5.55)), dimensionless

ϕ = association factor in the Wilke-Chang expression (Chapter 6), dimensionless

ϕ = Euler angle (Chapter 8), dimensionless

ϕ_i = species i probability distribution function for one-dimensional displacements (Chapter 8), L^{-1}

χ = Enskog frequency factor, dimensionless

ψ = composition-dependence function for the thermodynamic transport coefficient, α, such that D_{12} is composition-independent (Chapters 1 and 7), dimensionless

ψ_n = cross section-average integral defined in Equation (5.75), dimensionless

ψ = Euler angle (Chapter 8), dimensionless

Ω_d = collision integral for diffusion, dimensionless

ω = acentric factor, dimensionless

ω_i = species i weight fraction (Appendix 5), dimensionless

Subscripts

1 = solute

2 = solvent

A = solute (Tables 6.18 and 6.19)

B = solvent (Tables 6.18 and 6.19)

c = critical property

I = molecule I

i = interface (Section 1.2; Chapter 3)

i = ith site (Section 1.5)

i = ith principal direction (Equation 1.39; Equation 8.17)

J = molecule J

n = nth eigenvalue

o = solute inlet conditions

r = reduced quantity

Superscripts

+ = dimensionless quantity

0 = dilute limit

T = transposed

Overbars

- = partial molar quantity

^ = denotes value of a property for a specie in a mixture

• = time derivative

Underbars

- = vector

= = matrix, tensor

REFERENCES

B.J. Alder, W.E. Alley and J.H. Dymond, "Studies in molecular dynamics. XIV. Mass and size dependence of the binary diffusion coeffecient", J. Chem. Phys., **61**(4), 1415-1420, (1974).

B.J. Alder, W.G. Hoover and D.A. Young, "Studies in molecular dynamics. V. High-density equation of state and entropy for hard disks and spheres", J. Chem. Phys., **49**(8), 3688-3696, (1968).

B.J. Alder and T.E. Wainwright, "Studies in molecular dynamics. I. General method ", J. Chem. Phys., **31**(2), 459-466, (1959).

B.J. Alder and T.E. Wainwright, "Phase transition in elastic disks", Phys. Rev., **127**(2), 359-361, (1962).

B.J. Alder and T.E. Wainwright, "Velocity autocorrelations for hard spheres", Phys. Rev. Lett., **18**(23), 988-990, (1967).

B.J. Alder and T.E. Wainwright, "Decay of the velocity autocorrelation function", Phys. Rev. A, **1**(1), 18-21, (1970).

G. Allen, J.G. Watkinson, and K.H. Webb, "An infra-red study of the association of benzoic acid in the vapour phase, and in dilute solution in non-polar solvents", Spechtroch. Acta, **22**, 807-814, (1966).

E.N. da C. Andrade, "The Viscosity of Liquids", Nature, **125**, 309-310 (1930).

S. Angus, B. Armstrong and K.M. de Reuck, "Carbon Dioxide-International Thermodynamic Tables of the Fluid State-3", IUPAC, Division of Physical Chemistry, Commission on Thermodynamics and Thermochemistry, Thermodynamic Tables Project, Pergamon Press, Oxford, 1976.

V.S. Arpaci, "Conduction Heat Transfer", Addison-Wesley, Reading, Mass., 1966.

Z. Balenovic, M. Myers and J.C. Giddings, "Binary diffusion in dense gases to 1360 atm by the chromatographic peak-broadening method", J. Chem. Phys., **52**(2), 915-922, (1970).

V.J. Berry, Jr., and R.C. Koeller, "Diffusion in compressed binary systems", AIChE J., **6**(2), 274-280, (1960).

S.J. Bertucci and W.H. Flygare, "Rough hard sphere treatment of mutual diffusion in binary liquid mixtures", J. Chem. Phys., **63**(1), 1-9, (1975).

R.B. Bird, W.E. Stewart and E.N. Lightfoot, "Transport Phenomena", John Wiley and Sons, New York, 1960.

G. Brunner, "Mass transfer from solid material in gas extraction", Ber. Bunsenges. Phys. Chem., **88**, 887-891, (1984).

A.D. Buckingham and R.L. Disch, "The quadruple moment of the carbon dioxide molecule", Proc. Roy. Soc. A, 273, 275-289, (1963).

H.C. Burstyn and J.V. Sengers, "Decay rate of critical concentration fluctuations in a binary liquid", Phys. Rev. A, 25(1), 448-465, (1982).

D.M. Ceperley, "The relative performances of several scientific computers for a liquid molecular dynamics simulation", Supercomputers in Chemistry, P. Lykos and I. Shavitt, eds., ACS Symposium Series #173, Ch. 9, 125-134, (1981).

D. Chandler, "Rough hard sphere theory of the self-diffusion constant for molecular liquids", J. Chem. Phys., 62(4), 1358-1363, (1975).

D. Chandler, J. D. Weeks and H.C. Andersen, "van der Waals picture of liquids, solids and phase transformations", Science, 220, 787-794, (1983).

S. Chandrasekhar, "Stochastic problems in physics and astronomy", Rev. Mod. Phys., 15, 1-89, (1943).

S. Chapman and T.G. Cowling, "The Mathematical Theory of Non-Uniform Gases", 3rd edition, Cambridge University Press, Cambridge, 1970.

S. Chen, "A rough-hard-sphere theory for diffusion in supercritical carbon dioxide", Chem. Eng. Sci., 38(4), 655-660, (1983).

P.S.Y. Cheung and J.G. Powles, "The properties of liquid nitrogen. IV. A computer simulation", Mol. Phys., 30(3), 921-949, (1975).

K.J. Czworniak, H.C. Andersen, and R. Pecora, "Light scattering measurement and theoretical interpretation of mutual diffusion coefficients in binary liquid mixtures", Chem. Phys., 11, 451-473, (1975).

J. DeZwaan and J. Jonas, "Experimental evidence for the rough hard sphere model for liquids by high pressure NMR", J. Chem. Phys., 62(10), 4036-4040, (1975).

J.H. Dymond, "Corrected Enskog theory and the transport coefficients of liquids", J. Chem. Phys., 60(3), 969-973, (1974).

J.H. Dymond and B.J. Alder, "van der Waals theory of transport in dense fluids", J. Chem. Phys., 45(6), 2061-2068, (1966).

A. Einstein, "On the movement of small particles suspended in a stationary liquid demanded by the molecular-kinetic theory of heat", Ann. d. Phys., 17, 549, (1905).

J.F. Ely and J.K. Baker, "A review of supercritical fluid extraction", NBS Technical Note 1070, (1983).

D. Enskog, K. Svensk. Vet. - Akad. Handl., 63(4), (1921).

C.P. Enz (ed.), "Dynamical Critical Phenomena and Related Topics", Proceedings of the International conference on Dynamic Critical Phenomena, Geneva, 1979; Lecture Notes in Physics, No. 104; Springer-Verlag, Berlin, (1979).

R. Feist and G.M. Schneider, "Determination of binary diffusion coefficients of benzene, phenol, naphthalene and caffeine in supercritical CO_2 between 308 and 333 K in the pressure range 80 to 160 bar with supercritical fluid chromatography (SFC)", Sep. Sci. and Tech., **17**(1), 261-270, (1982).

M. Fury, G. Munie and J. Jonas, "Transport processes in compressed liquid pyridine", J. Chem. Phys., **70**(3), 1260-1265, (1979).

H. Goldstein, "Classical Mechanics", 2nd edition, Addison-Wesley, Reading, Mass., 1981.

K.E. Gubbins, K.S. Shing and W.B. Streett, "Fluid phase equilibria: experiment, computer simulation and theory", J. Phys. Chem., **87**, 4573-4585, (1983).

A.S. Gupta and G. Thodos, "Mass and heat transfer in the flow of fluids through fixed and fluidized beds of spherical particles", AIChE J., **8**(5), 608-610, (1962).

J.M. Haile, "Molecular dynamics simulations of simple fluids with three-body interactions included", Computer Modeling of Matter, P. Lykos, ed., ACS Symposium Series #86, Ch. 15, 172-190, (1978).

W.B. Hall, "Forced convective heat transfer to supercritical pressure fluids", Arch. Thermod. i Spalania, **6**(3), 341-352, (1975).

H.J.M. Hanley, R.D. McCarty and E.G.D. Cohen, "Analysis of the transport coefficients for simple dense fluids: applications of the modified Enskog theory", Physica, **60**, 322-356, (1972).

H.J.M. Hanley and E.G.D.Cohen, "Analysis of the transport coefficients for simple dense fluids: the diffusion and bulk viscosity coefficients", Physica, **83A**, 215-232, (1975).

G.S. Harrison and A. Watson, "Similarity and the formation of correlations for forced convection to supercritical fluids", Cryogenics, 147-151, March 1976.

E.G. Hauptmann and A. Malhotra, "Axial development of unusual velocity profiles due to heat transfer in variable density fluids", J. Heat Transf., **102**, 71-74, (1980).

W. Hayduk and S.C. Cheng, "Review of relation between diffusivity and solvent viscosity in dilute liquid solutions", Chem. Eng. Sci., **26**, 635-646, (1971).

P.T. Herman and B.J. Alder, "Studies in molecular dynamics. XI. Correlation functions of a hard-sphere test-particle", J. Chem. Phys., 56(2), 987-991, (1972).

J.O. Hirschfelder, C.F. Curtiss and R.B. Bird, "Molecular Theory of Gases and Liquids", John Wiley and Sons, New York, 1964.

C. Hoheisel, "The binary diffusion coefficient of benzene at high dilution in dense gas CO_2", Mol. Phys., 45(2), 371-377, (1983).

Y. I'Haya and T. Shibuya, "The dimerization of benzoic acid in carbon tetrachloride and chloroform", Bull. Chem. Soc. Japan, 38(7), 1144-1147, (1965).

K. Huang, "Statistical Mechanics", John Wiley and Sons, New York, 1963.

M.B. Iomtev and Y.V. Tsekhanskaya, "Diffusion of naphthalene in compressed ethylene and carbon dioxide", Russ. J. Phys. Chem., 38(4), 485-487, (1964).

J.A. Jossi, L.I. Stiel and G. Thodos, "The viscosity of pure substances in the dense gaseous and liquid phases", AIChE J., 8(1), 59-63, (1963).

C.R. Kakarala and L.C. Thomas, "Turbulent combined forced and free convection heat transfer in vertical tube flow of supercritical fluids", Int. J. Heat and Fluid Flow, 2(3), 115-120, (1980).

A.J. Karabelas, T.H. Wegner and T. J. Hanratty, "Use of asymptotic relations to correlate mass transfer data in packed beds", Chem. Eng. Sci., 26, 1581-1589, (1971).

R.T. Kurnik, Ph.D. Thesis, Massachusetts Institute of Technology, Cambridge, MA, 1981.

L.D. Landau and E.M Lifshitz, "Statistical Physics", 3rd edition, part 1; volume 5 of the Course of Theoretical Physics, revised and enlarged by E.M. Lifshitz and L.P. Pitaevskii, Pergamon Press, Oxford, 1980.

L.D. Landau and E.M. Lifshitz, "Mechanics", 3rd edition; volume 1 of the Course of Theoretical Physics, Pergamon Press, Oxford, 1982.

L.D. Landau and E.M. Lifshitz, "Fluid Mechanics", volume 6 of the Course of Theoretical Physics, Pergamon Press, Oxford, 1982.

G. Le Bas, "The Molecular Volumes of Liquid Chemical Compounds", Longmans, Green, New York, 1915.

M.A. Lusis and G.A. Ratcliff, "Diffusion in binary liquid mixtures at infinite dilution", Can. J. Chem. Eng., 46, 385-587, (1968).

S. Ma, "Modern Theory of Critical Phenomena", Benjamin/Cummings Publishing Company, Inc., Reading, MA, 1976.

G.C. Maitland, M. Rigby, E.B. Smith and W.A. Wakeham, "Intermolecular Forces, Their Origin and Determination", Clarendon Press, Oxford, 1981.

V.R. Maynard and E. Grushka, "Measurement of diffusion coefficients by gas-chromatography broadening techniques: a review", Adv. Chromatogr., 12, 99-140, (1975).

D.A. McQuarrie, "Statistical Mechanics", Harper and Row, New York, 1976.

B. Metais and E.R.G. Eckert, "Forced, mixed and free convection regimes", J. Heat Transfer, 86, 295-296, (1964).

N. Metropolis, A.W. Rosenbluth, M.N. Rosenbluth, A.H. Teller, and E. Teller, "Equations of state calculations by fast computing machines", J. Chem. Phys., 21, 1087-1092, (1953).

M. Modell and R.C. Reid, "Thermodynamics and its Applications", 2nd edition, Prentice-Hall, Englewood Cliffs, NJ, 1983.

V.S. Morozov and E.G. Vinkler, "Measurement of diffusion coefficients of vapours of solids in compressed gases. I. Dynamic method for measurement of diffusion coefficients", Russ. J. Phys. Chem., 49(9), 1404-1405, (1975).

V.S. Morozov and E.G. Vinkler, "Measurement of diffusion coefficients of vapours of solids in compressed gases. II. Diffusion coefficients of naphthalene in nitorgen and in carbon dioxide, Russ. J. Phys. Chem., 49(9), 1405-1406, (1975).

S. Murad and K.E. Gubbins, "Corresponding states correlation for thermal conductivity of dense fluids", Chem. Eng. Sci., 32, 499-505, (1977).

S. Murad and K.E. Gubbins, "Molecular dynamics simulation of methane using a singularity-free algorithm", Computer Modelling of Matter, P. Lykos, ed., ACS Symposium Series #86, ch. 5, 62-71, 1978.

S. Murad and K.E. Gubbins, "Prediction of thermal conductivity for dense fluids and fluid mixtures", AIChE J., 27(5), 864-866, (1981).

C.S. Murthy, K. Singer, and I.R. McDonald, "Interaction site models for carbon dioxide", Mol. Phys., 44(1), 135-143, (1981).

K. Nishikawa and T. Ito, "An analysis of free-convection heat transfer form an isothermal vertical plate to supercritical fluids", J. Heat Mass Transf., 12, 1449-1463, (1969).

K. Nishikawa, T. Ito, and H. Yamashita, "Free convective heat transfer to a supercritical fluid", J. Heat Transf., 187-191, May, (1973).

S. Nose and M.L. Klein, "A study of solid and liquid carbon tetrafluoride using the constant pressure molecular dynamics technique", J. Chem. Phys., 78(11), 6928-6939, (1983).

H.A. O'Hern and J.J. Martin, "Diffusion in carbon dioxide at elevated pressures", Ind. Eng. Chem., 47, 2081-2087, (1955).

L. Onsager, "Reciprocal Relations in Irreversible Processes. I", Phys. Rev., 37, 405-426, (1931)

L. Onsager, "Reciprocal Relations in Irreversible Processes. II", Phys. Rev., 38, 2265-2279, (1931).

A.C. Ouano, "Diffusion in liquid systems. I. A simple and fast method of measuring diffusion coefficients", Ind. Eng. Chem. Fund., 11(2), 268-271, (1972).

M.E. Paulaitis, V.J. Krukonis, R.T. Kurnik and R.C. Reid, "Supercritical fluid extraction", Rev. in Chem. Eng., 1(2), 179-250, (1983).

W. Pauli, "Pauli Lectures on Physics", volume 4, Statistical Mechanics, C.P. Enz, ed., MIT Press, 1981.

D.Y. Peng and D.B. Robinson, "A new two-constant equation of state", Ind. Eng. Chem. Fund., 15, 59, (1976).

R.H. Perry and C.H. Chilton, eds., "Chemical Engineers' Handbook", 5th edition, McGraw-Hill, New York, 1973.

R.H. Perry and D.H. Green, eds., "Perry's Chemical Engineers' Handbook", 6th edition, McGraw-Hill, New York, 1984.

P. Pfeuty and G. Toulouse, "Introduction to the Renormalization Group and to Critical Phenomena", John Wiley and Sons, Chichester, 1978.

K. Pitzer, D.Z. Lippmann, R.F. Curl, Jr., C.M. Huggins and D.E. Petersen, "The volumetric and thermodynamic properties of fluids. II. Compressibility factor, vapour rpessure and entropy of vaporization", J. Am. Chem. Soc., 77(13), 3433-3440, (1955).

K. Pitzer, "Inter-and intramolecular forces and molecular polarizability", Adv. Chem. Phys., 2, 59-83, (1959).

A. Rahman, "Correlations in the motion of atoms in liquid argon", Phys. Rev., 136(2A), A405-A411, (1964).

K. Reddy and L.K. Doraiswamy, "Estimating liquid diffusivity", Ind. Eng. Chem. Fund., 6(1), 77-79, (1967).

O. Redlich and J.N.S. Kwong, "On the thermodynamics of solutions. V. An equation of state. Fugacities of gaseous solutions", Chem. Rev., 44(1), 233-244, (1949).

R.C. Reid, J.M. Prausnitz and T.K. Sherwood, "The Properties of Gases and Liquids", 3rd edition, McGraw-Hill, New York, 1977.

P.J. Rossky and M. Karplus, "Solvation. A molecular dynamics study of a dipeptide in water", J. Am. Chem. Soc., 101(8), 1913-1937, (1979).

H. Saad and E. Gulari, "Diffusion of liquid hydrocarbons in supercritical CO_2 by photon correlation spectroscopy", Ber. Bunsenges. Phys. Chem., 88, 834-837, (1984).

E.G. Scheibel, "Liquid diffusivities", Ind. Eng. Chem., 46(9), 2007-2008, (1954).

G. Schmidt and H. Wenzel, "A modified van der Waals type equation of state", Chem. Eng. Sci., 35, 1503-1512, (1980).

W.M. Schmitt, private communication, 1984.

R.K. Shah and A.L. London, "Laminar Flow Forced Convection in Ducts", Academic Press, New York, 1978.

W. Shitsman, "Heat transfer to supercritical helium, carbon dioxide, and water: analysis of thermodynamic and transport properties and experimental data", Cryogenics, 77-83, February 1974.

K. Singer, A. Taylor and J.V.L. Singer, "Thermodynamic and structural properties of liquids modelled by '2 Lennard-Jones centres' pair potentials", Mol. Phys., 33(6), 1757-1795, (1977).

J.C. Slattery and R.B. Bird, "Calculation of the diffusion coefficient of dilute gases and the self-diffusion coefficient of dense gases", AIChE J., 4(2), 137-142, (1958).

G. Soave, "Equilibrium constants from a modified Redlich-Kwong equation of state", Chem. Eng. Sci., 27, 1197-1203, 1972.

H.E. Stanley, "Introduction to Phase Transitions and Critical Phenomena", Oxford University Press, New York, 1971.

K. Stefan and K. Lucas, "The Viscosity of Dense Fluids", Plenum Press, New York, 1979.

F.H. Stillinger and A. Rahman, "Improved simulation of liquid water by molecular dynamics", J. Chem. Phys., 60(4), 1545-1557, (1974).

W.B. Streett, D.J. Tildesley and G. Saville, "Multiple time step methods and an improved potential function for molecular dynamics simulations of molecular liquids", Computer Modelling of Matter, P. Lykos, ed., ACS Symposium Series #86, ch. 13, 144-158, 1978.

U.W. Suter, "Conformational characteristics of poly(methylvinyl ketone)s and of simple model ketones", J. Am. Chem. Soc., 101, 6481-6496, (1979).

I. Swaid and G.M. Schneider, "Determination of binary diffusion coefficients of benzene and some alkylbenzenes in supercritical CO_2 between 308 and 328 K in the pressure range 80 to 160 bar with supercritical fluid chromatography", Ber. Bunsenges. Phys. Chem., **83**, 969-974, (1979).

G.I. Taylor, "Dispersion of soluble matter in solvent flowing slowly through a tube", Proc. Roy. Soc. (London), **A219**, 186-203, (1953).

G.I. Taylor, "Diffusion and mass transport in tubes", Proc. Phys. Soc. (London), **B67**, 857-869, (1954).

L.S. Tee, S. Gotoh and W.E. Stewart, "Molecular Parameters for normal fluids", Ind. Eng. Chem., **5**(3), 356-363, (1966).

A.S. Teja, "The correlation and prediction of diffusion coefficients in liquids using a generalized corresponding states principle", AIChE annual meeting, Los Angeles, CA, 11-1982.

D.N. Theodorou and U.W. Suter, "Geometrical considerations in model systems with periodic boundary conditions", J. Chem. Phys., in press.

Y.V. Tsekhanskaya, "Diffusion in the system p-nitrophenol-water in the critical region", Russ. J. Phys. Chem., **42**(4), 532-533, (1968).

Y.V. Tsekhanskaya, "Diffusion of naphthalene in carbon dioxide near the liquid-gas critical point", Russ. J. Phys. Chem., **45**(5), 744, (1971).

J. van der Waals, Ph.D. Thesis, University of Leiden, 1873.

N.G. van Kampen, "Stochastic Processes in Physics and Chemistry", North-Holland, Amsterdam, 1983.

L. Verlet, "Computer 'experiments' on classical fluids. I. Thermodynamical properties of Lennard-Jones molecules", Phys. Rev., **159**(1), 98-103, (1967).

T. Wainwright and B.J. Alder, "Molecular dynamics computations for the hard sphere system", Nuovo Cimento, Supplemento al vol. IX, Ser IX, No. 1, 3° Trimestre, 116-132, (1958).

B. Widom, "Intermolecular forces and the nature of the liquid state", Science, **157**, 375-382, (1967).

C.R. Wilke and P. Chang, "Correlations of diffusion coefficients in dilute solutions", AIChE J., **1**(2), 264-270, (1955).

J.E. Williamson, K.E. Bazaire and C.J. Geankoplis, "Liquid-phase mass transfer at low Reynolds numbers", Ind. Eng. Chem. Fund., **2**, 126-129, (1963).

E.J. Wilson and C.J. Geankoplis, "Liquid mass transfer at very low Reynolds numbers in packed beds", Ind. Eng. Chem. Fund., **5**, 9-14, (1966).